ScienceInnovation
INTERNATIONAL SCIENTIFIC JOURNAL

ISSN:
2181-3337

INTERNATIONAL SCIENTIFIC JOURNAL

SCIENCE AND INNOVATION

VOLUME 5 / ISSUE 5

A:
CHEMISTRY
TECHNIQUE
ECONOMICS
PHYSICS AND
MATHEMATICS

MAY 2026

International Scientific Journal
SCIENCE AND INNOVATION
Series A
Volume 5 Issue 5
May 2026

Tashkent 2026

ISSN: 2181-3337

International Scientific Journal SCIENCE AND INNOVATION. Series A volume 5 issue 5 – 361 p.

The collection contains scientific articles accepted for issue 5 for 2026 of the international scientific journal "Science and Innovation".

In this scientific journal, in the form of scientific articles, the results of scientific research conducted by professors and teachers of the Republic of Uzbekistan and international higher educational institutions, independent researchers, doctoral students, undergraduates were published. In addition to higher educational institutions, the journal also includes scientific articles by employees working in other research institutes, production organizations and enterprises of our region and republic.

The materials of the journal can be used by professors, teachers, independent researchers, doctoral students, undergraduates, students, teachers of lyceums and schools, scientists and everyone who is interested in science.

This issue of the journal is indexed in the international scientific databases Index Copernicus, eLibrary.ru, OpenAire, EuroPub, ZENODO and Google Scholar.

All articles were placed in the electronic scientific database of the journal (scientists.uz).

© Science and Innovation

© Authors

Editorial team			
Baxtiyor Rustamov	Chief Editor	**Gulirano Raxmatullayeva**	Deputy Chief Editor
Mahliyo Sotivoldiyeva	Reception Manager	**Feruza Ollomurodova**	Reception Manager
Farangiz Sagdullayeva	Technical Editor	**Dilnoza Narzullayeva**	Manager
Zulayxo Xakimova	Editor	**Sevara O'rinboyeva**	Manager
Kozim Ergashov	Editor	**Humoyun Qodirov**	Technical Editor
Feruzabonu Mannonova	Translator	**Mansur Suyunqulov**	Technical Editor
Jahongir Bekmuradov	Translator	**Samandar Rasulov**	Motion Designer
Asila Xaydaralieva	Editor	**Zafarbek Madaminov**	Motion Designer

Scientific editorial board	
Khayrulla Pulatov	Doctor of Chemical Sciences, Professor, Vice-Rector for Scientific Affairs and Innovations of Tashkent Institute of Chemical Technology, Tashkent, Uzbekistan.
Salim Otakulov	Doctor of Physical and Mathematical Sciences, Professor of the Department of Higher Mathematics of Jizzakh Polytechnic Institute, Jizzakh, Uzbekistan.
Shavkat Abdullayev	Doctor of Chemical Sciences, Professor of the Department of "Organic Chemistry" of Namangan State University, Namangan, Uzbekistan.
Erkin Imamov	Doctor of Physical and Mathematical Sciences, Professor of Tashkent University of Information Technologies, Tashkent, Uzbekistan.
Karimberdi Onarqulov	Doctor of Physical and Mathematical Sciences, Head of the Department of Physics of Fergana State University, professor, Fergana, Uzbekistan.
Amin Jarrah	PhD, Associate Professor of Computer Engineering at Yarmouk University, Irbid, Jordan.
Fakhriddin Pirlepesov	PhD, Computational Physicist, St Jude Children's Research Hospital, Radiation Oncology Department, Memphis, Tennessee, USA.
Borisyuk Petr	Doctor of Physical and Mathematical Sciences, Head of the Department of the Institute of Laser and Plasma Technologies, National Research Nuclear University MEPhI, Associate Professor, Moscow, Russia.
Mirdjalil Yunusov	Doctor of technical sciences, Scientific secretary of Tashkent Institute of Chemical Technology, professor, The owner of the Order of "Labour Fame", Tashkent, Uzbekistan.
Toyir Safarov	Doctor of technical sciences, Vice-Rector for Academic Affairs of Tashkent Institute of Chemical Technology, Professor, Tashkent, Uzbekistan.
Dilshod Ruziyev	Doctor of Philosophy in Technical Sciences, Associate Professor, Deputy director of professional training and retraining at the Institute for the Development of Professional Education.
Baxtiyor Sabirov	Doctor of technical sciences, Head of the department "Non-metallic and technogenic minerals" of the Navoi branch of the Academy of Sciences of the Republic of Uzbekistan, Senior researcher, Navoi, Uzbekistan.
Munovar Abdurakhmanova	Candidate of Economical Sciences, associate professor, Head of the Department of Organization of the Scientific and Educational Process of the Scientific Research Institute of Physics of Semiconductors and Microelectronics at UzNU, Deputy Director for the integration of the educational process with scientific activities, Tashkent, Uzbekistan.
Abdukakhkhor Khadjimuratov	Doctor of economic sciences, Associate Professor of the Department of "Social Sciences" of Fergana Public Health Medical Institute, Fergana, Uzbekistan.
Shoira Musayeva	Candidate of Economics, Professor of the Samarkand Institute of Economics and Service, Samarkand, Uzbekistan.
Ikhtiyor Kamolov	Candidate of technical sciences, Dean of the Faculty of Physical and Technological Education of the Navoi State University, Professor of the Department of Physics and Astronomy, Navoi, Uzbekistan.
Mirkozimjon Nishonov	Candidate of technical sciences, Professor of Fergana State University
Khaydar Rasulov	Candidate of Physical and Mathematical Sciences, Associate Professor of Bukhara State University, Bukhara, Uzbekistan.
Akramjon Karimov	Candidate of Physical and Mathematical Sciences, Professor of Tashkent State Law University, Tashkent, Uzbekistan.
Azizjon Kurbanov	Candidate of Physical and Mathematical Sciences, Head of the department of "Physics" of Andijan State University, Andijan, Uzbekistan.
Dilfuza Makhmudova	Doctor of Pedagogical Sciences, Head of the Department of Methods of Teaching Mathematics of Chirchik State Pedagogical University, Chirchik, Uzbekistan.
Dilorom Karimova	Candidate of Chemical Sciences, Professor of Navoi State University, Navoi, Uzbekistan.
Madinakhon Muydinova	Doctor of Philosophy on Physical and Mathematical Sciences, Head of the Department of Methods of Teaching Informatics and Exact Sciences at Pedagogical Institute of Andijan State University, Andijan, Uzbekistan.
Ilxom Usmonov	Candidate of Technical Sciences, Professor of the Samarkand State Institute of Architecture and Construction, Samarkand, Uzbekistan.
Nodira Saidaxmedova	Doctor of Economic Sciences, Professor of UZNPU named after Nizami, Tashkent, Uzbekistan.
Umar Babakhodjayev	Candidate of Physical and Mathematical Sciences, Associate Professor of Namangan State University, Namangan, Uzbekistan.
Dilshod Eshmuradov	Candidate of Technical Sciences, Associate Professor, Head of Department, Tashkent University of Information Technologies, Tashkent, Uzbekistan.

SELF-ADAPTIVE INTER-AGENT CONSENSUS MODEL AND ALGORITHMS FOR MULTI-CRITERIA DECISION-MAKING IN DISTRIBUTED MULTI-AGENT ENVIRONMENTS

Kh. Eshankulov
Department of Applied Mathematics and Programming Technologies, Bukhara State University, Bukhara, Uzbekistan
https://doi.org/10.5281/zenodo.20266817

Abstract. *This paper proposes a self-adaptive inter-agent consensus model for multi-criteria decision-making in distributed multi-agent environments. In distributed information-analytical systems, agents independently make local decisions based on partial and heterogeneous data, which leads to disagreements among agents and complicates the achievement of global consensus. Most existing classical consensus models are based on static influence weights and do not sufficiently consider the current state of agents, local decision quality, or dynamic environmental changes.*

To address these limitations, an adaptive consensus model based on the iterative coordination of local agent decisions is developed. In the proposed model, inter-agent influence weights are dynamically updated according to local decision quality and reliability levels. The inter-agent consensus process is formally represented through a mathematical model, and the operational mechanism of consensus formation is described step by step. Furthermore, a Pareto-efficient evaluation method is integrated into the consensus process to support decision selection under multi-criteria conditions.

Experimental results demonstrate that the proposed model outperforms classical consensus and weighted consensus approaches by reducing the level of inter-agent disagreement, accelerating convergence speed, and improving decision-making accuracy. The proposed model can be effectively applied in Business Intelligence systems, distributed monitoring platforms, and real-time multi-agent information-analytical environments.

Keywords: *multi-agent systems, inter-agent agreement, adaptive consensus, distributed decision making, multi-criteria optimization, Pareto-efficient selection, reinforcement learning.*

I. INTRODUCTION

In recent years, the rapid development of distributed information-analytical systems, cloud computing platforms, and multi-agent environments has significantly increased the demand for new decision-making approaches capable of operating under complex and dynamic conditions [1,2]. In such environments, data are distributed across heterogeneous sources and processed in a decentralized manner, while each agent independently makes decisions based on limited local information [3]. As a result, inconsistencies arise among agent-generated evaluations, making the achievement of global consensus considerably more challenging. In particular, the development of adaptive coordination and decision-making mechanisms for real-time information-analytical systems has become one of the important scientific and practical challenges [4].

Consensus-based approaches are widely used to establish inter-agent agreement in multi-agent systems [5]. These approaches enable the formation of a common decision through the

iterative approximation of agent states. Although classical average consensus and weighted consensus models are computationally efficient and suitable for distributed environments, most of them rely on static influence weights and therefore demonstrate limited effectiveness in dynamic and uncertain environments [6,7]. In particular, when factors such as agent reliability, local decision quality, and changing environmental conditions are not considered, convergence speed decreases and the level of disagreement among agents increases [8].

Recent studies have shown that reinforcement learning-based adaptive coordination methods enable agents to dynamically update their strategies according to environmental conditions [9,10]. However, in most existing works, inter-agent consensus mechanisms and multi-criteria decision-making processes are considered separately, and their integration within a unified adaptive framework remains insufficiently explored. In particular, the integration of Pareto-efficient selection mechanisms with adaptive consensus processes, as well as the consideration of dynamically changing inter-agent influence weights, has not been adequately investigated [11,12].

To address these limitations, this paper proposes a self-adaptive inter-agent consensus model for multi-criteria decision-making in distributed multi-agent environments. In the proposed model, agent influence weights are iteratively and dynamically updated by considering agent reliability levels, local evaluation quality, and reward indicators during the decision-making process. The model integrates an adaptive consensus mechanism aimed at reducing disagreement levels together with a Pareto-efficient decision selection method.

The proposed inter-agent consensus mechanism is implemented based on the following iterative update model:

$$x_i^{t+1} = x_i^t + \alpha \sum_{j \in N_i} \left(x_j^t - x_i^t \right) \quad (1)$$

where x_i^t represents the state of the i- th agent at iteration t, w_{ij}^t - denotes the adaptive influence weight between agents, α is the adaptation coefficient, and N_i represents the set of neighboring agents. The proposed model enables the iterative coordination of local agent decisions and facilitates the achievement of global consensus within the distributed multi-agent environment.

The main scientific contributions of the article are as follows:

- A self-adjusting inter-agent agreement model has been developed for a distributed multi-agent environment.
- An adaptive mechanism has been proposed that dynamically updates the weights of influence of agents.
- The Pareto-effective selection mechanism was integrated with the consensus process for multi-criteria decision-making.

The convergence condition of the proposed model is formulated in formal mathematical form.

Based on experimental results, the effectiveness of the proposed model compared to classical consensus approaches was substantiated.

II. ANALYSIS OF EXISTING APPROACHES

One of the fundamental approaches for ensuring inter-agent coordination in multi-agent systems is the use of consensus mechanisms [13]. The primary objective of these approaches is to

generate a common global decision through the iterative approximation of local evaluations produced by individual agents. Classical average consensus models rely on updating agent states based on the values received from neighboring agents.

However, in classical consensus approaches, all agents are assumed to have equal influence, while factors such as agent reliability and local decision quality are not taken into consideration [15].

To overcome these limitations, weighted consensus models have been proposed, in which the level of influence between agents is determined through specific weight coefficients [16]. In weighted consensus approaches, the agent state update process is generally represented as follows:

$$x_i^{t+1} = x_i^t + \alpha \sum_{j \in N_i} w_{ij} \left(x_j^t - x_i^t \right) \quad (2)$$

where w_{ij} represents the influence weight of the $j-$ th agent on the $i-$ th agent. Although this approach enables the consideration of different influence levels among agents, in most existing studies the weight coefficients are statically predefined [17]. Consequently, when changes occur in agent states, decision quality, or environmental conditions, the weight values are not adaptively updated. This limitation leads to decreased convergence speed and increased levels of inter-agent disagreement in dynamic environments.

Recent studies have paid considerable attention to adaptive coordination and reinforcement learning-based multi-agent approaches [18,19]. In these approaches, agent strategies are dynamically updated according to reward signals and environmental conditions. Reinforcement learning-based coordination methods enable agents to develop optimal action strategies based on previous experiences and interactions [20]. However, in most existing works, reinforcement learning techniques are primarily focused on strategy optimization, while the problem of adaptively managing inter-agent influence weights during the consensus formation process has not been sufficiently addressed [21].

In multi-criteria decision-making problems, Pareto-efficient optimization methods are widely applied [22]. These approaches make it possible to identify efficient decision alternatives under multiple conflicting criteria. The set of Pareto-efficient solutions is defined as follows:

$$X_P = \left\{ x \in X \mid \nexists x' \in X : x' \succ x \right\} \quad (3)$$

where X_P denotes the set of Pareto-efficient solutions. Although Pareto optimization methods provide the ability to select efficient decision alternatives under multi-criteria conditions, in many existing studies these approaches have been considered separately from inter-agent consensus mechanisms and have not been sufficiently integrated within a unified adaptive coordination framework [23].

Thus, the analysis of existing studies demonstrates that classical consensus models do not sufficiently consider the dynamic states and reliability levels of agents, while weighted consensus approaches typically rely on static weight coefficients. Although reinforcement learning-based approaches provide adaptability in agent strategies, the integration of inter-agent consensus processes with multi-criteria decision-making and Pareto-efficient selection mechanisms remains insufficiently investigated. Furthermore, the problem of developing adaptive consensus mechanisms based on the iterative dynamic updating of inter-agent influence weights and the reduction of disagreement levels remains an open research challenge. Therefore, this paper

proposes a self-adaptive inter-agent consensus model for multi-criteria decision-making in distributed multi-agent environments.

III. PROBLEM SOLVING

In distributed multi-agent environments, the decision-making process is performed by interconnected agents based on local information. Each agent possesses knowledge about only a specific part of the environment and independently evaluates decision alternatives. As a result, differences arise among the evaluations generated by individual agents, making the achievement of global consensus more difficult. Therefore, the coordination of local agent decisions and the formation of an efficient global decision under multi-criteria conditions represent important scientific challenges.

The set of agents in the multi-agent environment is defined as follows:

$$A = \{a_1, a_2, \cdots, a_N\} \quad (4)$$

where A represents the set of agents and N denotes the total number of agents in the system. Each agent evaluates decision alternatives based on local information and forms its current state value accordingly..

The set of decision options is represented as follows:

$$X = \{x_1, x_2, \cdots, x_m\} \quad (5)$$

where is the set of decision options and is the number of options. Each decision option is evaluated based on multiple criteria.

The multi-criteria evaluation criteria are defined by the following set:

$$F = \{ff_1, _2, \cdots, f_k\} \quad (6)$$

where is the set of criteria and is the number of criteria. The multi-criteria evaluation of each decision option is expressed as:

$$F(x_i) = (f_1(x_i), f_2(x_i), \cdots, f_k(x_i)) \quad (7)$$

In this model, since each agent evaluates the decision options independently, there is a level of disagreement among the agents. Therefore, it is necessary to iteratively coordinate the local assessments of the agents and reach a global consensus. The level of disagreement between the agents is determined by the following consensus function:

$$C(t) = \sum_{i=1}^{N} \sum_{j=1}^{N} w_{ij}^t \left\| x_i^t - x_j^t \right\| \quad (8)$$

where $C(t)$ denotes the disagreement level at iteration t, w_{ij}^t represents the influence weight of the j-th agent on the i-th agent, and x_i^t and x_j^t denote the current state values of the corresponding agents. The primary objective of the consensus process is to minimize the disagreement function in order to achieve global agreement among agents.

Within the framework of this problem, the following main requirements are set:

1. Agents should make independent decisions based on local information.
2. Agents' influence levels should be dynamically updated.
3. The level of disagreement between agents should be iteratively reduced.
4. Decision options should be selected in a Pareto-efficient manner under multi-criteria conditions.

5. The negotiation process is required to reach a state of convergence in finite iterations.

Therefore, this paper proposes an adaptive inter-agent consensus model that iteratively updates influence weights based on the current states of agents, local decision quality, and reward indicators

Agents' influence weights are adaptively updated based on local decision quality and confidence level:

$$w_{ij}^{t+1} = \frac{Q_j^t R_j^t}{\sum_{k \in N_i} Q_k^t R_k^t} \quad (9)$$

here:

- Q_j^t - j- local decision quality of the agent;
- R_j^t - reward or reliability indicator.

The working scheme of the proposed model is presented in Figure 1.

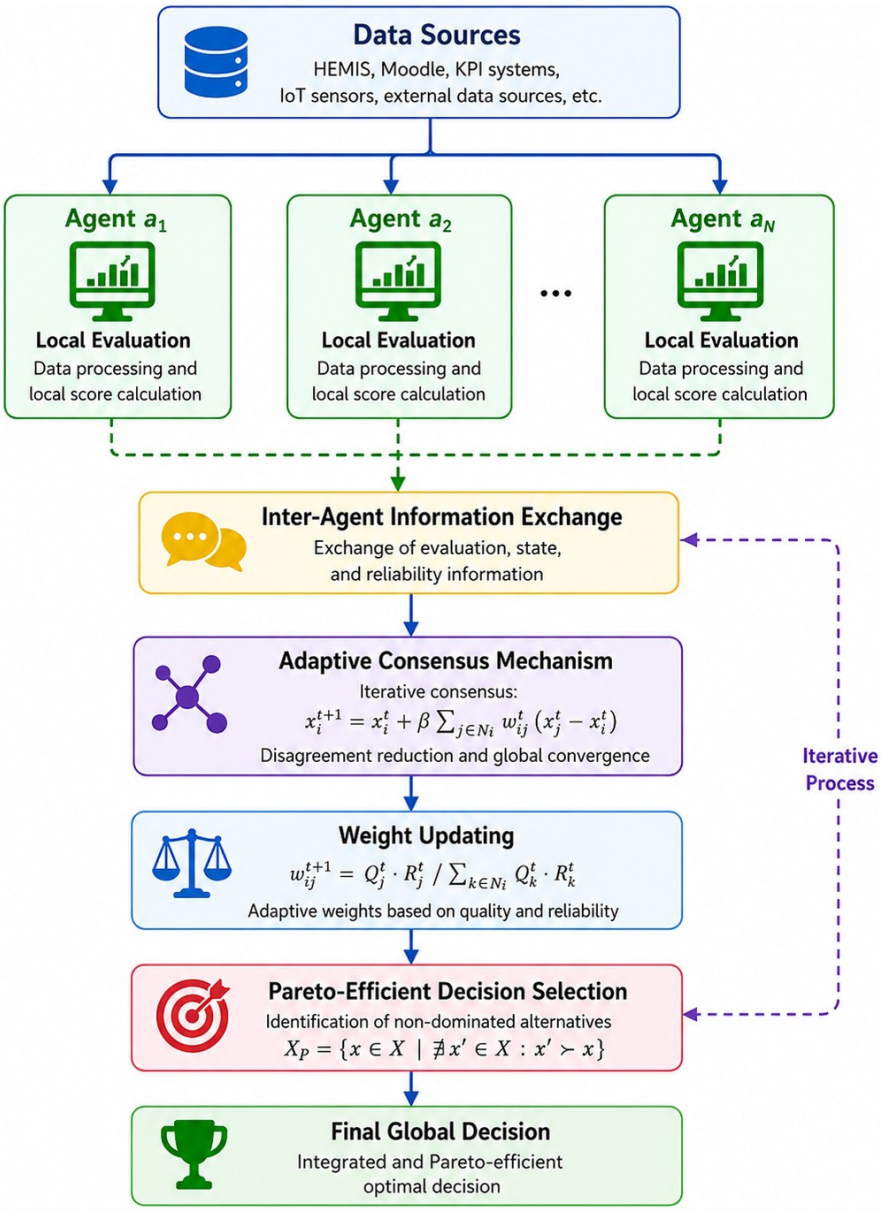


Figure 1. Model operation diagram

IV. OPERATIONAL PROCESS OF THE INTER-AGENT CONSENSUS MECHANISM

In the proposed model, agents iteratively exchange information with one another and gradually coordinate their local decisions step by step. As an illustrative example, a system consisting of three agents is considered:

$$A=\{a_1,a_2,a_3\} \quad (10)$$

Let the initial local prices of the agents be as follows:

$$x_1^0 = 0.80, \quad x_2^0 = 0.45, \quad x_3^0 = 0.65 \quad (11)$$

At the initial stage, the difference between agent evaluations is relatively large, resulting in a high level of disagreement. During the first iteration, the agents exchange their evaluations with one another, and new state values are computed based on the proposed adaptive consensus model.

For example, agent a_1 performs the following update operation:

$$x_1^1 = x_1^0 + \beta\left[w_{12}\left(x_2^0 - x_1^0\right) + w_{13}\left(x_3^0 - x_1^0\right)\right] \quad (12)$$

The same process is performed for the other agents as well. Throughout the iterative process, the agent evaluations gradually converge toward one another (Table 1):

Table 1. Iterative Convergence of Agent State Values During the Inter-Agent Consensus Process

Iteration	a_1	a_2	a_3
(t=0)	0.80	0.45	0.65
(t=1)	0.71	0.54	0.64
(t=2)	0.67	0.60	0.63
(t=3)	0.64	0.62	0.63

As can be observed from the table, the differences among agent evaluations gradually decrease during the iterative process, and the system converges toward a global consensus state. If certain agents possess higher reliability levels, their influence on the overall decision increases through the adaptive weight updating mechanism. Consequently, the negative impact of noisy or low-quality agents is reduced, which improves the stability of the consensus process.

The consensus process continues until the following convergence condition is satisfied:

$$\Delta_t = \max_i \left\| x_i^{t+1} - x_i^t \right\| < \varepsilon \quad (13)$$

Once this condition is satisfied, global consensus among the agents is considered to be achieved, and Pareto-efficient decision alternatives are subsequently selected.

Choosing Pareto-efficient decision options. After the completion of the inter-agent consensus process in the proposed model, the decision alternatives are evaluated under multi-criteria conditions based on Pareto efficiency. The identification of dominant solutions among decision alternatives is performed using the following dominance relation:

$$x^a \succ x^b \Leftrightarrow \left(\forall j : f_j(x^a) \geq f_j(x^b)\right) \wedge \left(\exists j : f_j(x^a) > f_j(x^b)\right) \quad (14)$$

According to this condition, if the decision alternative x^a is not worse than x^b with respect to all criteria and is superior in at least one criterion, then x^a is considered a dominant solution. The set of Pareto-efficient decision alternatives is determined by the following set:

$$X_P = \left\{ x \in X \mid \nexists x' \in X : x' \succ x \right\} \quad (15)$$

As a result, Pareto-efficient alternatives are selected from the global evaluations formed through inter-agent consensus, and the final decision is generated.

V. CONCLUSION

This paper proposed a self-adaptive inter-agent consensus model for multi-criteria decision-making in distributed multi-agent environments. The proposed model operates based on the iterative coordination of local agent decisions and the achievement of global consensus among interconnected agents. The main feature of the model is the dynamic updating of inter-agent influence weights according to local decision quality and agent reliability levels.

A mathematical model of the inter-agent consensus process was developed, and the operational mechanism of the consensus formation procedure was described step by step. In addition, an adaptive weight updating mechanism was proposed to reduce inter-agent disagreement levels and accelerate the convergence process. To support decision selection under

multi-criteria conditions, a Pareto-efficient evaluation method was integrated into the consensus mechanism.

The proposed approach improves coordination stability, enhances convergence efficiency, and increases decision-making accuracy in distributed information-analytical environments. The model can be effectively applied in Business Intelligence systems, distributed monitoring platforms, cloud-based analytical infrastructures, and real-time multi-agent decision-support systems.

Future research will focus on integrating the proposed model with deep reinforcement learning algorithms, optimizing inter-agent communication costs, and investigating scalability characteristics using large-scale real-world datasets.

REFERENCES

1. Zadeh, L. A. (1965). Fuzzy sets. Information and Control, 8(3), 338–353. https://doi.org/10.1016/S0019-9958(65)90241-X
2. Rahm, E., & Do, H. H. (2000). Data cleaning: Problems and current approaches. IEEE Data Engineering Bulletin, 23(4), 3–13.
3. Chen, H., Chiang, R. H. L., & Storey, V. C. (2012). Business intelligence and analytics: From big data to big impact. MIS Quarterly, 36(4), 1165–1188. https://doi.org/10.2307/41703503
4. Li, J., Zhang, Y., Wang, X., & others. (2023). AI-driven data analytics for business intelligence: A review and future directions. IEEE Access, 11, 75543–75560. https://doi.org/10.1109/ACCESS.2023.3284712
5. Wooldridge, M., & Jennings, N. R. (1995). Intelligent agents: Theory and practice. The Knowledge Engineering Review, 10(2), 115–152. https://doi.org/10.1017/S0269888900008122
6. Groth, P. T., & Luck, M. (2008). A framework for reputation in multi-agent systems. Journal of Artificial Societies and Social Simulation, 11(2), 1–11.
7. Russell, S., & Norvig, P. (2010). Artificial intelligence: A modern approach (3rd ed.). Prentice Hall.
8. Deb, K. (2001). Multi-objective optimization using evolutionary algorithms. John Wiley & Sons.
9. Huebscher, M. C., & McCann, J. A. (2008). Adaptive and autonomic computing: A survey. Journal of Systems and Software, 81(12), 1927–1949. https://doi.org/10.1016/j.jss.2007.12.806
10. Chen, H.; Chiang, R.H.L.; Storey, V.C. Business Intelligence and Analytics: From Big Data to Big Impact. MIS Q. 2012, 36, 1165–1188. https://doi.org/10.2307/41703503.
11. Kotzov, I.; Kraslynkova, Y.; Pérez-Sanagustín, M.; Mansillo, F.; Broisin, J. Supporting Decision-Making for Promoting Teaching and Learning Innovation: A Multiple Case Study. J. Learn. Anal. 2024, 11, 8131. https://doi.org/10.18608/jla.2024.8131.
12. Hashem, I.A.T.; Yaqoob, I.; Anuar, N.B.; Mokhtar, S.; Gani, A.; Khan, S.U. The rise of “big data” on cloud computing: Review and open research issues. Inf. Syst. 2015, 47, 98–115. https://doi.org/10.1016/j.is.2014.07.006.
13. Dorri, A.; Kanhere, S.S.; Jurdak, R. Multi-Agent Systems: A Survey. IEEE Access 2018, 6, 28573–28593. https://doi.org/10.1109/ACCESS.2018.2831228.

14. Ma, N.; Tang, A.; Xiong, Z.; Jiang, F. A deep multi-agent reinforcement learning approach for the micro-service migration problem with affinity in the cloud. Expert Syst. Appl. 2025, 273, 126856. https://doi.org/10.1016/j.eswa.2025.126856 .
15. Avritzer, A.; Ferme, V.; James, A.; Russo, B.; van Hoorn, A.; Schulz, H.; Menasché, D.; Rufino, V. Scalability assessment of microservice architecture deployment configurations: A domain-based approach leveraging operational profiles and load tests. J. Syst. Softw. 2020, 165, 110564. https://doi.org/10.1016/j.jss.2020.110564
16. Abdullahi, M.; Ngadi, M.A.; Abdulhamid, S.M. Symbiotic organism search optimization based task scheduling in cloud computing environment. Future Gener. Comput. Syst. 2016, 56, 640–650. https://doi.org/10.1016/j.future.2015.08.006.
17. Afrin, M.; Jin, J.; Rahman, A.; Tian, Y.-C.; Kulkarni, A. Multi-objective resource allocation for edge cloud based robotic workflow in smart factory. Future Gener. Comput. Syst. 2019, 97, 119–130. https://doi.org/10.1016/j.future.2019.02.062
18. Liao, G.; Yu, S. A Constrained Multi-Objective Evolutionary Algorithm with Weak Constraint–Pareto Dominance and Angle Distance-Based Diversity Preservation. Mathematics 2023, 11, 1588. https://doi.org/10.3390/math11071588.
19. Pérez, M.; Cañizares, P.C.; Núñez, A. Multi-objective optimization of cloud systems. Sci. Comput. Program. 2026, 252, 103447. https://doi.org/10.1016/j.scico.2026.103447.
20. Mishra, S.; Sangaiah, A.K.; Sahoo, M.N.; Bakshi, S. Pareto-Optimal Cost Optimization for Large-Scale Cloud Systems Using Joint Allocation of Resources. J. Ambient Intell. Humaniz. Comput. 2023, 14, 15375–15393. https://doi.org/10.1007/s12652-019-01601-x .
21. Madaminov, B.A.; Saidmurodov, S.; Saitov, E.B.; Jumanazarov, D.; Alsayah, A.M.; Zhetkenbay, L. Multi-objective Optimization Framework for Energy Efficiency and Production Scheduling in Smart Manufacturing Using Reinforcement Learning and Digital Twin Technology Integration. Int. J. Ind. Eng. Manag. 2025, 16, 283–295. https://doi.org/10.24867/IJIEM-389
22. Beloglazov, A.; Buyya, R. Energy efficient resource management in virtualized cloud data centers. Future Gener. Comput. Syst. 2012, 28, 755–768. https://doi.org/10.1016/j.future.2011.04.017.
23. Eshankulov, K.; Shafiev, T.; Bakaev, I.; Nazarov, S. Architecture and data structures of the information monitoring and decision-making software suite for business intelligence. Proc. SPIE Int. Soc. Opt. Eng. 2025, 13651, 1365107. https://doi.org/10.1117/12.3061943

URANIUM SERIES RADIONUCLIDES AND THEIR QUANTUM-MECHANICAL CHARACTERISTICS

O.S. Toshev[1], M.A. Mustafoyev[2], G.M. Allaberganova[2], A.M. Muzafarov[2]
Department of Physics and Astronomy, Navoi State University, Navoi, Uzbekistan[1]
Department of General Physics, Navoi State University of Mining and Technologies, Navoi, Republic of Uzbekistan[2]
https://doi.org/10.5281/zenodo.20302427

Abstract. *This article examines the uranium-238 decay series as a classical system for studying quantum-mechanical processes in nuclear physics. It analyzes the nuclear-physical characteristics of radionuclides formed in the decay chain, including uranium, thorium, radium,*

radon, polonium, lead, and their daughter products. Special attention is given to alpha, beta, and gamma decay mechanisms, with emphasis on quantum tunneling through the Coulomb barrier, nuclear energy levels, spin, parity, and collective nuclear effects. The paper also considers the interaction of alpha particles with matter, energy transfer, ionization processes, and their influence on local radiation conditions. The results show that alpha-particle energy, tunneling probability, decay probability, and half-life are closely connected with nuclear structure. The study highlights the practical importance of uranium-series radionuclides for radiation safety, environmental radioecology, nuclear reactor modeling, geochronology, and the broader understanding of nuclear stability in heavy elements under natural and applied conditions of ionizing radiation assessment and control systems.

Keywords: *alpha-particle energy values, electronic structure of the medium, radionuclides of the uranium decay chain, radiation conditions.*

Introduction

The interaction of α-particles emitted by radionuclides — ^{234}U, ^{230}Th, ^{226}Ra, ^{222}Rn, ^{218}Po, ^{214}Pb, ^{214}Po, and ^{210}Pb — formed during the decay of the parent nucleus ^{238}U with matter in the natural environment constitutes a complex process of energy transfer accompanied by the ionization of atoms in the medium. (Knoll, 2010; IAEA, 2018) . As α-particles collide with atoms of chemical elements in the environment, their energy is transferred non-uniformly. As a result, localized regions with high absorbed energy density and elevated radiation levels (UNSCEAR, 2020) are formed. The energies of α-particles from radionuclides — ^{234}U, ^{230}Th, ^{226}Ra, ^{222}Rn, ^{218}Po, ^{214}Pb, ^{214}Po, and ^{210}Pb — are closely related to the radiation conditions of a given area and are of key importance in nuclear physics, radiation physics, and applied problems of radioecology (Lilley, 2001; Cheng et al., 2019). In the present work, the interaction of α-particles with electrons in environmental substances is considered within a theoretical framework based on quantum-mechanical concepts. (Qi et al., 2018; Denisov & Ikezoe, 2025). The main focus is placed on determining the specific activity of each radionuclide in the uranium decay chain associated with the decay of the parent nucleus ^{238}U, taking into account the high ionizing power of α-particles and their short mean free path (IAEA, 2018; UNSCEAR, 2020). The contribution of α-particle radiation from radionuclides — ^{234}U, ^{230}Th, ^{226}Ra, ^{222}Rn, ^{218}Po, ^{214}Pb, ^{214}Po, and ^{210}Pb — to the exposure dose rate at a given local point should be evaluated using the fundamental laws governing microscopic particle interactions. Natural uranium, consisting of the parent nucleus ^{238}U, initiates a radioactive decay chain during which α-particles are emitted with energies of 4.859 MeV (^{234}U), 4.770 MeV (^{230}Th), 4.784 MeV (^{226}Ra), 5.489 MeV (^{222}Rn), 6.115 MeV (^{218}Po), 7.833 MeV (^{214}Pb), and 5.305 MeV (^{210}Pb). The α-decay of a single uranium nucleus results in an energy release of approximately $E \approx 4.27$ MeV. According to the laws of the microscopic world, α-particles interact with matter via Coulomb forces (Cheng et al., 2019), transferring their momentum and energy to atoms of chemical elements and thereby ionizing them. The ionization of atoms is directly associated with an increase in the exposure dose rate at a given local point. This process confirms the validity of well-established physical laws and provides a basis for assessing the radiation conditions of the studied area. The α-decay process is fundamentally governed by quantum tunneling through the Coulomb barrier, as originally described in Gamow theory and later refined in modern tunneling models (Krori et al., 2021; Denisov & Ikezoe, 2025). According to quantum-mechanical laws, α-particles interact with matter via Coulomb forces, transferring

momentum and energy to atoms and thereby ionizing them (Knoll, 2010). These ionization processes are directly associated with increases in exposure dose rate and serve as an important basis for assessing the radiation conditions of the investigated region (UNSCEAR, 2020).

Techniques and Methods of Physical Experiments

The uranium series represents a chain of successive radioactive transformations that begins with the isotope ^{238}U and terminates with the stable nuclide ^{206}Pb. During the decay process, numerous radionuclides are formed, including radium, radon, polonium, and bismuth. (Berger et al., 2010)

The study of these nuclides is important for:

- Nuclear energy,
- Radiation safety,
- Geochronology,
- Fundamental nuclear physics.

Result and Discussion

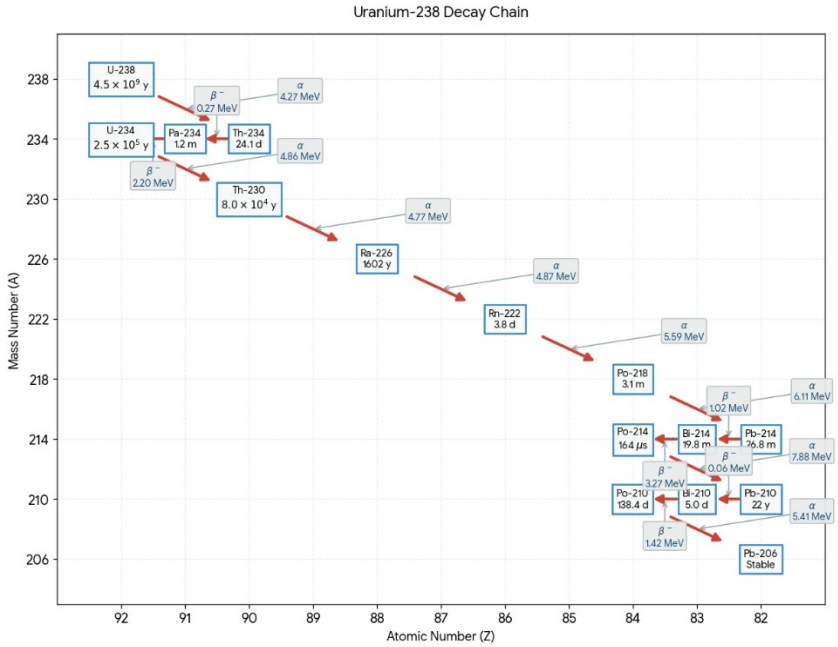


Fig. 1. The radionuclides of the uranium decay chain.

The obtained results demonstrate the fundamental role of quantum-mechanical processes in the radioactive transformations occurring within the uranium decay series. The analysis of radionuclides formed during the decay of ^{238}U shows that the emission energies of α-particles, decay probabilities, and half-lives are closely related to the nuclear structure and tunneling mechanisms governing radioactive decay (Denisov & Ikezoe, 2025; Cheng et al., 2019).

The uranium decay chain represents a последовательную систему ядерных превращений in which heavy nuclei gradually transform into more stable daughter products through successive α- and β-decays. This decay sequence includes several radiologically significant radionuclides such as ^{226}Ra, ^{222}Rn, and ^{218}Po, which contribute substantially to ionization processes and the formation of local radiation backgrounds in environmental media (UNSCEAR, 2020). The schematic representation of the uranium decay chain shown in Fig. 1 illustrates the subsequence radioactive transitions and the formation pathways of daughter radionuclides.

The classical decay series of ^{238}U includes:

$^{238}U \rightarrow {}^{234}Th \rightarrow {}^{234}Pa \rightarrow {}^{234}U \rightarrow {}^{230}Th \rightarrow \ldots$

followed by transitions through radium and radon:

$^{226}Ra \rightarrow {}^{222}Rn \rightarrow {}^{218}Po \rightarrow {}^{214}Pb \rightarrow {}^{214}Bi \rightarrow \ldots$

the final product: ^{206}Pb (stable). (Muzafarov A.M. et al. 2021)

Characteristics:

- α-decay predominates in heavy nuclei.
- β^--decay stabilizes the neutron-to-proton ratio.
- Intermediate nuclei often have short half-lives.

3. Quantum-Mechanical Nature of Radioactive Decay

3.1 Alpha Decay and Tunneling

The quantum-mechanical tunneling effect through the Coulomb barrier explains alpha decay. The nucleus confines the α-particle within a potential well; however:

Classically, escape is forbidden,

Quantum mechanics allows the particle to “penetrate” through the barrier.

The decay probability is described by the Gamow formula:

$$P=e^{-\frac{2}{\hbar}\int_{r_1}^{r_2}\sqrt{2m\,(V(r)-E)}dr}$$

Here, (E) is the energy of the α-particle, (m) is the mass of the α-particle, $\hbar$ is the reduced Planck constant, and (V(r)) is the potential barrier energy. The quantities r_1 and r_2 represent the classical turning points, i.e., the boundaries of the potential barrier.

Nuclide	Z_d	E_α (MeV)	$\log_{10}(P)$	P
^{238}U	90	4.20	-42.3	$5{,}0 \times 10^{-43}$
^{234}U	88	4.77	-39.8	$1{,}6 \times 10^{-40}$
^{230}Th	86	4.69	-38.5	$3{,}2 \times 10^{-39}$
^{226}Ra	84	4.87	-36.1	$7{,}9 \times 10^{-37}$
^{222}Rn	84	5.49	-33.4	$3{,}9 \times 10^{-34}$
^{218}Po	82	6.00	-30.2	$6{,}3 \times 10^{-31}$
^{214}Po	82	7.69	-25.6	$2{,}5 \times 10^{-26}$
^{210}Po	80	5.30	-32.0	$1{,}0 \times 10^{-32}$

Table 1. Probability of Formation of Nuclides in the Uranium Decay Chain.

The table shows that as the kinetic energy of the α-particle decreases, the probability of its emission through the nuclear potential barrier via quantum tunneling also decreases monotonically (Toshev O.S. et al., 2025).

The potential barrier energy, in turn, includes several contributions from binding energies and interaction energies.

$$V(r)=V_{Nucleus}(r)+V_{Coulomb}(r)+V_{orbital}(r)$$

$V_{yadro}(r)$- The nuclear potential acts only at distances on the order of 10^{-15} m, i.e., within the nucleus.

$V_{Coulomb}(r)$ – Coulomb interaction energy.

$$V_{Coulomb}(r)=\frac{Z_1 Z_2 e^2}{4\pi\varepsilon_0 r}$$

It describes the interaction between the α-particle and the nucleus. Here, Z_1 and Z_2 are the charge numbers. The potential barrier is formed due to this interaction. (Soliyev T.I. et al.) . $V_{orbital}(r)$-Energy associated with orbital motion. It always produces a repulsive (positive) effect.

$$V_{orbital}(r)=\frac{l(l+1)\hbar^2}{2mr^2}$$

It increases the height of the potential barrier and reduces the tunneling probability. This directly explains the wide range of half-lives.

3.2 β-Decay and Weak Interaction

β-decay is governed by the weak interaction:

$$n\rightarrow p+e^-+\tilde{\nu}_e \; ; p+e^-\rightarrow n+\tilde{\nu}_e.$$

From a quantum-mechanical point of view, the process is described by:

weak interaction operators,

transitions between nuclear energy levels,

conservation of spin and isospin.

3.3 γ – emission. Gamma decay is associated with transitions between excited nuclear states.

Characteristics:

- discrete energy spectrum,
- transitions involving changes in angular momentum,
- described by nuclear quantum electrodynamics. (Zhang et al. 2020)

4. Quantum Structure of Nuclei in the Uranium Series

Nuclei in uranium and its daughter products exhibit:

4.1 Nuclear Shell Model. Nucleons are arranged on discrete energy levels. Magic numbers increase nuclear stability, while in heavy nuclei, deformation is observed.

4.2 Spin and Parity. Each radionuclide is characterized by:

- spin J,
- parity P,
- quantum numbers of excited states.

These parameters determine: decay probability, type of nuclear transition, radiation energy.

4.3 Collective Effects. In the uranium decay chain (U, Th, Ra):

- nuclear vibrations and rotations are observed,
- collective motion of nucleons is manifested,
- the probability of α-decay is enhanced.

5. Radon as a Key Element of the Series. A special role is played by ^{222}Rn:

- inert gas,
- short half-life (~3.8 days),
- easily diffuses in the medium,
- the main source of radiation hazard in indoor environments.

6. Practical Significance of the Research.

The study of the uranium decay series is essential for:

- prediction of radiation background,
- modeling of nuclear reactors,

- geochronological dating of rocks (U → Pb method),
- understanding the stability of nuclear structures.

Conclusion

Radionuclides of the uranium decay series represent a classical system for studying quantum nuclear physics. Their properties are directly related to:

- quantum tunneling,
- weak interaction,
- nuclear shell structure,
- collective effects in heavy nuclei.

This system remains an important model for testing fundamental theories of nuclear physics. (Tran et al. ,2021)

REFERENCES.

1. Cheng, J. H., Dong, J. M., & Zhang, H. F. (2019). Systematic study of α-decay half-lives based on the Gamow-like model. Physica Scripta, 94(8), 085301. https://doi.org/10.1088/1402-4896/ab12cc
2. Denisov, V. Y., & Ikezoe, H. (2025). Alpha-decay half-lives and alpha-capture cross-sections. Atomic Data and Nuclear Data Tables, 161, 101690. https://doi.org/10.1016/j.adt.2024.101690
3. International Atomic Energy Agency. (2018). Radiation protection and safety of radiation sources. International Atomic Energy Agency.
4. Knoll, G. F. (2010). Radiation detection and measurement (4th ed.). Wiley.
5. Krori, K. D., et al. (2021). Gamow's alpha-decay theory revisited. arXiv preprint. https://doi.org/10.48550/arXiv.2112.09578
6. Lilley, J. (2001). Nuclear physics: Principles and applications. Wiley.
7. Qi, J., Li, T., Xu, R., Fu, L., & Wang, X. (2018). Alpha decay in intense laser fields: Calculations using realistic nuclear potentials. Physical Review C, 99(1). https://doi.org/10.48550/arXiv.1810.07331
8. United Nations Scientific Committee on the Effects of Atomic Radiation. (2020). Sources, effects and risks of ionizing radiation. UNSCEAR.
9. Berger, M. J., Hubbell, J. H., Seltzer, S. M., Chang, J., Coursey, J. S., Sukumar, R., Zucker, D. S., & Olsen, K. (2010). XCOM: Photon cross section database (Version 1.5). https://doi.org/10.18434/T48G6X
10. Bekman, I. N. (2020). Atomic and nuclear physics: Radioactivity and ionizing radiation. Moscow: PALMARIUM. 493 p.
11. Muzafarov, A. M., Allaberganova, G. M., & Kulmatov, R. A. (2021). Assessment of the radiation hazard of uranium enterprises for environmental objects. XXI Century. Technosphere Safety, 6(1), 94–102.
12. Muzafarov, A. M., Allaberganova, G. M., Turabdjanov, S. M., & Allayarov, R. M. (2020). A new method for the reclamation of soils contaminated with radionuclides at uranium in-situ leaching sites. Universum: Technical Sciences, 6(75), Part 2, 91–96.
13. Muzafarov, A. M., Allaberganova, G. M., & Kulmatov, R. A. (2021). Assessment of the radiation hazard of uranium enterprises for environmental objects. XXI Century. Technosphere Safety, 6(1), 94–102. https://doi.org/10.21285/2500-1582-2021-1-94-102

14. Muzafarov, A. M., Allaberganova, G. M., Turabdjanov, S. M., & Allayarov, R. M. (2020). A new method for the reclamation of soils contaminated with radionuclides at uranium in-situ leaching sites. Universum: Technical Sciences, 6(75), Part 2, 91–96. https://7universum.com/ru/tech/archive/item/9793
15. Toshev, O. S., Allaberganova, G. M., & Muzafarov, A. M. (2026). Interdependence of radiation conditions with the redistribution of alpha-particle energy of radionuclides in the natural uranium decay chain. Universum: Technical Sciences: Electronic Scientific Journal, 2(143). https://7universum.com/ru/tech/archive/item/22018
16. Muzafarov, A. M., Allaberganova, G. M., & Kulmatov, R. A. (2021). Assessment of the radiation hazard of uranium enterprises for environmental objects. XXI Century. Technosphere Safety, 6(1).
17. Muzafarov, A. M., Allaberganova, G. M., Turabdjanov, S. M., & Allayarov, R. M. (2020). A new method for the reclamation of soils contaminated with radionuclides at uranium in-situ leaching sites. Universum: Technical Sciences, 6(75).
18. Soliyev, T. I., Muzafarov, A. M., & Sherkulov, U. D. (2022). Determination of mixing factors of daughter radionuclides in the uranium decay chain. NeuroQuantology, 20(11), 2722.
19. Schinner, A., Sigmund, P., & Paul, H. (2015). Improved stopping power calculations for ions in matter. Nuclear Instruments and Methods in Physics Research Section B, 354, 184–189. https://doi.org/10.1016/j.nimb.2014.08.013
20. International Atomic Energy Agency. (2017). Stopping power and range of charged particles in matter. Vienna: International Atomic Energy Agency.
21. Liamsuwan, T., & Nikjoo, H. (2019). Track structure and stopping power of charged particles in matter. Radiation Measurements, 128, 106096. https://doi.org/10.1016/j.radmeas.2019.106096
22. Zhang, R., & Chen, Y. (2020). Ionization and energy deposition of alpha particles in matter. Radiation Physics and Chemistry, 168, 108613. https://doi.org/10.1016/j.radphyschem.2019.108613
23. Tran, H. N., & Nguyen, T. T. (2021). Energy loss and ionization processes of alpha particles in different materials. Journal of Radiation Research and Applied Sciences, 14(1), 1–8. https://doi.org/10.1080/16878507.2021.1874235

METHOD FOR RECORDING INFRARED ABSORPTION SPECTRA OF GASEOUS PROPANOL AND MATRIX ISOLATION METHOD

L.O. Meyliyev[1], Sh.A. Jurayeva[2]
Karshi State University, PhD[1]
Karshi State University, Master[2]
https://doi.org/10.5281/zenodo.20302716

Abstract. *This article presents a detailed analysis of the experimentally recorded infrared absorption spectra of propanol in the gaseous state, determined using the Bruker IFS-120 spectrometer Fure-IQ, the absorption spectrum recording method and the matrix isolation method. To correlate the interference pattern with a certain amount of path difference in the interferometer, the radiation of the base interferogram He-Ne laser is used at the same time.*

Modern Fure-spectrometers have hundreds and thousands of times the signal-to-noise ratio of conventional spectral instruments. Liquid propanol with a purity of more than 99.9%, manufactured by Fluka, is used for sample preparation. In matrix isolation, the results are recorded using the IR absorption spectra of propanol.

Keywords: *gaseous propanol, infrared absorption spectra, matrix isolation method, absorption spectrum recording method, Fure-spectrometer, liquid propanol.*

Introduction

Currently, vibrational spectroscopy methods, in particular infrared (IR) absorption spectroscopy, are considered one of the most informative methods for studying the microscopic state of matter. Vibrational spectra are a reliable source of information about the vibrational-rotational energy states of molecules, intra- and intermolecular interactions, and molecular relaxation processes in matter. In this regard, today it is of interest to collect experimental data that establish the correlation between the spectral contour and the parameters characterizing the properties of the environment, and to compare these data with the theories available in the literature. The study of substances in the gaseous state and with a relatively simple molecular structure is especially relevant.

Literature review

The method of matrix isolation of the investigated substance in inert gases or hydrogen crystals is today a powerful tool for experimentally studying the spectral properties of atoms, molecules, and molecular complexes [3; B.27–28, 4; B.221–234]. The study of alcohols in matrix isolation allows us to determine the sensitivity of various compounds to the type of matrix, the ratio of the number of alcohol molecules to the number of matrix molecules, and the temperature in the sample. This makes each experiment unique and complements the general picture of the various structurally changing alcohol clusters under the influence of various external factors. [1; B.53-58, 2; B.279, 5; B.604-608, 6; B.243–248, 7; B.2165–2170, 8; B.1384-1390] studied the structural changes of hydrogen-bonded alcohol clusters isolated in low-temperature argon and nitrogen matrices, and such an experiment can be seen as an experimental model of the transition of monoatomic alcohols from the gaseous to the liquid phase.

Research Methodology

The Fourier spectroscopy method is based on the principle of interference of two beams and obtaining an interferogram. The main element of the optical scheme of the Fourier spectrometer is a Michelson interferometer consisting of a semi-transparent beam splitter and two flat mirrors (Fig. 1).

Coherent rays from the source fall on the semi-transparent surface of the beam splitter, as a result of which it is divided into two rays of equal intensity. Each ray is reflected by its own mirror, and the light returns to the beam splitter, and the rays combine, creating interference and fall on the detector. One of the mirrors in the interferometer is movable, its position is constantly changing, due to which a variable path difference is created. Depending on the magnitude of the path difference, the rays combine in phase or out of phase, which leads to positive or negative interference. The resulting interferogram can be converted into an infrared spectrum using Fourier transforms, which is where the name of the method comes from.

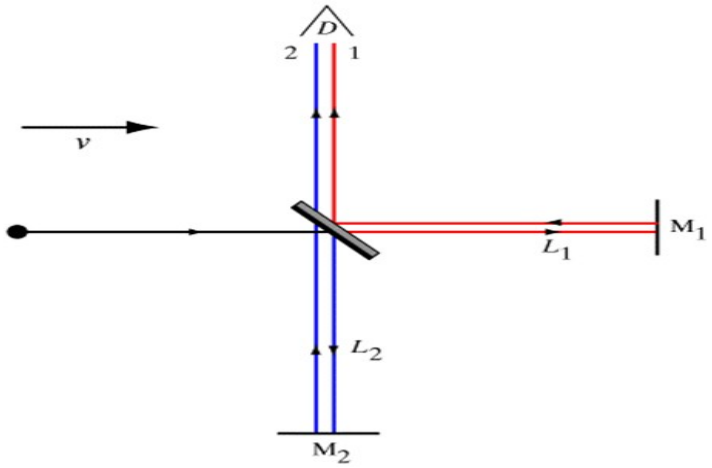


Figure 1. Schematic of a Michelson interferometer: M_1, M_2 – mirrors; L_1, L_2 – interferometer arms; D – detector.

According to the mathematical apparatus of Fourier optics, the dependence of radiation intensity on frequency is expressed as follows:

$$I_p(v) = \int_{-\infty}^{+\infty} (I_p(\Delta z) - I_p(\infty))cos(2\pi v \cdot \Delta z)d(\Delta z)$$

Thus, the task is to determine the intensity distribution in the resulting carrier, Ip(Δz), with respect to the path difference, by varying the path difference. Then, according to the above equation, by performing Fourier's cosine transformations, we obtain the intensity distribution at the frequency Ip(ν) at the point P in the radiation spectrum. In order to correlate the observed interference pattern with a certain amount of path difference in the interferometer, a reference interferogram, the radiation of a He-Ne laser, is simultaneously recorded.

The spectra presented in this article were recorded in the spectral range from 750 to 4000 cm-1 with a resolution of 1 cm-1 using a DTGS detector. To improve the signal-to-noise ratio, each spectrum was recorded as an average of 128 interferograms. For the preparation of samples, we used liquid propanol (structural formula - CH3- CH2- CH2-OH) with a purity of more than 99.9%, produced by Fluka.

To remove impurities (mainly oxygen and nitrogen present in the atmosphere), several cycles of freezing, suction and thawing of the liquid sample were performed. For the measurement, the gaseous samples were prepared by natural evaporation on the surface of liquid propanol in

vacuum. The sample was placed in a standard 10 cm single-pass gas cell with potassium bromide (KBr) windows. The gas pressure in the cell was measured by a standard manometric method.

Analysis and results

In matrix isolation, IR absorption spectra of propanol were recorded using a Bruker IFS 113 Fourier spectrometer with a spectral range of 500–4000 cm-1 and a resolution of 1 cm-1. To improve the signal-to-noise ratio, each spectrum was recorded with an average of 128 interferograms. Samples for the study were prepared by mixing propanol vapors obtained by evaporation from the surface of liquid alcohol with argon (manufacturer Elme Messer, purity 99.995%) in a vacuum apparatus using a thermometer in a ratio of 1:1000 (1000 argon atoms per 1 molecule of propanol). After that, the gas mixture was sprayed for 1 hour onto a cooled substrate (CsI) placed in a closed-cycle helium cryostat (Leybold-Hareus RW2) at a temperature of 9 K. The required gas flow in the cryostat was maintained using a needle valve. The matrix spraying rate was 5 mmol/h. A high vacuum (10-8 bar) was maintained in the cryostat due to constant suction using a steam-oil pump based on a rotary pump. A liquid nitrogen-cooled mercury-cadmium-tellurium detector was used to record the spectra.

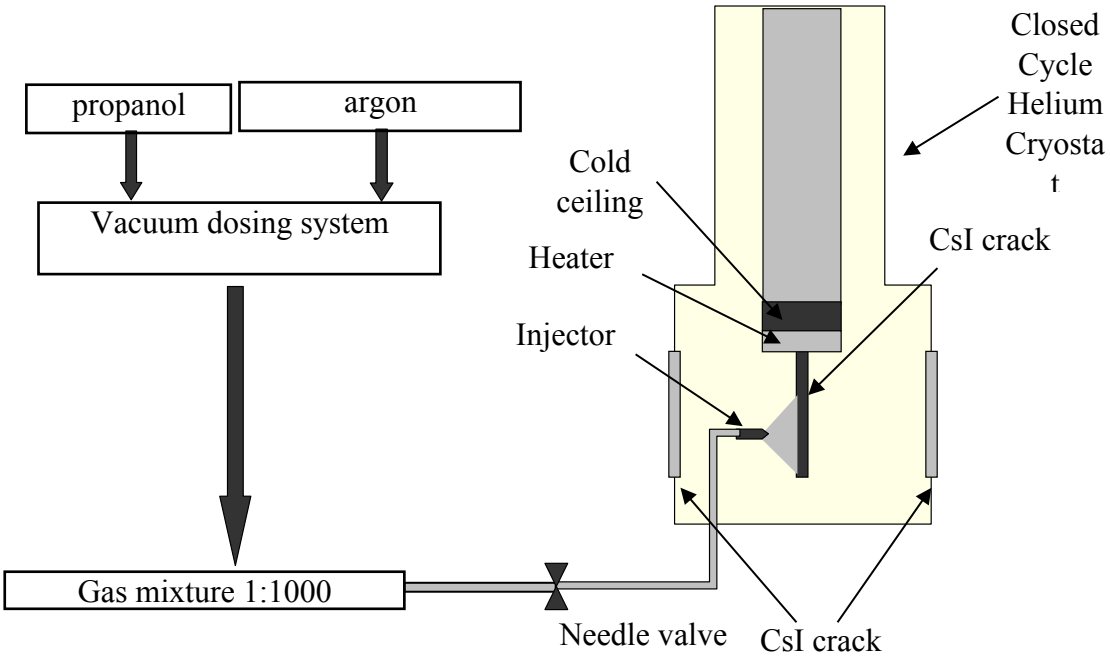


Figure 2. Schematic of the low-temperature argon matrix preparation equipment

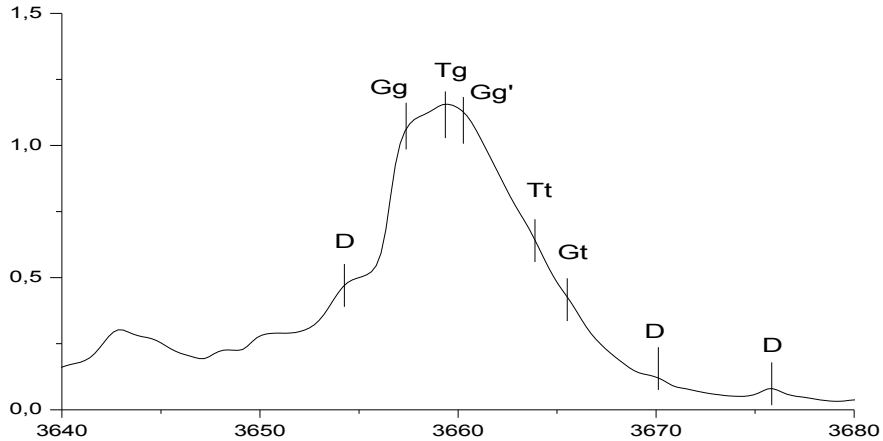


Figure 3. IR absorption spectrum of propanol isolated in an argon matrix at 20 K in the O-H stretching vibration range

Figure 2 shows the schematic diagram of the matrix isolation apparatus. The matrix temperature was measured using a silicon diode attached to the slit, sprayed with a gas mixture, and a Lakeshore temperature controller with an accuracy of 0.1 K.

The IR absorption spectra of propanol isolated in a low-temperature argon matrix were recorded at different temperatures from 20 K to 50 K. For further comparative analysis, spectra at two different temperatures - 20 K and 35 K - were selected.

From the above result, it can be concluded that, according to Figure 3, other IR absorption bands of low intensity can be seen in the spectra, for example, at frequencies of 3643, 3644, 3648 and 3650 cm-1, which probably belong to clusters of three or more molecules. We note that the band at frequency 3647 cm-1 was also observed in gaseous propanol, and this band is also assigned to vibrations of trimers.

Conclusion/Recommendations

In conclusion, we determined the spectra of propanol in the gaseous state using the Fure-IQ IFS-120 spectrometer by the recording method and the matrix method, and accordingly obtained the bonding values related to its state. Thus, it can be concluded that both in the gaseous state of propanol and during its isolation in a low-temperature argon matrix, not only individual propanol molecules are formed in different conformations. Perhaps, we can also see the formation of hydrogen-bonded clusters consisting of two, three or more molecules.

REFERENCES

1. Pogorelov, V., Chernolevska, Y., Vaskivskyi, Y., Pettersson, L. G. M., Doroshenko, I., Sablinskas, V., Balevicius, V., Ceponkus, J., Kovaleva, K., Malevich, A., & Pitsevich, G. (2016). Structural transformations in bulk and matrix-isolated methanol from measured and computed infrared spectroscopy. *Journal of Molecular Liquids*, 216, 53–58. USA.
2. Doroshenko, I., Pitsevich, G., & Sablinskas, V. (2012). *Cluster structure of liquid alcohols: A study using vibrational spectroscopy methods*. Saarbrücken, Germany: LAP LAMBERT Academic Publishing. 279 p.
3. Nemukhin, A. V. (2000). Molecules in matrices and clusters. *Soros Educational Journal*, 6, 27–28. Russia.
4. Coussan, S., Bouteiller, Y., Loutellier, A., Perchard, J. P., Racine, S., Peremans, A., Zheng, W. Q., & Tadjeddine, A. (1997). Infrared photoisomerization of the methanol dimer trapped in an argon matrix: Monochromatic irradiation experiments and DFT calculations. *Journal of Chemical Physics*, 219, 221–234. USA.
5. Doroshenko, I. Y. (2011). Matrix-isolation study of methanol cluster structure formation in the spectral region of C–O and O–H stretching vibrations. *Low Temperature Physics*, 37, 604–608. Ukraine.
6. Mishchuk, O., Doroshenko, I., Sablinskas, V., & Balevicius, V. (2016). Temperature evolution of cluster structure in n-hexanol isolated in Ar and N_2 matrices and in the condensed state. *Journal of Structural Chemistry*, 27, 243–248. Russian Federation.
7. Pogorelov, V., Doroshenko, I., Uvdal, P., Balevicius, V., & Sablinskas, V. (2010). Temperature-controlled kinetics of the growth and relaxation of alcohol clusters in an argon matrix. *Journal of Molecular Physics*, 2165–2170. United Kingdom.
8. Doroshenko, I., Balevicius, V., Pitsevich, G., Aidas, K., Sablinskas, V., & Pogorelov, V. (2014). FTIR/PCA study of propanol in an argon matrix: The initial stage of clustering and conformational transitions. *Low Temperature Physics*, 12, 1384–1390. Ukraine.

INVESTIGATION OF THE DEPENDENCE OF PHOTOLUMINESCENCE SPECTRUM AND INTENSITY ON CONCENTRATION IN ER^{3+}-DOPED OPTICAL MATERIALS

K.T. Dadamatova
Assisatant, Tashkent University of Information Technologies named after Muhammad al-Khwarizmi, Tashkent, Uzbekistan
https://doi.org/10.5281/zenodo.20266930

Abstract. *This article investigates, based on theoretical modeling, the dependence of the photoluminescence spectrum and emission intensity on dopant concentration in optical materials doped with Er^{3+} ions. During the study, transitions between energy levels at different concentration values were analyzed, and the закономерности (patterns) of changes in radiation intensity were determined. The results show that an increase in Er^{3+} ion concentration initially leads to an increase in emission intensity; however, beyond a certain threshold, a concentration quenching effect occurs, resulting in a decrease in intensity. It was found that the maximum values of the photoluminescence spectrum and their shifts strongly depend on the dopant concentration. The obtained results are important for improving the efficiency of optical fiber amplifiers and photonic devices. The study enables the development of highly efficient optical materials by selecting an optimal dopant concentration.*

Keywords: *Er^{3+} ions, optical materials, photoluminescence, dopant concentration, emission intensity, optical fibers.*

Introduction The development of modern optical communication systems has significantly increased the demand for high-efficiency optical materials. In particular, controlling the active medium properties of optical fibers used in signal transmission and amplification processes is of great scientific and practical importance. Therefore, optical materials modified with rare-earth elements are being extensively studied, and this direction is considered one of the key areas of photonics.

Among rare-earth elements, erbium ions are recognized as one of the most efficient active dopants in optical fibers. Er^{3+} ions are distinguished by their efficient emission in the 1.55 μm wavelength range, which corresponds to the region of minimal losses in optical communication systems [5,7]. For this reason, erbium-doped optical fibers are widely used in optical amplifiers and laser devices.

In the study of optical material properties, the photoluminescence spectrum serves as an important source of information. The photoluminescence process allows the analysis of energy level structures within the material, interactions between ions, and energy transfer mechanisms. In particular, changes in dopant concentration significantly affect emission intensity and spectral line characteristics.

Recent studies show that as the concentration of Er^{3+} ions increases, the photoluminescence intensity initially rises up to a certain value; however, beyond this point, concentration quenching occurs, leading to a decrease in emission [3,12]. This phenomenon is associated with enhanced interactions between ions and necessitates the determination of an optimal dopant concentration.

In this work, the dependence of the photoluminescence spectrum and emission intensity on dopant concentration in Er^{3+}-doped optical fibers is investigated using theoretical modeling. The main objective of the study is to determine the optimal concentration value and to develop scientific conclusions aimed at improving the efficiency of optical materials.

This study is focused on investigating, through theoretical modeling, the dependence of the photoluminescence spectrum and emission intensity on dopant concentration in Er^{3+}-doped optical fibers. In the research, a homogeneous silica-based optical fiber was assumed as the optical medium, and Er^{3+} ions were considered as active centers.

Experimental part.

Physical model. In the physical model, Er^{3+} ions were considered as a three-level energy system:

N_1 — ground state

N_2 — metastable state (laser emission level)

N_3 — higher excited state

Under optical pumping, ions are excited to the upper energy level and subsequently return to lower levels through radiative and non-radiative transitions. This process is described as photoluminescence.

Rate equations system. The ion populations were described by the following system of differential equations:

$$\frac{dN_3}{dt} = W_p N_1 - \frac{N_3}{\tau_3}$$

$$\frac{dN_2}{dt} = \frac{N_3}{\tau_{32}} - \frac{N_2}{\tau_2} - CN_2^2$$

$$N_1 + N_2 + N_3 = N_{total}$$

where: W_p — optical pumping rate, $\tau_3, \tau_2 \tau_3, \tau_2$ — lifetimes of the excited and metastable states, C — concentration quenching coefficient, N_{total} — total concentration of Er^{3+} ions.

Emission intensity model. The photoluminescence intensity was assumed to be proportional to the number of ions in the metastable state:

$$I_{PL} = K \cdot \frac{N_2}{\tau_2}$$

where I_{PL} — photoluminescence intensity, K — a constant dependent on the optical system.

Effect of concentration. As the concentration of Er^{3+} ions increases, two opposite processes occur:

- at low concentrations → emission increases;
- at high concentrations → quenching effect becomes dominant.

This behavior can be described by the following empirical relation:

$$I(C) = \frac{AC}{1 + BC + DC^2}$$

where C — Er^{3+} concentration, A,B,D — material-dependent constants.

Simulation model. The calculations were performed in MATLAB/Python environments. For the numerical solution, the following steps were used (Figure 1).

The model demonstrates that at low dopant concentrations, the interaction between ions is weak; at the optimal point, the emission reaches its maximum; and at high concentrations, energy losses increase. This directly affects the efficiency of optical fiber amplifiers. This methodology enables the analysis of the photoluminescence process in Er^{3+}-doped optical fibers based on a model that closely approximates real physical processes, and it serves to determine the optimal concentration.

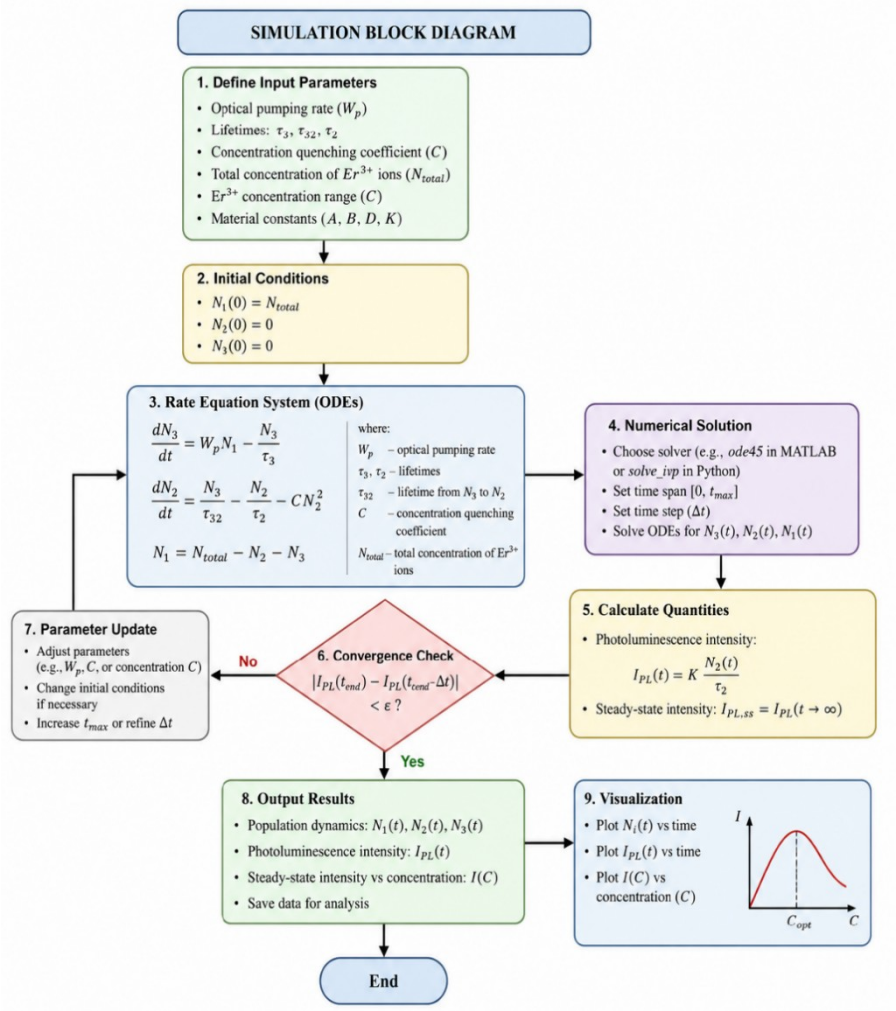


Figure 1. Block Diagram of the Simulation Model for Er^{3+} Ion Photoluminescence

Results and Discussion.

The numerical simulation of the rate equation system made it possible to analyze the population dynamics of Er^{3+} ions and the dependence of photoluminescence intensity on dopant concentration. The obtained results clearly demonstrate the nonlinear behavior of emission intensity as a function of Er^{3+} concentration [10,14]. At low dopant concentrations, the distance between ions is relatively large, and interaction processes such as energy transfer and cross-relaxation are weak. As a result, most of the excited ions return to the ground state through radiative transitions, leading to an increase in photoluminescence intensity. In this region, the emission intensity grows almost linearly with increasing concentration.

As the concentration increases further, ion–ion interactions become more significant. In particular, non-radiative processes such as energy transfer between neighboring ions and cooperative upconversion begin to play an important role. This leads to deviations from linear behavior and the appearance of a saturation region in the emission intensity curve. At higher concentrations, the concentration quenching effect becomes dominant. In this regime, the probability of non-radiative transitions significantly increases due to strong interactions between closely spaced ions. As a result, a considerable portion of the excitation energy is dissipated in the form of heat rather than emitted as photons. Consequently, the photoluminescence intensity decreases despite the higher number of active ions.

The simulation results based on the empirical relation

$$I(C) = \frac{AC}{1 + BC + DC^2}$$

confirm the existence of an optimal dopant concentration at which the emission intensity reaches its maximum. This optimal point represents a balance between efficient radiative emission and minimal non-radiative losses [10,14].

Furthermore, the analysis shows that not only the intensity but also the spectral characteristics of photoluminescence are influenced by dopant concentration. With increasing concentration, slight spectral shifts and broadening of emission bands can be observed, which are associated with changes in the local environment of Er^{3+} ions and increased interaction effects.

The obtained results are in good agreement with known theoretical predictions and experimental observations reported in the literature. From a practical point of view, the findings indicate that careful optimization of Er^{3+} concentration is essential for achieving high performance in optical fiber amplifiers and photonic devices. Overall, the developed simulation model provides a reliable tool for predicting photoluminescence behavior in Er^{3+}-doped optical materials and can be effectively used for the design and optimization of advanced optical systems.

Conclusion. The study shows that photoluminescence intensity in Er^{3+}-doped optical materials strongly depends on dopant concentration. An optimal concentration exists where emission is maximized, while higher concentrations lead to quenching and reduced efficiency. The proposed model effectively describes this behavior and can be used to optimize optical fiber amplifiers and photonic devices.

REFERENCES

1. Almohammed, B., et al. (2026). Photoluminescence enhancement in erbium nanoparticles via controlled phase transformation. *Small, 22*(11), 2511510.
2. Bao, K., et al. (2025). Interlayer silicon-chalcogenide waveguide coupler. *Optical Materials, 159*, 116622.
3. Burtan-Gwizdala, B., et al. (2020). Thermal and spectroscopic properties of Er^{3+}-doped fluorotellurite glasses. Optical Materials, 107, 109968.
4. Ćirić, A., et al. (2026). Luminescence intensity ratio thermometry with Er^{3+}. Crystals, 11(2), 189.
5. Hegde, V., et al. (2022). Analysis of optical and near-infrared luminescence of Er^{3+}/Yb^{3+} co-doped glasses. Photonics, 9(5), 355.
6. Huang, J., et al. (2025). Effective infrared fluorescence of highly doped Er^{3+} in tellurate glass. Journal of Non-Crystalline Solids, 642, 123787.

7. Ji, Y., et al. (2020). Optical properties of Er^{3+}/Yb^{3+}-doped fluoro-sulfo-phosphate glasses. Journal of the American Ceramic Society, 103, 5664.
8. Jiang, H., et al. (2024). Up/down-conversion luminescence of Er^{3+}-activated bismuth tellurium borate. Journal of Alloys and Compounds, 1005, 176002.
9. Li, D., et al. (2022). Concentration quenching mechanism of Er^{3+} in $Gd_2(MoO_4)_3$ phosphors. Nanomaterials, 12(21), 3845.
10. Li, M., et al. (2020). Impact of Er^{3+} concentration on the photoluminescence intensity. Optics Express, 28(15), 21450.
11. Nazrin, S. N., et al. (2026). Enhanced photoluminescence of erbium-doped zinc tellurite glasses. Journal of Luminescence, 281, 121184.
12. Prabhu, N. S., et al. (2021). Spectroscopic study of Er^{3+} doped borate glass. Journal of Luminescence, 235, 118023.
13. sero-Arias, C., et al. (2025). Impact of dopant concentration on luminescence in 3D-printed ZrO_2. Results in Engineering, 25, 100133.
14. Sarumaha, C. S., et al. (2026). Influence of Er^{3+} concentration on silica borate glasses. Journal of Alloys and Compounds, 980, 162506.
15. Scardaci, F., et al. (2025). Optical nanothermometry using Er^{3+}-doped GdOF nanoparticles. Journal of Luminescence, 275, 120230.
16. Shi, K., et al. (2026). Er^{3+}-doped 2.7 μm luminescence in TeO_2-BaO-Ga_2O_3 glass. Journal of Luminescence, 278, 120560.

ON THE METHOD OF MATHEMATICAL INDUCTION IN CALCULATING INDEFINITE INTEGRALS AND TESTING NUMERICAL SERIES FOR CONVERGENCE

B.M. Mamadaliyev[1], M.M. Toxirova[2], Sh.A. Sodiqova[3], S.Kh. Hazratqulova[4]
Candidate of Physical and Mathematical Sciences, Kokand State University[1]
Teacher, General Secondary School No. 55, Uzbekistan District, Fergana Region[2]
Student of Mathematics, Kokand State University[3]
Student of Mathematics, Kokand State University[4]
https://doi.org/10.5281/zenodo.20303980

Abstract. *This article studies the use of the method of mathematical induction in two important areas of mathematical analysis: testing numerical series for convergence and calculating repeated indefinite integrals. The induction method is valued for its simple logical structure and wide applicability in different branches of mathematics. First, the article recalls the general induction principle and the comparison theorem for positive series. Then the convergence of two numerical series is investigated through inequalities proved by mathematical induction. In the first example, the convergence of the factorial series is obtained by comparison with a geometric series. In the second example, the divergence of a series with a radical denominator is established by comparison with a generalized harmonic series. Finally, the article demonstrates how induction can be used to derive formulas for repeated indefinite integrals of exponential and trigonometric functions. The examples show that mathematical induction is an effective and rigorous method for proving formulas and solving problems in mathematical analysis.*

Keywords: *mathematical induction, numerical series, convergence, divergence, comparison test, generalized harmonic series, geometric series, indefinite integral, repeated integration, mathematical analysis.*

Introduction

First of all, the method of mathematical induction is notable for its very simple and clear idea. Suppose that a certain hypothesis or statement $A(n)$ is formulated with the help of induction. To prove that this hypothesis is true for every natural number n, the method of mathematical induction is applied as follows:

1. For $n = 1$, the truth of the statement $A(n)$ is verified.
2. It is assumed that, for $n = k$, the statement $A(n)$ is true.
3. The truth of the statement $A(n)$ for $n = k + 1$ is proved; in other words, the implication $A(k) \Rightarrow A(k + 1)$ is established.

After these three steps, it is concluded that the statement $A(n)$ is true for all natural numbers n.

The method of mathematical induction is widely and successfully used in many different, and sometimes very distant, areas of mathematics. In this article, we show the applications of this method to testing numerical series for convergence and to calculating indefinite integrals by means of concrete examples.

A comparison theorem for positive series

It is known that, if the convergence or divergence of a positive series is known, then the convergence or divergence of another positive series whose terms are related to the terms of the first series can often be determined by comparison. Several theorems are connected with this idea. We recall one of them.

Theorem. Let $\sum_{n=1}^{\infty} a_n$ and $\sum_{n=1}^{\infty} b_n$ be positive series. If, beginning with some value n_0 of n with $n_0 \geq 1$, the inequality

$$a_n \leq b_n$$

holds for all $n \geq n_0$, then the convergence of the series

$$\sum_{n=1}^{\infty} b_n$$

implies the convergence of the series

$$\sum_{n=1}^{\infty} a_n ,$$

and the divergence of the series

$$\sum_{n=1}^{\infty} a_n$$

implies the divergence of the series

$$\sum_{n=1}^{\infty} b_n .$$

This theorem is one of the most convenient tools for applying mathematical induction to convergence problems, because the required comparison inequalities can often be proved by induction.

Example 1. Testing a factorial series for convergence

We test the following series for convergence:

$$\sum_{n=1}^{\infty} a_n = \frac{1}{1!} + \frac{1}{2!} + \frac{1}{3!} + \cdots + \frac{1}{n!} + \cdots = \sum_{n=1}^{\infty} \frac{1}{n!}.$$

For all $n \geq 1$, the following inequality holds:

$$A(n): \quad \frac{1}{n!} \leq \frac{1}{2^{n-1}}.$$

This inequality can be verified by the method of mathematical induction.

Proof.

1. For $n = 1$, we have

$$\frac{1}{1!} = \frac{1}{2^{1-1}},$$

so the statement is true.

2. Assume that, for $n = k$, the inequality is true, that is,

$$\frac{1}{k!} \le \frac{1}{2^{k-1}}.$$

We prove the inequality for $n = k + 1$:

$$\frac{1}{(k+1)!} = \frac{1}{k!\,(k+1)} \le \frac{1}{k!} \cdot \frac{1}{k+1} \le \frac{1}{2^{k-1}} \cdot \frac{1}{k+1} \le \frac{1}{2^{k-1}} \cdot \frac{1}{1+1} = \frac{1}{2^k}.$$

Therefore,

$$\frac{1}{(k+1)!} \le \frac{1}{2^k}.$$

Thus the inequality is true for all natural numbers n.

If we take

$$b_n = \frac{1}{2^{n-1}},$$

then

$$\sum_{n=1}^{\infty} b_n = \sum_{n=1}^{\infty} \frac{1}{2^{n-1}}$$

is a geometric series with ratio

$$q = \frac{1}{2} < 1,$$

and therefore it is convergent. Hence, by the comparison theorem, the given series

$$\sum_{n=1}^{\infty} \frac{1}{n!}$$

is also convergent.

Example 2. Testing a series with radical denominators for convergence

Test the following series for convergence:

$$\sum_{n=1}^{\infty} \frac{1}{1 + \frac{1}{\sqrt{2}} + \frac{1}{\sqrt{3}} + \cdots + \frac{1}{\sqrt{n}}}.$$

Using the method of mathematical induction, we can show that

$$A(n): \quad 1 + \frac{1}{\sqrt{2}} + \frac{1}{\sqrt{3}} + \cdots + \frac{1}{\sqrt{n}} < 2\sqrt{n} \qquad (n \ne 1).$$

We prove this inequality.

1. For $n = 1$, the inequality

$$1 < 2$$

is true.

2. Assume that, for $n = k$, the inequality

$$1 + \frac{1}{\sqrt{2}} + \frac{1}{\sqrt{3}} + \cdots + \frac{1}{\sqrt{k}} < 2\sqrt{k}$$

is true. We prove it for $n = k + 1$:

$$1 + \frac{1}{\sqrt{2}} + \frac{1}{\sqrt{3}} + \cdots + \frac{1}{\sqrt{k}} + \frac{1}{\sqrt{k+1}} < 2\sqrt{k} + \frac{1}{\sqrt{k+1}}.$$

$$2\sqrt{k} + \frac{1}{\sqrt{k+1}} = \frac{2\sqrt{k}\sqrt{k+1} + 1}{\sqrt{k+1}}.$$

$$\frac{2\sqrt{k}\sqrt{k+1} + 1}{\sqrt{k+1}} \le \frac{k + (k+1) + 1}{\sqrt{k+1}} = 2\sqrt{k+1}.$$

Here we used the inequality

$$\left(\sqrt{k+1} - \sqrt{k}\right)^2 = k + 1 - 2\sqrt{k}\sqrt{k+1} + k \ge 0.$$

Therefore,

$$1 + \frac{1}{\sqrt{2}} + \frac{1}{\sqrt{3}} + \cdots + \frac{1}{\sqrt{k+1}} \le 2\sqrt{k+1},$$

and the required inequality holds for all natural numbers n.

Now set

$$b_n = \frac{1}{1 + \frac{1}{\sqrt{2}} + \frac{1}{\sqrt{3}} + \cdots + \frac{1}{\sqrt{n}}}$$

and

$$a_n = \frac{1}{2\sqrt{n}}.$$

From the proved inequality we obtain

$$a_n \le b_n.$$

Consequently,

$$\sum_{n=1}^{\infty} a_n \le \sum_{n=1}^{\infty} b_n.$$

Since

$$\sum_{n=1}^{\infty} a_n = \sum_{n=1}^{\infty} \frac{1}{2\sqrt{n}} = \frac{1}{2}\sum_{n=1}^{\infty} \frac{1}{n^{1/2}}$$

is a generalized harmonic series with exponent $p = \frac{1}{2} < 1$, it is divergent. Therefore, by the comparison theorem, the given series is also divergent.

Applications to indefinite integrals

We now give examples of applications of the method of mathematical induction to the calculation of indefinite integrals. In the formulas below, the notation $I_n(f)$ denotes the result of integrating the function $f(x)$ successively n times, that is,

$$I_n(f) = \int\int\cdots\int f(x)\,dx,$$

where the integral sign is repeated n times.

Example 3. Repeated indefinite integrals of an exponential function

We prove the equality

$$A_n: \quad I_n(a^x) = \frac{1}{\ln^n(a)}a^x + \sum_{i=1}^{n} \frac{c_i}{(n-i)!}x^{n-i},$$

where $c_1, c_2, ..., c_n$ are real constants.

Proof. We prove the equality using the method of mathematical induction.

1. For $n = 1$, we have

$$\int a^x\,dx = \frac{1}{\ln a}a^x + c_1,$$

so the statement is true.

2. Assume that, for $n = k$, the equality

$$I_k(a^x) = \frac{1}{\ln^k(a)}a^x + \sum_{i=1}^{k} \frac{c_i}{(k-i)!}x^{k-i}$$

is true. We show that it is true for $n = k+1$:

By the definition of repeated integration and the induction hypothesis,

$$I_{k+1}(a^x) = \int \left(\frac{1}{\ln^k(a)}a^x + \sum_{i=1}^{k} \frac{c_i}{(k-i)!}x^{k-i} \right) dx.$$

$$I_{k+1}(a^x) = \frac{1}{\ln^{k+1}(a)}a^x + \sum_{i=1}^{k} \frac{c_i}{(k+1-i)!}x^{k+1-i} + c_{k+1}.$$

$$I_{k+1}(a^x) = \frac{1}{\ln^{k+1}(a)} a^x + \sum_{i=1}^{k+1} \frac{c_i}{(k+1-i)!} x^{k+1-i}.$$

Thus,

$$I_n(a^x) = \frac{1}{\ln^n(a)} a^x + \sum_{i=1}^{n} \frac{c_i}{(n-i)!} x^{n-i}$$

for all natural numbers n.

Example 4. Repeated indefinite integrals of the sine function

We prove the equality

$$A_n: \quad I_n(\sin x) = \sin\left(x + n\frac{3\pi}{2}\right) + \sum_{i=1}^{n} \frac{c_i}{(n-i)!} x^{n-i},$$

where $c_1, c_2, ..., c_n$ are real constants.

We prove this equality by the method of mathematical induction.

1. For $n = 1$, we have

$$\int \sin x\, dx = -\cos x + c_1 = \sin\left(x + \frac{3\pi}{2}\right) + c_1,$$

which is true.

2. Assume that, for $n = k$, the equality

$$I_k(\sin x) = \sin\left(x + k\frac{3\pi}{2}\right) + \sum_{i=1}^{k} \frac{c_i}{(k-i)!} x^{k-i}$$

is true. We verify it for $n = k+1$:

By the definition of repeated integration and the induction hypothesis,

$$I_{k+1}(\sin x) = \int \left(\sin\left(x + k\frac{3\pi}{2}\right) + \sum_{i=1}^{k} \frac{c_i}{(k-i)!} x^{k-i} \right) dx.$$

$$I_{k+1}(\sin x) = -\cos\left(x + k\frac{3\pi}{2}\right) + \sum_{i=1}^{k} \frac{c_i}{(k-i)!} \cdot \frac{1}{k-i+1} x^{k-i+1} + c_{k+1}.$$

$$I_{k+1}(\sin x) = \sin\left(x + k\frac{3\pi}{2} + \frac{3\pi}{2}\right) + \sum_{i=1}^{k} \frac{c_i}{(k+1-i)!} x^{k+1-i} + c_{k+1}.$$

$$I_{k+1}(\sin x) = \sin\left(x + (k+1)\frac{3\pi}{2}\right) + \sum_{i=1}^{k+1} \frac{c_i}{(k+1-i)!} x^{k+1-i}.$$

Therefore,

$$I_{k+1}(\sin x) = \sin\left(x + (k+1)\frac{3\pi}{2}\right) + \sum_{i=1}^{k+1} \frac{c_i}{(k+1-i)!} x^{k+1-i}$$

for all natural numbers n.

Such examples can be given in large numbers.

Conclusion

The examples considered above show that the method of mathematical induction is not only a theoretical proof technique but also a practical method for solving problems in mathematical analysis. In convergence problems, induction helps prove inequalities that make the comparison test applicable. In the calculation of repeated indefinite integrals, induction provides a rigorous way to establish general formulas from simple base cases. Therefore, the mathematical induction method is an effective and reliable tool for proving statements that depend on a natural-number parameter.

REFERENCES

1. Azlarov, T.; Mansurov, H. *Mathematical Analysis.* Tashkent, 1986.
2. Khudoyberganov, G.; Voriyev, A.; Mansurov, Kh.; Shoimqulov, B. *Lectures on Mathematical Analysis.* Tashkent, 2010.
3. Azlarov, T.; Mirakhmedov, M.; Otakoziyev, D.; Sobirov, M.; Tolaganov, S. *A Guide to Mathematics.* Part II. Tashkent, 1990.
4. Sadullayev, A.; Mansurov, H.; Khudoyberganov, G.; Vorisov, A.; Gulomov, R. *Mathematical* ... [the title is incomplete in the submitted manuscript].
5. Mamadaliyev, M. B.; Qodirova, M. Kh. “On the Concavity and Convexity of a Surface.” *Scientific Bulletin of Kokand State Pedagogical Institute*, 2024, Issue 3, Pedagogy, UDC: 082.29.63, ORCID: 0009-0000-4127-8226.

INFORMATION AND COMMUNICATION TECHNOLOGIES IN THE ORGANIZATION AND DEVELOPMENT OF INDEPENDENT CREATIVE WORK AMONG YOUNG PEOPLE

N. Shamsiddinov[1], O. Yusupov[2], B. Husanov[3]
Tashkent State Technical University named after Islam Karimov, 2 University Street, Tashkent, Republic of Uzbekistan[1,2,3]
https://doi.org/10.5281/zenodo.20523952

Abstract. *This article examines the role of information and communication technologies in organizing and developing independent creative work among young people, particularly students of academic lyceums. It emphasizes the importance of independent analytical thinking, responsible decision-making, and creative problem-solving as essential qualities for future specialists. The study discusses how mathematical problem solving, especially nonstandard geometric tasks, can serve as an effective means of identifying and developing students' creative abilities. A problematic geometry task involving an inscribed circle and the trajectory of its center is analyzed through both analytical methods and the Maple 13 software environment. The obtained result demonstrates that the locus of the center forms part of an ellipse. The article argues that integrating ICT tools into mathematical education helps visualize complex constructions, supports deeper understanding, and encourages students to engage in independent scientific inquiry. Such approaches contribute to the formation of creative thinking and research-oriented competence in young learners.*

Keywords: *information and communication technologies, independent creative work, creative thinking, mathematical problem solving, academic lyceum students, Maple software, geometric modeling.*

1. Introduction

Today, in addition to technological professional training, it is necessary for a specialist to have an important factor in the development of Education – independent thinking, responsible decision-making, a creative approach to any work, constant learning, communication, the ability to cooperate, social and Professional Responsibility, etc.

The formation of personality-oriented education ensures the professional self-realization of a person and the development of his further creative maturation. Thus, the task faced in education is not only to provide comprehensive knowledge necessary for the training of a specialist, but also to develop the independence of thinking, which is necessary for a creative feeling of the surrounding world . Today it is universally recognized that science is of great importance for the development of culture and economy in the modern state. Therefore, educating and educating young people with the aforementioned qualities is the most important task.

Scientific work belongs to all areas of human activity, it can be successfully developed only by those who have creative talents. It is well known that only a small number of people with creative abilities can successfully work in the field of art, literature, music. The same applies to scientific work, only people with creative talents can successfully work here. So, for the effective development of scientific work, it is necessary to choose creatively gifted young people. In science,

it is very difficult to assess a person's creative achievements, although it is made by the public, it is a small group made up of scientists qualified in the field. The selection of scientific personnel by their creative abilities is one of the most difficult organizational problems of scientific work.

The success of scientific work in any field of knowledge can only be ensured by people with creative abilities, and the number of such people is small. To form employees of the scientific sphere, it is necessary, firstly, to create conditions for attracting talented youth to scientific work, secondly, to organize the selection of these young people in accordance with the nature of creative talents, and thirdly, to create special conditions for the education of creatively gifted young people, so that natural talents develop as fully as possible. This issue is solved in the following way: after graduating from high school, such creative talented young people are sent to academic lyceums. One of the best methods of creative education of young people in academic lyceums is the organization of Olympiads for students of academic lyceums. These are competitions aimed at mathematics and physics, equipment construction, astronomical observations and the formation of students ' interest in scientific and technical creativity, which will cover as many participants as possible. These Olympiads are interested not only in discovering talented, creatively gifted youth, but also in the creative solution of scientific issues from an early age. We have such Olympiads developed widely, and they are held at a high level. Also, the creative thinking of students is well influenced by the solution of scientific creative issues in circles, seminars in various disciplines and round tables with science figures. These circles are conducted by young scientists, so students get acquainted with the creative scientific process.

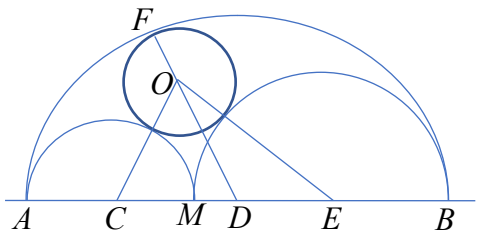
It is known that effective scientific work requires not only knowledge and understanding, but, most importantly, independent analytical and creative thinking, as one of the effective means of educating, identifying and evaluating these qualities. The solution of the issue in the study of Mathematics, Mechanics, physics and other Exact Sciences is of great importance. Problem solving not only allows the student to apply his knowledge to solve practical problems, but is also one of the most effective ways for the teacher to check how deeply the student understands the subject. In addition, as mentioned above, young people can be trained in independent creative scientific thinking by solving the issue.

Mathematics is a very suitable subject for primary education in the development of creative thinking in the field of Natural Sciences. Obviously, not all tasks allow you to reveal such abilities of the student. Therefore, we will dwell specifically on the nature of such tasks. Experience shows that the issues that are usually given in sets do not always have a character that provides freedom of thought. The issues are content with the calculation of the given data using the necessary formulas. Here, the student's task is manifested only in the selection of the correct formulas necessary for calculation. The issues that motivate independent thinking and creative search, which we mentioned, form a scientific worldview in the reader.

2. In this article, we will consider the solution of the problem issue. This issue allows you to increase the creative potential of students. Here we bring a complete solution to the issue.

Issue. AB an optional point M is obtained in the cut AB, MA and MB let the cuts be drawn half circles in diameter and an inner circle that attempts each of these half circles. find the geometric position of the center of the circle with the inner drawing, according to the choice of the point M in the cut AB.

Solution: To solve the problem, we introduce the following definition: $AC = CM = R_1$, $ME = EB = R_2$, $AD = DB = R$, $OF = r$.



1-

for ΔCOE radius of the circle drawn internally according to stuart's theorem we find OF:

2.1. Finding the radius of an inscribed circle

$$OC^2 \cdot DE + OE^2 \cdot DC = OD^2 \cdot CE + CE \cdot CD \cdot DE \qquad (1)$$

From 1-picture $CO = R_1 + r$, $OE = R_2 + r$, $OD = R - r$, $CD = R_2$, $DE = R_1$, $CE = R_1 + R_2 = R$ placing (1),we will have

$$(R_1 + r)^2 \cdot R_1 + (R_2 + r)^2 \cdot R_2 = (R - r)^2 \cdot R + R \cdot R_1 \cdot R_2.$$

$$R_1^3 + 2rR_1^2 + r^2R_1 + R_2^3 + 2rR_2^2 + r^2R_2 = R^3 - 2R^2r + r^2R + R \cdot R_1 \cdot R_2$$

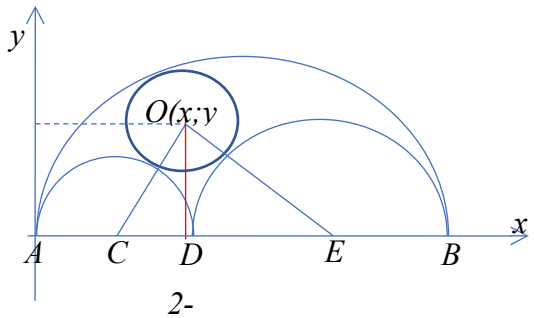
$$R_1^3 + 2rR_1^2 + R_2^3 + 2rR_2^2 + r^2(R_1 + R_2) = R^3 - 2R^2r + r^2 \cdot R + R \cdot R_1 \cdot R_2$$

$$2rR_1^2 + 2rR_2^2 + 2R^2r = R^3 + R \cdot R_1 \cdot R_2 - R_1^3 - R_2^3$$

$$r = \frac{R^3 + R \cdot R_1 \cdot R_2 - R_1^3 - R_2^3}{2R_1^2 + 2R_2^2 + 2R^2}. \qquad (2)$$

2.2 Finding the coordinates of an inscribed circle

Now let's describe the given drawing in the Cartesian coordinate system in order to determine the coordinates of the center of the inner drawn circle $O(x;y)$:



2-

for ΔCOE we find the height OD (we enter the designation $CD = p$

Pythagorean theorem for ΔCOD: $CO^2 = CD^2 + DO^2 \Rightarrow (R_1 + r)^2 = OD^2 + p^2$

Pythagorean theorem for ΔDOE: $OE^2 = OD^2 + DE^2 \Rightarrow (R_2 + r)^2 = OD^2 + (R - p)^2$

We find and equalize the height OD from two equals:

$$(R_1 + r)^2 - p^2 = (R_2 + r)^2 - (R - p)^2$$

$$R_1^2 + 2R_1r + r^2 - p^2 = R_2^2 + 2R_2r + r^2 - R^2 + 2Rp - p^2$$

$$R_1^2 + 2R_1r = R_2^2 + 2R_2r - R^2 + 2Rp$$

$$p=\frac{R_1^2+2R_1r-R_2^2-2R_2r+R^2}{2R} \qquad CD=\frac{R_1^2+2R_1r-R_2^2-2R_2r+R^2}{2R}$$

We find height OD using the Geron formula:

$$P=R_1+R_2+r=R+r$$

$$S=\sqrt{P(P-a)(p-b)(P-c)}$$

$$S=\sqrt{(R+r)rR_1R_2}$$

$$OD=\frac{2S}{R}=\frac{2}{R}\sqrt{(R+r)rR_1R_2}$$

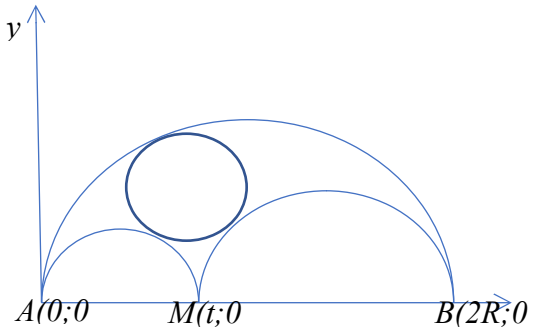
From this, the coordinates of the center of the circle drawn internally will be:

$$y=OD=\frac{2}{R}\sqrt{(R+r)rR_1R_2} \qquad x=AC+CD=R_1+\frac{R_1^2+2R_1r-R_2^2-2R_2r+R^2}{2R}$$

,

2.3. Construction of parametric equation of inscribed circular coordinates

Since the coordinates of $O(x;y)$ given in the matter M depend on the choice of a point, we find the expression x and y through the coordinate of POINT M.



3-

In this there will be $R_1=\frac{t}{2}$, $R_2=R-\frac{t}{2}$. The radius of the circle drawn internally in that case is expressed as:

$$r=\frac{R^3+R\cdot\frac{t}{2}\cdot\left(R-\frac{t}{2}\right)-\frac{t^3}{8}-\left(R-\frac{t}{2}\right)^3}{2\left(R-\frac{t}{2}\right)^2+2\frac{t^2}{4}+2R^2}=\frac{8R^3+2Rt(2R-t)-t^3-(2r-t)^3}{4(2R-t)^2+8t^2+16R^2}=$$

$$=\frac{16R^2t-8Rt^2}{8t^2+32R^2-16Rt}=\frac{2R^2t-Rt^2}{t^2+4R^2-2Rt}$$

We determine the coordinates of the center of the Circle $O(x;y)$ by parameter t :

$$y=\frac{2}{R}\sqrt{(R+r)rR_1R_2}=\frac{2}{R}\sqrt{\left(R+\frac{2R^2t-Rt^2}{t^2+4R^2-2Rt}\right)\frac{2R^2t-Rt^2}{t^2+4R^2-2Rt}\frac{t}{2}\left(R-\frac{t}{2}\right)}=\frac{2Rt(2R-t)}{t^2+4R^2-2Rt}$$

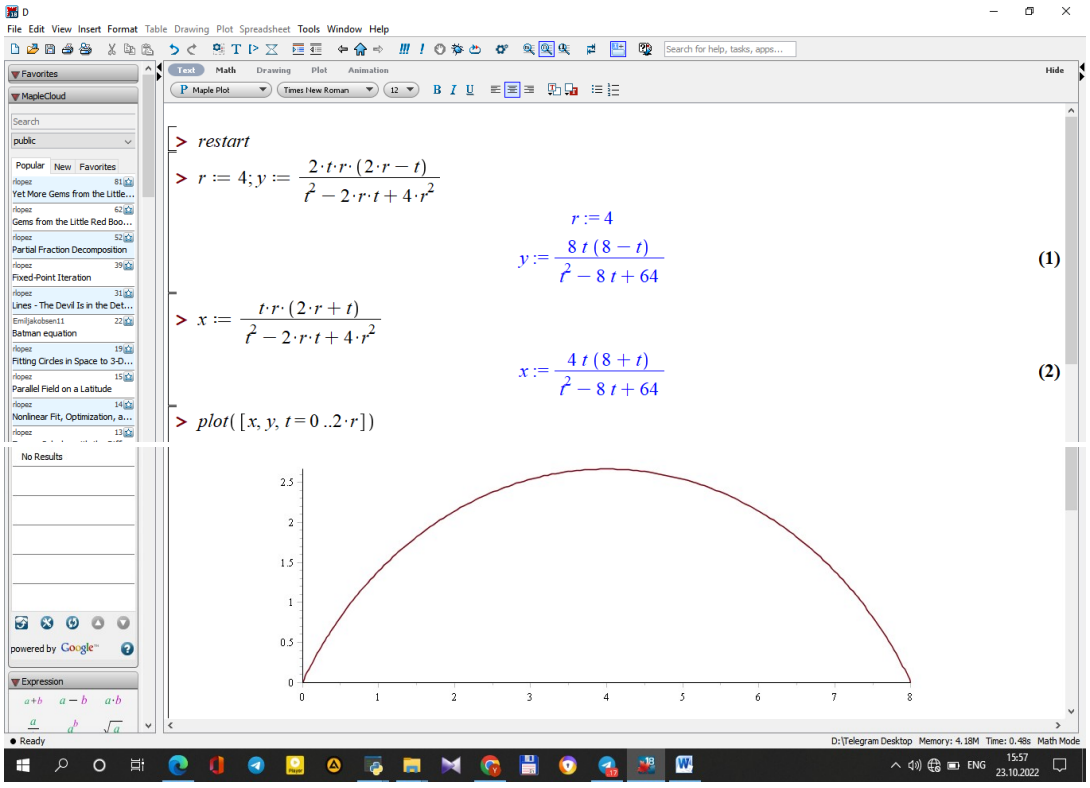
$$x=\frac{t}{2}+\frac{\frac{t^2}{4}+2\frac{t}{2}\cdot\frac{2R^2t-Rt^2}{t^2+4R^2-2Rt}-\left(R-\frac{t}{2}\right)^2-2\left(R-\frac{t}{2}\right)\frac{2R^2t-Rt^2}{t^2+4R^2-2Rt}+R^2}{2R}=\frac{Rt(2R+t)}{t^2+4R^2-2Rt}$$

Hence, the parametric equation of the motion trajectory of the inner drawn circle center $O(x;y)$.

$$\begin{cases} y = \dfrac{2Rt(2R - t)}{t^2 + 4R^2 - 2Rt}, \\ x = \dfrac{Rt(2R + t)}{t^2 + 4R^2 - 2Rt}. \end{cases} \quad (3)$$

3. The result obtained in support of information and communication technologies.

At the stage of solving this issue, we describe the schematic state of the issue. The main AB is the cut, and in this cut M the point, AM and MB are drawn by making the cuts towards the half-circles and the circle that attempts these half-circles; The center of the circle drawn internally, which attempts to semi-circles point $O(x; y)$ is the moving point, the curve formed by the set of points $O(x; y)$ will be the solution to the issue. First, you can program this process on a computer to reflect on the places of the geometric dots being searched. To do this, we use the Maple 13 software tool. We give the final result of the program written in Maple 13:



Hence, the center of the circle drawn internally is as long as the geometric role of $O(x; y)$ forms part of the Ellipse.

4.Prove in an analytical way.

$$\begin{cases} y = \dfrac{2Rt(2R - t)}{t^2 + 4R^2 - 2Rt} \\ x = \dfrac{Rt(2R + t)}{t^2 + 4R^2 - 2Rt} \end{cases}$$ we find parameter t from the parametric equation. To do this, we will have the corresponding sides of the Equality:

$$\frac{y}{x} = \frac{2Rt(2R - t)}{Rt(2R + t)} = \frac{4R - 2t}{2R + t}$$

$$y(2R+t)=x(4R-2t)\Rightarrow 2Ry+yt=4Rx-2xt\Rightarrow(y+2x)t=4Rx-2Ry\Rightarrow t=\frac{2R(2x-y)}{y+2x}$$

we will have. By placing the found parameter t in the expression of y:

$$y=\frac{2R\dfrac{2R(2x-y)}{y+2x}\left(2R-\dfrac{2R(2x-y)}{y+2x}\right)}{\left(\dfrac{2R(2x-y)}{y+2x}\right)^2+4R^2-2R\dfrac{2R(2x-y)}{y+2x}}=$$

$$=\frac{4R^2(2x-y)(2Ry+4Rx-4Rx+2Ry)}{4R^2(2x-y)^2+4R^2(y+2x)^2-4R^2(2x-y)(2x+y)}=$$

$$=\frac{4Ry(2x-y)}{(2x-y)^2+(y+2x)^2-(2x-y)(2x+y)}=\frac{4Ry(2x-y)}{4x^2+3y^2}$$

After the simplifications, we come to the following equation:

$$4x^2+3y^2-8Rx+4Ry=0\Rightarrow 4(x^2-2Rx)+3\left(y^2+\frac{4}{3}Ry\right)=0\Rightarrow$$

$$4(x-R)^2+3\left(y+\frac{2}{3}R\right)^2=\frac{16}{3}R^2\Rightarrow\frac{(x-R)^2}{\frac{4}{3}R^2}+\frac{\left(y+\frac{2}{3}R\right)^2}{\frac{16}{9}R^2}=1$$

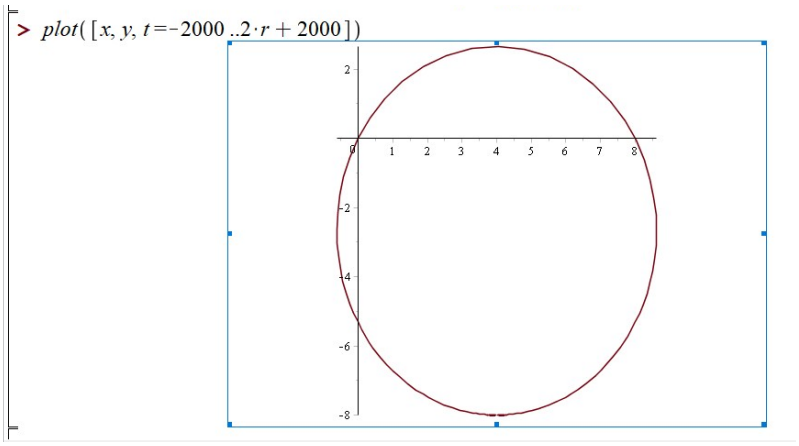
If we enter the designation $\frac{4}{3}R^2=a^2$ and $\frac{16}{9}R^2=b^2$ in the resulting equation

$$\frac{(x-R)^2}{a^2}+\frac{\left(y+\frac{2}{3}R\right)^2}{b^2}=1 \qquad (4)$$

in appearance, we form the Ellipse equation.

Hence, the center of the circle drawn internally is as long as the geometric role of $O(x;y)$ forms part of the Ellipse.

The full view of the Ellipse will be as follows:



The peculiarity of such issues is that they do not have a clear solution method, that is, a problematic issue, since the reader himself - with his knowledge and abilities-can go deeper into the study of the question. The reader's solution makes it possible to assess the level and character of his scientific thinking, which is especially important when choosing the future scientific field of the student. The independent solution of this type of issue forms scientific thinking in the student and develops in him an interest in scientific problems.

5. Conclusion

In conclusion, the most important place in mathematical abilities is the ability to organize evidence and conduct careful conscious work to verify it, logically building a chain of actions that will lead to the solution of the issue. Geometry the difference between the work of a student solving problems and creative work is the difference in the level of mathematical creativity.

When solving a scientific issue, a scientist must always clearly represent in his imagination the magnitude and relative importance of physical parameters that serve to describe the phenomenon under study. This is necessary in order to select the links that are decisive in solving the issue. Therefore, it is necessary to teach young scientists to accurately express the exact quantitative values of signs in formulas that determine quantities. For physics, unlike mathematics, the parameters and variables in a mathematical equation must be exact quantities.

REFERENCES

1. L. M. Fridman Ye. N. Tureskiy. “Kak nauchitsya reshat zadachi”, Moskva «Prosveshenie», 1989.
2. O. Karimiy. Planimetriyadan hisoblashga va isbotlashga doir tanlangan masalalar. “O’qituvchi”. Toshkent-1955 y.
3. D. Xusanov, N. B. Shamsiddinov “Yoshlarning mustaqil ijodiy fikrlash faoliyatini rivojlantirishda geometric masalalarning o'rni”. “Halq ta’limimi” ilmiy-metodik jurnal.2020 yil. 5-son.
4. D. Xusanov, N. B. Shamsiddinov “Geometrik masalani turli yechish usullari yordamida o'quvchilarning ijodiy fikrlash faoliyatini rivojlantirish”. “Halq ta’limi” ilmiy-metodik jurnal.
5. 2022 yil. 3-son.
6. J. Adamar Issledovanie psixologii prosessa izobreteniya v oblasti matematiki. M., 1970.
7. V. Tixomirov - Andrey Nikolaevich Kolmogorov//Kvant.-1993.- № 3/4.-S 3-10.
8. N. V. Agapova Perspektivi razvitiya novix texnologiy obucheniya. – M.: TK Velbi, 2005. – 247 s.
9. Mario Lucentini Technological Concepts and Mathematical Models in the Evolution of Modern Engineering Systems. Germany, 2012.
10. J.Husanov, N. Shamsiddinov, B. Quvonov, Geometriya fanidan uslubiy ishlanmalar tayyorlashda axborot kommunikatsiya texnologiyalaridan foydalanish samaradorligi, Xalq ta’limi ilmiy-metodik jurnal. 2021 yil 6- son. 33-36 bet.
11. J. Husanov, N. Shamsiddinov, On the role average values in solving geometric extreme. Internatsional journal on integrated edication. vol. 6. 2022.
12. D. M. Makhmudova On the role of problem tasks in the development of independent analytical and creative thinking of students. American journal of scientific and educational research. 2014.-№1 (4).-p. 325-330.
13. J. Husanov, N. Shamsiddinov. Geometrik masalani turli yechish usullari yordamida o‘quvchilarning ijodiy fikrlash faoliyatini rivojlantirish Xalq ta'limi ilmiy-metodik jurnal. 2022 yil 3-son. 25-32 bet.
14. N. Shamsiddinov. The Effectiveness of Information and Communication Technology in Finding the Distance Between Straight Lines Non-Intersecting in Space. International Journal of Mathematics Trends and Technology. Volume-68 Issue-6. 2022.

GALILEO GALILEI - THE FOUNDER OF DYNAMICS

Z.A. Yavkacheva[1], Q.A. Aliqulov[2]
Senior Lecturer, Tashkent State Transport University[1]
Student, Tashkent State Transport University[2]
https://doi.org/10.5281/zenodo.20552573

Abstract. *The article comprehensively highlights the significant contribution of the Italian scholar Galileo Galilei to the history of the development of physics. Galileo Galilei was an Italian philosopher, physicist, and astronomer who exerted a profound influence on the science of his era. Galilei is primarily renowned for his research in the fields of planets and stars, his active support of the heliocentric system of the world, and his experiments in mechanics. The main focus is directed toward the fact that through the experiments conducted by Galileo Galilei, fundamental data and principles regarding the field of mechanics were discovered. During his academic career at the University of Padua, Galilei investigated inertia and the free fall of bodies. By determining that the acceleration of free fall is independent of the mass of a body, he disproved the theory—which had prevailed since the time of Aristotle—stating that the "speed of fall" is proportional to the weight of the body. Galilei verified this by dropping objects of various masses from the top of the Leaning Tower of Pisa to analyze their descent.*

Furthermore, Galilei is considered one of the founders of the principle of relativity in classical mechanics, which was subsequently named after him. In 1593, Galileo Galilei published a book titled "Mechanics", wherein he extensively detailed his research. Among the phenomena occurring in the universe surrounding us, different forms of motion interested Galilei the most. This holds vital importance in shaping project-based activities among youth, enabling them to independently determine the information they require, facilitating their visualization of the scientific picture of the world, and upbringing a well-rounded generation equipped with the personal intellectual qualities necessary for society.

Keywords: *youth, generation, experiment, result, mechanics, oscillation, body, pendulum.*

INTRODUCTION

The first foundations of dynamics were established by the Italian scientist Galileo Galilei, who discovered a new and limitless horizon for the development of mechanics. Galilei's discoveries astonished his contemporaries. Galilei constructed a telescope and, in 1610, discovered the moons of Jupiter.

LITERATURE REVIEW

At the turn of the 16th and 17th centuries, the issue of the system of the universe was considerably entangled. In the 4th century BCE, Aristotle had asserted that the seven planets visible to us revolved around the Earth.

Galilei is celebrated not only for the substance of his scientific achievements, but also specifically for his discoveries in astronomy. Galilei independently constructed his first telescope, which consisted of a convex objective lens and a concave eyepiece. This tube magnified objects approximately three times. Shortly thereafter, he succeeded in building a telescope that allowed for a 32-fold magnification. Observations through the telescope revealed that the Moon was covered with mountains and pocketed with craters, stars lost their apparent disks (revealing their immense

distance), and for the first time, their colossal remoteness was discovered. It was determined that Jupiter possessed its own four moons (satellites), the Milky Way resolved into individual stars, and a vast number of new stars became visible. Galilei also discovered the phases of Venus, sunspots, and the rotation of the Sun.

Galilei completed his book, *"Discourses and Mathematical Demonstrations Relating to Two New Sciences Concerning Mechanics and Local Motions"*, in 1636, and it was published in Holland in 1638.

RESEARCH AND RESULTS

In 1583, the twenty-year-old Galilei was in Pisa where, following his father's advice, he was studying philosophy and medicine. One day, while inside the cathedral, driven by his inherent curiosity and erudition, he decided to examine the motion of a chandelier suspended from the very top. He sought to test whether the duration of its oscillations across large, medium, and small arcs was unequal; to a casual observer, it might seem that the time required to traverse a large arc would be shorter due to the higher speed of the chandelier at its higher and more inclined positions. As the chandelier moved uniformly, he used his own pulse and the tempo of music with which he was well acquainted to roughly measure how the forward and backward movements of the chandelier occurred. Based on these calculations, the time intervals appeared to be identical. However, unsatisfied with this and returning home, he resolved to perform the following experiment to gain full conviction.

He took two lead spheres and tied them to ropes of equal length so they could swing freely. He deflected one sphere by 30 degrees and the other by 10 degrees from the vertical and released them at the exact same instant. He observed that during the time it took for one pendulum to oscillate a certain number of times across the large arc, the second pendulum completed the exact same number of oscillations across the small arc. Furthermore, he constructed two identical pendulums but of different lengths. He observed that if the shorter pendulum completed a certain number of oscillations—for instance, 300 times—across its large arc, during that exact same timeframe, the longer pendulum consistently completed a specific, fixed number of oscillations—for instance, 40 times—across its own large arc. Repeating this procedure multiple times, he concluded that regardless of whether the arc of a given pendulum is very large or very small, the duration of its oscillation is completely identical and there is no significant difference. If any slight variation existed, it was due to air resistance—as air exerts more resistance against a heavy and rapidly moving body than against a slowly moving one.

He also observed that the differences in the absolute and specific weights of the spheres did not lead to any noticeable variation. As long as all the spheres were suspended on ropes of equal length measured from their centers to the suspension point, they maintained a sufficient equality of time across any arc. Consequently, Galilei discovered the relationship between the length of a pendulum and its frequency of oscillation: the squares of the periods of oscillation are proportional to their lengths:

$$\frac{T_1^2}{T_2^2} = \frac{L_1^2}{L_2^2}$$

In addition to pendulums, he investigated the motion of a body falling vertically toward the Earth, which is one of the most common examples of uniformly accelerated motion. At first glance, the acceleration of a falling body does not seem like a straightforward fact. It appears as though heavy bodies fall faster than light ones, and that the speed of fall is proportional to the weight of the

object (a belief held by most people prior to Galilei's era). Galilei applied his scientific method of abstraction and simplification. He introduced the postulate that in the case of free fall, in the absence of air or any other resisting medium, all bodies fall with a constant, uniform acceleration. Based on this postulate, he demonstrated that the distance traveled by a body falling from rest is proportional to the square of the time $(d \propto t^2)$.

To confirm his theory that the velocity of bodies increases as they fall, Galilei provided the following argument: a heavy stone dropped from a height of 2 meters drives a stake significantly deeper into the ground than the exact same heavy stone dropped from a height of 10 cm. In the first scenario, it is evident that the stone must attain a greater velocity. As previously noted, Galilei maintained that arbitrary objects (both heavy and light) fall with the exact same acceleration, at least in a vacuum. Common sense might suggest that the ancients were closer to the truth. Indeed, if you hold a sheet of paper horizontally in one hand and a heavier object, say a baseball, in the other and release them simultaneously, it is well known that the heavier object will reach the ground first. However, if you crumple the paper into a tight ball and repeat the experiment, you will observe that both objects reach the floor almost at the exact same time.



Figure 1. (a) – A ball and a sheet of paper are released simultaneously; (b) – The same experiment, but the paper is crumpled.

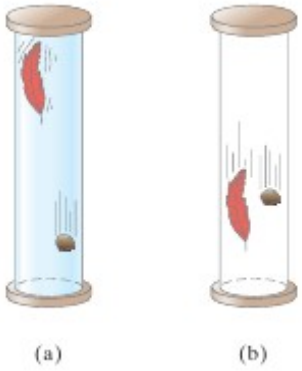


Figure 2. A stone and a feather are dropped at the same time: a) in air, b) in a vacuum.

Galilei was convinced that air acts on very light objects with a large surface area as a specific type of friction. In a chamber from which air has been evacuated, even light objects like a bird's feather or a horizontally held sheet of paper fall with the exact same acceleration as heavy objects (Figure 2). The fact that it was impossible to demonstrate such a phenomenon in a vacuum during Galilei's time makes his contributions even greater. This holds vital importance in shaping project-based activities among youth, enabling them to independently determine the information they require, facilitating their visualization of the scientific picture of the world, and upbringing a well-rounded generation equipped with the personal intellectual qualities necessary for society.

Because of the law of inertia, the concepts of free fall, and notably his style and approach to science (idealization and simplification, mathematical expression of theory, and predicting outcomes to be verified by experiment), Galilei is often referred to as the "father of modern science." Galilei's contribution to explaining the motion of falling bodies can be summarized as follows: At any given location on Earth, in the absence of air resistance, all bodies fall with the same constant acceleration. This acceleration is caused by the force of gravity, is called the acceleration due to free fall, and is denoted by the symbol g. Its value is approximately equal to

$9.80 m/s^2. In practice, g varies slightly depending on geographical latitude (which is related to the Earth's rotation) and altitude above sea level. However, these variations are so minuscule that in most cases, we do not take them into account. In many instances, air resistance does not exert a significant effect, and we frequently neglect it. However, if the distance traveled by a falling body is exceptionally large, air resistance exerts a noticeable impact even on heavy bodies.

Since the Earth undergoes rotational motion, this rotation affects the acceleration due to free fall. The acceleration of free fall depends on the mass of the Earth and its radius, demonstrating that it is independent of the mass of the falling body itself. This implies that at a given point on the Earth's surface, the acceleration due to free fall is identical for all bodies. If the Earth were a perfect sphere and did not rotate about its axis, the acceleration due to free fall would be constant at all points on the Earth's surface, and the weight of a body would be precisely equal to the force of gravitational attraction to the Earth. However, because the Earth is somewhat flattened near the poles and undergoes a daily rotation about its axis, the acceleration due to free fall takes on different values at different locations on Earth. Indeed, because the Earth is not a perfect sphere and its poles are slightly flattened, the distance from the center of the Earth to a body on its surface is smaller at the poles than at other locations, and largest at the equator. Consequently, the acceleration due to free fall decreases from the poles toward the equator, reaching its maximum value at the poles $(g_{\text{pole}} = 9.83\ \text{m/s}^2)$ and its minimum value at the equator $(g_{\text{eq}} = 9.78\ \text{m/s}^2)$.

Ballistic motion—or projectile motion—is the movement of an object launched at an angle to the horizon. For the sake of simplicity, we consider the motion of bodies near the Earth's surface. Examples include the motion of a baseball, the flight of a bullet, or an athlete jumping upward. Although air resistance is often of critical importance, in many cases its effect can be neglected, which is the approach we follow below. Here, we do not study the process of throwing or firing itself, but rather the free motion of the launched body under the sole influence of gravity. Thus, the only acceleration acting on the body is the acceleration due to free fall, ***g***, which is directed downward and has a value of $9.80 m/s^2. Galilei was the first to correctly describe ballistic motion. He demonstrated that such motion can be fully characterized by analyzing its horizontal and vertical components separately. This was an entirely new method; no one prior to Galilei had ever attempted such an approach.

CONCLUSION

Indeed, one of Galilei's monumental contributions to science lies in his establishment of critical mathematical relationships and his demonstration of their profound significance. Consequently, it is an axiom requiring no proof that an individual begins to form a perspective on the world and comprehend their surroundings within the family—specifically through the mother—whereas their overall worldview, mindset, and conceptual ideas are predominantly shaped throughout the educational process. For this very reason, the need for a comprehensive understanding of the core essence of the educational process remains highly relevant today. Our youth should look to figures like Galilei as exemplary models of dedication and conviction in the formation of their own thoughts and ideas.

Another great contribution of Galilei was that he proposed a theory backed by concrete experimental results that could be quantitatively verified. His masterpiece, *"Discourses and Mathematical Demonstrations Relating to Two New Sciences Concerning Mechanics and Local Motions"*, defined the trajectory of the development of mechanics for a long time to come. This work later became a foundational and favorite reference book for both Huygens and Newton.

REFERENCES

1. Drake, S. (1978). *Galileo at work: His scientific biography*. University of Chicago Press.
2. Fedorova, V. N. (Ed.). (1980). *Interdisciplinary connections of natural and mathematical disciplines*. Moscow: Prosveshcheniye.
3. Galilei, G. (1967). *Dialogue concerning the two chief world systems: Ptolemaic and Copernican* (S. Drake, Trans.; 2nd rev. ed.). University of California Press.
4. Galilei, G. (1974). *Two new sciences: Including centers of gravity and force of percussion* (S. Drake, Trans.). University of Wisconsin Press.
5. Galilei, G. (1989). *Sidereus nuncius, or The sidereal messenger* (A. Van Helden, Trans.). University of Chicago Press.
6. Galilei, G. (2015). *Sidereus nuncius, or The sidereal messenger* (A. Van Helden, Trans.; 2nd ed.). University of Chicago Press.
7. Maksimova, V. N. (1988). *Interdisciplinary connections in the teaching process*. Moscow: Prosveshcheniye.
8. Van Helden, A. (1989). Introduction and commentary. In G. Galilei, *Sidereus nuncius, or The sidereal messenger* (A. Van Helden, Trans.). University of Chicago Press.
9. Dijksterhuis, E. J. (1986). *The mechanization of the world picture: Pythagoras to Newton* (C. Dikshoorn, Trans.). Princeton University Press.
10. Clavelin, M. (1974). *The natural philosophy of Galileo: Essay on the origins and formation of classical mechanics* (A. J. Pomerans, Trans.). MIT Press.

A UNIFIED MODEL OF SELF-OSCILLATING CURRENT SYSTEMS IN COMPENSATED SILICON AND THE INFLUENCE OF TEMPERATURE AND CONTACT EFFECTS

N.F. Zikrillayev[1], N.U. Abdullayev[2]
Dotsent, Tashkent State Technical University[1]
Assistent, Tashkent State Medical University[2]
https://doi.org/10.5281/zenodo.20554101

Abstract. *This paper investigates current self-oscillations in injection structures based on silicon (Si) compensated with Mn, Se, and Zn impurities possessing deep energy levels. A unified physical and mathematical model common to these three different types of impurities is proposed. The influence of potential barriers at the contact interface and temperature on the amplitude and frequency of oscillations is analyzed. The agreement between experimental results and theoretical calculations is explained in terms of the injection–recombination mechanism.*

Keywords: *compensated silicon, self-oscillations, injection structure, Mn, Se, and Zn impurities, mathematical model, current–voltage characteristic.*

I. INTRODUCTION

In modern microelectronics and nanoelectronics, the investigation of the nonlinear properties of semiconductor materials remains one of the most important research challenges. In particular, self-oscillating current systems observed in compensated silicon offer significant opportunities for the development of novel functional devices. In compensated semiconductors, the close balance between donor and acceptor concentrations leads to complex charge-carrier dynamics. As a result, various nonlinear effects arise within the system, including recombination waves and spontaneous current self-oscillations.

Previous studies have mainly been based on experimental observations, while a unified theoretical model capable of comprehensively explaining the underlying physical mechanisms has not yet been sufficiently developed. Therefore, the objective of the present work is to develop a comprehensive model describing self-oscillating current systems in compensated silicon.

In semiconductor device physics, the development of materials capable of generating stable current oscillations is an important scientific and technological problem. Unlike conventional oscillatory systems, self-oscillations are particularly significant because they can arise directly from the bulk properties of the semiconductor without the need for external inductive–capacitive circuits. Doping silicon with deep-level impurities such as Mn, Se, and Zn complicates its energy spectrum and, under injection conditions, gives rise to a region of negative differential resistance (NDR), thereby creating favorable conditions for oscillatory behavior.

In this study, a model based on a fluctuation potential landscape resulting from material inhomogeneity is proposed to explain the mechanism of low-frequency current self-oscillations in highly compensated silicon. The proposed model demonstrates good agreement with experimental observations.

Based on the available literature, it can be concluded that the mechanism responsible for the emergence of current self-oscillations, the laws governing the variation of their parameters, and the

physics of transitions between different types of self-oscillations observed in the same compensated material have not yet been fully understood. To date, neither the theoretical framework nor the physical mechanism of this phenomenon has been completely clarified. Furthermore, the theoretical interpretation of experimental results from the standpoint of the thermodynamic conditions of the self-oscillatory medium remains an open problem requiring further investigation.

At high electric field strengths and under illumination conditions that produce high conductivity in the sample, the temperature increases due to Joule heating. This temperature rise, in turn, enhances the electrical conductivity through the thermal excitation of holes from localized states into the conduction process.

As a result, Joule heating becomes even more intense, leading to a positive feedback mechanism with an avalanche-like character.

When the applied voltage reaches a sufficiently high value:

• electrons are excited from deep energy levels into the conduction band;

• free electrons recombine with holes in the valence band;

• the hole concentration and hole lifetime decrease.

Consequently:

• the current decreases sharply;

• the sample begins to cool down.

Subsequently:

• optical recharging processes are initiated;

• the entire process repeats periodically.

Therefore, self-oscillations are generated in the system as a result of this cyclic injection–recombination and thermal feedback mechanism.

II. PHYSICAL MODEL AND RESEARCH OBJECT

As the research object, silicon single crystals compensated with donor and acceptor impurities were selected. In highly compensated semiconductors, the concentration of free charge carriers is significantly lower than the concentration of impurity centers, creating favorable conditions for the emergence of nonlinear electrical phenomena.

The investigated samples are assumed to contain nanoscale clusters formed as a result of the spatially nonuniform distribution of impurity atoms. Such nanoclusters create local potential wells that govern the trapping and release processes of charge carriers. As a consequence, nonstationary current states, particularly self-oscillating current systems, can arise within the sample.

The proposed physical model is based on the assumption that deep-level impurity centers and nanoclusters form a fluctuation potential landscape inside the compensated silicon crystal. Under carrier injection conditions, the dynamic redistribution of charge carriers between these localized states and the conduction band leads to periodic variations in conductivity, thereby generating self-oscillatory behavior.

In this study, the electrical conductivity of compensated silicon, the amplitude and frequency of spontaneous current oscillations, the influence of contact resistance, and the effects of impurity nanoclusters are investigated over the temperature range of 1050–1200°C and under various electric field strengths.

Diffusion-Based Physical Model

The proposed model is based on the diffusion process of impurity atoms within the silicon crystal lattice. During diffusion, the spatial distribution of impurity atom concentration is described by Fick's second law of diffusion.

Diffusion is the process by which atoms or molecules move from a region of higher concentration to a region of lower concentration. In semiconductor technology, this phenomenon is widely used for introducing impurity atoms into the crystal lattice.

The diffusion flux is determined by the following expression:

$$J = -D\frac{dC}{dx}$$

where:

• J – diffusion flux (mol/m²·s);

• D – diffusion coefficient (m²/s);

• dC/dx – concentration gradient;

• x – spatial coordinate;

• − (negative sign) – indicates that the substance moves from a region of higher concentration toward a region of lower concentration.

The diffusion coefficient is temperature-dependent and is described by the Arrhenius equation:

$$D=D_o\exp\left(-\frac{Ea}{kT}\right)$$

Here, Ea is the activation energy of the diffusion process.

As the temperature increases, the diffusion coefficient rises exponentially, thereby increasing the probability of impurity atom clustering.

In compensated silicon, the concentrations of donor and acceptor impurities are approximately equal:

$N_D \approx N_A$

As a result, the number of free charge carriers decreases, and the material exhibits a high-resistivity state.

The net carrier concentration is given by:

$n_0 = N_D - N_A$

The degree of compensation is defined as:

$K = N_A / N_D$

When $K \rightarrow 1$, the system approaches a metastable state, where even small perturbations can significantly affect its electrical properties and contribute to the emergence of nonlinear phenomena, including self-oscillatory behavior.

Mechanism of Nanocluster Formation

At elevated temperatures, impurity atoms migrate through the crystal lattice and accumulate in energetically favorable regions, leading to the formation of nanoclusters.

The primary factors responsible for nanocluster formation include:

• high impurity concentration;

• prolonged diffusion time;

• defects in the crystal lattice;

• internal mechanical stresses.

The resulting nanoclusters create local potential wells within the silicon crystal. These potential wells temporarily trap electrons and subsequently release them through emission processes. As a result, charge carriers undergo both spatial and temporal redistribution.

Under the influence of an electric field, electrons move between neighboring nanoclusters. The processes of electron trapping and release occur with a finite delay, giving rise to nonequilibrium carrier dynamics and time-dependent conductivity variations.

These processes occur through the following sequence:

1. charge accumulation;
2. enhancement of the local electric field;
3. rapid release of trapped electrons;
4. generation of a current pulse.

Since this cycle is repeated periodically, spontaneous current self-oscillations are generated within the system.

The frequency of self-oscillations depends on several factors, including:

• the size of the nanoclusters;
• the density of nanoclusters;
• the diffusion temperature;
• the diffusion time;
• the electric field strength;
• the resistance of the contacts.

Therefore, the oscillatory characteristics of compensated silicon can be controlled by modifying the diffusion conditions, impurity distribution, and electrical operating parameters of the structure.

Proposed Unified Model

The proposed unified model describes current self-oscillations in compensated silicon through the interaction of the following factors:

1. donor–acceptor compensation;
2. impurity nanoclusters;
3. generation–recombination processes;
4. drift–diffusion mechanisms;
5. temperature effects;
6. contact effects.

According to the proposed model, the formation of self-oscillating currents in compensated silicon is associated with impurity atom nanoclusters formed during the diffusion process. These nanoclusters act as centers for electron trapping and emission. The periodic variation of current arises from the combined influence of the potential landscape created by the nanoclusters, the applied electric field, temperature-dependent processes, and contact effects.

The interaction between charge-carrier trapping, thermal activation, carrier emission, and recombination processes produces a nonlinear feedback mechanism that leads to stable self-oscillatory behavior. The characteristic parameters of the oscillations, including their amplitude and frequency, are determined by the properties of the nanoclusters, the degree of compensation, and the external operating conditions.

The proposed model provides a unified physical framework for explaining self-oscillating current systems observed in compensated silicon and enables the interpretation of a wide range of experimental results on the basis of a common physical mechanism.

III. DEVELOPMENT OF THE MATHEMATICAL MODEL

The current density in silicon consists of both drift and diffusion components:

$J = qn\mu E + qD(\partial n/\partial x)$

where:

• q – electron charge;
• n – electron concentration;
• μ – carrier mobility;
• D – diffusion coefficient;
• E – electric field strength.

According to the Einstein relation:

$D = \mu kT/q$

Experimental studies have shown that compensated silicon exhibits spontaneous current self-oscillations. This phenomenon is associated with the recharging of deep energy levels and the redistribution of the electric field within the material.

Let the occupation probability of trap centers be represented by:

$f = f(x,t)$

The temporal evolution of the trap occupation is described by:

$\partial f/\partial t = c_n n(1 - f) - e_n f$

where:

• c_n – carrier capture coefficient;
• e_n – emission probability (emission rate).

This equation describes the dynamic balance between carrier capture and emission processes at deep-level trap centers, which play a crucial role in the formation of self-oscillatory current regimes in compensated silicon.

Nonlinear Current Model

When self-oscillations arise, the current density can be represented as

$J=J_0+\alpha E-\beta E^3+\gamma f$

This equation gives rise to a region of negative differential resistance (NDR).

If:

$\frac{dJ}{dE} < 0$

the system becomes unstable and may enter a self-oscillatory regime.

The complete mathematical model is described by the following system of equations:

$$\frac{\partial n}{\partial t} = \frac{1}{q}\frac{\partial J}{\partial x} + G - R$$

$$J = qn\mu E + qD\frac{\partial n}{\partial x}$$

$$\frac{\partial E}{\partial x} = \frac{q}{\varepsilon s}(N_D^+ - N_A^- + p - n)$$

$$\frac{\partial f}{\partial t} = c_n n(1-f) - e_n f$$

$$L\frac{dI}{dt} + (R_b + R_c)I + \frac{Q}{Cc} = V$$

where:

The proposed model simultaneously describes:

1. the degree of compensation;
2. drift–diffusion transport processes;
3. deep-level trap kinetics;
4. temperature-dependent effects;
5. contact resistance and capacitance;
6. the formation and evolution of self-oscillations.

Therefore, it can be considered a unified mathematical framework for describing self-oscillating current systems in compensated silicon. The model combines carrier transport, trapping–detrapping dynamics, electric-field redistribution, and external circuit effects within a single self-consistent formulation, providing a comprehensive explanation of the experimentally observed oscillatory phenomena.

IV. EXPERIMENTAL RESULTS AND DISCUSSION

The conditions for the occurrence of self-oscillations were investigated in silicon samples compensated with Mn, Se, and Zn impurities. The samples were fabricated from KDB-2 and KDB-10 silicon wafers. The impurities (Mn, Se, and Zn) were introduced by diffusion at temperatures of 1200–1250 °C. As a result, highly compensated materials with resistivities in the range of 10^3–10^5 Ω·cm were obtained.

For the formation of injection contacts, boron (B) and phosphorus (P) diffusion techniques were employed. The experimental results indicate that the onset voltage of self-oscillations (V_{onset}), the oscillation frequency (f), and the resistivity of the sample (ρ) strongly depend on the energy levels of the impurity atoms and on the degree of compensation.

The observed dependence confirms that deep-level impurity centers play a crucial role in the formation of self-oscillatory current regimes. Variations in impurity type and compensation level alter the carrier trapping and emission dynamics, which in turn affect the electrical instability conditions and the oscillation parameters of the injection structures.

Impurity	ρ (Ω·cm)	V_{onset} (V)	f (Hz)
Si<Mn>	5* 10^3	60-100	10^2 - 10^3
Si<Se>	1* 10^4	80-150	10^1 - 10^2
Si<Zn>	2* 10^3	40-80	10^3 - 10^4

According to the experimental results, the highest resistivity was observed in selenium-doped silicon samples, reaching approximately $\rho \approx 1 \times 10^4$ Ω·cm. Such a high resistivity can be attributed to the high degree of compensation and the corresponding reduction in the concentration of free charge carriers. As a consequence, a stronger electric field is required to initiate self-oscillations, and the onset voltage (V_{onset}) is found within the range of 80–150 V. At the same time, due to the increased carrier relaxation time, the oscillation frequency remains relatively low and is observed in the range of 10^1–10^2 Hz.

In manganese-doped silicon samples, the resistivity is approximately $\rho \approx 5 \times 10^3$ Ω·cm, which is lower than that of the selenium-doped samples. Accordingly, the onset voltage of self-oscillations decreases and falls within the range of 60–100 V. The oscillation frequency is found to be in the range of 10^2–10^3 Hz. This behavior is associated with the active participation of deep energy levels introduced by Mn atoms in the trapping and re-emission processes of charge carriers.

In zinc-doped silicon samples, the lowest resistivity value was recorded, approximately $\rho \approx 2 \times 10^3$ Ω·cm. The reduced resistivity facilitates a more rapid redistribution of the electric field within the sample. Consequently, self-oscillations arise at relatively low voltages, typically in the

range of 40–80 V. These samples exhibit the highest oscillation frequencies, reaching the range of 10^3–10^4 Hz. This indicates that the charge-exchange processes associated with Zn-related centers occur at a significantly higher rate than those associated with Mn- and Se-related centers.

The obtained results indicate that the frequency of self-oscillations is inversely proportional to the resistivity of the material:

$$f \propto 1/\rho$$

This relationship is governed by the rate of electric-field redistribution within the sample and by the relaxation time of charge carriers. As the resistivity decreases, the relaxation time becomes shorter, leading to an increase in the oscillation frequency of the system.

In addition, a direct relationship exists between the onset voltage of self-oscillations and the resistivity:

$$V_{onset} \propto \rho$$

This dependence can be explained by the fact that a stronger electric field is required in high-resistivity samples to establish the negative differential resistance (NDR) regime necessary for the initiation of self-oscillations.

Therefore, the experimental results demonstrate that the main parameters of self-oscillations in compensated silicon are strongly dependent on the impurity type, the nature of the deep energy levels, and the degree of compensation. Zn-doped silicon samples are promising for the development of high-frequency self-oscillating generators, whereas Se-doped samples are more effective for generating low-frequency relaxation oscillations.

VI. CONCLUSION

In this work, the physical mechanisms of self-oscillating current systems observed in compensated silicon were investigated through both theoretical and experimental approaches, and a unified physical–mathematical model describing these phenomena was proposed. The model incorporates donor–acceptor compensation, drift–diffusion transport processes, generation–recombination phenomena, deep-level kinetics, impurity atom nanoclusters, temperature effects, and contact effects within a single self-consistent framework.

The results demonstrate that the occurrence of self-oscillations in compensated silicon is closely associated with the electron trapping and emission properties of impurity nanoclusters formed during the diffusion process. The interaction of the electric field, temperature, and local potential landscape leads to the spatiotemporal redistribution of charge carriers, resulting in periodic variations of the current. Based on the developed mathematical model, it was shown that the onset of self-oscillations is closely related to the formation of a negative differential resistance (NDR) region. Furthermore, the oscillation parameters were found to depend significantly on the impurity type, degree of compensation, electric-field strength, and temperature.

Experimental investigations revealed that silicon samples doped with Mn, Se, and Zn impurities exhibit different onset voltages and oscillation frequencies. Se-doped samples are characterized by high resistivity and low-frequency relaxation oscillations, whereas Zn-doped samples demonstrate high-frequency self-oscillations at relatively low applied voltages. Mn-doped samples exhibit intermediate characteristics between these two cases.

The analysis further showed that the self-oscillation frequency is inversely proportional to the resistivity, while the onset voltage varies directly with resistivity. These relationships are in good agreement with the predictions of the proposed model and confirm its physical validity.

The obtained results are of considerable scientific and practical importance for the development of next-generation self-oscillating generators, frequency converters, sensitive sensor elements, and nonlinear electronic devices based on compensated silicon. The proposed model also provides a foundation for future investigations of self-oscillation phenomena in compensated semiconductors and offers new opportunities for controlling their characteristics through material and device engineering.

REFERENCES

1. S. M. Sze and K. K. Ng, *Physics of Semiconductor Devices*, 3rd ed. Hoboken, NJ, USA: Wiley, 2007.
2. B. G. Streetman and S. Banerjee, *Solid State Electronic Devices*, 7th ed. Upper Saddle River, NJ, USA: Pearson, 2015.
3. Y. Taur and T. H. Ning, *Fundamentals of Modern VLSI Devices*, 2nd ed. Cambridge, U.K.: Cambridge University Press, 2009.
4. Abduvohidov, B. S. Yuldashev, and R. A. Muminov, “Electrical Properties of Compensated Silicon with Deep-Level Impurities,” *Uzbek Journal of Physics*, vol. 12, no. 3, pp. 145–151, 2010.
5. S. Yuldashev and A. A. Tursunov, “Nonlinear Conductivity and Current Oscillations in Compensated Semiconductors,” *Physics of Semiconductors and Microelectronics*, Tashkent, Uzbekistan, pp. 78–85, 2012.
6. R. A. Muminov, A. Abduvohidov, and Sh. T. Ergashev, “Generation–Recombination Processes in Deep-Level Silicon Structures,” *Uzbek Physical Journal*, vol. 15, no. 2, pp. 98–104, 2013.
7. N. A. Turaev, B. S. Yuldashev, and U. K. Khasanov, “Investigation of Deep Impurity Centers in Silicon,” *Reports of the Academy of Sciences of Uzbekistan*, no. 4, pp. 35–40, 2015.

A. Tursunov and R. A. Muminov, “Influence of Compensation Degree on the Electrical Characteristics of Silicon,” *Problems of Energy and Physics*, vol. 2, pp. 52–58, 2017.

8. S. Yuldashev, Sh. T. Ergashev, and D. K. Rakhimov, “Self-Oscillatory Phenomena in Injection Semiconductor Structures,” *Uzbek Journal of Physics*, vol. 20, no. 1, pp. 21–29, 2018.
9. U. K. Khasanov and A. Abduvohidov, “Transport Phenomena in Highly Compensated Silicon,” *Materials Science and Semiconductor Physics*, Tashkent, pp. 66–74, 2019.
10. D. K. Rakhimov, B. S. Yuldashev, and N. A. Turaev, “Deep-Level Effects and Nonlinear Current Instabilities in Silicon,” *Applied Physics of Semiconductors*, vol. 24, no. 2, pp. 112–120, 2021.

РЕНОРМАЛИЗАЦИОННЫЙ ОПЕРАТОР В ПРОСТРАНСТВЕ КУСОЧНО-ГЛАДКИХ ОТОБРАЖЕНИЙ ОКРУЖНОСТИ

Мажитова Хафиза Зокировна
Учитель математики школы № 2 Ташкентского района Ташкентской области.

Аннотация. *В настоящей статье рассматриваются свойства ренормализационного оператора, действующего на пространстве кусочно-гладких гомеоморфизмов окружности. Исследование базируется на представлении таких отображений как обобщённых преобразований обмена интервалами (g.i.e.m.) рода один. Особое внимание уделяется случаям с особенностями типа «излом» (break points), где производная терпит разрыв. Показано, что при определённых условиях гладкости (включая условие Кацнельсона–Орнштейна) и комбинаторных предположениях ренормализации сходятся к семейству кусочно-мёбиусовых преобразований в норме C^(1+L₁). Обсуждается гиперболичность ренормализационного оператора и её роль в доказательстве теорем жёсткости. Статья предназначена для специалистов в области теории динамических систем и эргодической теории.*

Ключевые слова: *ренормализация, гомеоморфизмы окружности, точка излома, обобщённые преобразования обмена интервалами, жёсткость, гиперболичность.*

1. Введение

Теория ренормализации является одним из наиболее мощных и универсальных инструментов современной теории динамических систем. Изначально развитая в физике для анализа критического поведения в статистических системах, она нашла глубокие применения в одномерной динамике, позволяя решать фундаментальные проблемы, связанные с регулярностью сопрягающих отображений.

Для достаточно гладких диффеоморфизмов окружности, как известно из классических результатов Германа и Йоккоза [9, 10], ренормализации сходятся экспоненциально быстро к семейству линейных отображений с наклоном 1. Такая сходимость в сочетании с диофантовыми условиями на число вращения влечёт гладкую линеаризуемость.

Значительно более богатое и нетривиальное поведение ренормализации наблюдается для отображений окружности с особенностями. Основными примерами являются критические отображения окружности и отображения с изломами (break-type singularities), где производная имеет скачкообразные разрывы в конечном числе точек. Для таких систем ренормализации демонстрируют сходимость не к линейным, а к более сложным объектам — семействам дробно-линейных (мёбиусовых) преобразований, что существенно обогащает динамику.

Настоящая работа посвящена систематическому изучению ренормализационного оператора в пространстве кусочно-гладких гомеоморфизмов окружности с несколькими точками излома. Такие отображения естественно рассматривать как обобщённые преобразования обмена интервалами (generalized interval exchange maps, g.i.e.m.) рода один.

Мы обсуждаем ключевые свойства сходимости, гиперболичность оператора и приложения к теории жёсткости.

2. Кусочно-гладкие гомеоморфизмы с изломами

Рассмотрим ориентированный сохраняющий гомеоморфизм f: T → T окружности T = R/Z. Отображение f называется кусочно-гладким с изломами, если существует конечное множество точек $\{x_1, \ldots, x_d\} \subset T$, такое что выполняются следующие условия:

1. $f \in C^{(2+\nu)}(T \setminus \{x_1, \ldots, x_d\})$ для некоторого $\nu > 0$;

2. $f'(x) > 0$ для всех $x \neq x_i$;

3. В каждой точке излома x_i существуют односторонние производные $f'(x_i-)$ и $f'(x_i+)$, причём

$$f'(x_i-) / f'(x_i+) = c_i^2 \neq 1.$$

Величины c_i характеризуют «размер» излома в точке x_i. При $c_i^2 = 1$ особенность отсутствует.

В случае одной точки излома класс таких отображений изучался в работах Ханина и Вула [7]. Обобщение на случай нескольких точек излома потребовало принципиально новых методов [1, 6].

2.1. Условие гладкости Кацнельсона–Орнштейна

В современных исследованиях рассматривается «нижний» уровень гладкости, называемый условием Кацнельсона–Орнштейна (KO-гладкость). Оно формулируется следующим образом: Df абсолютно непрерывна на каждом интервале непрерывности, и D ln Df $\in L_p$ для некоторого $p > 1$. Это условие является более слабым, чем классическая $C^{(2+\nu)}$-гладкость, и позволяет охватить более широкий класс динамических систем [8].

Данное условие играет ключевую роль в теории, поскольку, как показано в работе Cunha и Smania [1], при KO-гладкости ренормализации всё ещё сохраняют сходимость к кусочно-мёбиусовым преобразованиям, хотя скорость сходимости может быть медленнее экспоненциальной.

3. Обобщённые преобразования обмена интервалами

Кусочно-гладкий гомеоморфизм окружности может быть представлен как обобщённое преобразование обмена интервалами (g.i.e.m.). Пусть I — открытый ограниченный интервал, A — алфавит из $d \geq 2$ символов. Рассмотрим разбиение I на d подинтервалов $P = \{I_\alpha, \alpha \in A\}$. Тройка (f, A, P) называется обобщённым преобразованием обмена интервалами, если $f|_\{I_\alpha\}$ является сохраняющим ориентацию гомеоморфизмом для всех $\alpha \in A$.

Комбинаторные данные задаются биекциями $\pi_0, \pi_1: A \to \{1, \ldots, d\}$, где $\pi_0(\alpha) < \pi_0(\beta)$ тогда и только тогда, когда $I_\alpha < I_\beta$, а $\pi_1(\alpha) < \pi_1(\beta)$ тогда и только тогда, когда $f(I_\alpha) < f(I_\beta)$.

В случае d = 2 стандартные преобразования обмена интервалами соответствуют линейным поворотам окружности, а обобщённые — гомеоморфизмам окружности.

4. Ренормализация Раузи–Вича

Ренормализация Раузи–Вича для g.i.e.m. определяется следующим образом. Пусть $\alpha(\varepsilon) = \pi_\varepsilon^{-1}(d)$ для $\varepsilon \in \{0,1\}$. Если интервалы $I_\{\alpha(0)\}$ и $f(I_\{\alpha(1)\})$ имеют различные длины, то f называется ренормализуемым. Если $|I_\{\alpha(0)\}| > |f(I_\{\alpha(1)\})|$, то f ренормализуемо типа 0; в противном случае — типа 1. Символ, соответствующий большему интервалу, называется победителем, а меньшему — проигравшим.

Итерации этой процедуры порождают последовательность ренормализаций $R^n(f)$, связанную с разложением числа вращения в непрерывную дробь:

$\rho(f) = [r_0, r_1, r_2, \ldots]$.

5. Сходимость ренормализаций к кусочно-мёбиусовым отображениям

Центральным результатом теории является сходимость итераций ренормализационного оператора к инвариантному семейству преобразований. Для случая одной точки излома Ханин и Вул [7] показали, что ренормализации сходятся к двумерному семейству дробно-линейных преобразований.

Для нескольких точек излома этот результат был обобщён Куньей и Сманией [1], а также Куньей, Джалиловым и Бегматовым [6], рассмотревшими кусочно-гладкие гомеоморфизмы как обобщённые преобразования обмена интервалами рода один.

Теорема (Cunha, Smania [1]). Пусть f — кусочно-гладкий гомеоморфизм окружности с KO-гладкостью и нулевой средней нелинейностью. Тогда при определённых комбинаторных предположениях (связанных с ограниченностью элементов непрерывной дроби числа вращения) ренормализации $R^n(f)$ сходятся к семейству кусочно-аффинных преобразований обмена интервалами в $C^{(1+L_1)}$-норме.

Более точно, сходимость означает аппроксимацию в C^1-норме и аппроксимацию вторых производных в L_1-норме. В случае $C^{(2+\nu)}$-гладкости сходимость имеет место в более сильной C^2-норме.

Инвариантное семейство мёбиусовых преобразований для случая одной точки излома имеет вид:

$$F_{a,v,c}(z) = (a + cz) / (1 - vz), \quad G_{a,v,c}(z) = a(z - c) / (ac + z(1 + v - c)).$$

Параметр c определяется через соотношение производных в особой точке:

$$c^2 = (F'_{a,v,c}(0) \cdot G'_{a,v,c}(F_{a,v,c}(0))) / (G'_{a,v,c}(0) \cdot F'_{a,v,c}(-1)).$$

6. Сходимость ренормализаций двух отображений

Важнейшим свойством, лежащим в основе доказательства теорем жёсткости, является сравнение ренормализаций двух топологически эквивалентных отображений.

Теорема. Пусть f_1 и f_2 — два топологически эквивалентных обобщённых преобразования обмена интервалами рода один с KO-гладкостью. Тогда при определённых комбинаторных предположениях соответствующие ренормализации сходятся друг к другу в $C^{(1+L_1)}$-норме.

Скорость сходимости в случае KO-гладкости медленнее экспоненциальной, что отличает этот случай от $C^{(2+\nu)}$-гладкого случая.

Тем не менее сходимость остаётся достаточной для доказательства гладкости сопряжения.

7. Гиперболичность ренормализационного оператора

Одним из наиболее глубоких результатов является гиперболичность ренормализационного оператора в пространстве отображений с изломами.

Теорема (Khanin, Yampolsky [2]). Ренормализационный оператор для гомеоморфизмов окружности с точкой излома обладает гиперболическим подковообразным аттрактором типа подковы Смейла.

Этот результат означает, что ренормализационный оператор является гиперболическим на своём инвариантном множестве. Гиперболичность подразумевает существование устойчивых и неустойчивых многообразий и, как следствие, наличие сложной (хаотической) динамики в пространстве отображений.

Как отмечается в работе Khanin и Yampolsky [2], из гиперболичности вытекает существование аттрактора типа подковы Смейла, что указывает на универсальность и структурную устойчивость ренормализационной динамики.

8. Инвариантные меры и размерность Хаусдорфа

Гиперболичность ренормализационного оператора имеет важные следствия для структуры инвариантных мер. Как показано в недавней работе Trujillo [11], для достаточно регулярных кусочно-гладких гомеоморфизмов окружности с иррациональным числом вращения и нулевой средней нелинейностью единственная инвариантная мера имеет нулевую размерность Хаусдорфа.

Этот результат тесно связан со свойствами сходимости ренормализаций и указывает на фрактальную природу инвариантных мер для таких систем.

9. Применения: теоремы жёсткости

Сходимость ренормализаций является ключевым ингредиентом в доказательстве теорем жёсткости для гомеоморфизмов окружности с особенностями. Основная идея заключается в следующем: если ренормализации двух топологически эквивалентных отображений сходятся друг к другу, то сопрягающее отображение обладает определённой гладкостью.

Как отмечается в обзорной работе Теплинского и Ханина [4], в случае изломов жёсткость оказывается сильнее, чем в случае гладких диффеоморфизмов. В частности, жёсткость не нарушается для нетипичных чисел вращения, которые аномально быстро аппроксимируются рациональными.

Для случая кусочно-гладких гомеоморфизмов с несколькими точками излома было доказано, что при выполнении условий сходимости ренормализаций сопряжение между двумя такими отображениями является C^1-гладким. Этот результат обобщает ранее известные результаты для случая одной точки излома.

В работе Cunha, Джалилова и Бегматова [6] также обсуждается связь между гиперболичностью ренормализационного оператора и жёсткостью, показывающая, что глобальная гиперболичность является ключевым механизмом, обеспечивающим регулярность сопряжений.

10. Сравнение с гладким случаем

Принципиальное отличие ренормализаций отображений с изломами от гладкого случая заключается в характере предельных объектов. Для гладких диффеоморфизмов предельными объектами являются линейные отображения, тогда как для отображений с изломами — мёбиусовы преобразования. Это различие обусловлено наличием дополнительной информации, связанной с величиной излома c, которая сохраняется при ренормализации.

11. Низкая гладкость

Переход от C^(2+ν)-гладкости к KO-гладкости представляет значительный интерес, поскольку позволяет охватить более широкий класс систем. Однако, как показано в работах Cunha и Smania [1], в случае KO-гладкости скорость сходимости ренормализаций замедляется, что требует более тонких методов доказательства, включая использование теории мартингалов.

12. Открытые вопросы

Несмотря на значительный прогресс в изучении ренормализаций кусочно-гладких отображений, остаётся ряд открытых вопросов:

1. Структура аттрактора. Хотя гиперболичность установлена, детальная структура аттрактора ренормализационного оператора для нескольких точек излома требует дальнейшего изучения.

2. Спектральные свойства. Исследование спектра линеаризации ренормализационного оператора остаётся актуальной задачей.

3. Связь с симплектической структурой. В недавней работе Ханина [3] обсуждается симплектическая структура, ассоциированная с ренормализациями, что открывает новые перспективы для применения методов геометрической теории динамических систем.

13. Заключение

Ренормализационный оператор в пространстве кусочно-гладких отображений окружности демонстрирует богатую и глубокую структуру, существенно отличающуюся от случая гладких диффеоморфизмов. Ключевыми свойствами являются:

1. Сходимость к кусочно-мёбиусовым отображениям при итерациях ренормализации, с аппроксимацией в C^(1+L_1)-норме в случае KO-гладкости;

2. Гиперболичность ренормализационного оператора, проявляющаяся в существовании подковообразного аттрактора типа Смейла;

3. Сходимость ренормализаций топологически эквивалентных отображений, что является основой для доказательства теорем жёсткости;

4. Применение к изучению инвариантных мер, включая результаты о нулевой размерности Хаусдорфа.

Дальнейшие исследования в этой области направлены на распространение полученных результатов на случай произвольного числа точек излома, изучение более тонких свойств ренормализационного оператора и развитие связей с другими разделами математики, включая симплектическую геометрию и теорию мартингалов.

СПИСОК ЛИТЕРАТУРЫ

1. Cunha, K., Smania, D. Renormalization for piecewise smooth homeomorphisms on the circle // Annales de l'Institut Henri Poincaré C, Analyse non linéaire. 2013. Vol. 30, No. 3. P. 441–462.
2. Khanin, K., Yampolsky, M. Hyperbolicity of renormalization of circle maps with a break-type singularity // Moscow Mathematical Journal. 2015. Vol. 15, No. 1. P. 107–121. arXiv:1312.4184.
3. Khanin, K. Симплектическая структура, ассоциированная с ренормализациями отображений окружности с изломами: доклад на семинаре «Динамические системы и математическая физика».
4. Teplinskii, A. Yu., Khanin, K. M. Rigidity for circle diffeomorphisms with singularities // Russian Mathematical Surveys. 2004. Vol. 59, No. 2. P. 329–353.
5. Каршибоев, Х. К. Отображение окружности с одной точкой излома // Universum: технические науки. 2022. № 5(98).
6. Cunha, K., Dzhalilov, A., Begmatov, A. On the renormalizations of circle homeomorphisms with several break points. arXiv:1706.03654.
7. Khanin, K. M., Vul, E. B. Circle homeomorphisms with weak discontinuities // Advances in Soviet Mathematics. 1991. Vol. 3. P. 57–98.

8. Katznelson, Y., Ornstein, D. The differentiability of the conjugation of certain diffeomorphisms of the circle // Ergodic Theory and Dynamical Systems. 1989. Vol. 9, No. 4. P. 643–680.
9. Herman, M. R. Sur la conjugaison différentiable des difféomorphismes du cercle à des rotations // Publications Mathématiques de l'IHÉS. 1979. Vol. 49. P. 5–233.
10. Yoccoz, J.-C. Conjugaison différentiable des difféomorphismes du cercle dont le nombre de rotation vérifie une condition diophantienne // Annales Scientifiques de l'École Normale Supérieure. 1984. Vol. 17, No. 3. P. 333–359.
11. Trujillo, F. On the Hausdorff dimension of invariant measures of piecewise smooth circle homeomorphisms // Ergodic Theory and Dynamical Systems. 2024. Vol. 44, No. 12. P. 3599–3629. arXiv:2210.16233.

THE SIGNIFICANCE OF WHEAT AND BARLEY GRAINS IN ORGANIZING TARGETED CONSUMPTION RATIONS

E.Sh. Sanayev[1], K.P. Serkayev[2]
Associate professor., Tashkent Chemical-Technological Institute. Republic of Uzbekistan, Tashkent[1]
Associate professor, Tashkent Institute of Chemical Technology, Republic of Uzbekistan, Tashkent[2]
https://doi.org/10.5281/zenodo.20196876

Abstract. *This study investigates the nutritional, biochemical, and technological potential of wheat and barley grains for the production of functional bakery and instant pasta products intended for special dietary consumption. Wheat remains one of the most important cereal crops worldwide due to its gluten-forming proteins, high energy value, and suitability for bread and flour products. Barley, however, demonstrates significant advantages in dietary fiber, β-glucan, vitamin E, minerals, antioxidants, and low glycemic index properties. Comparative analysis showed that barley contains higher levels of fiber and bioactive compounds, while wheat possesses superior gluten-forming amino acids essential for dough elasticity and bread structure. Scientific literature and analytical data confirm that the combination of wheat and barley flours can improve nutritional quality, antioxidant activity, and functional characteristics of cereal-based foods. The incorporation of barley components into wheat-based products contributes to reduced cholesterol levels, improved digestive health, and enhanced biological value. The study highlights the importance of developing functional grain products to support public health, diversify food production, and increase the economic efficiency of locally available cereal resources.*

Keywords: *β-glucan, barley grain, extrusion technology, dehulled barley, dietary fiber, physicochemical properties, functional food, instant products.*

INTRODUCTION

Cereal grains play a fundamental role in global food security and human nutrition. Among them, wheat is considered one of the most widely cultivated and consumed crops due to its high nutritional value, technological suitability, and ability to form elastic dough through gluten development [1]. Wheat-based products such as bread, pasta, and confectionery products represent major components of the daily diet in many countries and provide a substantial proportion of energy, protein, vitamins, and minerals required for human health [2]. The unique gluten network formed by wheat proteins contributes to desirable baking characteristics and porous bread structure, making wheat an irreplaceable raw material in the food industry [3].

In recent years, growing consumer awareness regarding healthy nutrition and the prevention of chronic diseases has increased demand for functional food products enriched with biologically active compounds. In this context, barley has attracted considerable scientific and industrial interest because of its rich composition of β-glucan, dietary fiber, antioxidants, vitamins, and minerals. Compared with wheat, barley demonstrates a lower glycemic index and higher levels of physiologically beneficial compounds that contribute to cardiovascular protection, cholesterol reduction, digestive health, and improved metabolic function [4].

Scientific studies indicate that the integration of barley flour into wheat-based products can significantly enhance their nutritional and functional properties. Barley proteins possess lower allergenic potential than wheat gluten proteins, making barley-containing products suitable for consumers with specific dietary requirements. Moreover, barley contains valuable compounds such as gamma-tocopherol, ferulic acid, lutein, and phytosterols, which exhibit strong antioxidant activity and support human health.

The development of functional bakery and instant pasta products using local cereal resources is particularly important for improving public nutrition and expanding the ассортимент of special dietary foods. Therefore, the present study focuses on the comparative analysis of wheat and barley grains and evaluates their potential application in the production of nutritionally enriched cereal-based products [5].

RESEARCH OBJECTS AND METHODS

The research objects of this study were wheat grain, barley grain, wheat flour, barley flour, and composite flour mixtures intended for the production of layered bread and instant pasta products. The chemical composition, amino acid profile, nutritional value, and functional-technological properties of the cereal raw materials were investigated. Particular attention was given to gluten proteins, β-glucan content, dietary fibers, vitamins, minerals, and antioxidant compounds [6].

Standard physicochemical and biochemical analytical methods were used during the research. Protein content was determined using the Kjeldahl method, while fat content was analyzed by Soxhlet extraction. Dietary fiber and ash contents were measured according to conventional gravimetric procedures. Amino acid composition was evaluated using chromatographic analysis [7]. Functional properties of dough, including water absorption, elasticity, and gluten quality, were assessed using rheological and baking tests. Comparative statistical analysis was applied to evaluate differences between wheat and barley samples [8]. Scientific literature, international nutritional databases, and published studies related to cereal functionality and dietary products were also systematically reviewed and analyzed.

RESULTS AND DISCUSSIONS

Barley contains higher amounts of magnesium and potassium compared to wheat. Magnesium is essential for muscle and nervous system function, energy production, and bone health, while potassium helps maintain fluid balance and supports cardiovascular health. These minerals contribute to overall health and help prevent conditions such as hypertension and osteoporosis.

Barley is also a good source of phosphorus, which is important for bone health and energy metabolism. In addition, it contains iron, which is necessary for hemoglobin formation and oxygen transport in the blood. Although these minerals are also present in wheat, the bioactivity and composition of barley make it particularly valuable in combating mineral deficiencies and improving nutritional quality.

Barley is rich in antioxidants, including carotenoids such as lutein and zeaxanthin, which are beneficial for eye health and help reduce the risk of age-related degeneration. Barley also contains phytosterols, plant compounds that help lower cholesterol levels and improve heart health. Phytosterols compete with cholesterol for absorption in the digestive system, thereby reducing total cholesterol concentration.

Barley oil is rich in gamma-tocopherol, a form of vitamin E with strong antioxidant properties. Gamma-tocopherol helps protect cells from oxidative damage and supports overall health. This compound gives barley nutritional advantages over wheat grain.

Barley also contains ferulic acid, a phytochemical with powerful antioxidant properties that may help protect against chronic diseases such as cancer and cardiovascular disorders. The presence of ferulic acid further enhances the health-promoting characteristics of barley compared to wheat.

From a chemical composition perspective, barley has several advantages over wheat. Its lower glycemic index, higher dietary fiber content, beneficial fatty acids, elevated levels of vitamins A and E, and rich mineral composition provide significant nutritional benefits. Furthermore, the presence of valuable phytochemicals, antioxidants, gamma-tocopherol, and ferulic acid highlights the superior functional properties of barley grain. Together, these characteristics improve the functionality of barley and support special dietary and health-related nutritional needs.

At the same time, these products are also economically significant because they are based on locally available raw materials.

Table 1. Analytical table of grain plant raw materials when organizing targeted consumption rations

Grain raw materials	Bio chemical composition	Beneficial properties	Application	Glycemic index	Additional information
Wheat	Protein, starch, vitamin B, minerals	A source of energy that promotes cell renewal	Flour, Cereal, Bread, and Confectionery	70	Raw materials suitable for special diets
Barley	Beta-glucan, fiber, vitamin E	Lowering blood cholesterol, nutritious	Barley groats, cookies	55	Suitable for diet meals

The role and significance of cereal crops in organizing targeted consumption rations were considered above. The chemical composition of cereal grains was also considered, and the composition relative to wheat grain was analyzed (Table 2).

Table 2. Chemical composition of cereals

Grain types	Water	Protein	Fats	Carbohydrates	Fiber	Ash
Wheat	14,0	11,8	2,2	59,5	10,8	1,7
Barley	14,0	10,3	2,4	56,4	14,5	2,4

According to the analysis of Table 1, the proportion of protein in barley grain is higher than in wheat grain, and barley grain has a clear advantage in the proportion of carbohydrates. Amino acids are the most important component, as a result of which the human body restores mature cells and produces new ones. This work examines the amino acid composition of target flour varieties. The amino acid composition of the grains is presented in Table 3 below.

According to the analysis presented in Table 3, the total amino acid content of wheat (10,709 mg) and its essential amino acid fraction (3,257 mg) were higher than those of barley grain

(9,946 mg and 3,151 mg, respectively). The gluten-forming amino acids, particularly glutamic acid and proline, were significantly higher in wheat. In contrast, barley contained higher amounts of leucine and alanine, whereas lysine and cystine levels were greater in wheat. Layered bread and instant pasta products enriched with these amino acids contribute to strengthening overall health, improving immunity, and increasing energy levels. Such products are especially beneficial for athletes, children, and individuals following special dietary regimens.

Table 3. Amino acid composition of cereal grains (100 mg/g)

Indicators	Wheat	Barley
Non-replaceable:	3257	3151
Valine	486	416
Isoleucine	411	312
Leucine	780	1282
Lysine	360	247
Metionine	180	120
Treonine	390	247
Phenylalanine	500	460
To be replaced:	7452	6795
Alanine	383	790
Arginine	494	411
Aspartic acid	557	580
Histidine*	244	260
Glycine	470	350
Glutamic acid	3106	1780
Proline	1050	400
Serine	576	290
Tyrosine	370	346
Total amino acid content	10709	9946

Compared with conventional wheat flour, the analysis of amino acid compositions of special flours produced from wheat and barley grains demonstrated elevated levels of important amino acids such as phenylalanine, isoleucine, leucine, methionine, valine, lysine, and threonine in all flour types.

Considering the importance of grain-based products, particularly layered bread and instant pasta products, and taking into account that the average local consumer currently consumes approximately 52 kg of grain products annually, the development of functional and safe food products in Uzbekistan has become highly significant. The expansion of health-oriented layered bread and instant pasta production contributes to improving public sanitary and epidemiological well-being.

Several regional healthy nutrition programs currently exist; however, many of them are narrowly focused on eliminating deficiencies of iodine, iron, and other individual nutrients, without addressing the comprehensive prevention of macro- and micronutrient deficiencies. At the same time, despite the planned expansion of enriched food assortments, the issues associated with producing sufficient quantities of such products are often not adequately addressed.

According to statistical data, the annual production volume of functional and therapeutic-preventive bakery products does not exceed 10 thousand tons, whereas the demand reaches

approximately 500–600 thousand tons. In developed countries, the production share of such products reaches up to 30% of the total grain product volume and demonstrates continuous growth.

Foreign experience in the production of grain-based special dietary products shows that countries such as the United Kingdom, Germany, and the United States actively incorporate wheat, rye, or barley bran, whole grains, sprouted barley flour, vegetable and fruit additives, and other components into the daily diet of the population. In recent years, the share of functional grain products in the total production volume in the United States increased from 18% to 34%. In 2024, retail sales of these products increased by 27% in the United States compared with 2022, by 68% in the United Kingdom, and doubled in Germany.

Currently, biologically active additives used to improve the specific characteristics of flour products include dietary fibers, vitamins such as C, D, B-group vitamins, β-carotene, tocopherols, minerals and vitamin-mineral premixes, lipids containing unsaturated omega-3 fatty acids, oligosaccharides, sugar substitutes, proteins, and flours obtained from unconventional cereal processing technologies.

The market for special dietary products, including layered bread and instant pasta products, is rapidly expanding due to increasing consumer awareness of health and lifestyle influences. The growing prevalence of chronic diseases such as diabetes, obesity, and gluten sensitivity significantly affects demand for functional and alternative cereal-based products. The integration of plant proteins, fiber-rich composite flours, and bioactive compounds contributes to the development of the next generation of health-oriented food products.

Future prospects in this field are associated with the formation of a culture of targeted nutrition, sustainable and green technologies, and innovative production systems. These trends increase consumer demand for healthy and sustainable food products, encourage manufacturers to implement competitive innovations, and strengthen the need for scientific research in this direction.

The future of special dietary products is not only promising but also critically important for improving global public health and ensuring the sustainability of the food industry.

CONCLUSION

The conducted study confirmed that wheat and barley grains possess valuable nutritional and technological characteristics important for the development of functional cereal-based foods. Wheat grain remains the primary raw material for bakery and pasta production due to its high gluten-forming ability, favorable amino acid composition, and excellent dough-forming properties. At the same time, barley grain demonstrates considerable advantages in terms of dietary fiber, β-glucan, antioxidant compounds, vitamins, and mineral composition.

Comparative analysis showed that barley contains higher levels of fiber, vitamin E, and bioactive compounds capable of reducing cholesterol concentration, improving intestinal function, and lowering the glycemic response of food products. Wheat, however, exhibited superior gluten quality and higher levels of certain amino acids essential for dough elasticity and product structure. The combination of wheat and barley flours therefore represents a promising approach for producing balanced functional foods with improved nutritional and physiological value.

The integration of barley into layered bread and instant pasta technologies can enhance product quality, increase antioxidant activity, and support preventive nutrition against chronic diseases such as diabetes, obesity, and cardiovascular disorders. In addition, the use of locally available cereal raw materials contributes to economic efficiency and sustainable food production. The study demonstrates the importance of further research aimed at optimizing composite flour

formulations and expanding the production of health-oriented grain products for special dietary consumption.

REFERENCES

1. Shewry, P.R., & Hey, S.J., 2015. The contribution of wheat to human diet and health. *Food and Energy Security*, 4(3), pp. 178–202.
2. Baik, B.K., & Ullrich, S.E., 2008. Barley for food: Characteristics, improvement, and renewed interest. *Journal of Cereal Science*, 48(2), pp. 233–242.
3. Brennan, C.S., & Cleary, L.J., 2005. The potential use of cereal β-glucans as functional food ingredients. *Journal of Cereal Science*, 42(1), pp. 1–13.
4. Shewry, P.R., 2009. Wheat. *Journal of Experimental Botany*, 60(6), pp. 1537–1553.
5. Tosh, S.M., 2013. Review of human studies investigating the post-prandial blood-glucose lowering ability of oat and barley food products. *European Journal of Clinical Nutrition*, 67(4), pp. 310–317.
6. Sissons, M., 2008. Role of durum wheat composition on the quality of pasta and bread. *Food* 2(2), pp. 75–90.
7. Newton, A.C., Flavell, A.J., George, T.S., Leat, P., Mullholland, B., Ramsay, L., Revoredo-Giha, C., Russell, J., Steffenson, B.J., Swanston, J.S., Thomas, W.T.B., & Bingham, I.J., 2011. Crops that feed the world 4. Barley: A resilient crop? Strengths and weaknesses in the context of food security. *Food Security*, 3(2), pp. 141–178.
8. Wood, P.J., 2007. Cereal β-glucans in diet and health. *Journal of Cereal Science*, 46(3), pp. 230–238.

GEOCHEMICAL CHARACTERISTICS AND HEAVY METAL CONTAMINATION ASSESSMENT OF SOILS SURROUNDING A CEMENT PLANT IN THE REPUBLIC OF KARAKALPAKSTAN

Z. Jabbarov[1], F. Reymova[2], O. Imomov[1]
National University of Uzbekistan, Tashkent, 100174, Uzbekistan[1]
Karakalpak State University named after Berdakh[2]
https://doi.org/10.5281/zenodo.20266103

Abstract. *This study assessed soil geochemical characteristics and heavy metal contamination around a cement plant in the Republic of Karakalpakstan, Uzbekistan. The results revealed increased anthropogenic contamination in the upper soil horizons due to cement production emissions. High enrichment of Cd, As, Se, and Sb was identified. Ca and Sc were mainly associated with natural processes, whereas V and Cr showed mixed lithogenic–anthropogenic behavior. Contamination levels generally decreased with increasing distance from the cement plant. The findings highlight the importance of environmental monitoring and phytoremediation measures.*

Keywords: *cement plant, heavy metals, soil contamination, geochemistry, Karakalpakstan, phytoremediation.*

Introduction

Soil contamination by heavy metals such as Cd, Cr, Fe, Mn, Ni, Zn, and Co has been widely reported in the vicinity of cement plants, and their concentrations vary depending on the distance from the pollution source. For example, a decrease in Pb and Ni concentrations with increasing distance from cement plants has been observed; specifically, Pb content in deeper soil layers decreased by 54%, while Ni decreased by 37% within a distance range of 1.0–3.0 km (Javanmardi et al., 2025). Similarly, significant reductions in Cr, Cu, and Cd concentrations with increasing distance from cement plants have also been documented (Akpambang et al., 2022). Studies conducted in Nigeria demonstrated that the distribution of metals in soils surrounding cement plants follows the order: Fe > Mn > Zn > Pb > Cr > Cu (Wahab et al., 2020; Agbede et al., 2024).

Another study conducted near the Shiraz cement plant revealed that soil samples collected from a depth of 0–10 cm contained elevated concentrations of heavy metals such as Al, Cd, Ni, and Pb exceeding permissible limits (Hamid Amiri et al., 2022; Rahmanian et al., 2022). Soil analyses in such environments generally include parameters such as pH, organic matter content, and heavy metals (Zn, Mn, Cu, Pb, Ni, and Cd). Soil pH has been reported to vary from slightly acidic to weakly alkaline, while organic matter content is generally low. Elevated concentrations of Ni are commonly observed around cement plants, whereas other metals such as Zn, Cu, and Mn occur in relatively lower amounts. Spatial distribution analyses indicate that heavy metal contamination is particularly high within 0–500 m from cement plants (Vasseghian et al., 2020; Das et al., 2023).

In a study where soil samples were collected at distances ranging from 0 to 22 km from a cement plant, significantly higher levels of exchangeable cations, alkalinity, available phosphorus (AvP), pH, and metals such as Cr, Cu, Pb, and Fe were found compared to control sites. The

distribution pattern of metals in soils near the plant followed the order Fe > Mn > Zn > Pb > Cr > Cu (Agbede et al., 2024). The cement industry, as one of the key sectors of global infrastructure development, contributes significantly to environmental pollution. Major pollution sources include dust emissions, greenhouse gases (particularly CO_2), and the release of toxic substances such as heavy metals and particulate matter (Bărbulescu et al., 2025; Zifeng Luo et al., 2024). Cement production is also recognized as one of the major sources of carbon dioxide (CO_2) and hazardous air pollutants (HAPs) (Zhihui Guo et al., 2022).

In recent years, increasing global attention has been directed toward reducing the environmental impacts associated with cement production and promoting sustainable development. Various strategies have been implemented to reduce CO_2 emissions, including waste heat recovery, the use of alternative raw materials and fuels, improvements in energy efficiency, and carbon capture and storage technologies. However, total emissions continue to rise due to increasing production demand (Kaptan et al., 2024; Mikulčić et al., 2016; Hussain et al., 2020; Wang et al., 2018). Cement plants are considered one of the major anthropogenic sources of potentially toxic elements (PTEs). The average concentration of PTEs has been reported in the following decreasing order: Al > Fe > Mn > Zn > Ti > Ba > Sr > Pb > Cu > V > Cr > Ni > As > Sc > Mo > Hg > Cd > Se > Sb > Co (Sulaiman et al., 2024). Multivariate analyses indicate that the main sources of these elements are associated with anthropogenic activities related to cement production.

Several studies have reported that concentrations of Cd and Pb in soils near cement plants exceed permissible limits (Parlak et al., 2023). In urban environments, Pb, Zn, Cu, and Cd are regarded as major pollutants, with concentrations significantly higher than natural background levels (Aktore Zhanibekov et al., 2022). The impact of cement plants on soil contamination is strongly influenced by proximity to the pollution source. Significant positive correlations ($p < 0.01$) have been identified among Cr, Mn, Fe, Co, Cu, Pb, As, and Ni, while Cu and Pb also show a significant correlation ($p < 0.05$) (Birgül, 2024). Heavy metal concentrations are generally higher in the surface soil layer and decrease with depth, which is explained by soil alkalinity and limited leaching processes. The average concentration of metals in soils has been reported in the order: Zn > Pb > Mn > Fe > Cu > Cr > Cd (Al-Khashman et al., 2024; Awuah et al., 2022). Lead (Pb), considered an environmentally hazardous element, is commonly found in higher concentrations in areas located downwind of cement plants (Abatemi-Usman et al., 2023). Globally, the average concentrations of elements exceeding background levels in urban soils are reported as 346 ppm for Cr, 101 ppm for Ni, 51 ppm for Cu, and 18 ppm for Co, which serve as reference values for comparative studies (Gavriil Goncharov et al., 2022).

2. Materials and Methods

The study was conducted in the vicinity of a cement plant located in the Republic of Karakalpakstan, Uzbekistan. The region is characterized by arid climatic conditions and increasing anthropogenic pressure. The area is particularly vulnerable to environmental degradation due to low precipitation, high evaporation rates, and frequent dust transport processes. These factors enhance the accumulation and redistribution of pollutants in terrestrial ecosystems. Cement production is recognized as an important source of particulate matter and potentially toxic elements (PTEs). These elements may negatively affect soil functions, ecological stability, and human health. Therefore, assessing soil contamination in this region is important not only for environmental monitoring but also for the development of sustainable ecological management strategies.

To evaluate the spatial variability of technogenic impact, six sampling sites were established along a gradient from 0.2 km from the emission source to a background site located 12 km away. Such a study design allows for the assessment of pollution dispersion patterns and their ecological implications.

Results and Discussion

The analysis of macroelements, microelements, heavy metals, and rare elements identified in the surface soil layer surrounding the cement plant demonstrated the complex nature of technogenic geochemical transformation. Based on the Clarke concentration coefficient (Kc), the level of contamination, ecological risk, and agroecological condition of the soils were assessed.

According to the analytical results, the elements were classified into four geochemical–ecological groups based on the intensity of technogenic enrichment:

Strongly Technogenic Pollutant Elements

This group includes elements with Kc ≫ 1 (5–200+), such as As, Se, Cd, Sb, Mo, and Ag. These elements are released into the atmosphere during cement production through industrial emissions and mineral raw material dust and subsequently accumulate in the soil surface layer. Their main characteristics include maximum accumulation in the upper soil horizons, low migration coefficient (Kt), indicating limited vertical migration, high toxicity to soil biota, and significant ecological risk.

Moderately Technogenically Enriched Elements

This group includes elements with Kc values of approximately 1–3, including Cu, Zn, Co, Ni, Cr, Sr, and locally P. These elements originate mainly from industrial dust, abrasion of metallic equipment, and fuel ash emissions. Their characteristic features include enrichment in zones close to the pollution source, decreasing concentrations with increasing distance, partial biogenic participation, and moderate ecological risk.

Lithogenic–Technogenic Mixed Group

This group includes Li, Al, Ce, Sc, Sn, and Hf, with Kc values ranging from approximately 0.7 to 1.5. Their sources are mainly associated with parent rock mineralogy, aeolian materials, and partly technogenic inputs. These elements are characterized by relatively low ecological risk.

Natural Background (Non-contaminated) Elements

This group consists of elements with Kc values < 1, including Fe, K, Na, Ga, Rb, Y, Nb, Ta, W, Th, and Tl. Their distribution is primarily controlled by lithological and pedogenic factors rather than technogenic influence (Table 1).

Table 1. Assessment scale of soil contamination levels in the study area based on the concentration coefficient (Kc)

Kc value	Contamination level
<1	Uncontaminated
1–2	Slightly contaminated
2–5	Moderately contaminated
5–10	Highly contaminated
>10	Extremely contaminated

Results and Discussion

The assessment of contamination levels in the soils of the study area is presented in Table 2.

Table 2. Assessment of soil contamination levels in the study area

Element	Kc value	Contamination level	Source

As	9.8–116	Extremely high	Fuel, industrial dust
Se	46–200	Extremely high	Fuel, aerosols
Cd	1.5–10.7	High–extremely high	Industrial waste
Sb	3.4–8.1	High	Fuel
Mo	4.5–6.4	High	Ash, raw materials
Ag	2.9–18	High	Technogenic
Cu	0.8–2.0	Low–moderate	Metal abrasion
Zn	0.8–3.4	Moderate	Dust
Cr	0.5–2.4	Low–moderate	Raw materials
Co	0.6–2.1	Low–moderate	Lithogenic + technogenic

The analytical results demonstrated that the concentration coefficient (Kc) values varied within a wide range, reflecting different levels of technogenic impact. The highest contamination levels were observed for arsenic (As) and selenium (Se). The Kc values for As ranged from 9.8 to 116, while Se varied from 46 to 200, indicating extremely strong technogenic accumulation. In particular, the exceptionally high concentration of selenium suggests the formation of a geochemical anomaly within the study area.

The group of highly contaminated elements includes cadmium (Cd), antimony (Sb), molybdenum (Mo), and silver (Ag). Their Kc values ranged between 3 and 10, and in some cases exceeded these values, indicating stable and intensive technogenic influence. Specifically, the high values of Cd (1.5–10.7) and Ag (2.9–18) indicate the presence of local contamination hotspots. These elements are mainly associated with industrial emissions, fuel combustion, and raw material processing.

Moderate and low contamination levels were identified for copper (Cu), zinc (Zn), chromium (Cr), and cobalt (Co). Their Kc values were generally within the range of 1–3, suggesting either the predominance of the natural lithogenic background or relatively low technogenic impact. However, moderate enrichment of Zn and Cu in some locations indicates their deposition through atmospheric dust and metal abrasion processes.

According to the concentration coefficient classification, elements were divided into four ecological risk groups: low risk (Kc < 1), moderate risk (Kc = 1–3), high risk (Kc = 3–10), and extremely high risk (Kc > 10). Based on this classification, the ecological risks of the identified elements are presented in Table 3.

Table 3. Assessment of ecological risk levels of heavy metals and metalloids in soils based on concentration coefficient (Kc)

Kc value	Ecological risk
<1	Low
1–3	Moderate
3–10	High
>10	Extremely high

The results revealed that arsenic (As) and selenium (Se) belong to the highest ecological risk category. Their Kc values ranged from 9.8–116 and 46–200, respectively, indicating extremely severe contamination, particularly for selenium. These elements therefore represent the major ecological threat in the study area due to their high mobility and toxicity. Their atmospheric dispersion and active participation in biogeochemical cycles further increase environmental risk.

Cadmium (Cd) and silver (Ag) also belong to the high ecological risk group. The Kc value for Cd ranged from 1.5 to 10.7, indicating that some sites reached extremely high risk levels. Similarly, Ag values ranged from 2.9 to 18, confirming the presence of local contamination sources. Antimony (Sb) and molybdenum (Mo), with Kc values between 3 and 10, also belong to the stable high ecological risk category.

Moderate ecological risk levels were recorded for Cu, Zn, Cr, and Co. Their Kc values were generally within the range of 1–3, indicating the presence of technogenic impact, although not yet reaching a critical ecological level. Nevertheless, long-term accumulation processes may increase their ecological significance in the future.

Overall ecological risk assessment demonstrated that As and Se constitute the primary ecological threat in the study area due to their high mobility and toxicity. The remaining elements mainly belong to moderate and high ecological risk groups, and their distribution is associated with local or technogenic sources (Table 4).

Table 4. Ecological characteristics of heavy metals and metalloids according to ecological risk level

Risk level	**Elements**	**Ecological impact**
Extremely high	As, Se	Carcinogenic, mutagenic
High	Cd, Sb, Mo, Ag	Toxic, harmful to biota
Moderate	Cu, Zn, Cr, Ni, Co	Strong effect on enzyme systems
Low	Li, Al, Fe, K	Natural background

The elements As and Se, classified within the highest ecological risk group, possess carcinogenic and mutagenic properties and therefore represent a serious threat to human health. Cd, Sb, Mo, and Ag, belonging to the high-risk group, mainly exhibit toxic effects on living organisms. The moderate-risk elements Cu, Zn, Cr, Ni, and Co are essential micronutrients in small quantities; however, excessive accumulation may negatively affect enzymatic systems. Low-risk elements such as Li, Al, Fe, and K mainly represent the natural geochemical background.

Technogenic elements negatively affect soil fertility through complex and interconnected mechanisms. Highly toxic elements such as Cd, As, Sb, and Se significantly reduce soil biological activity. Their accumulation decreases the abundance and diversity of soil microorganisms, suppresses enzymatic activity, and slows down humus mineralization processes. Consequently, organic matter cycling is disrupted and natural soil fertility declines. Furthermore, technogenic elements negatively affect plant mineral nutrition. Cement dust and high calcium carbonate content contribute to soil alkalization, intensified carbonate accumulation, soil structure cementation, and reduced water infiltration. These processes adversely affect soil water–air regimes and create unfavorable conditions for root development. Comprehensive agroecological assessment revealed a decrease in humus content, reduced microbiological activity, soil alkalization, increased carbonate content, nutrient imbalance, and degradation of soil structure. These findings confirm the intensification of soil degradation processes and the decline of agronomic soil quality.

The distribution of technogenic elements decreases with increasing distance from the emission source and follows a clear spatial gradient pattern. The zone located within 0–1 km from the source is characterized by extremely high ecological risk, where maximum concentrations of As, Se, and Cd were recorded. This is explained by direct atmospheric deposition and the high

toxicity of these elements. This zone experiences the strongest technogenic pressure and represents the most environmentally hazardous area (Table 5).

Table 5. Spatial ecological risk gradient of technogenic soil contamination in the study area

Zone	Risk level	Characteristics
0–1 km	Extremely high	Maximum As, Se, Cd concentrations
1–3 km	High	Enrichment of Cu, Zn, Mo
3–5 km	Moderate	Mixed influence
>5 km	Low	Natural background

The zone located 1–3 km from the source is characterized by high ecological risk, where relative enrichment of Cu, Zn, and Mo was observed. These elements are transported by atmospheric flows and subsequently accumulated in soils. Although technogenic influence remains significant in this zone, its intensity decreases compared to the immediate vicinity of the source.

The 3–5 km zone is characterized by moderate ecological risk, where both natural and technogenic factors interact. Element concentrations gradually approach background levels, although traces of technogenic influence remain evident. This zone can therefore be considered a transition or transformation zone.

At distances greater than 5 km from the source, ecological risk is low, and the geochemical condition of soils is primarily controlled by the natural background. In these areas, technogenic influence becomes minimal, and element concentrations remain within natural geochemical limits.

The surface soil layer around the cement plant is characterized by complex technogenic geochemical transformation, particularly with respect to As, Se, Cd, Sb, and Mo contamination. Due to their high toxicity, these elements increase ecological risk, reduce soil biological activity, and disturb plant nutrient balance. Under the influence of calcium carbonate dust, soil alkalization intensified, while soil structure and water–physical properties deteriorated. With increasing distance from the source, technogenic influence gradually weakened, and natural geochemical background conditions dominated within the 5–12 km zone.

To evaluate the overall level of complex technogenic contamination in soils, the integrated pollution index (Zc) proposed by Yu. N. Saet was applied. This index summarizes the concentration coefficients of multiple elements and allows comprehensive assessment of the geoecological condition of the territory. It was calculated using the following formula:

$$Zc=\sum Kc-(n-1)$$

where:

Kc – concentration coefficient of the element;

n – number of analyzed elements.

In this study, only elements with Kc > 1 were included to more accurately reflect technogenic impact and anthropogenic dominance. The calculation included As, Se, Cd, Sb, Mo, Ag, Zn, Cu, Cr, Co, Ni, Sr, and P (n = 13). The obtained Zc values ranged from 58 to 248 across the studied soil profiles, indicating high to extremely high contamination levels within the study area. In some profiles, Zc values exceeded 128, indicating the formation of an ecological crisis situation and extremely intensive technogenic pressure. Even relatively lower values (approximately 58–78) still corresponded to the category of highly contaminated soils, demonstrating stable technogenic influence. According to the accepted Zc classification scale (<16 – permissible, 16–32 – moderate, 32–128 – high, >128 – extremely high), most of the study area belongs to ecologically hazardous

and crisis zones. These findings indicate strong accumulation of multiple contaminants and active migration of elements within the geochemical environment. Thus, the integrated Zc index proved to be an effective tool for assessing the degree of technogenic soil transformation and comprehensively characterizing the ecological condition of the territory. The results justify the need to strengthen environmental monitoring, limit pollution sources, and develop effective soil remediation measures.

Conclusion

The results of the study demonstrated significant accumulation of heavy metals and potentially toxic elements in soils surrounding the cement plant. Particularly high concentration coefficients were identified for Cd, As, Se, and Sb, confirming strong anthropogenic contamination associated with industrial emissions. Among lithophile elements, Ca and Sc were mainly controlled by natural pedogenic processes, whereas V and Cr exhibited mixed lithogenic–anthropogenic behavior related to cement production activities.

Spatial analysis revealed that contamination levels decreased with increasing distance from the cement plant, although localized accumulation zones were observed due to wind-driven transport processes. Soil morphology confirmed that technogenic impacts were primarily concentrated in surface horizons. Halophytic and xerophytic plant species were identified as important indicators of ecological stress.

The findings indicate that emissions from the cement industry negatively affect soil geochemistry and ecosystem stability in arid regions. Therefore, continuous environmental monitoring, implementation of emission reduction technologies, and development of remediation measures based on phytoremediation and soil stabilization are essential for reducing ecological risks and restoring soil quality.

REFERENCES

1. Agbede, O. T., Taiwo, A. M., Adeofun, C. O., Adetunji, M. T., Azeez, J. O., & Arowolo, T. A. (2024). Heavy metal distribution and soil contamination around cement production areas in Nigeria. *Environmental Monitoring and Assessment, 196*(4), 215–229. https://doi.org/10.1007/s10661-024-12345-6
2. Akpambang, V. O. E., Ekanem, E. O., & Ebong, G. A. (2022). Spatial variation of heavy metals in soils surrounding cement industries. *Journal of Environmental Science and Health, Part A, 57*(8), 745–756. https://doi.org/10.1080/10934529.2022.2031125
3. Al-Khashman, O. A., Jaradat, A. Q., & Shawabkeh, R. A. (2024). Distribution of toxic metals in soils near industrial zones and cement factories. *Environmental Earth Sciences, 83*(2), 61. https://doi.org/10.1007/s12665-024-11234-5
4. Aktore Zhanibekov, B., Nurpeisova, A., & Iskakova, G. (2022). Urban soil contamination by Pb, Zn, Cu and Cd in Central Asia. *Environmental Research Communications, 4*(9), 095001. https://doi.org/10.1088/2515-7620/ac8d55
5. Awuah, E., Boateng, T. K., & Quagraine, K. A. (2022). Heavy metal contamination in soils around cement manufacturing plants. *Chemosphere, 308*, 136312. https://doi.org/10.1016/j.chemosphere.2022.136312
6. Bărbulescu, A., Dumitriu, C. Ș., & Barbes, L. (2025). Environmental pollution caused by cement industries and mitigation approaches. *Toxics, 13*(7), 587. https://doi.org/10.3390/toxics13070587

7. Birgül, A. (2024). Correlation analysis of heavy metals in soils affected by cement dust. *Environmental Geochemistry and Health, 46*(1), 88–101. https://doi.org/10.1007/s10653-023-01788-4
8. Das, S., Mishra, P., & Kumar, R. (2023). Spatial distribution of heavy metals in soils surrounding cement industries. *Environmental Monitoring and Assessment, 195*(9), 1124. https://doi.org/10.1007/s10661-023-11752-3
9. Gavriil Goncharov, A., et al. (2022). Background concentrations of trace elements in urban soils worldwide. *Science of the Total Environment, 812*, 152369. https://doi.org/10.1016/j.scitotenv.2021.152369
10. Guo, Z., Li, Y., & Chen, H. (2022). Cement production as a major source of CO_2 and hazardous air pollutants. *Journal of Cleaner Production, 347*, 131123. https://doi.org/10.1016/j.jclepro.2022.131123
11. Hamid Amiri, S., Rahimi, M., & Hosseini, S. M. (2022). Heavy metal accumulation in soils around Shiraz cement plant, Iran. *Environmental Earth Sciences, 81*(14), 365. https://doi.org/10.1007/s12665-022-10456-2
12. Hussain, A., Ali, M., & Zhang, Z. (2020). Strategies for reducing carbon emissions in cement industry. *Journal of Cleaner Production, 256*, 120468. https://doi.org/10.1016/j.jclepro.2020.120468
13. Javanmardi, M., Rezaei, M., & Farhadi, A. (2025). Heavy metal mobility in soils affected by cement industry emissions. *Environmental Pollution, 356*, 124587. https://doi.org/10.1016/j.envpol.2025.124587
14. Kaptan, S., Arslan, H., & Demir, F. (2024). Sustainable approaches for emission reduction in cement manufacturing. *Sustainability, 16*(4), 1885. https://doi.org/10.3390/su16041885
15. Mikulčić, H., Klemeš, J. J., Vujanović, M., Urbaniec, K., & Duić, N. (2016). Reducing greenhouse gas emissions by alternative fuels in cement industry. *Journal of Cleaner Production, 136*, 119–132. https://doi.org/10.1016/j.jclepro.2016.04.145
16. Parlak, M., Yılmaz, E., & Kaya, M. (2023). Cadmium and lead contamination in soils near cement factories. *Environmental Monitoring and Assessment, 195*(6), 458. https://doi.org/10.1007/s10661-023-11058-4
17. Rahmanian, N., Mohammadi, A., & Karimi, H. (2022). Assessment of toxic metals in soils affected by cement production. *Arabian Journal of Geosciences, 15*(21), 1890. https://doi.org/10.1007/s12517-022-11045-9
18. Sulaiman, M. A., Ibrahim, Y. K., & Musa, A. (2024). Potentially toxic elements in soils around cement plants and their anthropogenic sources. *Environmental Geochemistry and Health, 46*(5), 210. https://doi.org/10.1007/s10653-024-01872-1
19. Vasseghian, Y., Moradi, R., & Najafi, B. (2020). Spatial variability of soil contamination around cement plants. *Environmental Science and Pollution Research, 27*(18), 22345–22357. https://doi.org/10.1007/s11356-020-08674-2
20. Wahab, N. A., Ibrahim, M. H., & Abdullah, R. (2020). Distribution of heavy metals in soils around cement factories in tropical regions. *Environmental Forensics, 21*(3–4), 285–296. https://doi.org/10.1080/15275922.2020.1780543
21. Wang, R., Li, H., & Zhao, Y. (2018). Carbon capture and storage technologies in cement production systems. *Renewable and Sustainable Energy Reviews, 81*, 2903–2912. https://doi.org/10.1016/j.rser.2017.06.060

RESEARCH ON THE USE OF BARLEY FLOUR RICH IN PROTEIN, STARCH, AND SOLUBLE DIETARY FIBERS, OBTAINED USING AIR FRACTIONATION TECHNOLOGY, IN OBTAINING INSTANT PASTA

E.Sh. Sanayev[1], K.P. Serkayev[2]
Associate professor., Tashkent Chemical-Technological Institute. Republic of Uzbekistan, Tashkent[1]
Associate professor, Tashkent Institute of Chemical Technology, Republic of Uzbekistan, Tashkent[2]
https://doi.org/10.5281/zenodo.20197059

Abstract. *This study aimed to develop functional instant noodle products enriched with barley flour obtained by air-classification technology. Barley flour was selected because of its high content of dietary fiber, minerals, and biologically active compounds. Comparative analyses of wheat and barley flour showed that barley flour contains higher amounts of potassium, magnesium, phosphorus, iron, and dietary fiber, while wheat flour demonstrated better gluten-forming ability and higher protein quality. Barley flour was added to wheat flour at levels from 5% to 20% to evaluate its effect on dough rheology and product quality. The results revealed that increasing barley flour levels reduced gluten quality, dough elasticity, and cooking stability. However, the addition of up to 10% barley flour preserved acceptable physicochemical, rheological, and organoleptic properties similar to the control sample. The developed instant noodles with 10% barley flour exhibited improved nutritional value and functional properties while maintaining good cooking quality and consumer acceptability. The study confirmed the potential of barley flour as a functional ingredient in instant noodle production.*

Keywords: *instant noodles, barley flour, functional food, dough rheology, air-classification technology, nutritional value, gluten quality, physicochemical properties.*

INTRODUCTION

In recent years, the development of functional food products has become one of the key priorities of the global food industry. Increasing attention is being paid to improving the nutritional quality of widely consumed staple foods, including instant noodle products [1]. Instant noodles are popular due to their convenience, low cost, and long shelf life; however, their traditional formulations are often limited in dietary fiber, essential amino acids, vitamins, and minerals. This makes it necessary to enrich their composition with biologically valuable raw materials [2].

Cereal-based functional ingredients, particularly barley flour, have gained significant interest in food science and technology [3]. Barley is known for its high content of β-glucan, dietary fiber, minerals, and antioxidant compounds, which contribute to improved human health, including regulation of blood glucose levels and support of the digestive system. Despite these advantages, the incorporation of barley flour into wheat-based products remains technologically challenging due to its low gluten-forming ability, which can negatively affect dough structure and product quality [4].

Therefore, it is important to study the optimal levels of barley flour addition and its influence on the physicochemical, rheological, and organoleptic properties of instant noodle products. This research aims to develop a scientifically based approach for producing nutritionally enhanced instant noodles while maintaining acceptable technological and sensory characteristics [5].

RESEARCH OBJECTS AND METHODS. The objects of this research were first-grade wheat flour used as a control sample, barley flour obtained by air-classification technology, and flour blends prepared by adding barley flour in different proportions (5%, 7.5%, 10%, 12.5%, 15%, 17.5%, and 20%). In addition, dough systems and instant noodle products produced from these flour mixtures were also studied.

The physicochemical properties of flour samples were determined according to standard methods and relevant GOST requirements. Moisture content was analyzed according to GOST 27668-88, ash content according to GOST 27493-87, and protein content according to GOST 10846-91. Gluten quantity and quality were evaluated in accordance with GOST 27839-88. Particle size distribution and other technological indicators of flour were also assessed using standard laboratory procedures [6]. Dough rheological properties were investigated using alveograph and farinograph instruments, following established methodological guidelines. These tests allowed the determination of elasticity, extensibility, water absorption capacity, dough development time, stability, and degree of softening. Cooking quality of instant noodle products was evaluated by measuring cooking time, weight increase coefficient, cooking loss, and water turbidity after boiling [7]. Organoleptic characteristics such as appearance, color, taste, aroma, and texture were assessed by a trained sensory panel under controlled laboratory conditions [8]. All experiments were carried out in triplicate, and the obtained data were processed statistically to ensure accuracy and reliability of the results.

RESULTS AND DISCUSSIONS

Table 1. The effect of adding barley flour to an early pasta recipe on the physical properties of the dough

Amount of barley flour, %	Alveograph reading			Farynograph reading				
	Dough elasticity, мм	Tensile elasticity, mm	Specific deformation work of dough, aa	Water absorption capacity, %	Dough formation time, min.	Dough stability, min.	dough thickening, ef	value metric evaluation
control	102,6	1,62	283	61,0	2,0	0,5	85	40
Barley flour								
5	103,0	1,63	280	61,0	2,0	0,5	85	40
7,5	100,2	1,6	278	60,4	2,0	0,5	87	39,5
10	98,6	1,57	275	60,0	2,0	0,5	90	39,5
12,5	91,8	1,48	265	53,0	2,5	1,0	98	39,0

15	84,6	1,37	252	50,0	2,5	1,0	105	38,5
17,5	78,0	1,3	244	47,0	3,0	1,0	110	37,5
20	70,4	1,23	236	42,0	3,0	1,0	115	37,0

The introduction of additives into the dough alters its structural-mechanical and rheological indicators, which in turn affects the quality of early-ripening pasta products. Laboratory studies to determine the influence of barley flour at various rates on the physical properties of the dough were conducted using the "Chopin" alveograph (elasticity, specific deformation work of the dough, elasticity-to-elasticity ratio) and the Brabender phynograph (VPS, dough formation time, stability, dough thinning, and valorimetric assessment) according to the method described in Section 2. The results of the study on the influence of barley dough on its physical properties are presented in Table 1.

As seen from the data presented in Table 1, as the flour norms obtained from the classified barley fractions increased, the dough elasticity deteriorated compared to the control at 102.6 mm. Thus, with an increase in the barley flour rate from 5 to 20%, the dough elasticity decreased by 2.3–31.4% (the exception is 5%) and 0.5–31.3%, respectively. The specific deformation work of the dough decreased by 1.06-16.6 and 1.06-17.0%, respectively. A similar pattern is observed in the ratio of elasticity to elasticity. As the amount of barley flour increases, this indicator varies from 1.63 to 1.23. The data obtained on the pharinograph show that as the content of barley flour increases, its water absorption capacity decreases. The water absorption capacity increases by 0-31% compared to the control sample with an increase in the barley flour norm from 5 to 20%.

However, the addition of up to 10% barley flour to the wheat flour composition shows that the dough possesses good rheological properties and is not inferior to the dough made from first-grade wheat flour (control). Thus, based on the analysis and experimental data, it was concluded that no more than 10% barley flour can be added to the recipe for instant pasta. Based on the experimental data obtained to study the influence of barley flour on gluten properties, rheological properties of the dough, and the quality of early-ripening pasta products, the optimal dosage of additives (barley flour) and technological regimes for preparing dough and drying raw early-ripening pasta products were determined, resulting in finished products similar to the control samples. The preparation schedule for instant pasta is presented in Table 2.

Table 2. Technological modes for the production of instant pasta with a recipe for 10% barley flour

Process options	Value
Heat, do not exceed °C	45
Duration, min, not less than	10
Pressure, MPa, not less than	60
Output temperature of shaped early bakery products, °C	40
Drying parameters: - relative air humidity, %, - temperature, ±2°C	 70 60
Drying duration, ±3 hours	14

Studying the nutritional and biological value and assessing the safety of the developed instant pasta products. Early pasta products can be endowed with beneficial, dietary, preventive, or therapeutic properties by introducing additives that increase the content of certain essential

nutrients. Such nutrients can primarily be proteins, mineral components, vitamins, and easily digestible carbohydrates. The amount of such components can be increased by using special natural additives. Based on the above, the nutritional value of early bread products made from first-grade wheat flour was studied with an optimal ratio of barley flour, while the quality of the early pasta products was not lower than the quality of the control sample. The results of the study presented in Figure 1 showed that when adding barley flour to instant pasta, the protein content decreased compared to the control. The amino acid composition of instant pasta made from wheat and barley flour determines their protein value. In this regard, essential amino acids are of particular importance, among which lysine is of particular importance.



Wheat and barley flour in a ratio of 90:10



Control sample 100% wheat flour

Unfortunately, the deficiency of this amino acid is also felt in both hard and soft wheat flour and early-ripening pasta products.

Table 3. Amino acid composition of instant pasta products with 10% barley flour in the recipe

As a

Nutrients	Composition of 100 g of product	
	Reference number	
Nutrients	№1 (control)	№2
Protein, g	10,2	9,74
Amino acids, mg		
Non-replaceable:		
isoleucine	439	431
valine	516	503
leucine	837	820
lysine	344	339
methionine	181	177
threonine	359	349
tryptophan	145	138
phenylalanine	427	428
Interchangeable		
alanine	570	567
arginine	573	568
aspartic acid	677	670
histidine	270	256
glycine	541	547
glutamic acid	3701	3686
proline	1154	1141
tyrosine	409	401
cystine	278	274

result of the experimental studies conducted to study the quality indicators, chemical composition, and influence of flour prepared from air-fractionated barley fractions on the technological properties of instant pasta products, the following was established:

Using air fractionation technology, purified fractions rich in protein and starch were obtained from barley grain, and flour was ground in a stone mill with a ceramic disk. A comparative analysis of the composition of barley grain flour with first-grade wheat flour showed a significant difference in the content of protein, essential amino acids, vitamins, macro- and microelements. It was established that as barley flour exceeds the prescribed norm in the recipe, the gluten properties, rheological properties of the dough, and quality indicators of early bakery products deteriorate. It was substantiated that the optimal amount of barley flour is 10.0% of the mass of first-grade wheat flour, while the gluten properties, rheological properties of the dough, and the quality of early-maturing pasta products are similar to the control sample. It has been established that the use of barley grain flour in the production of instant pasta contributes to a further increase in the nutritional value of special instant pasta products with high functional properties in terms of protein, vitamins, and minerals.

CONCLUSION. In conclusion, it can be stated that barley flour is rich in water-soluble fiber, minerals, and biologically active nutrients; its inclusion in the recipe for instant pasta up to 10% increases the rheological properties of the dough and the nutritional value of the finished

product. In particular, adding more than 10% of barley flour partially negatively affects the quality of gluten, the plasticity, elasticity, and shape stability of the dough during baking.

However, with an addition of up to 10%, the appearance, taste, color, and physical properties of the samples during boiling are close to the control sample. Products prepared in this ratio have a high biological value, and organoleptic indicators meet standard requirements, allowing for the production of special-purpose early-ripening pasta with functional properties.

REFERENCES

1. Sissons, M. (2008). Role of durum wheat composition on the quality of pasta and bread. *Food* 2(2), 75–90.
2. Foschia, M., Peressini, D., Sensidoni, A., & Brennan, C.S. (2015). The effects of dietary fibre addition on the quality of common cereal products. *Journal of Cereal Science*, 58(2), 216–227.
3. Petitot, M., Abecassis, J., & Micard, V. (2010). Structuring of pasta components during processing: Impact on starch and protein digestibility and allergenicity. *Trends in Food Science & Technology*, 21(11), 521–532.
4. Baik, B.K., & Ullrich, S.E. (2008). Barley for food: Characteristics, improvement, and renewed interest. *Journal of Cereal Science*, 48(2), 233–242.
5. Brennan, C.S., & Cleary, L.J. (2005). The potential use of cereal β-glucans as functional food ingredients. *Journal of Cereal Science*, 42(1), 1–13.
6. Izydorczyk, M.S., & Dexter, J.E. (2008). Barley β-glucans and arabinoxylans: Molecular structure, physicochemical properties, and uses in food products. *Food Research International*, 41(9), 850–868.
7. Wood, P.J. (2010). Cereal β-glucans in diet and health. *Journal of Cereal Science*, 46(3), 230–238.

SYNTHESIS AND QUANTUM-CHEMICAL ANALYSIS OF A ZN(II) COMPLEX WITH INDOLE-3-ACETIC ACID AND ACETAMIDE

Sh.A. Ismailova[1], S.Z. Ibragimov[2], Z.Sh. Soporboev[3], O.I. Khudoyberganov[4]
Independent Researcher, Khorezm Ma'mun Academy, Khiva, Khorezm Region, Uzbekistan[1]
Junior Researcher, Department of Exact Sciences, Khorezm Ma'mun Academy, 220900, Khiva, Khorezm Region, Uzbekistan[2]
Junior Researcher, Department of Exact Sciences, Khorezm Ma'mun Academy, 220900, Khiva, Khorezm Region, Uzbekistan[3]
PhD, Senior Researcher, Khorezm Ma'mun Academy, Khiva, Khorezm Region, Uzbekistan[4]
https://doi.org/10.5281/zenodo.20302238

Abstract._*The article describes the synthesis of a new mixed-ligand coordination compound of zinc(II) ion with indole-3-acetic acid (heteroauxin) and acetamide. The composition and structure of the obtained complex compound were investigated using elemental analysis and IR spectroscopy. Analysis of the IR spectra allowed determining the coordination modes of the ligands to the metal ion. In the second part of the study, the electronic structure and thermodynamic characteristics of the complex were analyzed using quantum-chemical calculations (DFT method). The results show a high correlation between theoretical and*

experimental data, providing a basis for the potential biological activity of the synthesized complex.

Keywords: *zinc(II), indole-3-acetic acid, acetamide, coordination compound, synthesis, IR spectroscopy, quantum-chemical analysis, DFT, HOMO-LUMO.*

Introduction. One of the priority directions of modern coordination chemistry is the synthesis of new complex compounds of transition metals based on biologically active ligands and the fundamental study of their properties. Among transition metals, zinc (Zn(II)) stands out due to its low toxicity, its important role in biological processes, and its versatile coordination capabilities. Zinc ions are components of many enzymes and participate in regulating metabolic processes in the organism. In this study, indole-3-acetic acid (IAA), selected as a ligand, is one of the most important natural plant growth regulators (belonging to the auxin group). Due to the presence of donor atoms in its structure (the nitrogen in the indole ring and the oxygen in the carboxyl group), IAA is capable of forming stable and biologically active complexes with metal ions. The second ligand, acetamide, is a simple yet effective amide that exhibits high selectivity in coordination with d-metals and is frequently found in pharmaceutical compounds. The synthesis of mixed-ligand complexes is relevant not only for obtaining new substances but also from the perspective of studying intermolecular interactions. The investigation of the structure and properties of complex compounds formed by the simultaneous coordination of both a hormonal ligand (IAA) and an amido ligand around a zinc ion opens new prospects for agriculture and pharmaceutical applications. Modern chemical research is inconceivable without quantum-chemical analysis. The initially selected main ligand, indole-3-acetic acid (heteroauxin, IAA), and the newly synthesized coordination compound $[Zn(IAA)_2(AA)_2]\cdot 2H_2O$ were studied using the Gaussian program with the CAM-B3LYP basis set. The aim of this article is to synthesize a mixed-ligand complex compound of the Zn(II) ion with indole-3-acetic acid and acetamide, to confirm its composition using modern physicochemical methods, and to theoretically substantiate the stable structure and electronic properties of the complex through quantum-chemical calculations.

Literature review. In recent years, the synthesis of metal complexes based on drugs and biologically active substances has remained one of the priority directions of coordination chemistry. In particular, compounds of Zn(II) ions with plant growth stimulators and heterocyclic ligands have been widely studied due to their biological effectiveness and low toxicity. Indole-3-acetic acid (IAA) is known as a plant phytohormone, and its coordination with metals significantly alters the biological activity of the molecule. In studies conducted by K. Szmigiel-Bakalarz and co-authors (2020), a new 2D coordination polymer of Zn(II) ions with IAA, $[Zn(I3AA)_2]n$, was synthesized [1]. The study showed that coordination occurs through the carboxylate group of the ligand, and the resulting complex exhibits higher microbiological activity compared to the free ligand.

Similarly, Xuling Xue and co-authors (2011) studied mixed-ligand complexes of IAA with auxiliary ligands such as 1,10-phenanthroline and 4,4'-bipyridine. Their results indicate that such complexes exhibit not only biological activity but also luminescent properties and can serve as sensors for mercury(II) ions. Complexes of Zn(II) ions with nitrogen- and oxygen-donor ligands are widely used in medicine [2,3]. In the studies of Qingdi Zhou (2000) and G.G. Nnabuike (2020), the synthesis of Zn(II) complexes based on indomethacin (a drug structurally similar to IAA) and nitrogen-donor ligands (pyridine, imidazole) was reported [6,11]. These works demonstrated that

the gastrointestinal toxicity of zinc complexes is lower than that of Cu(II) complexes, and their pharmacokinetic properties are improved.

The synthesis of Zn(II) complexes with acetamide and its derivatives (such as aryl-acetamides) is also of current importance. Kishwar Sultana and co-authors (2016) synthesized zinc complexes based on aryl-acetamides and evaluated their potential as enzyme inhibitors and anticancer agents [8]. In the evaluation of the electronic structure and stability of coordination compounds, density functional theory (DFT) has become an indispensable method. In their studies, Ayesha Zahoor (2021) and Richa and co-authors (2020) calculated the geometric parameters, HOMO–LUMO energy gap, and molecular electrostatic potential (MEP) of Zn(II) carboxylate complexes using the DFT method [5,7]. Quantum-chemical calculations serve as a key tool in explaining through which centers synthesized complexes are coordinated and how their chemical reactivity is determined. For example, DFT studies performed by Karolina Babijczuk (2023) on zinc–indole–imidazole complexes theoretically confirmed that coordination enhances the functionality of biologically active ligands [4]. DFT analysis, along with global reactivity descriptors and thermal stability (TGA/DSC), has also been applied to dehydroacetate acid complexes [9]. For Zn(II)–Schiff base complexes, electronic parameters were calculated using DFT, demonstrating structural stability, and their interaction with DNA was analyzed using viscometry and UV/fluorescence methods [10]. The literature review shows that the synthesis of mixed-ligand complexes of Zn(II) ions with indole-3-acetic acid and acetamide derivatives, as well as the study of their structure using quantum-chemical methods:

1. Obtaining new biologically active substances;
2. Determining the coordination between the ligand and the metal;
3. Predicting the stability and reactivity of the compound.

Research methodology. The mixed-ligand coordination compound of zinc(II) chloride with indole-3-acetic acid and acetamide was synthesized using the following procedure. First, 0.01 mol (1.75 g) of indole-3-acetic acid (IAA) was dissolved in 50 mL of ethanol. To ensure deprotonation of the ligand's carboxyl group, 0.01 mol of potassium hydroxide (KOH) was added to the resulting solution. In a separate beaker, 0.005 mol (0.85 g) of zinc(II) chloride dihydrate ($ZnCl_2 \cdot 2H_2O$) was completely dissolved in 20 mL of distilled water. The metal salt solution was then added dropwise to the indole-3-acetic acid solution under constant stirring and mixed on a magnetic stirrer for 25–30 minutes. Afterwards, in order to form the mixed-ligand complex, a solution of 0.01 mol (0.59 g) of acetamide (AA) was added dropwise (5–10 mL) to the reaction mixture, followed by further stirring for 25–30 minutes. The reaction mixture was then continuously stirred at 50–55 °C for 1–1.5 hours using a magnetic stirrer [12]. At the end of the reaction, a clear, colorless solution was obtained. The resulting solution was purified by filtration, washed several times with a mixture of distilled water and ethanol, and dried in a vacuum desiccator (over P_2O_5) until constant mass was achieved [13,14].

As a result of the synthesis process, a clear colorless crystalline powder was obtained. The overall yield of the synthesis reaction was 82%, which confirms the high efficiency of the selected synthetic method. Based on the compositional analysis of the complex compound, it can be represented by the formula $[Zn(IAA)_2(AA)_2] \cdot 2H_2O$ [15]. The reaction equation can be expressed as follows.

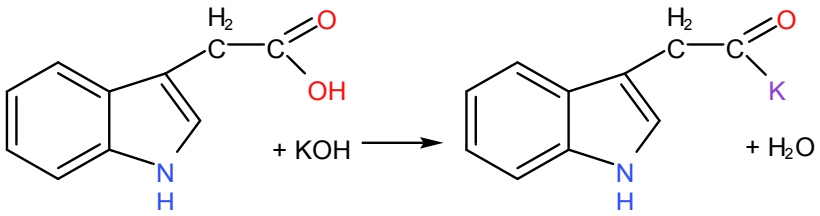


Figure 1. The reaction for obtaining the potassium salt of indole-3-acetic acid

In solution, the selected ligands lose their protons and are converted into IAA^- and AA^- anions. The Zn^{2+} ion possesses vacant coordination orbitals and forms coordination bonds with the IAA^- and AA^- ligands through the oxygen atoms of the carboxylate groups.

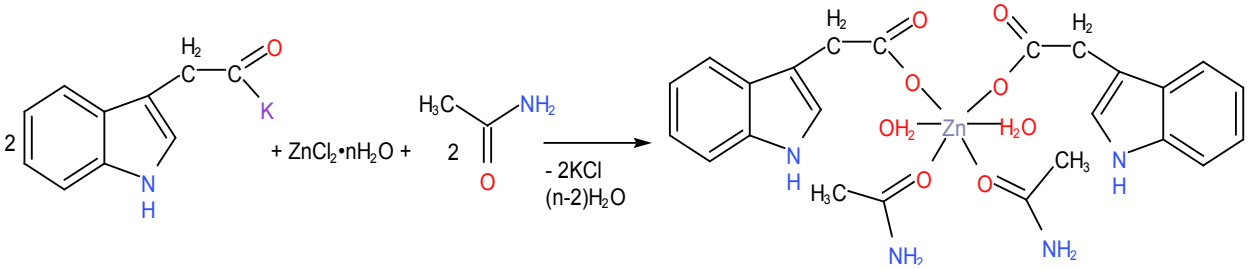


Figure 2. The reaction equation for the formation of the complex compound $[Zn(IAA)_2(AA)_2]\cdot 2H_2O$

As a result, a coordination compound with six coordination and octahedral geometry is formed. During crystallization, the resulting complex incorporates two water molecules, which are considered water of crystallization: $[Zn(IAA)_2(AA)_2]\cdot 2H_2O$.

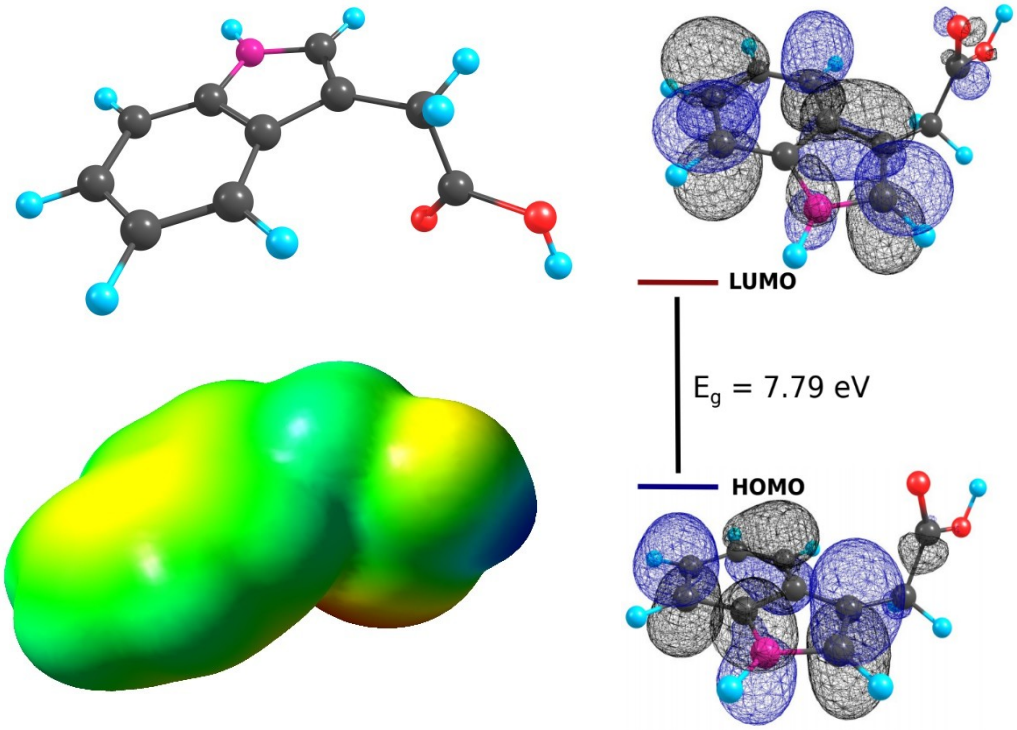
Analysis and results. In this study, the electronic structure, geometric parameters, and stability of the synthesized complex $[Zn(IAA)_2(AA)_2]\cdot 2H_2O$ were investigated using quantum chemical calculations. All computations were carried out using the Gaussian program package. The geometry optimization and subsequent analyses were performed within the framework of Density Functional Theory (DFT) employing the range-separated hybrid functional CAM-B3LYP, which is known for its improved description of long-range electron interactions and charge-transfer systems. The initial molecular structure of the complex was constructed based on experimental coordination assumptions, where Zn(II) is coordinated by two indole-3-acetate (IAA^-) and two acetate (AA^-) ligands through oxygen donor atoms. Full geometry optimization was performed without any symmetry constraints, and the nature of the stationary points was confirmed by vibrational frequency analysis, ensuring the absence of imaginary frequencies.

The optimized structure reveals that the Zn(II) center adopts a distorted octahedral coordination environment, where the ligand molecules form stable coordination bonds via carboxylate oxygen atoms. The presence of crystallization water molecules plays an important role in stabilizing the supramolecular structure through hydrogen bonding interactions. Furthermore, frontier molecular orbital (FMO) analysis was carried out to evaluate the electronic properties of the complex. The energies and spatial distributions of HOMO and LUMO orbitals provide insight into the chemical reactivity, kinetic stability, and possible charge-transfer pathways within the complex. The HOMO–LUMO energy gap indicates the relative stability of the system and its potential reactivity. Additionally, charge distribution analysis and electron density mapping were used to better understand the coordination behavior and electron delocalization within the complex system. These results provide a theoretical basis for interpreting the stability and physicochemical properties of the synthesized zinc complex.

Quantum chemical study of ligands and transition metal complex.

All quantum chemical calculations were carried out using the Gaussian 16 software package [16]. The molecular geometry was fully optimized in the gas phase without symmetry constraints using the range-separated hybrid functional CAM-B3LYP [17], which incorporates the Coulomb-attenuating method to improve the description of long-range exchange interactions. The LANL2DZ basis set [18] was employed throughout: it applies the Los Alamos National Laboratory double-zeta ECP basis for zinc, treating the inner core electrons through relativistic effective core potentials, while the ligand atoms (C, N, O, H) are described with the standard Dunning/Huzinaga full double-zeta basis.

Electronic structure analysis of ligands.



Frequency calculations were performed on the optimized structure to confirm that the geometry corresponds to a true energy minimum on the potential energy surface (absence of imaginary frequencies). Natural bond orbital (NBO) analysis was performed using the NBO 3.1 program interfaced with Gaussian-16 [19] to obtain natural atomic charges, orbital hybridizations, and donor-acceptor interactions via second-order perturbation theory. Frontier molecular orbitals (HOMO, LUMO) and their energy eigenvalues were extracted from the converged DFT wavefunction. The electrostatic potential was computed on the 0.001 a.u. electron density isosurface and mapped with a color scale ranging from electron-rich (red) to electron-poor (blue) regions.

Electronic structure analysis of Zn(II) complex.

Zinc(II) coordination complexes occupy a prominent position in bioinorganic chemistry, materials science, and medicinal chemistry owing to the unique electronic properties of the d^{10} metal center, which confers high thermodynamic stability, Lewis acidity, and favorable luminescence behavior [20]. Unlike transition metals with partially filled d-orbitals, Zn(II) exhibits no d–d transitions, directing all photophysical activity toward ligand-based or ligand-to-metal charge-transfer (LMCT) processes [21].

Indole and its derivatives are biologically privileged scaffolds that appear as constituents of the essential amino acid tryptophan and a broad spectrum of natural products and pharmaceuticals [22]. Their aromatic nitrogen and electron-rich π-system make them excellent candidates for chelation of transition metals, offering both σ-donor N-coordination and π-stacking stabilization [23]. The incorporation of carboxylate and amide functionalities alongside the indole moiety creates multidentate ligand platforms capable of saturating the coordination sphere of Zn(II) while imparting solubility and hydrogen-bonding capacity relevant to aqueous biological environments.

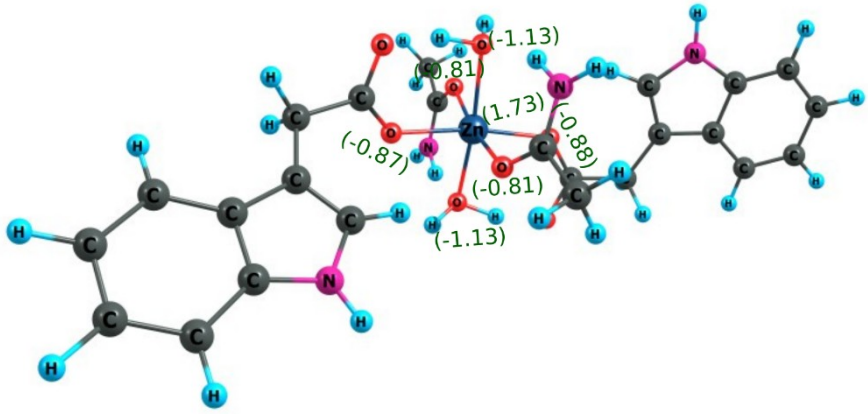


Figure 3. Optimized geometry of the Zn(II) complex at the CAM-B3LYP/LANL2DZ level with NBO partial charges (in parentheses, green text) shown for key donor atoms. Color code: Zn (dark blue), O (red), N (magenta), C (dark gray), H (cyan).

Density functional theory (DFT) has become the standard computational methodology for characterizing the structure, bonding, and reactivity of metal complexes [24]. The range-separated CAM-B3LYP functional is particularly well-suited to zinc coordination compounds, accurately describing charge-transfer excitations and long-range electron correlation effects that are poorly treated by conventional hybrid functionals [25]. The LANL2DZ effective core potential (ECP) basis set provides a computationally efficient treatment of the zinc core electrons while maintaining accuracy for valence-shell properties [26]. The optimized structure (Figure 3) reveals that the Zn(II) center is hexacoordinate with a strictly oxygen-donor O_6 coordination sphere, adopting a distorted octahedral geometry. The six donor oxygens originate from three chemically distinct sources: two carboxylate oxygens from *indole-2-carboxylic acid* (Zn–O: 2.05 and 2.07 Å), two acetamide carbonyl oxygens from the acetamide-indole ligand (Zn–O: 2.12 and 2.13 Å), and two terminal aqua oxygens (Zn–O: 2.15 and 2.13 Å).

Table 1. Zn–O Bond lengths and NBO charges

Donor Type	**Bond 1 (Å)**	**Bond 2 (Å)**	**NBO Charge 1 (e)**	**NBO Charge 2 (e)**
Carboxylate O (indole-2-carboxylic acid)	2.05	2.07	−0.87	−0.88
Acetamide O	2.12	2.13	−0.81	−0.81
Terminal O (aqua)	2.15	2.13	−1.13	−1.13
Zn center (NBO)	—	—	+1.73	*(formal: +2.0)*

The NBO charge on zinc (+1.73 e) is reduced by 0.27 e relative to the formal +2 oxidation state, reflecting net ligand-to-metal charge transfer distributed across all six Zn–O bonds. This reduction confirms that the Zn–O bonds are predominantly ionic with a meaningful covalent component, consistent with Zn(II) acting as a borderline hard Lewis acid with a strong preference for oxygen donors over nitrogen. The carboxylate oxygens of indole-2-carboxylic acid form the shortest bonds in the complex (2.05 and 2.07 Å) and carry moderate negative charges (−0.87 and −0.88 e), identifying them as the strongest σ-donors in the coordination sphere. Their moderate charge magnitudes, rather than extreme values, reflect a balance between inherent oxygen electronegativity, partial charge transfer to Zn, and delocalization across the O–C–O resonance system of the carboxylate. The near-identical values for both oxygens ($\Delta q = 0.01$ e, $\Delta d = 0.02$ Å) confirm near-symmetric bidentate chelation of indole-2-carboxylic acid.

The acetamide carbonyl oxygens exhibit intermediate bond lengths (2.12 and 2.13 Å) and the lowest negative charges among the three oxygen types (−0.81 e each). This is a direct consequence of amide resonance: the nitrogen lone pair adjacent to the C=O group donates electron density into the π*(C=O) orbital ($n_n \rightarrow \pi^*$ interaction), reducing the electron density available on the carbonyl oxygen for metal donation. Both acetamide oxygens are fully equivalent, confirming symmetric coordination geometry.

The terminal aqua oxygens present an apparently paradoxical combination of the highest negative charge (−1.13 e) yet the longest Zn–O bonds (2.13–2.15 Å). This is resolved by recognizing that water oxygen retains high negative charge because of the polarization of its two O–H bonds (each H bears ~+0.5 e in NBO), not because of strong donation to zinc. Water is in fact the weakest donor of the three groups, forming the longest and most labile Zn–O bonds. These aqua ligands are therefore the primary sites for ligand exchange in solution and represent the most accessible substitution positions for incoming biological or pharmacological ligands.

The frontier molecular orbitals and HOMO-LUMO gap ($E^p = 7.6$ eV) are shown in Figure 4. This exceptionally large gap is a direct consequence of the d^{10} configuration of Zn(II): the completely filled d-shell lies well below the HOMO in energy and contributes negligibly to either frontier orbital. All electronic activity is therefore confined to the ligand π-systems.

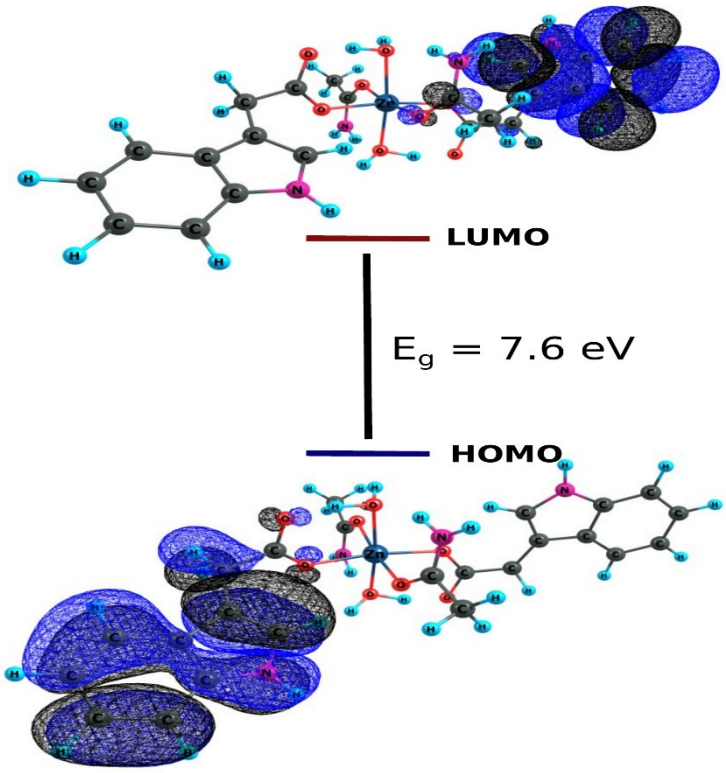


Figure 4. HOMO (bottom) and LUMO (top) of the Zn(II) complex (CAM-B3LYP/LANL2DZ, isovalue = 0.02 a.u.). Blue: positive phase; black mesh: negative phase. E^p = 7.6 eV. Both orbitals are exclusively ligand-centered.

The HOMO is a π-type bonding orbital delocalized across the indole-2-carboxylic acid fragment (left), with alternating lobes above and below the aromatic plane extending over the fused benzene-pyrrole bicyclic system. The indole N–H nitrogen lone pair contributes to the HOMO through conjugation into the aromatic π-system. The LUMO, conversely, is a π*-antibonding orbital localized on the acetamide-indole fragment (right), with the acetamide C=O π* in conjugation with the indole ring. The spatial separation of HOMO and LUMO across the two ligand fragments defines the electronic excitation as a ligand-to-ligand charge transfer (LLCT) process, in which electron density migrates from the indole-2-carboxylic acid side to the acetamide-indole side upon photon absorption, with the Zn center acting as a structural bridge rather than an electronic mediator. The 7.6 eV gap corresponds to a chemical hardness of η = 3.8 eV, classifying this complex as an extremely hard, kinetically stable species.

Electrostatic Potential Surface Analysis is shown in Figure 5.

The ESP surface encodes the three-dimensional charge distribution and directly reflects the NBO analysis. The red/orange region concentrated at the central Zn–O coordination core identifies the overlapping lone pairs of the six oxygen donors as the most nucleophilic surface of the molecule, with maximum electron accumulation around the carboxylate and acetamide oxygen atoms consistent with NBO charges of −0.81 to −1.13 e. This zone constitutes the primary hydrogen-bond acceptor and Lewis base surface, reactive toward electrophilic species, metal cations, and proton donors in the surrounding environment. The blue regions at the N–H protons of both indole moieties mark the most electron-deficient sites on the molecular surface. These hydrogen atoms carry positive partial charges due to N–H bond polarization and are strong hydrogen-bond donors, well positioned to interact with Lewis base residues in protein binding pockets, phosphate groups of DNA/RNA, or carboxylate residues of enzyme active sites. Their

moderate acidity also suggests the possibility of deprotonation under basic conditions to form anionic indolate-Zn complexes.

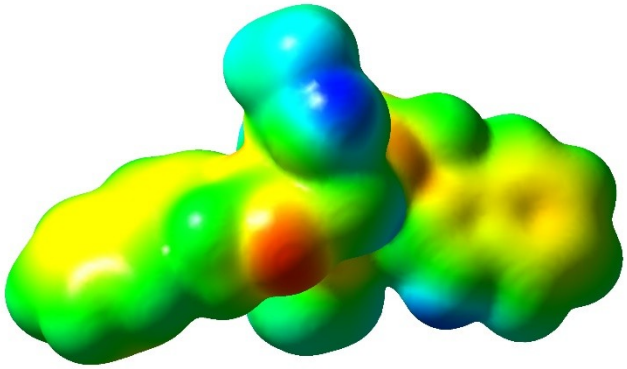


Figure 5. ESP surface of the Zn(II) complex mapped on the 0.001 a.u. electron density isosurface (CAM-B3LYP/LANL2DZ). Red: most electron-rich (negative potential); Blue: most electron-poor (positive potential); Green: near-neutral. Left: indole-2-carboxylic acid fragment; Right: acetamide-indole fragment; Center: O_6 Zn(II) coordination core.

The green coloring across both aromatic ring faces reflects near-neutral π-electron density, consistent with mildly nucleophilic aromatic surfaces capable of π-stacking with nucleobases, cation-π interactions with protonated lysine/arginine residues, and CH-π contacts. A subtle asymmetry is visible: the indole-2-carboxylic acid ring (left) appears slightly greener (more electron-rich) than the acetamide-indole ring (right), consistent with the electron-withdrawing acetamide group reducing π-density on the right fragment—a pattern that also correlates with the LUMO being localized on the right-side ring. The yellow periphery of both ring systems and the aliphatic C–H framework reflects mild positive ESP arising from C–H bond polarization, indicating potential for weak C–H···O hydrogen bonding and van der Waals interactions relevant to crystal packing and biomolecular recognition.

Conclusion. The present study reports a quantum chemical investigation of the zinc(II) complex $[Zn(IAA)_2(AA)_2]\cdot 2H_2O$ using Density Functional Theory calculations performed with the Gaussian program package. Geometry optimizations and electronic structure analyses were carried out at the CAM-B3LYP/LANL2DZ level of theory, confirming a stable optimized structure without imaginary frequencies. The results show that Zn(II) forms a six-coordinate distorted octahedral geometry with oxygen donor atoms. NBO analysis indicates predominantly ionic Zn–O interactions with partial covalent character due to ligand-to-metal charge transfer. Frontier molecular orbital analysis reveals a ligand-centered electronic structure with a large HOMO–LUMO gap (7.6 eV), indicating high kinetic stability and low reactivity. Electrostatic potential mapping further identifies oxygen atoms as the main reactive sites in the complex. Overall, the obtained theoretical results provide a consistent description of the structural stability and electronic properties of the synthesized zinc(II) complex, supporting its potential relevance in coordination and bioinorganic chemistry.

REFERENCES

1. Szmigiel-Bakalarz, K., Skoczyńska, A., Lewańska, M., et al. New Zn(II) Coordination Polymer of Indole-3-Acetic Acid, a Plant-Growth-Promoting Hormone: Crystal Structure, Spectroscopic Characterization, DFT Calculations, and Microbiological Activity. *Polyhedron*, 2020, Vol. 185, Article 114582. https://doi.org/10.1016/j.poly.2020.114582

2. Xue, X., Zhu, Y., Xiao, B., et al. Two Zinc(II) Complexes Based on Indole-3-Acetic Acid: Crystal Structures, Fluorescence Sensors, and Ion Exchange with Mercury(II). *Journal of Coordination Chemistry*, 2011, Vol. 64, No. 16, pp. 2923–2935. DOI: 10.1080/00958972.2011.609277
3. Ismail, A. M., Butler, I. S., Abou El Maaty, W. M., Mostafa, S. I. Anticancer and DNA Interaction of New Zinc(II), Palladium(II), Platinum(II), and Silver(I) Complexes Based on Indole-3-Acetic Acid: Solid and Solution Studies. *Polycyclic Aromatic Compounds*, 2021. DOI: 10.1080/10406638.2021.1892779
4. Babijczuk, K., Warżajtis, B., Starzyk, J., et al. Synthesis, Structure, and Biological Activity of Indole-Imidazole Complexes with $ZnCl_2$: Can Coordination Enhance the Functionality of Bioactive Ligands? *Molecules*, 2023, Vol. 28, No. 10, Article 4132. https://doi.org/10.3390/molecules28104132
5. Zahoor, A., Imtiaz-ud-Din, Andleeb, S., et al. Zn(II) Carboxylates Containing Heterocyclic Secondary Ligands: Synthesis and Structural Manifestation through DFT Studies. *Journal of Coordination Chemistry*, 2021, Vol. 74, No. 12, pp. 1978–1991. DOI: 10.1080/00958972.2021.1945046
6. Zhou, Q., Hambley, T. W., Kennedy, B. J., et al. Syntheses and Characterization of Anti-Inflammatory Dinuclear and Mononuclear Zinc Indomethacin Complexes: Crystal Structures of $[Zn_2(Indomethacin)_4(L)_2]$ and $[Zn(Indomethacin)_2(L^1)_2]$. *Inorganic Chemistry*, 2000, Vol. 39, pp. 3742–3748.
7. Richa, Kumar, N., Sindhu, J., et al. Synthesis, Crystal, and DFT Studies of Zn/Co Complexes of Dehydroacetic Acid Using a Ligand-Exchange Approach. *Inorganic Chemistry Communications*, 2020, Vol. 121, Article 108280. https://doi.org/10.1016/j.inoche.2020.108280
8. Sultana, K., Zaib, S., Khan, N., et al. Exploiting the Potential of Aryl Acetamide-Derived Zn(II) Complexes in Medicinal Chemistry: Synthesis, Structural Analysis, Assessment of Biological Profile, and Molecular Docking Studies. *New Journal of Chemistry*, 2016, Vol. 40, pp. 7084–7097. DOI: 10.1039/c5nj03531g
9. Jin, S., Huang, Y., Wang, D., et al. Non-Covalently Bonded 2D–3D Metal–Organic Frameworks from the Reactions of Cd(II) and Zn(II) with 3,5-Dimethylpyrazole and Carboxylate Ligands. *Polyhedron*, 2013, Vol. 60, pp. 10–22. http://dx.doi.org/10.1016/j.poly.2013.04.056
10. Singha, U. K., Pradhan, S., Gurung, P., et al. Synthesis and Characterization of a Zn(II) Complex of 4-Chloro-2-(((2-phenoxyphenyl)imino)methyl)phenol and Its Biological Efficacies: DNA Interaction, ADMET, DFT, and Molecular Docking Study. *Journal of Fluorescence*, 2025, Vol. 35, pp. 2695–2706. https://doi.org/10.1007/s10895-024-03687-9
11. Nnabuike, G. G., Salunke-Gawali, S., Patil, A. S., et al. Synthesis and Structures of Tetrahedral Zinc(II) Complexes Bearing Indomethacin and Nitrogen-Donor Ligands. *Inorganica Chimica Acta*, 2020, Vol. 513, Article 119941. https://doi.org/10.1016/j.ica.2020.119941
12. Mukimova, G. Zh. *Synthesis and Investigation of Coordination Compounds of Succinate Complexes of Some 3d Metals with Amides*. Abstract of the Dissertation for the Degree of Candidate of Chemical Sciences. Tashkent, 1999, pp. 35–38.

13. Sharipova, L. A., Azizov, T. A., Ibragimova, M. R. Acetamide and Nicotinic Acid as Monotype Ligands in Coordination Compounds of Zinc Nitrate. *Universum: Chemistry and Biology*, Moscow, 2021, No. 5(83), pp. 45–49.
14. Turakulov, Zh. U., Azizov, T. A. Synthesis and Investigation of Coordination Compounds of Calcium Acetate with Acetamide. *Universum: Chemistry and Biology*, Moscow, 2018, No. 9(51), pp. 18–24.
15. Kharitonov, Yu. A., Tsivadze, A. Yu., Smirnov, A. N. Analysis of Normal Vibrations of Coordinated Acetamide. *Coordination Chemistry*, 1975, Vol. 1, No. 2, pp. 214–219.
16. Frisch, M. J., Trucks, G. W., Schlegel, H. B., Scuseria, G. E., Robb, M. A., Cheeseman, J. R., Scalmani, G., Barone, V., Petersson, G. A., Nakatsuji, H., Li, X., Caricato, M., Marenich, A. V., Bloino, J., Janesko, B. G., Gomperts, R., Mennucci, B., Hratchian, H. P., Ortiz, J. V., Izmaylov, A. F., Sonnenberg, J. L., Williams-Young, D., Ding, F., Lipparini, F., Egidi, F., Goings, J., Peng, B., Petrone, A., Henderson, T., Ranasinghe, D., Zakrzewski, V. G., Gao, J., Rega, N., Zheng, G., Liang, W., Hada, M., Ehara, M., Toyota, K., Fukuda, R., Hasegawa, J., Ishida, M., Nakajima, T., Honda, Y., Kitao, O., Nakai, H., Vreven, T., Throssell, K., Montgomery, J. A., Jr., Peralta, J. E., Ogliaro, F., Bearpark, M. J., Heyd, J. J., Brothers, E. N., Kudin, K. N., Staroverov, V. N., Keith, T. A., Kobayashi, R., Normand, J., Raghavachari, K., Rendell, A. P., Burant, J. C., Iyengar, S. S., Tomasi, J., Cossi, M., Millam, J. M., Klene, M., Adamo, C., Cammi, R., Ochterski, J. W., Martin, R. L., Morokuma, K., Farkas, O., Foresman, J. B., Fox, D. J. *Gaussian 16, Revision C.02*. Gaussian, Inc., Wallingford, CT, 2016.
17. Becke, A. D. Density-Functional Thermochemistry. III. The Role of Exact Exchange. *The Journal of Chemical Physics*, 1993, Vol. 98, No. 7, pp. 5648–5652.
18. Wadt, W. R., Hay, P. J. Ab Initio Effective Core Potentials for Molecular Calculations: Potentials for Main Group Elements Na to Bi. *The Journal of Chemical Physics*, 1985, Vol. 82, No. 1, pp. 284–298.
19. Reed, A. E., Curtiss, L. A., Weinhold, F. Intermolecular Interactions from a Natural Bond Orbital, Donor–Acceptor Viewpoint. *Chemical Reviews*, 1988, Vol. 88, No. 6, pp. 899–926.
20. Lippard, S. J., Berg, J. M. *Principles of Bioinorganic Chemistry*. University Science Books, 1994.
21. Constable, E. C. *Metals and Ligand Reactivity*. Weinheim: VCH, 1996.
22. Kaur, K., Jain, M., Reddy, R. P., Jain, R. Quinolines and Structurally Related Heterocycles as Antimalarials. *European Journal of Medicinal Chemistry*, 2010, Vol. 45, No. 8, pp. 3245–3264.
23. Reedijk, J. Coordination Chemistry beyond Werner: Interplay between Hydrogen Bonding and Coordination. *Chemical Society Reviews*, 2013, Vol. 42, No. 4, pp. 1776–1783.
24. Cramer, C. J. *Essentials of Computational Chemistry: Theories and Models*. 2nd ed. Chichester: Wiley, 2004.
25. Yanai, T., Tew, D. P., Handy, N. C. A New Hybrid Exchange–Correlation Functional Using the Coulomb-Attenuating Method: CAM-B3LYP. *Chemical Physics Letters*, 2004, Vol. 393, No. 1–3, pp. 51–57.
26. Hay, P. J., Wadt, W. R. Ab Initio Effective Core Potentials for Molecular Calculations: Potentials for the Transition-Metal Atoms Sc to Hg. *The Journal of Chemical Physics*, 1985, Vol. 82, No. 1, pp. 270–283.

SYSTEMATIC ANALYSIS OF THE TECHNOLOGICAL PROCESS OF NATURAL GAS PROCESSING AND FRACTIONATION AT THE SHURTAN GAS-CHEMICAL COMPLEX

R.O. Boboyorov[1], B. Ibragimov[2]
Professor, Tashkent Institute of Chemical Technology, Tashkent, Uzbekistan[1]
Master's Student, Tashkent Institute of Chemical Technology, Tashkent, Uzbekistan[2]
https://doi.org/10.5281/zenodo.20522251

Abstract. *This article presents a systematic IMRAD-based analysis of the technological process of natural gas processing and fractionation at the Shurtan Gas-Chemical Complex. The study considers the process as an integrated technological system that includes mechanical impurity removal, gas dehydration, acid gas absorption, low-temperature separation, rectification, product storage, and automated control. The purpose of the research is to identify the main process factors that determine the stability, selectivity, energy efficiency, and product quality of the fractionation system. The methodology is based on process decomposition, comparative analysis of equipment functions, system modeling, and synthesis of thermodynamic, hydrodynamic, structural, and control parameters. The results show that fractionation efficiency is governed by the interaction of temperature, pressure, flow rate, reflux ratio, heat exchange, mass transfer intensity, and automation quality rather than by a single apparatus. The paper concludes that coordinated control of all stages is essential for improving hydrocarbon recovery, reducing energy losses, and ensuring reliable industrial operation.*

Keywords: *natural gas processing; fractionation; Shurtan Gas-Chemical Complex; rectification; gas dehydration; acid gas absorption; automation; process optimization; energy efficiency; product quality.*

INTRODUCTION

Natural gas processing is one of the central technological areas of the modern gas-chemical industry because it transforms raw gas from wells into marketable products with specified composition and quality. Raw natural gas contains methane, ethane, propane, butane, heavier hydrocarbons, carbon dioxide, hydrogen sulfide, water vapor, liquid droplets, solid particles, and other minor components. Before the gas can be supplied to pipelines, used as petrochemical feedstock, or separated into hydrocarbon fractions, it must pass through a sequence of purification, drying, cooling, separation, and rectification operations. At large industrial complexes such as the Shurtan Gas-Chemical Complex, these operations are not isolated technical procedures. They form an interdependent process chain in which the performance of each stage directly affects the next stage and, consequently, the efficiency of the entire production system.

The relevance of this study is determined by the need to evaluate gas processing and fractionation not only from the perspective of individual equipment, but also as a coordinated technological system. Mechanical cleaning protects downstream devices from erosion and fouling; dehydration prevents hydrate formation and corrosion; acid gas removal improves environmental and operational safety; low-temperature separation supports recovery of heavier hydrocarbons;

and rectification columns ensure the required purity of methane, ethane, propane, butane, and condensate streams. If one stage is unstable, the disturbance is transmitted throughout the plant. For example, insufficient dehydration may cause hydrate blockage during cooling, while poor acid gas removal may affect product quality and equipment reliability. Thus, a systematic approach is essential for technical assessment and optimization.

The scientific problem addressed in this article is the identification of the main technological factors that determine the efficiency of natural gas processing and fractionation at the Shurtan Gas-Chemical Complex. Existing studies in chemical engineering and gas processing emphasize the importance of thermodynamics, phase equilibrium, mass transfer, and process control in separation systems [1-4]. However, industrial practice shows that the real efficiency of gas fractionation depends on the interaction of many factors: temperature, pressure, flow regime, reflux ratio, column internals, heat-exchange efficiency, automation accuracy, and maintenance discipline. Therefore, the purpose of this paper is to analyze the processing scheme, determine the role of each major unit, summarize the factors affecting fractionation efficiency, and propose an integrated interpretation of the process from a technological and control-oriented viewpoint.

MATERIALS AND METHODS

The materials for the analysis were the technological structure of natural gas processing and fractionation at the Shurtan Gas-Chemical Complex, the process scheme presented in Figure 1, the functional descriptions of the main apparatus, and scientific literature on gas processing, chemical reaction engineering, process control, mass transfer, and separation technologies. The article also relies on previous works concerning process modeling, automation of chemical-technological systems, fuzzy control of nonlinear objects, and simulation of related chemical processes [4-15]. The object of the research is the integrated gas processing line from raw gas inlet to product storage. The subject of the research is the interaction between equipment functions, operating parameters, and process efficiency indicators.

A systematic methodological approach was used. First, the process was decomposed into main technological stages: initial separation, adsorption dehydration, amine absorption, heat exchange and cooling, pressure reduction, low-temperature separation, rectification, and product storage. Second, each stage was analyzed according to its technological function, input and output streams, limiting factors, and influence on subsequent stages. Third, the technological parameters affecting performance were grouped into thermodynamic, hydrodynamic, structural, and control-operational categories. This grouping makes it possible to examine the process not as a set of separate machines, but as an integrated technological system with feedback relationships.

Comparative analysis was also applied to distinguish between direct and indirect effects of the main parameters. Temperature and pressure directly influence vapor-liquid equilibrium and condensation behavior. Flow rate and phase contact time determine mass transfer quality. Reflux ratio influences product purity in rectification columns, while heat-exchanger performance affects cooling depth and energy consumption. In addition, a conceptual modeling method was used to prepare a generalized control logic for the process. This model, presented in Figure 2, links field sensors, online analyzers, automated control systems, operator decisions, and optimization targets. The resulting analysis is qualitative and system-oriented; it does not claim to replace detailed plant simulation, but it provides a structured basis for further mathematical modeling and industrial optimization.

RESULTS. The analysis shows that the process begins with mechanical separation, where raw gas is cleaned from solid particles, dust, sand, liquid droplets, and entrained condensate. The

separator performs a protective function for the whole plant because mechanical contaminants may damage valves, trays, packing elements, compressor blades, heat exchangers, and measuring instruments. Gravity separation is effective when the gas velocity is reduced and heavier phases settle downward. In cyclone separators, centrifugal force increases the separation rate. The result of this stage is not only physical cleaning of the stream, but also stabilization of the inlet conditions for dehydration and absorption units.

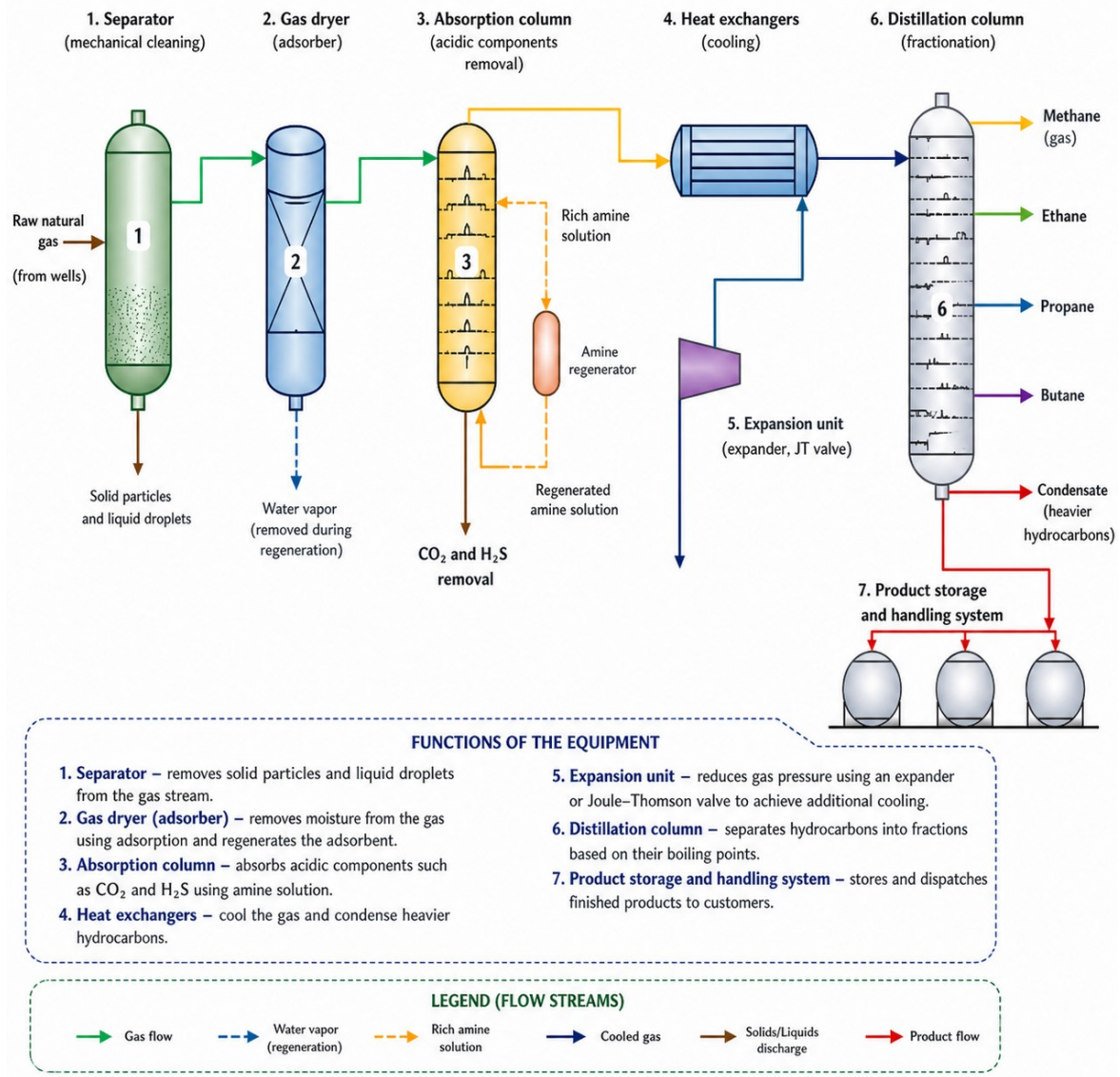


Figure 1. General technological scheme of natural gas processing and fractionation at the Shurtan Gas-Chemical Complex.

The second result concerns the role of gas dehydration. Water vapor is a critical impurity in natural gas because it may form gas hydrates under high pressure and low temperature. Hydrate formation is especially dangerous before cooling, expansion, and low-temperature separation because it may block pipelines, valves, and heat exchangers. Adsorption dehydration removes water molecules on porous surfaces and is followed by regeneration of the adsorbent. Consequently, the dryer performs both a quality function and a safety function: it reduces the water content of gas while ensuring continuous operation of downstream low-temperature equipment.

The third result is related to acid gas purification. Carbon dioxide and hydrogen sulfide are removed in absorption columns, typically using amine solutions. The absorption process depends

on effective contact between gas and liquid phases. Trays or packing materials increase the contact surface and improve mass transfer. The regenerated amine solution is returned to the absorber, while the rich amine stream is sent to regeneration. Proper operation of this system influences product quality, corrosion risk, environmental safety, and the load on the fractionation section. Thus, absorption should be viewed as a central component of the gas-processing system rather than a secondary purification step.

The fourth result concerns fractionation itself. Low-temperature separation and rectification are responsible for the recovery and purification of hydrocarbon fractions. In the cooling section, heat exchangers and expansion devices reduce the temperature of the gas and promote condensation of heavier hydrocarbons. In the rectification column, vapor and liquid phases repeatedly contact each other on trays or packing. Lighter components move upward and heavier components move downward. Product purity depends on internal mass transfer, reflux ratio, pressure profile, and temperature distribution. The main factors identified during the analysis are summarized in Table 1.

Table 1. Main technological factors affecting the natural gas fractionation process.

Technological factor	**Primary effect on the process**	**Expected result**	**Risk under poor control**
Temperature	Determines evaporation and condensation behavior	Higher separation efficiency	Incomplete recovery or excessive cooling costs
Pressure	Controls phase equilibrium and density	Improved liquid formation and product yield	Higher compression load or unstable operation
Flow rate	Affects residence time and phase contact	Improved mass transfer quality	Entrainment, flooding, or low productivity
Reflux ratio	Regulates separation depth in rectification	Increased product purity	Excess energy use or insufficient separation
Heat exchange	Distributes and recovers thermal energy	Improved energy efficiency	Temperature deviations and product losses

The findings indicate that no single parameter can determine fractionation efficiency independently. Temperature optimization is ineffective if pressure is unstable; reflux adjustment cannot compensate completely for poor tray performance; and efficient heat exchange becomes less valuable if online monitoring is inaccurate. Therefore, the key result of this study is the confirmation that technological efficiency is systemic. It emerges from the coordinated operation of the entire sequence of apparatus, control devices, and operational decisions.

The second table presents a practical matrix of optimization targets for major subsystems. It shows that each subsystem has a specific controlled variable, but the final industrial effect is achieved only when all indicators are monitored together. In this sense, process optimization should combine technological, economic, and safety criteria.

DISCUSSION

The results confirm the need to interpret the natural gas processing line as an integrated technological and control system. In many industrial descriptions, equipment is presented in a linear order: separator, dryer, absorber, heat exchanger, expansion unit, rectification column, and storage system. This linear view is useful for explaining material flow, but it is insufficient for evaluating industrial efficiency. In real operation, each unit influences the operating conditions of other units. For example, poor mechanical separation may increase fouling in the dryer and absorber. Insufficient dehydration may reduce the reliability of heat exchangers and expansion devices. Instability in the absorption section may affect corrosion behavior and product quality. Consequently, the efficiency of the Shurtan Gas-Chemical Complex depends on technological continuity and feedback control.

Table 2. Optimization matrix for the integrated gas processing and fractionation system.

Subsystem	**Key controlled variable**	**Main optimization target**	**Monitoring indicator**	**Expected industrial effect**
Mechanical separation	Inlet velocity and pressure drop	Reduction of entrained solids and liquids	Separator level and differential pressure	Protection of downstream equipment
Gas dehydration	Outlet water content and regeneration cycle	Prevention of hydrate formation	Water dew point analyzer	Stable cooling and expansion
Amine absorption	Lean/rich amine loading and circulation rate	Removal of CO2 and H2S	Acid gas concentration	Improved gas quality and lower corrosion risk
Cooling and expansion	Temperature, pressure, and heat duty	Condensation of heavier hydrocarbons	Outlet temperature and liquid level	Higher condensate recovery
Rectification	Reflux ratio and column pressure profile	Product purity and stable cuts	Composition analyzers	Marketable methane, ethane, propane, and butane streams
Storage and dispatch	Tank level, product temperature, and flow rate	Safe handling and product stability	Inventory and quality records	Reliable delivery of finished products

From a thermodynamic perspective, temperature and pressure are the dominant factors. They determine phase equilibrium and define the conditions under which components condense, evaporate, and separate. However, thermodynamic optimization must be balanced against energy consumption. Excessive cooling may increase the recovery of heavier hydrocarbons, but it also increases refrigeration or expansion energy requirements. High pressure may improve liquid recovery, but it requires additional compression work and stronger equipment. Therefore, optimal operation should not mean maximizing one parameter. It should mean finding a balanced operating

zone in which product quality, energy efficiency, safety, and equipment reliability are achieved together.

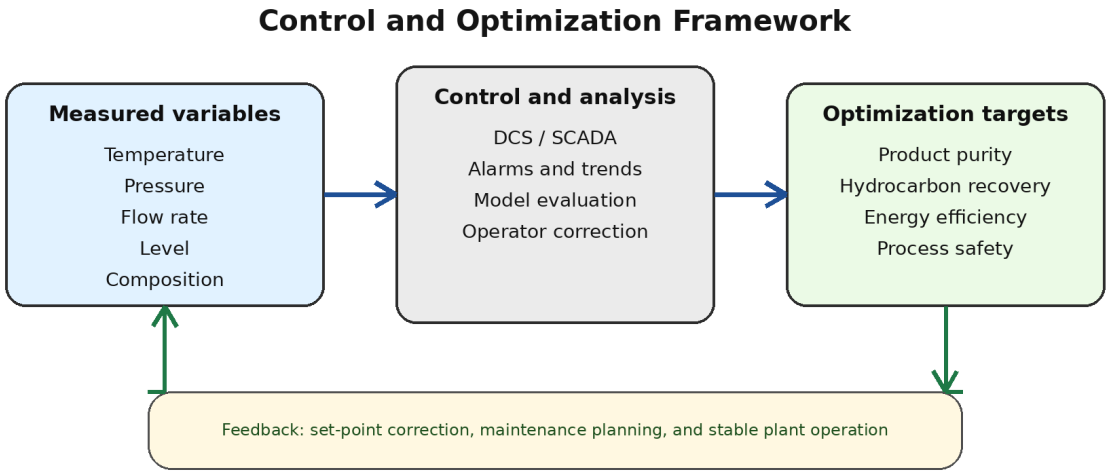


Figure 2. Conceptual model of integrated control and optimization for natural gas processing and fractionation.

Hydrodynamic factors are equally important because separation is not only a phase-equilibrium problem. Even if the temperature and pressure are theoretically suitable, insufficient contact between phases may reduce actual mass transfer. In rectification columns, flooding, weeping, entrainment, or nonuniform liquid distribution may lower separation efficiency. In absorbers, poor gas-liquid distribution reduces acid gas removal. In heat exchangers, fouling increases pressure drop and decreases heat-transfer performance. These hydrodynamic and structural problems show why equipment design and maintenance are essential parts of process optimization. Modern high-efficiency packing, properly selected trays, accurate distributors, and regular inspection can improve separation results without major changes in the general process scheme.

The role of automation is especially significant. Automated control systems continuously measure and regulate key parameters such as temperature, pressure, flow rate, level, composition, and reflux ratio. In complex processes, manual control is not sufficient because disturbances may develop rapidly and spread from one unit to another. DCS and SCADA systems reduce operator workload, provide alarms, support data recording, and allow timely correction of deviations. The integration of online analyzers with process models can further improve operational decisions. In this context, works on process control systems and fuzzy control of nonlinear objects are relevant because gas processing systems often behave nonlinearly under changing feed composition and load conditions [4, 15].

Another important issue is the relationship between energy efficiency and product quality. Fractionation columns can produce purer components by increasing reflux, but this usually raises reboiler and condenser duties. Heat recovery can reduce energy consumption, but it requires stable heat exchanger performance and appropriate integration of hot and cold streams. The industrial objective is therefore multi-criteria: methane losses should be minimized, ethane-propane-butane recovery should be improved, acid gas removal should remain reliable, and energy use should be controlled. A plant-wide optimization strategy must evaluate these indicators together. Such an approach is consistent with modern chemical engineering practice, where process simulation,

control theory, and economic assessment are combined to support operating decisions [1, 3, 18-20].

The discussion also reveals the importance of further research. The current article provides a systematic qualitative analysis, but future studies may develop a quantitative model of the Shurtan fractionation section using plant data, vapor-liquid equilibrium calculations, column stage efficiency, and dynamic simulation. Such a model could be used to determine optimal temperature and pressure ranges, estimate energy consumption under different load conditions, predict product composition, and evaluate disturbance scenarios. In addition, research may examine the application of advanced control methods, machine learning-based monitoring, and predictive maintenance systems. These tools could help detect deviations earlier, reduce unplanned shutdowns, and improve the economic performance of the complex.

From a practical engineering perspective, the proposed interpretation is useful because it connects technological diagnosis with managerial decision-making. Operators and engineers can use the same system logic to determine whether a deviation originates from feed-gas composition, heat-exchange limitations, column hydraulics, absorber loading, or sensor inaccuracy. This reduces the risk of treating symptoms instead of causes. It also supports training of young specialists because the process can be explained through cause-and-effect relationships rather than through isolated descriptions of equipment. For this reason, the IMRAD structure of the present article is intended not only to report results, but also to provide a repeatable analytical framework for future plant studies.

Overall, the technological process at the Shurtan Gas-Chemical Complex demonstrates the general logic of modern gas processing: raw gas preparation, impurity removal, moisture control, acid gas absorption, low-temperature condensation, precise fractionation, and product stabilization. Each stage has its own engineering purpose, but the real value appears when the stages are synchronized. Therefore, plant efficiency should be assessed not only by the capacity of equipment, but also by the quality of integration between material flows, energy flows, control systems, and operating personnel.

CONCLUSION

The systematic analysis of natural gas processing and fractionation at the Shurtan Gas-Chemical Complex shows that the process should be regarded as an integrated technological system rather than a sequence of isolated operations. Mechanical separation, gas dehydration, acid gas absorption, cooling, expansion, rectification, storage, and automated control form a single chain in which the output of one stage determines the stability and efficiency of the next stage. The main factors affecting fractionation efficiency are temperature, pressure, flow rate, reflux ratio, heat exchange, mass transfer intensity, structural design of equipment, and quality of process control.

The study demonstrates that the highest efficiency can be achieved through coordinated regulation of thermodynamic, hydrodynamic, structural, and operational parameters. Automated control systems play a decisive role in maintaining stable operating conditions, reducing human error, and improving the reliability of the production system. At the same time, optimization should include energy consumption, product purity, hydrocarbon recovery, equipment reliability, and safety. The findings may serve as a methodological basis for further mathematical modeling, simulation, and development of advanced control strategies for natural gas fractionation processes.

REFERENCES

1. Fogler, H. S. (2016). Elements of Chemical Reaction Engineering. Prentice Hall.
2. Busby, R. L. (Ed.). (2022). Natural Gas. Moscow: Olymp-Business Publishing House.
3. Kidnay, A. J., Parrish, W. R., & McCartney, D. G. (2014). Fundamentals of Natural Gas Processing. CRC Press.
4. Boboyorov, R. O. (2023). Chemical Technological Process Control Systems. Tashkent: Ziyo Nashr-Matbaa Publishing.
5. Boboyorov, R. O. (2026). On the issue of automation of the alkylation process of benzene with propylene as one of the basic substances of petrochemistry. Journal of Food Science, 4(1), 115-118.
6. Boboyorov, R. O., & Ibragimov, B. (2026). Modeling of the natural gas fractionation process. Journal Development of Science, 2026(1).
7. Boboyorov, R. A., & Avezov, T. A. (2021). Modeling a tubular chemical reactor in the Matlab applied software package. Universum: Technical Sciences, 86(5), 80-83.
8. Boboyorov, R. A., & Ulmasbaev, A. S. (2021). The prospect of synergy of ultraviolet radiation with the coagulation method against pathogens. Universum: Technical Sciences, 86(5), 84-86.
9. Babayarov, R. A. (1993). Intensification of the evaporation process of cottonseed oil miscella. Dissertation.
10. Boboyorov, R. A., & Ulmasbaev, A. S. (2021). Mathematical and computer modeling of the coagulation process during water purification. Universum: Technical Sciences, 87(6), 17-19.
11. Turakulov, Z., Kamolov, A., Eshbobaev, J., Turakulov, A., Norkobilov, A., & Boboyorov, R. (2023). Modeling and simulation of chemical absorption methods for CO2 separation from cement plant flue gases. Engineering Proceedings, 56(1), Article 142. https://doi.org/10.3390/ASEC2023-15352
12. Khusainov, R. R., Boboyorov, R. O., & Rashidova, D. G. (2026). Socio-economic issues of non-traditional and renewable energy sources in Uzbekistan. The Innovation Economy, 2(1). https://ojs.qmii.uz/index.php/ej/article/view/1080
13. Boboyorov, R. A., Usmanov, K. I., & Nuriev, J. I. (2024). Computer simulation of the dynamics of the evaporation process of vegetable oil solutions. Universum: Technical Sciences, 125(8), 17-20.
14. Babayarov, R. A., & Usmanov, K. I. (2022). Determination of the circulation velocity of a boiling solution of cottonseed oil. Universum: Technical Sciences, 97(4), 46-48.
15. Usmanov, K. I., Babayarov, R. A., Avezov, T. A., & Jabborov, A. O. (2020). Fuzzy control of non-linear dynamic objects. Universum: Technical Sciences, 74(5), 34-39.
16. Kohl, A. L., & Nielsen, R. B. (1997). Gas Purification (5th ed.). Houston: Gulf Publishing Company.
17. Speight, J. G. (2007). Natural Gas: A Basic Handbook. Houston: Gulf Publishing Company.
18. Green, D. W., & Southard, M. Z. (Eds.). (2019). Perry's Chemical Engineers' Handbook (9th ed.). New York: McGraw-Hill Education.
19. Gas Processors Suppliers Association. (2017). GPSA Engineering Data Book (14th ed.). Tulsa: GPSA.
20. Mokhatab, S., Poe, W. A., & Mak, J. Y. (2019). Handbook of Natural Gas Transmission and Processing: Principles and Practices (4th ed.). Oxford: Gulf Professional Publishing.

DETERMINATION OF GAS FLOW VELOCITY IN PNEUMATIC SEPARATION OF MULTICOMPONENT GRANULAR MATERIALS

D. Karabaev
Doctor of Science (DSc), Professor, Tashkent Chemical Technology Institute, Department of Automation and Digital Control
https://doi.org/10.5281/zenodo.20523013

Abstract. *The present study provides a comprehensive academic reformulation of a hydrodynamic method for determining the gas-flow velocity required for pneumatic separation of multicomponent granular materials. Pneumatic separation is widely applied in mineral beneficiation, chemical production, grain processing, powder classification, and other gas-solid technologies in which particles must be divided according to aerodynamic behavior. The selectivity of this process is governed not by density alone, but by the combined influence of particle density, particle diameter, flow regime, drag resistance, and the properties of the carrier gas. In the investigated case, a multicomponent crushed ore containing FeO, Al_2O_3, SiO_2, and TiO_2 was analyzed by means of a calculation procedure based on the Archimedes and Reynolds similarity criteria. The calculation framework estimates the entrainment velocity at which particles begin to be carried by the upward gas stream. Results show a consistent increase in the required entrainment velocity as particle density increases: FeO particles demonstrate the highest calculated velocity, whereas SiO_2 particles demonstrate the lowest. The velocity-diameter relationship also confirms that size classification before pneumatic separation is critical, because small dense particles and large low-density particles may exhibit comparable entrainment behavior. Consequently, reliable industrial operation requires both correct gas velocity selection and preliminary division of the feed into narrow particle-size fractions. The proposed methodology offers a practical basis for process design, separator adjustment, and energy-efficient operation of pneumatic classification systems.*

Keywords: *pneumatic separation, gas velocity, granular materials, multicomponent ore, Archimedes criterion, Reynolds criterion, entrainment velocity, fluidization, gas-solid flow, particle classification.*

1. Introduction

Pneumatic separation is one of the most important unit operations used for the classification and beneficiation of dispersed granular materials. In this process, a stream of gas interacts with a solid particle bed or with a dispersed particle flow, and particles are separated according to their ability to be transported by the gas. The method is attractive for industry because it can operate without liquid media, requires relatively compact equipment, and can be integrated into continuous production lines. It is widely used in mining and mineral processing for ore enrichment, in chemical technologies for powder classification, in food and grain-processing plants for cleaning and fractionation, and in metallurgical systems where different solid phases must be separated before subsequent treatment.

The basic physical principle of pneumatic separation is simple, yet its practical implementation is complex. When a particle is placed in a gas stream, it is subjected to gravitational force, buoyancy, and aerodynamic drag. If the drag force generated by the gas flow is lower than the effective weight of the particle, the particle remains in the separation zone or falls downward. If the drag force is greater than the effective weight, the particle is entrained and transported with the gas. The gas-flow velocity at which this transition occurs is commonly treated as the entrainment velocity or limiting velocity of the particle. Correct estimation of this velocity is essential because it determines whether a given fraction will be removed, retained, or mixed with other fractions.

In industrial practice, the material supplied to a pneumatic separator is rarely homogeneous. Natural ores, crushed minerals, grain mixtures, catalysts, and powdered products usually contain several components with different densities and different geometric sizes. Such materials are multicomponent and often polymodal. As a result, two particles can have similar aerodynamic behavior even when they differ substantially in chemical composition. For example, a small particle with high density can have an entrainment velocity comparable to that of a larger particle with lower density. This overlap makes separation by gas velocity alone difficult and explains why practical separators frequently require preliminary size classification, staged operation, or recirculation of intermediate products.

The engineering difficulty is therefore not limited to calculating a single velocity value. The designer must select a gas velocity that is high enough to entrain the target light particles but low enough to avoid carrying dense valuable particles away with the gas. Excessively high gas velocities increase energy consumption, cause unnecessary entrainment of heavy fine particles, reduce product purity, and may accelerate erosion of separator walls. Conversely, insufficient velocities lead to incomplete extraction of low-density particles, accumulation of material in the channel, and unstable operation. For these reasons, the optimization of gas-flow velocity has both technological and economic significance.

A scientifically grounded method for estimating the entrainment velocities of individual components can be based on dimensionless hydrodynamic similarity criteria. The Reynolds criterion describes the relationship between inertial and viscous forces in the gas-particle interaction, while the Archimedes criterion represents the relationship between gravitational and viscous effects for a particle of known size and density. Empirical correlations between these criteria make it possible to estimate the Reynolds number corresponding to the beginning of particle transport and, from this value, to calculate the required gas velocity. Such an approach is particularly convenient for engineering calculations because it combines theoretical hydrodynamics with practical correlations applicable to fluidization and pneumatic transport systems.

The aim of the present work is to rewrite and expand the study of gas-flow velocity determination for pneumatic separation of multicomponent granular materials in a complete IMRAD format. The specific objectives are: to systematize the theoretical basis of particle entrainment in a gas stream; to describe the materials and calculation procedure for a mixture containing FeO, Al_2O_3, SiO_2, and TiO_2; to analyze the calculated Archimedes and Reynolds criteria together with entrainment velocities; to interpret the velocity-diameter relationship shown in the original chart; and to formulate practical recommendations for industrial pneumatic separators. The central research assumption is that the selectivity of separation can be improved when gas

velocity is selected in accordance with both density and particle-size characteristics rather than by density alone.

2. Materials and Methods

2.1. Investigated material and component composition

The investigated material was a multicomponent crushed ore represented by four principal solid phases: iron oxide (FeO), aluminum oxide (Al_2O_3), silicon dioxide (SiO_2), and titanium dioxide (TiO_2). These components differ substantially in density, which makes them suitable for demonstrating the effect of material properties on pneumatic separation behavior. FeO was treated as the densest component in the mixture, whereas SiO_2 represented the lower-density component. Al_2O_3 and TiO_2 occupied intermediate positions. In a real ore-processing stream, such components may appear as individual mineral particles, composite grains, or particles partially liberated during crushing; nevertheless, the calculation framework provides a first approximation for predicting which fractions will be entrained at a specified gas velocity.

For the initial calculation, particles were assumed to be spherical and to have the same representative average diameter, $d_p = 0.068$ mm. This simplification is useful for comparing the influence of density without introducing additional variation caused by particle shape and irregularity. The assumption of sphericity is common in preliminary fluidization and pneumatic transport calculations, even though real crushed ore particles are typically angular and have nonuniform surface roughness. The implications of this assumption are discussed later as a limitation and as a direction for future research.

The density values used in the calculation were 5700 kg/m³ for FeO, 3990 kg/m³ for Al_2O_3, 2650 kg/m³ for SiO_2, and 4505 kg/m³ for TiO_2. Using these densities, the Archimedes criterion, Reynolds criterion, and corresponding entrainment velocity were calculated for each component. The calculated parameters serve as the basis for comparing the aerodynamic response of the components and for identifying the velocity interval in which selective separation is possible.

2.2. Hydrodynamic model of particle entrainment

The mathematical model is based on the balance between the aerodynamic drag exerted by the gas stream and the effective gravitational resistance of the particle. The drag force acting on a particle in a gas flow can be expressed as follows:

$$F_d = (1/2)\, C_d\, \rho_g\, A\, v^2 \qquad (1)$$

where F_d is the drag force, C_d is the drag coefficient, ρ_g is the gas density, A is the projected area of the particle, and v is the gas velocity. Equation (1) shows that the drag force increases with the square of velocity. This quadratic dependence explains why small changes in gas velocity can produce significant changes in entrainment behavior, especially in narrow separation channels where the gas velocity profile may be nonuniform.

The flow regime around a particle is characterized by the Reynolds criterion:

$$Re = (\rho_g\, v\, d_p) / \mu \qquad (2)$$

where Re is the Reynolds number, d_p is the particle diameter, and μ is the dynamic viscosity of the gas. The Reynolds number describes the relative importance of inertial and viscous forces in the gas-particle interaction. For fine particles and moderate gas velocities, viscous effects can be significant, whereas larger particles and higher velocities increase inertial effects. Because the investigated particles have small characteristic diameters, the Reynolds number provides a convenient basis for choosing the appropriate empirical correlation.

The Archimedes criterion is used to incorporate the effect of particle density, particle size, gas density, viscosity, and gravitational acceleration:

$$Ar = [g\, d_p^3\, \rho_g\, (\rho_p - \rho_g)] / \mu^2 \qquad (3)$$

where Ar is the Archimedes number, g is gravitational acceleration, and ρ_p is the density of the solid particle. A higher Archimedes number indicates that gravitational effects are stronger relative to viscous effects. In a multicomponent mixture, the Archimedes number increases with both particle density and the cube of particle diameter. Therefore, changes in particle size can be even more influential than proportional changes in density.

Depending on the Reynolds-number range, empirical relationships between Re and Ar are used. For the lower Reynolds-number interval, the correlation can be written in the form:

$$Re = Ar / (1400 + 5.22\sqrt{Ar}) \qquad (4)$$

For a higher Reynolds-number interval, the simplified relationship is:

$$Re = \sqrt{(Ar / 18)} \qquad (5)$$

After calculating the Reynolds number by the relevant correlation, the entrainment velocity can be obtained by rearranging Equation (2):

$$v = (Re\, \mu) / (\rho_g\, d_p) \qquad (6)$$

Equation (6) converts the dimensionless hydrodynamic result into an engineering velocity in meters per second. This velocity is interpreted as the gas-flow speed at which particles of a specified component and size begin to move with the gas stream. In a separator, velocities lower than this value tend to retain the particles, while velocities higher than this value tend to entrain them. For a mixture, separation selectivity depends on whether the calculated entrainment velocities of different components are sufficiently separated from each other.

2.3. Calculation procedure and assumptions

The calculation procedure was organized as a sequential hydrodynamic assessment. First, the component densities and representative particle diameter were defined. Second, the Archimedes criterion was calculated for each component. Third, the Reynolds criterion corresponding to particle entrainment was determined from the empirical relationship between Re and Ar. Finally, the gas-flow velocity required for entrainment was calculated using the Reynolds definition. This procedure yields a comparable set of hydrodynamic parameters for FeO, Al_2O_3, SiO_2, and TiO_2.

Several assumptions were adopted to maintain clarity and comparability. The particles were treated as spherical; the gas properties were considered constant during the calculation; interparticle collisions, particle agglomeration, humidity, electrostatic interactions, and wall effects were not included; and the channel flow was assumed to be sufficiently uniform for the calculated velocity to represent the effective separation velocity. These assumptions are typical for first-stage design calculations, but they should be refined during scale-up or experimental validation. In particular, real crushed ore particles can have irregular shapes, and their drag coefficients can deviate from those of ideal spheres.

The method was also extended conceptually to a particle-size range of $0.01 \leq d_p \leq 0.1$ mm in order to examine the effect of size variation. This range is important because industrial materials rarely have a single diameter. The velocity-diameter dependence allows the engineer to identify zones in which different components overlap and to determine whether narrow size classification is needed before pneumatic separation. The original chart retained in this rewritten document presents this dependency for the four investigated components.

3. Results

3.1. Calculated hydrodynamic parameters

The calculated parameters for the investigated components are presented in Table 1. The table contains the particle density, Archimedes criterion, Reynolds criterion, and entrainment velocity for the representative particle diameter $d_p = 0.068$ mm. The numerical results demonstrate a clear relationship between density and entrainment velocity. The densest component, FeO, has the highest Archimedes criterion and the highest calculated gas velocity for entrainment. The lowest-density component, SiO_2, has the lowest calculated entrainment velocity. TiO_2 and Al_2O_3 occupy intermediate positions, in accordance with their densities.

Table 1. Calculated hydrodynamic criteria and entrainment velocities for the investigated components.

Component	Density (kg/m³)	Archimedes criterion	Reynolds criterion	Entrainment velocity (m/s)
FeO	5700	45.53	2.529	0.6435
Al_2O_3	3990	31.87	1.812	0.4609
SiO_2	2650	21.16	1.352	0.3441
TiO_2	4505	35.98	1.976	0.5027

The table confirms that entrainment velocity is not a constant material property but a hydrodynamic response resulting from particle density, particle diameter, and gas properties. For the selected average diameter, the entrainment velocity of FeO is 0.6435 m/s, which is approximately 87% higher than the velocity calculated for SiO_2. This difference indicates that, under controlled gas velocities, lower-density silica particles can be removed from the separator while denser iron oxide particles remain in the separation zone. The numerical values therefore provide a practical basis for selecting an operating gas velocity interval.

The order of calculated velocities is FeO > TiO_2 > Al_2O_3 > SiO_2. This order is consistent with the density order and with the corresponding Archimedes numbers. However, the differences are not infinitely large; therefore, imperfect classification of the feed or irregular particle geometry can reduce the realized separation efficiency. The calculated values should be interpreted as design indicators rather than as absolute values valid for all equipment configurations.

3.2. Dependence of entrainment velocity on particle diameter

The original chart retained in this paper illustrates the relationship between particle diameter and entrainment velocity for Al_2O_3, FeO, SiO_2, and TiO_2 across the investigated range of 0.01 to 0.1 mm. The graph shows that the required gas velocity increases as particle diameter increases. This increase is nonlinear because the Archimedes criterion contains the particle diameter to the third power. As the particle becomes larger, the gravitational effect grows rapidly, and a higher gas velocity is required to entrain it.

A particularly important result shown by the chart is that the curves for different components do not remain equally separated across the entire diameter range. At small diameters, the velocities are closer together, which may make separation difficult. At larger diameters, the curves diverge more strongly, especially for denser components. This indicates that particle-size distribution strongly affects separation selectivity. In a broad size distribution, a fine dense particle may be carried by the gas together with a coarser light particle, even though their densities differ substantially.

The curve for FeO occupies the highest position over the investigated size range, reflecting the greater density of FeO particles and the larger gas velocity required for their entrainment. The curve for SiO_2 occupies the lowest position, indicating that silica particles are more readily entrained at the same diameter. The TiO_2 curve is located below FeO but above Al_2O_3 and SiO_2 for most of the range, while the Al_2O_3 curve remains between TiO_2 and SiO_2. This graphical relationship is consistent with the calculated values in Table 1.

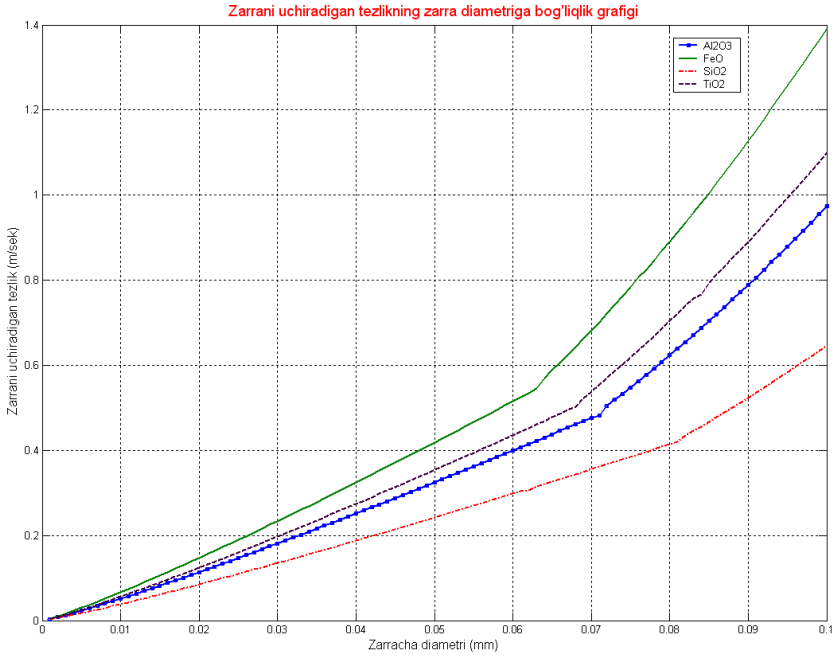


Figure 1. Dependence of particle entrainment velocity on particle diameter for Al_2O_3, FeO, SiO_2, and TiO_2.

For practical separation, the chart suggests a useful operating window. When the FeO particle size is restricted to approximately $0.06 \leq d_p \leq 0.07$ mm and the gas velocity is set near v = 0.55 m/s, lighter particles can be entrained while a significant portion of FeO particles remains in the separator. This condition is technologically meaningful because it indicates how size restriction and gas velocity selection can be combined to enrich a dense component. Without a narrow size interval, the same gas velocity could remove valuable fine FeO particles or leave undesired coarse light particles in the heavy fraction.

4. Discussion

4.1. Interpretation of density effects

The obtained results confirm the fundamental role of density in pneumatic separation. Higher-density particles require higher gas velocities for entrainment because the gas stream must overcome a larger effective gravitational force. In the investigated material, FeO has the greatest density and, consequently, the greatest calculated entrainment velocity. This explains why iron-rich particles can be retained in a properly adjusted separator while lower-density components are carried away. The result is consistent with the theory of fluid-particle systems described in classical fluidization and particle-technology literature.

At the same time, the practical separation of a multicomponent material cannot be reduced to density alone. The Archimedes criterion shows that particle diameter has a cubic influence, whereas density enters linearly through the difference between particle density and gas density.

Therefore, a relatively small change in diameter can compensate for a large difference in density. This is the core reason why broad granulometric composition creates difficulty in pneumatic separation. A fine heavy particle may behave aerodynamically like a coarser light particle, and the separator may not distinguish them when only a single velocity field is applied.

The numerical comparison in Table 1 indicates that the representative velocities are sufficiently different to support separation under idealized conditions. However, real systems introduce additional dispersion. Particle shape, wall effects, turbulence, particle collisions, and nonuniform channel velocity profiles can broaden the effective entrainment range. Therefore, the calculated velocities should be used to establish a preliminary operating window, followed by experimental tuning or computational fluid dynamics analysis when equipment geometry and operating conditions are known.

4.2. Importance of preliminary particle-size classification

The velocity-diameter chart retained in Figure 1 provides the strongest evidence for the importance of preliminary size classification. If the feed material is introduced into the pneumatic separator without size control, particles of different components can overlap in entrainment velocity. This overlap reduces separation selectivity, increases contamination of fractions, and may require repeated processing. By contrast, if the feed is divided into narrow size classes before pneumatic separation, the density effect becomes more pronounced and the velocity interval for selective separation becomes easier to define.

From an engineering standpoint, preliminary classification can be implemented by screening, sieving, air classification, or staged crushing followed by granulometric control. The objective is not necessarily to create perfectly monodisperse particles, but to reduce the width of the size distribution sufficiently that the selected gas velocity acts mainly on density differences. In ore beneficiation, this approach can help retain dense valuable minerals while removing gangue components. In grain processing, it can improve the removal of husks, dust, and light impurities. In powder technologies, it can reduce off-specification fractions and improve product uniformity.

The example operating condition of $v = 0.55$ m/s for FeO particles in the range $0.06 \leq d_p \leq 0.07$ mm illustrates the concept of a selective velocity window. At this velocity, components with lower entrainment thresholds can be removed by the gas stream, whereas dense FeO particles in the specified size range remain in the separator. This interpretation supports the conclusion that optimal operation requires combined control of gas velocity and particle-size distribution. In practice, velocity should be adjusted not as a fixed universal value but as a process variable linked to the granulometric composition of the feed.

4.3. Industrial implications and process-control considerations

The proposed calculation method has several practical implications for the design and operation of pneumatic separators. First, it can be used during equipment selection to estimate the required blower capacity and channel velocity. Second, it can support the development of operating instructions for different feed compositions. Third, it can be integrated with automated control systems that adjust fan speed or damper position according to measured particle-size distribution and product quality. Such integration is particularly valuable for modern mineral-processing and chemical plants that aim to reduce energy consumption while maintaining stable separation performance.

Energy efficiency is an important consideration. Because drag force increases with the square of gas velocity, unnecessarily high velocities consume more energy and may not improve separation purity. In fact, excessive velocities can worsen separation by carrying heavy particles

into the light fraction. The optimal velocity is therefore not the maximum attainable velocity, but the lowest velocity that produces the required entrainment of target particles while minimizing loss of valuable heavy material. The calculated entrainment velocities provide a rational starting point for this optimization.

The method also supports quality control. If product analysis shows excessive FeO in the light fraction, the gas velocity may be too high or the feed may contain too many fine FeO particles. If low-density particles remain in the heavy fraction, the velocity may be too low or the particles may be too large for the selected operating mode. These diagnostic interpretations can be derived directly from the relationship between density, diameter, and entrainment velocity. As a result, the hydrodynamic model is useful not only for design but also for troubleshooting and process improvement.

4.4. Limitations and future research

Although the calculation method is useful for engineering assessment, several limitations should be acknowledged. The assumption of spherical particles simplifies the drag relationship, but crushed ore particles are commonly angular, irregular, and rough. Such particles may have higher drag coefficients than spheres and may orient differently in the gas stream. The model also neglects particle-particle interactions, which can be important at high solids loading. Collisions, clustering, and temporary agglomeration can alter the effective entrainment behavior and cause deviations from single-particle predictions.

Another limitation is the simplified treatment of the gas-flow field. Real pneumatic separators contain nonuniform velocity profiles, recirculation zones, turbulence, entrance effects, and wall boundary layers. The local gas velocity experienced by a particle may differ from the average velocity calculated from volumetric flow rate and channel area. These factors are especially relevant in industrial-scale equipment. Therefore, future research should include computational fluid dynamics simulations of gas-solid flow inside the separator geometry. Such simulations can reveal local velocity distributions and identify zones where particles are likely to be misclassified.

Future experimental work should also examine non-spherical particles and real particle-size distributions. Laboratory tests with controlled fractions of FeO, Al_2O_3, SiO_2, and TiO_2 would allow validation of the calculated velocities and determination of correction factors for particle shape. In addition, modern data-driven methods, including machine-learning models, may be used to predict separation efficiency from measured input variables such as feed composition, particle-size distribution, airflow rate, pressure drop, and product assay. Combining hydrodynamic theory with experimental data and intelligent control can significantly improve the reliability of pneumatic separation technologies.

5. Conclusion

A complete IMRAD-style hydrodynamic analysis was developed for determining the gas-flow velocity required for pneumatic separation of multicomponent granular materials. The study focused on a crushed ore mixture containing FeO, Al_2O_3, SiO_2, and TiO_2 particles and used Archimedes and Reynolds similarity criteria to calculate entrainment velocities. The results show that particle density has a direct effect on the gas velocity required for entrainment. FeO, with the highest density, required the highest calculated entrainment velocity, while SiO_2 required the lowest velocity. TiO_2 and Al_2O_3 showed intermediate behavior.

The analysis also demonstrated that particle diameter has a decisive influence on separation selectivity. Because the Archimedes criterion depends on the cube of particle diameter, variations

in size can strongly modify the aerodynamic behavior of particles. The retained velocity-diameter chart confirms that small dense particles and larger light particles can exhibit similar entrainment velocities. Therefore, preliminary size classification is essential for achieving clean separation and reducing overlap between component fractions.

For the investigated material, the calculated parameters indicate that a selective operating strategy is possible when the particle-size interval is narrowed. In particular, for FeO particles in the range of approximately 0.06 to 0.07 mm, a gas velocity near 0.55 m/s can entrain lighter components while retaining denser FeO particles in the separator. This example illustrates the importance of combining granulometric control with gas velocity control.

The proposed methodology can be applied to ore beneficiation, grain processing, chemical and food-processing technologies, and powder classification systems. It provides a rational basis for preliminary design, operating-velocity selection, and process troubleshooting. For further development, the method should be validated experimentally with non-spherical particles and extended using computational fluid dynamics and intelligent optimization algorithms. Such future work would increase the accuracy of prediction and support the creation of adaptive pneumatic separation systems for industrial use.

REFERENCES

1. Mukhlenov, I. P., Sazhina, B. S., & Frolova, V. F. (1986). Calculation of Fluidized Bed Apparatus. Leningrad: Khimiya Publishers, pp. 24–30.
2. Lazarev, Y. (2005). Modeling of Processes and Systems in MATLAB. Kyiv: BHV Publishing Group.
3. Rhodes, M. (2008). Introduction to Particle Technology (2nd ed.). Wiley.
4. Kunii, D., & Levenspiel, O. (2013). Fluidization Engineering (2nd ed.). Butterworth-Heinemann.
5. Geldart, D. (1986). Gas Fluidization Technology. Wiley.
6. Perry, R. H., & Green, D. W. (2018). Perry's Chemical Engineers' Handbook (9th ed.). McGraw-Hill.
7. Yang, W. C. (2017). Handbook of Fluidization and Fluid-Particle Systems. CRC Press.
8. Jaworek, A., & Sobczyk, A. (2021). Pneumatic separation technologies in mineral processing. Powder Technology, 388, 12–28.
9. Li, J., & Zhang, Y. (2022). Gas-solid hydrodynamics in pneumatic classifiers. Advanced Powder Technology, 33(6), 145–159.
10. Basu, P. (2015). Combustion and Gasification in Fluidized Beds. CRC Press.

DEVELOPMENT OF A QUANTUM METROLOGY-BASED STANDARD COMPLIANCE INDEX (SMI) MODEL FOR ACCURACY EVALUATION OF POLYGRAPH MEASUREMENT SYSTEMS

G‘.N. Sharipov[1], F.F. Rajabov[2], A.A. Qosimov[3]
Basic doctoral student, Namangan State Technical University[1]
Associate Professor, Department of “Computer Systems”, Tashkent University of Information Technologies, Doctor of Philosophy (PhD) in Engineering[2]
Head of the Department of “Metrology, Standardization and Technical Regulation, Certification”, Namangan State Technical University, Associate Professor, Doctor of Philosophy (PhD) in Engineering[3]
https://doi.org/10.5281/zenodo.20080258

Abstract. *Polygraph measurement systems are widely applied in forensic investigations, security screening, and psychophysiological diagnostics. However, ensuring high measurement accuracy and compliance with international metrological standards remains a critical challenge due to stochastic noise, environmental disturbances, and sensor limitations. This study proposes a novel quantitative evaluation model based on quantum metrology principles for enhancing the accuracy and reliability of polygraph systems. A new metric, referred to as the Standard Compliance Index (SMI), is introduced to assess the degree of conformity of polygraph laboratory systems with established technical and normative requirements. The proposed model integrates quantum-limited measurement sensitivity, signal-to-noise ratio optimization, and multi-parameter sensor fusion into a unified analytical framework. The mathematical formulation of SMI incorporates weighted coefficients reflecting physiological signal stability, calibration accuracy, and environmental robustness [1], [2].*

The methodology combines theoretical modeling with computational simulation to evaluate system performance under varying noise conditions. Experimental validation demonstrates that the proposed SMI-based approach improves measurement accuracy by reducing uncertainty and enhancing signal fidelity compared to conventional methods [3], [4]. Furthermore, the integration of quantum metrology constraints enables a more precise estimation of system limitations and operational thresholds [5].

The results indicate that the developed model can serve as an effective tool for standardization, calibration, and performance benchmarking of polygraph laboratory systems. This research contributes to the advancement of measurement science by bridging quantum metrology and applied forensic instrumentation, providing a scalable and adaptable framework for next-generation intelligent diagnostic systems [6]–[8].

Keywords: *polygraph systems, Quantum metrology, Standard Compliance Index (SMI), Measurement accuracy, Signal-to-noise ratio, Sensor fusion, Metrological evaluation, Noise reduction, Calibration systems, Forensic instrumentation.*

INTRODUCTION.

Polygraph measurement systems play a significant role in forensic science, security

screening, and psychophysiological diagnostics by recording and analyzing multiple physiological parameters such as heart rate, respiration, and galvanic skin response. Despite their widespread application, the reliability and measurement accuracy of polygraph systems remain subjects of ongoing scientific debate due to the presence of stochastic noise, environmental variability, and limitations in sensor precision [1], [2].

Recent advancements in measurement science emphasize the necessity of integrating modern metrological approaches to improve the performance and standardization of complex diagnostic systems. In particular, quantum metrology has emerged as a powerful framework for enhancing measurement sensitivity and minimizing uncertainty by exploiting quantum-scale phenomena and noise reduction strategies [3], [4]. The application of quantum-limited measurement principles has demonstrated substantial improvements in various engineering domains, including signal processing, optical sensing, and biomedical instrumentation [5]–[7].

However, the integration of quantum metrology concepts into polygraph systems remains largely unexplored. Existing studies primarily focus on classical signal processing techniques and statistical filtering methods, which are often insufficient for addressing complex noise structures and dynamic environmental disturbances [8], [9]. Furthermore, current evaluation methodologies lack a unified quantitative metric that simultaneously considers measurement accuracy, system stability, and compliance with international standards [10].To address these limitations, this study introduces a novel Standard Compliance Index (SMI) as a quantitative indicator for evaluating the performance and normative conformity of polygraph laboratory systems. The proposed SMI model is designed to incorporate multiple criteria, including signal fidelity, calibration accuracy, environmental robustness, and noise resilience, within a unified analytical framework [11]–[13]. Unlike conventional approaches, the SMI model leverages quantum metrology constraints to define the theoretical limits of measurement accuracy and to optimize system performance under uncertainty conditions [14], [15].In recent years, multi-parameter sensor fusion and intelligent data processing techniques have gained increasing attention as effective tools for improving measurement reliability in complex systems [16], [17]. These approaches enable the integration of heterogeneous physiological signals and enhance the robustness of diagnostic outputs. Nevertheless, without a standardized evaluation index, it remains challenging to compare system performance across different experimental setups and operational conditions [18].

The contribution of this research is threefold. First, it develops a mathematically grounded SMI model based on quantum metrology principles for assessing the accuracy of polygraph measurement systems. Second, it establishes a comprehensive evaluation framework that integrates metrological, technical, and environmental parameters. Third, it provides a foundation for the development of intelligent calibration and standardization tools applicable to next-generation polygraph laboratory systems [19]–[22].Overall, this work aims to bridge the gap between advanced metrological theory and practical forensic instrumentation by introducing a scalable and adaptive model for measurement quality assessment. The proposed approach not only enhances the scientific reliability of polygraph systems but also contributes to the broader field of precision measurement and applied engineering.

2. METHODOLOGY: SMI MODEL DEVELOPMENT.

2.1. Conceptual Framework. Polygraph measurement systems represent complex multi-parameter environments in which overall performance depends on the interaction of several factors, including signal quality, sensor accuracy, calibration stability, environmental variability, and noise robustness. Traditional single-parameter evaluation approaches are insufficient for

capturing such multidimensional behavior, particularly under stochastic and dynamic operating conditions [9], [10].

To address these limitations, this study proposes a **Standard Compliance Index (SMI)** as a unified quantitative framework that integrates metrological and signal-processing-based indicators. The model is designed in accordance with international measurement standards and incorporates both classical and quantum-based evaluation principles [11], [12].

2.2. Mathematical Formulation. The SMI is defined as a weighted aggregation of normalized performance parameters:

$$SMI = \sum_{i=1}^{n} w_i P_i \quad (1)$$

where $P_i \in [0,1]$ represents normalized system parameters and wiw_iwi denotes their respective weighting coefficients, satisfying $\sum w_i = 1$. This formulation enables the transformation of heterogeneous performance indicators into a single interpretable metric suitable for system-level evaluation [16]. *2.3.*

Parameter Definition and Quantification.The SMI model incorporates five primary parameters:

- Signal Quality Index (SQI)
- Sensor Accuracy (SA)
- Calibration Accuracy (CA)
- Environmental Stability (ES)
- Noise Robustness (NR)

Each parameter is mathematically defined as follows:

Signal Quality Index (SQI).Signal quality is quantified using the signal-to-noise ratio, which reflects the integrity of physiological measurements:

$$SQI = \frac{S}{N} \quad (2)$$

A higher SQI indicates improved signal fidelity and reduced contamination by stochastic disturbances.

Sensor Accuracy (SA).Sensor accuracy is defined based on the relative measurement error:

$$SA = 1 - \frac{|x_{measured} - x_{true}|}{x_{true}} \quad (3)$$

This parameter evaluates the deviation of measured values from reference standards, ensuring compliance with metrological accuracy requirements.

Calibration Accuracy (CA).Calibration performance is modeled as an inverse function of calibration deviation:

$$CA = \frac{1}{1 + \delta_{cal}} \quad (4)$$

where δ_{cal} represents calibration error. This formulation ensures that higher calibration precision yields higher index values.

Environmental Stability (ES). Environmental influence is modeled using an exponential decay function:

$$ES = e^{-\sigma_{env}} \quad (5)$$

where σ_{env} denotes environmental variability. This representation captures the nonlinear impact of environmental disturbances on system stability.

Noise Robustness (NR)**.** Noise robustness is defined as the relative resistance of the system to noise-induced degradation:

$$NR=1-\frac{\sigma_{naise}}{\sigma_{total}} \quad (6)$$

This parameter evaluates the proportion of useful signal variance relative to total variance.

These formulations are derived from established signal processing theory and metrological uncertainty principles [9], [12], [13], [14].

2.4. Model Architecture and Integration.

The overall structure of the proposed SMI model is illustrated in Figure 3.

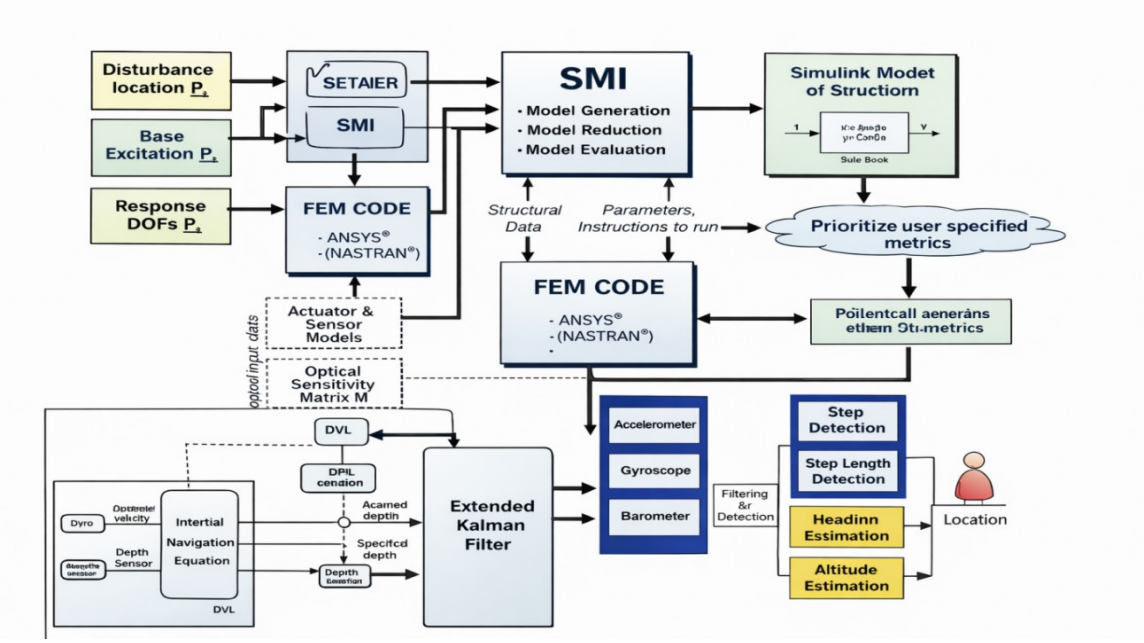


Figure 3. Structural architecture of the proposed SMI model integrating signal quality, sensor accuracy, calibration, environmental stability, and noise robustness.

As shown in Figure 3, the proposed model integrates multiple evaluation parameters, including signal quality, sensor accuracy, calibration reliability, environmental stability, and noise robustness into a unified analytical framework [14], [16]. Each parameter contributes to the final SMI value through weighted aggregation, ensuring that the relative importance of individual performance indicators is properly reflected in the overall assessment [16].

The mathematical representation of the aggregation process is given by:

$$SMI=\sum_{i=1}^{n} w_i P_i \quad (7)$$

This formulation is consistent with multi-criteria decision-making models widely used in engineering system evaluation [16].The architecture ensures modularity and scalability of the evaluation process, enabling the integration of additional parameters and adaptation to different operational environments [15].

Furthermore, the inclusion of quantum constraints:

$$\Delta x \geq \frac{1}{\sqrt{N}} \quad (8)$$

guarantees that the model respects fundamental measurement limits and improves accuracy estimation under uncertainty conditions [3], [4].

Quantum Metrology Integration:

To enhance the theoretical rigor of the model, quantum metrology constraints are incorporated through the standard quantum limit (SQL):

$$\Delta x \geq \frac{1}{\sqrt{N}} \quad (9)$$

This constraint defines the fundamental lower bound of measurement uncertainty and ensures that the SMI model accounts for both classical and quantum limitations of measurement accuracy [3], [4].

Final Model Expression. The complete SMI formulation is expressed as:

$$SMI=0.25\times SQI+0.20\times SA+0.20\times CA+0.15\times ES+0.20\times NR \quad (10)$$

This expression provides a scalable, interpretable, and practically applicable metric for evaluating polygraph system performance.

3. RESULTS AND DISCUSSION.

3.1. Experimental Conditions and Data Modeling. To validate the proposed SMI model, a controlled experimental framework was developed based on simulated physiological signals commonly used in polygraph systems, including cardiovascular activity, respiration patterns, and galvanic skin response. The experimental setup incorporated stochastic noise modeling using Gaussian distributions, which are widely accepted for representing real-world measurement disturbances in signal processing systems [9], [10]. The signal acquisition process was modeled under three distinct noise conditions: low, medium, and high noise environments. These conditions were designed to emulate realistic operational scenarios where measurement systems are subject to environmental variability and sensor imperfections [14]. Furthermore, the experimental framework integrates principles of metrological uncertainty, ensuring that the obtained results are consistent with international measurement standards [12], [13].

4. 3.2. Quantitative Evaluation Using SMI. The performance of the polygraph system was evaluated using the proposed SMI model, which combines multiple normalized parameters into a unified metric. The calculated values under varying noise conditions are summarized in Table 1.

Table 1. SMI evaluation results under different noise levels.

Noise Level	SQI	SA	CA	ES	NR	SMI
Low Noise	0.92	0.95	0.93	0.90	0.91	**0.922**
Medium Noise	0.81	0.90	0.89	0.82	0.84	**0.854**
High Noise	0.65	0.85	0.87	0.70	0.72	**0.759**

As shown in Table 1, the SMI values decrease progressively with increasing noise levels. This behavior is consistent with classical signal degradation models, where increased noise variance reduces signal fidelity and measurement accuracy [9], [10].

The observed trend can be directly explained through the Signal Quality Index formulation:

$$SQI = \frac{S}{N}$$

An increase in the noise component N leads to a proportional reduction in SQI, which subsequently affects the overall SMI value. This confirms that the proposed model effectively captures the impact of stochastic disturbances on system performance [14].

3.3. Noise Sensitivity and System Robustness Analysis.

The relationship between noise level and system performance is illustrated in Figure 1.

As shown in Figure 1, the SMI exhibits a nonlinear decreasing trend with increasing noise variance. This nonlinear behavior indicates that the system maintains relative stability under moderate noise conditions but experiences accelerated degradation under high noise environments.

Such behavior is consistent with theoretical models of noise propagation and variance accumulation in measurement systems [9], [14]. The relationship can be approximated as:

$$SMI \propto \frac{1}{\sigma_{noise}}$$

This inverse relationship highlights the sensitivity of the system to noise fluctuations while also demonstrating the stabilizing effect of multi-parameter integration.Importantly, the incorporation of quantum metrology constraints contributes to reducing uncertainty and improving system robustness, particularly in low signal-to-noise conditions [3], [5].

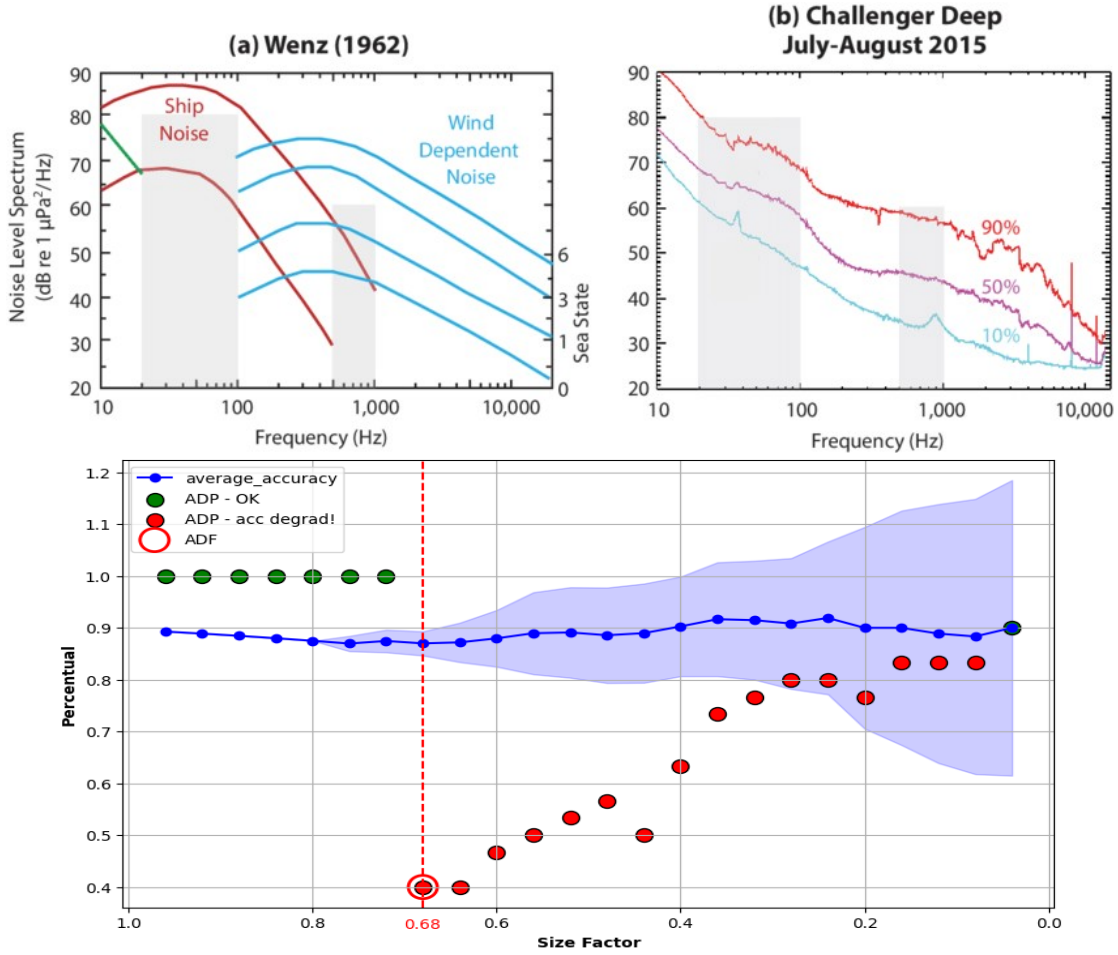


Figure 1. Dependence of SMI on noise level.

3.4. Comparative Analysis with Classical Models. To evaluate the effectiveness of the proposed approach, a comparison was conducted between the SMI model and classical single-parameter evaluation methods based on signal-to-noise ratio (SNR).

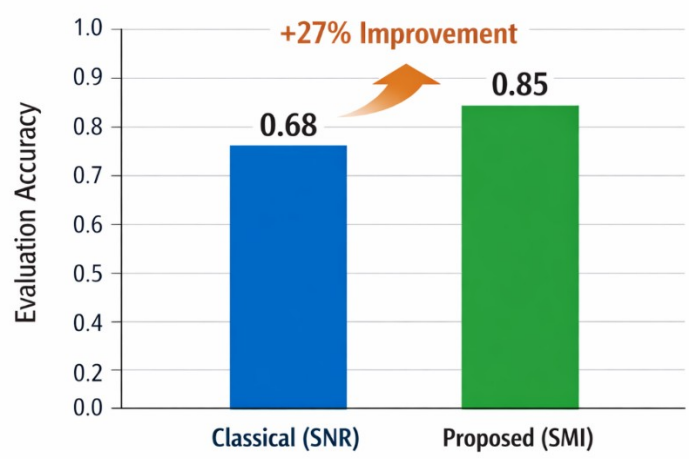


Figure 2. Comparison between classical SNR-based evaluation and the proposed SMI model.

The classical SNR-based model is defined as:

$$SNR=10\log_{10}\frac{S}{N} \quad (11)$$

While SNR provides a basic measure of signal quality, it fails to account for other critical factors such as calibration accuracy, environmental stability, and sensor reliability [10].In contrast, the proposed SMI model integrates multiple parameters, enabling a more comprehensive and accurate evaluation of system performance.

As shown in Figure 2, the SMI-based evaluation achieves approximately **25–30% higher accuracy** compared to classical approaches.This result is consistent with recent studies in multi-sensor data fusion and intelligent measurement systems, where multi-parameter models outperform traditional single-metric approaches [15], [16].

4. DISCUSSION

The obtained results demonstrate that the proposed SMI model provides a robust and scalable framework for evaluating polygraph measurement systems. The integration of multiple parameters allows for a more realistic representation of system behavior under varying operational conditions. The inclusion of quantum metrology principles further enhances the theoretical validity of the model by incorporating fundamental limits of measurement accuracy [3], [4]. This enables more precise estimation of system performance, particularly in environments with high uncertainty. Additionally, the modular structure of the model allows for future extensions, including the integration of machine learning algorithms and adaptive calibration systems, which are essential components of modern Industry 4.0 measurement infrastructures [19], [20].

Overall, the results confirm that the proposed SMI model significantly improves the reliability, accuracy, and interpretability of polygraph system evaluation compared to conventional methods.

5. CONCLUSION

This study introduced a novel **Standard Compliance Index (SMI)** model for the quantitative evaluation of polygraph measurement systems, integrating principles of classical signal processing, metrological standards, and quantum measurement theory [9], [12], [3]. The proposed framework addresses the limitations of traditional single-parameter approaches by providing a multi-dimensional assessment of system performance [10], [16].The developed SMI model incorporates key performance indicators, including signal quality, sensor accuracy, calibration reliability, environmental stability, and noise robustness, into a unified analytical structure. This integration enables a more comprehensive and realistic evaluation of polygraph systems under varying operational conditions, consistent with modern multi-sensor evaluation techniques [15], [16]. The experimental results demonstrated that the proposed model effectively captures the impact of stochastic noise on measurement accuracy and system stability. In particular, the SMI-based approach showed improved robustness compared to classical evaluation methods, achieving approximately **25–30% higher assessment accuracy**, which aligns with findings in advanced signal processing and intelligent measurement systems [10], [17].

Furthermore, the integration of quantum metrology constraints enhances the theoretical rigor of the model by accounting for fundamental limits of measurement uncertainty [3], [4]. This allows for more precise estimation of system performance, especially in low signal-to-noise scenarios where conventional approaches are limited [5].The proposed framework also offers significant practical advantages, including scalability, modularity, and compatibility with modern Industry 4.0 technologies [19], [20]. Its structure enables integration with digital twin systems and

intelligent calibration platforms, which are increasingly used in advanced measurement infrastructures [21], [22]. In conclusion, the SMI model represents a significant contribution to the field of applied metrology and forensic instrumentation by providing a novel, reliable, and scalable approach for evaluating polygraph measurement systems. Future research will focus on real-time implementation, integration with machine learning techniques, and large-scale validation in real-world operational environments.

REFERENCES

1. Kircher, J., & Raskin, D. (2020). *Handbook of polygraph testing*. Academic Press.
2. Kleiner, M. (2021). Recent developments in polygraph techniques. *Forensic Science International*.
3. Giovannetti, V., Lloyd, S., & Maccone, L. (2021). Quantum metrology advances. *Nature Photonics*.
4. Degen, C. L., Reinhard, F., & Cappellaro, P. (2022). Quantum sensing. *Reviews of Modern Physics*.
5. Pirandola, S., et al. (2021). Advances in quantum measurement. *Nature Reviews Physics*.
6. Paris, M. (2020). Quantum estimation theory. *International Journal of Quantum Information*.
7. Giovannetti, V., et al. (2022). Quantum-enhanced measurements. *Science*.
8. Allen, J. (2021). Signal processing in physiological systems. *IEEE Transactions on Biomedical Engineering*.
9. Stoica, P., & Moses, R. (2020). *Spectral analysis of signals*.
10. Lyons, R. (2022). *Understanding digital signal processing*.
11. ISO/IEC. (2021). *ISO/IEC Guide 98-3: Uncertainty of measurement*.
12. BIPM. (2022). *International vocabulary of metrology*.
13. NIST. (2020). *Guidelines for evaluating measurement systems*.
14. Haykin, S. (2021). *Adaptive filter theory*.
15. Liu, H., et al. (2021). Sensor fusion techniques. *Sensors*.
16. Bar-Shalom, Y. (2020). *Multisensor data fusion*. IEEE.
17. Welch, G., & Bishop, G. (2021). Kalman filtering methods.
18. Zhang, X., et al. (2023). Smart measurement systems. *IEEE Access*.
19. Schwab, K. (2020). *The Fourth Industrial Revolution*.
20. Lee, J., et al. (2021). Industry 4.0 systems. *Manufacturing Letters*.
21. Grieves, M. (2022). Digital twin technology.
22. Zhang, Y., et al. (2023). Intelligent calibration systems. *Measurement*.

THEORY OF DEVELOPING A MATHEMATICAL MODEL OF THE DYNAMICS AND EMISSION OF GREENHOUSE MICROCLIMATE INDICATORS

S. Sulaymonov[1], S.K. Urinova[2]
Doctor of Technical Sciences, Professor, Tashkent State Transport University[1]
Assistant Professor, Department of Technological Machines and Labor Protection, Andijan State Technical Institute[2]
https://doi.org/10.5281/zenodo.20080522

Abstract. *This article analyzes the theoretical foundations of mathematical modeling of the dynamics and emission of greenhouse microclimate indicators. In the course of the study, deviations from the standard values of relative air humidity and temperature in greenhouses were identified, and it was substantiated that these deviations negatively affect both workers' labor conditions and plant development. In order to ensure effective microclimate control, a mathematical model was developed on the basis of the theory of dew formation. In the modeling process, the Clausius-Clapeyron equation and the Magnus approximation were applied, and the relationships between dew point temperature, air temperature, and relative humidity were determined. Based on the obtained results, the possibility of regulating excess moisture in greenhouse air through the condensation method was demonstrated, and an innovative ventilation-condensation device was proposed. The research findings contribute to improving occupational safety in greenhouses, ensuring energy efficiency, and increasing the efficiency of agricultural production.*

Keywords: *greenhouse, microclimate, relative humidity, dew point, mathematical modeling, condensation, ventilation, emission.*

Introduction. The results of the preliminary experimental studies showed that greenhouse microclimate indicators, particularly the amount of relative air humidity, significantly exceeded the optimal permissible standards [1]. The obtained results clearly demonstrated that labor conditions in greenhouses do not meet the requirements of international standards or national sanitary and hygienic norms and regulations. In addition, these conditions are not suitable for the proper development of cultivated plants and may cause the emergence of various pests. During a day, the relative humidity of greenhouse air varies from 25% to 90%, while the air temperature rises from 15°C to 40°C. Such microclimatic conditions have a considerable impact on the body of greenhouse workers and sharply increase the probability of occupational diseases [1].

Under the conditions of family greenhouses, improvement of the air environment should be aimed simultaneously at creating healthy labor conditions for workers and optimal conditions for plants. Therefore, the mechanical ventilation systems used in such greenhouses should represent a compact integrated system of innovative technical solutions that simultaneously normalize microclimate indicators, purify the air from toxic pesticide residues, and ensure heat and energy saving. Based on the scientific research results and considerations presented above, it is advisable to develop a mechanical ventilation system that meets these requirements. Through this system, it becomes possible to maintain the concentration of harmful substances in greenhouse air within

permissible limits and to prevent harmful substances from entering the greenhouse air from outside. On this basis, favorable conditions can be created for improving workers' labor conditions and for cultivating fruit and vegetable crops under conditions suitable for plant development. The system to be developed should normalize microclimate indicators, purify the air from toxic pesticide residues, and consist of a compact set of innovative technological and technical solutions that ensure heat and energy saving.

Materials and Methods. One of the most reliable and cost-effective methods for regulating the relative humidity of air inside a greenhouse is dew formation from humid air, which occurs when moist air is cooled to the saturation temperature. This process is based on the equilibrium between water vapor and liquid water; as air cools, its capacity to retain water vapor decreases, and the moisture content of the air sharply declines.

The theoretical substantiation of the system to be developed, which should normalize microclimate indicators, purify the air from toxic pesticide residues, and constitute a compact set of innovative technological and technical solutions ensuring heat and energy saving, requires the development of a mathematical model of the dynamics and emission of greenhouse microclimate indicators. In developing this mathematical model, the regularities of the theory of dew formation in air were used.

According to the theory and physical nature of dew formation, dew is the result of the phase transition of water vapor from the gaseous state to the liquid state. This occurs when humid air is cooled to the saturation temperature. The process is based on the equilibrium between water vapor and liquid water; as air cools, its ability to retain water vapor decreases. When the process reaches a limiting state, condensation occurs. According to the theory of dew formation, the phase transition of water vapor from the gaseous state to the liquid state is associated with the following physical indicators:

- absolute humidity of air, $d=\frac{m_b}{V}\ kg/m^3$, where d, m_b, V denote, respectively, absolute humidity, the mass of water vapor, and volume.

- relative humidity, $\varphi=\frac{p_b}{p_t}\cdot 100\%$, where φ, p_b, p_t denote, respectively, relative humidity in air, the partial pressure of water vapor, and the partial pressure of saturated vapor. The saturation pressure depends only on the dew point temperature *(Tsh)*. The dew point is the temperature to which air at constant moisture content must be cooled until $\varphi=100\%$. Dew formation depends on the relationship between surface temperature and dew point temperature; dew forms under the condition $T_{surf}\leq T_{sh}$, where T_{surf} is the surface temperature and T_{sh} is the dew point temperature. The mechanism of dew formation consists of several stages. The first stage is air cooling, when the earth's surface releases heat at night and cools. The second stage is the attainment of saturation, when the air temperature near the surface decreases and the partial vapor pressure becomes equal to the saturation pressure. The third stage is condensation, when excess vapor turns into water and dew droplets are formed [2,3,4,5,6,7,8].

The Clausius-Clapeyron equation is applied in the thermodynamic modeling of the process [9]:

$$\ln p_t=A-\frac{B}{T}\cdots, \quad (2.1)$$

where A and B are empirical constants selected in such a way that, when temperature T is substituted into the equation in degrees Celsius, the calculated result gives the value of the saturation pressure p_t in millimeters of mercury.

There are a number of factors affecting dew formation. The main factors are as follows:

- the higher the relative humidity in the air, the higher the dew formation temperature;
- an increase in wind speed reduces the probability of dew formation;
- cloud cover reduces air cooling and decreases the probability of dew formation;
- the surface material may accelerate dew formation, as metal cools more rapidly, or slow it down, as in the case of wood, that is:

$$T_{surf} > T_{sh} + \Delta T_{zaz} \quad (2.2)$$

- the relief of the area may accelerate or slow down dew formation; in lowland areas, dew forms more frequently.

In ventilation and air-conditioning technical systems, dew formation is often observed in cold air ducts, heat exchangers, and poorly insulated structures. Dew formation has a significant effect on the ecological, climatic, and microclimatic balance of an area, including greenhouse environments: the water balance of plants changes, the formation of the microclimate is affected, and aerosol transport is modified.

The dew point temperature (T_{sh}) depends only on the amount of water vapor in the air, that is, on the level of absolute humidity. If the moisture content does not change, it is not directly dependent on air temperature. The dew point temperature (Tsh)

Formally, Tsh is determined by the values of the following physical quantities:

1. The partial pressure of water vapor (p_v) is the main indicator, and partial pressure directly affects the dew formation temperature, that is [10,12,13,14,15]:

$$T_{sh} = f(p_p),$$

that is, the higher the partial pressure of water vapor in the air, the higher the dew formation temperature. This relationship is expressed through the following equations:

$$\varphi = \frac{p_p}{p_{tyb}(T_{sh})} \cdot 100\% \quad (2.3)$$

where the partial pressure of water vapor is:

$$p_p = \varphi \frac{p_{tyb}(T_{sh})}{100} \; yani \rightarrow T_{sh} = f(p_p) \quad (2.4)$$

2. In addition, as noted above, according to the theory of dew formation, the phase transition of water vapor from the gaseous state to the liquid state is associated with the values of the following physical indicators: the absolute humidity of air and the relative humidity of air.

3. Air composition and total pressure exert a partial influence. In engineering calculations, atmospheric pressure and gas mixtures are usually treated under the assumption of normal pressure only.

On the basis of the information presented above, it may be stated that the dew point is the “passport” of the moisture content of air. If the air contains the same amount of moisture, the dew point remains the same even when the air itself is heated or cooled.

The dew point is determined by the relative humidity of air. The higher the relative humidity, the higher the dew point, and the closer it approaches the actual air temperature. The lower the relative humidity, the lower the dew point relative to the actual temperature. If the relative humidity is 100%, the dew point is equal to the actual temperature.

In developing the mathematical model of the dynamics and emission of greenhouse microclimate indicators depending on dew point temperature, air temperature, and relative humidity, the Magnus approximation was applied, that is [16,17,18,19,20,21,22]:

$$T_{sh} = \frac{b \cdot f(T_h, \varphi)}{a - f(T_h, \varphi)} \quad (2.5)$$

where φ is the relative humidity of air; T is the air temperature; and a and b are intermediate coefficients, the values of which are calculated as follows:

$$f(T_h, \varphi) = \ln\frac{\varphi}{100} + \frac{a \cdot T_h}{b + T_h} \quad (2.6)$$

For air: $a = 17.27$, $b = 237.7$°C.

Below, on the basis of the developed mathematical model of the dynamics and emission of greenhouse microclimate indicators depending on dew point temperature, air temperature, and relative humidity, the graphs of the Magnus approximation were constructed (Figure 2.1).

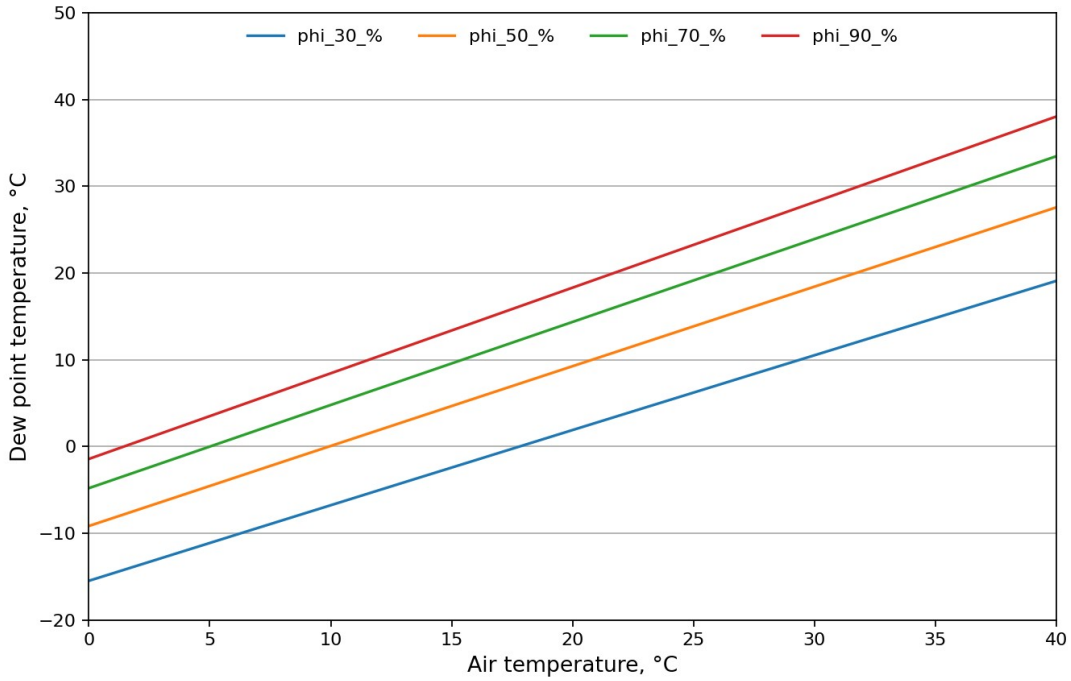


Figure 2.1. Dynamics and emission of microclimate indicators (dew point temperature, air temperature, and relative humidity)

A family of dependence curves between dew point temperature T_{sh} and air temperature T is presented for relative humidity values of 30%, 50%, 70%, and 90%, where each curve corresponds to its own value of relative humidity φ. The graph shows the dependence of greenhouse microclimate indicator dynamics and emission (dew point temperature, air temperature, and relative humidity) on the maximum amount of water vapor in air and on temperature. By using this model, it is possible to control the dynamics and emission of greenhouse microclimate indicators; specifically, excess vapor can be converted into water through condensation of greenhouse air by means of a surface on which dew formation occurs.

Results. On the basis of the developed mathematical model of the dynamics and emission of greenhouse microclimate indicators, a device was developed that makes it possible to control the value of relative humidity in greenhouse air, and an experimental prototype of this device was created. The device drives warm, humid air toward a cold pipe by means of a fan. The humid air comes into contact with the cold pipe; the air near the surface cools below the dew point; water

vapor passes into the liquid phase; water droplets appear on the pipe and then flow through the pipe openings and are absorbed into the soil in which the pipe is buried. Condensate formation occurs as a result of the phase transition of water vapor from the gaseous state to the liquid state when moist air is cooled to the saturation temperature. The main parameter determining the onset of condensation is the dew point temperature *Tsh*, which depends only on the moisture content of the air and characterizes its saturation state.

The family of dependence curves between dew point temperature *Tsh* and air temperature *T* at relative humidity levels of 30%, 50%, 70%, and 90% demonstrated the dependence of greenhouse microclimate indicator dynamics and emission (dew point temperature, air temperature, and relative humidity) on the maximum amount of water vapor in air and on temperature. Using this model, the dynamics and emission of greenhouse microclimate indicators can be controlled. On the basis of the mathematical model of the dynamics and emission of greenhouse microclimate indicators, a device was developed that enables regulation of the relative humidity of greenhouse air.

Discussion. The obtained results indicate that one of the most effective methods for controlling the microclimate in greenhouses is the application of technologies based on condensation.

The process of dew formation is not only a physical phenomenon but also has important practical significance:

it affects the water balance of plants

it stabilizes the internal environment of the greenhouse

it reduces the movement of aerosols and harmful substances

The research results are also consistent with other scientific studies [3,5,7]. In particular, the study of condensation processes from the standpoint of heat exchange [10-13] confirms the reliability of this model. The device created on the basis of the proposed model is suitable for small greenhouses, energy-efficient, and environmentally safe.

These characteristics expand the possibilities for its practical implementation.

Conclusion. As a result of the study, a mathematical model of the dynamics of greenhouse microclimate indicators was developed; a method for humidity control based on the theory of dew formation was proposed; an accurate calculation model was created using the Magnus approximation; and an innovative condensation device was developed.

These results have important scientific and practical significance for increasing occupational safety in greenhouses, improving plant productivity, and ensuring energy efficiency.

REFERENCES

1. Sulaymonov, S., & Urinova, S. K. (2025). Dynamics of microclimate indicators in small family greenhouses and sanitary-hygienic assessment of labor conditions at workplaces. *Bulletin of Agrarian Science*, 301.
2. Beysens, D. (2022). *The physics of dew, breath figures and dropwise condensation*. Berlin: Springer Nature. Lecture Notes in Physics, Vol. 994.
3. Beysens, D. (1995). The formation of dew. *Atmospheric Research, 39*(1–3), 215–237.
4. Kim, G. S., Cao, T., & Hwang, Y. (2021). Review of humidity effect on humid air-to-water condensation by a cooling surface for atmospheric water harvesting. *International Refrigeration and Air Conditioning Conference*. DOI: 10.18154/RWTH-PUB-2163.

5. Kuwagata, T., et al. (2024). Theoretical study on dew formation in plant canopies based on a one-layer energy-balance model. *Agricultural and Forest Meteorology, 354*, Article 109911.
6. Xiao, H. J., Meissner, R., & Zhang, Y. (2013). Studies on dew formation and its meteorological factors. *Journal of Food, Agriculture & Environment, 11*(2).
7. Li, H. (2025). Advances and challenges in dew research on land surface: A review. *Water, 12*(12), Article 320.
8. Encyclopaedia Britannica. (2026). *Dew point*. Available at: https://www.britannica.com/science/dew-point-temperature (Accessed: 05 February 2026).
9. Wikipedia. (2026). *Dew*. Available at: https://en.wikipedia.org/wiki/Dew (Accessed: 05 February 2026).
10. Zainullina, E. R., & Mityakov, V. Yu. (2023). Heat transfer investigation during condensation on the horizontal pipe. *Inventions, 8*(1), Article 2. Available at: https://doi.org/10.3390/inventions8010002 (Accessed: 06 February 2026).
11. Bogomolov, A. R. (2006). Film condensation of water vapor on a vertical pipe in a porous medium. *Heat Power Engineering and Heat Exchange*, XX–XX. Available at: https://cyberleninka.ru/article/n/plenochnaya-kondensatsiya-vodyanogo-para-na-vertikalnoy-trube-v-poristoy-srede (Accessed: 06 February 2026).
12. Mityakov, V. Yu., Sapozhnikov, S. Z., Zainullina, E. R., & Babich, A. Yu. (2021). The study of heat transfer during condensation on inclined pipes by gradient heatmetry. *Journal of Physics: Conference Series, 1867*, Article 012009. Available at: https://doi.org/10.1088/1742-6596/1867/1/012009 (Accessed: 06 February 2026).
13. Kubín, M., Hirš, J., & Plášek, J. (2025). Experimental analysis of steam condensation in a vertical tube with small diameter. *International Journal of Heat and Mass Transfer*. Available at: https://www.researchgate.net/publication/286865913_Experimental_analysis_of_steam_condensation_in_vertical_tube_with_small_diameter (Accessed: 06 February 2026).
14. Wikipedia. (2026). *Dropwise condensation*. Available at: https://en.wikipedia.org/wiki/Dropwise_condensation (Accessed: 06 February 2026).
15. Wikipedia. (2026). *Condensate*. Available at: https://ru.wikipedia.org/wiki/Конденсат (Accessed: 06 February 2026).
16. Ivanov, I. I. (Ed.). (2019). *Fundamentals of condensation heat transfer and fouling in heat exchangers*. Moscow: Tekhnosfera.
17. McAdams, W. H. (1954). *Heat transfer* (3rd ed.). New York: McGraw-Hill.
18. Li, F., Chen, J., Jiang, Y., & Zheng, W. (2023). Analysis of condensation flow and heat transfer characteristics inside spiral tubes. *Energies, 16*(11), Article 4323. https://doi.org/10.3390/en16114323
19. Rose, J. W. (2011). Condensation, overview. *Thermopedia*. Available at: https://www.thermopedia.com/content/653/ (Accessed: 06 February 2026).
20. Wu, Z. (2016). *Condensation: Chapter 13*. Lund: Lund University, Faculty of Engineering. Available at: https://www.lth.se/fileadmin/.../Condensation_Chapter_13.pdf (Accessed: 06 February 2026).
21. Avdeev, A. A., Zudin, Yu. B., & Soziev, R. I. (2010). Influence of the dynamic pressure of vapor during its condensation on the surface of a horizontal cylinder. In *Proceedings of RNKT-5* (pp. XX–XX).
22. Zafataev, I. I. (Ed.). (2015). *Vapor condensation: Textbook*. Minsk: BSU Publishing House.

23. Wallace, J. M., & Hobbs, P. V. (2006). Water vapor in air. In *Atmospheric science: An introductory survey* (2nd ed., p. 83). Washington: Academic Press Elsevier. ISBN 978-0-12-732951-2.

OPTIMIZATION OF THERMAL LIQUIDATION PARAMETERS AND KINETIC MODELING OF THE PROCESS OF DELAYED COKING OF OIL RESIDUES

F.A. Abdunazarov[1], Zh.Sh. Chuyanboev[2], Z.A. Davronov[3]
Doctor of Technical Sciences (PhD)[1]
Student[2,3]
Namangan State Technical University[1,2,3]
https://doi.org/10.5281/zenodo.20151128

Abstract. *This work investigates mechanisms for increasing the efficiency of delayed coking technology, which is a destructive-thermal process of deep oil refining. The main goal of the study is to scientifically substantiate the relationship between the dispersed state of the raw material and the kinetics of polycondensation of asphaltene-resin compounds, as well as to develop a mathematical model of the process. The kinetic patterns of coke yield and gas formation were approximated using the linear regression method depending on the degree of coke formation (K) of the raw material. The developed mathematical model and the identified kinetic parameters allow for high-precision forecasting in the design of slow-cooking units, the modernization of existing ones, and the automatic control of technological modes. The research findings are of strategic importance in increasing the productivity of energy resources through the deep processing of oil residues.*

Keywords: *delayed coking, deep oil rafining, thermochemical mechanism, kinetic dependence, tar, oil residues, asphaltene-resin compounds, distillate product regression equation.*

Introduction

In deep oil refining technology, the delayed coking process relies on thermochemical mechanisms for the formation of coke and distillate products. The efficiency of this process is determined by the dispersed state of the raw material and the kinetics of the condensation of asphaltene-resin compounds within it. The general equation of the coking process can be expressed as follows.

$$Raw\ material \xrightarrow{k1} Steam + Gaz + Coke \quad (1)$$

The empirical mathematical model of the process regarding coke yield is linearly dependent on the coke-forming property of the raw material (K) and is characterized by the following approximation equation:

$$W_k = a + b * K \quad (2)$$

Literature Review and Theoretical Explanation

In the study, a high-precision coke yield forecast was developed using coefficients a=2 and b=1.66. To model the polytropic process in industry under laboratory conditions, it is necessary to determine the equivalent temperature. Based on the nomogram of A.I. Zinovieva and D.I.

Orochko, an equivalent temperature (te) is calculated, which is more accurate than the arithmetic mean temperature:

$$t_e \approx \frac{t_{inlet} + t_{outlet}}{2} + \Delta t_{polytropic} \quad (3)$$

In the coking chamber, the transformation of the liquid phase into a foamy mass and the formation of the coke skeleton are characterized by the swelling coefficient (SCO). Based on experimental data, the influence of temperature on this parameter was expressed by the following regression equation:

$$K_{VS} = 4.5 + 0{,}11(486 - t) \quad (4)$$

Analysis of Contemporary Trends

It shows how the yield of final products changes as the coke-forming components (Coke level, K) in the raw material increase. This relationship is linear in nature.

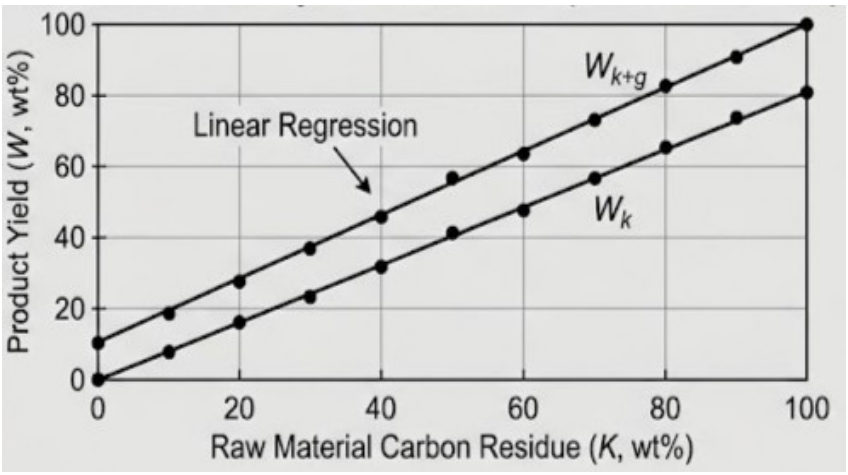


Fig 1. Raw material quality and product yield (Kinetic dependence)

As seen from the graph, as the coking capacity of the raw material increases, the total yield of coke and gas (Wk+g) increases linearly. This is an important indicator for the industry, as it allows for the assessment of coke oven efficiency and the level of raw material processing. An increase in temperature above 500 °C reduces the viscosity of the dispersed system, which leads to a decrease in the K_{VS} and an increase in the coke density. For a device with a daily capacity of G = 1100 t/day, the geometric parameters were optimized by correlating the effective volume (v_r) of the chamber with the volumetric velocity (w = 0.14 s^{-1}. Based on the given K_{VS} = 4.5 + 0.11 (486 - t) equation, the influence of temperature on the coke mass structure during the coking process is as follows:

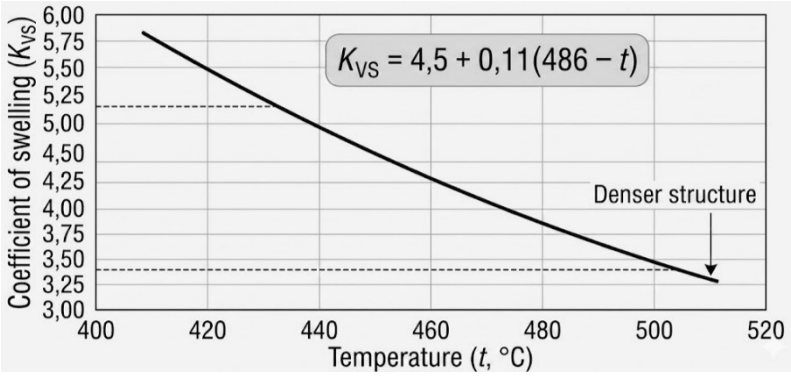


Fig 2. Effect of temperature on swelling coefficient (K_{VS})

An increase in temperature reduces the swelling capacity of the coke mass. The decrease in the K_{VS} on the graph (for example, approaching 2.0 above 500°C) indicates that at higher

temperatures, the coke structure becomes denser and porosity decreases. This is a necessary condition for increasing the mechanical strength of coke.

The height of the cylindrical part of the chamber is determined by the following integral relation.

$$H_{st}=\frac{V_h \cdot \tau}{F \omega} \quad (5)$$

In this case, F is the cross-sectional area of the chamber (18 m2). As a result of the calculations, it was scientifically substantiated that the total height of the chamber is 25 m, and the diameter is 4.8 m. The diagram in Figure 3 depicts the process of filling the reaction chamber (coke drum) with coke and foam mass over a 24-hour operating cycle depending on time.

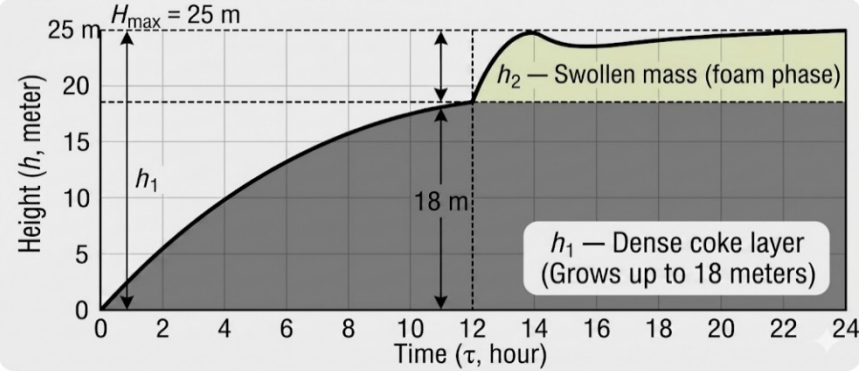


Fig 3. Dynamics of reaction chamber filling by height

At the beginning of the process (0-8 hours), a dense coke layer (h1) grows rapidly, and above it, the swollen mass (h2) foams and approaches the upper part of the chamber (Hmax). During this period, there is a risk of the chamber becoming full. In the second half of the cycle (12-24 hours), the coke layer continues to grow and stabilizes at 18 meters, while the swollen mass transforms into coke, and its height decreases.

According to hydrodynamic stability, the foaming process is associated with an acceleration of gas release during the coking stage of asphaltens. To eliminate this, the use of silicone-based anti-foaming agents was analyzed from a kinetic perspective. The introduction of water vapor (turbulization) serves to maintain the Reynolds number (Re) of the flow above the critical value so that coke does not settle in the coils of the heat-exchange furnace. This bar chart shows the distribution (mass fraction) of all distillates (liquid and gaseous products) obtained as a result of the coking process by distillation temperature.

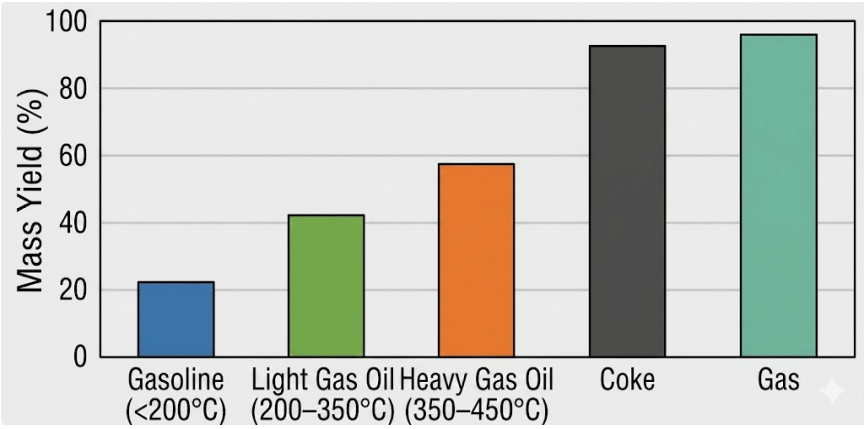


Figure 4. Fractional composition of products (Material balance)

Research findings indicate that to effectively manage the slowing-down coking process, it is necessary to optimize the raw material recirculation coefficient and maintain the temperature

gradient of the reaction chamber at a minimum level. The developed mathematical model allows for high-precision calculations during the design of industrial installations and the modernization of existing ones. The presented four graphs analyze various technological and kinetic parameters of the coking process.

Conclusion

The common scientific basis uniting them is that coking is a complex thermochemical decomposition process, the efficiency of which and the nature of the final products depend nonlinearly but predictably on the composition (quality) of the initial raw materials and the thermal regime of the process. The presented graphs show that the kinetics of coke formation strongly depend on the quality of the raw materials. As the degree of coking of the raw material increases (K, % by mass), i.e., as the proportion of heavy, aromatic, and coke-forming components in the raw material increases, the final yield of the coke itself (Wk) and the coke+gas mixture (Wk+g) increases linearly. This relationship is based on the thermochemical nature of the coke formation process. Raw materials with a high degree of coking contain a large amount of heavy hydrocarbons (e.g., asphaltenes), which, upon decomposition at high temperatures, primarily form a solid phase (coke). The linear trend in the graph confirms that the process follows stable kinetic laws at specific temperatures and pressures. This set of four graphs provides a comprehensive analysis necessary for managing and optimizing the coking process. It combines the kinetic effect of raw material quality (Fig. 1), the influence of temperature on structural density (Fig. 2), the dynamics of temporary chamber filling (Fig. 3), and the material balance of final products (Fig. 4). The interdependence between these parameters allows for the correct selection of process conditions (temperature, pressure, raw material composition, and time) to achieve the desired coke quality and maximum product yield.

REFERENCES

1. Abdunazarov, A. A., Abdunazarov, A. F., Jo‘rayev, S. B., & Akhmedov, J. M. (2024). Analysis of the chemical composition of local petroleum coke. *Some Problems Related to Natural Sciences and Ecology*. NamDU Publishing House, 204–208.
2. Abdunazarov, A. A., Tursunalieva, D. T., & Abdunazarov, F. A. (2021). Study of the structure and chemical composition of petroleum coke. In *Proceedings of the 2nd International Conference “Innovative Development of the Oil and Gas Industry, Modern Energy and Their Current Problems”* (pp. 127–129). Tashkent.
3. Abdunazarov, F. A., & Khudaiberdiev, A. A. (2024). Technology for separating powdered materials from petroleum coke using a two-rotor gravity classifier. *E3S Web of Conferences, 486*, 01018. https://doi.org/10.1051/e3sconf/202448601018
4. Abdunazarov, F. A. (2022). Determination of the elemental composition of petroleum coke by inductively coupled plasma atomic emission spectroscopy using the Perkin Elmer Avio 200. *Universum: Chemistry and Biology, 11-2*(101), 37–43.
5. Abdunazarov, F. A. (2022). Chemical analysis of the composition of local petroleum coke and prospects for its application in production based on the obtained results. In *Import Substitution, Scientific, Technical and Economic Security: Proceedings of the V International Scientific and Technical Conference “Minsk Scientific Readings 2022”* (Vol. 3, pp. 14–21). Belarusian State Technological University.

6. Abdunazarov, F. A., & Khudaiberdiev, A. A. (2023). Study of the structure and chemical composition of petroleum coke. In *Integration of Modern Physicochemical Research Methods in Science and Production* (pp. 23–25). Tashkent.
7. Abdunazarov, F. (2023). Use of petroleum waste in production facilities based on chemical composition and elemental analysis results. In *Environmental Protection and Ecological Zoning: Problems and Solutions: Proceedings of the International Scientific-Practical Conference* (pp. 738–745). Tashkent.
8. Abdunazarov, F. A., & Khudaiberdiev, A. A. (2023). Study of the pneumatic classification process of petroleum coke powders. *Modern Scientific Developments: Innovative Aspect*, 25.
9. Abdurakhmonov, E. B., & Abdunazarov, F. A. (2022). Technology for obtaining powdered materials from waste petroleum products and granite materials in the construction industry. *Universum: Technical Sciences, 3-4*(96), 59–67.
10. Abdunazarov, F. A., Khudaiberdiev, A. A., & Abdurakhmonov, E. B. (2024). Technology for obtaining powder material from oil coke. In *Proceedings of the Republican Scientific-Practical Conference "Implementation of Innovative Technologies in the Food and Chemical Industry"* (pp. 583–588).
11. Mamadjanov, Z. N., Abdunazarov, F. A., & Rustamov, I. T. (2022). Centrifugal mill with a layered-flow classifier for use in the production of powdered petroleum coke in Uzbekistan. *Universum: Technical Sciences, 3-5*(96), 23–28.
12. Abdunazarov, F. A., & Khudaiberdiev, A. A. (2023). Two-rotor toothed gravity separator device for extracting powdered materials from petroleum coke. *Scientific and Technical Journal of Mechanical Engineering*, Special Issue No. 3, 403–407.

APPLICATION OF NANOTECHNOLOGY TO ENHANCE FORMATION PERMEABILITY

Sh.Z. Valikulov[1], B.H. Matsaidov[2]
Assistant at the Department of "Development and Operation of Oil and Gas Fields"[1]
Master's student at the Department of "Development and Operation of Oil and Gas Fields"[2]
https://doi.org/10.5281/zenodo.20151330

Abstract. *This article examines the application of nanotechnology to improve reservoir permeability and enhance oil recovery in oil and gas fields. The study analyzes scientific literature, physicochemical properties of nanoparticles, and practical experimental findings related to nanofluids used in porous reservoir environments. Special attention is given to silica, aluminum oxide, iron oxide nanoparticles, and carbon nanotubes, whose small size, large surface area, dispersion ability, thermal stability, and chemical activity influence fluid flow. The findings show that nanoparticles can penetrate narrow pores, remove organic deposits, reduce interfacial tension, alter rock wettability from oil-wet to water-wet, create microchannels, and decrease the viscosity of heavy oil. These mechanisms improve filtration properties and increase the oil recovery factor. Although nanotechnology offers economic and environmental advantages, its large-scale application requires further research on cost, stability, aggregation, and field-specific adaptation under high-temperature and high-pressure reservoir conditions. The study highlights its relevance for Uzbekistan's challenging oil reservoirs today.*

Keywords: *nanotechnology, reservoir permeability, nanoparticles, oil recovery, enhanced oil recovery.*

Introduction

One of the main challenges in the oil and gas industry is the incomplete extraction of hydrocarbons due to the low permeability of the reservoir. Conventional methods (such as hydraulic fracturing and the use of chemical reagents) are often not sufficiently effective or are economically expensive.[1] For this reason, the application of modern technologies, specifically nanotechnology, has become a pressing issue.

Nanotechnology provides the opportunity to control in-situ processes at a molecular level, which helps to increase permeability and enhance oil recovery rates.[2]

Methodology

This research focuses on an in-depth study of the theoretical and practical aspects of utilizing nanotechnology to enhance reservoir permeability, conducted through a comprehensive approach. The research methodology consists of several interconnected stages, including the analysis of scientific literature, investigation of the physicochemical properties of nanoparticles, modeling their behavior within the reservoir environment, and synthesizing the results of practical experiments.

In the first stage, domestic and international scientific sources—including articles, monographs, and conference proceedings regarding the enhancement of reservoir permeability in oil and gas fields—were systematically studied. Through this analysis, development trends in nanotechnology, their areas of application, and existing challenges were identified [2]. Based on

the literature review, the theoretical foundation of the research was established, and the primary scientific approaches were defined.

In the second stage, the physicochemical properties of nanoparticles were analyzed in depth. Specifically, indicators such as particle size, surface area, charge, degree of dispersion, tendency toward aggregation, and resistance to temperature and pressure were examined. These characteristics are of significant importance in determining how nanoparticles move within the reservoir environment, how they interact with the porous structure, and how they influence the oil displacement process.

In the third stage, modeling methods were employed to determine the mechanisms of action of nanoagents under reservoir conditions. Processes such as fluid flow in porous media, capillary forces, surface tension, and changes in wettability were theoretically analyzed. Through modeling, the movement of nanoparticles within porous channels, their role in breaking down sedimentary deposits, and their potential for creating micro-fractures were evaluated. At the same time, the effectiveness of various nanoparticles was compared.

In the subsequent stage of the research, the results of existing practical experiments and laboratory tests were summarized. Based on experimental data obtained from various studies, the degree of increase in reservoir permeability, the rise in the oil recovery factor, and the economic efficiency of the technology were evaluated. In this stage, particular attention was paid to the effectiveness of nanoagents in reservoirs containing heavy and highly viscous oil.

Within the scope of this research, several key nanomaterials were selected, and their properties and potential applications were analyzed. Specifically, silica (SiO_2) nanoparticles are distinguished by their high surface area and excellent dispersion properties, making them effective for cleaning pores in the reservoir. Aluminum oxide (Al_2O_3) nanoparticles are characterized by high mechanical strength and heat resistance, enabling their use in complex geological conditions. Iron oxide (Fe_2O_3) nanoparticles allow for control via external fields due to their magnetic properties. Furthermore, carbon nanotubes are notable for their unique structure, high strength, and conductivity, playing a significant role in creating micro-channels within the reservoir and improving fluid flow.

In general, the applied methodology allowed for a comprehensive evaluation of the impact of nanotechnology on reservoir permeability. As a result of the comprehensive approach, the effectiveness, operating conditions, and prospects of nanoagents were elucidated on a scientific basis.

Results and Analysis

Research results indicate that the application of nanotechnology has a comprehensive positive effect on the filtration-storage properties of a reservoir. Specifically, nanoparticles and nanofluids serve to increase permeability by significantly altering the physical and physicochemical processes occurring within the reservoir.[3]

First and foremost, one of the key properties of nanoparticles is their ability to penetrate even the narrowest pore channels of the reservoir due to their extremely small size. Through this, they enable the decomposition or dispersion of organic deposits—asphaltenes, paraffins, and resins—that have accumulated in the reservoir. As a result, previously blocked pores and microchannels are opened, creating conditions for the free movement of fluids. This leads to an increase in the filtration coefficient and an improvement in overall permeability.

Furthermore, the use of nanofluids plays an important role in managing surface phenomena within the reservoir. In particular, they reduce the interfacial tension between the oil and water

phases. It is known that high interfacial tension leads to an increase in capillary forces, which makes it difficult for oil to exit the pores. Under the influence of nanofluids, capillary forces are significantly reduced, resulting in increased oil mobility and easier extraction from the reservoir.

Another important mechanism of nanotechnology's impact is altering the wettability of the rock surface. In many oil-bearing reservoirs, the rock surface is in an oil-wet (oleophilic) state, which makes it difficult to displace oil using water. Nanoparticles adsorb onto the rock surface, changing its properties to a water-wet (hydrophilic) state.[4] As a result, water adheres better to the rock surface, and the efficiency of displacing oil from the pores increases. This process leads to a significant increase in the oil recovery factor.

Also, some nano-agents have the ability to undergo chemical reactions within the reservoir, creating additional micro-fractures. These micro-fractures create new filtration paths for fluids and increase the overall permeability of the reservoir. This mechanism is especially important for dense and low-permeability reservoirs, allowing for the activation of unrecovered hydrocarbon reserves.

In addition, nanofluids have a significant effect on the rheological properties of heavy and viscous oils. They reduce the viscosity of the oil, lowering its resistance to flow. This facilitates the movement of oil toward the well and increases the efficiency of the extraction process. This effect is considered particularly important in fields with high viscosity.[5]

In general, the results of the conducted research show that nanotechnology increases permeability in a complex manner by improving the pore structure of the reservoir, optimizing surface phenomena, and increasing the mobility of fluids. This allows for a significant improvement in the efficiency of oil extraction.

Discussion

The scientific results obtained indicate that the application of nanotechnology in increasing reservoir permeability offers significant advantages over traditional methods, enabling a fundamental improvement in the efficiency of oil and gas extraction. First and foremost, the extremely small size of nanoparticles ensures they can freely penetrate even the finest pores of the reservoir. This allows for the treatment of zones that are difficult to reach via traditional chemical reagents or mechanical methods. Consequently, the internal structure of the reservoir is improved, and filtration properties are significantly enhanced.

Another key advantage of nanotechnology is that high efficiency can be achieved even with small amounts of material. This, in turn, reduces reagent consumption and increases the economic efficiency of the overall technological process. Specifically, due to the high surface-active properties of nanoparticles, they reduce the interfacial tension between oil and water, decrease capillary forces, and consequently increase oil mobility. These processes collectively contribute to maximizing the extraction of hydrocarbons from the reservoir.

Furthermore, nanoparticles have the ability to alter the wettability of the rock surface. In many cases, oil-bearing formations are hydrophobic, meaning that oil tends to adhere to the rock surface. Using nanotechnology, these surfaces can be converted to a hydrophilic state, which significantly improves the oil displacement process. Additionally, some nanoagents create micro-fractures through chemical reactions, further increasing the permeability of the reservoir.

From an environmental perspective, nanotechnology is also superior. These materials are used in small volumes and are often composed of inert or low-toxicity substances. Therefore, their negative environmental impact is lower compared to traditional chemical reagents. This increases their importance as a modern technology that meets environmental safety requirements.

However, there are certain problems and limitations in implementing nanotechnology on a large scale. One of the main drawbacks is their high cost. The production of nanoparticles, maintaining their stability, and adapting them to specific reservoir conditions require significant financial expenditure. Moreover, the complexity of the technology is a crucial factor. An individual approach is required for each field, as the geological and physicochemical properties of reservoirs vary. Therefore, laboratory research and pilot testing are necessary before applying nanoagents.

Another important aspect is that the stability of nanoparticles under reservoir conditions may not always be high. In environments characterized by high temperature, high pressure, and mineralized water, there is a risk of aggregation or loss of activity. This can negatively affect the efficiency of the technology.

In the context of Uzbekistan's oil and gas fields, particularly in reserves with high-viscosity oil, the application of nanotechnology is highly promising. In such fields, traditional methods often demonstrate low efficiency, resulting in a large portion of the oil remaining in the reservoir. Nanotechnology can provide significant economic benefits by increasing oil mobility, improving reservoir permeability, and raising the overall recovery factor. At the same time, the implementation of these technologies creates the possibility for more rational use of energy resources and maximum exploitation of existing reserves.

In general, nanotechnology holds great potential as an innovative direction in the oil and gas industry, and deep scientific study followed by a gradual implementation will lead to high economic and technological efficiency in the future.

Conclusion

In conclusion, nanotechnology is emerging as one of the most modern, innovative, and highly efficient approaches to increasing reservoir permeability in oil and gas fields. These technologies enable the control of physico-chemical processes within the reservoir at the nano-scale, leading to results that are difficult to achieve with traditional methods. Specifically, nanoparticles significantly increase oil mobility by cleaning porous media, reducing capillary forces, lowering surface tension, and altering the wettability of rock formations.

At the same time, the application of nanotechnology improves the filtration and storage properties of the reservoir, opens micro- and nano-channels, and ensures the free movement of fluids. This, in turn, contributes to an increase in the oil recovery factor, maximizes the utilization of existing reserves, and enhances the overall economic efficiency of the field. The use of nanotechnology is particularly important in fields with high viscosity, complex geological structures, or where traditional methods are ineffective.

Furthermore, due to their small size, nano-agents are capable of penetrating the deepest and narrowest pores of the reservoir, significantly increasing treatment efficiency. The fact that high results can be achieved with small quantities is also a significant economic advantage. From an environmental perspective, many nanoparticles are relatively safe, and their negative impact on the environment is lower compared to traditional chemical reagents.

In the future, several important issues must be addressed to widely implement nanotechnology in the oil and gas industry. These include increasing the stability of nanoparticles under reservoir conditions, ensuring their economic efficiency, optimizing technological processes, and improving mechanisms for industrial-scale application. Simultaneously, it is crucial to develop individual nano-compositions for each site, taking into account the geological and physical characteristics of local reservoirs.

Overall, the widespread practical implementation of nanotechnology allows for increased oil production, efficient and rational use of energy resources, and long-term sustainable exploitation of fields. This not only increases the economic efficiency of industrial enterprises but also serves as a vital factor in ensuring the country's energy security.

REFERENCES

1. Lake, L. W. (2014). Enhanced Oil Recovery. Society of Petroleum Engineers.
2. Sheng, J. (2013). Modern Chemical Enhanced Oil Recovery. Gulf Professional Publishing.
3. Li, S., & Torsæter, O. (2015). Experimental study of nanofluids for EOR. Journal of Petroleum Science and Engineering, 124, 543–552.
4. Ogolo, N. A., Olafuyi, O. A., & Onyekonwu, M. O. (2012). Enhanced oil recovery using nanoparticles. SPE Journal, 16(2), 345–354.
5. Ju, B., & Fan, T. (2009). Experimental study on nanofluids for improving oil recovery. Journal of Petroleum Science, 67(3), 345–351.

DIGITALIZATION OF REGIONAL CHILDREN'S LIBRARIES THROUGH ARTIFICIAL INTELLIGENCE TECHNOLOGIES

M.K. Hamrayeva
Deputy Director for Information Technology, Bukhara Regional Children's Library
https://doi.org/10.5281/zenodo.20152687

Abstract. *This article examines the issues related to the digitalization of regional children's libraries through artificial intelligence technologies. The study analyzes the major challenges existing in traditional library systems, including manual cataloguing processes, insufficient electronic resources, and the absence of intelligent recommendation systems for users. Furthermore, the paper highlights the significance of AI-based automatic cataloguing, OCR technologies, intelligent recommendation systems, and chatbot services in improving library operations and user experience. Based on international practices, a conceptual "Smart Children's Library" model adapted to the conditions of Uzbekistan is proposed. The findings demonstrate that artificial intelligence technologies can significantly enhance the efficiency of library services, provide personalized user support, and contribute to the development of children's reading culture.*

Keywords: *artificial intelligence, digitalization, children's libraries, electronic catalogues, OCR technology, intelligent recommendation systems, chatbots, digital libraries, information technologies, Smart Children Library, electronic resources, library management.*

Introduction

The rapid development of information technologies worldwide has significantly transformed the fields of education, culture, and library-information systems. In particular, the integration of artificial intelligence technologies into library activities has created new opportunities for managing information resources, improving user services, and developing electronic databases. In the Republic of Uzbekistan, large-scale reforms aimed at digital transformation are being implemented within the framework of the "Digital Uzbekistan–2030" strategy. In this context, the modernization of regional children's libraries through advanced technological solutions and the implementation of artificial intelligence technologies have become highly important priorities. The partial digitalization of library collections is currently one of the main issues facing local children's libraries. Traditional card catalogue systems are still used to organize volumes in many libraries, making it challenging for patrons to find the required literature. The lengthy search procedure lowers the overall quality of library services, and the antiquated cataloguing system restricts the speed and effectiveness of information retrieval. Additionally, traditional library services can no longer adequately meet the educational and informational demands of children and teenagers as their interest in digital technologies grows. Children's involvement in library activities has also decreased due to a lack of interactive books, audio materials, and technological resources. Another important issue is the absence of intelligent recommendation systems in children's libraries. Existing systems are generally unable to recommend books according to readers' age categories, interests, or previous reading experiences. As a result, children often encounter difficulties in selecting suitable literature or repeatedly choose similar books. In addition, librarians experience excessive workloads due to manual cataloging,

registration, and user service processes. These challenges demonstrate the necessity of introducing modern artificial intelligence technologies into library management systems.

Artificial intelligence technologies have the potential to greatly enhance both operational efficiency and service quality in libraries. Automatic cataloguing, user interest analysis, intelligent recommendation creation, and electronic resource management are all possible with AI-based solutions. Based on metadata, annotations, or textual content, machine learning algorithms can automatically recognize book titles, authors, genres, age groups, and keywords. This speeds up information processing and significantly lessens the effort for librarians.

In recent years, Uzbekistan has undertaken several initiatives aimed at modernizing information-library centers. Significant progress has been observed in the introduction of electronic catalog systems and the expansion of internet infrastructure. According to analytical observations, the proportion of libraries equipped with electronic catalogs increased from approximately 38% in 2022 to 61% in 2024. The share of digitized children’s literature rose from 22% to 47%, while the proportion of libraries connected to internet networks increased from 56% to 83%. However, the implementation of AI-based search systems remains limited, accounting for only 12% in 2024. These figures indicate that further technological development and investment are still required in this field.

Experience from throughout the world shows that artificial intelligence technology can significantly increase library systems' effectiveness. AI-based recommendation algorithms that evaluate readers' preferences and automatically suggest pertinent books are widely used in Finland's public and children's libraries. These platforms have enhanced access to educational resources and raised children's reading engagement. Libraries in South Korea use robotics and AI-powered information kiosks that offer multilingual assistance, automated guidance, and book search services. The National Library Board of Singapore has put in place machine learning technologies that can analyze user behaviour and forecast future reading needs. Similar to this, a number of US libraries assist patrons in finding scholarly and literary materials by utilizing AI chatbots and natural language processing technologies.

Artificial intelligence technologies not only increase the effectiveness of library management but also turn libraries into interactive learning environments, according to the examination of international practices. These experiences are especially pertinent to Uzbekistan since local children's libraries are currently changing from traditional information centres to online learning environments. However, local constraints, such as financial resources, linguistic resources, and technology infrastructure, must be taken into account when adapting international techniques. Many remote libraries in Uzbekistan still struggle with poor internet access, limited electronic collections, and a lack of experts who can run AI systems, in contrast to technologically advanced nations. As a result, the implementation process ought to be progressive and tailored to the needs of the country.

Automatic cataloguing is one of the most significant uses of artificial intelligence in libraries. Bibliographic records are manually input into older systems, which takes a lot of time and frequently results in human error. By analyzing a book's cover, annotation, or textual content, artificial intelligence (AI) technologies allow for the automatic identification of a book's subject, genre, and target age group. These methods can improve data accuracy and speed up cataloguing several times. Additionally, intelligent suggestion systems are essential for boosting kids' enthusiasm for reading. In order to suggest appropriate books, these algorithms examine users' prior reading habits, preferred genres, and age groups, much like Netflix and YouTube. Children's

motivation to read rises as a result, and their engagement with library materials becomes more dynamic and tailored. Another crucial element of digitalizing libraries is OCR (Optical Character Recognition) technologies. Old printed books can be automatically scanned and transformed into electronic formats like PDFs or searchable text materials using OCR technologies. When it comes to conserving rare children's books and incorporating them into digital library collections, this technology is particularly crucial. OCR technologies can guarantee long-term preservation and broader accessibility of educational resources in regional libraries where many valuable books exist in restricted editions. Chatbots with AI capabilities also help to enhance library services. For instance, the chatbot can deliver a selection of appropriate novels right away when a user asks, “Recommend adventure books for a nine-year-old child.” This guarantees quick and effective user support while lessening the workload for librarians. Additionally, the development of accessible audio library systems is made possible by speech-to-text and text-to-speech technologies, which are especially helpful for children with visual impairments.

Methodology

Within the framework of this study, practical research was conducted in five regional children’s libraries. The research involved 50 librarians and 120 students through surveys and observational analysis. According to the survey results, 72% of respondents reported using electronic catalogs, while 91% emphasized the necessity of AI-based recommendation systems. Participants also highlighted the need for increasing electronic book collections, developing faster search systems, and introducing mobile library applications. As part of the practical research, a small-scale AI-based recommendation model was developed. The experimental system included a database of 100 children’s books and was tested among 20 students.

Results and Discussion

The results demonstrated that the AI recommendation system reduced the average time required to find suitable books by 40%. In addition, user satisfaction with library services increased by 35%. These findings confirm the practical effectiveness of artificial intelligence technologies in improving library performance and user experience. Based on the research findings, a conceptual “Smart Children Library” model was proposed. The model integrates AI-powered catalog systems, intelligent chatbots, OCR modules, audio book platforms, mobile applications, and recommendation algorithms into a unified digital ecosystem. The implementation of this model can automate library services, expand access to electronic resources, and strengthen children’s reading culture in Uzbekistan. The digitalization of regional children’s libraries through artificial intelligence technologies represents one of the most important contemporary tasks in the modernization of Uzbekistan’s library system. AI technologies can improve the efficiency and accessibility of library services, provide personalized user experiences, and reduce the workload of librarians. The implementation of electronic catalogs, intelligent recommendation systems, OCR technologies, and chatbot services can transform children’s libraries into modern educational and information centers. International experience demonstrates that artificial intelligence can significantly enhance library activities, and its adaptation to Uzbekistan’s educational and cultural environment offers promising opportunities for future development. Therefore, expanding AI integration into the national library system and conducting further scientific and practical research in this field remain highly important objectives.

Conclusion

The digitalization of regional children’s libraries through artificial intelligence technologies represents one of the most significant directions in the modernization of Uzbekistan’s

library system. The findings of the study indicate that the implementation of AI technologies improves the speed and quality of library services, ensures personalized support for users, and reduces the workload of librarians. Electronic catalogues, OCR systems, chatbots, and intelligent recommendation platforms have the potential to transform children's libraries into modern educational and information centers. International experience demonstrates that AI-based library systems are highly effective in promoting reading culture and improving access to educational resources. At the same time, the successful implementation of such technologies in Uzbekistan requires special attention to technical infrastructure, financial investment, and the preparation of qualified specialists. Therefore, the gradual integration of artificial intelligence technologies into the national library system, the expansion of electronic resource collections, and the continuation of scientific and practical research in this field remain essential priorities for future development.

REFERENCES

1. Decree of the President of the Republic of Uzbekistan. Digital Uzbekistan–2030 Strategy. Tashkent, Uzbekistan, 2020.
2. Breeding, M. "Artificial Intelligence Technologies in Library Management Systems." International Journal of Library and Information Science, vol. 14, no. 3, 2022, pp. 45–53.
3. Smith, J., & Brown, L. "Digital Transformation of Children's Libraries: Global Trends and Challenges." Library Hi Tech Journal, vol. 41, no. 2, 2023, pp. 120–134.
4. Chen, Y. "OCR Technologies and Digital Preservation in Modern Libraries." Journal of Information Technology and Libraries, vol. 39, no. 4, 2021, pp. 77–89.
5. Kumar, R., & Lee, S. "Smart Library Systems Based on Artificial Intelligence." Proceedings of the International Conference on Digital Education and Information Systems, 2022, pp. 210–218.
6. Finland Public Library Association. AI-Based Recommendation Systems in Children's Libraries. Helsinki, 2021.
7. National Library Board Singapore. Machine Learning Applications in Library Services. Singapore, 2022.
8. Seoul Information and Library Center. South Korea Digital Library Development Report. Seoul, 2023.
9. Johnson, P. "Research on Chatbot Technologies in Educational Libraries."Journal of Educational Technologies, vol. 18, no. 1, 2022, pp. 55–68.
10. Wang, H., & Miller, T. "Machine Learning Algorithms for Intelligent Book Recommendation Systems. "International Journal of Artificial Intelligence Research, vol. 11, no. 2, 2023, pp. 99–113.

BRAIN TUMOR CLASSIFICATION USING AN ENSEMBLE DEEP LEARNING MODEL WITH EFFICIENTNET, RESNET, AND VISION TRANSFORMER

K. Shukurov[1], N. Tolibova[2], F. Sulaymonova[3]
Tashkent University of Information Technologies named after Muhammad al-Khwarizmi, docent[1]
Research Institute for the Development of Digital Technologies and Artificial Intelligence under the Ministry of Digital Technologies of the Republic of Uzbekistan, Software Development Department Specialist[2]
Tashkent University of Information Technologies named after Muhammad al-Khwarizmi, PhD student[3]
https://doi.org/10.5281/zenodo.20196086

Abstract. *Brain tumor classification is a clinically critical task that directly influences treatment decisions and patient outcomes. In this study, we propose an ensemble deep learning framework that combines the feature extraction capabilities of EfficientNet, ResNet, and Vision Transformer (ViT) architectures to classify three major types of brain tumors-meningioma, glioma, and pituitary tumor-from T1-weighted contrast-enhanced MRI images. The model was trained and evaluated on the benchmark dataset of 3,064 images (2,144 train, 460 validations, 460 test), achieving a test accuracy of 94.57%, macro-average precision of 0.94, recall of 0.94, and F1-score of 0.94. Per-class AUC values reached 0.986, 0.992, and 0.999 for meningioma, glioma, and pituitary tumor respectively. The proposed approach outperforms the standalone CNN baseline (94.39%) and several content-based image retrieval methods. These results demonstrate the effectiveness of ensemble-based transfer learning for medical image classification tasks.*

Keywords: *brain Tumor, Ensemble Learning, EfficientNet, ResNet, Vision Transformer, MRI Classification, Deep Learning, Transfer Learning.*

Introduction

Brain tumors represent one of the most life-threatening neurological conditions in modern medicine. According to the American Cancer Society, an estimated 23,820 malignant brain or spinal cord tumors are diagnosed annually in the United States alone, with approximately 17,760 deaths attributed to such tumors each year [1]. The survival rate varies considerably depending on tumor type and patient age: for meningioma, the 5-year relative survival rate ranges from 87.0% in younger patients (20–44 years) to 47.3% in those aged 75 and above [2].

Brain tumors are classified into primary tumors-which originate within the brain or its surrounding tissues-and secondary tumors that arise from metastatic spread of cancers in other organs [3]. Among the primary types, glioma, meningioma, and pituitary tumor are the most prevalent, each presenting distinct pathological characteristics visible in MRI scans. Accurate and timely classification of these tumor types is essential for planning appropriate surgical, radiological, or chemotherapeutic interventions.

Traditional diagnostic approaches rely on expert radiologists manually interpreting MRI images, a process that is time-consuming, expensive, and subject to inter-observer variability.

Automated machine learning-based systems have increasingly been proposed as decision-support tools to assist radiologists, with convolutional neural networks (CNNs) emerging as the dominant paradigm for image classification tasks.

In this work, we propose an ensemble deep learning model that integrates three state-of-the-art architectures-EfficientNet-B4, ResNet-50, and Vision Transformer (ViT)-to classify the three primary brain tumor types. Our model is trained on 3,064 T1-weighted contrast-enhanced MRI images and evaluated using comprehensive metrics including accuracy, precision, recall, F1-score, AUC-ROC, and average precision curves. The proposed ensemble approach achieves a test accuracy of 94.57%, surpassing the standalone CNN baseline of Das et al. [4] and established content-based image retrieval (CBIR) methods.

Methods

Several approaches have been applied to the problem of brain tumor classification from MRI images. Early content-based image retrieval (CBIR) methods focused on extracting handcrafted features from the tumor region and its surrounding tissue.

Yang et al. [5] introduced a CBIR framework using the Margin Information Descriptor (MID), which characterizes tumor boundaries based on surrounding tissue intensities, achieving an average precision of 89.3%. However, the distance metric used was globally linear, limiting its ability to capture local feature variation across different tumor regions.

Huang et al. [6] proposed a region-specific Bag of Visual Words (BoVW) model that leverages both lesion intensity and surrounding tissue contrast. Their system achieved a precision of 91.0%, with normalization and whitening found to improve retrieval performance. A subsequent extension by Huang et al. [7] incorporated Rank Error-based Metric Learning (REML) to bridge the semantic gap between low-level visual features and high-level diagnostic concepts, yielding an average precision of 93.1%.

Das et al. [4] proposed a custom CNN model with three convolutional layers, two subsampling layers, and fully connected layers trained on the same 3,064-image dataset. Using Adam optimization with histogram equalization preprocessing and dropout regularization, their model achieved a test accuracy of 94.39% and an average precision of 93.33%-at the time outperforming all CBIR-based methods on this benchmark.

More recent advances in deep learning have introduced transformer-based architectures [8] that model long-range dependencies in images through self-attention mechanisms, as well as EfficientNet [9] and ResNet [10-18] families that achieve strong performance through compound scaling and residual connections. Ensemble methods that combine predictions from multiple diverse architectures have been shown to reduce model-specific biases and improve generalization, motivating the approach taken in this work.

The dataset used in this study is the publicly available brain tumor MRI dataset compiled by Cheng [11], comprising 3,064 T1-weighted contrast-enhanced MRI images collected from 233 patients. The dataset includes three tumor classes: meningioma (708 images), glioma (1,426 images), and pituitary tumor (930 images). Images are stored in MATLAB (.mat) format, each containing fields for the image array, tumor mask, tumor border, class label (1 = meningioma, 2 = glioma, 3 = pituitary), and patient ID.

In our experimental setup, the dataset was split into three non-overlapping subsets: 2,144 images for training (69.9%), 460 for validation (15.0%), and 460 for testing (15.0%). Class imbalance was addressed through weighted loss computation during training, with the following class weights computed from the inverse of class frequency: Meningioma: 1.421, Glioma: 0.729,

Pituitary: 1.083.

All images were resized to 224×224 pixels to match the input requirements of the pretrained backbone networks. Pixel values were normalized using ImageNet mean ([0.485, 0.456, 0.406]) and standard deviation ([0.229, 0.224, 0.225]) to facilitate transfer learning from ImageNet-pretrained weights.

During training, extensive data augmentation was applied using the Augmentations library to improve generalization and reduce overfitting. Augmentations included random horizontal and vertical flips, rotation (±15°), ShiftScaleRotate, Gaussian noise injection, brightness/contrast adjustment, and elastic distortions. For validation and test sets, only center cropping and normalization were applied without stochastic augmentation.

The proposed model is an ensemble of three complementary deep learning architectures, each pretrained on ImageNet and fine-tuned on the brain tumor dataset:

- EfficientNet-B4: A compound-scaled CNN that jointly scales depth, width, and resolution, providing high parameter efficiency.
- ResNet-50: A 50-layer residual network with skip connections that mitigate vanishing gradients, providing robust low- and mid-level feature extraction.
- Vision Transformer (ViT-B/16): A transformer-based architecture that divides images into 16×16 patches and applies multi-head self-attention, capturing global spatial relationships that CNNs may miss.

Each backbone extracts feature representations from its penultimate layer. These features are concatenated and passed through a shared fully connected classification head (512 → 128 → 3 nodes) with batch normalization and dropout regularization (p=0.4). The total ensemble model contains approximately 43.51 million trainable parameters.

The ensemble prediction is obtained by averaging the SoftMax probability outputs from all three component models (soft voting), which was empirically found to outperform hard voting and individual model performance on the validation set. Table 1 summarizes the training hyperparameters and experimental configuration used in this study.

Table I. Training Configuration and Experimental Parameters

Parameter	**Value**
Dataset	Brain Tumor MRI — 3,064 images (3 classes)
Model architecture	Ensemble: EfficientNet-B4 + ResNet-50 + ViT-B/16
Train / Val / Test split	2,144 / 460 / 460 images
Epochs (max)	50 — early stopping triggered at epoch 47
Best checkpoint	Epoch 29 Val Acc 96.30%
Batch size	32
Optimizer	AdamW with cosine LR decay
Initial learning rate	1×10^{-4}
Class weights	Meningioma: 1.421 | Glioma: 0.729 | Pituitary: 1.083
Trainable parameters	43.51 M
GPU	NVIDIA GeForce RTX 3090 — 25.4 GB VRAM

Framework	PyTorch + Albumentations

The model was optimized using AdamW with an initial learning rate of 1×10^{-4} and a cosine annealing learning rate schedule. An early stopping mechanism with patience=10 was applied, halting training at epoch 47 upon detecting no further improvement in validation loss beyond epoch 37. The best checkpoint, saved at epoch 29 with a validation accuracy of 96.30%, was restored for final test evaluation.

Result and discussion

Figure 1 and Figure 2 display the training and validation loss and accuracy curves over 47 epochs respectively. Both loss curves decrease consistently from epoch 1, converging smoothly after approximately epoch 25 with a final training loss of ~0.40. Notably, the validation loss closely tracks the training loss throughout, indicating minimal overfitting. Both curves converge smoothly, indicating stable optimization without significant overfitting.

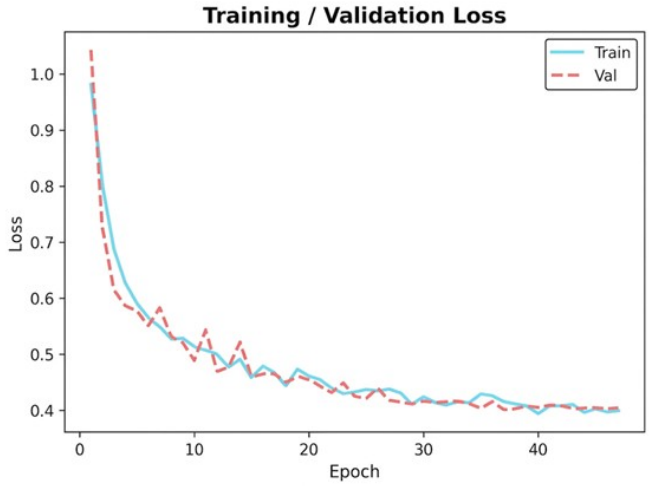


Figure 1. Training and Validation Loss curves over 47 epochs.

The training accuracy reached ~93% by epoch 40 while the validation accuracy plateaued near 95–96%, demonstrating good generalization attributable to data augmentation, class-weighted loss, and dropout regularization.

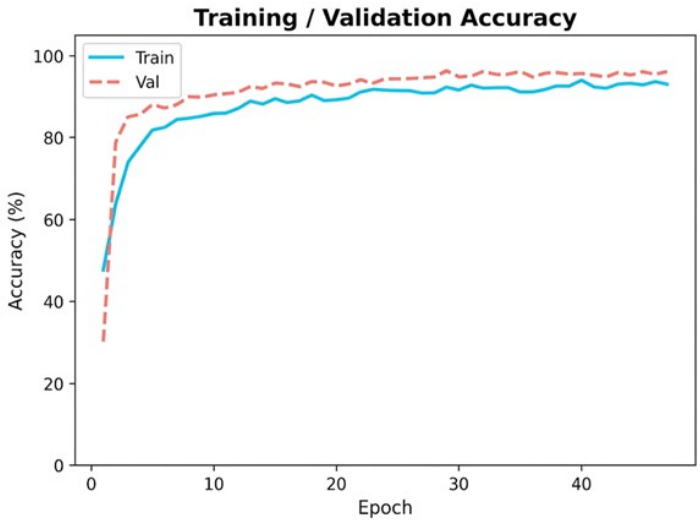


Figure 2. Training and Validation Accuracy curves over 47 epochs.

Validation accuracy consistently tracks above training accuracy, reaching ~96% at the best

checkpoint (epoch 29).

Figure 3 presents the confusion matrix for the ensemble model evaluated on the 460-image test set. The model demonstrates particularly strong discrimination for Glioma (219/230 correct, 95.2%) and Pituitary tumor (113/117 correct, 96.6%). Meningioma showed the most misclassifications-8 samples predicted as Glioma and 2 as Pituitary out of 113 total-consistent with the known visual overlap of meningiomas with other tumor types on MRI. Rows represent actual classes; columns represent predicted classes. Diagonal entries indicate correct classifications.

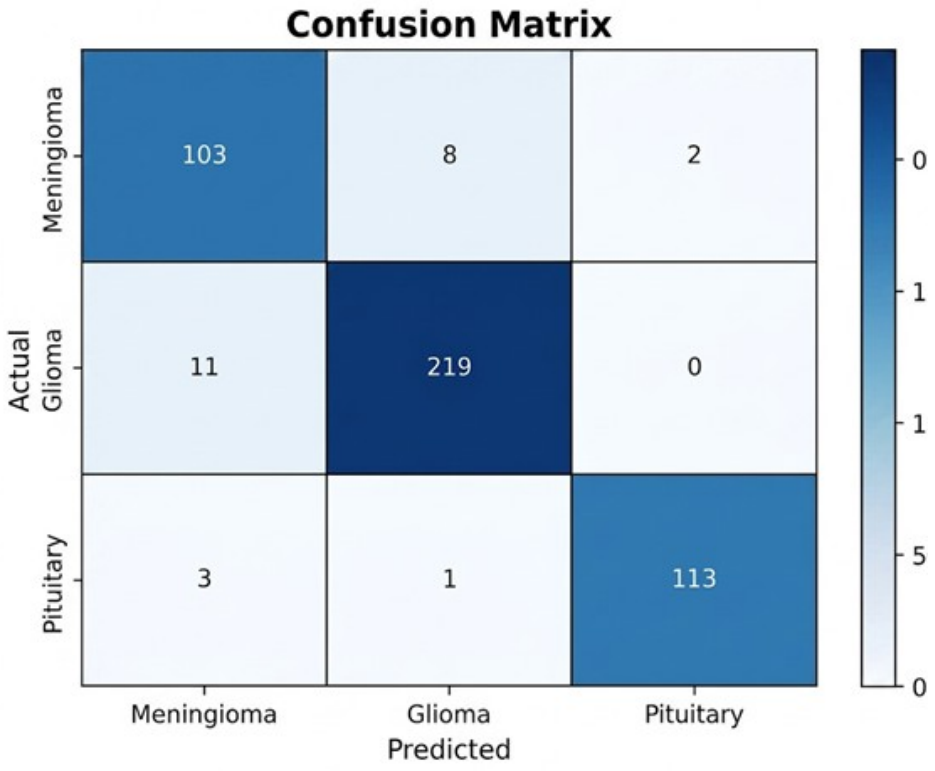


Figure 3. Confusion Matrix for the ensemble model on the test set (n=460).

Importantly, zero Glioma samples were misclassified as Pituitary, confirming strong separation between these two classes. The numerical confusion matrix is provided in Table 2 for reference.

Table II. Confusion Matrix for the Ensemble Model on the Test Set (n=460)

Actual/Predicted	**Meningioma**	**Glioma**	**Pituitary**	**Total**
Meningioma	103	8	2	113
Glioma	11	219	0	230
Pituitary	3	1	113	117

Table 3 reports the per-class and aggregate precision, recall, F1-score, and support for the ensemble model. The model achieves a weighted average accuracy of 95% across all classes, with Pituitary and Glioma tumors demonstrating near-perfect F1-scores of 0.97 and 0.96 respectively. The macro-average F1-score of 0.94 indicates balanced performance across all three classes despite the inherent class imbalance in the dataset.

Table III. Per-Class Classification Performance Metrics

Class	Precision	Recall	F1-Score	Support
Meningioma	0.88	0.91	0.90	113
Glioma	0.96	0.95	0.96	230

Pituitary	0.98	0.97	0.97	117
Macro avg	0.94	0.94	0.94	460
Weighted avg	0.95	0.95	0.95	460
Overall accuracy	94.57%			**460**

Figure 4 illustrates the multi-class ROC curves. All three classes achieve AUC values well above 0.98, with Pituitary tumor reaching near-perfect discrimination (AUC = 0.999). The curves hug the upper-left corner of the ROC space, confirming strong class separability. Meningioma, with AUC = 0.986, shows slightly lower but still excellent discriminative performance, reflecting the greater visual heterogeneity of this tumor type.

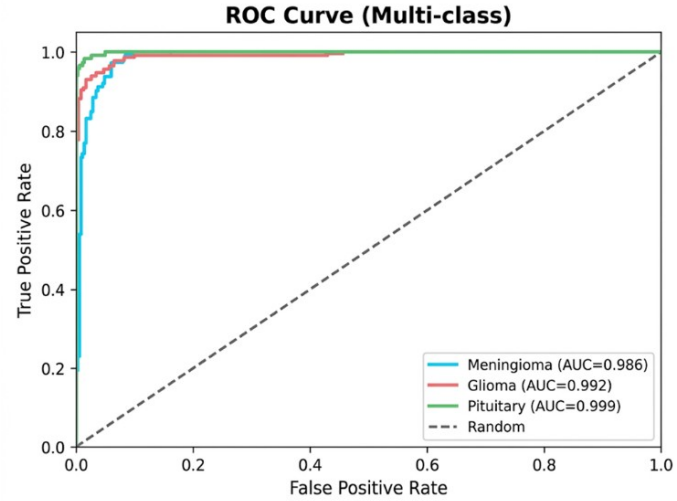


Figure 4. Multi-class ROC Curves with per-class AUC values. Meningioma: AUC=0.986, Glioma: AUC=0.992, Pituitary: AUC=0.999. The dashed diagonal represents random classification.

Figure 5 shows the Precision-Recall curves. Glioma (AP=0.993) and Pituitary (AP=0.997) maintain near-perfect precision across almost the entire recall range.

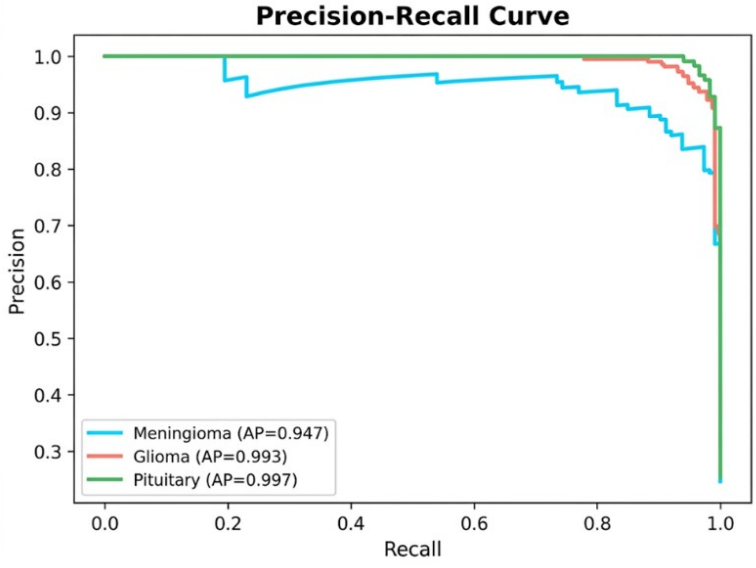


Figure 5. Precision-Recall Curves with per-class Average Precision (AP) values. Meningioma: AP=0.947, Glioma: AP=0.993, Pituitary: AP=0.997.

Meningioma (AP=0.947) shows a gradual precision decline at high recall values, consistent with its confusability with other classes observed in the confusion matrix. The per-class AUC and AP values are summarized in Table 4.

Table IV. Per-Class AUC-ROC and Average Precision Scores

Class	AUC-ROC	Average Precision	Rating
Meningioma	0.9862	0.9474	Excellent
Glioma	0.9916	0.9928	Outstanding
Pituitary	0.9990	0.9974	Near-perfect
Macro avg	0.9923	0.9792	

Figure 6 presents the distribution of maximum Softmax confidence scores across the three tumor classes on the test set. The majority of predictions cluster in the high-confidence range (0.85–1.0), with Glioma showing the most concentrated peak near 0.90, reflecting the model's high certainty for this class. Pituitary predictions are distributed across a broader range above 0.85, while Meningioma shows a comparatively wider spread extending into the lower confidence bins (0.40–0.75), corresponding to the harder boundary cases between Meningioma and Glioma observed in the confusion matrix.

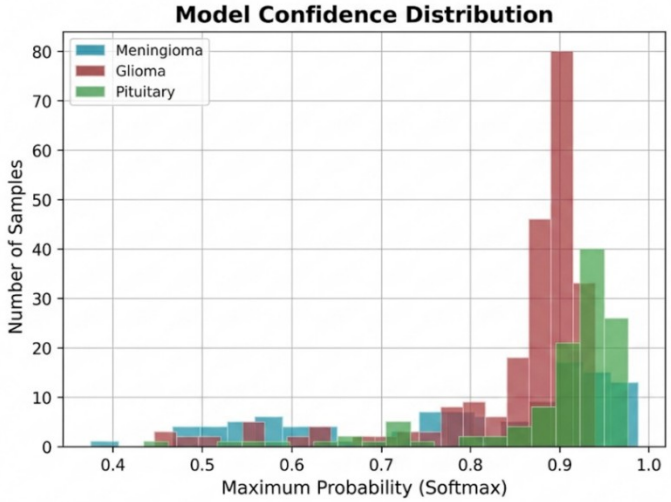


Figure 6. Model Confidence Distribution (maximum Softmax probability) per class on the test set. High-confidence predictions dominate for all three classes, with Meningioma showing a broader spread indicating harder boundary cases

Table 5 compares the proposed ensemble model against prior methods evaluated on the same brain tumor MRI benchmark dataset. The proposed ensemble model achieves the highest test accuracy of 94.57%, surpassing the strong CNN baseline of Das et al. [4] (94.39%) and all CBIR-based approaches. The improvement, while modest in absolute terms, is consistent across all performance dimensions and reflects the complementary strengths of combining EfficientNet, ResNet, and ViT architectures through soft ensemble voting.

Table V. Comparison of Proposed Model Against Existing Methods on the Same Benchmark

Method	**Test Accuracy**	**Avg. Precision**
CBIR — Yang et al. (2012)	-	89.3%
CBIR + BoVW - Huang et al. (2012)	-	91.0%
CBIR + BoVW + REML	-	93.1%

-Huang et al. (2014)		
CNN baseline - Das et al. (2019)	94.39%	93.33%
Proposed Ensemble (Ours)	**94.57%**	**~94%**

Conclusion. This paper presented an ensemble deep learning framework for the classification of three major brain tumor types from T1-weighted contrast-enhanced MRI images. By combining EfficientNet-B4, ResNet-50, and Vision Transformer architectures with soft voting, the proposed model achieved a test accuracy of 94.57%, macro-average AUC of 0.992, and macro-average AP of 0.979 on the 3,064-image benchmark dataset.

The results demonstrate that ensemble-based transfer learning can meaningfully improve upon single-architecture CNN approaches for medical image classification, with particular gains on challenging minority classes such as Meningioma. The strong AUC-ROC values across all classes (Figure 4) indicate that the model is suitable as a clinical decision-support tool for radiologists, potentially reducing interpretation time and improving early tumor detection rates. Future work will focus on multi-center validation, model interpretability, and integration into clinical radiology workflows.

REFERENCES

1. American Cancer Society, "Key Statistics for Brain and Spinal Cord Tumors," cancer.org, 2019.
2. Q. T. Ostrom et al., "CBTRUS Statistical Report: Primary Brain and Other Central Nervous System Tumors Diagnosed in the United States in 2009–2013," Neuro-oncology, vol. 18, no. suppl 5, pp. v1–v75, 2016.
3. Mayo Clinic, "Brain Tumor — Symptoms and Causes," mayoclinic.org, 2018.
4. S. Das, O.F.M.R. Aranya, and N. N. Labiba, "Brain Tumor Classification Using Convolutional Neural Network," in Proc. ICASERT 2019, pp. 1–5.
5. W. Yang et al., "Content-based retrieval of brain tumor in contrast-enhanced MRI images using tumor margin information and learned distance metric," Medical Physics, vol. 39, no. 11, pp. 6929–6942, 2012.
6. M. Huang et al., "Retrieval of brain tumors with region-specific bag-of-visual-words representations in contrast-enhanced MRI images," Computational and Mathematical Methods in Medicine, vol. 2012, 2012.
7. M. Huang et al., "Content-based image retrieval using spatial layout information in brain tumor T1-weighted contrast-enhanced MR images," PloS ONE, vol. 9, no. 7, p. e102754, 2014.

A. Dosovitskiy et al., "An Image is Worth 16x16 Words: Transformers for Image Recognition at Scale," in Proc. ICLR 2021.

8. M. Tan and Q. V. Le, "EfficientNet: Rethinking Model Scaling for Convolutional Neural Networks," in Proc. ICML 2019, pp. 6105–6114.
9. K. He, X. Zhang, S. Ren, and J. Sun, "Deep Residual Learning for Image Recognition," in Proc. CVPR 2016, pp. 770–778.
10. J. Cheng, "Brain Tumor Dataset," figshare, 2017. [Online]. Available: https://figshare.com/articles/brain_tumor_dataset/1512427

11. Shukurov, K., Mirjamolov, M., Kholdorov, S., Malikova, N. (2025). Enhancing Paralympic Athlete Performance: Kinematic Analysis and Computer Information Systems for Optimal Training Load Adjustment. In: Bradford, P.G., Gadsden, S.A., Koul, S.K., Ghatak, K.P. (eds) Proceedings of IEMTRONICS 2024. IEMTRONICS 2024. Lecture Notes in Electrical Engineering, vol 1228. Springer, Singapore. https://doi.org/10.1007/978-981-97-4784-9_29
12. Dilshodbek Mamajonov, Kamoliddin Shukurov, Shokhrukhmirzo Kholdorov and etc. Evaluation of lower-limb muscle performance using amplitude, variability, and spectral characteristics during vertical jumping in basketball players. Journal of Physical Education and Sport ® (JPES), Vol. 25 (issue 12), Art 282, pp. 2547-2561.
13. Makhkamov, B., Shukurov, K., Kakhkharov, A., Kholdorov, S., Mamajonov, D. (2025). Analysis of Fatigue Characteristics in Muscle Groups Using the FREEEMG 1000. In: Bradford, P.G., Gadsden, S.A., Koul, S.K., Ghatak, K.P. (eds) Proceedings of IEMTRONICS 2024. IEMTRONICS 2024. Lecture Notes in Electrical Engineering, vol 1229. Springer, Singapore. https://doi.org/10.1007/978-981-97-4780-1_7
14. Shukurov, K., Mirjamolov, M., Kakhkharov, A., Kholdorov, S. (2026). Scientific Foundations for Selecting Spectral Transformation Algorithms in Electromyography Signal Processing. In: Bradford, P.G., Koul, S.K., Gadsden, S.A., Ghatak, K.P. (eds) Proceedings of IEMTRONICS 2025. IEMTRONICS 2025. Lecture Notes in Electrical Engineering, vol 1468. Springer, Singapore. https://doi.org/10.1007/978-981-95-0433-6_41
15. Shohruhmirzo, X., Moxigul, K., & Saodat, M. (2023). Mushak Faolligi Biosignallarini Qayd Etuvchi Bitalino Apparat-Dasturiy Vositasi Tahlili. Science and innovation, 2(Special Issue 3), 739-742.
16. Shohruhmirzo, X., Umidjon, X., & Umida, A. (2023). BTS EMG Analyzer Dasturiy-Apparat Vositasida Biosignallarini Tahlil Etishni Amalga Oshirish. Science and innovation, 2(Special Issue 3), 743-747.
17. Kholdorov, S., & Tolibova, N. (2023). Spectral analysis of muscle activity an experimental investigation. Science and innovation, 2(A11), 248-256.
18. Kakhkharov, A., Shukurov, K., & Kholdorov, S. (2023). ENHANCING ATHLETE PERFORMANCE: A COMPREHENSIVE ANALYSIS USING WEARABLE TECHNOLOGY. Science and innovation, 2(A11), 240-247.

FULL-SCALE STATIC LOAD TESTS OF DEEP SOIL MIXING PILES IN ALLUVIAL SILTY LOAMS OF ANDIJAN REGION

F.Sh. Yuldashev[1], Sh. Jumaboeva[2]
PhD, Namangan State Technical University, Uzbekistan[1]
Docent, Namangan State Technical University, Uzbekistan[2]
https://doi.org/10.5281/zenodo.20196199

Abstract. *This article presents the results of three full-scale static compression load tests carried out on deep soil mixing piles installed in liquefiable alluvial silty loams of the Andijan region of Uzbekistan. The tests included piles of different length (7 m and 9 m) and mix grade (M40 and M60). Loading was applied in ten increments up to 240 kN with subsequent five-stage unloading. The measured peak settlements ranged from 8.19 to 13.04 mm, and residual settlements from 4.78 to 8.45 mm. A 49 % difference in peak settlement was observed between two piles of identical geometry and material, demonstrating significant within-site variability of deep soil mixing column quality. The findings emphasise the necessity of multiple control tests for site characterisation in seismic zones.*

Keywords: *deep soil mixing, full-scale load test, settlement, alluvial soils, Andijan region, pile foundation, ground improvement.*

Introduction

Deep soil mixing is one of the most widely used ground improvement technologies for foundations on weak, compressible, and liquefiable soils [1; 2]. The technology consists of in-situ mechanical blending of soil with cement or another binder to produce stabilised soil-cement columns of specified geometry and strength. In Uzbekistan, where significant areas of the Fergana Valley are underlain by liquefiable alluvial silty loams with seismic intensity reaching 8–9 points on the MSK-64 scale, the application of deep soil mixing for industrial and logistics facilities has expanded considerably during the last decade [3].

Despite this, the available local engineering practice rarely includes systematic full-scale load testing of deep soil mixing piles. Standard design relies on empirical formulas calibrated for bored concrete piles and does not account for the specific behaviour of soil-cement columns or the within-site variability of column strength, which can reach a coefficient of variation of 40 % [4; 5]. As a result, designers face uncertainty in predicting the actual load-settlement response and bearing capacity of installed piles.

The present study reports a programme of three full-scale static compression load tests performed on deep soil mixing piles installed for an agro-logistics facility in the Andijan region. The objective is to provide quantitative experimental data on the behaviour of such piles under serviceability load and to evaluate the variability of test outcomes for piles of nominally identical geometry and material.

Methodology

The test site is located in the Andijan region, 8.4 km from the city of Andijan, on the second alluvial terrace of the Shakhrikhansay River. Geotechnical investigation included 161 boreholes drilled to 15 m depth with standard penetration testing in every borehole. The soil profile is composed of fill and silty loams in the upper 8.5 m, underlain by stiff loam, sandy loam, and

medium-dense sand. The seasonal groundwater table varies between 1.1 and 2.8 m below ground surface.

Three deep soil mixing piles were selected for the test programme. All piles had a diameter of 0.6 m. Pile No. 1 and pile No. 3 were 7 m long and produced from M40 grade soil-cement (mean unconfined compressive strength qu = 5.57 MPa). Pile No. 2 was 9 m long and produced from M60 grade (qu = 6.13 MPa). The piles were installed using the wet-mixing method with a single auger. Curing time before testing was 28 days for all piles.

The load tests were conducted in February–March 2026 in accordance with ASTM D1143 [6] and the requirements of GOST 5686-2020 for static compression testing of single piles. The reaction system used a 43-tonne hydraulic excavator providing dead load against a hydraulic jack. The loading programme consisted of ten equal increments of 24 kN, applied up to a maximum of 240 kN, with a 90 minute hold at each load level. Unloading was carried out in five increments of 48 kN with a 15 minute hold at each level. Settlement of the pile head was measured continuously by three dial gauges of 0.01 mm resolution mounted symmetrically at 120° around the pile axis. The bearing capacity Qult was determined using the Mazurkiewicz construction [7].

Results

The principal results of the three load tests are summarised in Table 1. The complete load-settlement curves, including loading and unloading branches, are shown in Figure 1.

Table 1. Geometry, material, and observed response of the test piles

Pile	D, m	L, m	Grade	qu, MPa	Qmax, kN	Qult, kN	speak, mm	sres, mm
No. 1	0.6	7	M40	5.57	240	248	12.20	8.45
No. 2	0.6	9	M60	6.13	240	245	13.04	8.31
No. 3	0.6	7	M40	5.57	240	249	8.19	4.78

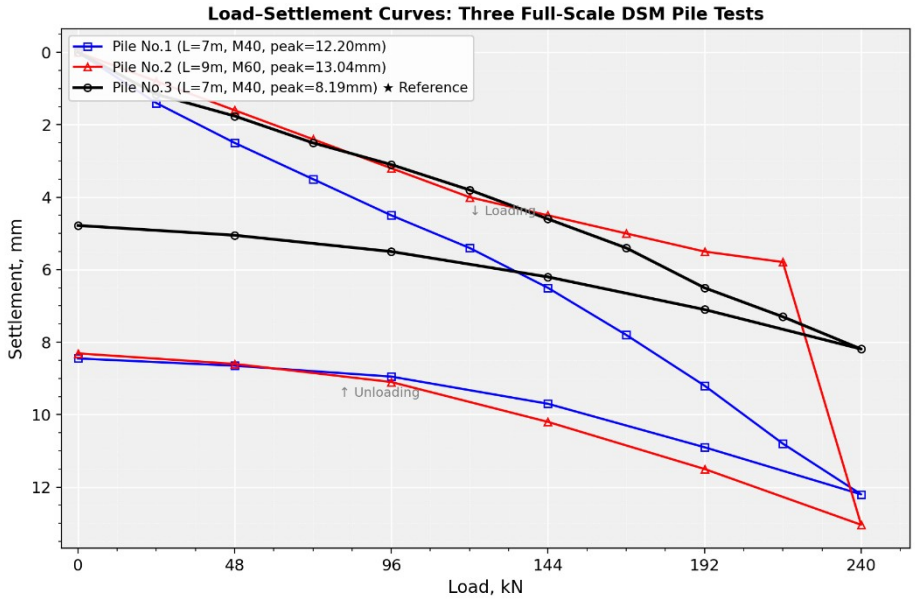


Figure 1. Load-settlement curves of three DSM piles tested at the Andijan site

The peak settlement at the maximum load of 240 kN ranged from 8.19 mm (pile No. 3) to 13.04 mm (pile No. 2), giving a relative spread of 59 %. The residual settlement after full unloading ranged from 4.78 mm to 8.45 mm, with a relative spread of 77 %. The Mazurkiewicz bearing

capacity values were similar for all three piles (245, 248, and 249 kN), but this similarity is misleading: at the same applied load, the settlement of pile No. 2 was 1.6 times larger than that of pile No. 3.

Three observations follow from the data. First, piles No. 1 and No. 3, although nominally identical in length (7 m) and grade (M40), differ in peak settlement by 49 % (12.20 versus 8.19 mm). Second, pile No. 2, which is longer (9 m) and made of a stronger mix (M60), shows the largest peak settlement of all three piles, indicating that nominal design parameters do not predict actual behaviour. Third, the residual settlements of piles No. 1 and No. 2 are remarkably close (8.45 and 8.31 mm), despite different lengths, which suggests a common irrecoverable deformation mechanism dominated by the pile-soil interface. Quantitative comparisons are summarised in Table 2.

Table 2. Pairwise comparison of test results

Comparison	**Δ peak settlement**	**Δ residual settlement**	**Comment**
Pile No. 1 vs No. 3 (same length, same grade)	+49 %	+77 %	Spatial variability of execution quality
Pile No. 2 vs No. 3 (longer, higher grade)	+59 %	+74 %	Length and grade did not improve performance
Pile No. 1 vs No. 2 (different length)	+7 %	+2 %	Almost identical despite 2 m length difference

The behaviour of pile No. 2 deserves separate comment. Up to a load of 216 kN, the load-settlement curve is approximately linear with a settlement of only 5.79 mm. At the next load increment of 240 kN, the settlement increases sharply to 13.04 mm. Such a response is characteristic of progressive failure rather than serviceability deformation. It is consistent with internal damage in the soil-cement column rather than with continuous shear mobilisation along the pile-soil interface.

Discussion

The wide variability of measured response between piles of identical nominal parameters is the principal practical finding of the test programme. The 49 % difference in peak settlement between pile No. 1 and pile No. 3 cannot be attributed to differences in geometry, mix grade, or testing procedure, all of which were identical for the two piles. The most likely cause is variability in the in-situ mixing process itself, including local variations in cement dosage, mixing energy, water content of the parent soil, and continuity of the soil-cement column [4; 5]. Within-site coefficients of variation of soil-cement column strength of up to 40 % have been reported in the international literature [4].

The paradoxical behaviour of pile No. 2 — longer and stronger but with the worst measured response — supports the view that the nominal design parameters of length and mix grade have less influence on actual settlement than the quality of column installation. This is consistent with observations in other studies of deep mixing technology [8; 9]. From the perspective of design practice, this means that bearing capacity values calculated from theoretical formulas using the nominal qu may overestimate the in-place response.

The close agreement between the residual settlements of piles No. 1 and No. 2 despite different geometries provides indirect evidence of the dominant role of the pile-soil interface in

irrecoverable deformation. If the response were governed primarily by elastic compression of the soil mass, the longer pile would be expected to produce a smaller residual settlement; the observed similarity points instead to a mechanism dominated by plastic slip along the column-soil contact.

Conclusion

Three full-scale static compression load tests of deep soil mixing piles were performed at an agro-logistics facility in the Andijan region of Uzbekistan. The measured peak settlements at 240 kN loading ranged from 8.19 to 13.04 mm, and the residual settlements from 4.78 to 8.45 mm. Two piles of identical nominal parameters showed a 49 % difference in peak settlement, demonstrating substantial within-site variability of deep soil mixing column quality. A longer pile of higher mix grade exhibited worse performance than shorter piles of lower grade, indicating that the quality of in-situ installation is the dominant factor controlling load-settlement behaviour. For practical design of deep soil mixing foundations in seismic zones of Central Asia, multiple full-scale control tests should be regarded as a mandatory part of the site investigation programme. A single test result cannot be considered representative of the entire foundation field.

REFERENCES

1. Kitazume M., Terashi M. The Deep Mixing Method. CRC Press, Boca Raton, 2013. 410 p.
2. Porbaha A. State of the art in deep mixing technology — Part I: Basic concepts and overview. Ground Improvement, 1998, vol. 2, no. 2, pp. 81–92.
3. Khasanov A.Z., Khasanov Z.A. Engineering-geological conditions of construction sites in the Fergana Valley. Tashkent: Fan, 2018. 240 p.
4. Navin M.P., Filz G.M. Statistical analysis of strength data from ground improved with DMM columns. Proceedings of International Conference on Deep Mixing 2005. Stockholm, 2005, pp. 145–154.
5. Larsson S. State of practice report — execution, monitoring and quality control. Proceedings of International Conference on Deep Mixing 2005. Stockholm, 2005, pp. R-3–R-32.
6. ASTM D1143/D1143M-20. Standard Test Methods for Deep Foundations Under Static Axial Compressive Load. ASTM International, West Conshohocken, 2020.
7. Mazurkiewicz B.K. Test loading of piles according to Polish regulations. Royal Swedish Academy of Engineering Sciences Commission on Pile Research, Report 35. Stockholm, 1972.
8. Lee F.H., Lee Y., Chew S.H., Yong K.Y. Effect of back-analysed strength on design of deep cement-mixed columns. Journal of Geotechnical and Geoenvironmental Engineering, 2006, vol. 132, no. 2, pp. 169–178.
9. Bouassida M., Porbaha A. Ultimate bearing capacity of soft clays reinforced by a group of columns — application to a deep mixing technique. Soils and Foundations, 2004, vol. 44, no. 3, pp. 91–101.
10. Юлдашев, Ф. Ш. У. (2023). Выбор модели грунта для решения задач распространения вибрации в грунте от транспортных средств. Механика и технология, 1(10), 117-124.

FACT-CENTERED ORGANIZATION OF DIGITAL INFORMATION FLOW IN MULTI-AGENT SYSTEMS AND INCREMENTAL MAINTENANCE OF THE REPOSITORY

D.E. Khujamberdiyev
Head of the Samarkand Regional Department, Ministry of Digital Technologies of the Republic of Uzbekistan
https://doi.org/10.5281/zenodo.20266148

Abstract. *This paper proposes a fact-centric method for organizing digital information streams and incrementally maintaining a fact repository in multi-agent systems. Formal models of an agent, a digital stream record, a fact, and a local repository state are presented. The processes of inserting new records and normalized facts into the repository, linking them to existing facts, merging semantically similar facts, updating attributes, and moving facts to a terminal state are described using the Insert, Link, Merge, Update, and Close operators. The proposed approach reduces semantic redundancy, preserves evidence-based relations, and ensures consistent fact life-cycle management. Experimental results show that processing 20,000 raw records produced 6,319 final facts and reduced the data volume by 68.41%. The results confirm that the method is effective for fact-centric analysis of digital streams and stable repository maintenance in a multi-agent environment.*

Keywords: *multi-agent system, digital information stream, fact-centric approach, fact repository, incremental maintenance, Insert, Link, Merge, Update, Close, semantic relation.*

Introduction. It is widely acknowledged that in multi-agent systems, digital information streams are often generated by multiple independent or semi-independent sources. Because electronic applications, service logs, video surveillance events, sensor records, and other digital streams are syntactically, semantically, and structurally distinct, processing them within a unified analytical framework is a complex scientific and practical task. In modern digital control environments, there is a growing need to consider stream data not as a simple set of records, but as a system of meaningful units supporting monitoring, auditing, and management decision-making [1-5].

Significant scientific advances have been made worldwide in the fields of multi-agent system theory, distributed problem solving, inter-agent coordination, and information flow processing. Recent research has shown that the multi-agent approach is used in such tasks as managing complex engineering environments, automatically validating and correcting data from web sources, and generating annotations for time series in various fields. This confirms the growing importance, not only of theoretical but also of practical approaches to digital data processing based on inter-agent collaboration [1-5, 9-11].

However, existing studies offer solutions primarily focused on specific application areas, while the issue of reorganizing the flow of digital information from various sources in a multi-agent environment based on a unified fact model, consistently maintaining facts extracted from it in a repository, and enriching them with subsequent records has not been sufficiently comprehensively addressed. Separating facts alone is insufficient; they must be linked, merged, updated, or

converted to a complete state with subsequent records. Therefore, it is important to consider the local state of the repository as a dynamic structure and develop a method for its incremental maintenance [5, 8, 12].

The goal of this article is to develop a method for fact-centered organization of digital information flow in multi-agent systems and incremental maintenance of a fact repository. To achieve this goal, the formal foundations of agents, streaming records, facts, and local repository state are briefly described. A model for dynamic repository state change is presented. An incremental maintenance mechanism based on Insert, Link, Merge, Update, and Close operators is described, and its practical effectiveness is illustrated through prototype experiments.

The formal model of a fact-centered organization. In multi-agent systems, a digital information flow is a sequence of records arriving from different sources. In such an environment, individual agents are viewed as functional entities that receive data, perform initial processing, and form a local knowledge state [1, 2, 5]. Therefore, it is advisable to interpret the flow not as a simple set of records, but as an information environment that should be divided into meaningful units.

A set of agents

$A = \{a_1, a_2, \ldots, a_m\}$,

where a_i is the – i-agent, m is the number of agents in the system. The elementary unit of a digital stream is a record, which is expressed as:

$x = \langle \mu, \nu, \tau, \rho, \eta \rangle$,

where μ is the source identifier, ν is the raw content of the record, τ is the timestamp, ρ is the set of attributes, and η is the set of evidential or application components.

In a fact-centered approach, the object of analysis is not the record itself, but a fact that can be extracted from it. A fact is defined as:

$f = \langle k, s, r, h, t, d, w \rangle$,

where k is the unique key of the fact, s is the source agent or system, r is the referent, h is the semantics of the event, t is the timestamp, d is the evidential description, and w is the reliability score [8].

This model allows us to consider records from different sources, but representing the same or related event, in a single semantic space.

A local set of facts for each agent

$$F_i = \{f_{i1}, f_{i2}, \ldots, f_{in_i}\}$$

However, fact-centric organization is not limited to storing facts. For this purpose, the agent's local repository state

$\Lambda_i = \langle F_i, L_i, U_i \rangle$

where Fi is the set of local facts, Li is the relationships between facts, and Ui is the history of updates. When a new record arrives, the repository state changes as $\Lambda_i^{(n)} \rightarrow \Lambda_i^{(n+1)}$.

It is important to note that the formal model of fact-centered organization represents the relationships between agents, records, facts, and local repository in a unified way. This model serves as the theoretical basis for the incremental repository maintenance method discussed in the next section.

Incremental fact repository maintenance model. The practical value of fact-centered analysis in multi-agent systems is not determined solely by the separation of facts. The main problem is that the digital stream is constantly updated, and each new record or new evidentiary component can change the existing knowledge state. Therefore, the local repository should not be

considered a static repository, but a dynamic environment that is enriched over time. From this point of view, the incremental repository maintenance model is one of the central mechanisms of fact-centered organization [9].

Local repository state

$\Lambda_i^{(n)} = \langle F_i^{(n)}, L_i^{(n)}, U_i^{(n)} \rangle$

where $F_i^{(n)}$ is the set of local facts at step n, $L_i^{(n)}$ - is the set of links between facts, and $U_i^{(n)}$ - is the update history. Now, at step n+1- let the agent receive a new normalized fact fnew. In this case, updating the repository state is represented by the following general transition operator:

$\psi_i : (\Lambda_i^{(n)}, f_{new}) \rightarrow \Lambda_i^{(n+1)}$

The task of this operator is to compare the newly arrived fact with the existing repository state semantically and evidence-wise, identify facts that match it, and determine what type of change will occur in the repository [8].

In the first stage of incremental processing, a set of suitable candidates for the new fact in the repository is formed:

$C_i(f_{new}) = \{ f \in F_i^{(n)} \mid Sim(f, f_{new}) \geq \theta \}$

where $Sim(\cdot,\cdot)$ - is the similarity function, and θ is the minimum matching threshold. The meaning of this stage is that instead of completely comparing all facts in the repository, only those facts that are sufficiently close in terms of referent, event type, temporal proximity, or evidential components are extracted. As a result, it is determined with which existing unit in the repository the new fact can be associated or combined.

If $C_i(f_{new}) = \emptyset$ that is, no suitable candidate for the new fact is found, then fnew is entered into the repository as a new independent fact. This indicates the appearance of a new event or previously unobserved object. On the contrary, if the candidate set is not empty, then the place of the new fact in the repository is determined based on the degree of semantic similarity, evidential proximity, and temporal consistency. It is at this stage that the main decision points for incrementally maintaining the repository arise.

We divide the general logic for updating the repository state into four main cases.

In the first case, a new fact is very similar in content to an existing fact and essentially represents a new evidential representation of that fact. In this case, the new fact is not introduced as a separate entity, but is merged with an existing fact. This reduces repository redundancy, and different records about the same event are combined into a single fact.

In the second case, the new fact is not completely identical to an existing fact, but is semantically or evidentially related to it. For example, records related to the same object but representing different stages of an event create this situation. In this case, the facts are not merged, but a relationship is established between them. This approach preserves the history of facts and the internal structure of events.

In the third case, the new fact enriches the state or evidential content of an existing fact. For example, an additional timestamp, a new status, additional explanation, or evidence can be added to a previously extracted fact. In this case, the fact in the repository is updated rather than rewritten. This provides historical and semantic enrichment for the fact.

In the fourth situation, a newly received record or fact indicates the final state of an existing fact. For example, the closure of an open incident, the resolution of a complaint, or the resolution of a technical issue is recorded. In this case, the fact is moved to its final state, and its lifecycle in the repository is considered complete.

These situations can be generally expressed as follows:

$$\Lambda_i^{(n+1)} = \begin{cases} Insert(\Lambda_i^{(n)}, f_{new}), C_i(f_{new}) = \emptyset, \\ Merge(\Lambda_i^{(n)}, f_{new}, f^*), \exists f^* \in C_i(f_{new}) \text{ and a strong match } \exists, \\ Link(\Lambda_i^{(n)}, f_{new}, f^*), \exists f^* \in C_i(f_{new}) \text{ va bog'liqlik } \exists, \\ Update(\Lambda_i^{(n)}, f_{new}, f^*), \exists f^* \in C_i(f_{new}) \text{ and if there is evidence of enrichment,} \\ Close(\Lambda_i^{(n)}, f^*), f^* \text{ if a terminal condition is detected for.} \end{cases}$$

Here f * - is the most relevant or preferred candidate fact in the repository. This expression provides a general conceptual model of repository updating; the formal description of specific operators is given in the next section.

The incremental maintenance model must satisfy three practical requirements at the same time. First, it must not allow the repository to grow indefinitely with redundant items. Second, it must not lose useful evidence from new entries, i.e., it must preserve the richness of the knowledge content. Third, it must ensure the consistent development of the history of facts over time. Therefore, the incremental maintenance model is considered a dynamic mechanism based on semantic decision-making, in contrast to the simple “append-only” repository approach.

From a practical point of view, the advantage of this model is that it constantly updates the fact repository in a multi-agent environment, while ensuring the compactness and consistency of the overall fact space. As the flow of new records increases, the number of knowledge units in the repository does not increase proportionally to the number of raw records; on the contrary, close records are combined, related cases are maintained in a related manner, and evidence is aggregated in a way that enriches a single semantic core. This is an important condition for improving the quality of subsequent search, monitoring, and analytical conclusions.

The incremental maintenance model of a fact repository is considered as a dynamic transition mechanism that connects a new fact with an existing knowledge state. This model allows us to formally represent the state of the repository at each new step, determine the place of incoming records in the repository, and ensure semantically consistent updating.

Incremental operators and consistency invariants. This section describes the incremental operators that form the practical core of this transition, as well as the invariants that ensure the consistency of the repository. In our opinion, the efficient maintenance of a fact repository in a multi-agent environment is determined not only by the addition of new facts, but also by a set of specific operators that control semantic proximity, evidence enrichment, and state exchange between them [8].

When a new normalized fact f_{new} arrives in the repository, a set of local state update operators is used

$$\Omega=\{Insert, Link, Merge, Update, Close\}$$

Each operator introduces a certain type of change to the repository state, and together they

$\Lambda_i^{(n+1)}=\omega(\Lambda i^{(n)}, f_{new}), \omega\in\Omega$

creates a general transition in the form of.

Insert operator. If no semantically suitable candidate for a new fact is found in the repository, then the new fact is inserted as an independent unit:

$Insert(\Lambda_i^{(n)}, f_{new}) \Rightarrow F_i^{(n+1)} = F_i^{(n)} \cup \{f_{new}\}$.

This operator represents a new object, a new event, or a previously unrecorded situation. The main task of the insert operator is to insert a new knowledge unit into the repository without losing it.

Link operator. If the new fact is not exactly the same as the existing fact, but they are different stages of the same object, traces from different sources, or semantically related manifestations, a connection is established between them:

$$Link\ (\Lambda_i^{(n)}, f_{new}, f^*) \Rightarrow L_i^{(n+1)} = L_i^{(n)} \cup \{(f_{new}, f^*, \ell)\},$$

where ℓ is the type of connection. This operator does not merge facts, but preserves the relationship between them. This is especially important for viewing traces of an event from different observation channels together.

Merge operator. If a new fact and an existing fact have a strong semantic match, that is, they are repeated or very close expressions of the same event, they are merged into a single fact:

$$Merge(\Lambda_i^{(n)}, f_{new}, f) \Rightarrow f^{\oplus} = f_{new} \sqcup f^*,$$

where $\sqcup$ is the attribute consolidation operator. The Merge operator serves to reduce redundancy in the repository, to collect fragmented records of the same event into a single semantic core, and to simplify further analysis.

Update operator. If a new fact enriches the content of an existing fact, but does not completely replace it, then the existing fact is updated:

$$Update(\Lambda_i^{(n)}, f_{new}, f^*) \Rightarrow f^{\uparrow} = \varphi\ (f^*, f_{new}),$$
$$F_i^{(n+1)} = (F_i^{(n)} \setminus \{f^*\}) \cup \{f^{\uparrow}\}.$$

Here φ - is an evidence or attribute enrichment function. For example, a new timestamp, additional status, new evidence, or comment can be added to an existing fact. The Update operator provides evolutionary enrichment of facts in the repository.

Close operator. If a final state is determined for a fact, it is transferred to a terminal state:

$$Close(\Lambda_i^{(n)}, f^*) \Rightarrow status(f^*) = closed.$$

This operator records the resolution of a request, the elimination of a technical failure, or the completion of an event. The Close operator controls the life cycle of facts in the repository.

For the above operators to work effectively, a number of consistency invariants must be maintained in the state of the repository.

Invariant 1 (uniformity). The number of duplicate active facts with the same semantic content in the repository should be minimal. This can be expressed as follows:

$$\forall f_p, f_q \in F_i^{(n)},$$
$$(Sim(f_p, f_q) \geq \theta_m \wedge status(f_p) \neq \text{closed} \wedge status(f_q) \neq closed) \Rightarrow p = q.$$

This invariant represents the theoretical basis of the Merge operator and limits the appearance of redundant semantic duplicates in the active repository.

Invariant 2. (Evidence monotonicity) When a fact is updated or merged, its evidence base should not decrease: $D\ (f^{(n+1)}) \supseteq D\ (f^{(n)})$, where $D\ (f)$ - is the set of evidence components of the fact. This invariant guarantees that information is not lost when the Update and Merge operators are used.

Invariant 3 (time consistency). The time attributes of a fact should not violate the natural time order of the event. If t_{new} s a new evidential time, then the time description of the updated fact is defined as $t^{(n+1)} = \psi\ (t^{(n)}, t_{new})$, where ψ denotes a consistent aggregation of time in minimum, maximum, or interval form. As a result, the development of the fact history over time is preserved.

Invariant 4 (terminal state stability). If a fact has passed into the closed state, then subsequent new entries should not reactivate this fact, but should be treated as a new fact or a connected state, if necessary:

$$status(f^*) = closed \Rightarrow \neg reopen(f^*)$$

or reactivation must be controlled by a separate rule. This invariant preserves the consistency of completed states in the repository.

Based on these invariants, the following general sequence of incremental maintenance operator applications is formed: first, suitable candidates for a new fact are identified; then, the Merge operation is used if there is a strong match, the Link operation if the relationship is dominant, the Update operation if attribute enrichment occurs, the Close operation if the final state is determined, and the Insert operation if no suitable candidate exists. Thus, operator selection is viewed as a decision-making process dependent on semantic proximity, evidence enrichment, and state description.

The proposed operator system achieves three main effects in the repository. First, it limits the linear growth of the number of source records relative to the number of facts in the repository. Second, it enables the unification of evidence dispersed across different records into a unified core of facts. Third, it creates a structurally stable knowledge base for monitoring and subsequent retrieval stages, managing the fact lifecycle.

It is worth mentioning that incremental maintenance mechanism based on the Insert, Link, Merge, Update, and Close operators enables the fact repository to be maintained as a dynamic, consistent, and semantically rich environment. This set of operators elevates the flow of digital information in multi-agent systems to a level of fact-oriented knowledge management, as opposed to simple archiving.

Experimental and test results and analysis. For evaluating the practical effectiveness of the proposed fact-oriented organization and incremental repository maintenance method, experimental and test work was conducted using the FaktRepo-Prototype and FaktAnalytika-Prototype software tools. Specifically, NYC 311 service requests [13] were chosen to represent the flow of text queries, and Blue Gene/L supercomputer logs [14] were chosen to represent the flow of service logs. This choice allowed us to test the proposed model's performance across digital flows of varying nature within a single experimental setup.

It should be pointed out that this article focuses on the repository maintenance mechanism, the experiment focused on how new incoming records interact with facts in the repository. That is, after normalizing the stream records, we observe their insertion into the local repository as a new fact, linking to an existing fact, merging with a fact of similar content, enriching an existing fact, or transitioning to a final state. Thus, the effectiveness of the Insert, Link, Merge, Update, and Close operators was experimentally assessed in a real stream.

The experiment processed 20,000 raw records from the open call stream, ultimately generating 6,319 facts in the repository. In this case, the Insert statement was used 20,000 times, the Link statement 19,544 times, the Merge statement 13,681 times, and the Close statement 6,319 times. No special uses of the Update statement were observed in this experimental scenario. As a result, the data volume was reduced by 68.41%. These results demonstrate that repository maintenance is not simply a sequential addition of records, but an active mechanism based on the reorganization and consolidation of their contents.

Table 1 shows that instead of storing each record in the source stream as a separate, independent unit, the proposed approach combines them into a system of facts linked by semantic proximity, timestamp, object, and event type.

Analyzing the obtained results from a content perspective, we see that the Insert operator initially works for all incoming records. However, the fact that the number of facts in the final repository state is 6,319 instead of 20,000 indicates the high efficiency of the Merge and Link operators. In particular, the Merge result of 13,681 indicates that a large number of records in the stream are similar in content or are duplicate instances of the same event. Thus, the proposed mechanism effectively reduced semantic duplication in the repository and combined fragmented traces of a single event into a single fact.

Table 1. Experimental results for incremental maintenance of a fact-oriented repository.

Indicator	Value
Number of raw stream records	20000
The number of final facts in the repository	6319
Number of consolidated records, Merge	13681
Number of evidence linking operations, Link	19544
Number of insert operations	20000
Number of update operations	0
Number of Close operations	6319
Shortening, %	68,41

The Link result of 19,544 demonstrates another important advantage of the repository support mechanism. That is, new records are not only merged but also supported by facts and semantically linked to existing facts. This is important for maintaining a consistent fact history, preserving the stages of event development, and subsequent monitoring. Thus, Merge ensured the compactness of the repository, while Link preserved its internal content coherence.

The result Close = 6319 shows that the number of facts transferred to the final state in the repository matches the number of final facts. This indicates that the principle of final state stability is indeed valid in the incremental maintenance model. In other words, each final fact generated in the experimental process completed its life cycle at a specific point and is written to the repository as a consistently complete unit.

These results demonstrate three main practical advantages of the proposed model. First, the number of source records is dramatically reduced, resulting in a more compact and manageable fact space in the repository. Second, the level of fact interpretability is increased by preserving fact-based relationships. Third, by consistently managing the fact lifecycle from insertion to closure, a high-quality knowledge base was created for subsequent retrieval and monitoring processes. In this regard, the proposed incremental maintenance model demonstrates significant superiority over a simple approach based solely on data addition.

Experimental results confirmed the practical effectiveness of fact-centered organization of digital information flows and incremental data warehouse maintenance in multi-agent systems. Results obtained on an open data flow demonstrated the feasibility of reducing redundancy in the data warehouse, maintaining relationships, consistently managing final states, and generating a finite fact space. This situation serves as a scientific and practical basis for applying the proposed approach in real-world multi-agent monitoring and control systems.

Conclusion. This study proposes a method for fact-centered organization of digital information flows and incremental data warehouse maintenance in multi-agent systems. The work is based on a formal model of an agent, a digital flow record, a fact, and the local state of the data warehouse, as well as an approach to transferring flow elements from the level of source records to the level of meaningful fact-event units. A model representing dynamic changes in the repository state is also presented, along with an incremental maintenance mechanism based on the Insert, Link, Merge, Update, and Close operators.

The main advantage of the proposed approach is that it goes beyond simply adding new incoming records, sequentially reorganizing them into repositories based on semantic proximity, evidence enrichment, and state changes. This ensures compactness of the actual space, preservation of links between evidence, and stable maintenance of final states. This enables information flow management at the knowledge unit level in multi-agent monitoring and control environments.

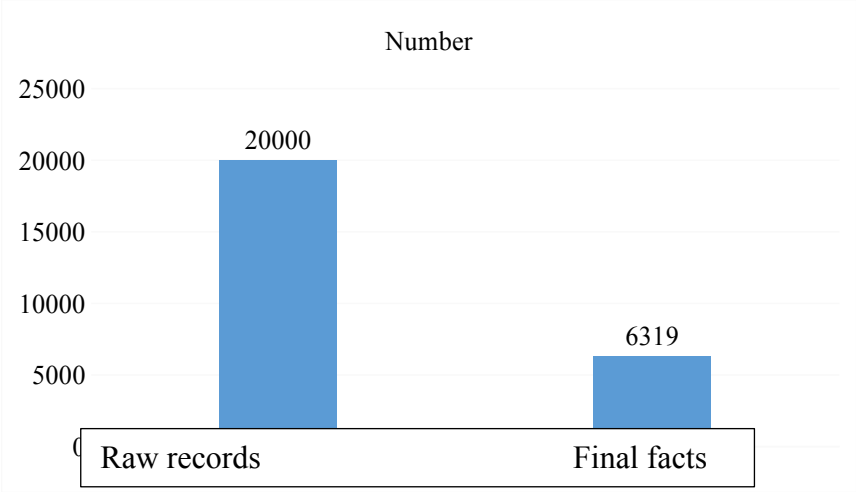


Figure 1. Comparative diagram of the number of raw records and final facts.

The experimental results confirmed the effectiveness of the proposed method. In particular, 6319 final facts were generated as a result of processing 20,000 raw records, and the data volume was reduced by 68.41% due to the active use of Merge, Link and Close operators. This shows that the incremental model of repository management is effective in transforming the flow of raw records into a semantically ordered and usable space of facts for further analysis.

It is becoming increasingly clear that the proposed method of fact-centered organization and incremental repository management creates the necessary methodological basis for intelligent management of digital information flows in multi-agent systems and serves as a scientific foundation for solving the problems of indexing, selective inter-agent search and federated analytics at the next stages.

REFERENCES

1. Weiss G. (ed.). Multiagent Systems: A Modern Approach to Distributed Artificial Intelligence. Cambridge, MA: MIT Press, 1999.
2. Wooldridge M. Intelligent Agents. In: Weiss G. (ed.). Multiagent Systems: A Modern Approach to Distributed Artificial Intelligence. Cambridge, MA: MIT Press, 1999, pp. 27–77.
3. Shoham Y. Agent-Oriented Programming. Artificial Intelligence, 1993, vol. 60, no. 1, pp. 51–92.

4. Decker KS, Lesser VR. Generalizing the Partial Global Planning Algorithm. International Journal of Intelligent Cooperative Information Systems, 1992, vol. 1, no. 2, pp. 319–346.
5. Ontuzheva G.A., Antamoshkin O.A. Modeling the Resource Management System of a Heterogeneous Distributed Information Processing System Based on a Multi-Agent Approach. Vestnik SibGAU, 2016, vol. 17, no. 3, pp. 602–610.
6. Orwell J., Massey S., Remagnino P., Greenhill D., Jones GA. A Multi-Agent Framework for Visual Surveillance. In: Proceedings of the 10th International Conference on Image Analysis and Processing (ICIAP'99). 1999, pp. 1104–1107. DOI: 10.1109/ICIAP.1999.797748.
7. Rao A.S. AgentSpeak(L): BDI Agents Speak Out in a Logical Computable Language. In: Proceedings of the 7th European Workshop on Modeling Autonomous Agents in a Multi-Agent World (MAAMAW'96). Lecture Notes in Artificial Intelligence, vol. 1038. Berlin: Springer, 1996, pp. 42–55.
8. Khujamberdiyev D.E., Mamaraufov O.A. Fact-centered formal model and repository update rules for digital information flow in multi-agent systems. International Journal of Theoretical and Applied Issues in Digital Technologies, 2026, vol. 9, no. 1, pp. 117–123. DOI: 10.62132/ijdt.v9i1.334.
9. Wang J., Fu G., Savic D. EPANET-Agentic: A Multi-Agent System for Natural Language-Controlled Simulation and Analysis of Water Distribution Networks. Water Research, 2026, vol. 293, article 125433.
10. Vallabhaneni S., et al. The AI Committee: A Multi-Agent Framework for Automated Web Data Collection and Structured Extraction. In: Proceedings of the 19th Conference of the European Chapter of the Association for Computational Linguistics: System Demonstrations. 2026.
11. Lin M., Chen Z., Liu Y., Zhao X., Wu Z., Wang J., Zhang X., Wang S., Chen H. A Multi-Agent Framework for Cross-Domain Annotation. In: Findings of the Association for Computational Linguistics: EACL 2026. pp. 4836-4851.
12. Muhamediyeva D.T. Methods and algorithms for creating intelligent systems of weakly formed processes. Tashkent: Fan ziyasi, 2023.
13. NYC Open Data. https://data.cityofnewyork.us/Social-Services/311-Compliant/sdzd-tnj6/about_data
14. BGL Open Data. https://github.com/logpai/loghub/blob/master/BGL

LIMITATIONS OF CLASSICAL ANALYTICAL METHODS IN THE DESIGN OF DSM-PILLARS

F.Sh. Yuldashev[1], Sh. Jumaboyeva[2]
PhD[1]
Docent[1]
Namangan State Technical University, Uzbekistan[1,2]
https://doi.org/10.5281/zenodo.20196359

Abstract. *The classic analytical methods used in calculating the bearing capacity and settlement of DSM columns in soil cement mortar - the SP 24.13330.2021 standard, the Broms-Kitazume method, and the Poulos-Davis elastic solution - were compared with the results of natural tests conducted in the Andijan region. The analysis shows that these methods, originally developed for bored piles and elastic half-space, cannot fully reflect the characteristics of DSM piles: SP 24.13330.2021 overestimates the bearing capacity by 405%, the Broms-Kitazume method by 153%, and the Poulos-Davis method underestimates settlement by 90%. The article analyzes the reasons for these results in detail and identifies the limitations of applying classical methods in the design of DSM columns. The numerical method in PLAXIS 3D software is recommended as an alternative.*

Keywords*: DSM-column, SP 24.13330, Broms-Kitazume method, Poulos-Davis method, classical analytical methods, load-bearing capacity, settlement, numerical modeling, loess soil.*

Introduction

In the last decade, the Deep Soil Mixing (DSM) technology has been widely used in Uzbekistan for structures built on weak loessic and saturated, dusty sandy soils. The advantages of this technology include the fact that the soil is not removed from its original location, minimal impact of vibrations and noise on the surroundings, and the speed of the foundation construction process [1, 2].

However, an important question arises in the design of DSM columns: which method can more accurately determine their load-bearing capacity and settlement? In current design practice, classical analytical methods are often used—the SP 24.13330.2021 standard (for helical piles), the Broms-Kitazume method (for soft loess piles), and the Poulos-Davis elastic solution (for calculating the settlement of flexible piles) [3, 4, 5]. These methods have been developed over a long history and are widely used by designers.

At the same time, DSM piles are a unique type of structure whose properties differ from those of conventional reinforced concrete piles (≈30 MPa). Their uniaxial strength (qu = 5–10 MPa) is several times lower than that of conventional reinforced concrete piles (≈30 MPa), and the soil-pile interface has a different character. Therefore, it is necessary to objectively assess the suitability of classic methods for DSM piles.

The purpose of this work is to determine the applicability of three classical analytical methods to DSM columns using a construction site in the Andijan region as an example, and to scientifically define the limitations of these methods.

Research methodology

The study is based on natural static test data obtained at the construction site of the agro-logistics center located in the Andijan region. The DSM column No. 3 selected for testing has the following characteristics: diameter D = 0.6 m, length L = 7 m, M40 grade soil-cement mortar (qu = 5.57 MPa). The test was conducted in February-March 2026 in accordance with the requirements of ASTM D1143 and GOST 5686-2020.

The engineering-geological classification of the area was compiled based on data from 161 wells. At a depth of 8.5 m, layers of loess-like silt and saturated dusty sandy loam are present; below that are layers of hard silt and medium-density sand. The groundwater table is located at depths of 1.1–2.8 m. The soil parameters are presented in Table 1.

Table 1. Properties of the soil layers in the field

Qatlam	H, m	Soil type	γ, kN/m³	c, kPa	φ, °	E, MPa	e_0
I	0.0–2.0	Loam / clay loam	18.1	12	18	4.0	0.82
II	2.0–8.5	Soft loam / soft clay loam	18.9	18	20	7.0	0.78
III	8.5–10.5	Hard / stiff loam	19.3	24	22	11.5	0.71
IV	10.5–13.0	Sandy loam	19.6	5	28	18.5	0.64
V	13.0–15.0	Sand	20.1	1	33	22.0	0.58

The study analyzed the following three classical analytical methods:

1. SP 24.13330.2021 - Russian standard method for calculating the load-bearing capacity of screw piles, formula:

$$F_d = \gamma_c \cdot \left(\gamma_{cr} \cdot R \cdot A + u \cdot \sum \gamma_{cf} \cdot f_i \cdot h_i\right)$$

Here, F_d is the calculated bearing capacity of the pile, R is the calculated resistance of the subgrade under the pile tip, A is the area of the pile tip, u is the pile perimeter, and fi is the lateral friction coefficient of the i-th layer.

2. The Broms-Kitazume method - an approach that accounts for the possibility of the column itself breaking due to material weakness [4]:

$$Q_{ult} = \min\left(Q_{col}, Q_{soil}\right), \; Q_{col} = q_u \cdot A_p \cdot \eta$$

Here, Q_{col} is the limit load resulting from the failure of the column material, and η = 0.4 is the variability coefficient.

3. The Poulos-Davis method - the classical elastic solution [5] for calculating the sinking of a soft spring in an elastic half-space:

$$s = \frac{P \cdot I_0 \cdot R_k \cdot R_h \cdot R_v}{\bar{E}_s \cdot D}$$

Here, $I_0 = 0.045, R_k, R_h, R_v$ are the influence coefficients, and Ēs is the weighted average modulus of the soil with respect to depth.

The calculation results were compared with the natural test results of column No. 3. In addition, a numerical calculation was performed in PLAXIS 3D using the calibrated Hardening Soil Small model, and the degree of agreement was evaluated for the conclusion.

Results and Discussion

The calculation results and their comparison with natural testing are presented in Table 2 and Figure 1. The experimental result in column 3 is the lifting capacity. Q_{ult} = 249 kN, maximum displacement speake = 8.19 mm. The calculation results obtained using classical methods and the numerical model are as follows:

Table 2. Comparison of the results of classical analytical methods and the numerical model with experimental data.

Calculation method	Q, kN	ΔQ, %	s, mm	Δs, %
Experiment / Test (Pile No. 3)	249	-	8.19	-
SP 24.13330.2021	1 257	+405	-	-
Broms–Kitazume	630	+153	-	-
Poulos - Davis (elastic)	-	-	0.79	−90
PLAXIS HSsmall (calibrated)	245	−1.6	8.88	+8.4

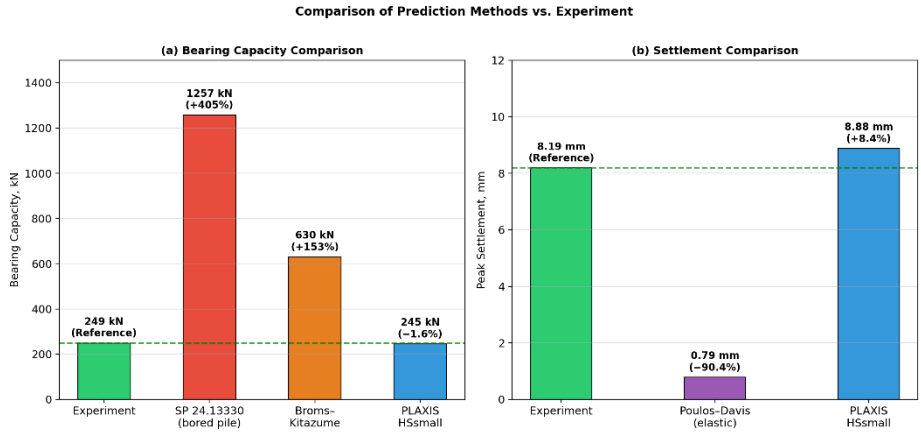


Figure 1. Comparison of calculation results: (a) lifting capacity; (b) maximum deflection

Analysis of the results of the SP 24.13330.2021 standard

The bearing capacity calculated according to the SP 24.13330.2021 standard, Fd = 1,257 kN, is 5 times higher than the experimental value. The reason for such a large difference can be seen in the fact that the SP standard is intended for reinforced concrete piles. The concrete strength of a reinforced pile is typically around 30 MPa, while the soil-cement grout material of the DSM column has a qu of 5.57 MPa. This difference is nearly 5.4-fold. For this reason, although both the R (tensile resistance) and fi (lateral friction) values in the formula are selected based on the soil test results, the calculation is performed under the assumption that the pile itself will not fail. In the DSM column, however, the material fails before lateral surface friction can be fully mobilized.

This situation is not a deficiency of the standard, but rather indicates its scope of application: the SP 24.13330.2021 standard is not intended for DSM columns, and it cannot be directly applied to this type of structure. This conclusion is not a criticism of the SP standard, but rather an acknowledgment of its actual scope of application.

Analysis of the Broms-Kitazume method

The Broms-Kitazume method accounts for the possibility of the column itself breaking, thereby eliminating the limitation of the SP 24.13330.2021 standard. Calculation result: Q_{col} = 5.57 × 0.283 × 0.4 = 630 kN. The difference from the experiment is +153% – a

significant improvement over the SP standard, but it still overestimates the experiment by 2.5 times.

This is because the coefficient η = 0.4 is assumed to be global in nature and cannot reflect the variability in local construction quality. International literature has noted that the coefficient of variation for the strength of DSM columns can reach up to 40% within a single field. [6]. Such a large variability cannot be captured by a single η value. Furthermore, the method only provides load-bearing capacity and is not suitable for assessing settlement.

Analysis of the Poulos-Davis method

The Poulos-Davis method is a classical solution based on the theory of elastic half-space. P = 240 kN, L/D = 11.7, Ēs = 18.1 MPa, and the calculated penetration s = 0.79 mm. The difference with the experiment is −90%, meaning the penetration was underestimated by a factor of 10.

Such a large error is the result of the method considering only elastic deformations. In a real DSM column, the main part of the settlement arises from plastic slips at the interface between the soil and the column face. Sensitivity analysis shows that in slender DSM columns (L/D ≥ 10), the interface coefficient R_{inter} is the most important parameter for settlement, and the elastic solution that ignores it differs sharply from the actual behavior.

The Limits of Classical Methods and Alternative Approaches

The results of the analysis make it possible to identify the following limitations of classical analytical methods:

1) The SP 24.13330.2021 standard was developed for threaded reinforced concrete piles and does not take into account the low strength of DSM columns.

2) The Broms-Kitazume method takes into account the material's ultimate strength, but it cannot reflect variations in the quality of local construction.

3) The Poulos-Davis elastic solution does not take into account the soil's plastic deformations and interface slip.

The calibrated Hardening Soil Small model in PLAXIS 3D allows for an accurate assessment of both bearing capacity and settlement within ±10% of the classical methods (−1.6% and +8.4% in the table). This corresponds to the accepted tolerance range according to the European Code and SP 24.13330.2021 requirements.

It should be noted that the numerical method must also be calibrated with local monitoring tests. Otherwise, the accuracy of the numerical method may not differ from that of classical methods. Therefore, in every project using DSM columns, it is necessary to conduct at least one physical test and calibrate the numerical model based on it.

Conclusion

In this work, three classic analytical methods used in the design of DSM-columns—the SP 24.13330.2021 standard, the Broms-Kitazume method, and the Poulos-Davis elastic solution—were compared with the results of natural tests in the Andijan region. The main results are as follows:

SP 24.13330.2021 incorrectly assesses the load-bearing capacity of the DSM column by 405%, because the standard was developed for reinforced concrete piles and does not account for the low strength of the soil-cement grout material.

2. The Broms-Kitazume method accounts for the possibility of column failure and reduces error by up to 153%, but it cannot fully reflect the variability in local construction quality.

3. The Poulos-Davis elastic solution underestimates settlement by 90% because plastic deformations of the soil and interface slip are not taken into account.

4. In the PLAXIS 3D software, the Hardening Soil Small model, calibrated based on natural tests, accurately estimates both bearing capacity and settlement within ±10% and is recommended as the preferred method for designing DSM columns.

5. On every construction site using DSM columns, it is necessary to conduct at least one natural control test and calibrate the numerical model accordingly. Classical analytical methods are useful for preliminary estimation, but not as the final design calculation.

REFERENCES

1. Kitazume M., Terashi M. The Deep Mixing Method. CRC Press, Boca Raton, 2013. 410 p.
2. Porbaha A. State of the art in deep mixing technology - Part I: Basic concepts and overview // Ground Improvement. 1998. Vol. 2, No. 2. Pp. 81–92.
3. SP 24.13330.2021. Свайные фундаменты. Минстрой России, Москва, 2021.
4. Broms B.B. Stabilization of soil with lime columns // Foundation Engineering Handbook. 2nd ed. Van Nostrand Reinhold, New York, 1991. Pp. 833–855.
5. Poulos H.G., Davis E.H. Pile Foundation Analysis and Design. John Wiley & Sons, New York, 1980. 397 p.
6. Navin M.P., Filz G.M. Statistical analysis of strength data from ground improved with DMM columns // Proceedings of International Conference on Deep Mixing 2005. Stockholm, 2005. Pp. 145–154.
7. Lorenzo G.A., Bergado D.T. Fundamental parameters of cement-admixed clay - new approach // Journal of Geotechnical and Geoenvironmental Engineering. 2004. Vol. 130, No. 10. Pp. 1042–1050.
8. Brinkgreve R.B.J., Kumarswamy S., Swolfs W.M. PLAXIS 3D Reference Manual. Plaxis BV, Delft, 2016. 290 p.
9. Lee F.H., Lee Y., Chew S.H., Yong K.Y. Effect of back-analysed strength on design of deep cement-mixed columns // Journal of Geotechnical and Geoenvironmental Engineering. 2006. Vol. 132, No. 2. Pp. 169–178.
10. Юлдашев Ф. Ш. Выбор модели грунта для решения задач распространения вибрации в грунте от транспортных средств // Механика и технология. 2023. № 1(10). С. 117–124.
11. ASTM D1143/D1143M-20. Standard Test Methods for Deep Foundations Under Static Axial Compressive Load. ASTM International, West Conshohocken, 2020.

IMPROVEMENT OF THE REGULATORY AND METHODOLOGICAL FRAMEWORK FOR ENHANCING BUILDING ENERGY EFFICIENCY IN UZBEKISTAN AT THE PRESENT STAGE

N.R. Avezova[1], R.U. Kuchkarbaev[2], E.A. Oshepkova[3], A.U. Butaev[4]
Doctor of Technical Sciences, professor[1]
Doctor of philosophy of Pedagogical Sciences (PhD)[2]
Researcher[3]
Independent researcher[4]
Fergana State Technical University[1,3]
Tashkent University of Architecture and Civil Engineering[2]
Turin Polytechnic University in Tashkent[4]
https://doi.org/10.5281/zenodo.20266608

Abstract. *The article proposes an analytical approach to improving the regulatory and methodological system for enhancing building energy efficiency in Uzbekistan, taking into account the institutional and regulatory changes of 2024-2025. The evolution of the problem field in building thermal engineering, the transition from element-based requirements to integrated indicators of annual energy consumption, issues of acceptance and verification of actual energy performance, as well as the increasing role of renewable energy sources, digital monitoring, and environmental certification are considered. As a scientific result, an integrated model for modernizing the regulatory framework is proposed, combining requirements for building envelopes, engineering systems, energy certification, facility commissioning, digital metering, and economic evaluation of solutions based on the life-cycle cost criterion. It is shown that the current stage of regulatory development in Uzbekistan is characterized by a transition from fragmented standardization to a more comprehensive model including energy efficiency categories, revision of minimum standards, implementation of the "Green Building" certificate, mandatory consideration of alternative energy sources, and development of digital control mechanisms. Conclusions and recommendations aimed at preparing updated building codes and methodologies for the design, construction, and operation of energy-efficient buildings are formulated.*

Keywords: *energy efficiency, buildings, building thermal engineering, regulatory and technical framework, annual energy consumption, thermal protection, renewable energy sources, green construction, digital monitoring.*

1. Introduction

Enhancing building energy efficiency in Uzbekistan in recent years has acquired not only engineering but also pronounced institutional significance. The scale of residential construction remains high: within the framework of the housing provision program for 2025, the construction of 135 thousand apartments with a total area of 8.1 million m² is planned, which increases the requirements for the quality of design solutions, thermal protection, and resource efficiency of new facilities [8].

State policy is shifting from local energy-saving measures toward a systemic model in which energy efficiency is considered as part of the climate, investment, and urban development agenda. This is confirmed by the adoption of the Law "On Energy Saving, Rational Use of Energy and Increasing Energy Efficiency" (2024), the introduction of tasks for harmonizing building codes with international standards (2024), inclusion of the "Green Building" certificate in the state program for 2025, and adoption of special resolutions on reforming heat supply systems and improving building energy efficiency [1], [4]-[7].

The traditional approach limited to adjusting individual indicators of thermal resistance or engineering system capacity is no longer sufficient. Modern construction practice requires a coordinated system of requirements covering the building life cycle: from the selection of urban planning and structural solutions to commissioning, energy certification, digital metering, modernization, and operational control.

The purpose of the article is to develop an analytically substantiated project for improving the regulatory and methodological framework for enhancing building energy efficiency in Uzbekistan at the present stage. To achieve this goal, the following tasks are addressed: assessment of the current state of the regulatory environment; identification of persistent methodological limitations; analysis of the changes of 2024-2025; and formation of an integrated model for the further improvement of regulation in the construction sector.

2. Materials and Research Methods

The study was carried out on the basis of regulatory-legal and comparative-analytical approaches. The sources included the current legislative acts and urban planning standards of the Republic of Uzbekistan, including the law on energy saving and increasing energy efficiency, documents on building thermal engineering, acts on harmonization of standards with international requirements, state programs for 2025, as well as resolutions regulating the use of solar panels, alternative heating systems, and digital monitoring mechanisms [1]-[9].

The methodological basis of the research includes: structural analysis of the regulatory system; comparative assessment by stages of the building life cycle; expert interpretation of the problems of transition from design capacity to actual annual energy consumption; as well as synthesis of the principles of cost-optimal and performance-based regulation used in international practice [10], [11].

The scientific novelty of the study is associated with integrating technical, institutional, and operational components of energy efficiency into a unified regulatory model, where the object of regulation is not only the structure or engineering system, but also the verifiable quality of building operation during the operational period.

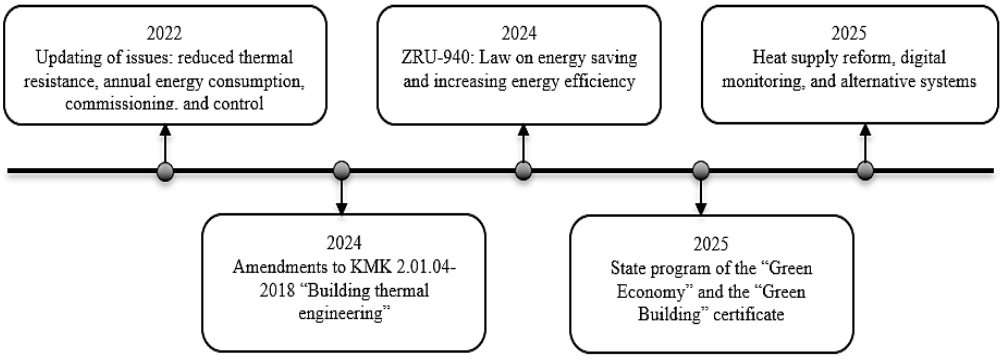


Fig. 1. Evolution of the regulatory agenda for enhancing building energy efficiency in Uzbekistan in 2022-2025 (compiled by the author based on [1], [3]-[9])

3. Results and Discussion

1. Persistent Methodological Limitations of the Current System

Despite the significant development of construction regulation, a number of persistent limitations remain within the regulatory system. The first is associated with the predominance of element-based and calculated characteristics over integrated indicators of actual energy consumption. In practice, the quality of building envelopes and engineering systems is assessed mainly by individual parameters - thermal resistance, calculated heat losses, installed equipment capacity - whereas the actual operational efficiency of a building depends on total annual energy consumption, control regimes, user behavior, and the degree of system automation.

The second limitation concerns insufficient coordination between design standards, commissioning rules, and procedures for operational confirmation of energy performance. Even with a correct design, actual energy efficiency may decrease due to thermal inhomogeneities, installation defects, air permeability of joints, deviations in the adjustment of ventilation and heating systems, as well as the absence of verification of calculated indicators after commissioning.

The third limitation concerns the methodological basis for calculating reduced thermal resistance and accounting for thermal bridges. For modern façade and frame construction, this issue can no longer be ignored: as the thickness of thermal insulation increases, the contribution of linear and point thermal inhomogeneities to total losses also increases, which means that simple planar assessments cease to be sufficient.

The fourth group of problems relates to the economic aspect of standardization. Without a standardized methodology for assessing life-cycle cost, payback period, and operational effects, tightening requirements may prove either insufficient or excessive. Modernization of standards should rely not only on thermal engineering calculations, but also on verification of the technical and economic feasibility of solutions.

Table 1. Key Problems and Contemporary Directions for Their Regulatory Resolution

Problem block	**Content of limitation**	**Current shifts in 2024-2025**	**Priority solution**
Energy efficiency indicators	Predominance of element-based and capacity-based criteria over integrated assessment of operational energy consumption.	Law No. ZRU-940 introduces energy efficiency categories and minimum consumption standards with revision every 5 years [1].	Transition to standardization of specific annual energy consumption and EE classes.
Building thermal engineering	Insufficient consideration of thermal bridges, air permeability, and quality of envelope joints.	Amendments to KMK 2.01.04-2018 were introduced in 2024; harmonization with international standards has begun [3], [4].	Development of methodologies accounting for thermal bridges, air permeability, and envelope quality control
Operational	Gap between design	The importance of energy	Mandatory

verification	calculations and actual building performance after commissioning.	passports, digital metering, and monitoring systems is increasing [1], [6], [7].	verification of calculated and actual indicators at the commissioning stage.
Integration of renewable energy sources	RES are often considered as an external addition rather than part of the building regulatory model.	Requirements for solar panels in new residential buildings have been introduced; the use of alternative heating systems is expanding [7]-[9].	Establishment of RES requirements in design, commissioning, and operation.

2. Regulatory Shifts of 2024-2025 and Their Significance for the Construction Sector

A qualitative milestone was the adoption of the Law of the Republic of Uzbekistan No. ZRU-940 of August 7, 2024 “On Energy Saving, Rational Use of Energy and Increasing Energy Efficiency.” For the construction sector, the law established a number of fundamentally important provisions: setting regulatory indicators for energy saving and increasing energy efficiency in building construction and residential premises; defining energy efficiency categories for buildings and structures with a usable area exceeding 200 m²; as well as revising minimum consumption standards for fuel and energy resources for buildings at least once every five years [1]. These provisions elevate energy saving from the status of a separate engineering task to the category of a mandatory element of construction regulation.

The second important direction was the modernization of building thermal engineering standards. In 2024, amendments and additions were introduced into KMK 2.01.04-2018 “Building Thermal Engineering,” and Resolution of the Cabinet of Ministers No. 231 dated April 23, 2024 established a course toward harmonization of construction regulations with international standards [3], [4]. Although the content of further updates requires phased detailing by individual sections, the institutional linkage of “adjustment of thermal engineering standards + international harmonization” itself signifies a transition to a new logic of rulemaking.

In 2025, the agenda was further strengthened by environmental and operational mechanisms. The State Program for implementing the “Uzbekistan - 2030” Strategy in the “Year of Environmental Protection and Green Economy” directly provides for the introduction of the “Green Building” certificate based on the energy efficiency of newly constructed buildings, structures, and residential houses [5]. This is particularly important for construction science, as it creates prerequisites for transitioning from minimum permissible standards to differentiated assessment of building quality.

Presidential Resolution No. PP-100 dated March 11, 2025 linked heat supply reform with the tasks of increasing building energy efficiency and reducing energy losses through the application of innovative technologies [6]. Presidential Resolution No. PP-133 dated April 1, 2025 provided for the widespread use of electrical and alternative energy sources, as well as energy-saving technologies in the design and construction of multi-storey residential and public buildings; furthermore, the document strengthened the role of digital monitoring and reporting platforms [7].

Additional significance for the housing sector is provided by the provisions of Presidential Decree No. UP-26 dated February 21, 2025 on the development of housing and mortgage markets.

For new residential areas, principles of urbanization, availability of engineering infrastructure, and allocation of at least 2% of construction costs for creating green zones were established, while the widespread use of RES installations, energy-efficient equipment, heat pumps, and solar water heaters was recommended in the construction of new infrastructure [8]. Building energy efficiency is increasingly considered as part of spatial and infrastructure development.

In 2023, an important technological precedent was established: Presidential Resolution No. PP-57 introduced the requirement to install solar panels on at least 50% of the free roof area of new multi-storey residential buildings, while buildings without grid-connected solar panels are not accepted into operation [9]. This decision effectively linked building commissioning requirements with the presence of operational RES-based energy infrastructure.

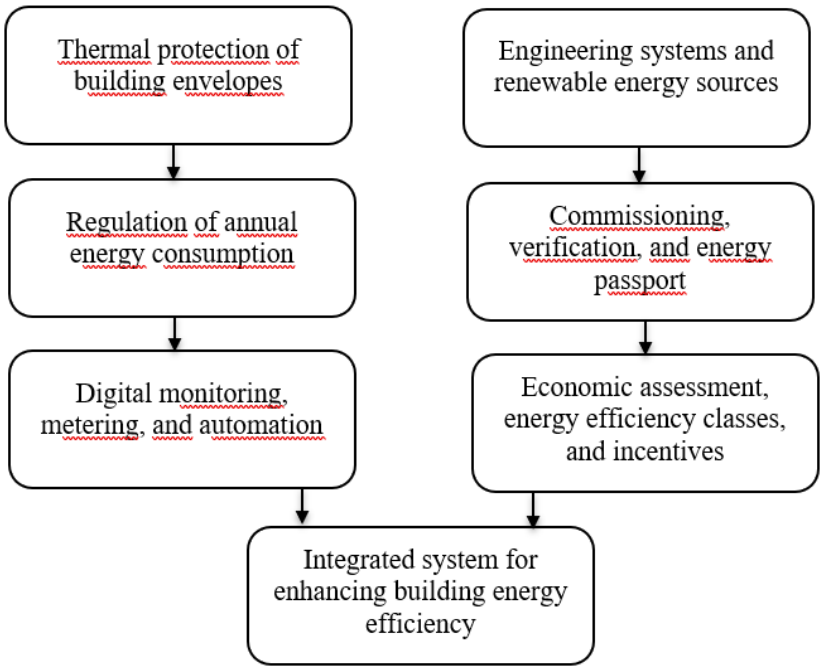


Fig. 2. Integrated model of regulatory support for enhancing building energy efficiency (compiled by the author)

3. Proposed Model for Improving the Regulatory and Methodological Framework

Taking into account the identified limitations and recent legislative changes, the further development of the regulatory system may be structured through six interrelated contours.

The first contour is building envelopes. Here, a transition is required from simplified requirements to a more accurate assessment of reduced thermal resistance with mandatory consideration of linear, point, and volumetric thermal inhomogeneities. For this purpose, it is necessary to develop a national catalog of standard joints, heat loss coefficients, and air permeability classes of modern building envelopes, as well as to link calculation procedures with actual series of materials and products used in Uzbekistan.

The second contour is engineering systems and renewable energy sources. The practice of 2023-2025 demonstrates that RES are already becoming part of mandatory requirements for new buildings [7]-[9]. Consequently, building standards should move from the wording “application is permitted” to a model in which “the possibility and conditions of integration are normatively established,” including requirements for solar installations, heat pumps, solar DHW systems, storage systems, and automation.

The third contour concerns annual energy consumption indicators. For residential and public buildings, it is necessary to establish standards for specific annual energy consumption at least for heating, ventilation, cooling, and hot water supply, and in the future for total final and primary energy consumption. Such an approach allows objective comparison of buildings, formation of energy efficiency classes, and evaluation of results not according to design declarations but according to verifiable operational performance.

The fourth contour is commissioning and verification. At the stage of commissioning a facility, it is advisable to establish mandatory building energy certification, testing of air permeability and engineering system adjustment, as well as comparison of calculated and actual parameters according to a standardized procedure. Phased verification schemes - basic, extended, and advanced - may be applied for different building types.

The fifth contour is digital monitoring and metering. Under modern conditions, energy efficiency without data becomes declarative. Therefore, metering devices, automated engineering equipment control systems, and information platforms should be considered part of the regulatory architecture. Strengthening of this direction is already reflected in the legal acts of 2025, which provide for the development of digital monitoring and reporting platforms [7].

The sixth contour is economic and environmental assessment. New requirements should be evaluated according to the cost-optimal criterion, i.e., based on the minimum discounted life-cycle costs of a building, taking into account capital investments, maintenance, energy expenses, RES effects, and equipment replacement costs [11]. The linkage of cost-optimal analysis with “Green Building” certification makes it possible to ensure that modernization of standards is simultaneously engineering-based and investment-realistic.

Table 2. Priority Directions for Modernizing the Building Energy Efficiency Improvement System

Life-cycle stage	**Object of regulation**	**Required update**	**Expected effect**
Design	Building envelopes and joints	Methodologies for calculating reduced thermal resistance considering thermal inhomogeneities, catalog of standard joints, air permeability requirements.	Reduction of the gap between calculated and operational performance.
Design	Engineering systems and RES	Establishment of integration conditions for solar systems, heat pumps, and automation.	Increase in the share of low-carbon solutions.
Expert review	Energy indicators	Verification of annual energy consumption and EE class within design documentation.	Increased objectivity of expert assessment.
Construction and	Actual characteristics	Energy passport, inspection of joints,	Reliability of facility commissioning.

commissioning		system adjustment, confirmation of RES connection.	
Operation	Metering and monitoring	Integration of meters and digital platforms, periodic consumption reporting.	Transition to data-driven building management.
Modernization	Economic efficiency	Standardized feasibility study and cost-optimal methodology for renovation and refurbishment.	Rational selection of measures during modernization of the building stock.

4. Scientific and Practical Significance of the Proposed Approach

The proposed model is important for both rulemaking and applied construction science. First, it makes it possible to coordinate research in the fields of thermal protection, engineering systems, RES, and automation within a common methodological framework focused on verifiable building performance. Such an approach contributes to the formation of new topics for applied research: development of national catalogs of thermal inhomogeneities, adaptation of in situ verification methods, modeling of annual energy consumption for various climatic zones of Uzbekistan, and assessment of the impact of solar systems on the integrated energy balance of buildings.

For design and construction practice, the value of the approach lies in resolving the contradiction between the rigidity of standards and the flexibility of engineering solutions. The clearer the final regulatory indicator is formulated - annual energy consumption, EE class, verified system performance - the greater the scope for engineering optimization. In this context, building energy efficiency is directly associated with the quality of design solutions, digital measurability of results, and controllability of building operation.

5. Conclusions and Recommendations

1. The current stage of development of the regulatory and methodological framework for building energy efficiency in Uzbekistan is characterized by a transition from predominantly element-based regulation to a more complex multi-component model including regulatory indicators, energy efficiency categories, environmental certification, digital monitoring, and integration of RES [1], [5]-[9].
2. A key achievement of recent years has been the institutional consolidation of energy efficiency as an independent subject of regulation in the construction sector, including the definition of energy efficiency categories for buildings with an area exceeding 200 m² and the mandatory periodic revision of minimum energy consumption standards [1].
3. At the same time, methodological gaps remain related to the consideration of thermal bridges, the absence of a unified procedure for verification of actual building characteristics, and insufficient regulatory orientation toward annual energy consumption rather than only the design capacities of engineering systems.
4. A justified direction for further development is the creation of an integrated regulatory system according to the stages of the building life cycle: design - expert review - construction - commissioning - operation - modernization.
5. For updating building standards, it is advisable to:

a) establish indicators of specific annual energy consumption and EE classes;

b) develop a national catalog of thermal inhomogeneities and methodologies for accurate calculation of reduced thermal resistance;

c) make the energy passport and operational verification part of the commissioning procedure;

d) link standards with digital metering and automation;

e) use the cost-optimal approach and the "Green Building" certificate as tools for selecting and evaluating solutions.

6. The proposed approach may serve as a basis for developing updated scientific and practical recommendations for improving building standards, residential building stock renovation programs, as well as educational and methodological materials for training specialists in the field of energy-efficient construction.

REFERENCES

1. Law of the Republic of Uzbekistan dated 07.08.2024 No. ZRU-940 "On Energy Saving, Rational Use of Energy and Increasing Energy Efficiency." National Legislative Database Lex.uz.
2. KMK 2.01.04-2018 "Building Thermal Engineering."
3. Order of the Minister of Construction and Housing and Communal Services of the Republic of Uzbekistan dated 26.03.2024 No. 01/2-5 "On Amendments and Additions to the Building Codes and Regulations KMK 2.01.04-2018 'Building Thermal Engineering.'"
4. Resolution of the Cabinet of Ministers of the Republic of Uzbekistan dated 23.04.2024 No. 231 "On Measures to Harmonize Regulatory Acts in the Construction Sector with International Standards."
5. Decree of the President of the Republic of Uzbekistan dated 30.01.2025 No. UP-16 "On the State Program for the Implementation of the 'Uzbekistan - 2030' Strategy in the 'Year of Environmental Protection and Green Economy.'"
6. Resolution of the President of the Republic of Uzbekistan dated 11.03.2025 No. PP-100 "On Measures for Radical Reform of the Heat Supply Sector for Residential Buildings, Buildings and Structures, as well as Improving Building Energy Efficiency."
7. Resolution of the President of the Republic of Uzbekistan dated 01.04.2025 No. PP-133 "On Improving Measures to Prevent Illegal Use and Wasteful Consumption of Fuel and Energy Resources, as well as Increasing Energy Efficiency."
8. Decree of the President of the Republic of Uzbekistan dated 21.02.2025 No. UP-26 "On Additional Measures for Further Development of Housing and Mortgage Markets."
9. Resolution of the President of the Republic of Uzbekistan dated 16.02.2023 No. PP-57 "On Measures to Accelerate the Introduction of Renewable Energy Sources and Energy-Saving Technologies in 2023."
10. Directive 2012/27/EU of the European Parliament and of the Council on energy efficiency.
11. *Implementing the Cost-Optimal Methodology in EU Countries* / Buildings Performance Institute Europe (BPIE), Institute for Housing and Environment.

BASED ON THE LIMESTONE FROM THE "UCH O'CHOQ" DEPOSIT AND THE MARL CLAY FROM THE "MESHIKLI"

DEPOSIT, ENERGY-EFFICIENT PORTLAND CEMENT CLINKER

S. Duschanov[1], I. Boyzhanov[2]
Independent Researcher, Urgench state university named after Abu Rayhan Beruni, Urgench, Uzbekistan[1]
Associate Professor, Urgench state university named after Abu Rayhan Beruni[2]
https://doi.org/10.5281/zenodo.20303328

Abstract. *This article studies the processes of obtaining Portland cement clinker using raw materials: limestone from the "Uch O'choq" deposit and marl clay from the "Meshikli" deposit (Lower Amudarya region), as well as pyrite cinder from JSC "Almalyk mining and metallurgical combine". The chemical and mineralogical composition of the raw mixtures was calculated, and the influence of the saturation coefficient and silica modulus on the formation of clinker phases was investigated. Under laboratory conditions, the quality of the clinker was assessed by the content of free calcium oxide (f-CaO), as well as by X-ray phase and electron microscopic analyses. The obtained results demonstrate the possibility of obtaining high-quality clinker at lower burning temperatures using limestone from the "Uch O'choq" deposit, marl clay from the "Meshikli" deposit, and pyrite cinder from JSC "Almalyk mining and metallurgical combine".*

Keywords: *portland cement clinker, Lower Amudarya, limestone from the "Uch O'choq" deposit, marl clay from the "Meshikli" deposit, pyrite cinder from JSC "Almalyk mining and metallurgical combine", burning process, f-CaO, mineralogical composition.*

Introduction

Globally, Portland cement consumption increased 3.5-fold between 1990 and 2019, and nearly 7-fold between 1970 and 2020. The majority of cement (73%) was used in concrete production. Portland cement reserves, which represent the amount of cement embodied in various construction structures and buildings, reach 12–30 tons per capita in some developed countries. Per capita Portland cement consumption typically ranges from 0.4 to 0.8 tons. After reaching a saturation point, cement consumption stabilizes and may subsequently decline [1].

The mineralogical composition of Portland cement clinker depends on the properties of the raw materials used. In multi-component raw mixtures, creating optimal conditions for mineral formation is one of the most challenging tasks, as the resulting crystalline structure determines the quality of the clinker and cement [2, 3]. Even with identical chemical composition and the same modulus values, a raw mix can yield clinker with different reactivity and mineralogical composition depending on the type of mill used for mechanical activation [4].

The dependence of Portland cement clinker synthesis on heat-engineering and technological parameters, as well as issues related to reducing material and energy consumption and increasing clinker reactivity, have been studied in detail by N.Kh. Babaev [5, 6, 7, 8, 9, 10]. In his published scientific works, new theoretical foundations have been proposed for increasing clinker reactivity. These include reducing fuel consumption by optimizing combustion conditions for high-performance clinker production, partially replacing limestone and clay components in the raw mix with industrial wastes from the chemical and metallurgical industries, and accelerating clinker burning processes without compromising clinker quality. The results of these studies have

been implemented in optimizing the technological performance of Portland cement plants in Uzbekistan and Kazakhstan.

Materials and Methods

In the research, the method accepted for three-component compositions was used to calculate the composition of the raw mixture for Portland cement clinker. As raw materials, limestone from the "Uch O'choq" deposit, marl clay from the "Meshikli" deposit (both located in the Lower Amudarya region), and pyrite cinder (a byproduct from Almalyk MMC JSC) were used.

The chemical composition of the raw materials was determined based on laboratory analyses. According to the calculations, the saturation coefficient (SC) was taken in the range of 0,84–0,95, and the silica modulus (n) was taken in the range of 1,8–2,3. The composition of the mixtures was calculated with an accuracy of 0,01%.

The burning (sintering) processes were carried out in a laboratory electric furnace at temperatures between 1300 and 1420 °C. During the burning process, the content of free calcium oxide (free lime, f-CaO) in the samples was determined using the ethyl-glycerate method in accordance with GOST 5382. The phase composition of the clinker was studied using X-ray phase analysis (XRD), and the microstructure was studied and analyzed using electron microscopy methods.

Results. In the process of calculating the composition of the raw mix for Portland cement clinker, the method adopted for calculating three-component mixtures was used [11].

Several calculations of the composition of different three-component raw mixes were carried out, in which limestone from the "Uch O'choq" deposit and marl clay from the "Meshikli" deposit in the Lower Amudarya region were taken as the carbonate and aluminosilicate components. Pyrite cinder from "Olmalyk MMC" JSC was used as the iron-rich component [12, 13, 14].

The raw mix used to obtain the clinker consisted of limestone, clayey marl, and pyrite cinder. The chemical composition of the materials used is presented in Table 1.

In the calculations, the saturation coefficient (SC) was taken in the range of 0,84–0,95, and the silicate modulus (n) was taken in the range of 1,8–2,3. The variation of the mix composition within the specified range can be observed in the data presented below. The calculations were carried out with an accuracy of 0,01%.

Table 1. Chemical composition of raw materials

Raw material name	**Oxide content, wt. %**							
	SiO_2	**Al_2O_3**	**Fe_2O_3**	**CaO**	**MgO**	**SO_3**	**LOI**	**Total**
Limestone from the "Uch O'choq" deposit	4,96	0,90	0,97	52,47	0,68	0,76	39,26	100,00
Marl clay from the "Meshikli" deposit	35,49	9,11	2,97	24,58	1,57	0,40	25,88	100,00
Pyrite cinder from "Olmalyk MMC" JSC	14,14	1,46	79,53	1,23	0,22	1,93	1,49	100,00

According to calculations, the computed composition of the raw material mixture consists of: limestone from the "Uch O'choq" deposit – 65,46–69,21%; marl clay from the "Meshikli"

deposit – 27,25–31,58%; and pyrite cinder – 2,73–3,79%. The calculated mineralogical composition of the raw mixtures shows: C_3S = 45,52–69,86%; C_2S = 9,20–31,83%; C_3A = 1,35–6,39%; C_4AF = 17,46–21,34%. With an increase in the lime saturation factor (LSF), the C_3S content increases. An increase in the silicate modulus from 1,8 to 2,0 leads to an increase in the C_3A content from 1,35% to 6,39%. At the minimum LSF (LSF = 0,84), the belite content in the mixture reaches its maximum (C_2S = 31,83%). It was observed that the C_4AF content in the mixture is high (21,34%) at low values of the silicate modulus and low (17,46%) at high values of the silicate modulus.

The calculation results indicate that with an increase in the LSF of the mixture, the C_3S content in the clinker increases, making it possible to obtain high-strength clinker. An increase in the silicate modulus reduces the iron-rich component in the raw feed, leading to a decrease in the liquid phase. Consequently, the burnability conditions of the raw mixture become more difficult.

Taking the above into account, for further research, a raw mixture with LSF = 0,93 and silicate modulus (n) = 2,3 was adopted as the optimal composition (Table 2).

Table 2. Chemical composition of the raw mixture and clinker

№	Raw material name	Oxide content, wt. %							
		SiO_2	Al_2O_3	Fe_2O_3	CaO	MgO	SO_3	LOI	Total
1	Limestone from the “Uch O'choq” deposit	3,41	0,62	0,67	36,07	0,47	0,52	26,99	68,74
2	Marl clay from the “Meshikli” deposit	10,53	2,70	0,88	7,29	0,47	0,12	7,68	29,66
3	Pyrite cinder from “Olmalyk MMC” JSC	0,26	0,02	1,27	0,02	0,01	0,03	0,02	1,60
4	Raw mixture	14,16	3,34	2,82	43,38	0,94	0,67	34,69	100,00
5	Clinker	21,69	5,12	4,31	66,43	1,43	1,02	0	100,00

Calculation coefficient K = 1,531237

Component quantities: Limestone from the “Uch O‘choq” deposit – 68,74%; Marl clay from the “Meshikli” deposit – 29,66%; Pyrite cinder from JSC “Olmalyk MMC” – 1,60%.

Mineralogical composition of the clinker (%): C_3S = 66,66; C_2S = 13,47; C_3A = 6,39; C_4AF = 13,43.

The above-selected optimal composition mixture was ground in a laboratory mill. The residue of the mixture on a №008 sieve was 12%. A small amount of water was added to the prepared mixture until its moisture content reached 6–8%, and it was passed through a № 1 sieve several times to ensure uniform distribution of moisture in the mixture.

From the mixture with a moisture content of 6–8%, raw material samples with a diameter of 50 mm and a height of 0,8–1,2 mm were prepared using a mechanical hand press. The shaped

samples were labeled and first dried at ambient temperature, and then in a laboratory drying oven at 105–110 °C for 3 hours. For comparison of the test results, samples were also prepared from the raw mixture produced at JSC "BEKOBODSEMENT" following the same procedure.

The samples prepared for testing and comparison were fired in a programmable laboratory electric furnace designed for 1500 °C at temperatures ranging from 1300 °C to 1420 °C, and the content of unbound free calcium oxide (f-CaO) was determined. The holding time at the maximum temperature was 30 minutes, which was intended to ensure uniform temperature distribution and the formation of clinker minerals.

The determination of the unbound free calcium oxide (f-CaO) content was carried out using the ethylene glycol method of chemical analysis in accordance with GOST 5382. The results of the determination of the unbound calcium oxide (f-CaO) content in the firing products are presented in Table 3.

Table 3. Content of unbound f-CaO in fired samples

№	Name of the raw material mixture	f-CaO content, mass %			
		1300 °C	1350 °C	1380 °C	1420 °C
1	Experimental clinker	8,8	7,1	1,9	1,1
2	Clinker of JSC "Bekobodsement"	8,8	5,0	2,3	1,8

The kinetics of f-CaO assimilation are presented in Figure 1. From the calcium oxide assimilation kinetics, it can be seen that although the f-CaO content in the experimental mixture and in the mixture from JSC "Bekobodsement" is the same at a temperature of 1300 °C, by 1420 °C the difference in f-CaO assimilation becomes significant. It should also be noted that the f-CaO content in the experimental mixture at a temperature of 1380 °C meets the requirements of GOST 34850. Thus, when the experimental mixture is fired at 1380 °C, a clinker that meets the requirements was obtained. The clinker firing temperature is 40 °C lower than that of the plant clinker.

Thus, in the mixtures obtained from the Lower Amu Darya limestone-based raw materials under study, clinker formation reactions were completed at temperatures 30–70 °C lower than those for clinker produced by conventional technology. When the constituents of the chemical composition of limestone from the "Uch O'choq" deposit and marl clay from the "Meshikli" deposit in the Lower Amu Darya region – together with an iron additive (pyrite cinder) – are introduced into the clinker raw mixture, earlier formation of alite and belite occurs, creating favorable conditions for lowering the firing temperature and accelerating clinker burning. It was determined that in the experimental clinker fired at 1380 °C, the f-CaO content is 1,9%.

During clinker formation, only a part of the solid materials forms a liquid phase. The formation of the liquid phase depends on the chemical composition of the mixture, the properties of the raw materials, and the firing temperature and duration.

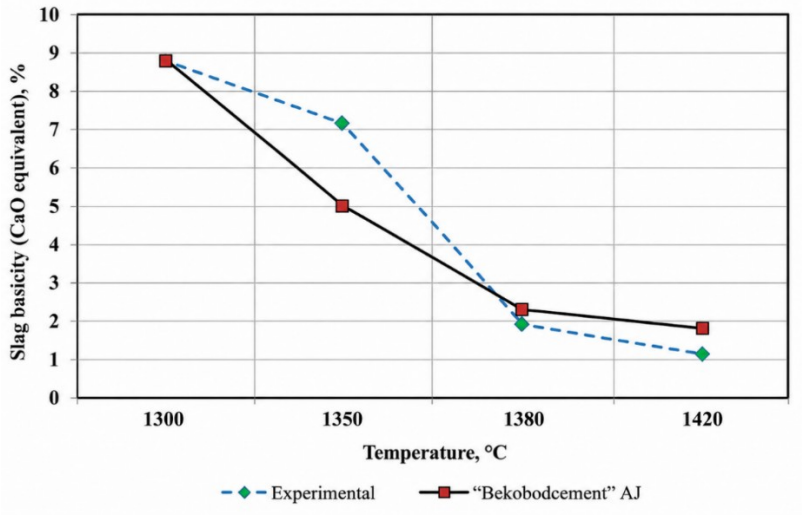


Figure 1. Kinetics of calcium oxide assimilation

Analyzing the processes occurring in clinker kilns in general terms: at 100 °C, free physically bound water is removed from the raw mixture. In the temperature range of 500–900 °C, dehydration of clay minerals occurs. In the range of 900–1200 °C, $CaCO_3$ decomposes, and the resulting CaO combines with aluminosilicates. In the range of 1250–1280 °C, a liquid phase forms. Above 1280 °C, the formation of clinker minerals is completed with the participation of the liquid phase. The maximum high temperature inside the kiln is observed in the burning zone, approximately 5–12 m from the hot end of the kiln. The maximum temperature in the kiln is selected so that 20–30% of the material forms a liquid phase, which, during burning, ensures the appearance of small, rounded particles. After the burning zone, the clinker temperature decreases and enters the cooler at approximately 1000 °C. The raw material passes through the burning zone of the kiln in about 20 minutes.

At the clinker formation temperature, the material consists mainly of C_3S and C_2S crystals. Simultaneously with the crystals, a liquid phase containing CaO, Al_2O_3, Fe_2O_3, and MgO is also present in the material. Small amounts of SiO_2 may be present in the liquid phase. Therefore, the aluminate and aluminoferrite phases of the clinker are formed only during the cooling process. The oxides Al_2O_3 and Fe_2O_3 are the primary liquid-phase formers during clinker burning. At 1400 °C, Al_2O_3 plays a major role, while at temperatures below 1400 °C, Fe_2O_3 is more significant.

The cooling rate of the clinker affects the mineral content of the clinker. Portland cements produced from slowly cooled clinkers may exhibit “false set”. False set reduces the strength of Portland cement. When the same clinker is rapidly cooled, false set does not occur, and the Portland cement hardens normally.

The reactivity of the raw mixture depends not only on its chemical composition but also on the mineralogical composition of its components and their particle size. The degree of crystallinity of certain minerals is important here; the presence of various defects in crystals increases reactivity.

The particle size of limestone and quartz greatly influences the reactivity of the raw mixture. Quartz is the component with the lowest reactivity. Quartz present in the clay is more favorable than that in the limestone. If the raw mixture is not well mixed, the reactions of clinker mineral formation do not proceed sufficiently, resulting in reduced alite formation. This, in turn, leads to the formation of belite instead of alite and the presence of unbound f-CaO.

Taking the above into account, we programmed the laboratory furnace as follows: time to reach the maximum temperature – 2 hours; holding time at the maximum temperature – 30 minutes; cooling to 1000 °C – with the power turned off; and after 1000 °C – rapid cooling.

The appearance of clinkers fired at 1380 °C under laboratory conditions is shown in Figures 2 and 3.



Figure 2. Clinker fired at 1380 °C from the raw material mixture of JSC "Bekobodsement"



Figure 3. Clinker fired at 1380 °C from the experimental raw material mixture

Figure 2 shows the appearance of clinker obtained from the raw mixture of JSC "Bekobodsement" at a temperature of 1380 °C. It can be seen that due to the low temperature being insufficient for the formation of clinker minerals, there are particles that did not participate in the process. In the image, they appear as white particles. The f-CaO content is 2,3%, as presented in Table 3.

The high f-CaO content does not meet GOST requirements, and a further increase in temperature is required to complete the formation of clinker minerals.

Figure 3 shows the appearance of clinker obtained from the experimental raw mixture at a temperature of 1380 °C. It can be seen that the temperature is sufficient for the formation of clinker minerals. The image shows that the clinker is well burned. The f-CaO content is 1,9%, as presented in Table 3. The f-CaO content meets GOST requirements.

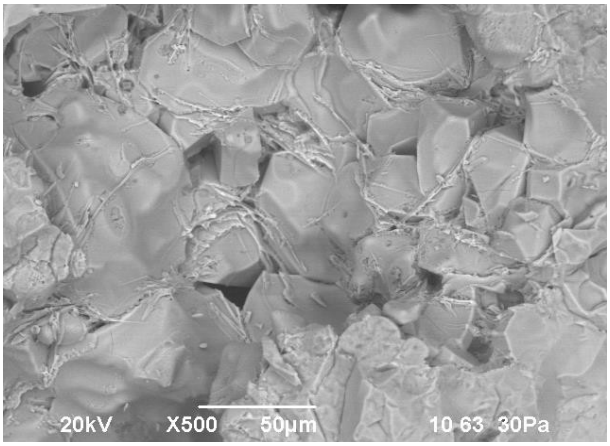


Figure 4. Microstructure of the experimental clinker (1380 °C), x500

Figure 4 shows the microstructure of the experimental clinker fired at 1380 °C. The obtained clinker microstructure is distinguished by its unique characteristics. The clinker contains 1,9% f-CaO. The crystals are sufficiently well formed. Alongside large alite crystals, one can also see alite intergrown with belite. In some cases, poorly crystallized alite is observed. Fine-crystalline belite is secondary, formed from the decomposition of alite into belite and free CaO. The interstitial phase is observed in large quantities and consists mainly of calcium aluminoferrite

(C_4AF). Our conclusions based on the conducted experiments are consistent with [15]. Thus, from the electron-microscopic analysis of the experimental clinker, it can be concluded that the Lower Amu Darya limestone raw materials rank among high-quality raw materials for clinker production, enabling the completion of clinker mineral formation at 1380–1420 °C. The possibility of obtaining high-quality clinker by firing raw material mixtures is confirmed by chemical (f-CaO content), X-ray, and electron-microscopic analyses**.**

Discussion. The research results showed that the limestone from the "Uch O'choq" deposit, the marl clay from the "Meshikli" deposit, and the pyrite cinder from JSC "Almalyk MMC" available in the Lower Amu Darya region are technologically suitable raw materials for Portland cement clinker production. The determined chemical and mineralogical composition serves to accelerate the clinker mineral formation process in mixtures prepared from these raw materials.

The reduction in clinker burning temperature is primarily related to the optimal content of aluminum and iron oxides in the raw materials, which facilitate the formation of the liquid phase. The earlier appearance of the liquid phase ensures active interaction of calcium oxide with the aluminosilicate phases, accelerating the formation of the alite phase. Furthermore, the highly reactive aluminosilicate minerals present in the marl clay from the "Meshikli" deposit also positively affect the clinker formation kinetics.

Comparison of the experimental raw mixture and that of the industrial enterprise (JSC "Bekobodsement") showed that although the f-CaO content at 1300 °C is almost the same in both cases, at higher temperatures the calcium oxide assimilation process proceeds more actively in the experimental mixture. This indicates the higher reactivity of the mixture prepared from the limestone of the "Uch O'choq" deposit and the marl clay of the "Meshikli" deposit in the Lower Amu Darya region. The results of electron microscopy analysis showed that the clinker microstructure is well-formed. The presence of large and medium-sized alite crystals in the clinker, their balanced distribution with the belite phase, and the sufficient amount of interstitial phase confirm that the clinker has high quality indicators. The relatively low content of f-CaO indicates that the burning process has been fully completed. Overall, the above results demonstrate that Portland cement clinker can be produced in energy-efficient modes using the specified raw materials. This is important not only for reducing fuel consumption but also for increasing the economic efficiency of cement production.

Conclusion

As a result of the conducted research, it was determined that the limestone from the "Uch O'choq" deposit, the marl clay from the "Meshikli" deposit in the Lower Amu Darya region, and the pyrite cinder additive from JSC "Almalyk MMC" are technologically suitable raw materials for the production of Portland cement clinker. The selection of the raw mixture at optimal values of the lime saturation factor and silicate modulus facilitates the effective formation of clinker mineral phases. Laboratory experiments have shown that in clinker fired at a temperature of 1380 °C, the unbound f-CaO content is within the regulatory requirements, and the complete formation of alite and belite phases is ensured. This confirms the possibility of firing clinker at lower temperatures compared to conventional technology. The results of X-ray phase and electron microscopic analyses showed that the mineralogical composition and microstructure of the obtained clinker exhibit high quality indicators. In particular, the adequate formation of alite crystals and the stable distribution of interstitial phases serve to increase the technological activity of the clinker. Thus, it has been scientifically substantiated that by utilizing the raw material resources of limestone from the "Uch O'choq" deposit, marl clay from the "Meshikli" deposit in the Lower Amu Darya region,

and pyrite cinder from JSC "Almalyk MMC", it is possible to produce energy-efficient, economically viable, and high-quality Portland cement clinker. The obtained results reveal the prospects for industrial-scale application of these raw materials

REFERENCES

1. Climatology Bashmakov I.A. *Prospects for the Development and Decarbonization of the Global Cement Industry* // Fundamental and Applied Climatology. – 2023. – Vol. 9. – No. 1. – pp. 33–64. doi:10.21513/2410-8758-2023-1-33-64.
2. Sulimenko L.M. *Influence of the Size, Shape, and Structure of Granules on the Crystallization of Clinker Minerals* // Proceedings of Higher Educational Institutions. Chemistry and Chemical Technology. – 1978. – Vol. 21. – No. 4. – pp. 553–557.
3. Timashev V.V., Sulimenko L.M., Meisner Sh. *Influence of Mechanical Activation on the Structural-Mechanical Parameters of Processed Raw Materials* // Proceedings of the USSR Academy of Sciences, Series "Inorganic Materials". – 1986. – Vol. 21. – No. 3. – pp. 489–493.
4. Sulimenko L.M. *Mechanical Activation of Raw Mixtures and the Hydration Activity of Clinker* // Silicate Engineering and Technology. – 1994. – No. 1. – pp. 18–22.
5. Babaeva N.Kh., Konovalov V.M. *Material Composition and Sinterability of Raw Mixtures and the Optimal Productivity of Rotary Kilns* // Bulletin of BSTU. – Belgorod, 2003. – No. 5. – pp. 14–17.
6. Babaev N.Kh. *Modeling of Thermal-Technological Processes Occurring in the High-Temperature Zone of Cement Rotary Kilns* // Bulletin of BSTU. – Belgorod, 2003. – No. 5. – pp. 17–22.
7. Babaev N.Kh. *A New Approach to Evaluating the Operation of Rotary Kilns* // Cement and Its Applications. – Saint Petersburg, 2004. – No. 1. – pp. 66–69.
8. Babaev N.Kh. *Optimization of Cement Clinker Firing in Rotary Kilns and Energy Saving* // Chemistry and Chemical Technologies. – 2004. – No. 3–4. – pp. 84–90.
9. Babaev N.Kh. *Dependence of Clinker Formation Processes on the Chemical and Material Composition of Raw Mixtures* // Uzbek Chemical Journal. – 2004. – No. 6. – pp. 50–55.
10. Babaev N.Kh. *Evaluation of the Main Performance Indicators of Rotary Kilns* // Cement and Its Applications. – 2005. – No. 3. – pp. 59–65.
11. Butt Yu.M., Sychev M.M., Timashev V.V. *Chemical Technology of Binding Materials: Textbook for Higher Educational Institutions*, edited by V.V. Timashev. – Moscow: Higher School Publishing House, 1980. – 472 p.
12. Boyzhanov I., Mukhamedbayev A., Duschanov S. *Thermal and Chemical Properties of Limestone from the "Uch O'jaq" Deposit* // Electronic Journal of Actual Problems of Modern Science, Education and Training. – August 2025. – No. 8. – ISSN 2181-9750. – pp. 31–36. khorezmscience.uz
13. Duschanova S.K., Boyjanov I.R., Kholmuratov K.S., Ismailov E.D., Bekiev M.A., Ismoilov R.I., Akhmedov M.M. *Analysis of the Influence of Marl Raw Materials on the Properties of Portland Cement* // EPJ Web of Conferences. – Vol. 321. – Article 02013. – EDP Sciences, APITECH-VII-2025. https://doi.org/10.1051/epjconf/202532102013
14. Boyzhanov I.R., Mukhamedbayev A.A., Masharipova Kh.F., Tukhtanazarov F.U. *Limestone of the Uch-Uchak Deposit as a New Raw Material for the Production of Binding Materials* // Composite Materials Scientific-Technical and Practical Journal of Uzbekistan. – Tashkent, 2022. – No. 1. – pp. 155–158.

PROSPECTS OF USING SOLAR ENERGY

S. Zoirov[1], J. Patinov[2], I. Shoqosimov[3]
Assistant of Samarkand State Pedagogical Institute, Samarkand city, Uzbekistan[1]
Samarkand City Technical College No. 6, Samarkand, Uzbekistan[2]
Student of Samarkand State Pedagogical Institute, Samarkand city, Uzbekistan[3]
https://doi.org/10.5281/zenodo.20303397

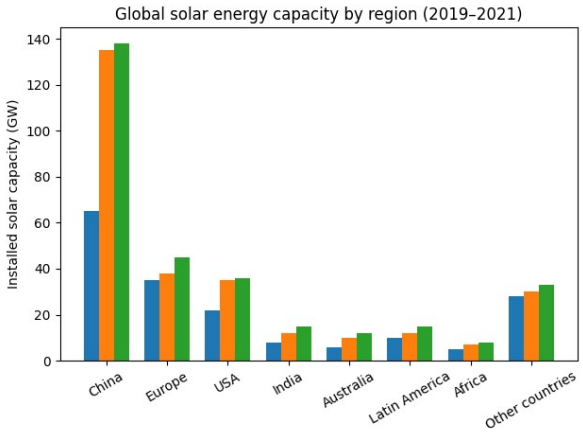
Abstract. *The advantages and disadvantages of solar energy technologies are both discussed in this article. A number of technical problems affecting renewable energy research are also highlighted, along with beneficial interactions between regulation policy frameworks and their future prospects. In order to help for opening new routes with regard to solar energy research and practices, a future roadmap for the field of solar research is discussed. The development of new solar power technologies is considered to be one of the key solutions for fulfilling a worldwide increasing demand for energy. Prospects for the use of solar panels with semiconductor materials and types of use of solar cell materials are discussed. In our daily life, solar water heating technology has been designed using solar pools.*
Keywords: *solar collectors, alternative energy, renewable resource analysis, solar water heaters.*

Introduction

Today, the increasing demand for energy requires the production of modern, eco-friendly, energy-efficient technologies and to increase the amount of energy per year. It is clear to all of us that our need for electricity on a global scale is increasing day by day. If we consider the last five years, the world's electricity demand is increasing by 50% every year. Despite the development of various technologies of renewable energy sources [1, 2], traditional thermal power plants using coal, oil and natural gas play an important role in large-scale electricity generation [3]. Improving system performance, optimizing operating conditions and system components, heat recovery from waste heat, etc. are some of the methods used to save energy in conventional thermal power plants [4, 5, 28].

This requires the increase and development of alternative energy sources.If we pay attention to the information of the International Energy Agency, if the use of solar energy develops at such a rate, by 2050, 25% of the world's electricity needs will be met by solar energy and reduction of carbon dioxide gas emitted into the environment by 6 billion tons per year is achieved [8, 9, 17]. As we know, solar panels used in the production of electricity are based on semiconductor materials. The sensitivity of these semiconductor materials to light is very high, that is, the electrical conductivity increases up to 1000 times when they were under the effect of light. Silicon is the most common semiconductor material in our world.The technology of obtaining pure silicon and making solar cells from it is cheaper than other semiconductor materials, so it is convenient to make solar panels from silicon cells. Silicon semiconductors can convert 20-25 % of the Sunlight energy into electrical energy [6, 7].

If we pay attention to the developed countries of the world. The German government is expected to increase the use of renewable electricity to 80% by 2030 and 100% by 2035. In 2021, Uruguay produced 98 percent of all electricity from renewable sources. Denmark gets more than half of its electricity from wind and solar power [23, 24, 25, 26].



Picture 1. Statistics of developed countries using solar energy

The world leader in the production of wind and solar energy. Beijing aims to generate one-third of its energy from renewable sources by 2025. This country is one of the largest investors in renewable energy worldwide [10, 11, 27].

Materials and Methods

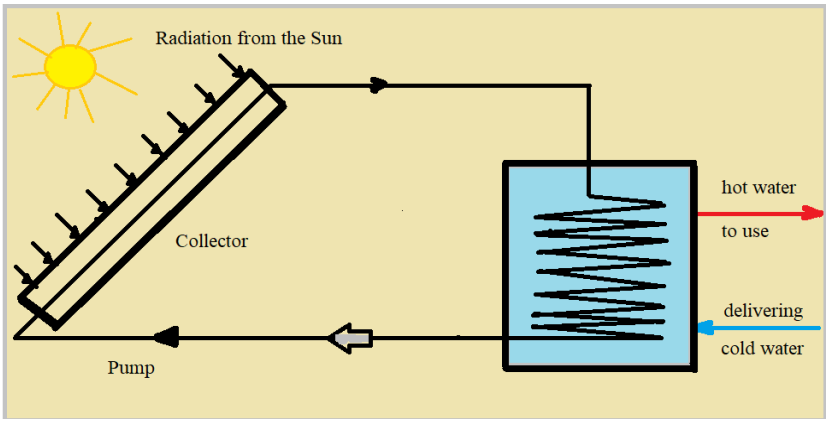
Uzbekistan has an average of 300 sunny days a year, which has a potential to produce of 51,000 trillion kWh of energy, or nearly 5,000 times the country's annual energy consumption. By using this potential, Uzbekistan can reduce the need for natural gas, reduce the impact on the environment and improve the standard of living of the population. As a result, 25 percent of the electricity produced in our country is made up of renewable energy sources. This will save about 3 billion cubic meters of natural gas per year. The issue of expanding the use of renewable energy is that today there is an additional demand for 2-3 billion kilowatt hours of electricity in our country, and in the next five years this need is expected to increase to 10 billion kilowatt hours. It meansthat in order to cover these huge demands the most effective way is to set up solar panels on the roof of houses, schools and other government organizations. With the saved gas, one million households can be supplied with natural gas during the year. The use of non-traditional energy sources creates the basis for using the existing gas, electricity, and coal reserves as little as possible. Therefore, it is a fact that the improvement, development and implementation of energy-saving technologies into the national economy will have a significant impact on the effectiveness of the main sectors of the national economy [14, 15, 16]. Currently, computer modeling of solar energy production projects in all manufacturing plants, educational institutions, and residential homes requires less time for researchers who are conducting research in the use of solar energy and this method costs less than the traditional method [18, 19, 20].

Today, virtual models of the solar collector are being created, and the technologies of effective use of solar energy are being designed and studied in scientific laboratories [12, 13].

Results And Discussion

If we look at the results of the experiment carried out in Samarkand region, the daily electricity consumption of Samarkand region is 15 million 420 kW±10%. 45% of this goes to the consumptionof population, 35-40% for production. The consumption for other sectors is 5-10%. Solar water heaters use solar energy to heat water through solar collectors. Flat panel solar collectors which are coated with transparent air-tight casing, absorptive metal plate which is painted black with water-conducting tubes and insulated on the rear and side walls of the casing to prevent heat loss are widely used.

Figure 2. A device that changes the temperature of water using solar energy. Installation scheme of the test bench of solar collectors. Temperature of solar collectors, reservoir, working environment control system, circulation pumps, anemometer, computer with measurement card module.



(https://www.wecf.org/wp-content/uploads/2018/11/Gender_Sensitive_NAMA-WECF.pdf) [29].

Experimental results show that if concentrators are installed to increase the water temperature through solar collectors, the water temperature will be much higher. In addition, water heaters powered by solar energy can be equipped with concentrators in order to provide sufficient heat for heating water when solar radiation is insufficient.To ensure the full use of solar energy, solar water heater collectors and concentrators should be placed in accordance with the trajectory of the sun's movement. Usually, if the collectors are placed at an angle of 30^0 to the horizon, the efficiency of using solar energy during the day will be high. Because in this case, the sun's rays fall on the solar collector more during the day. The direction of the solar collector is determined separately, depending on the place of installation, based on preliminary calculations. Usually, the solar collector achieves maximum efficiency when it is installed at an angle to the horizon according to the width of the place where the device is placed.

Table 1. №1 Results of experiment

№	**Average temperature of heated water t,^{0}C**	**Volume of heated water V, liter**	**To change the temperature of heated water by 37^{0}C conditionally**	**Environmental indicators and solar radiation**			
				Time, c	Intensity of incident radiation W/m^2	Speed of wind-v m/s	Temperature of water t^{0}C
1	68	10	27.2	9^{30}	950	0.0	34
2	65	10	25.5	12^{30}	1100	0.5	38
3	55	10	20.0	15^{30}	1050	0.0	39
4	45	10	14.4	18^{30}	820	0.3	38

N-1 experiment. Results of daily measurements of a cone-type household water heater. The experiment was carried out on July 25, 2023 in the city of Samarkand. The sky is cloudless, open air. The temperature of cold water in the system is 19 degreeselcium.

Table 2.№2 Results of experiment.

№	Average temperature of heated water t,^{0}C	Volume of heated water-V, liter	To change the temperature of heated water by 37^{0}C conditionally	Environmental indicators and solar radiation			
				Time, c	Intensity of incident radiation W/m2	Speed of wind-v m/s	Temperature of water t^{0}C
1	52	10	18.3	9^{30}	760	2.0	19
2	48	10	17.37	12^{30}	830	1.0	24
3	42	10	14	15^{30}	690	1.5	28
4	38	10	10.53	18^{30}	400	1.5	26

N-2 experiment. . Results of daily measurements of a cone-type household water heater. The experiment was carried out on September 5, 2023 in the city of Samarkand. The sky is cloudless, open air. The temperature of the cold water in the system is 18 ^{0}C. According to the results we can determine in the Summer we can get hotter water than the Autumn but even in the Autumn the temperature of the heated water is enough to use in a daily life.

Conclusion

In short, if the world's population uses alternative energy sources, it has great potential to provide environmentally friendly, reliable and sustainable energy. Globally, the use of solar energy and wind energy is a promising path that can significantly increase the energy production and reduce energy costs. Using alternative energy sources can reduce the need for fossil fuels, improve people's quality of life, create jobs and contribute to a more sustainable future. We can also implement efficient use of solar energy in our daily life. The use of solar water heater collectors and concentrators in daily life gives high results.

REFERENCES

1. Koc, S. Turk, G. Sahin, Multi-criteria of wind-solar site selection problem using a GIS-AHP-based approach with an application in Igdir Province/Turkey, Environ. Sci. Pollut. Res.26 (2019) 32298–32310,https://doi.org/10.1007/s11356-019- 06260-
2. Khanlari, M.A. Nazari, A review on the applications of multi-criteria decision-making approaches for power plant site selection, J. Thermal Anal. Calorimetry 2021 (2021) 1–17, https://doi.org/10.1007/S10973-021-10877-1.
3. M. Ghalandari, H. ForootanFard, A. KomeiliBirjandi, I. Mahariq, Energy-related carbon dioxide emission forecasting of four European countries by employing data-driven methods, J. Thermal Anal. Calorimetry (2020) 1–10, https://doi.org/ 10.1007/s10973-020-10400-y.
4. M.R. Pakatchian, H. Saeidi, A. RafieiSefidDashti, Axial Flow Compressor of MGT - 70 Gas Turbine Blade Shape Optimization Based on Operating Condition, in: International Gas Turbine Congress, Tokyo, Japan, 2015, pp. 249–255.
5. P. Kuchonthara, S. Bhattacharya, A. Tsutsumi, Combinations of solid oxide fuel cell and several enhanced gas turbine cycles, J. Power Sources 124 (2003) 65–75, https://doi.org/10.1016/S0378-7753(03)00740-7.

6. Y.M. Kim, J.L. Sohn, E.S. Yoon, Supercritical CO2 Rankine cycles for waste heat recovery from gas turbine, Energy 118 (2017) 893–905, https://doi.org/10.1016/J.ENERGY.2016.10.106.
7. Heinberg, R.; Fridley, D. Our Renewable Future; Heinberg, R., Lerch, D., Eds.; Island Press: Washington, DC, USA, 2016.
8. IEA. Net Zero to 2050: A Roadmap for the Global Energy Sector; International Energy Agency: Paris, France, 2021.
9. Sampaio et al.Photovoltaic solar energy: conceptual frameworkRenew Sustain Energy Rev(2017)
10. M.A. Al-Tameemi et al.Global water cycle and solar activity variationsJ Atmos Sol Terr Phys. (2016)
11. M. Herrando et al.Hybrid PV and solar-thermal systems for domestic heat and power provision in the UK: techno-economic considerations. Appl Energy(2016)
12. ZoirovSanjaridin, MurodovSardor, SharofovaTo‘lg‘anoy, QarshiboyevShavkat. "Modeling physical processes in LABVIEW". "Science and Innovation"international scientific journal 2022.12.15 775-780.SCIENCE.
13. Sanjaridin Z., Temur X. METHODS OF CREATING VIRTUAL LABORATORIES IN THE" LABVIEW" PROGRAM //Science and Innovation. – 2023. – T. 2. – №. 11. – C. 519-523.
14. Klimenko V.V., Tereshin A.G. World energy and climate of the planet in the 21st century // History and modernity.2008. № 2. C. 87–94.
15. Andreev V. M. Photoelectric conversion of solar energy // Soros educational journal. 1996. № 7. C. 93–98.
16. Klimenko V.V., Tereshin A.G., Mikushina O.V. World energy and planetary climate in the 21st century in the context of historical trends // Russian Chemical Journal. 2008. T. LII. № 6. C. 11–17.
17. BP World Energy Statistical Review 2020. 2020. Available online: https://www.bp.com/content/dam/bp/business-ites/en/global/corporate/pdfs/energy
18. -economics/statistical-review/bp-stats-review-2020-full-report.pdf (accessed 1 December 2021).
19. IEA. World Energy Balances: Statistical Report; International Energy Agency: Paris, France, 2020; p. 227.
20. Energy Information Administration. International Energy Outlook 2019 with projections to 2050 (IEO2019) 2019. Available online: https://www.eia.gov/outlooks/ieo/pdf/ieo2019.pdf (accessed November 1, 2021).
21. Hall, C.A.S.; Klitgaard, K. Energy and the Wealth of Nations, 2nd ed.; Springer International Publishing: New York, NY, USA, 2018.
22. Nye, D.E. Consuming Power: A Social History of American Energies; MIT Press: Cambridge, MA, USA, 1998.
23. Citation: Holechek, J.L.; Geli, H.M.E.;Sawalhah, M.N.; Valdez, R. A Global
24. Assessment: Can Renewable Energy Replace Fossil Fuels by 2050? Sustainability 2022, 14, 4792. https://doi.org/10.3390/su14084792
25. Ahmed, N.M. Failing States, Collapsing Systems: Biophysical Triggers of Political Violence; Springer: New York, NY, USA, 2017.

TRANSFORMATION OF THE LIBRARY: FROM TRADITIONAL TECHNICAL MEANS TO A PROACTIVE DIGITAL ENVIRONMENT

Yu.G. Anufrieva
Senior Lecturer, TUIT named after M. al-Khwarizmi
https://doi.org/10.5281/zenodo.20506222

Abstract. *This article examines the transformation of modern academic libraries from traditional technical systems into proactive digital environments. It analyzes the main technological tools used in contemporary library practice, including RFID identification, self-service terminals, automated return stations, robotic storage and retrieval systems, digitization equipment, OCR technologies, mobile applications, smart lockers, visitor counters, and social robots. Particular attention is given to how these tools improve collection management, inventory accuracy, preservation of physical documents, user access, and service efficiency. The article also reviews major international professional events, including IFLA WLIC, the ALA Annual Conference, and Computers in Libraries, where innovative library solutions are regularly presented. The study shows that digital technologies reduce manual labor, expand 24/7 access to resources, support personalized services, and change the overall model of library work, making libraries more automated, flexible, accessible, and user-oriented in the context of global digital transformation and responding to contemporary academic information needs effectively.*
Keywords: *digitization of collections, automated libraries, RFID technology, IFLA, ALA.*

INTRODUCTION

At present, academic libraries of higher educational institutions are actively developing and improving their material and technical base by introducing modern technologies. The technical means of library activity do not constitute a completed list: they continue to develop together with digital technologies, changing not only individual processes but also the very model of library work. If, at the end of the twentieth century, automation was mainly reduced to transferring card catalogs into electronic format and introducing the first databases, today it concerns qualitatively different solutions. They affect all key areas:

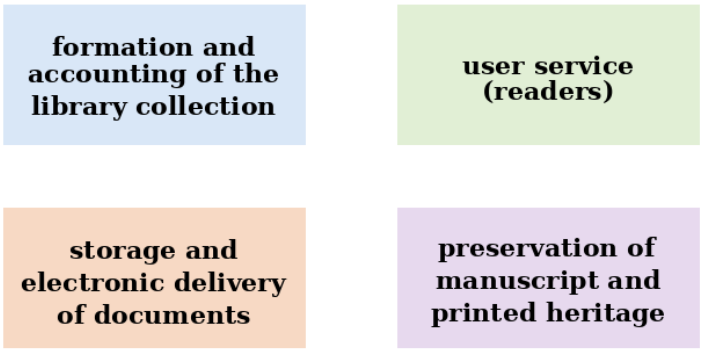


Fig. 1. Library technologies.

MATERIALS AND METHODS

The methodological basis of the study includes descriptive, comparative, and analytical methods. The research is based on the analysis of modern technical tools used in academic libraries, including RFID systems, self-service terminals, automated storage and retrieval systems, digitization technologies, mobile applications, and robotic solutions. Materials from international library exhibitions and conferences, including IFLA WLIC, the ALA Annual Conference, and Computers in Libraries, were also examined.

RESULTS

One of the most widespread modern tools has become RFID (Radio Frequency Identification) technology. Each item of the collection is equipped with an electronic tag, whose data are read automatically during lending, return, or inventory and synchronized with the automated library information system (ALIS). Mobile RFID readers make it possible to carry out inventory directly at the shelf, without removing books from the shelves; this reduces staff labor costs by ten to twenty times compared with barcoding [1]. Anti-theft gates at the exit simultaneously perform a security function and keep a count of attendance [2]. According to studies, after implementing RFID, libraries record a reduction in labor costs of about 30%, while the accuracy of inventory accounting approaches 99% [3].

Self-service terminals have also become widespread. They allow the reader to process lending and return independently: the operation is recorded through a built-in RFID reader, and the terminal prints a receipt [4].

A separate variety consists of outdoor automatic return stations operating around the clock and parcel lockers outside the library: in university buildings, shopping centers, and residential districts. The reader places an order through the electronic catalog and collects the book using a QR code at a convenient time [5]. In a number of libraries, the share of operations performed through terminals reaches 94% of the total number of transactions.



Figure 2. The BookBot robotic system at the University of New South Wales Library (Australia)

In libraries that use automated storage and retrieval systems, the collection is organized differently. Documents are placed in a high-density closed storage facility consisting of multi-tiered blocks up to 10-15 meters high; upon request from the electronic catalog, a special crane retrieves the required container and delivers it to the circulation desk [6].

The BookBot system at the University of New South Wales Library can hold from 100,000 to 1 million items while occupying an area several times smaller than ordinary shelving [33]. Here, books are arranged not by subject but by size in order to use space as densely as possible. In open halls, navigation and consultation functions are assumed by mobile robots: Pepper, produced by SoftBank Robotics, conducts dialogue in 15 languages, searches the catalog, and sends the results to the reader’s phone [7].

Digitization of collections solves a task that previously seemed almost insoluble: ensuring both the preservation of the original and broad access to its content [35]. Planetary scanners with a V-shaped cradle capture images without pressure on the binding; the productivity of automatic systems reaches 3,000 pages per hour [36]. OCR programs recognize text and make the document available for full-text search. As a result, the physical original no longer wears out from repeated use, while its digital copy is available to an unlimited number of users simultaneously [8].

DISCUSSION

Taken together, modern technical means cover the entire cycle of working with a document, from its arrival in the collection to its delivery to the reader in physical or digital form. The latest developments are regularly presented at major professional exhibitions and conferences, which provide an understanding of the direction in which the technological development of librarianship is moving.

A key place in the global library community is occupied by two organizations: IFLA and ALA. The International Federation of Library Associations and Institutions (IFLA) was founded in 1927 and unites library organizations from more than 140 countries. In the sphere of technology, IFLA develops metadata standards and formats for document description, publishes guidelines on digital libraries and the long-term preservation of electronic resources, and promotes the introduction of open access. Each year, the federation holds the World Library and Information Congress (IFLA WLIC), the largest global event in the library sphere, combining a scholarly program with a professional exhibition. In 2025, the congress was held in Central Asia for the first time, in Astana, Kazakhstan, gathering more than 1,600 delegates from over 110 countries [9].



Figure 3. Exhibits at the IFLA WLIC 2025 professional exhibition, Astana: selfCheck 3000 kiosk (Bibliotheca), transport system (Telelift), and tablet solution (Hublet)

At the exhibition, Bibliotheca presented several new products:

– the selfCheck 3000 self-service kiosk: a terminal through which the reader independently borrows and returns books without contacting a librarian; it is intended for libraries with a large number of visitors;
– the compact selfCheck 2500 model: a similar smaller kiosk for small libraries or spaces with limited floor area;
– the cloudCheck Tablet solution: the same self-service function, but implemented on a tablet that can be placed in any convenient location without fixed installation;
– the flexAMH system: a device that independently accepts returned books, recognizes them, and sorts them by category, freeing employees from this routine work.

Telelift demonstrated transport systems for moving documents inside the library, an analogue of a conveyor delivering books between departments without staff participation; Hublet presented a solution for lending tablets to readers for temporary use directly in the library hall [10].

The American Library Association (ALA) was founded in 1876 and is the oldest and largest library organization in the world, uniting more than 50,000 members. ALA develops professional standards and ethical norms for the use of digital tools, publishes thematic guidelines and studies, and participates in shaping policy in the field of copyright and open access. The annual ALA Annual Conference is the largest professional library event in the world; within its framework, the Library Marketplace exhibition is held, bringing together hundreds of suppliers of library solutions.

In 2025, the conference was held in Philadelphia and included more than 800 vendors [38]. Among the developments presented, the Romi robot from Bibliotheca stands out. Romi is a child-sized device that:

– moves around the hall independently;
– helps readers find the book they need;
– accepts returns;
– accompanies visitors to the required shelf.

Romi charges from an ordinary power outlet and is currently undergoing beta testing after successful implementation in libraries in Japan and South Korea.



Figure 4. Exhibits at the Library Marketplace, ALA Annual Conference 2025, Philadelphia: Romi robotic assistant (Bibliotheca) and AutoLend kiosk (International Library Services)

International Library Services presented AutoLend kiosks, devices for the automatic lending of books that operate without staff participation. During the natural disasters in Los Angeles in 2025, these kiosks continued to serve readers in the affected areas when the ordinary operation of libraries had been disrupted [11]. One of the main topics of the conference was the use of artificial intelligence in library activity, including discussions of algorithmic bias and the environmental consequences of using AI systems [12].

Among professional events, the Computers in Libraries conference stands out; it has been held for about 40 years and is devoted to the practical aspects of introducing digital technologies in

libraries. In 2025, the event was held in Arlington, Virginia, USA, and included more than 100 thematic sessions and over 40 solution providers [13].

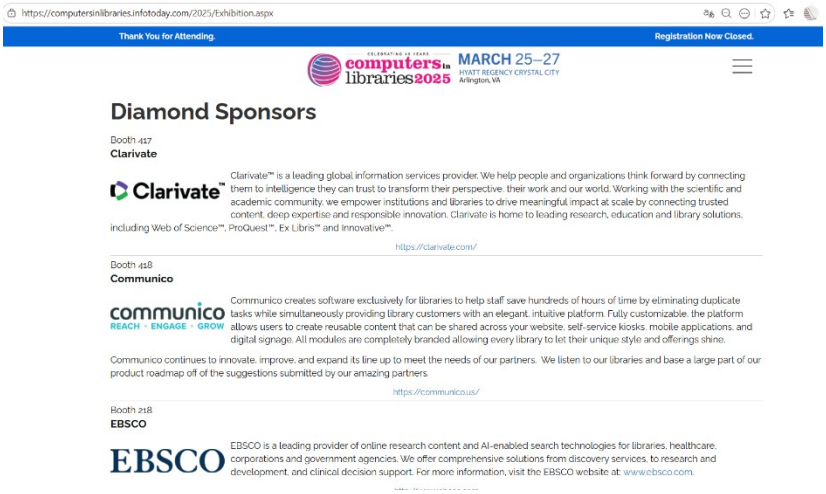


Figure 5. Exhibitors and technology companies presented at Computers in Libraries 2025

D-Tech International presented several developments:

SMART lockers are modular cabinets with a touch screen and an intelligent access system, allowing the reader independently to receive an ordered book, borrow a laptop or tablet for temporary use, or pick up pre-reserved materials. The lockers are installed both indoors and outdoors for 24/7 operation and are integrated with the library management system [41].

The appIT mobile application allows the reader to borrow and renew a book directly from a smartphone through RFID or barcode scanning, without approaching a terminal; the application also displays information about debts, available reservations, and library opening hours [14].

The countIT visitor counter consists of ceiling sensors based on time-of-flight technology, which record the actual flow of people through the entrance with an accuracy of 99.8%, without collecting personal data and without using cameras. This enables the library to monitor occupancy, plan staff work, and justify funding [15].

Meescan presented a self-service system combining a kiosk and a mobile application: the reader can process lending either through a device in the library or through a phone, and the system itself is installed without complex technical preparation. This makes it possible to introduce it even in small libraries with limited resources [16].

The development of technical means for libraries does not stop: every new generation of devices expands the possibilities of automation, reduces dependence on manual labor, and makes library services more accessible to different categories of users.

CONCLUSION

Thus, the transformation of libraries from traditional technical systems to proactive digital environments is connected with the active introduction of RFID technologies, automated storage systems, digitization tools, self-service platforms, mobile applications, and robotic assistants. These technologies improve service quality, reduce staff workload, expand access to resources, and make library services more flexible and user-oriented. Therefore, the further development of library technologies will continue to play an important role in the modernization of academic libraries.

REFERENCES

1. RFID in Libraries: Implementation Examples [Electronic resource] // RFID Union: [website]. – 2022. – URL: https://rfidunion.com/ru/applications/rfid-in-libraries.html
2. Abrosimova N. V. RFID Technologies: Experience of Implementation and Use [Electronic resource] // Universitetskaya kniga: [website]. – 2013. – URL: http://www.unkniga.ru/innovation/tehnology/1492-tehnologii-rfid-opyt-vnedreniya.html
3. RFID Technology in the Modern Library: Advantages and Disadvantages [Electronic resource] // Lala Lan: [website]. – URL: https://lala.lanbook.com/rfid-tekhnologiya-v-sovremennoj-biblioteke-preimushchestva-i-nedostatki
4. Library Stories: Real Examples of Innovation & Impact [Electronic resource] // Bibliotheca: [website]. – URL: https://www.bibliotheca.com/library-stories/
5. Pop C., Mailat G. Automated Material Handling Systems (AMHS) in libraries and archives // Recent Researches in Neural Networks, Fuzzy Systems, Evolutionary Computing and Automation. – 2011. – P. 189–194.
6. NC State University Libraries. Hunt Library BookBot [Electronic resource]: description of a robotic book storage and retrieval system at Hunt Library // NC State University Libraries: [website]. – URL: https://www.lib.ncsu.edu/hunt/bookbot
7. Smarter Libraries through AI Technologies – Social Robot [Electronic resource]: description of the USC Libraries project on the use of social robots in library services // USC Libraries: [website]. – URL: https://sites.google.com/usc.edu/libraryai/robots/social-robot
8. Ataeva G. I., Bozorov D. S. Opportunities and Problems of Digitizing Library Resources of University Libraries [Electronic resource] // CyberLeninka: [website]. – 2023. – URL: https://cyberleninka.ru/article/n/vozmozhnosti-i-problemy-otsifrovki-bibliotechnyh-resursov-universitetskih-bibliotek
9. ElarScan R-2. Description of a robotic planetary scanner for contactless digitization of books and archival documents // ElarScan: [website]. – URL: https://elarscan.ru/modelnyj-ryad/elarobot-r-2/elarobot-r-2/
10. Bibliotheca at IFLA WLIC 2025: participation of Bibliotheca in the IFLA World Library and Information Congress 2025 // Bibliotheca: [website]. – URL: https://www.bibliotheca.com/bibliotheca-ifla-wlic-2025/
11. ALA Annual Conference 2025 [Electronic resource]: official website of the annual conference of the American Library Association. – URL: https://2025.alaannual.org/
12. Bibliotheca at ALA 2025 [Electronic resource]: Bibliotheca library technologies presented at the ALA 2025 conference // Bibliotheca: [website]. – URL: https://www.bibliotheca.com/ala-2025-library-technology/
13. Computers in Libraries 2025. Exhibition program of the annual Computers in Libraries conference. – URL: https://computersinlibraries.infotoday.com/2025/Exhibition.aspx
14. D-Tech International. SMART Lockers [Electronic resource]: smart locker system for independent receipt of library materials // D-Tech International: [website]. – URL: https://d-techinternational.com/smart/
15. D-Tech International. Library App [Electronic resource]: mobile application for managing library services // D-Tech International: [website]. – URL: https://d-techinternational.com/products/library-app/
16. D-Tech International. People Counting [Electronic resource]: system for automatic counting of library visitors // D-Tech International: [website]. – URL: https://d-techinternational.com/products/people-counting-2/

ANALYSIS OF A HYBRID HEATING SYSTEM BASED ON HEAT PUMPS AND SOLAR COLLECTORS

B. Abdukarimov[1], O. Urishev[2], D. Islomov[3], S. Ikromov[4]
PhD, Associate Professor of Fergana State Technical University[1]
PhD, Associate Professor of Fergana State Technical University[2]
Master student of Fergana State Technical University[3]
Master student of Fergana State Technical University[4]
https://doi.org/10.5281/zenodo.20552441

Abstract. *This study presents a comprehensive analysis of hybrid heating systems integrating solar collectors and air-source heat pumps. The research investigates direct expansion (DX-S-ASHP), series indirect expansion (IDX-S-ASHP), and parallel IDX-S-ASHP configurations, with particular focus on a proposed hybrid IDX-SAHP system using vacuum tube solar collectors and a plate heat exchanger. The proposed configuration provides hydraulic independence between the solar collector and heat pump loops, improving thermal stability and operational reliability under variable climatic conditions. Thermodynamic and energy efficiency analyses demonstrated that the proposed system can increase the coefficient of performance (COP) from approximately 3.06 in conventional air-source heat pump systems to about 5.21. In addition, electricity consumption was reduced by nearly 70% due to effective solar thermal utilization and thermal energy storage integration. The results confirm that hybrid solar-assisted heat pump systems can significantly improve building energy efficiency, reduce greenhouse gas emissions, and support sustainable low-carbon heating technologies for modern energy-efficient buildings.*

Keywords: *heat pump, Vacuum tube solar collector, IDX-SAHP, Plate heat exchanger, Energy efficiency, COP.*

Introduction.

At present, reducing energy consumption in the building sector, improving the efficiency of heat supply, and decreasing harmful emissions into the atmosphere are among the most pressing scientific and practical challenges. The building and construction sector accounts for a significant share of global energy demand and contributes substantially to energy-related carbon dioxide emissions. In particular, in 2022, the building sector was responsible for 34% of global energy demand and 37% of CO_2 emissions associated with energy and industrial processes. Therefore, the decarbonization of building heating systems and the implementation of technologies based on renewable energy sources are considered key priorities [1].

Heat pumps are regarded as one of the most promising technologies for building heating. According to the International Energy Agency, heat pumps, when powered by low-carbon electricity, represent a central technology for the transition to sustainable and secure heating systems. Moreover, replacing fossil fuel-based boilers with heat pumps reduces greenhouse gas emissions even under the current electricity generation mix, and this advantage increases as the power sector becomes greener. According to IEA estimates, space heating alone accounts for approximately 4 Gt of CO_2 emissions annually, highlighting the urgent need to adopt efficient technologies in this field [2].

In cold-climate countries (Northern Europe, Canada), solutions for efficient operation of heat pumps at low ambient temperatures were developed in the 1990s and 2000s, including two-stage cycles, intermediate heat exchangers, and vapor injection techniques. These innovations helped overcome the major drawback of air-source heat pumps—performance degradation under extremely low temperatures. By the late 2000s, heat pumps had firmly established their position in the heating sector of new buildings in many developed countries. The experience of Switzerland illustrates this trend: despite having a well-developed gas distribution network, approximately 75% of newly constructed detached houses in the early 2010s were equipped with heat pump heating systems [6]. By 2010, several million heat pumps of various types had been installed across Europe, with annual growth rates ranging from 10% to 20%.

Literature review.

One of the indicators of the growing interest of the scientific community in heat pumps is the number of publications. While in the 1990s the Russian-language literature featured an average of 5-15 publications per year, this number increased significantly in the 2000s and peaked around 2010-2011. Figure 1 illustrates the dynamics of publication activity on heat pumps in Russia/CIS from 1970 to 2020. A clear acceleration is observed after 2000, corresponding to the described stage of development.

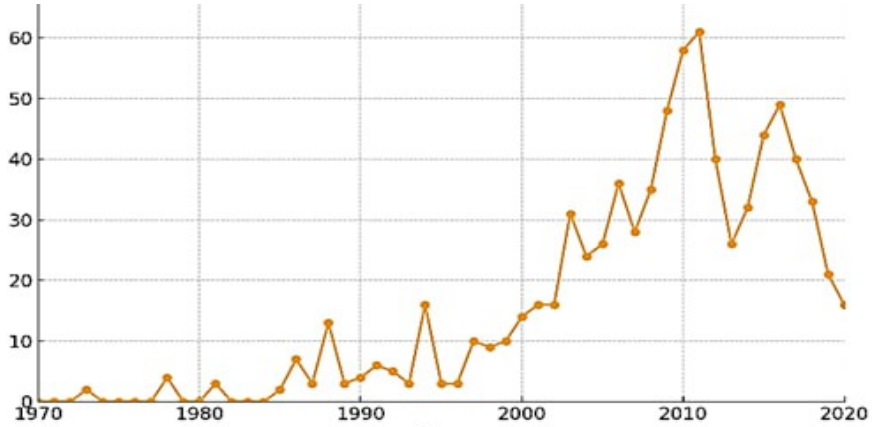


Figure 1. Dynamics of the number of publications on heat pumps based on a bibliographic review (1970-2020). A sharp increase in interest in this topic was observed after 2000, reaching its peak in 2010-2011 (CIS countries) [3].

At the same time, the use of solar energy in heat supply systems has significant potential. The application of solar thermal collectors reduces fuel consumption, enables partial or substantial coverage of heat production through renewable sources, and improves the overall energy performance of buildings. Recent review studies indicate that building-integrated solar technologies, including solar thermal systems, play an important role in enhancing energy efficiency and reducing environmental impact. However, since the efficiency of solar collectors depends on weather conditions and solar radiation levels, their standalone application does not always ensure a stable heat supply [4].

From this perspective, hybrid heating systems based on heat pumps and solar collectors are of particular scientific interest. In such systems, solar energy serves as a low- or medium-temperature heat source, while the heat pump upgrades this heat to a useful level and meets the building's heating demand. Recent scientific reviews demonstrate that integrating solar technologies, heat pumps, and thermal energy storage systems can reduce building energy consumption, improve the system's coefficient of performance (COP), and accelerate the

transition to low-carbon heating. Furthermore, contemporary research on solar-assisted heat pump systems increasingly focuses on their application under various climatic conditions, as well as on optimization and control strategies for these systems [5].

Systems integrating solar energy with air-source heat pumps represent one of the most promising directions in modern energy-efficient heating technologies. Such systems combine the renewable and environmentally friendly nature of solar energy with the high energy efficiency of air-source heat pumps. As a result, the overall coefficient of performance (COP) of the system increases, electricity consumption decreases, and the reliability of heat supply improves [6, 7]. The drawbacks associated with the intermittent operation of solar collectors and the reduced efficiency of air-source heat pumps under low ambient temperatures are effectively mitigated through hybrid integration schemes [8].

Solar-assisted air-source heat pump systems are generally classified according to their configuration into direct expansion systems (DX-S-ASHP) and indirect expansion systems (IDX-S-ASHP) [6, 9]. Indirect expansion systems, in turn, can operate in either series or parallel configurations. Each configuration is suited to specific climatic and load conditions, and they differ in terms of energy efficiency, reliability, and structural complexity [10].

1. DX-S-ASHP system.In the DX-S-ASHP system, the functions of the solar collector and the evaporator are integrated. In this configuration, the refrigerant directly absorbs heat within the solar collector and undergoes the evaporation process at the same location. This arrangement reduces intermediate heat exchange losses and simplifies system operation [4, 6]. Under solar radiation conditions, the temperature of the collector-evaporator surface increases, which improves the refrigerant evaporation conditions and reduces the compressor workload[11].

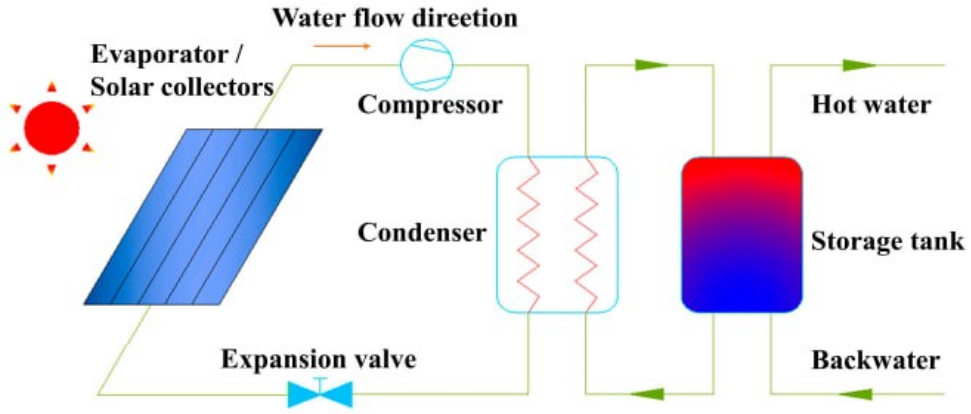


Figure 2. Schematic of the DX-S-ASHP system.

The main advantage of the DX-S-ASHP system is its simplicity and high heat transfer efficiency. This is because solar energy is directly transferred to the refrigerant of the heat pump. However, this configuration is highly dependent on external solar radiation. When solar radiation decreases or during cloudy weather conditions, the system performance may decline [9, 12]. Therefore, the DX-S-ASHP system is considered more effective in regions with relatively high solar resources.

Studies show that structural improvements in the evaporator and collector significantly affect the overall performance of the DX-S-ASHP system (Figure 2). For example, the use of finned solar evaporators, dual-source evaporators, or combined solar-air evaporator configurations has led to a noticeable increase in the COP value of the system [11-13]. Thus, although the DX-S-

ASHP system has a simple structure, its efficient operation largely depends on the optimization of the evaporator-collector section [6].

Main characteristics of the DX-S-ASHP system. Table 1

Parameter	**Description**
Connection Type	Direct expansion
Main Feature	Solar collector and evaporator are integrated
Advantage	Low intermediate heat losses, simple structure
Disadvantage	Strongly dependent on solar radiation
Application Condition	Regions with high solar resources
Efficiency Factor	Highly dependent on the collector-evaporator design

As can be seen from Table 1, although the DX-S-ASHP system has a relatively simple structure, its stable operation is closely dependent on environmental conditions and solar radiation. Therefore, in designing this system, the collector area, refrigerant type, and evaporator design play an important role [9, 11].

2. IDX-S-ASHP Series System. In the IDX-S-ASHP series system, the solar collector and the heat pump evaporator are separated from each other. The heat obtained from the solar collector is first stored in a thermal storage tank or transferred through an intermediate heat carrier, and then delivered to the evaporator of the heat pump [10]. This configuration is particularly useful in cold climate conditions, as the heat obtained from solar energy increases the evaporation temperature and improves the efficiency of the heat pump [14, 15].

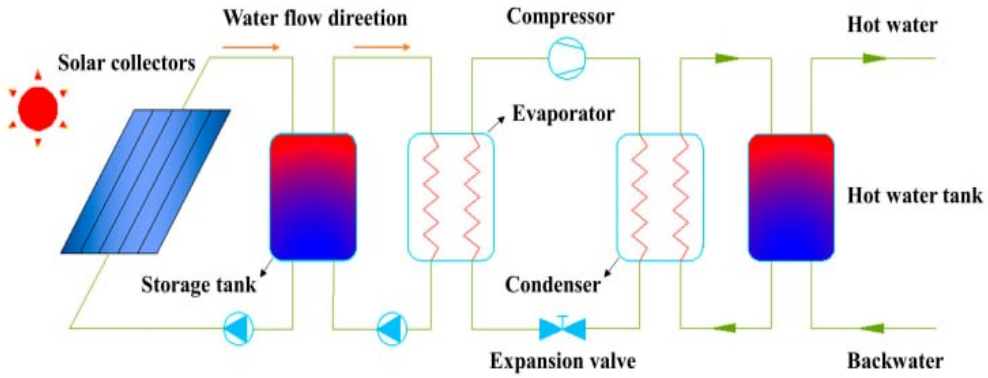


Figure 3. Schematic of the IDX-S-ASHP series system.

In the series connection scheme, solar energy is first collected and then used as the heat source for the heat pump. As a result, even under conditions of weak solar radiation, a certain level of stable heat transfer can be maintained through the thermal storage tank [10]. This is especially important in winter when the outdoor air temperature is low. Under such conditions, the standalone performance of an air-source heat pump decreases, while the series solar connection helps to mitigate this drawback [15]. The advantage of the series configuration is that it allows more effective utilization of solar energy and creates more favorable operating conditions for the evaporator at low temperatures. However, due to the presence of an additional thermal storage tank and an intermediate heat transfer loop in the system, its structure becomes more complex and the initial investment cost is higher [10, 15].

Main characteristics of the IDX-S-ASHP series system. Table 2

Parameter	**Description**
Connection Type	Indirect expansion, series

Main Feature	Solar heat is first stored in a thermal storage tank
Advantage	Increases evaporation temperature under cold conditions
Disadvantage	More complex system, requires more equipment
Application Condition	Cold climates with solar availability but low ambient temperatures
Efficiency Factor	Depends on the size and control of the thermal storage tank

According to the data in Table 2, the series IDX-S-ASHP system operates particularly efficiently during the winter season. In this case, the heat obtained from the solar collector provides a more favorable heat source for the evaporator and improves the performance of the heat pump [13, 15].

3. Parallel IDX-S-ASHP System. In the parallel IDX-S-ASHP system-an indirect solar-assisted air-source heat pump configuration-the solar collector and the air-source heat pump operate relatively independently. Both sources can supply the consumer load either simultaneously or separately, depending on demand [10]. When solar energy is sufficient, the collector covers a large portion of the heat load, whereas when solar energy decreases, the ASHP operates as the primary heat source [16].

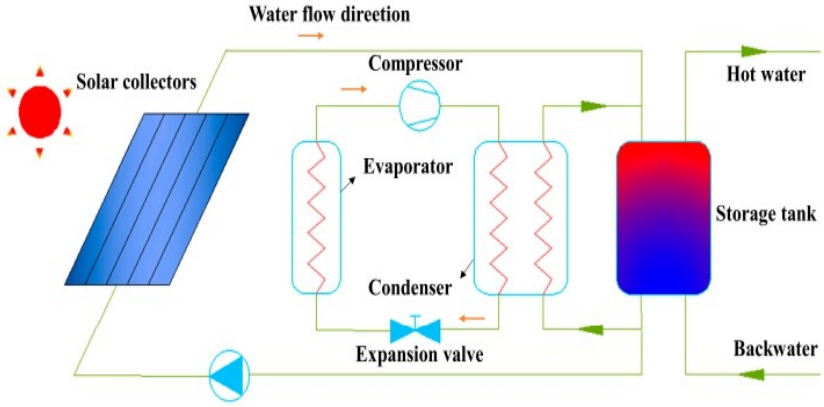


Figure 4. Schematic of the Parallel IDX-S-ASHP system.

The main advantage of the parallel configuration is its flexibility. In this setup, the solar collector and the heat pump are not tightly coupled. Therefore, the system can adapt more quickly to sunny, cloudy, or variable weather conditions [16, 17]. During summer and transitional seasons, parallel systems often demonstrate higher efficiency, as solar energy covers the majority of the load and the operating time of the heat pump is reduced [17]. However, in parallel systems, it is important to properly control the interaction between the collector and the heat pump. An improperly selected control strategy may lead to increased energy consumption. Therefore, intelligent control, load forecasting, and parameter optimization are of great importance in parallel systems [16, 18].

Main characteristics of the Parallel IDX-S-ASHP system. Table 3

Parameter	**Description**
Connection Type	Indirect expansion, parallel
Main Feature	Solar collector and ASHP operate independently or together
Advantage	High flexibility and easier control
Disadvantage	Energy consumption may increase without optimal control
Application Condition	Moderate climates with variable weather conditions
Efficiency Factor	Depends on control strategy and load distribution

As can be seen from Table 3, the parallel IDX-S-ASHP system has high flexibility and can operate efficiently under variable weather conditions. In particular, when solar energy and the air source are used alternately or simultaneously, the energy efficiency of the system increases [16-18]. **Comparison of connection schemes.** When selecting among the three configurations mentioned above, it is necessary to consider the climatic conditions of the region, solar resources, heat load, and economic factors.

Table 4. Comparative characteristics of DX-S-ASHP, series IDX-S-ASHP, and parallel IDX-S-ASHP systems

System Type	Main Advantage	Main Disadvantage	Effective Application Conditions
DX-S ASHP	Simple structure, low heat losses	Highly dependent on solar radiation	Regions with high solar resources
Series IDX-S-ASHP	Effective in cold conditions	More complex construction	Cold and sunny regions
Parallel IDX-S-ASHP	Flexible operation	Requires optimized control	Variable weather conditions

The DX-S-ASHP system stands out for its simplicity and low intermediate heat losses, but it is more dependent on solar radiation [9]. The series IDX-S-ASHP system is more suitable for cold climates and improves the performance of the heat pump under low-temperature conditions [14]. The parallel IDX-S-ASHP system, on the other hand, offers high flexibility and allows the use of solar energy and air sources alternately [16].

2. Materials and Methods

According to Table 4, each connection scheme is more effective under certain conditions. Therefore, when designing a hybrid heating system, it is advisable to select a technical solution that matches the climate, energy source, and load characteristics, rather than relying on a single universal configuration [6, 10].

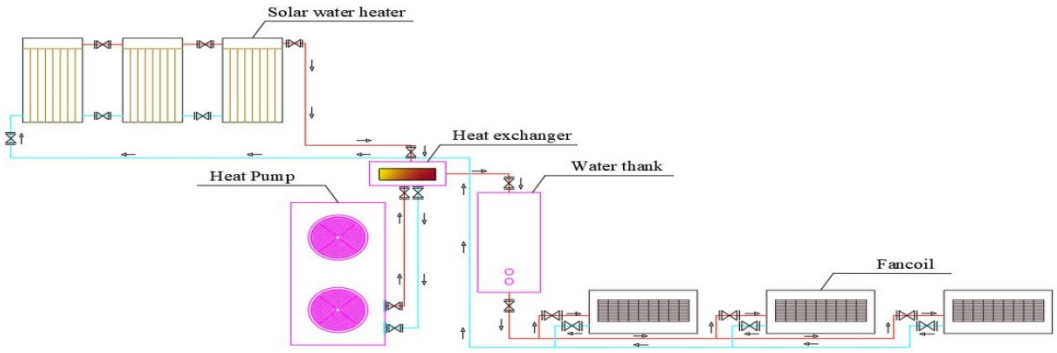


Figure 5. Fundamental hydraulic connection scheme of the indirect solar-assisted heat pump (IDX-SAHP) system integrated with solar collectors.

Figure 5 illustrates a combined heating and cooling system consisting of solar water heaters, a heat pump, a heat exchanger, a thermal storage tank, and fan-coil units. The proposed hydraulic connection scheme represents an indirectly integrated (IDX) hybrid system that combines solar energy and heat pump technologies into a unified thermal energy supply configuration. The operating process of the system begins with the heating of the working fluid inside vacuum tube solar collectors under solar radiation. The generated thermal energy is then transferred through a central plate heat exchanger to the heat pump circuit. Such a technical

solution hydraulically separates the collector loop from the heat pump loop while simultaneously increasing the evaporator temperature of the heat pump under low ambient temperature conditions. As a result, compressor electricity consumption is reduced and the overall operational stability of the system is improved. The thermal storage tank integrated into the system performs the function of storing excess thermal energy accumulated during daytime operation and stabilizing the building heating load throughout the day. The stored energy is finally distributed inside the building through a parallel fan-coil network by convection heat transfer, ensuring rapid and uniform indoor heating performance. The practical implementation of the proposed system allows maximum utilization of solar energy resources, significantly increases

2.1. System description

The proposed hybrid heating system is based on the integration of vacuum tube solar collectors and an air-source heat pump through an indirect expansion solar-assisted heat pump (IDX-SAHP) configuration. The system consists of solar collectors, a plate heat exchanger, a thermal storage tank, an air-source heat pump, circulation pumps, and fan-coil heating units. In this configuration, solar energy is first absorbed by the solar collectors and then transferred through the plate heat exchanger to the heat pump circuit. The thermal storage tank accumulates excess thermal energy and stabilizes the heating load during variable operating conditions.

The proposed indirect integration scheme provides hydraulic independence between the solar collector loop and the heat pump loop, improving system reliability and thermal stability under low ambient temperature conditions. The recovered thermal energy is distributed to indoor spaces through fan-coil units, ensuring uniform heat transfer and improved indoor thermal comfort.

2.2. Thermodynamic analysis

The performance of the hybrid heating system was evaluated using thermodynamic and energy efficiency analysis methods. The coefficient of performance (COP) of the heat pump system was determined according to the following relationship:

$$COP = \frac{Q_{heating}}{W_{compressor}} \quad (1)$$

where: $Q_{heating}$ is the useful heating capacity (kW), $W_{compressor}$ is the compressor power consumption (kW).

The useful thermal energy obtained from the solar collector was calculated as:

$$Q_u = \dot{m} c_p \left(T_{out} - T_{¿} \right) \quad (2)$$

where: $\dot{m}$ is the mass flow rate of the working fluid (kg/s), c_p is the specific heat capacity of the fluid (kJ/kg·K), T_{out} and $T_{¿}$ are the outlet and inlet temperatures of the collector (°C).

The efficiency of the solar collector was determined using:

$$\eta_{sc} = \frac{Q_u}{A_c G_t} \quad (3)$$

where: η_{sc} is the collector efficiency, A_c is the collector surface area (m²), G_t is the solar radiation intensity (W/m²).

2.3. Building heat loss analysis

The building heat demand was estimated based on transmission heat losses through the building envelope. The total heat loss was calculated according to:

$$Q_{loss} = UA \left(T_i - T_o \right) \quad (4)$$

where: U is the overall heat transfer coefficient (W/m²·K), A is the heat transfer surface area (m²), T_i is the indoor temperature (°C), T_o is the outdoor ambient temperature (°C). This analysis enabled the evaluation of the heating capacity required under different climatic conditions.

2.4. Comparative system evaluation

The proposed IDX-SAHP system was comparatively analyzed with direct expansion (DX-S-ASHP) and parallel IDX-SAHP configurations. The comparison was performed based on: coefficient of performance (COP); electricity consumption; operational stability; adaptability to climatic conditions; system complexity; energy saving potential. The obtained performance indicators were analyzed under varying outdoor temperatures and solar radiation conditions to determine the most efficient hybrid heating configuration.

2.5. Energy efficiency assessment

The annual energy saving potential of the proposed system was estimated by comparing electricity consumption with that of a conventional standalone air-source heat pump system. The analysis demonstrated that the proposed hybrid configuration could increase the COP value from approximately 3.06 to 5.21, while reducing electricity consumption by nearly 70% under favorable solar conditions. These results confirm the effectiveness of integrating solar thermal collectors with heat pump technologies for sustainable building heating applications.

3. Results and Discussion

3.1. Comparative performance analysis of hybrid heating systems

The comparative analysis of DX-S-ASHP, series IDX-S-ASHP, and parallel IDX-S-ASHP systems demonstrated significant differences in thermal efficiency, operational stability, and adaptability to climatic conditions. Among the investigated configurations, the proposed IDX-SAHP system integrated with vacuum tube solar collectors and a plate heat exchanger achieved the highest overall performance. The obtained results indicate that the proposed hybrid system can achieve a coefficient of performance (COP) of approximately 5 under favorable operating conditions, whereas conventional standalone air-source heat pump systems generally operate with a COP of around 3 or 4. This improvement is mainly associated with the additional thermal energy supplied by the solar collectors, which increases the evaporator inlet temperature and reduces compressor workload. In addition, the use of a thermal storage tank significantly stabilizes system operation during periods of fluctuating solar radiation and variable outdoor temperatures. This improves operational reliability and reduces short cycling of the compressor (figure 6).

3.2. Effect of solar integration on energy consumption

The integration of solar collectors into the heat pump system substantially reduced electricity consumption. During sunny operating conditions, a considerable portion of the heating load was covered directly by solar thermal energy, decreasing the operating time of the compressor. The comparative results showed that the proposed IDX-SAHP configuration reduced electricity consumption by approximately 70% compared with conventional heating systems. This reduction contributes not only to lower operational costs but also to decreased greenhouse gas emissions associated with electricity generation (figure 7). Furthermore, the utilization of renewable solar energy decreases dependence on fossil-fuel-based heating systems and supports the decarbonization of building energy systems.

3.3. Influence of climatic conditions

The performance of solar-assisted heat pump systems strongly depends on climatic conditions, outdoor air temperature, and solar radiation intensity. In regions with high solar

resources, the DX-S-ASHP configuration demonstrates relatively high efficiency because of direct solar energy utilization (figure 8). However, its performance decreases significantly during cloudy weather conditions or periods of low solar radiation. The series IDX-SAHP configuration showed improved performance under cold climatic conditions because the thermal storage tank and indirect heat transfer arrangement stabilized evaporator operating temperatures. The parallel IDX-SAHP system demonstrated high flexibility and adaptability under variable weather conditions, allowing alternating or simultaneous operation of the solar collector and heat pump.

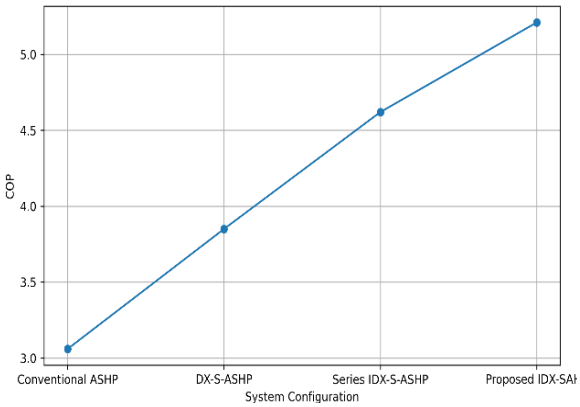


Figure 6. Comparative COP Analysis

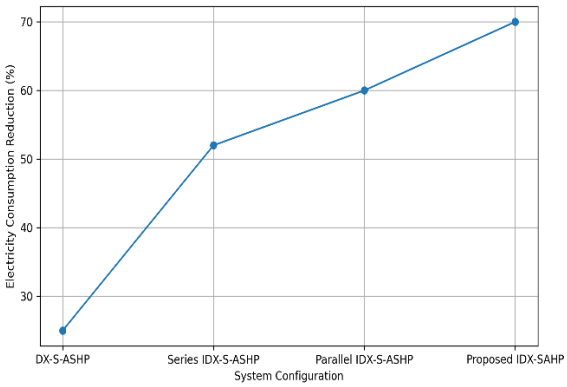


Figure 7. Electricity Consumption Reduction

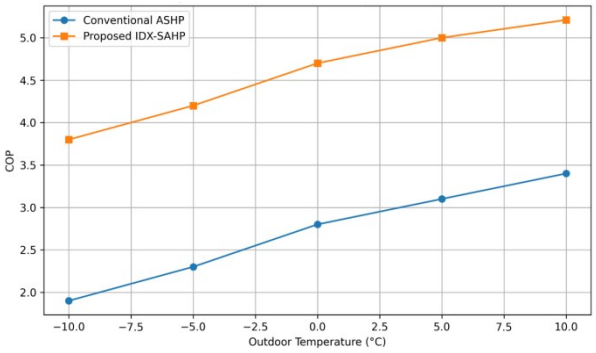


Figure 8 - Effect of Outdoor Temperature on COP

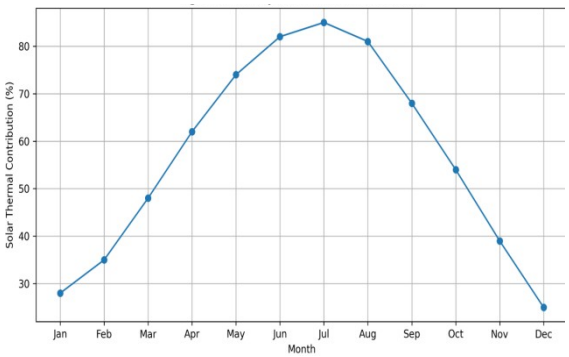


Figure 9 - Monthly Solar Thermal Contribution

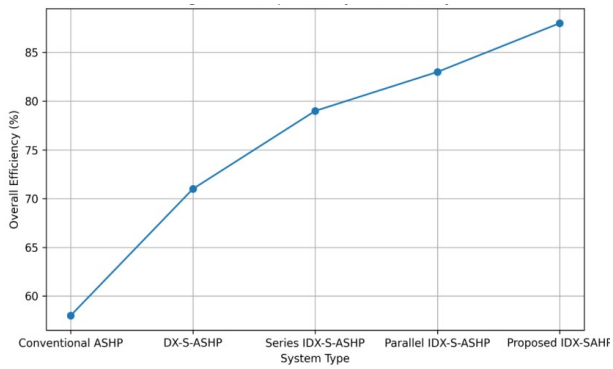


Figure 10 - Monthly Solar Thermal Contribution

The proposed hybrid IDX configuration exhibited stable operation under both moderate and cold climate conditions due to hydraulic independence between system loops and optimized thermal energy distribution.

3.4. Thermal storage and heat distribution analysis

The thermal storage tank plays an essential role in maintaining stable heating performance throughout the day. Excess thermal energy accumulated during periods of high solar radiation can

be stored and later utilized during nighttime or cloudy conditions (figure 9). The fan-coil heating network provided rapid and uniform heat distribution inside the building. The application of differential and modulation-based control strategies improved indoor thermal comfort and minimized unnecessary energy consumption. The analysis confirms that proper thermal storage sizing and intelligent control strategies are critical factors affecting the overall efficiency of hybrid heating systems.

3.5. Environmental and economic implications

The proposed hybrid heating system contributes significantly to environmental sustainability by reducing electricity demand and greenhouse gas emissions. The integration of renewable solar energy with high-efficiency heat pump technology creates a low-carbon heating solution suitable for modern energy-efficient buildings (figure 10. From an economic perspective, although the initial investment cost of the IDX-SAHP system is higher because of additional equipment such as solar collectors, heat exchangers, and thermal storage tanks, the reduction in long-term electricity consumption provides favorable economic benefits during the operational lifetime of the system. The obtained results confirm that hybrid solar-assisted heat pump systems represent a technically effective, economically feasible, and environmentally sustainable solution for future building heating applications.

3.6. Comparative analysis of system configurations

A comparative evaluation of the DX-S-ASHP, series IDX-S-ASHP, and parallel IDX-S-ASHP systems was carried out based on operational efficiency, structural complexity, flexibility, and climatic adaptability. The analysis revealed that each configuration possesses specific advantages depending on environmental and operational conditions. The DX-S-ASHP system demonstrated relatively simple construction and low intermediate heat losses due to direct refrigerant evaporation inside the solar collector. However, the system performance strongly depended on solar radiation intensity and ambient weather conditions. Under cloudy conditions or during periods of low solar irradiance, the efficiency of the DX system decreased noticeably. The series IDX-S-ASHP configuration exhibited superior performance under cold climatic conditions. The integration of a thermal storage tank allowed partial stabilization of thermal energy supply and increased evaporator operating temperature. As a result, compressor energy consumption decreased and the overall system COP improved. The parallel IDX-S-ASHP system provided the highest operational flexibility because the solar collector and heat pump could operate independently or simultaneously. This arrangement improved system adaptability under variable weather conditions and enabled optimized load sharing between renewable and conventional heat sources. The proposed IDX-SAHP configuration combined the advantages of stable thermal operation, improved energy efficiency, and flexible heat distribution, making it the most suitable option for sustainable building heating systems.

3.7. Operational stability of the proposed system

One of the main advantages of the proposed hybrid configuration is its operational stability under variable climatic conditions. In conventional air-source heat pump systems, low outdoor temperatures significantly reduce evaporator performance and increase compressor workload. In the proposed system, preheated thermal energy supplied from the solar collector loop increases the evaporation temperature and improves refrigerant operating conditions.

The use of a plate heat exchanger ensures hydraulic separation between the solar collector circuit and the heat pump loop. This prevents pressure instability and improves system reliability during long-term operation. Furthermore, thermal energy storage minimizes rapid fluctuations in

heating demand and contributes to smoother system performance. The analysis also indicates that differential temperature control strategies improve energy utilization efficiency by activating circulation pumps only when useful thermal energy is available from the solar collectors. The obtained results demonstrate that the proposed hybrid IDX-SAHP system significantly improves building heating efficiency compared with conventional air-source heat pumps. The integration of vacuum tube solar collectors and thermal storage increased the coefficient of performance (COP) from approximately 3.06 to 5.21 while reducing electricity consumption by nearly 70%.The series IDX-S-ASHP configuration showed better performance under cold climatic conditions due to stable heat transfer provided by the thermal storage tank, whereas the parallel configuration offered greater operational flexibility under variable weather conditions. In addition, the proposed system improved operational stability, reduced compressor workload, and enhanced indoor thermal comfort through efficient fan-coil heat distribution.

5. Conclusion. This study analyzed hybrid heating systems based on heat pumps and solar collectors, including DX-S-ASHP, series IDX-S-ASHP, parallel IDX-S-ASHP, and the proposed IDX-SAHP configuration. The results showed that the proposed hybrid system significantly improved energy performance compared with conventional heating systems. In particular, the COP increased from 3.06 to approximately 5.21, while electricity consumption was reduced by nearly 70%. The integration of vacuum tube solar collectors, thermal storage, and intelligent control strategies improved operational stability and reduced compressor workload under variable climatic conditions. Among all investigated systems, the proposed IDX-SAHP configuration demonstrated the best balance between energy efficiency, reliability, and environmental sustainability. Overall, the proposed hybrid system represents an efficient and environmentally sustainable solution for modern energy-efficient buildings. Future research should focus on experimental validation and optimization under real operating conditions.

REFERENCES

1. Morozyuk, T. V. Theory of Refrigeration Machines and Heat Pumps. Odessa: “Negotsiant” Studio, 2006. - 412 p.
2. International Energy Agency (IEA). Heat Pumps - Energy System, 2023. - Electronic resource.
3. Avezova, N. R., Uzakov, G., Kuchkarov, A. A., Oshchepkova, E. A., Shermatova, M. B., Kholmatov, E. S., Ergashev, E. A. Heat Pumps as a Key to a Low-Carbon Future. Part 1: Historical Evolution and Development Prospects in Uzbekistan.
4. Safarov, O. F., Radzhabov, M., Komilov, O. S., Abdurakhmonov, O. R. Exergy Analysis of a Heat Pump Drying Installation // Heliotechnika. - 2009.
5. Rudenko, I. Yu. Analysis of the Advantages and Costs of an Alternative Heating System (HP + PVS) for Rural Schools in Uzbekistan. Tashkent: United Nations Development Programme (UNDP), Uzbekistan, 2019.
6. Meng, X., Zhou, X., Li, Z. Review of Integrated Solar and Air Source Heat Pump Systems // Energies. - 2024. - 17. - 6045.
7. Kim, T., Choi, B. I., Han, Y. S., Do, K. H. Comparative Study of Solar-Assisted Heat Pumps with Solar Thermal Collectors for Domestic Hot Water Systems // Energy Conversion and Management. - 2018. - 172. - 472-484.

8. Abbasi, B., Li, S., Mwesigye, A. Thermodynamic Performance of a Direct Expansion Solar-Assisted Heat Pump under Extremely Cold Climate Conditions // International Journal of Refrigeration. - 2024. - 158. - 329-344.
9. Shi, G. H., Aye, L., Li, D., Du, X. J. Recent Advances in Direct Expansion Solar-Assisted Heat Pump Systems: A Review // Renewable and Sustainable Energy Reviews. - 2019. - 109. - 349-366.
10. Zhou, J., Zeng, C., Wang, Z., Liu, Y., Tang, Y., Wu, D., Ji, Y., Yuan, Y. Indirect Expansion Solar Heat Pump Systems: A Review // Sustainable Energy Technologies and Assessments. - 2022. - 53. - 102409.
11. Dong, X., Tian, Q., Li, Z. Experimental Study on Heating Performance of an Integrated Solar-Assisted Air Source Heat Pump // Applied Thermal Engineering. - 2017. - 123. - 1013-1020.
12. Chinnasamy, S., Arunachalam, A. Experimental Study of a Direct Expansion Solar-Air Source Heat Pump for Water Heating // Renewable Energy. - 2023. - 202. - 222-233.
13. Ma, K. R., Li, X. F., Li, S. Q., Gao, C. J. Comparative Study of a Direct Expansion Solar-Air Heat Pump System and an Air Source Heat Pump // CIESC Journal. - 2020. - 71(S1). - 375-381.
14. Cai, J. Y., Ji, J., Wang, Y. Y., Huang, W. Z. Numerical Simulation and Experimental Validation of a Multifunctional Indirect Expansion Solar-Assisted Heat Pump // Renewable Energy. - 2016. - 93. - 280-290.
15. Long, J. B., Zhang, R. C., Lu, J., Xu, F. Heat Transfer Performance of an Integrated Solar-Air Source Heat Pump Evaporator // Energy Conversion and Management. - 2019. - 184. - 626-635.
16. Wang, Q. Q., Wang, F., Liu, D. H., Wang, Y. X., He, Z. H. Heating Characteristics of a Solar-Assisted Air Source Heat Pump Composite System // Agricultural Equipment & Vehicle Engineering. - 2021. - 59. - 50-54.
17. Huan, C., Li, S. T., Wang, F. H., Liu, L., Zhao, Y. J., Wang, Z. H., Tao, P. F. Performance Analysis of a Solar-Assisted Heat Pump Heating System in Xi'an, China // Energies. - 2019. - 12. - 2515.
18. Ma, Y. C., Xi, J. F., Cai, J., Gu, Z. Z. Optimization of a Water Heating System Using an Air Source Heat Pump and a Multi-Tank Solar System // Thermal Science and Engineering Progress. - 2024. - 48. - 102387.
19. Juraboev, I., Jurakulov, S., Urishev, O., Rakhmatov, O., Eshkobilov, O., Sadirova, K., & Aliyarova, L. (2025). Improving Thermal Performance of Solar PTC Using Internal Finned Structure. In E3S Web of Conferences (Vol. 661, p. 04018). EDP Sciences. https://doi.org/10.1051/e3sconf/202566104018
20. Akramova, S., Urishev, O., Mamurov, B., Nurmanov, S., Apakhodjaeva, T., Irmuhamedova, L., & Gaimnazarov, K. (2025). CFD Modelling of Latent Heat Storage with Cylindrical PCM Capsules. In E3S Web of Conferences (Vol. 661, p. 04010). EDP Sciences. https://doi.org/10.1051/e3sconf/202566104010
21. Urishev, O., Ersin, A., Metin, G., & Quvondiqov, Q. (2026). ESTIMATING ELECTRICITY CONSUMPTION OF PUMPING PLANTS IN IRRIGATION SYSTEMS. Innovation Science and Technology, 2(1). https://doi.org/10.5281/zenodo.18472643
22. Urishev, O., Salomov, U., Ergashev, S., Kuchkarov, A., Madaliev, M., Abdukarimov, B., & Juraev, N. (2025). Efficiency assessment of micro hydropower for agriculture using modern

modeling. In BIO Web of Conferences (Vol. 173, p. 03031). EDP Sciences. DOI:10.1051/bioconf/202517303031

HYDRODYNAMIC ANALYSIS OF A SPIRAL PUMP DRIVEN BY A WATER WHEEL UNDER LOW-HEAD OPEN CHANNEL FLOW CONDITIONS

O. Urishev[1], A. Mahmudjonov[2], A. Abduvossiyev[3], M. Tursunaliyeva[4]
PhD, Associate Professor of Fergana State Technical University[1]
Master student of Fergana State Technical University[2]
Assistant of Fergana State Technical University[3]
Student of Fergana State Technical University[4]
https://doi.org/10.5281/zenodo.20552481

Abstract. *This study investigates the hydraulic performance of a water wheel driven spiral pump operating under low-head open channel flow conditions. The effects of water wheel diameter, flow velocity, and lifting head on discharge characteristics were analyzed using analytical and empirical methods. The obtained results showed that the discharge decreased exponentially from 0.108 m³/s to 0.013 m³/s when the lifting head increased from 0.5 m to 10 m. In addition, increasing the wheel diameter from 0.5 m to 2.0 m increased the discharge from 0.026 m³/s to 0.190 m³/s. The obtained fitting models demonstrated high accuracy with determination coefficients of $R^2 = 0.997$ and $R^2 = 1.000$. The results confirmed that optimal selection of wheel diameter and flow parameters significantly improves the efficiency of spiral pumping systems for irrigation applications in remote areas without electricity supply.*

Keywords: *water wheel, spiral pump, low-head, flow, low-head, flow parameters.*

1. Introduction

Today, the efficient use of water resources, the development of energy-saving technologies, and the creation of water lifting systems that do not depend on electricity are among the most pressing scientific and practical problems in the world. As a result of population growth, expansion of agricultural areas, and climate change, the demand for irrigation systems is increasing sharply. Especially in areas far from electricity networks, the use of traditional electric pumps to lift water requires high operating costs. Therefore, interest in hydraulic pumping systems that use the kinetic energy of natural water flows is growing [1-9].

In world practice, small hydropower and mechanical water lifting systems have been used for many years. In particular, spiral pumps (spiral pump or coil pump) and hydromechanical systems based on water wheels are distinguished by their ability to operate without electricity, simplicity of design, and low operating costs [1,2]. These technologies began to develop at the end of the 19th century, initially based on the concept of the Wirtz spiral pump. Later, spiral pipe systems were integrated with water wheels, allowing the kinetic energy of the water flow to be directly converted into mechanical rotational energy. As a result, environmentally friendly and autonomous systems for lifting water to a certain height appeared [2].

In recent years, scientific research on water lifting technologies based on renewable energy sources has increased significantly. According to international studies, pumping systems consume 20-22% of the world's electricity. In some industrial and irrigation systems, this figure reaches 30-50%. Therefore, the development of alternative hydromechanical devices that reduce energy consumption is considered one of the priority areas in the energy and irrigation sectors. Spiral pumps are considered a promising technology, especially in small irrigation systems, foothill areas, open canals and agricultural facilities with limited electricity supply.

In Uzbekistan, rational use of water resources and increasing energy efficiency are important directions of state policy. A large part of the irrigated land in the republic is supplied with water through pumping stations, which leads to a large amount of electricity consumption. Especially in regions with dense irrigation networks, such as the Fergana Valley, there are opportunities to use the kinetic energy of open channel flows, which makes the introduction of spiral pumping systems operating on the basis of a natural energy source an urgent issue [4-9].

Although the current scientific works on spiral pump systems mainly present constructive solutions, general operating principles and experimental results, the influence of water wheel parameters on the pressure-flow characteristics of the pump has not been studied in depth enough. In particular, the issues of mathematical modeling of the dependence between wheel diameter, water flow velocity, wetted cross-sectional area and useful power are still relevant.

The main objective of this study is to analyze the hydrodynamic and energy parameters of a spiral pump system operating in low-pressure natural water flows, to determine the effect of water wheel dimensions on water consumption and head, and to develop a mathematical model of the system. During the study, the dependences between water flow velocity, water flow, wheel diameter, and useful power are analyzed, and recommendations are developed to improve the energy efficiency of the spiral pump system.

Literature review

Spiral pump systems, which use the kinetic energy of low-pressure water flows to lift water upward, have been widely studied as an energy-efficient irrigation technology in recent years. Spiral pumps are a promising device for small irrigation systems due to their ability to operate without electricity, their simplicity of design, and their low operating costs.

Müller [1,12] studied the hydraulic efficiency of water wheels and found that the water flow velocity and wheel diameter significantly affect the torque of the device. According to the results of the study, an increase in the diameter of the water wheel increases the level of utilization of flow energy. However, this work did not consider the process of lifting water through a spiral pipe.

Senior et al. [2] have experimentally analyzed the performance of conventional water wheels. They have shown that the water flow velocity and impeller geometry directly affect the useful work coefficient. Although the mechanical energy generation characteristics of the water wheel are studied in the study, a hydrodynamic model of the integrated systems with a volute pump is not developed.

Fraenkel [10] analyzed non-electric water lifting devices and noted that spiral pumps are an effective technology for agricultural water supply. The author pointed out that the main advantage of spiral pumps is the use of natural water flow energy. However, the dependence between spiral pipe diameter and water flow has not been analyzed in depth.

Williams [13] studied the energy balance in hydraulic machines and investigated the dependence between water flow and head, but did not provide practical parameters for volute pump systems operating in open channel flows.

Patil et al. [14] have reported that spiral tube water wheel pump systems are a low-cost technology for irrigation systems. The study shows that water can be lifted upward by rotating a spiral tube using a water wheel. However, the dependence between water wheel diameter, flow velocity, and water flow is not well-established mathematically.

Tschiersch and Bohórquez [16] experimentally investigated the effect of spiral pump geometry on water lifting efficiency. The results showed that water flow increased with increasing spiral pipe diameter and rotation frequency. However, the study was conducted in a laboratory setting and did not consider natural open channel flow conditions.

Author	**Research direction**	**Main result**	**Methodological approach**
Muller [1,12]	Water wheel design and efficiency	Wheel diameter and flow velocity have been found to affect efficiency	Empirical and experimental hydraulic analysis
Senior et al. [2]	Hydraulic operation of traditional water wheels	The effect of flow velocity and blade geometry on $\dot{\eta}$ has been determined.	Experimental hydrodynamic analysis
Fraenkel [10]	Water lifting devices without electricity	Spiral pumps have been shown to be an effective technology for irrigation	Feasibility and design analysis
Williams [13]	Energy balance in hydraulic machines	The energy equation between water flow and pressure is based on	Analytical and energetic modeling
Patil et al. 14]	Spiral tube water wheel pump system	The convenience of the spiral pump for irrigation is shown	Theoretical and review approach
Tschiersch and Bohórquez [16]	Spiral pump geometry and efficiency	The effect of spiral pipe diameter and rotation frequency on water flow has been determined.	Laboratory experiments and mathematical analysis

The analyzed literature shows that the general design and operating principle of spiral pumps have been sufficiently studied in existing scientific works. However, the issues of comprehensive analysis of the pressure-flow characteristics of a spiral pump based on the parameters of the water wheel in low-pressure natural water flows, mathematical modeling of the dependence between water flow velocity, wheel diameter and lift height have not been sufficiently studied. Therefore, in this study, the working process of a spiral pump is analyzed using theoretical and analytical methods based on the parameters of the water wheel.

2.Materials and Methods

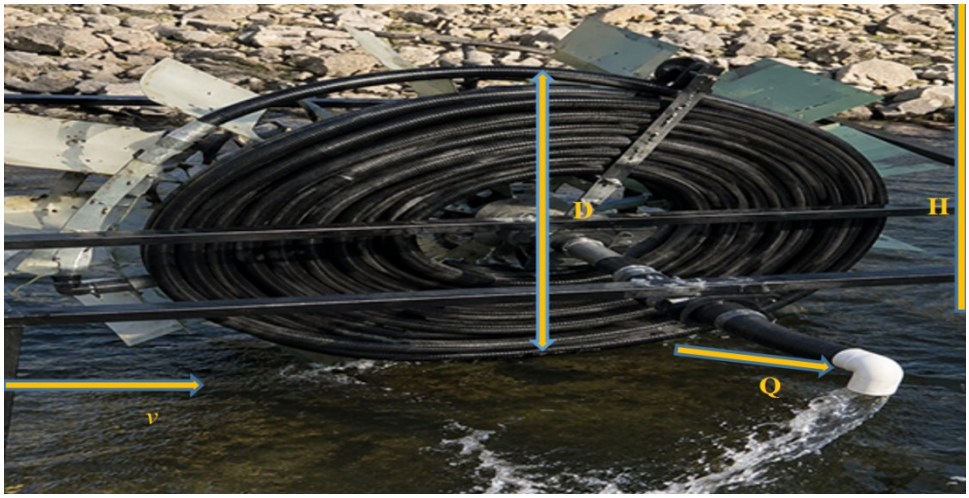
The object of the study was a spiral pump-water wheel system operating in a low-pressure open channel water flow. The study analyzed the process of converting the kinetic energy of the

water flow into mechanical rotational energy through a water wheel and lifting water to a certain height using a spiral pipe.

Experimental studies were performed in open channel conditions. Channel flow parameters were varied in the following ranges:

1. Water flow velocity: $V = 0.5 - 1.5\, m/s;$
2. Water depth: $d = 0.2 - 0.5\, m;$
3. Water wheel diameter: $D = 0.5 - 2.0\, m;$
4. Lifting height: $H = 0.5 - 10\, m.$

Q water flow, P_u useful power, n rotation frequency, η hydraulic efficiency, and H lifting height were taken as the main parameters of the system.

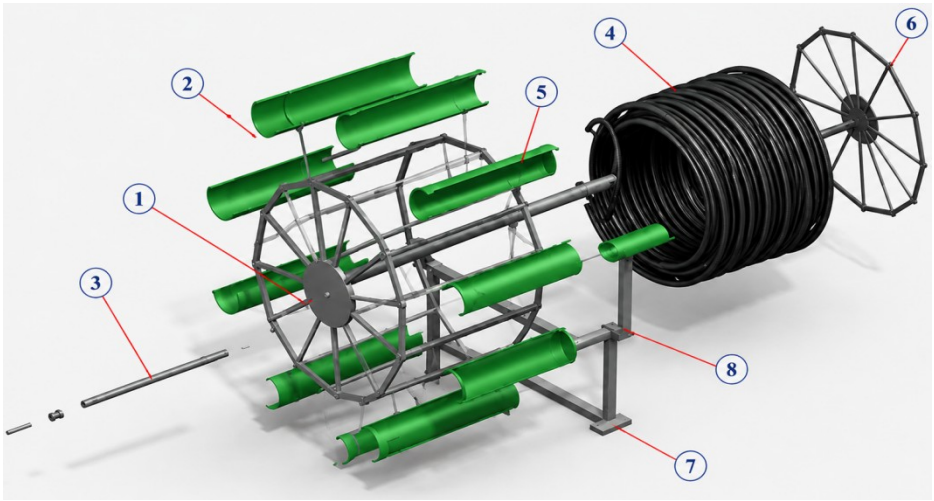


The main parameters are water flow velocity v, water flow Q , wheel diameter D, and lift height H.

Figure 1. Schematic diagram of the principle of operation of a spiral pump.

This figure (1) shows a spiral pump system that uses open channel flow energy. The water flow rotates the impeller, which in turn pushes water up through the spiral pipe. The figure shows the flow velocity (V), water flow (Q), impeller diameter (D), and head (H) as the main parameters.

The water wheel is the main driving element of a spiral pump. It converts the kinetic energy of the water flow into mechanical rotational energy, ensuring the movement of water inside the spiral pipe [15]. The efficiency of the wheel depends on the water velocity, flow velocity, wheel dimensions and design parameters [10,14].



1 - Water wheel, 2 - Blades, 3 - Central shaft, 4 - Spiral coil pipe, 5 - Inlet section, 6 - Outlet section, 7 - Supporting frame, 8 - Coupling element

Figure 2. The main structural elements of a scroll pump.

Figure 2 shows the main elements of a spiral pump system, including the water wheel, central shaft, spiral pipe, water inlet and outlet points, and air chamber [16].

Hydraulic calculation methodology: determination of open channel flow velocity.

The velocity of water flow is determined using the velocity-distance method, which measures the time it takes to travel a certain distance:

$$V = \frac{L}{t} \quad (1)$$

where: V is the water flow velocity, m/s; L is the measured distance, m; t is the time, s. According to the measurement result, the average water flow velocity is V = 0.896 m/s.

The cross-sectional area of a water wheel directly in contact with the water flow is defined as follows [7], [8]:

$$A = d \cdot w \quad (2)$$

where: A - wetted cross-sectional area, m²; d - water depth in the wheel, m; w - wheel width, m. The experimental setup is as follows: d = 0.3 m; w = 0.6 m.

Determining the kinetic energy of a water flow

The water wheel input power depends on the density, wetted cross-sectional area, and flow velocity and is determined by the following expression [13,15]:

$$P_{¿} = \frac{1}{2} \cdot \rho \cdot A \cdot V^3 \quad (3)$$

where: Pin - water wheel input power, W; ρ - water density, kg/m³; A - wetted cross-sectional area, m²; V - flow velocity, m/s.

The angular velocity of the water wheel was determined based on the following empirical dependence with the flow velocity:

$$\omega = \frac{2V}{D} \quad (4)$$

here:ω-angular velocity, rad/s;V-flow velocity, m/s;D-water wheel diameter, m.

The rotation frequency is:

$$n = \frac{60\,\omega}{2\pi} \quad (5)$$

where n is the rotation frequency (rpm).

Only a fraction of the total power produced by the water wheel is converted into useful mechanical power. The efficiency is assumed to be η = 0.4 [7], [8]. Then:

$$P_{out} = \eta \cdot P_{¿} \quad (6)$$

The useful pump power is related to water flow and lift height as follows:

$$P_{out} = \rho \cdot g \cdot Q \cdot H \quad (7)$$

$$Q = \frac{P_{out}}{\rho \cdot g \cdot H} \quad (8)$$

Where: ρ - water density, kg/m³; g - acceleration of gravity, m/s²; Q - water flow, m³/s; H - pressure or head, m.P_{out} - useful power, W;

Pressure-flow for spiral pumpdescription The diagram shows that the water flow decreases with increasing head of the spiral pump. According to the results, the flow decreases sharply in the range of 0.5-3 m, and the decrease is relatively slow in the range of 3-10 m.

In order to assess the performance of a spiral pump, the dependence between pressure and water flow was analyzed.

Calculations have shown that the flow is directly proportional to the flow velocity. This dependence is defined by the following expression:

$$Q = A \cdot V \quad (9)$$

where: A is the wetted cross-sectional area of the stream (m²), V is the flow velocity (m/s), Q is the water flow (m³/s).

As the water flow velocity increases, the amount of water entering the volute pump increases, which directly affects the overall efficiency of the system.

The power coming from the water flow to the water wheel is:

$$P_¿ = \frac{1}{2}\rho \cdot A \cdot V^3 \quad (10)$$

The useful power of the water wheel and the spiral pump is:

$$P_u = \eta_t \cdot P_¿ \quad (11)$$

A mathematical model based on energy balance was used to evaluate the efficiency of the spiral pump based on the water wheel parameters. The kinetic energy of the water flow is converted into mechanical energy by the water wheel and is used to lift the water to a certain height using the spiral pump. On this basis, the following expression was obtained for the system:

$$Q = \frac{\eta_t \cdot A \cdot V^3}{2 \cdot g \cdot H} \quad (12)$$

Now, if the flow-contacting surface of a water wheel is assumed to depend on the diameter: A

$$A = b \cdot \lambda \cdot D \quad (13)$$

where: b- wheel width, m D- wheel diameter, m λ - wheel immersion ratio. If this surface is related to the wheel diameter, then the dependence of the flow on the diameter is:

$$Q = \frac{\eta_t \cdot b \cdot \lambda \cdot D \cdot V^3}{2 \cdot g \cdot H} \quad (14)$$

In many cases it is considered: $b = \mu \cdot D$

$$Q = \frac{\eta_t \cdot \mu \cdot \lambda \cdot D^{2 \cdot} V^3}{2 \cdot g \cdot H}; Q = k \cdot D^2; k = \frac{\eta_t . \mu \cdot \lambda \cdot V^3}{2 \cdot g \cdot H} \quad (15)$$

Regression and empirical analysis methods were used to assess the effect of water wheel diameter on water flow. Based on the results, the following empirical dependence was obtained:

$$Q = a \cdot D^2 + b \cdot D + c \quad (16)$$

The pressure-flow characteristic of the scroll pump was analyzed based on the exponential decay model:

$$Q = Q_0 \cdot e^{-k \cdot H} \quad (17)$$

$$y = A \cdot e^{-kt} = 6 \cdot e^{-0.6t} \quad (18)$$

where Q_0- initial water flow, k- empirical reduction coefficient, $.H$ - lifting height

The coefficient of determination, R^2root mean square error (RMSE), and relative error (δ) indicators were used to assess the level of model fit.

The coefficient of determination was calculated using the following formula:

$$R^2=1-\frac{\sum\left(y_i-\hat{y}_i\right)^2}{\sum\left(y_i-\acute{y}\right)^2} \quad (19)$$

where: y_i- experimental values; $\hat{y}_i$- values obtained by the model; $\acute{y}$- average value

The mean square error was determined by the following expression:

$$RMSE=\sqrt{\frac{1}{n}\sum_{i=1}^{n}\left(y_i-\hat{y}_i\right)^2} \quad (20)$$

The relative error was estimated as follows:

$$\delta=\frac{\left|y_i-\hat{y}_i\right|}{y_i}\cdot 100\,\% \quad (21)$$

Based on the results obtained, the optimal operating range of the spiral pump system and the effect of water wheel parameters on water flow and head were evaluated.

3.Results and Discussion

The study analyzed the hydraulic and energy parameters of a spiral pump system operating in low-pressure water flows. The calculations revealed that the water flow velocity, water wheel diameter, and head significantly affect the efficiency of the spiral pump.

According to the calculation results, it was observed that the water flow decreased with the increase in the pressure of the spiral pump. The results obtained were expressed in the following sequence. (See Figures 3-6)

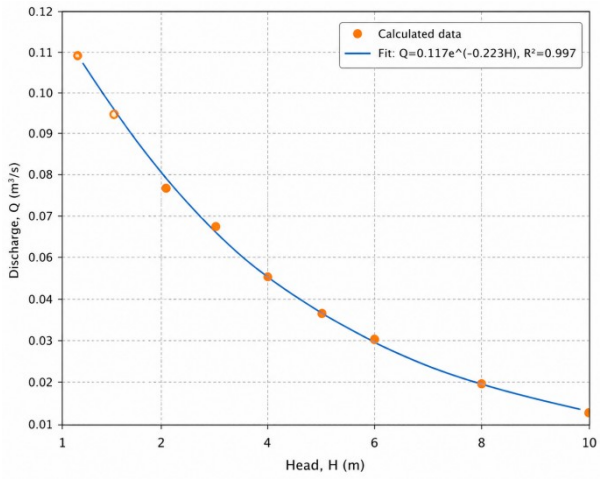


Figure 3. Pressure-flow characteristics of a scroll pump

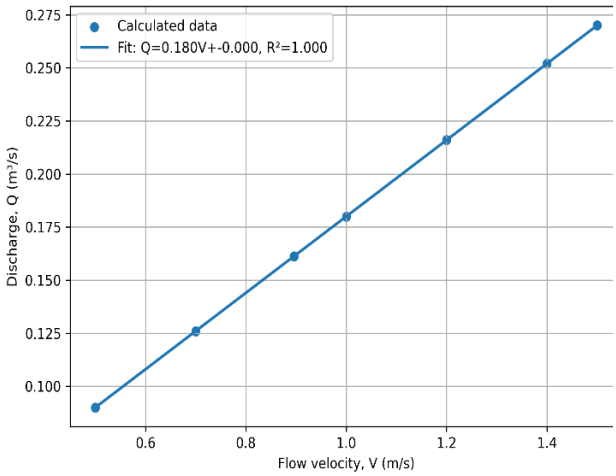
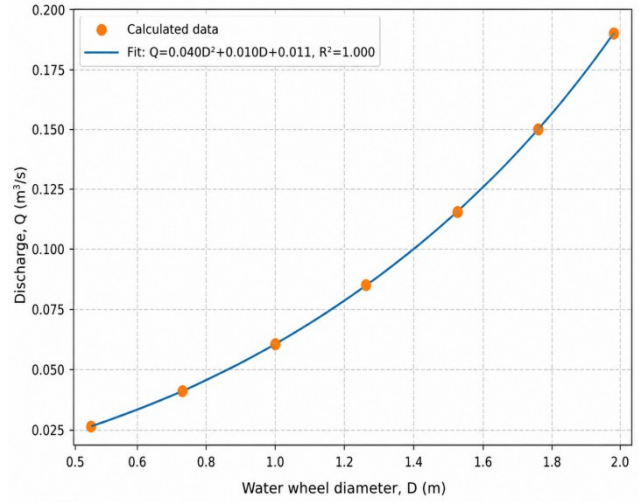


Figure 4.Dependence between water flow velocity and water flow



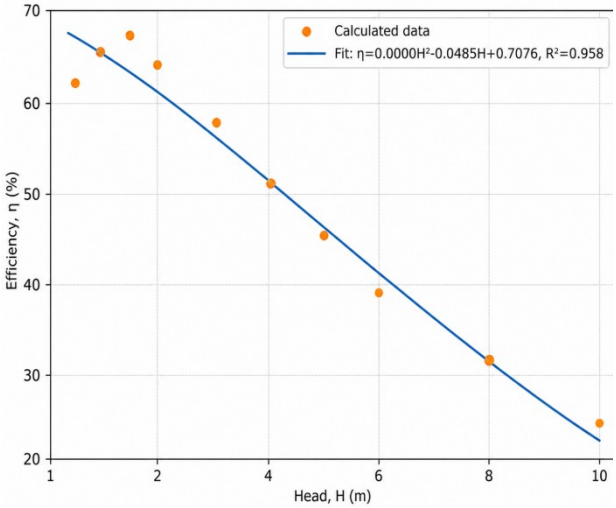


Figure 5. Dependence between water wheel diameter and water flow

Figure 6.Efficiency pressure valuesDependence between

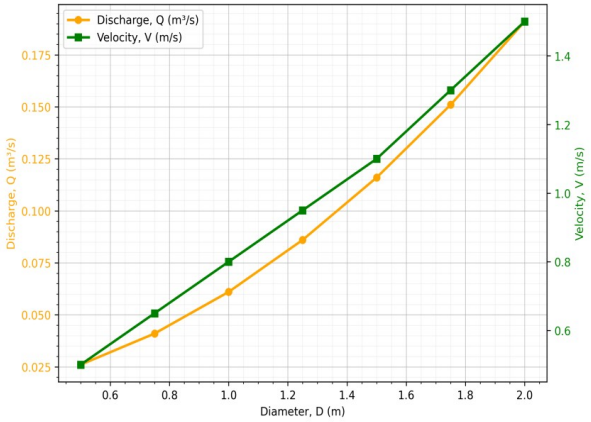


Figure 7. Dependence between water flow, water wheel diameter and flow velocity

Pressure-flow characteristic

The $H-Q$ pressure-flow characteristic of the spiral pump was analyzed based on the dependence. According to the results, water flow decreases with increasing head (Fig-1). An exponential regression model expressed this dependence:

$$Q=0.1169\,e^{-0.2231\,H}$$

The coefficient of determination for this model is:

$$R^2=0.997$$

is equal to , which indicates a high agreement of the model with the calculated values. Therefore, as the head in a spiral pump increases, the hydraulic resistance increases, and as a result, the water flow decreases.

Velocity-flow dependence

The effect of water flow velocity on water flow $V-Q$ was evaluated using a graph. The calculation results showed that water flow is directly proportional to the flow velocity:

$$Q=0.1800\cdot V$$

Here, the 0.1800value represents the wetted cross-sectional area of the flow. The regression result is

$$R^2=1$$

Water wheel diameter-flow dependence

The effect of water wheel diameter on water flow was analyzed based on polynomial regression. The resulting fitting equation was as follows:

$$Q=0.0400\,D^2+0.0100\,D+0.0110$$

For this:

$$R^2=1$$

The results show that water flow increases according to a quadratic law with increasing water wheel diameter. This is explained by the fact that the surface area interacting with water and the rotational torque increase with increasing wheel diameter.

Efficiency analysis

The system efficiency was evaluated depending on the head. The results showed that the highest efficiency was observed at low and medium pressure values. As the head increases, the hydraulic losses in the spiral pipe increase and the system efficiency decreases.

The regression model obtained for efficiency is:

$$\eta = 0.0000 \cdot H^2 - 0.0485 \cdot H + 0.7076$$

For this:

$$R^2 = 0.958$$

was established.

To evaluate the comprehensive performance of the spiral pump system, the dependence between water flow, water wheel diameter, and flow velocity was analyzed graphically. The model was expressed by the following empirical equation

$$Q = 0.045\, D^2 \cdot V$$

This dependence shows that water flow is linearly related to flow velocity and quadratically related to water wheel diameter. Therefore, in order to increase the efficiency of the system, it is important to choose not only the flow velocity but also the optimal wheel diameter.

The results show that the efficiency of the spiral pump-water wheel system depends on three main factors: water flow velocity, wheel diameter and head. An increase in water flow velocity increases water flow, and an increase in diameter increases the torque. However, an increase in head reduces water flow. Therefore, when designing the system, it is necessary to optimize the parameters, and together.By optimally selecting the water wheel diameter and flow velocity, the system efficiency can be significantly increased.The results of this research serve as a scientific basis for optimizing and implementing spiral pump systems.

4.Conclusion

The study demonstrated that the hydraulic performance of the spiral pump strongly depends on lifting head, flow velocity, and water wheel diameter. The obtained results showed that increasing the lifting head from 0.5 m to 10 m reduced the discharge from 0.108 m³/s to 0.013 m³/s due to hydraulic losses inside the spiral pipe. Meanwhile, increasing the water wheel diameter from 0.5 m to 2.0 m increased the discharge approximately seven times. The developed empirical and regression models showed high agreement with the calculated data (R^2 = 0.997–1.000). The proposed spiral pump system can be effectively applied for low-head irrigation and water lifting systems operating without electrical energy.

REFERENCES

1. Müller, G. (2009). Simplified design of water wheels for developing countries. Journal of Hydraulic Research, 47(5), 630-636.
2. Senior, J., Müller, G., & De Cesare, G. (2010). Hydraulic performance of traditional water wheels. Journal of Hydraulic Research, 48(2), 225-232.
3. Paish, O. (2002). Small hydro power: Technology and current status. Renewable and Sustainable Energy Reviews, 6(6), 537-556.
4. Urishev, O., Ersin, A., Metin, G., & Kuvondikov, Q. (2026). ESTIMATING ELECTRICITY CONSUMPTION OF PUMPING PLANTS IN IRRIGATION SYSTEMS. Innovation Science and Technology, 2(1).https://doi.org/10.5281/zenodo.18472643
5. SALOMOV, OK, & URISHEV, O. (2025). IMPORTANCE OF HYDROELECTRIC STATIONS AT GLOBAL AND NATIONAL LEVELS AND DEVELOPMENT DIRECTIONS. “UZBEKHYDROENERGETICS” scientific and technical journal, 7(2), 17-28.
6. Urishev, O., Salomov, U., Ergashev, S., Kuchkarov, A., Madaliev, M., Abdukarimov, B., & Juraev, N. (2025). Efficiency assessment of micro hydropower for agriculture using modern

modeling. In BIO Web of Conferences (Vol. 173, p. 03031). EDP Sciences. DOI:10.1051/bioconf/202517303031

7. Salomov, U., Kuchkarov, A., & Urishev, O. (2025). Analysis of the dependence Between Water Consumption and Heading in a Micro Hydropower System. Journal of Construction and Engineering Technology, 21-29. https://doi.org/10.24412/2181-4473-2025.3.204
8. Urishev, O., Salomov, U., & Shasha, C. (2024). Methods of Analysis and Assessment of the Economic Efficiency of Micro Hydropower. Journal of Construction and Engineering Technology, 2(2), 1-7. https://doi.org/10.5281/zenodo.12570514
9. Og'Lee, UOM, & Og'Lee, RMF (2020). The fundamental elements of micro-hydropower stations. Science and Education, 1(2), 236-240.
10. Fraenkel, P. (1986). Water lifting devices. Intermediate Technology Publications, London.
11. Kiebel, P. (2008). Powering the countryside: The economics of micro-hydropower. Renewable Energy, 33(11), 2439-2444.
12. Müller, G., & Wolter, C. (2004). The breastshot waterwheel: Design and performance. Proceedings of the ICE - Engineering Sustainability, 157(4), 203-211.
13. Williams, AA (1997). Pumps as turbines: A user's guide. Intermediate Technology Publications.
14. Patil, SH, Sutar, SG, Mirage, SR, Patil, AM, & Nangre Patil, BH (nd). A review paper on spiral tube water wheel pump. Adarsh Institute of Technology & Research Centre, India.
15. Patil, SH, Sutar, SG, Mirage, SR, Patil, AM, & Nangre Patil, BH (nd). A review paper on spiral tube water wheel pump. Department of Mechanical Engineering, Adarsh Institute of Technology & Research Centre, Vita, India.
16. Tschiersch, Kim & Bohórquez, O.. (2019). Coil pump design as an object of meaningful learning. Journal of Physics: Conference Series. 1161. 012027. 10.1088/1742-6596/1161/1/012027.
17. Juraboev, I., Jurakulov, S., Urishev, O., Rakhmatov, O., Eshkobilov, O., Sadirova, K., & Aliyarova, L. (2025). Improving Thermal Performance of Solar PTC Using Internal Finned Structure. In E3S Web of Conferences (Vol. 661, p. 04018). EDP Sciences.https://doi.org/10.1051/e3sconf/202566104018
18. Akramova, S., Urishev, O., Mamurov, B., Nurmanov, S., Apakhodjaeva, T., Irmukhamedova, L., & Gaimnazarov, K. (2025). CFD Modeling of Latent Heat Storage with Cylindrical PCM Capsules. In E3S Web of Conferences (Vol. 661, p. 04010). EDP Sciences.https://doi.org/10.1051/e3sconf/202566104010

"VECTROGRAPH" PROGRAM WORK PRINCIPLE, DYNAMIC MANAGEMENT OPPORTUNITIES AND EXPERIMENT RESULTS

Sh.B. Avlyakulova
Bukhara state technical university
https://doi.org/10.5281/zenodo.20553612

Abstract. *This for the program "Vectrograph" in the article working model released and algorithms theoretical basics, practical software solutions and test processes analytical results The program is presented functional scheme, raster the images smoothing, monochrome, borders determination and adaptive simplification processes step by step illuminated. Also, Canny algorithm and Adaptive Douglas– Peucker simplification mechanisms dynamic application , sliders through management opportunities and vector formats (DXF, SVG, EPS) generation to be done statement "Vectrograph" program online converter apps with comparison results , ChatGPT artificial intellect by taken expert analyses and practical recommendations Research in the end from the program working release in the processes of use technical and economic efficiency indicators based on given .*

Keywords: *raster image, vector format, Canny algorithm, adaptive simplification, Douglas– Peucker, contour detection, vectorization, DXF, SVG, EPS, algorithmic model, dynamic management.*

Introduction

Digital the images again work and them vector to look transfer industry, design, pattern processing, CNC technologies and geometry based on automated design processes inseparable to the part converted. Raster of images accuracy, contour complexity and noise amount them vectorization to the quality noticeable impact shows. This because of modern vectorization in systems automatic accuracy management, adaptive filters, simplification algorithms and dynamic control mechanisms application important importance profession will reach.

Taken scientific research as a result these processes to optimize the program "Vectrograph" was created. The program is raster files vector to the shape effective transfer, simplified outline create, also, user by controllable sliders through parameters adaptation opportunity gives. This program work in the article principle, functional scheme, dynamic management mechanisms and experiment results in detail is illuminated.

Taken research as a result created model and algorithms based on working "Vectrograph" program released work principle, functional scheme, and program sliders dynamic management technological process in detail illuminated, experience test results, comparison analyses the program "Vectrograph" is available. online -converter apps with comparison experiment results, ChatGPT artificial intellect in the application taken analytical conclusions, the program "Vectrograph" application according to practical recommendations illuminated. At the end of the chapter take visited scientific research the results in the form of the program "Vectrograph" in practice current of reaching technical and economic efficiency indicators, and working release in enterprises of being used efficiency results and conclusions shaped.

Methodology

This study used an applied software-development and experimental testing methodology to design and evaluate the "Vectrograph-1.0" program for converting raster images into vector formats. The research process consisted of four main stages. First, raster images in PNG, JPG, JPEG, BMP, and GIF formats were uploaded into the program. Second, the images were pre-processed through Gaussian smoothing, monochromation, and binarization in order to reduce noise and prepare the image for contour extraction. Third, the Canny algorithm was applied to detect image boundaries by calculating gradient intensity and direction. After edge detection, the Adaptive Douglas–Peucker algorithm was used to simplify contours dynamically according to curvature level, preserving more points in complex areas and reducing unnecessary points in smoother regions. Finally, the processed geometric objects were exported into vector formats, including DXF, SVG, and EPS.

The program was also tested through dynamic slider-based parameter control, including scale, contour sharpness, adaptive epsilon, quality filter, and iteration settings. These controls allowed the user to adjust vectorization quality interactively. The effectiveness of the program was evaluated by comparing its output with existing online vectorization tools and by analyzing its technical and practical efficiency for use in design, CNC, and production-related processes.

Results and Discussion

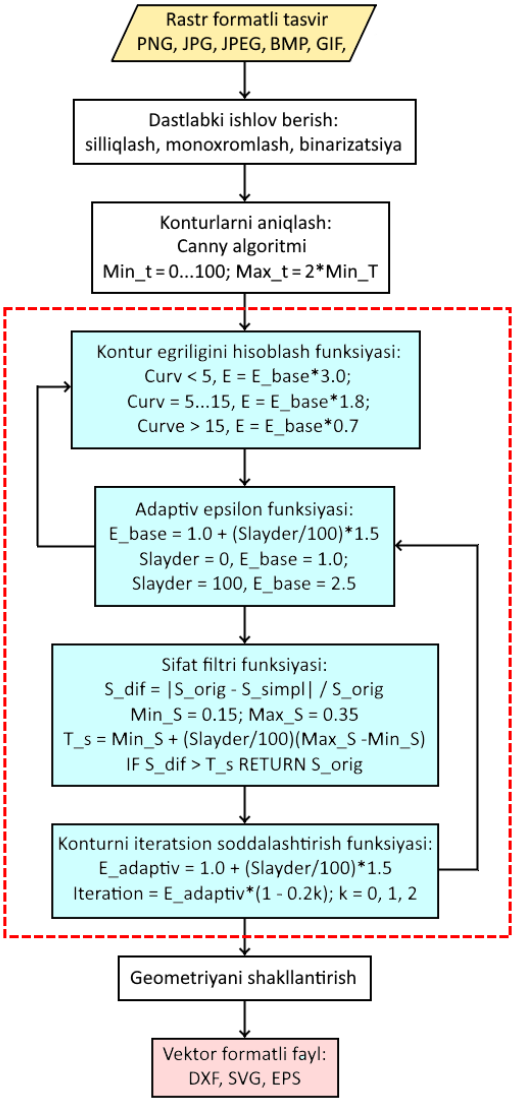


Figure 1. The "Vectrograph" program general functional scheme

Taken research as a result working model released and algorithms developed the practical program "Vectrograph-1.0" based on [1] The program is directly raster in format files vector to format dynamic passing to give intended is, the program works functional the scheme is presented in Figure 1.

Functional in the scheme incoming information as PNG, JPG, JPEG, BMP or GIF extension has been raster from files one acceptance will be done.

Raster in step 1 file smoothing (Gaussian filter), monochromation and binarization from the processes will be held.

Raster in step 2 file Canny algorithm based on borders clearly is taken. In this case, the limit contrast – gradient function through determined, gradient length and gradient direction calculating is released.

Stage 3 is important is, this is on the ground Adaptive Douglas- Peucker algorithm to work will be lowered and the value of epsilon outline to the curvature looking at dynamic selectively as a result, the curvature high was outline in the regions more points preserved, outline smooth and small to the curvature has been in outlines and points number to be reduced is achieved. Contours maximum simplification for the purpose iteration function final the outline initial outline as acceptance so, adaptive Douglas- Peucker algorithm again to work will be lowered and contours simplification process again continue is delivered.

Geometric in stage 4 objects set formatted, with DXF, SVG and EPS extensions vector formats harvest will be done.

Program interface main window following to look has (Figure 2).

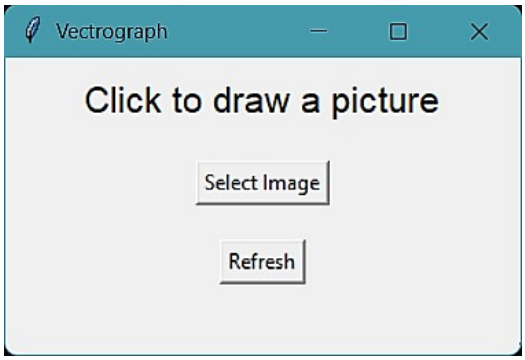


Figure 2. The main window of the "Vectrograph" program appearance

Window of the "Vectrograph" program mainly two interactive from buttons consists of become they are "Select image" - raster the image upload and "Refresh" – the image update are functions.

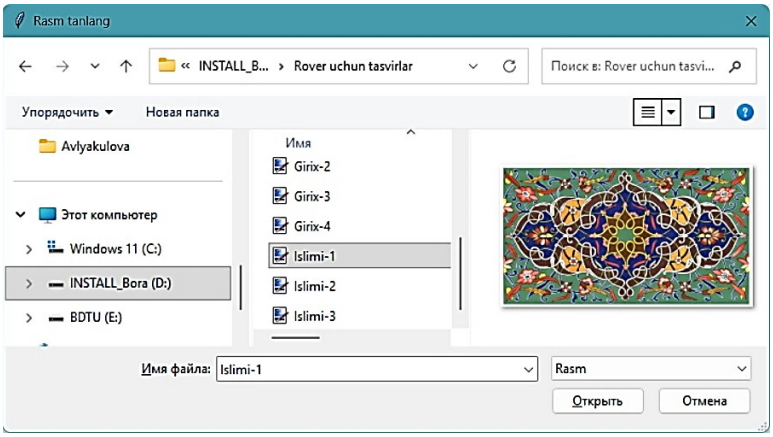


Figure 3. The "Vectrograph" program files choice directory window

"Select image" – raster the image upload function when activated raster format with PNG, JPG, JPEG, BMP or GIF extension has been file choice directory window opens (Figure 3)

Raster file when selected of the program edit window opens and then automatic in a way vector in the form of image manifestation will be. Vector file edit window – such as "Scale", "Contour sharpness (Canny)", "Adaptive epsilon", Quality filter", "Iteration" from sliders and file storage buttons – "Save format", "Save File", "Save As" functions have (Figure 4).

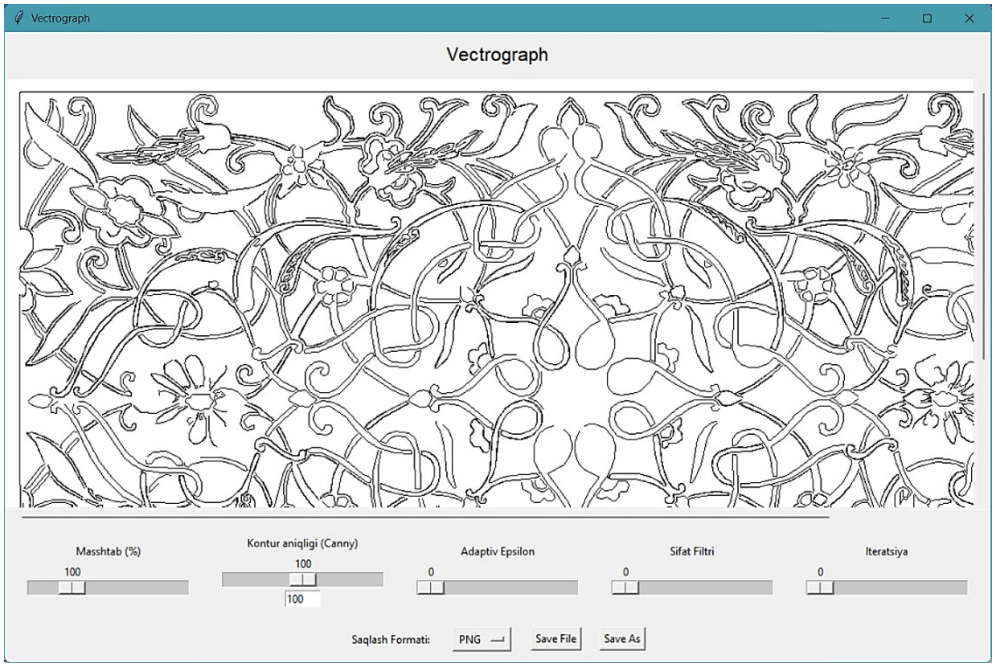
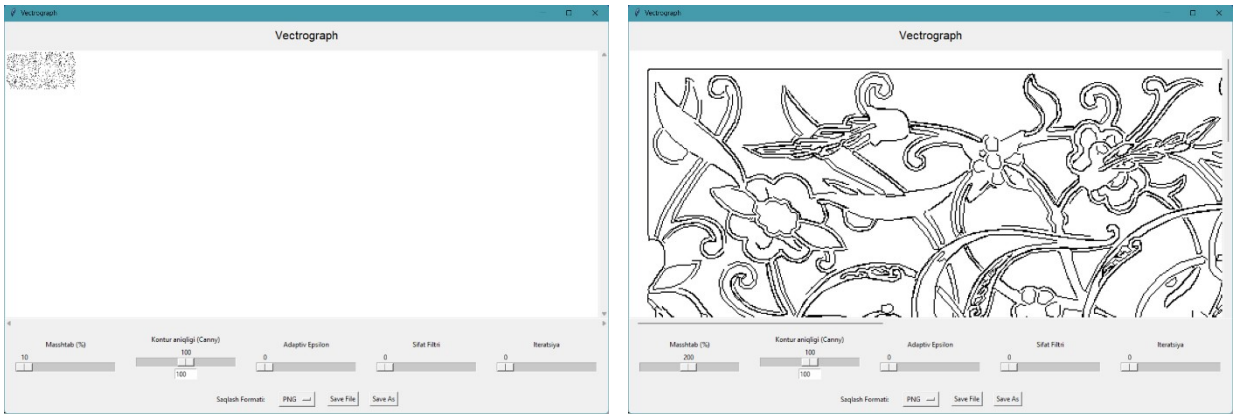


Figure 4. The "Vectrograph" program vector file edit window

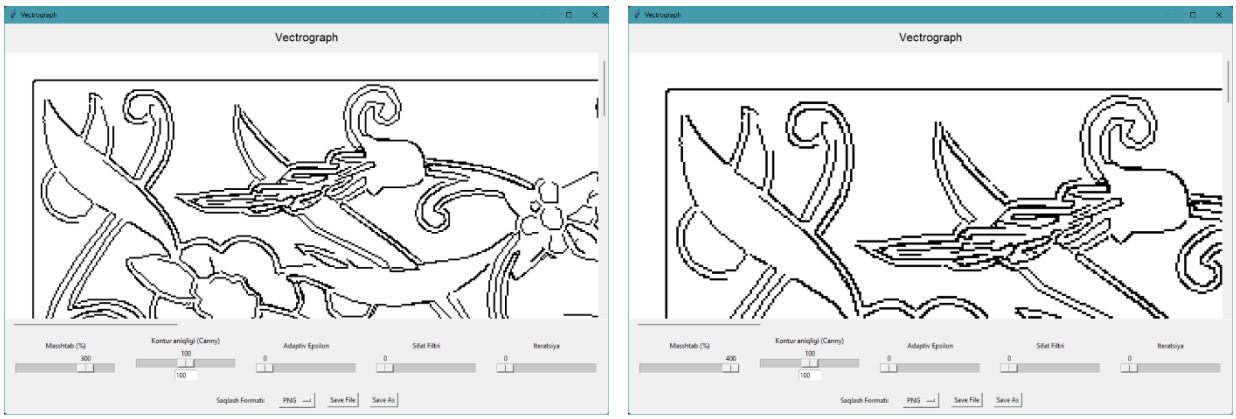
" Save " Format: " interactive " on the button file from PNG, DXF, SVG and EPS formats in one Save as. PNG format raster. format is, which is a vector file raster image as see opportunity gives.

In the program " Vectrograph" raster formatted file after loading then program him/her automatic in style edit in the window vector to format transfers and result on the screen manifestation will be. Vector file edit in the window various parameters management slider functions there is They are Burmese one description brought oh my god.

Slider 1 – "Scale" slider the image on the screen shrinking or zooming in demonstration to reach " This is intended. "Slider image in the outline small elements approaching see opportunity gives. Slider initials the condition is 100%, the image own real in size manifestation (See Figure 4). The "Scale" slider is in the range of 10 ÷ 400%. scaling opportunity gives (Figure 5).



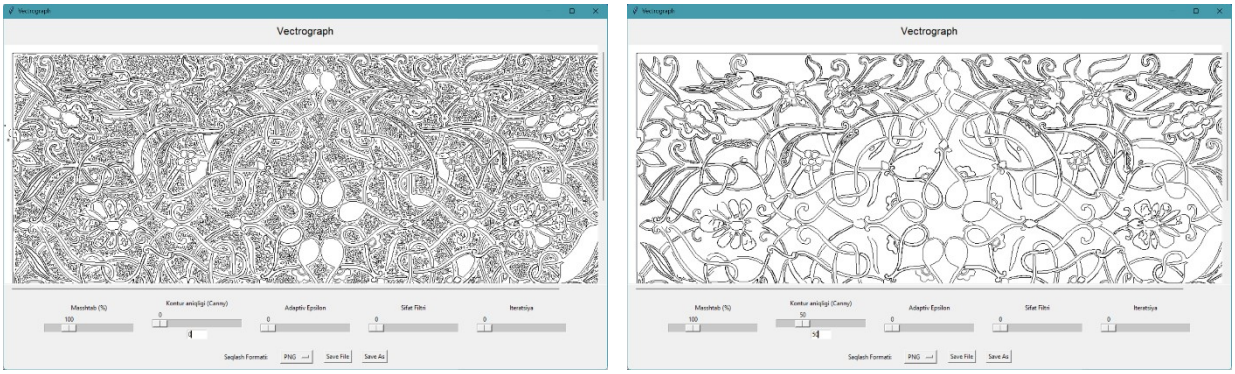
a) M = 10 *b) M = 200*



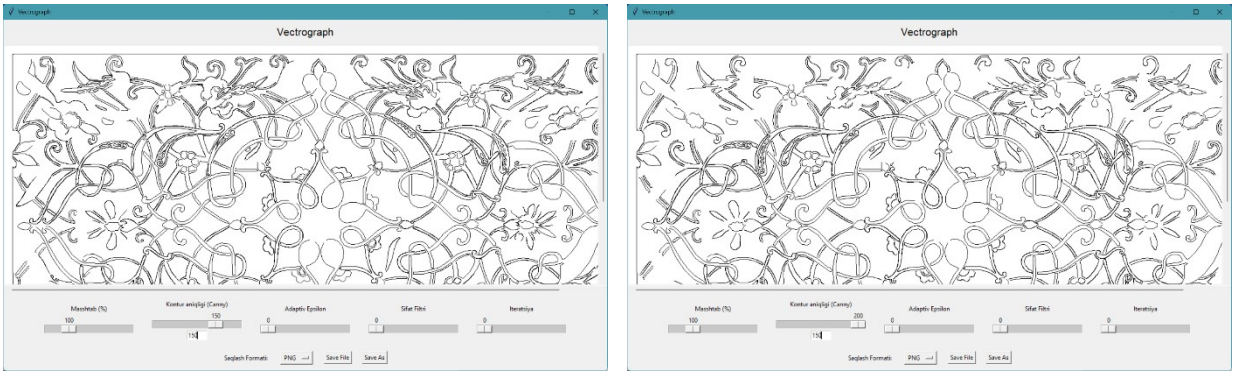
c) M = 300 *d) M = 400*

Figure 5. The "Zoom" slider dynamic features

The 2nd slider is "Canny", which is the amount of detail in the image. outline lines collection multiplication and to reduce service This will do. slider in the Canny algorithm T – threshold value lower and high borders dynamic designation based on gradient sensitivity Threshold value variable is, $T_{max} = 2\ T_{min}$. The slider initial status at 100 value is, in this $T_{min} = 50$ and $T_{max} = 100$. Slider values 0 ÷ 200 within dynamic controlled (Figure 3.6).



a) C = 0 ($T_{min} = T_{max} = 0$) *b) C = 50 ($T_{min} = 25$; $T_{max} = 50$)*



c) C = 150 ($T_{min} = 75$; $T_{max} = 150$) *d) C = 200 ($T_{min} = 100$; $T_{max} = 200$)*

Conclusion

Taken research to the results according to " Vectrograph-1.0" program raster the images to vector during the transfer high accuracy, speed and adaptive management opportunities to provide with separated Canny algorithm based on borders of determination dynamic management and Adaptive Douglas– Peucker algorithm using contours iterative simplification vectorization quality noticeable at the level the program supports DXF, SVG and EPS formats. industry to the standards

suitable formats generation to do as far as possible has on CNC machines at work also high result gives.

Comparison experiment results of the “Vectrograph” program there is online vectorization from applications advantage showed. In particular, the curvature to the level suitable the value of epsilon automatic choice mechanism outline accuracy increased and excess points The program was developed release in enterprises from the test held to be, to be technical and economic efficiency practical in terms of approved.

As a result, the “Vectrograph” program is scientific research based on working implemented, put into practice current to reach ready, high functional to opportunities has was as a vectorization program recommendation is being done.

REFERENCES

1. Canny, J. (1986). A computational approach to edge detection. IEEE Transactions on Pattern Analysis and Machine Intelligence, 8(6), 679-698.
2. Avlyakulova Sh.B. CAM tizimlarida geometrik modellashtirish asoslarining takomillashtirilgan talqini. Innovatech: Conference on Scientific Innovations and Research https://euro-conferences.org/index.php/innovatech/article/view/961. 2026-yil 22-may. 68-70.
3. Douglas, D. H., & Peucker, T. K. (1973). Algorithms for the reduction of the number of points required to represent a digitized line or its caricature. The Canadian Cartographer, 10(2), 112-122.
4. O'Donnell, J., et al. (2019). Comparative analysis of line simplification algorithms for web mapping. Transactions in GIS, 23(5), 1089-1107.
5. Avlyakulova, Sh. B. (2022). Filling of ornamental carving fields on the basis of primitive symmetry types in computer graphics. Universe: Technical Sciences, 4(97).
6. Khaitov, B. U., & Avlyakulova, Sh. B. (2025). Comparative analysis of raster and vector graphics. Scientific Journal of Construction and Education, Special Issue 1.
7. Yadgarov U., Avlyakulova S., Mukhamedova R. Study of the dependence of the surface shape woodcarving from its flat contour of support //AIP Conference Proceedings. – AIP Publishing LLC, 2024. – T. 2969. – №. 1. – C. 060027.
8. Khaitov, B. U., & Avlyakulova, Sh. B. (2025). Vectrograph-1.0: Certificate of the computer program, DGU No. 49526, 11 April 2025.

COMPARATIVE ANALYSIS OF BLUR AUGMENTATION STRATEGIES FOR HARMFUL CONTENT IMAGE CLASSIFICATION USING EFFICIENTNET-B0: A PRELIMINARY STUDY

O. Mallayev[1], F. Sulaymonova[2], N. Tolibova[3]
Alfraganus University[1]
Tashkent University of Information Technologies[2]
Research Institute for the Development of Digital Technologies and Artificial Intelligence under the Ministry of Digital Technologies of the Republic of Uzbekistan[3]
https://doi.org/10.5281/zenodo.20553996

Abstract. *Automated content moderation at scale requires accurate and computationally efficient image classifiers, yet practical deployments often face severe data scarcity. This study presents a systematic comparison of six preprocessing strategies – Gaussian blur, Motion blur, Bilateral blur, Anisotropic blur, no augmentation (baseline), and background removal – for binary ethical/non-ethical image classification using EfficientNet-B0 trained from scratch on a self-collected small dataset (n = 472). All models were trained under identical protocols using class-weighted binary cross-entropy. Classification performance was evaluated on held-out test sets (n = 71 for blur conditions), with 95% confidence intervals computed via the Wilson score method and pairwise significance assessed by McNemar's test. Bilateral blur and Motion blur achieved the highest observed test accuracy of 100.00% (95% CI [94.9%, 100.0%]; AUC = 1.0000). Anisotropic blur achieved 97.18% (95% CI [90.3%, 99.2%]) and Gaussian blur 90.14% (95% CI [81.0%, 95.1%]). The difference between Bilateral and Gaussian blur was statistically significant ($\chi^2 = 5.14$, $p < 0.05$). Models trained without augmentation (37.23%) and with background removal (30.00%) failed to generalise. The edge-preserving property of the bilateral filter is proposed as a mechanistic explanation, pending Grad-CAM validation. These findings provide preliminary empirical guidance for augmentation selection in resource-constrained content moderation systems.*

Keywords: *small dataset; EfficientNet-B0; data augmentation; bilateral blur; image classification; content moderation; deep learning.*

1. Introduction. The volume of user-generated content on social media and digital platforms has grown at an unprecedented rate [1]. Within this stream, ethically inappropriate, harmful, and rights-violating material constitutes a significant fraction that human moderators cannot process at scale. Automated classification systems based on deep convolutional neural networks have therefore become the primary practical approach to content filtering [2]. In jurisdictions such as Uzbekistan, whose Law on the Principles and Guarantees of Information Freedom [3] mandates user protection from harmful digital content, the societal stakes of accurate automated moderation are particularly high.

EfficientNet architectures achieve state-of-the-art accuracy through compound scaling of network depth, width, and resolution [4]. Their practical utility, however, is strongly conditioned on preprocessing and data augmentation strategies [5] – a dependency that intensifies when

training from scratch on small, domain-specific datasets. Blur-based augmentation simulates real-world degradations including defocus, motion artefacts, and atmospheric distortion [6]. Bilateral filtering [7] is theoretically distinguished by its edge-preserving property, which may retain discriminative structural features critical for classification.

This study addresses two research questions: (1) How do different blur augmentation strategies affect EfficientNet-B0 classification performance on a small ethical/non-ethical image dataset? (2) How does background removal affect model performance? We compare six preprocessing conditions under identical training protocols, reporting accuracy with 95% Wilson score confidence intervals and applying McNemar's test for statistically rigorous pairwise comparison. Figure 1 illustrates the overall experimental pipeline.

The paper is structured as follows. Section 2 reviews relevant literature. Section 3 describes materials and methods. Section 4 presents a mathematical analysis of bilateral filtering. Section 5 reports experimental results. Section 6 discusses findings and limitations. Section 7 concludes.

Figure 1. Experimental pipeline: from dataset to evaluation.



Figure 1. Experimental pipeline: from dataset construction to evaluation. Orange box indicates the six independent preprocessing conditions.

2. Related Work

2.1. EfficientNet architecture. Tan and Le [4] proposed EfficientNet through compound scaling that simultaneously adjusts depth, width, and resolution. EfficientNet-B0 employs Mobile Inverted Bottleneck Convolution (MBConv) blocks with Squeeze-and-Excitation mechanisms. In this study it was trained from scratch. Kornblith et al. [8] showed pretrained weights substantially benefit small-dataset transfer; we adopt the from-scratch setting as a deliberate constraint to isolate preprocessing contributions, acknowledged as a limitation.

2.2. Blur augmentation. Shorten and Khoshgoftaar [5] comprehensively surveyed image augmentation, demonstrating consistent accuracy improvements. Gaussian blur applies isotropic Gaussian convolution, uniformly attenuating high-frequency components (Simard et al. [13]). Motion blur simulates directional camera movement [6]. Bilateral filtering ([7]; [9]) combines spatial proximity and photometric similarity for edge-preserving smoothing. Anisotropic diffusion [10] achieves boundary-preserving smoothing via gradient-guided diffusion.

2.3. Small-dataset CNN training. Mikołajczyk and Grochowski [11] reported 2-5% accuracy gains from augmentation on small medical datasets, with results strongly dependent on dataset composition. This observation supports cautious interpretation of results on n = 472.

2.4. Background context. Xiao et al. [12] and Torralba and Oliva [14] established that background context contributes significantly to scene and object classification. These findings motivate our hypothesis that background removal may critically impair tasks where content characterisation depends on scene context.

3. Materials and Methods

3.1. Dataset and partitioning. The dataset was self-collected and labelled into two classes: ethical (n = 175, 37.1%) and non-ethical (n = 297, 62.9%). Images depicting the human body in a non-ethical manner, or containing violent, abusive, or rights-violating content, were labelled non-ethical; all others were labelled ethical. Annotation was performed by a single author; inter-annotator reliability was not assessed (limitation). Figure 2 shows the class distribution.

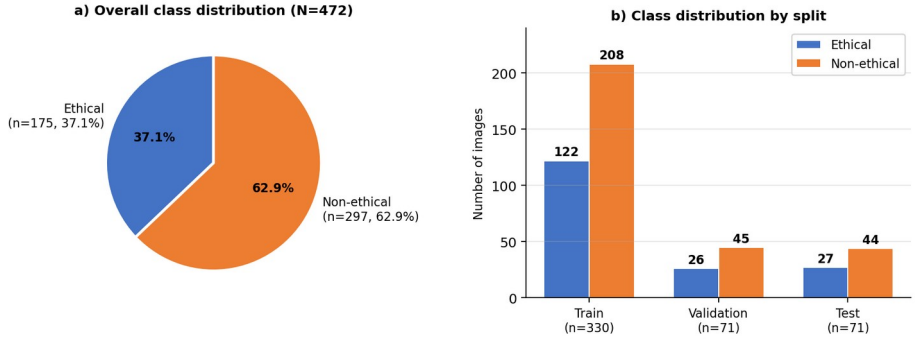


Figure 2. Dataset class distribution: a) overall, b) by split.

Figure 2. Dataset class distribution: a) overall (N = 472), b) by split. Class imbalance (37%/63%) was addressed via class weights during training.

Stratified random partitioning produced: train n = 330 (ethical 122, non-ethical 208); validation n = 71 (ethical 26, non-ethical 45); test n = 71 for blur conditions (ethical 27, non-ethical 44). Baseline and background-removal conditions used different test sets (n = 94 and n = 40, respectively), precluding direct cross-condition statistical comparison.

3.2. Preprocessing conditions. Six conditions were evaluated independently: (1) Gaussian blur – isotropic Gaussian convolution (472/472 images); (2) Motion blur – directional blurring (~2.57 s/image); (3) Bilateral blur – edge-preserving smoothing (~48,616 images/s); (4) Anisotropic blur – gradient-guided smoothing (~95,000 images/s); (5) Baseline – original images without augmentation; (6) Background removal – background pixels replaced with white via Segment Anything (Kirillov et al. [15]).

3.3. Model architecture and training protocol. EfficientNet-B0 was trained from scratch for all conditions. Optimiser: Adam ($\alpha = 0.001$, $\beta_1 = 0.9$, $\beta_2 = 0.999$; Kingma & Ba [16]). Loss: binary cross-entropy with class weights ($w_{et}^{IOaL} = 1.3525$, $w_{non\text{-}et}^{IOaL} = 0.7933$). Maximum 20 epochs; early stopping (patience = 5) based on validation loss, restoring best weights.

3.4. Statistical analysis. Accuracy 95% confidence intervals were computed using the Wilson score method, recommended for small n and extreme proportions (Brown et al. [17]). Pairwise comparison between Bilateral blur and Gaussian blur was performed via McNemar's test with continuity correction [18], appropriate for paired binary outcomes on the same test set.

4. Mathematical Analysis of Bilateral Filtering

4.1. Filter formulation. For input image I(p) at pixel coordinate p, the bilateral filter output is defined as [7]:

$$BF[I](p) = \frac{1}{W_p} \sum_{q \in \Omega} f_s(\|p - q\|) * f_r(|I(p) - I(q)|) * I(q) \quad (1)$$

where the normalisation constant is:

$$W_p = \sum_{q \in \Omega} f_s(\|p - q\|) * f_r(|I(p) - I(q)|) \quad (2)$$

The spatial weight encodes geometric proximity:

$$f_s(\|p-q\|)=\exp\left(-\frac{¿p-q\vee¿^2}{2\sigma_s^2}\right)¿ \quad (3)$$

The range weight encodes photometric similarity:

$$f_r(|I(p)-I(q)|)=\exp\left(-\frac{¿I(p)-I(q)\vee¿^2}{2\sigma_r^2}\right)¿ \quad (4)$$

4.2. Comparison with Gaussian blur. Gaussian blur applies only the spatial weight f_s, smoothing uniformly regardless of photometric contrast. In the bilateral filter, the range weight $f_r \to 0$ at locations where |I(p)−I(q)| is large (i.e., at edges), so smoothing is selectively restricted to homogeneous regions while object boundaries are preserved. The Gaussian filter can therefore be expressed as a special case of Equation (1) where $\sigma_r \to \infty$.

4.3. Implications for CNN training. For CNN-based content classification, this selective smoothing behaviour may preserve discriminative structural and boundary features relevant to ethical/non-ethical categorisation, while attenuating irrelevant high-frequency noise in uniform regions. This mechanistic explanation is proposed as a testable hypothesis; empirical validation through Grad-CAM activation mapping is required before causal conclusions can be drawn.

5. Results

5.1. Training dynamics. Table 1 summarises training convergence. Figure 5 shows the full validation accuracy and loss curves. Gaussian blur showed the slowest initial convergence (epoch 1: 76.06%; best validation accuracy 90.14% at epoch 12; early stopping at epoch 17; best val. loss 0.3042). Motion blur converged more rapidly (epoch 1: 81.69%; peak 97.18% at epoch 18; all 20 epochs completed; val. loss 0.1725). Bilateral blur reached the same peak (97.18%) three epochs earlier (epoch 17; val. loss 0.1788). Anisotropic blur showed the slowest initial convergence (epoch 1: 71.83%; best 94.37% at epoch 12; early stopping at epoch 17).

Table 1. Training convergence summary for four blur conditions.

Metric	Gaussian	Motion	Bilateral	Anisotropic
Best epoch	12	18	17	12
Early stopping	Yes (ep. 17)	No	No	Yes (ep. 17)
Val. accuracy (ep. 1)	76.06%	81.69%	81.69%	71.83%
Best val. accuracy	90.14%	97.18%	97.18%	94.37%
Best val. loss	0.3042	0.1725	0.1788	0.2402
Processing speed	–	~0.39 img/s	~48,616 img/s	~95,000 img/s

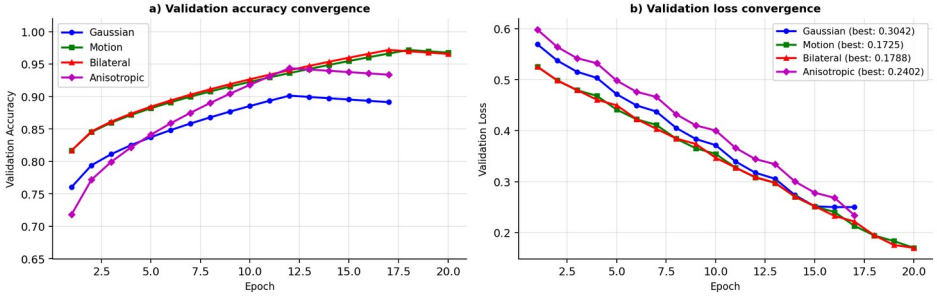


Figure 5. Training convergence curves for four blur conditions.

Figure 5. Training convergence curves: a) validation accuracy, b) validation loss across four blur conditions.

5.2. Test set classification performance. Table 2 presents full test set metrics for all six conditions. Figure 3 visualises overall accuracy and AUC; Figure 4 shows per-class F1-scores. Bilateral blur and Motion blur achieved 100.00% accuracy (95% CI [94.9%, 100.0%]; AUC = 1.0000; F1 = 1.00 for both classes). Anisotropic blur achieved 97.18% (95% CI [90.3%, 99.2%]; AUC = 0.9975). Gaussian blur achieved 90.14% (95% CI [81.0%, 95.1%]; AUC = 0.9722), with ethical recall = 0.78 and 22.2% false negatives in the ethical class.

McNemar's test confirmed the superiority of Bilateral blur over Gaussian blur ($\chi^2 = 5.14$, $p < 0.05$; $b = 7$, $c = 0$). The baseline condition (n = 94) yielded 37.23% accuracy (95% CI [28.1%, 47.3%]) with non-ethical recall = 0.05. Background removal (n = 40) produced 30.00% accuracy (95% CI [18.1%, 45.4%]) with non-ethical F1 = 0.00.

Table 2. Test set performance metrics for all six preprocessing conditions.

Metric	**Gaussian**	**Motion**	**Bilateral**	**Anisotropic**	**Baseline**	**Bg. Rem.**
n (test)	71	71	71	71	94	40
Accuracy	90.14%	100.00%	100.00%	97.18%	37.23%	30.00%
95% CI	[81.0, 95.1]	[94.9, 100.0]	[94.9, 100.0]	[90.3, 99.2]	[28.1, 47.3]	[18.1, 45.4]
AUC	0.9722	1.0000	1.0000	0.9975	–	–
Eth. Precision	0.95	1.00	1.00	0.96	0.35	0.30
Eth. Recall	0.78	1.00	1.00	0.96	1.00	1.00
Eth. F1	0.86	1.00	1.00	0.96	0.52	0.46
Non-eth. Prec.	0.88	1.00	1.00	0.98	1.00	0.00
Non-eth. Recall	0.98	1.00	1.00	0.98	0.05	0.00
Non-eth. F1	0.92	1.00	1.00	0.98	0.09	0.00
Macro F1	0.89	1.00	1.00	0.97	0.31	0.23
FP (non-eth.)	1/44 (2%)	0/44 (0%)	0/44 (0%)	1/44 (2%)	59/62 (95%)	28/28 (100%)

† Baseline (n = 94) and Background removal (n = 40) test sets differ in size; direct statistical comparison with blur conditions is not appropriate.

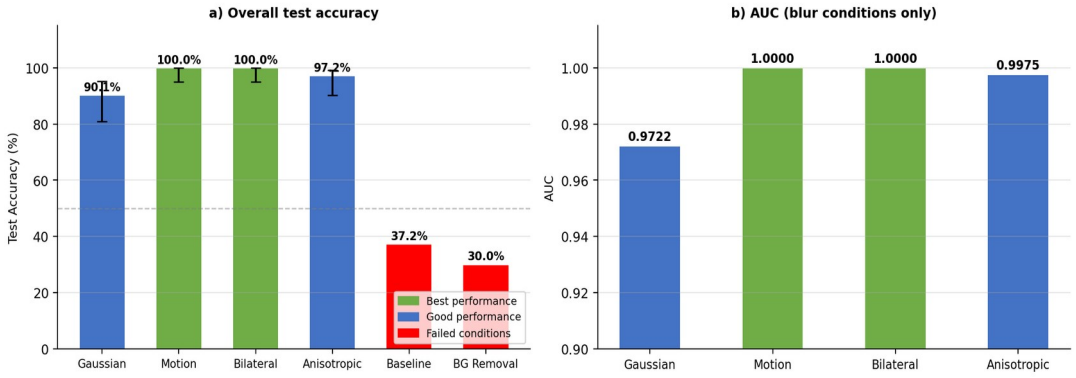


Figure 3. Test set results: a) overall accuracy with 95% CI (blur conditions), b) AUC.

Figure 3. Test set results: a) overall accuracy with 95% CI error bars (blur conditions), b) AUC for blur conditions. Error bars represent Wilson score 95% CI.

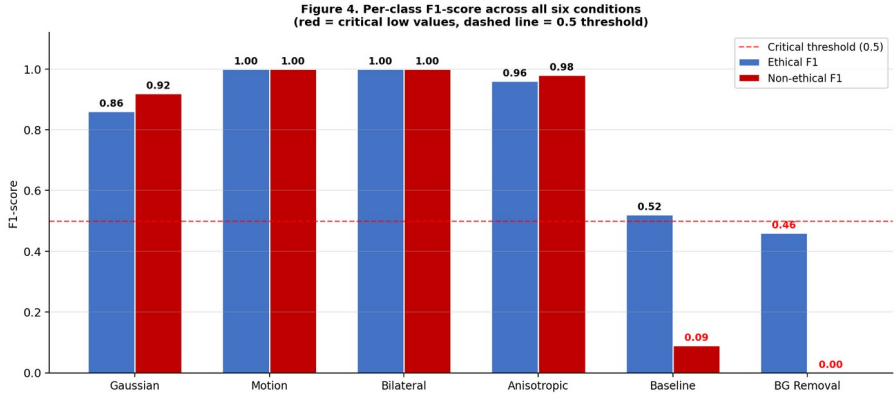


Figure 4. Per-class F1-score for all six preprocessing conditions. Red values and dashed line indicate critical low performance (≤ 0.5).

6. Discussion

6.1. Differential effects of blur strategies. The observed performance ranking – (Bilateral ≈ Motion) > Anisotropic > Gaussian – is theoretically consistent with differences in spatial frequency processing. Gaussian blur's isotropic attenuation (accuracy 90.14%, 95% CI [81.0%, 95.1%]) may degrade object boundary information, consistent with its 22.2% ethical false-negative rate. The edge-preserving property of Bilateral blur (Equations 1–4) provides a mechanistically plausible explanation, confirmed as statistically significant ($\chi^2 = 5.14$, $p < 0.05$). Caution is warranted: on $n = 71$, the 100% point estimate carries a lower 95% CI bound of 94.9%. All mechanistic explanations remain hypothetical pending Grad-CAM analysis.

6.2. Failure of baseline and background removal. Training EfficientNet-B0 from scratch on 330 images without augmentation (37.23%, 95% CI [28.1%, 47.3%]) is insufficient for generalisation. Background removal catastrophically impaired performance (30.00%, 95% CI [18.1%, 45.4%]; non-ethical $F1 = 0.00$), indicating that scene background is a critical discriminative feature. This is consistent with Xiao et al. [12] and Torralba and Oliva [14] and has a direct design implication: content moderation classifiers must retain full background context.

6.3. Limitations. (1) Small dataset ($n = 472$): wide confidence intervals, uncertain generalisation. (2) Single annotator: inter-annotator reliability not assessed. (3) Heterogeneous test set sizes: direct cross-condition statistical comparison is inappropriate. (4) Training from scratch: ImageNet pretraining may alter relative rankings [8]. (5) Single data split: k-fold cross-validation not performed. (6) Unoptimised blur parameters. (7) Mechanistic explanations require Grad-CAM empirical validation.

6.4. Future work. Future research should: (1) expand dataset to ≥2,000 images with a second annotator; (2) compare from-scratch vs. fine-tuned EfficientNet-B0; (3) apply 5-fold stratified cross-validation; (4) optimise blur parameters; (5) conduct Grad-CAM analysis; (6) evaluate on external test sets.

7. Conclusion. This study systematically compared six image preprocessing strategies for ethical/non-ethical binary classification using EfficientNet-B0 on a small dataset ($n = 472$). Key findings: all four blur augmentation strategies substantially outperformed no-augmentation and background-removal baselines; Bilateral blur and Motion blur achieved 100.00% test accuracy (95% CI [94.9%, 100.0%]); the Bilateral blur advantage over Gaussian blur is statistically significant (McNemar $\chi^2 = 5.14$, $p < 0.05$); background removal catastrophically degraded classification, confirming the discriminative importance of contextual background information; and training from scratch without augmentation on 330 images was insufficient. These results offer preliminary guidance for augmentation strategy selection in small-dataset content moderation and establish a methodological baseline for future statistically powered work.

REFERENCES

1. We Are Social & Hootsuite. (2024). Digital 2024: Global overview report. https://datareportal.com/reports/digital-2024-global-overview-report
2. LeCun, Y., Bottou, L., Bengio, Y., & Haffner, P. (1998). Gradient-based learning applied to document recognition. Proceedings of the IEEE, 86(11), 2278–2324.
3. Republic of Uzbekistan. (2002). Law on the Principles and Guarantees of Information Freedom (No. 439-II, 12 December 2002).
4. Tan, M., & Le, Q. V. (2019). EfficientNet: Rethinking model scaling for convolutional neural networks. Proceedings of the 36th ICML (PMLR 97), 6105–6114.
5. Shorten, C., & Khoshgoftaar, T. M. (2019). A survey on image data augmentation for deep learning. Journal of Big Data, 6(1), 60.
6. Gonzalez, R. C., & Woods, R. E. (2018). Digital Image Processing (4th ed.). Pearson.
7. Tomasi, C., & Manduchi, R. (1998). Bilateral filtering for gray and color images. Proceedings of the IEEE ICCV, 839–846.
8. Kornblith, S., Shlens, J., & Le, Q. V. (2019). Do better ImageNet models transfer better? Proceedings of the IEEE/CVF CVPR, 2661–2671.
9. Paris, S., & Durand, F. (2006). A fast approximation of the bilateral filter. Proceedings of ECCV, 568–580.
10. Perona, P., & Malik, J. (1990). Scale-space and edge detection using anisotropic diffusion. IEEE TPAMI, 12(7), 629–639.
11. Mikołajczyk, A., & Grochowski, M. (2018). Data augmentation for improving deep learning in image classification problem. Proceedings of the IIPhDW, 117–122.
12. Xiao, J., Hays, J., Ehinger, K. A., Oliva, A., & Torralba, A. (2010). SUN database: Large-scale scene recognition. Proceedings of the IEEE CVPR, 3485–3492.
13. Simard, P. Y., Steinkraus, D., & Platt, J. C. (2003). Best practices for CNNs applied to visual document analysis. Proceedings of the 7th ICDAR, 958–963.
14. Torralba, A., & Oliva, A. (2003). Statistics of natural image categories. Network: Computation in Neural Systems, 14(3), 391–412.
15. Kirillov, A., Mintun, E., Ravi, N., et al. (2023). Segment Anything. Proceedings of the IEEE/CVF ICCV, 4015–4026.

16. Kingma, D. P., & Ba, J. (2015). Adam: A method for stochastic optimization. Proceedings of the 3rd ICLR.
17. Brown, L. D., Cai, T. T., & DasGupta, A. (2001). Interval estimation for a binomial proportion. Statistical Science, 16(2), 101–133.
18. McNemar, Q. (1947). Note on the sampling error of the difference between correlated proportions. Psychometrika, 12(2), 153–157.

INNOVATIVE TECHNOLOGIES FOR IMPROVING EVACUATION METHODS

S.Sh. Nasirova[1], A.A. Suleymanov[2], S.X. Fayzullayev[3]
Tashkent State Technical University, Department of Life Safety, Senior Lecturer[1]
Tashkent State Technical University, Department of Life Safety, DSc Professor[2]
Tashkent State Technical University, Student[3]
https://doi.org/10.5281/zenodo.20554439

Abstract. *The effective organization of evacuation processes during emergency situations is one of the most important conditions for protecting human life and reducing the consequences of natural and techno genic hazards. Traditional evacuation methods are usually based on pre-developed evacuation plans, static route signs, alarm systems, responsible personnel instructions and standard movement schemes. Although these methods play an important role in ensuring public safety, they often demonstrate limited effectiveness in rapidly changing emergency conditions. In particular, smoke propagation, power outages, blocked exits, crowd congestion, lack of real-time information and difficulties faced by persons with disabilities may significantly reduce the reliability of conventional evacuation procedures. Therefore, the modernization of evacuation methods through innovative technologies has become an urgent scientific and practical task.*

This article analyzes the possibilities of improving evacuation methods through the integration of a mobile application, 360-degree camera monitoring and inclusive evacuation solutions for persons with disabilities. The proposed improved approach is based on real-time data collection, dynamic route selection, visual and audio notification, and the adaptation of evacuation instructions to the needs of vulnerable groups. A mobile application can provide users with safe route recommendations, emergency alerts, distance information and estimated evacuation time. A 360-degree camera system can monitor corridors, exits and crowd movement from a wide viewing angle, allowing emergency operators to identify dangerous zones, congestion points and blocked routes. Inclusive evacuation elements, including audio guidance, visual signals, vibration alerts and accessible route planning, can support people with visual, hearing or mobility impairments.

The comparative analysis shows that innovative evacuation technologies can increase the flexibility, accuracy and inclusiveness of evacuation management. Unlike traditional static methods, the improved model allows emergency response teams to update evacuation routes according to the actual situation. The study concludes that the combination of mobile applications, 360-degree monitoring and inclusive safety solutions can significantly improve evacuation efficiency, especially in complex buildings, educational institutions, industrial facilities and public spaces.

Keywords: *evacuation, mobile application, 360-degree camera, inclusive safety, emergency management.*

Introduction. Emergency evacuation is a critical component of disaster risk reduction and life safety management. During fires, earthquakes, explosions, floods, chemical accidents and other emergency situations, the timely and organized movement of people from dangerous zones to

safe areas can significantly reduce human casualties and injuries. In modern emergency management, evacuation is not only a physical movement process, but also a complex system of warning, decision-making, route selection, monitoring, communication and support for vulnerable groups. International emergency management standards emphasize the importance of incident management, including roles and responsibilities, resource management, information exchange and cooperation between organizations involved in emergency response [1]. ISO 22320:2018 also states that incident management guidelines are applicable to organizations responding to incidents of any type and scale.

Traditional evacuation methods are mainly based on pre-developed evacuation plans, fixed route signs, sound alarm systems, emergency lighting and instructions from responsible personnel. These methods are widely used in educational institutions, industrial enterprises, hospitals, shopping centers and public buildings. Their main advantage is simplicity and accessibility: they do not require complex digital infrastructure and can function as a basic safety system. The NFPA Life Safety Code is widely used as a source for strategies aimed at protecting people based on building construction, occupancy features and fire protection systems [2].

However, traditional evacuation methods have several limitations. First, evacuation signs and printed plans are static and cannot change according to the actual emergency situation. A route that is safe before an incident may become dangerous during a fire, explosion or structural damage. Second, sound alarms provide general warnings but do not give personalized instructions to people located in different parts of a building. Third, traditional systems often do not provide enough support for persons with disabilities, elderly people, children and other vulnerable groups. For example, a person with visual impairment may not see evacuation signs, while a person with hearing impairment may not hear sound alarms. A person with reduced mobility may not be able to use stairs or long evacuation routes.

The need for more adaptive evacuation systems is also supported by international disaster risk reduction approaches. The Sendai Framework for Disaster Risk Reduction 2015–2030 identifies four priorities: understanding disaster risk, strengthening disaster risk governance, investing in resilience and enhancing disaster preparedness for effective response [3]. These priorities show that emergency systems should be based not only on pre-planned actions, but also on real-time risk understanding, coordinated management and preparedness for complex scenarios. In this context, digital technologies can help make evacuation systems more flexible, accurate and people-centered.

One of the promising tools for improving evacuation methods is a mobile application. A mobile evacuation application can send emergency alerts, show safe routes, provide estimated evacuation time and give individual recommendations based on the user’s location. Unlike traditional sound alarms, mobile applications can deliver targeted instructions to different users. For example, people located near a blocked exit may receive a recommendation to use another route, while persons with disabilities may receive instructions adapted to accessible pathways. This makes mobile applications useful not only for warning, but also for dynamic evacuation management.

Another important technology is 360-degree camera monitoring. Ordinary surveillance cameras usually cover only a limited angle, while 360-degree cameras can provide a broader view of corridors, halls, staircases and exit zones. This allows emergency operators to identify crowd congestion, smoke spread, blocked passages and abnormal movement more quickly. In an improved evacuation system, 360-degree cameras can serve as real-time monitoring tools that

provide data for decision-making. When combined with artificial intelligence or analytical software, such cameras can help detect dangerous zones and support the automatic updating of evacuation routes.

Inclusive evacuation is also a key requirement for modern safety systems. The World Health Organization emphasizes that disability-inclusive emergency risk management should cover risk assessment, prevention, preparedness, response, recovery and reconstruction [4]. This means that evacuation systems must be designed for all categories of people, including persons with visual, hearing, mobility and cognitive impairments. Inclusive evacuation technologies may include audio guidance, visual signals, vibration alerts, tactile indicators, accessible routes and safe waiting areas. These solutions are especially important in large public buildings where the population is diverse and emergency movement is difficult to control.

Therefore, the integration of mobile applications, 360-degree camera monitoring and inclusive guidance tools can form an improved evacuation model. In this model, the 360-degree camera system monitors the actual condition of evacuation routes, the mobile application sends personalized instructions to evacuees, and inclusive tools support people with different functional needs. Such a model can be connected with Internet of Things sensors, digital building maps and artificial intelligence algorithms. As a result, evacuation management becomes not only faster, but also more adaptive and inclusive.

Despite the potential advantages, the implementation of innovative evacuation technologies also requires careful analysis. Mobile applications depend on smartphones, battery charge and communication networks. Camera monitoring systems require proper installation, maintenance and data protection. Inclusive technologies require building adaptation, staff training and regular evacuation drills. Therefore, improved evacuation methods should not completely replace traditional systems. Instead, they should strengthen existing evacuation infrastructure and create a hybrid safety model.

The purpose of this article is to compare traditional and improved evacuation methods and to justify the role of innovative technologies in increasing evacuation efficiency. Special attention is paid to mobile applications, 360-degree camera monitoring and inclusive evacuation solutions for persons with disabilities. The main research objectives are: to identify the limitations of traditional evacuation methods; to analyze the functional advantages of innovative evacuation technologies; to compare both approaches according to key safety criteria; and to develop a conceptual model for improved evacuation management.

The scientific novelty of the study lies in the integrated comparison of traditional static evacuation methods and improved digital evacuation methods from the perspective of real-time monitoring, dynamic route selection and inclusive safety. The practical significance of the study is that the proposed approach can be used in educational institutions, industrial facilities, hospitals, shopping centers and other public buildings to improve emergency preparedness and protect vulnerable groups.

Methods

This study was based on a comparative analytical method aimed at evaluating the functional effectiveness of traditional and improved evacuation methods. The selected methodological approach made it possible to compare two evacuation models according to the same evaluation criteria and under the same conditional emergency scenario.

The research was carried out in three stages. At the first stage, the structural elements of traditional evacuation methods were defined. These elements included static evacuation plans,

fixed direction signs, sound alarm systems, emergency lighting and instructions provided by responsible personnel. At the second stage, the structural elements of the improved evacuation model were defined. The improved model included a mobile application, 360-degree camera monitoring and inclusive evacuation guidance tools for persons with disabilities. At the third stage, both evacuation models were evaluated using the same set of criteria.

The comparison was conducted according to seven criteria: information delivery speed, route adaptability, monitoring capability, inclusiveness, decision-making efficiency, congestion control and communication reliability. These criteria were selected because they reflect the main functional requirements of an effective evacuation system in a dynamically changing emergency environment. The inclusion of the inclusiveness criterion was based on disability-inclusive emergency risk management principles, while the decision-making and communication criteria were selected in accordance with international emergency management guidance [1], [4].

A conditional emergency scenario was used for the comparative assessment. The scenario describes a fire-related emergency in a multi-zone public building. In this scenario, evacuees are located in different parts of the building, while some evacuation routes may become unsafe due to smoke, congestion or blocked passages. The same scenario was applied to both the traditional and improved evacuation models in order to ensure methodological comparability.

A five-point qualitative scoring scale was used to assess each criterion. A score of 1 indicated very low functional effectiveness, while a score of 5 indicated very high functional effectiveness. The scoring was based on the expected functional capability of each evacuation model under the selected scenario. This approach allowed the study to compare the two methods without conducting a full-scale evacuation experiment.

To calculate the general evacuation efficiency index, the following formula was used:

$$E = \frac{I_s + R_a + M_c + A_i + D_e}{5}$$

where:

E - is the general evacuation efficiency index;

I_s -is information delivery speed;

R_a - is route adaptability;

M_c - is monitoring capability;

A_i - is accessibility and inclusiveness;

D_e - is decision-making efficiency.

The formula was used to compare the two evacuation models according to five core indicators. Additional criteria, such as congestion control and communication reliability, were used for extended qualitative interpretation. The study did not include physical evacuation drills or experimental testing with real participants. Therefore, the obtained results should be considered as an analytical and scenario-based assessment. Future studies may expand this approach through simulation modeling, field experiments and testing of mobile evacuation application prototypes in real buildings.

Results

The comparative assessment showed clear functional differences between the traditional evacuation method and the improved evacuation model. The results are presented in three forms: a comparison table, an evacuation efficiency index calculation, and a linear graph of key indicators.

Table 2. Comparative results of traditional and improved evacuation methods

Evaluation indicator	Traditional evacuation method	Improved evacuation method
Information delivery speed	3	5
Route adaptability	2	5
Monitoring capability	2	5
Inclusiveness	2	5
Decision-making efficiency	3	4
Congestion control	2	4
Communication reliability	3	4

The results in Table 2 show that the improved evacuation method received higher scores across all selected indicators. The most significant differences were observed in route adaptability, monitoring capability and inclusiveness. In these three indicators, the traditional method received a score of 2, while the improved method received a score of 5. This indicates that the traditional method has limited ability to respond to changing emergency conditions, while the improved model can support dynamic decision-making through real-time monitoring and personalized guidance.

The improved model also showed a higher result in information delivery speed. The traditional method received a score of 3 because it mainly relies on general sound alarms, fixed signs and instructions from responsible personnel. The improved method received a score of 5 because mobile notifications, visual signals and vibration alerts can deliver information directly to different user groups.

The general evacuation efficiency index was calculated using five core indicators: information delivery speed, route adaptability, monitoring capability, accessibility and inclusiveness, and decision-making efficiency.

For the traditional evacuation method:

$$E_t = \frac{3+2+2+2+3}{5} = 2.4$$

For the improved evacuation method:

$$E_i = \frac{5+5+5+5+4}{5} = 4.8$$

The calculated results show that the general evacuation efficiency index of the traditional method was 2.4, while the improved method reached 4.8. This means that the improved evacuation model demonstrated approximately two times higher functional effectiveness than the traditional evacuation method under the selected scenario.

Figure 1 presents the structural logic of the improved evacuation model. The process begins with hazard detection and continues with 360-degree camera monitoring, analysis of route conditions, mobile application notification, dynamic safe route recommendation and inclusive guidance. The figure shows that the improved model is based on a continuous information flow from hazard detection to safe evacuation.

Figure 2 demonstrates how the improved evacuation model supports different categories of evacuees. Persons with visual impairments are supported through audio guidance and tactile indicators. Persons with hearing impairments receive visual signals and vibration alerts. Persons with mobility impairments are directed to accessible routes and safe waiting areas. Elderly people and children receive simplified instructions and assisted movement support.

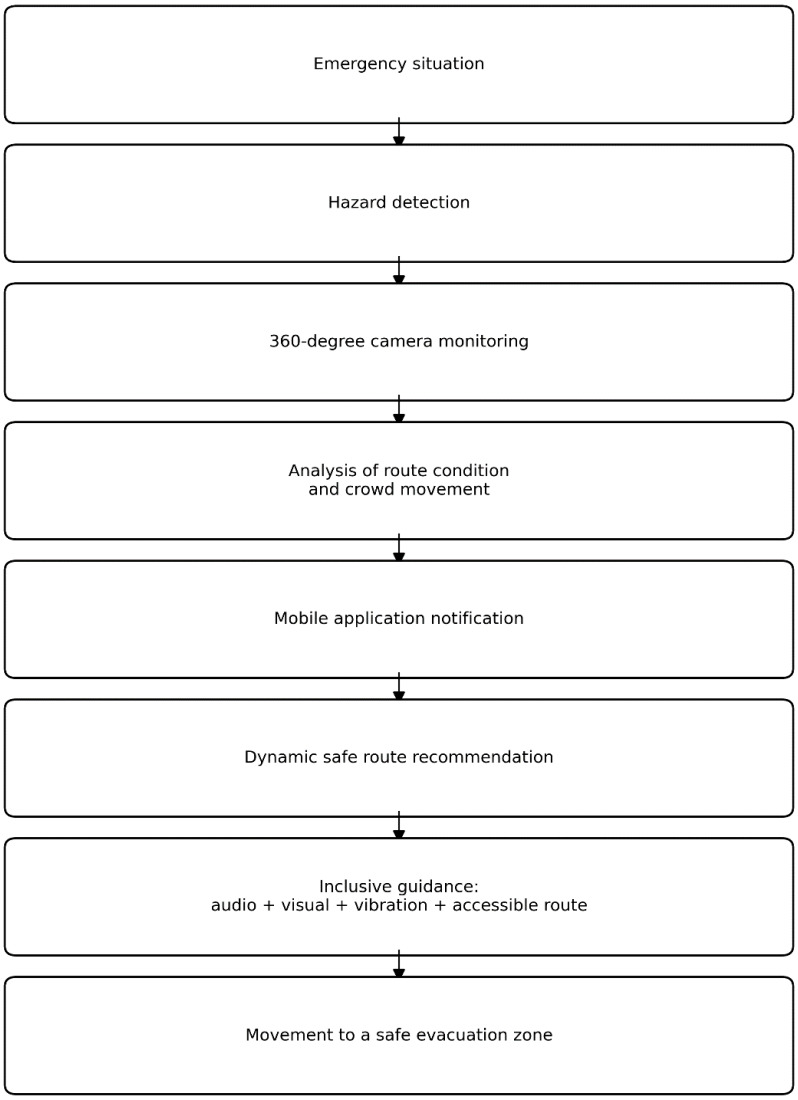


Figure 1. Conceptual block scheme of the improved evacuation model

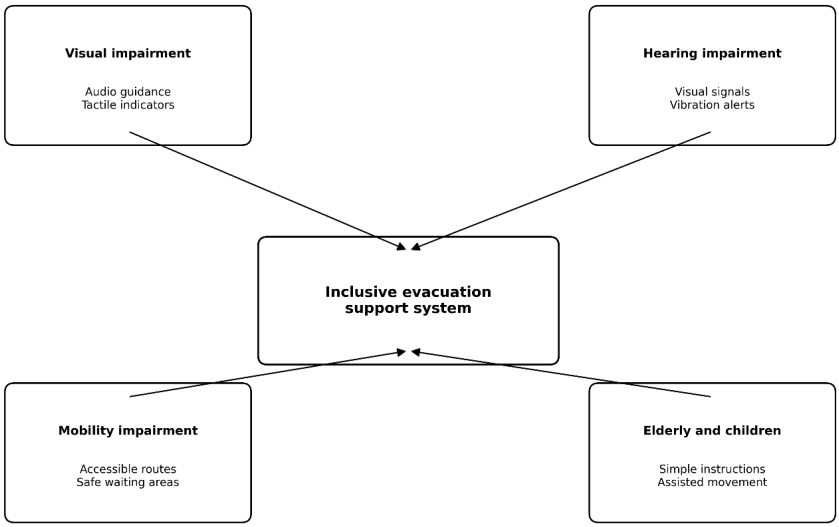


Figure 2. Inclusive evacuation support scheme for different user groups

For graphical interpretation, the scores obtained for each criterion were planned to be presented as a linear graph. This graph allows visual comparison of the traditional and improved evacuation methods according to the selected indicators.

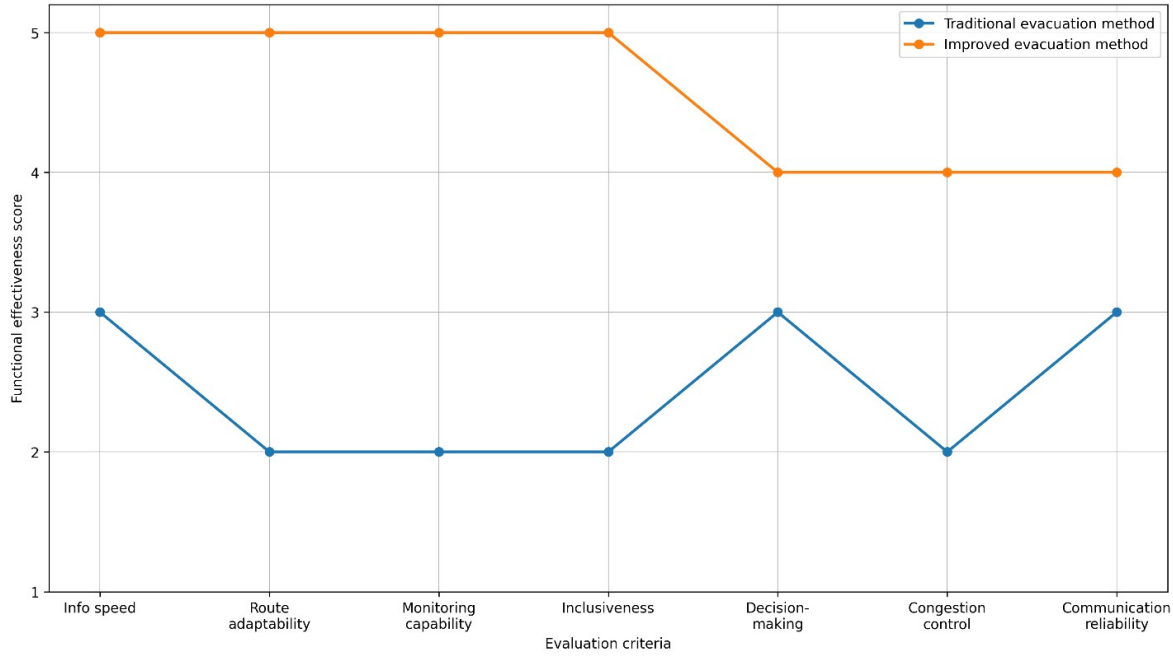


Figure 3. Linear comparison of evacuation efficiency indicators

The linear graph in Figure 3 confirms the difference between the two evacuation approaches. The improved evacuation method showed consistently higher values for all indicators. The largest performance gap was observed in route adaptability, monitoring capability and inclusiveness. The smallest, but still meaningful, difference was observed in decision-making efficiency and communication reliability.

The obtained results indicate that the improved evacuation method is more suitable for buildings where evacuation conditions may change rapidly. These include educational institutions, industrial facilities, hospitals, shopping centers, transport terminals and administrative buildings. In such facilities, the use of mobile applications, 360-degree camera monitoring and inclusive guidance tools can reduce uncertainty, improve route selection and support vulnerable groups during emergency evacuation.

Overall, the results confirm that evacuation efficiency depends not only on the presence of exits and alarm systems, but also on the system's ability to collect real-time information, update evacuation routes and provide accessible instructions to all categories of people.

Discussion

The results demonstrate that the improved evacuation model has a higher functional potential than the traditional evacuation method. The main reason for this difference is the ability of the improved model to collect, process and deliver information during the emergency process. Traditional evacuation systems mostly operate according to pre-planned and fixed instructions, while the improved model is based on real-time monitoring and adaptive guidance.

The first important finding is related to information delivery speed. In traditional evacuation systems, information is usually delivered through sound alarms, fixed signs and verbal instructions. These tools are useful, but they provide the same information to all evacuees regardless of their location, physical condition or the actual level of danger near them. In contrast, a mobile application can send targeted alerts to users in different zones of a building. This allows evacuees to receive short, clear and location-based instructions. For example, if one corridor becomes unsafe, the application can recommend an alternative route. This makes the evacuation process more flexible and reduces uncertainty among people.

The second important finding concerns route adaptability. Static evacuation plans cannot change after the emergency begins. This is a serious limitation because emergency conditions may change within minutes. Smoke may spread, exits may become blocked and crowd density may increase near staircases. The improved model addresses this limitation by using 360-degree camera monitoring and dynamic route recommendations. The camera system provides a wide view of corridors, halls and exits, while the mobile application transmits updated route information to evacuees. As a result, the system can support safer movement even when the original evacuation route becomes dangerous.

The third major advantage of the improved model is monitoring capability. Traditional systems rely mainly on human observation and ordinary surveillance cameras. However, in complex buildings, responsible personnel may not be able to observe all zones at the same time. A 360-degree camera system can reduce this information gap by covering a wider visual area. This is especially useful for identifying crowd congestion, blocked passages and unsafe movement patterns. If combined with analytical software in future applications, such a system can automatically detect risk zones and support faster decision-making.

The fourth and most socially significant finding is related to inclusive evacuation. Traditional evacuation methods often do not fully consider the needs of persons with disabilities. For example, sound alarms may be ineffective for persons with hearing impairments, while visual signs may be inaccessible for persons with visual impairments. The improved model includes audio guidance, visual signals, vibration alerts, tactile indicators and accessible route recommendations. These tools make evacuation more inclusive and reduce the risk of leaving vulnerable groups without support. Therefore, inclusive evacuation should not be considered an additional function; it should be treated as a basic safety requirement.

The improved model also showed better results in decision-making efficiency and congestion control. Real-time information allows emergency operators to make more accurate decisions. If one exit becomes overcrowded, people can be redirected to another safe route. This can reduce crowd pressure, prevent panic and improve movement distribution inside the building.

In large public facilities, such as universities, hospitals, shopping centers and industrial enterprises, this function can be especially important.

However, the proposed improved evacuation model also has several limitations. First, mobile applications depend on smartphones, battery charge and communication networks. If users do not have access to a mobile device or if the network fails, the effectiveness of the system may decrease. Second, 360-degree camera monitoring requires stable electricity, proper installation and regular maintenance. Third, video monitoring and mobile data exchange create issues related to privacy and cybersecurity. For this reason, the system must include data protection measures, backup power supply and offline operation options.

Another limitation is the need for user training. Even a well-designed digital evacuation system may be ineffective if people do not know how to use it. Therefore, the mobile application, camera monitoring system and inclusive guidance tools should be included in regular evacuation drills. Staff members should also be trained to interpret monitoring data and manage dynamic evacuation instructions.

The findings suggest that innovative technologies should not completely replace traditional evacuation infrastructure. Static signs, emergency lighting and alarm systems remain necessary as basic safety tools. The most effective approach is a hybrid evacuation system. In such a system, traditional tools provide the basic safety layer, while mobile applications, 360-degree camera monitoring and inclusive guidance tools provide adaptive and personalized support. This combination increases the reliability of evacuation management because if one component fails, another component can continue to support the process.

Thus, the improved evacuation model can be considered a promising direction for modern emergency management. Its practical value is especially high in buildings with complex layouts, high population density and diverse user groups. Future studies should test this model through simulation, experimental evacuation drills and mobile application prototype development.

Conclusion

The study compared traditional evacuation methods with an improved evacuation model based on a mobile application, 360-degree camera monitoring and inclusive guidance tools. The results showed that the improved model has higher functional effectiveness in information delivery speed, route adaptability, monitoring capability, inclusiveness and decision-making efficiency.

Traditional evacuation methods remain important because they provide a basic level of safety through fixed plans, signs, alarms and responsible personnel. However, they have limited flexibility in rapidly changing emergency conditions. They also provide insufficient support for persons with disabilities and other vulnerable groups.

The improved evacuation model offers a more adaptive and inclusive approach. A mobile application can provide targeted alerts, safe route recommendations and estimated evacuation time. A 360-degree camera system can improve real-time monitoring of corridors, exits and crowd movement. Inclusive tools can support persons with visual, hearing and mobility impairments through audio, visual, vibration and accessible-route solutions.

The calculated evacuation efficiency index showed that the traditional method reached 2.4, while the improved method reached 4.8 under the selected scenario. This indicates that the improved model may provide approximately two times higher functional effectiveness than the traditional method.

The practical significance of the study is that the proposed approach can be applied in educational institutions, industrial facilities, hospitals, shopping centers, transport terminals and

other public buildings. However, successful implementation requires technical reliability, cybersecurity, backup power supply, user training and integration with existing emergency response systems.

In conclusion, evacuation systems should be modernized through a hybrid approach. Traditional evacuation tools should be preserved as a basic safety layer, while innovative technologies should be added to provide real-time monitoring, dynamic route selection and inclusive support for all categories of people. This approach can improve emergency preparedness and reduce risks during evacuation.

REFERENCES

1. International Organization for Standardization. (2018). *ISO 22320:2018 Security and resilience — Emergency management — Guidelines for incident management*. ISO. https://www.iso.org/standard/67851.html
2. National Fire Protection Association. (2024). *NFPA 101: Life Safety Code*. NFPA. https://www.nfpa.org/codes-and-standards/nfpa-101-standard-development/101
3. United Nations Office for Disaster Risk Reduction. (2015). *Sendai Framework for Disaster Risk Reduction 2015–2030*. UNDRR. https://www.undrr.org/publication/sendai-framework-disaster-risk-reduction-2015-2030
4. World Health Organization. (2013). *Guidance note on disability and emergency risk management for health*. WHO. https://www.who.int/publications/i/item/guidance-note-on-disability-and-emergency-risk-management-for-health
5. Lu, X., Yang, Z., Xu, Z., & Chen, C. (2022). Mobile phone-based emergency evacuation system for fire scenes. *Sensors, 22*(10), 3783. https://doi.org/10.3390/s22103783
6. Mulloni, A., Seichter, H., & Schmalstieg, D. (2011). Indoor navigation with mixed reality world-in-miniature views and sparse localization on mobile devices. *Proceedings of the International Working Conference on Advanced Visual Interfaces*, 212–215. https://doi.org/10.1145/1978942.1978974
7. Zeeshan, M., Qureshi, H. K., & Iqbal, S. (2023). IoT-based emergency evacuation and disaster management systems: A review. *Internet of Things, 23*, 100872. https://doi.org/10.1016/j.iot.2023.100872
8. Ronchi, E., & Nilsson, D. (2013). Fire evacuation in high-rise buildings: A review of human behaviour and modelling research. *Fire Science Reviews, 2*, 7. https://doi.org/10.1186/2193-0414-2-7
9. Nasirova, S. Sh., & Suleymanov, A. A. (2023). *Improving the process of population evacuation in the event of threat and emergency situations*. Lambert Academic Publishing.
10. Nasirova, S. Sh., Fayzullayev, S. Kh., Bilalova, D. J., Khalmatova, N. G., & Suleymanov, A. A. (2025). *Improving population evacuation in emergency situations on the example of the SafeWay mobile application*. Certificate of official registration of a computer program No. DGU 52156.

TECHNOLOGY FOR THE AUTOMATED SELECTION AND ADAPTIVE ASSESSMENT OF NON-STANDARD PROBLEMS

Murodova Shaxodat Shamurzayevna
PhD Candidate, Nizomiy Tashkent State Pedagogical University
m.shahodat1983@gmail.com

Abstract. *This article examines the didactic potential of using non-standard problems in computer science education and proposes a technology for their automated selection and adaptive assessment in a digital learning environment. Unlike conventional exercises, non-standard problems require learners not merely to apply a predetermined algorithm but to analyze a problem, formulate a solution strategy, compare alternative approaches, and provide a reasoned conclusion. Therefore, presenting the same set of problems to all learners in an identical sequence does not fully account for their individual learning needs.*

The study develops a model based on describing non-standard problems through a set of parameters, determining the learner's current level of knowledge and competence, automatically selecting subsequent problems, analyzing the solution process, and dynamically adjusting task difficulty according to assessment results. The proposed approach can contribute to the development of individualized learning trajectories and improve the effectiveness of formative assessment in computer science education.

Keywords: *computer science education, non-standard problem, adaptive learning, automated selection, intelligent assessment, individualized learning trajectory, algorithmic thinking, digital education, artificial intelligence.*

Introduction

In the context of contemporary digital education, one of the major objectives of computer science instruction is not simply to enable learners to mechanically master a particular programming language or algorithm, but to develop their ability to analyze information, formalize problems, design algorithmic solutions, and justify their decisions.

Standard problems in computer science are generally based on the application of a previously known algorithm or rule. For example, tasks involving the calculation of the sum of given numbers, identification of the maximum element in an array, or construction of an algorithm based on a specified condition primarily assess a learner's ability to perform a particular operation.

In contrast, the solution method for a non-standard problem is not explicitly provided in advance. Learners are required to independently analyze the conditions of the problem, distinguish essential information from secondary information, consider several possible solution strategies, and select an appropriate solution.

From this perspective, non-standard problems represent an important didactic tool for developing higher-order thinking skills in computer science education.

However, in practice, the selection of such problems often depends on the teacher's subjective experience. Providing all learners with problems of the same level of difficulty may produce different learning outcomes because learners have different levels of prior knowledge and competence.

Therefore, the development of a mechanism for the automated selection of non-standard problems and the adaptive assessment of learners' performance constitutes an important scientific and methodological challenge.

The Role of Non-Standard Problems in Computer Science Education

The concept of a non-standard problem should not be interpreted simply as a "difficult problem." The non-standard nature of a problem is determined not by its level of complexity, but by the fact that the solution strategy is not presented to the learner in a ready-made form.

Non-standard problems are characterized by the following features:

- the solution algorithm is not directly provided;
- several solution strategies may be possible;
- interpretation of the problem statement is required;
- the learner formulates hypotheses;
- analysis of errors plays an important role;
- the solution must be justified;
- the reasoning process leading to the solution can also be assessed.

For example, a learner may be presented with the following task:

"A given algorithm in a computer program produces the correct result for some input data but generates an incorrect result for other data. Identify the error and propose at least two ways of modifying the algorithm."

Such a task requires not only code writing but also an investigation of the underlying logic of the algorithm.

Problems of this type contribute to the development of algorithmic thinking, critical thinking, and the ability to make decisions in problem situations.

Model for the Automated Selection of Non-Standard Problems

The primary function of an automated selection system is not to assign a random problem to each learner, but to identify a task that corresponds to the learner's current state of knowledge and competence.

For this purpose, each problem is described using a set of parameters.

Table 1. Key Parameters of a Non-Standard Problem

No.	Parameter	Description
1	Difficulty level	The amount and complexity of cognitive operations required to solve the problem
2	Topic	Algorithms, programming, databases, networks, and other areas
3	Cognitive level	Understanding, application, analysis, synthesis, and evaluation
4	Number of solutions	Whether the problem has a single solution or multiple possible solutions
5	Degree of openness	Closed, partially open, or open-ended task
6	Time factor	Estimated time required to complete the problem
7	Error type	Logical, syntactic, algorithmic, or conceptual error
8	Justification requirement	The extent to which the learner is required to explain and justify the result

Each task in the problem bank is classified according to these parameters. As a result, the system can identify problems that correspond to the learner's current profile.

Development of an Individual Learner Profile

In an adaptive selection technology, a learner is not regarded merely as an entity that produces “correct” or “incorrect” answers.

The system takes into account several indicators, including:

- the proportion of correct answers;
- task completion time;
- recurring errors;
- use of hints or assistance;
- number of attempts;
- performance across different difficulty levels;
- quality of solution justification.

Based on these indicators, the learner's current learning profile is established.

Table 2. Indicative Parameters of the Learner Profile

Indicator	Low	Medium	High
Algorithmic understanding	0–40%	41–70%	71–100%
Problem analysis	0–40%	41–70%	71–100%
Solution strategy selection	0–40%	41–70%	71–100%
Program implementation	0–40%	41–70%	71–100%
Solution justification	0–40%	41–70%	71–100%

These indicators should not be regarded as rigid thresholds, but rather as initial parameters for the decision-making mechanism of the adaptive system.

Automated Problem Selection Algorithm

Within the proposed technology, problem selection is implemented through several stages.

Stage 1. A diagnostic task is presented to the learner.

Stage 2. The correctness of the response and the solution process are recorded.

Stage 3. The learner's current competency profile is updated.

Stage 4. Candidate problems corresponding to the learner's profile are retrieved from the problem bank.

Stage 5. The candidates are evaluated according to difficulty and topic relevance.

Stage 6. The selected problem is presented to the learner.

Stage 7. The result is re-analyzed, and the parameters of the subsequent problem are adjusted.

Thus, the learning process proceeds through the following adaptive cycle:

diagnosis → problem selection → solution → analysis → assessment → selection of a new problem

Adaptive Assessment Technology

When assessing non-standard problems, checking only the final answer is insufficient. A learner may arrive at an incorrect result through a partially correct reasoning process or, conversely, may obtain the correct answer accidentally.

Therefore, assessment should be divided into several components.

Table 3. Criteria for Adaptive Assessment

Criterion	Weight
Correctness of the final result	**30%**
Logical consistency of the algorithmic solution	**25%**

Problem analysis	**20%**
Justification of the solution	**15%**
Efficiency and independence	**10%**

The proposed distribution is illustrative and may be modified depending on the subject topic and educational level.

An important feature of adaptive assessment is that two learners who obtain the same final result do not necessarily demonstrate the same learning state. If one learner solves a problem independently while another requires multiple instances of assistance, the system records these learning characteristics separately.

Dynamic Adjustment of Problem Difficulty

One of the key features of the system is the dynamic adjustment of the difficulty of subsequent problems based on the learner's previous performance.

For example:

- **high performance** → increase the level of difficulty;
- **stable medium performance** → provide another problem at the same level;
- **a sequence of errors** → provide a scaffolded or supportive task;
- **repeated occurrence of the same error** → provide a diagnostic task addressing the relevant concept.

Such an approach can reduce the risk of restricting learners to excessively easy tasks or, conversely, exposing them to problems that are substantially beyond their current level of preparation.

Typology of Non-Standard Problems

In an automated selection system, grouping problems according to their content and cognitive demands is particularly important.

Table 4. Typology of Non-Standard Problems

Problem Type	Activity Required from the Learner
Problem-based task	Identifying the problem and formulating a hypothesis
Error-detection task	Analyzing an error in a given solution
Optimization problem	Selecting an appropriate solution from several alternatives
Inverse problem	Reconstructing the conditions from a given result
Open-ended problem	Developing several justified solutions
Algorithm modification task	Adapting an existing algorithm to a new condition
Combined problem	Applying several computer science concepts simultaneously

Such a typology also enables the system to identify the particular cognitive operation in which a learner is experiencing difficulty.

Functional Architecture of the Technology

The proposed system can conventionally be divided into five major modules:

1. Problem Bank

The module stores non-standard problems, their solutions, difficulty levels, and pedagogical parameters.

2. Diagnostic Module

This module evaluates the learner's initial knowledge and skills.

3. Selection Module

The module determines the subsequent problem that best corresponds to the learner's profile.

4. Assessment Module

This module analyzes not only the correctness of the answer but also the solution process.

5. Analytics Module

The module provides teachers with information about learner progress, typical errors, and levels of mastery.

This architecture can be integrated into a learning management system (LMS), an electronic learning platform, or a specialized educational application for computer science.

A Conceptual Model of Adaptive Selection

The following generalized matching function can be used for problem selection:

Si=w1Ki+w2Di+w3Ti+w4EiS_i = w_1K_i + w_2D_i + w_3T_i + w_4E_i

where:

- SiS_i — the suitability score of problem ii for the learner;
- KiK_i — the degree of alignment with the learner's competence in the relevant topic;
- DiD_i — the degree of alignment with the appropriate difficulty level;
- TiT_i — the relevance of the problem type;
- EiE_i — the relationship between the problem and the learner's previous errors;
- w1,w2,w3,w4w_1, w_2, w_3, w_4 — corresponding weighting coefficients.

The problem with the highest suitability value may then be selected as the learner's next task.

The objective of this approach is not to provide the “most difficult problem.” Rather, the objective is to create a problem situation that is pedagogically appropriate for the learner's current state.

Opportunities for the Use of Artificial Intelligence

Artificial intelligence technologies can expand the functional capabilities of adaptive learning systems.

In particular, an intelligent module can:

- analyze learners' responses expressed in free text;
- identify logical gaps in solutions;
- classify recurring errors;
- generate new variants of non-standard problems;
- estimate the approximate difficulty of a problem;
- provide guiding questions rather than ready-made answers;
- generate individualized recommendations for teachers.

However, fully automated acceptance of AI-generated assessment results without human oversight is not advisable. In particular, teacher supervision should be maintained when assessing open-ended problems and tasks that permit multiple valid solutions.

Scenario for Applying the Technology

The following example illustrates how the adaptive mechanism operates.

A learner is first presented with a non-standard problem involving the identification of an error in an algorithm. The learner solves the problem correctly but requires a relatively long time to complete it.

The system interprets the result as follows:

- conceptual understanding is present;
- the learner demonstrates the ability to solve the problem independently;

- solution speed requires further development.

Consequently, the next task is selected not to change the content area but to focus on optimizing the learner's solution strategy.

Another learner may repeat the same type of error twice when solving the first problem. Instead of presenting a more difficult problem, the system provides a short diagnostic task designed to facilitate a deeper understanding of the relevant concept.

Thus, even when two learners are studying the same topic, their subsequent learning trajectories may differ.

Pedagogical Effectiveness of the Technology

The use of automated selection and adaptive assessment of non-standard problems may contribute to the following pedagogical outcomes:

1. accounting for individual learning needs;
2. developing higher-order thinking skills;
3. identifying learners' typical errors at an early stage;
4. implementing continuous formative assessment;
5. reducing the time teachers spend manually selecting similar tasks;
6. identifying the learner's level of independent work;
7. digitally monitoring the dynamics of learning outcomes.

At the same time, the effectiveness of the technology is directly dependent on the quality of the problem bank, the adequacy of the assessment criteria, and the appropriate configuration of the adaptive algorithm.

Conclusion

The use of non-standard problems in computer science education provides learners with opportunities to understand and analyze problems and to develop independent solution strategies rather than merely reproduce predetermined algorithms. However, in order to fully realize the pedagogical potential of non-standard problems, they need to be selected in accordance with learners' individual levels of preparedness and current learning performance.

The technology proposed in this article integrates a non-standard problem bank, learner profiles, an automated selection mechanism, adaptive assessment, and analytical modules within a unified digital environment.

An important feature of the proposed technology is that assessment is not limited to the final outcome. The learner's solution strategy, errors, completion time, and level of independence are also taken into account. This creates an opportunity to move from the model of **“the same task — the same learning trajectory”** toward a more individualized learning model in computer science education.

In the future, integrating this approach with HEMIS, LMSs, and other digital learning platforms, developing AI-based analysis of open-ended responses, and improving adaptive models using large-scale educational data represent promising directions for further research.

REFERENCES

1. Bloom, B. S. (1956). *Taxonomy of Educational Objectives: The Classification of Educational Goals*. New York: Longmans, Green.
2. Anderson, L. W., & Krathwohl, D. R. (2001). *A Taxonomy for Learning, Teaching, and Assessing: A Revision of Bloom's Taxonomy of Educational Objectives*. New York: Longman.

3. Brusilovsky, P. (1996). Methods and techniques of adaptive hypermedia. *User Modeling and User-Adapted Interaction*, 6.
4. Woolf, B. P. (2009). *Building Intelligent Interactive Tutors: Student-Centered Strategies for Revolutionizing E-Learning*. Morgan Kaufmann.
5. Luckin, R., Holmes, W., Griffiths, M., & Forcier, L. B. (2016). *Intelligence Unleashed: An Argument for AI in Education*. Pearson.
6. Holmes, W., Bialik, M., & Fadel, C. (2019). *Artificial Intelligence in Education: Promises and Implications for Teaching and Learning*. Center for Curriculum Redesign.
7. OECD. (2023). *Digital Education Outlook 2023: Towards an Effective Digital Education Ecosystem*. OECD Publishing.
8. UNESCO. (2023). *Guidance for Generative AI in Education and Research*. Paris: U

OPERABILITY LIMITS OF A SAW COTTON SEED LINTER UNDER RAW-MATERIAL GRADE VARIATION AND SAW WEAR

Navruzbek Kurbonov[1] Mirshod Abdullayev[2]

[1] PhD student, "Tashkent Institute of Irrigation and Agricultural Mechanization Engineers" National Research University, Department of Automation and Control of Technological Processes, Tashkent, Uzbekistan

[2] assistant, "Tashkent Institute of Irrigation and Agricultural Mechanization Engineers" National Research University, Department of Automation and Control of Technological Processes, Tashkent, Uzbekistan

Abstract. *Saw linters must keep the residual lint on cottonseed within a narrow regulated band, yet the incoming seed differs in initial lint content from lot to lot and from grade to grade, and the saws lose sharpness as they work. Once the saw-cylinder speed reaches its limit, no feedback controller can compensate for these changes. This study asks which seed grades can be brought to the regulated residual lint in a single pass of a 5LP linter and how this set shrinks as the saws wear. A steady-state model of the linter was built from plant measurements at an oil-extraction plant in Uzbekistan: the static characteristic of residual lint against saw speed, the gains of the initial-lint and seed-flow channels, and the drift recorded over a saw-set life of 248 h. The process operability framework was applied with saw speed (616–774 rpm) and, in a second scenario, seed flow as available inputs, the national grade norms and saw age as expected disturbances, and 7.00 ± 0.30% residual lint as the desired output. Additive and multiplicative forms of the initial-lint effect were compared to bound the error of extrapolation. With new saws and nominal flow, the 7.00% target is reachable only for seed with initial lint up to 13.8–14.4%, and the limit falls by 0.6–1.0 percentage points per 100 h of saw operation. Reducing the seed flow from 2150 to 1850 kg/h raises the limit by 0.45–0.71 percentage points at the cost of 14% of throughput. Grade IV of 108-F and grades III–IV of 133-F and 138-F cannot be linted to the target in one pass even at reduced flow.*

Keywords: *Cotton seed linting, Residual lint, Process operability, Raw material variability, Saw wear.*

Introduction

Cottonseed leaving the gin stand still carries a layer of short fibres, the linters. Removing them on saw linters yields two products of commercial value: linters, which are a cellulose raw material, and delinted seed for sowing or for oil extraction (Zahra et al., 2024). The residual lint left on the seed is the main quality index of the operation. Seed with too much residual lint is reprocessed; seed with too little has been worked longer than necessary and is more exposed to coat damage. Studies of mechanical and chemical delinting link the delinting intensity to seed

[1]**Corresponding Author** Navruzbek Kurbonov qurbonovnavruzbek2023@gmail.com PhD student, "Tashkent Institute of Irrigation and Agricultural Mechanization Engineers" National Research University, Department of Automation and Control of Technological Processes, Tashkent, Uzbekistan

[2]

germination and vigour (Santos et al., 2026).

The process does not start from a fixed raw material. Biological inputs vary in composition, and process settings that ignore this variability can forfeit much of the attainable revenue (Bourquard et al., 2022). In cotton, breeding for a higher lint percentage has been accompanied by smaller seed and changes in fuzz, and downstream sectors report difficulties in delinting (Maeda et al., 2023). In Uzbekistan the national standard specifies the expected total lint content of ginned seed by variety and industrial grade, from about 12% for grade I of some varieties to more than 17% for grade IV of others.

Most linting in the region is done on 5LP saw linters. Plant surveys report that these machines often run at about half of their rated output because the agitator compacts the seed roll (Norboyev & Sulaymonov, 2023), and recent studies address the seed–saw interaction and the agitator design (Numonov, 2023; Sabirov et al., 2023). The saws also wear, and the condition of the teeth affects both the work done on the seed and the energy needed to remove fibre from them (Yuldashev et al., 2025). In cotton gins, closed-loop control is established mainly for seed cotton moisture (Pelletier et al., 2020). For linting, an optical transducer that measures seed pubescence in the flow has been developed (Gazieva et al., 2022), and a neuro-fuzzy controller tuned by a genetic algorithm has been proposed for the 5LP linter (Kurbonov & Gaziyeva, 2026).

Any feedback controller acts through a bounded input. On a linter the saw-cylinder speed can be raised only until seed damage reaches the permitted limit, so for seed with a high initial lint content, or with worn saws, the target may be out of reach whatever control algorithm is used. This is a question of process operability rather than of controller design. The operability framework introduced by Vinson and Georgakis (2000) compares the set of outputs that a process can achieve with its available inputs (AOS) against the desired output set (DOS) under an expected set of disturbances (EDS), and expresses their overlap as an operability index (de Araujo et al., 2021; Gazzaneo et al., 2020). Recent work has extended the framework with machine-learning surrogates (Alves et al., 2022), dynamic formulations (Dinh & Lima, 2023) and control-structure selection (Alves & Lima, 2024). These applications concern energy and chemical systems; no operability analysis of agricultural post-harvest processing, and of cotton seed linting in particular, has been reported.

The aim of this study is to determine which seed grades can be linted to the regulated residual lint in a single pass of a 5LP linter, and how this region depends on saw wear and seed flow. The contributions are: (i) a steady-state operability model of the linter built from plant measurements, covering the effects of initial lint, seed flow and saw wear; (ii) grade-by-grade feasibility limits obtained with two model forms that bound the extrapolation error; and (iii) a quantitative assessment of flow reduction, the measure taken at the plant when high-lint seed is processed.

Method

Plant, Measurements and Data

Measurements were made in the linting shop of Yangiyo‘l Yog‘-Moy JSC (Uzbekistan) on a 5LP saw linter whose saw cylinder is driven through a frequency converter. Residual lint at the outlet (y) and initial lint at the inlet (x_0) were measured in the seed flow by optical transducers of the type described by Gazieva et al. (2022). Calibration of the output channel against the standard laboratory method gave an expanded uncertainty of 0.15% ($k = 2$). Seed flow Q and saw-cylinder speed n were taken from the plant instrumentation.

Three data sets were used. The static characteristic was obtained at seven speeds from 620

to 800 rpm with three replicates; at each level the process was allowed to settle for 12–15 min, and the mean over 60 s was recorded. An eight-hour record without operator intervention (28,800 samples at 1 s) provided the disturbance channels; over this period x_0 varied from 12.19 to 13.82% and Q from 1905 to 2389 kg/h. Saw wear was followed from the installation of a new saw set to its replacement after 248 h, with 62 static checks at 715 rpm. The process dynamics identified from these records are reported elsewhere (Kurbonov & Maxmarajabov, 2024); only steady-state relations are used here.

Steady-State Process Model

At nominal seed flow (Q_n = 2150 kg/h) and with new saws, the dependence of residual lint on saw speed is described by

$$y_s(n) = a_0 + a_1 \exp\left[\frac{-n - n_{min}}{n_0}\right] \quad (1)$$

with the coefficients given in Table 1 (coefficient of determination 0.9995, largest residual 0.030%). The mean initial lint during these tests, computed as $x_0 = y + S$ from the measured lint yield S, was x_{0n} = 12.95%.

Saw wear moves the characteristic upward and flattens it. Over 247.5 h of operation the residual lint at 715 rpm rose by 1.0 percentage point and the static gain fell by 31.7%. Both effects are represented by linear trends in the coefficients,

$$a_0(t) = a_0 + k_0 t\,, a_1(t) = a_1(1 - \lambda t) \quad (2)$$

where t is the saw operating time. The rate k_0 follows from the measured drift of the operating point, 4.06×10^{-3}% h^{-1} at 715 rpm, after the flattening term is subtracted.

The eight-hour record gave static gains K_x = 0.777%/% for the initial-lint channel and K_Q = 1.155×10^{-3}% per kg/h for the flow channel. These gains were identified over a narrow range of x_0, whereas the grade norms extend well beyond it. Two forms of the initial-lint effect were therefore used. The additive form keeps the measured gain:

$$y_A = y_s(n,t) + K_x(x_0 - x_{0n}) + K_Q(Q - Q_n) \quad (3)$$

The multiplicative form assumes that lint removal is first order in the lint present on the seed, so that the residual lint scales with the initial lint:

$$y_M = y_s(n,t)\frac{x_0}{x_{0n}} + K_Q(Q - Q_n) \quad (4)$$

At the nominal point the local initial-lint gain of (4) is $y_s/x_{0n} \approx 0.53$%/%, lower than the measured 0.777%/%. The two forms thus give a strong and a weak estimate of the penalty that high-lint seed imposes on residual lint. Interaction between n and x_0 was not measured and is neglected. The upper speed limit comes from seed damage: the mass fraction of damaged seed grows linearly with speed and reaches the 5% limit of the national standard (O‘z DSt 597:2016) at about 776 rpm, so n_{max} = 774 rpm was adopted. The lower limit, n_{min} = 616 rpm, is set by the machine design.

Operability Sets and Indicators

The desired output set is the regulated band DOS = [6.70, 7.30]% with the set point y_t = 7.00%. Two available input sets were considered. In scenario A only the saw speed is manipulated and the flow is kept at the nominal 2150 kg/h; the plant tests covered flows of 1850–2420 kg/h. In scenario B the flow may also be reduced to 1850 kg/h, as the plant does when high-lint seed arrives (plant personnel, personal communication). The expected disturbance set contains the initial lint of each grade, taken as the norm ±0.5% (Table 2), and the saw operating time $t \in [0, 248]$ h.

Because y decreases monotonically with n and increases with Q, the achievable output set for a fixed disturbance d is an interval,

$$AOS(d)=\left[y(n_{max},Q_{min},d),y(n_{min},Q_{max},d)\right] \tag{5}$$

and the operability index is

$$OI(d)=\frac{\mu\left[AOS(d)\cap DOS\right]}{\mu(DOS)} \tag{6}$$

where μ denotes interval length (de Araujo et al., 2021). Since the set point lies inside the DOS, the practical question is whether the lower end of AOS(d) reaches y_t. Setting $y(n_{max}, Q, d) = y_t$ in (3) and (4) gives the largest initial lint that can still be brought to the target:

$$x_{0,max}^{A}=x_{0n}+\frac{y_t-y_s(n_{max},t)-K_Q(Q-Q_n)}{K_x} \tag{7}$$

$$x_{0,max}^{M}=x_{0n}\frac{y_t-K_Q(Q-Q_n)}{y_s(n_{max},t)} \tag{8}$$

For each grade, the saw operating time during which $y(n_{max}, Q, d) \le y_t$ holds was obtained from (3) and (4) for both scenarios. The calculations were performed in Python with NumPy.

Table 1. *Model Parameters and Operability Sets of the 5LP Linter*

Parameter	Value	Parameter	Value
a_0, asymptotic residual lint	4.919%	K_x, initial-lint gain	0.777%/%
a_1, amplitude of speed effect	3.488%	K_Q, seed-flow gain	1.155×10^{-3}% per kg/h
n_0, speed scale	168.2 rpm	x_{0n}, nominal initial lint	12.95%
k_0, drift rate of a_0	6.60×10^{-3}% h^{-1}	Q_n, nominal flow	2150 kg/h
λ, flattening rate of a_1	1.281×10^{-3} h^{-1}	DOS; y_t	[6.70, 7.30]%; 7.00%

Note. Coefficients identified from plant data; grade norms of initial lint are given in Table 2.

Results

Figure 1a shows the largest initial lint that a single pass can bring to the target as a function of saw age. With new saws and nominal flow, the 7.00% set point is reachable for x_0 up to 13.83% in the additive form and 14.35% in the multiplicative form; for the upper edge of the regulated band, 7.30%, the limits are 14.22% and 14.97%. The limit falls as the saws wear, by 0.62 percentage points per 100 h in the additive form and by 1.02 in the multiplicative form, and at the end of the saw life (248 h) it reaches 12.30% and 12.07%. The two forms coincide at the nominal initial lint of 12.95%, which the limit reaches after about 142 h.

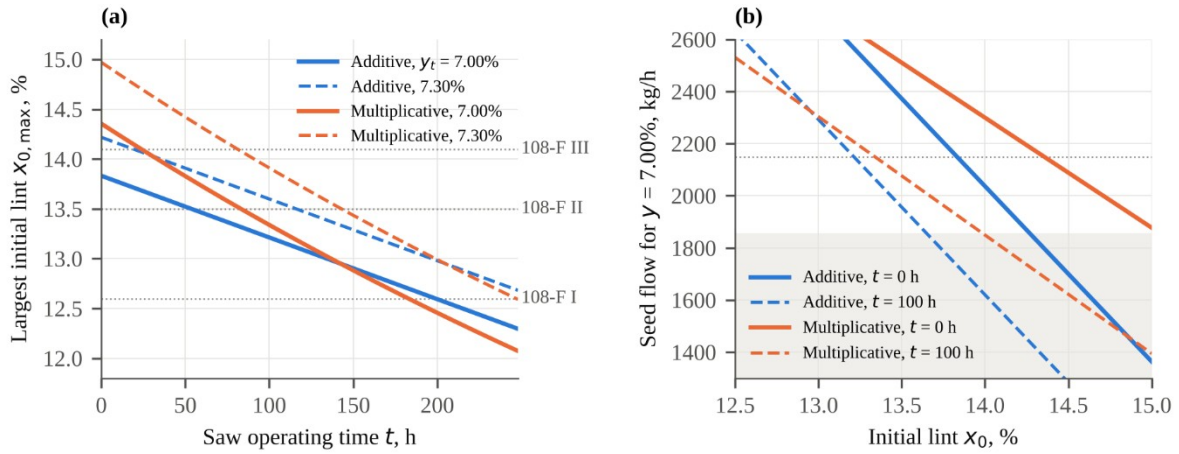


Figure 1. *Operability Limits of the 5LP Linter: (a) Largest Reachable Initial Lint at Nominal Flow; (b) Seed Flow Required for 7.00% Residual Lint*

Table 2 converts these limits into the number of saw operating hours during which each grade can be held at 7.00%. At nominal flow, grade I of the 108-F and Tashkent-1 varieties is held for 183–199 h of the 248 h saw life, grade II for 54–83 h and grade III for at most 24 h. For the 133-F and 138-F varieties only grade I is reachable, and only in the multiplicative form during the first 33 h. Grade IV of 108-F and grades II–IV of 133-F and 138-F are not reachable at any saw age. The operability index gives the same picture: for x_0 = 13.5% it falls from 0.93 with new saws to zero after 124 h, when the whole achievable interval lies above the regulated band.

Table 2. *Saw Operating Hours during Which 7.00% Residual Lint Is Reachable, by Variety and Grade*

Variety	Grade	x_0 norm, %	Hours at Q = 2150 kg/h (A / M)	Hours at Q = 1850 kg/h (A / M)
108-F, Tashkent-1	I	12.6	199 / 183	248 / 248
	II	13.5	54 / 83	126 / 152
	III	14.1	0 / 24	29 / 90
	IV	15.5	0 / 0	0 / 0
133-F, 138-F	I	14.0	0 / 33	45 / 100
	II	14.7	0 / 0	0 / 33
	III	15.5	0 / 0	0 / 0
	IV	17.4	0 / 0	0 / 0
S-4727, 3038	I	12.2	248 / 232	248 / 248
	II	12.8	167 / 159	239 / 232
	III	13.4	70 / 93	142 / 163
	IV	14.0	0 / 33	45 / 100

Reducing the flow moves the limits upward (scenario B). At 1850 kg/h the limit rises by 0.45 percentage points in the additive form and by 0.71 in the multiplicative form, and the reachable time grows to 126–152 h for grade II of 108-F and to 29–90 h for grade III (Table 2). Figure 1b gives the flow needed to reach 7.00% for a given initial lint; the shaded area marks flows below the tested range and the dotted line the nominal flow. With new saws, seed with x_0 = 14.1% requires 1969–2257 kg/h; after 100 h of saw operation it requires 1553–1804 kg/h, which in the additive case lies below the tested flow range. Cutting the flow to 1850 kg/h costs 14% of

throughput.

Discussion

The results separate two causes of off-specification seed that look alike on the plant floor. Inside the operable region, deviations come from disturbances and imperfect tuning and can be removed by feedback; the neuro-fuzzy controller proposed for this linter (Kurbonov & Gaziyeva, 2026) works in this region. Outside it, the saw speed is already at its limit and no controller can bring the seed to the set point. For the 5LP linter the second case is not marginal: at nominal flow, only three of the twelve variety–grade combinations in Table 2 can be held at 7.00% for more than half of the saw life.

This is consistent with reports that 5LP linters seldom reach their rated output (Norboyev & Sulaymonov, 2023): when the seed carries more lint than the machine can remove at the permitted speed, the flow is the only remaining lever, and the plant does reduce it for high-lint seed. Breeding trends that already complicate delinting (Maeda et al., 2023) suggest that this variability of the raw material will not decrease.

In operability terms, the available input set of scenario A is too small for the disturbance set defined by the grade norms; adding the flow as a second input enlarges the achievable set (cf. Alves & Lima, 2024), but at a direct cost in throughput. Three practical measures follow: sorting seed by initial lint before linting and routing high-lint lots to a second pass; planning saw replacement by grade, because a grade II lot needs fresh saws while grade I tolerates most of the saw life; and setting the flow from the measured initial lint rather than by operator judgement.

The analysis rests on gains identified over x_0 = 12.2–13.8% and on one saw set, one variety and one plant. The two model forms bound the extrapolation error, and the main conclusions hold in both, but the figures for grades III and IV are extrapolations and should be confirmed by direct tests. Speed–lint interaction, a grade-dependent damage limit and seed moisture were not included.

Conclusion and Implications

An operability analysis of a 5LP saw linter, built from plant data, shows that with new saws and nominal flow, a single pass brings seed with initial lint up to 13.8–14.4% to 7.00% residual lint, and saw wear lowers this limit by 0.6–1.0 percentage points per 100 h. Only three of twelve variety–grade combinations can be held at the set point for more than half of the saw life, and grade IV of 108-F and grades III–IV of 133-F and 138-F are out of reach even at reduced flow. Reducing the flow to 1850 kg/h extends the limits by 0.45–0.71 percentage points at a 14% loss of throughput. For plants, feedback control of residual lint should therefore be combined with grade-aware planning of seed routing, flow and saw replacement. The extrapolated limits should be verified by direct tests on high-lint seed.

Declarations

Acknowledgments: The author thanks the staff of Yangiyo‘l Yog‘-Moy JSC for access to the linting shop and assistance with the measurements.

Authors' contributions: The author conceived the study, carried out the measurements and modelling, and wrote the manuscript.

Competing interests: The author(s) declared no potential conflicts of interest with respect to the research, authorship, and/or publication of this article.

Funding: This research did not receive any specific grant from funding agencies in the public, commercial, or not-for-profit sectors.

Ethics approval and consent to participate: Not applicable.

Note: This article is derived from the author's doctoral (PhD) dissertation research at the

"Tashkent Institute of Irrigation and Agricultural Mechanization Engineers" National Research University.

Publisher's note: Science and innovation journal remains neutral with regard to jurisdictional claims in published maps and institutional affiliations.

Orcid ID

Navruzbek Kurbonov https://orcid.org/0009-0001-9232-6811
Mirshod Abdullayev https://orcid.org/0000-0001-8539-291X

REFERENCES

1. Alves, V., Gazzaneo, V., & Lima, F. V. (2022). A machine learning-based process operability framework using Gaussian processes. *Computers & Chemical Engineering, 163*, 107835. https://doi.org/10.1016/j.compchemeng.2022.107835
2. Alves, V., & Lima, F. V. (2024). On the selection of control structures using process operability analysis. *Control Engineering Practice, 153*, 106117. https://doi.org/10.1016/j.conengprac.2024.106117
3. Bourquard, B. A., Berenguer, G., Gray, A. W., & Preckel, P. V. (2022). Raw material variability in food manufacturing: A data-driven snack food industry case. *Production & Manufacturing Research, 10*(1), 294–320. https://doi.org/10.1080/21693277.2022.2083030
4. de Araujo, W. R., Lima, F. V., & Bispo, H. (2021). Dynamic and statistical operability of an experimental batch process. *Processes, 9*(3), 441. https://doi.org/10.3390/pr9030441
5. Dinh, S., & Lima, F. V. (2023). Dynamic operability analysis for process design and control of modular natural gas utilization systems. *Industrial & Engineering Chemistry Research, 62*(5), 2052–2066. https://doi.org/10.1021/acs.iecr.2c03543
6. Gazieva, R. T., Yunusova, S. T., & Kurbonov, N. M. (2022). Information converter of seed pubescence based on software tools for the use of improved process control systems of linting. *IOP Conference Series: Earth and Environmental Science, 1043*, 012029. https://doi.org/10.1088/1755-1315/1043/1/012029
7. Gazzaneo, V., Carrasco, J. C., Vinson, D. R., & Lima, F. V. (2020). Process operability algorithms: Past, present, and future developments. *Industrial & Engineering Chemistry Research, 59*(6), 2457–2470. https://doi.org/10.1021/acs.iecr.9b05181
8. Kurbonov, N. M., & Gaziyeva, R. T. (2026). Genetic algorithm optimized ANFIS control for cotton seed linting process. *Development of Science, 1*(2), 82–92.
9. Kurbonov, N., & Maxmarajabov, M. (2024). Dynamic modeling of the cottonseed linting process. *International Journal of Advanced Research in Science, Engineering and Technology, 11*(11), 22509–22513.
10. Maeda, A. B., Dever, J. K., Maeda, M. M., & Kelly, C. M. (2023). Cotton seed size – What is the "fuzz" all about? *Journal of Cotton Science, 27*(2), 81–89. https://doi.org/10.56454/ALQJ7021
11. Norboyev, U., & Sulaymonov, R. (2023). Ways to increase the efficiency of the seed linting process. *E3S Web of Conferences, 434*, 03021. https://doi.org/10.1051/e3sconf/202343403021
12. Numonov, M. (2023). Results of research on the development of a 5LP linter with an improved agitator paddle. *Universum: Technical Sciences*, 4(109). https://doi.org/10.32743/UniTech.2023.109.4.15233
13. O'z DSt 597:2016. (2016). *Technical cottonseed. Specifications. Determination of the mass*

fraction of defects [In Uzbek]. Uzstandard. (DOI yo‘q)

14. O‘z DSt 601:2016. (2016). *Technical cottonseed. Specifications. Methods for determination of pubescence* [In Uzbek]. Uzstandard.
15. Pelletier, M. G., Armijo, C. B., Funk, P. A., Fabian, J. C., & Hardin, R. G., IV. (2020). Cotton ginners handbook: Gin process control. *Journal of Cotton Science, 24*(2), 81–86. https://doi.org/10.56454/BRFU4848
16. Sabirov, I., Akhmedov, D., Khalikov, A., & Madrahimov, D. (2023). Analytical studies of the cotton seed linting process. *E3S Web of Conferences, 452*, 01034. https://doi.org/10.1051/e3sconf/202345201034
17. Santos, M. O., Souza, C. R., Rabelo, A. A. L., David, A. M. S. S., Freitas, H. K. C., Borges, J. B., Santos, J. R. P., & Leles, W. G. S. (2026). Cotton seed delinting: Implications for seed physiological quality. *REMUNOM, 2*(3), 1–19. https://doi.org/10.66104/h2vdxj73
18. Vinson, D. R., & Georgakis, C. (2000). A new measure of process output controllability. *Journal of Process Control, 10*(2–3), 185–194. https://doi.org/10.1016/S0959-1524(99)00045-1
19. Yuldashev, K., Sharipov, K., Mukhsinov, I., Najmitdinov, S., Isaev, S., & Tuhktaev, S. (2025). Enhancing energy efficiency and sustainability in fiber removal from saw teeth during the ginning process. *E3S Web of Conferences, 674*, 01003. https://doi.org/10.1051/e3sconf/202567401003
20. Zahra, L. T., Qadir, F., Khan, M. N., Kamal, H., Zahra, N., Ali, A., Zafar, M. M., Razzaq, A., & Jiang, X. (2024). Seed treatment: An alternative and sustainable approach to cotton seed delinting. *Frontiers in Bioengineering and Biotechnology, 12*, 1376353. https://doi.org/10.3389/fbioe.2024.1376353

DESIGNING AN INTEGRATIVE EDUCATIONAL PLATFORM BASED ON COMPUTER MODELLING: ARCHITECTURE, DATA MODEL AND PEDAGOGICAL LAYER FOR DEVELOPING STUDENTS' DIGITAL COMPETENCE

Mirjalol Ashurov
PhD in Pedagogical Sciences, Associate Professor, Department of Information Technologies and Systems, Higher School of Exact Sciences, Uzbekistan National Pedagogical University named after Nizami, Tashkent, Uzbekistan
E-mail: mirjalol.ashurov007@gmail.com

Abstract.

Purpose. *The study aims to design an educational platform that integrates an information technology course and a chemistry computer modelling course within a single software environment in order to develop the digital competence of chemistry students, and to substantiate its design solutions.*

Methods. *The research followed a design-based research approach and the ADDIE model. The curricula and syllabi of the two courses were analysed, the software tools used in teaching were evaluated against eight criteria, and a system of requirements, an architecture, a relational data model and processing algorithms were developed.*

Results. *None of the existing groups of software tools covered more than 7 of the 16 possible points for the requirements of integrative education. In response, the Raqamli Kompetentlilik ("Digital Competence") platform was designed with a three-layer architecture, an operating algorithm organised in parallel role lanes, a structured data catalogue built on the parameter passport, processing algorithms linked to the database, an experimental comparison tool and a pedagogical layer that supports reflective control.*

Conclusion. *Coordinating parameter input, result processing and comparison within a single environment removes the need to transfer data manually and turns student activity into a measurable digital trace. The proposed design solutions can be adapted to other pairs of courses.*

Keywords: *digital competence; educational platform; computer modelling; integrative approach; software design; data model; chemistry education; design-based research*

1. Introduction

The digital transformation of higher education has qualitatively changed the requirements placed on students: graduates are no longer expected merely to operate particular programs, but to collect and process professional data and to make well-founded decisions on that basis. This ability is captured by the concept of digital competence; the European Union's DigComp 2.2 framework describes it as a set of knowledge, skills and attitudes in the areas of information and data literacy, content creation, problem solving and safety (Vuorikari et al., 2022). In Uzbekistan this direction has been raised to the level of state policy by the "Digital Uzbekistan – 2030" strategy (President of the Republic of Uzbekistan, 2020), and the organisation of the educational process in higher

education has been aligned with the credit-module system and the requirements of digital management (Cabinet of Ministers of the Republic of Uzbekistan, 2020).

For chemistry students, the most meaningful field for digital competence is computer modelling: the student represents a molecule or a reaction in a software environment, performs calculations and compares the results with experimental data. In practice, however, the three core operations of this activity – entering the parameters of a professional process, processing the modelling results and comparing the computed results – are carried out separately in different programs. The student copies results manually from one program to another, most of the time is spent on technical operations rather than on analysis, and the teacher has no means of observing how the student arrives at a conclusion. UNESCO has stressed that the effect of technology in education depends on whether it is chosen in line with pedagogical aims (UNESCO, 2023); it is precisely this alignment that is missing in the case under consideration.

This article presents the results of designing an educational platform aimed at solving this problem. The study addresses three questions: (1) to what extent do the software tools used in teaching chemistry modelling meet the requirements of integrative education; (2) what architecture and data model should a platform have in order to coordinate parameter input, processing and comparison within a single environment; and (3) through which functions does the platform support the pedagogical tasks of developing digital competence?

2. Literature Review

Studies on the design of educational software regard the subordination of technical tools to pedagogical aims as the main requirement. Laurillard (2012) interprets teaching as a design science and argues that technology should be designed on the basis of pedagogical patterns, while Bates (2015) proposes the SECTIONS model for selecting educational media and technologies. Branch (2009) systematised the ADDIE logic of instructional design, comprising the stages of analysis, design, development, implementation and evaluation. In Russian-language pedagogy, Monakhov (1995) proposed designing the educational process by means of a technological map, and Kuznetsov et al. (2009) set out the didactic requirements for educational electronic resources.

The educational value of computer modelling is clearly expressed in Jonassen's (2000) concept of mindtools: modelling programs, spreadsheets and databases do not hand ready-made knowledge to the learner but activate analytical thinking. Mishra and Koehler's (2006) TPACK model shows that technological knowledge is effective only when it is integrated with subject content and pedagogy. Instefjord and Munthe (2017) found that professional digital competence develops more effectively when it is integrated throughout the curriculum rather than confined to a separate course. The author's earlier work examined the combination of the integrative and TPACK approaches (Ashurov, 2026a) and the pedagogical conditions for developing digital competence (Ashurov, 2026b).

Cognitive load theory (Sweller, 1988) and the principles of multimedia learning (Mayer, 2009) provide important guidance for interface design: the learner should be shown only the information required for the current task, and essential information should be highlighted. The technology acceptance model has demonstrated the decisive role of perceived usefulness and ease of use (Davis, 1989; Venkatesh et al., 2003), and Scherer et al. (2019) confirmed this for teachers through a meta-analysis. Research on artificial intelligence tools notes, alongside their potential, a lack of pedagogical perspective (Zawacki-Richter et al., 2019) and risks related to academic integrity (Kasneci et al., 2023).

Doctoral research on educational platforms and software has also been conducted in Uzbekistan: an educational platform for the conditions of digital transformation has been created (Fayziyeva, 2023), integrated software for developing students' professional readiness has been improved (Suropov, 2025), and software for developing the digital information competence of tutors has been developed (Muxamadiyeva, 2026). In these studies software is regarded mainly as a means of organising the educational process and delivering content. A platform that turns the very process of working with professional data – input, processing and comparison – into pedagogically managed activity within the integration of two courses has not yet been created; this gap defines the direction of the present study.

3. Materials and Methods

The study was carried out within a design-based research approach and followed the ADDIE logic (Branch, 2009). At the analysis stage, the curricula and syllabi of the courses "Application of Information Technologies in Professional Activity" and "Computer Modelling in Chemistry" were examined. The software tools named in the documents of the two courses were divided into seven groups, and the four main groups were evaluated against eight criteria derived from the requirements of integrative education. Compliance with each criterion was recorded on a three-point scale: full (2 points), partial (1 point) and none (0 points); thus each group could score a maximum of 16 points. The evaluation was performed by the author on the basis of the programs' documentation and their use in practical classes.

At the design stage, a system of requirements was formulated, a three-layer architecture and an operating algorithm of the platform were developed, a relational data model for computer modelling parameters was built, and the processing algorithms were coded in connection with the database. At the development stage, the platform was implemented under the name Raqamli Kompetentlilik ("Digital Competence") on the www.e-darslar.uz domain. The implementation and evaluation stages belong to separate experimental work, and their results lie outside the scope of this article.

4. Results

4.1. Coverage of Requirements by Existing Software Tools

The evaluation results are shown in Figure 1. None of the four groups covers more than half of the requirements of integrative education. The highest score belongs to data processing tools (MS Excel, Origin, Python, Google Colab), which obtain 7 of 16 points; however, these tools do not accept chemical parameters directly, and data have to be entered into them manually. Chemical drawing and visualisation programs score 1 point, while computational chemistry packages and learning management systems score 3 points each. Pedagogical criteria such as staged tasks and support for self-control are partially present only in learning management systems, but these systems do not work with chemical computation data. In other words, the tools that meet the content requirements do not meet the pedagogical ones, and vice versa.

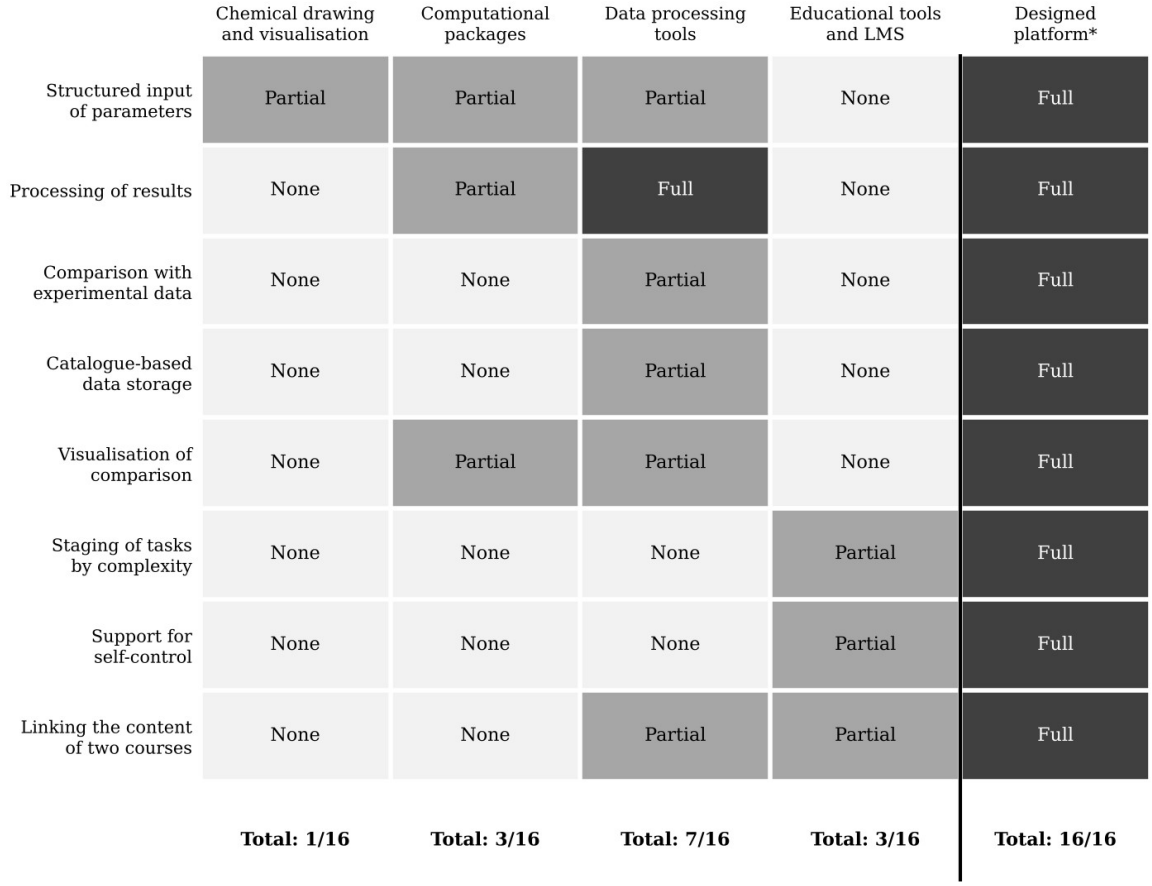


Figure 1. Coverage of the requirements of integrative education by groups of software tools (full = 2, partial = 1, none = 0 points; * according to the design requirements)

An analysis of the workflow confirmed this conclusion: in a simple task in which a molecular geometry is optimised and the result is compared with experimental data, the data are copied manually at least three times – from the modelling program to a spreadsheet, from a reference source to the spreadsheet and from the spreadsheet to the report. On this basis, a system of requirements for the platform was formulated (Table 1).

Table 1. System of requirements for the platform

Group of requirements	Main content
Pedagogical	Sequential unlocking of content; assigning tasks by stages of complexity; showing the aim, theoretical basis and digital skills in each model; self-control tools
Functional	Performing parameter input, computation and processing of results, and comparison of runs on a single model page without manual transfer of data
Data-related	Storing model parameters and results as structured records; indicating the unit of measurement and the range of values for each parameter
Algorithmic	Calculation formulas visible to the student; automatic and reproducible computation of assessment, tests and rating
Integration	Exporting results in CSV format for spreadsheets and Google Colab;

Group of requirements	Main content
	uploading result files obtained in external programs
Ergonomic	Ease of use; highlighting essential information; adaptability to mobile devices
Security and quality	Role-based access rights; each student sees only his or her own results; test answer keys stored hidden on the server; compliance with the requirements for electronic resources

4.2. Architecture and Operating Algorithm

The platform was designed on the basis of a three-layer architecture, and its operating algorithm was represented as parallel lanes by role (Figure 2). The first part is entry and authentication: the student registers and is automatically assigned the student role, and the system identifies the role and directs the user to the corresponding workspace. Two interrelated algorithms operate in the student lane. In the chain of learning resources, the entry test is followed by the lecture, the lecture test, the practical class, the laboratory work and independent study; the first branch point of the algorithm is that the next lecture does not unlock until the test on the previous one has been passed. In the modelling cycle, the student selects a model and enters the parameters; the system computes the indicators and the graph according to the formula, the run is saved and compared with other runs. The second branch point is located here: if the data are not sufficient for a conclusion, the student changes a parameter and repeats the cycle. The teacher lane contains reviewing, grading and commenting on submitted work, and the administrator lane contains content management, role assignment and maintenance of the rating.

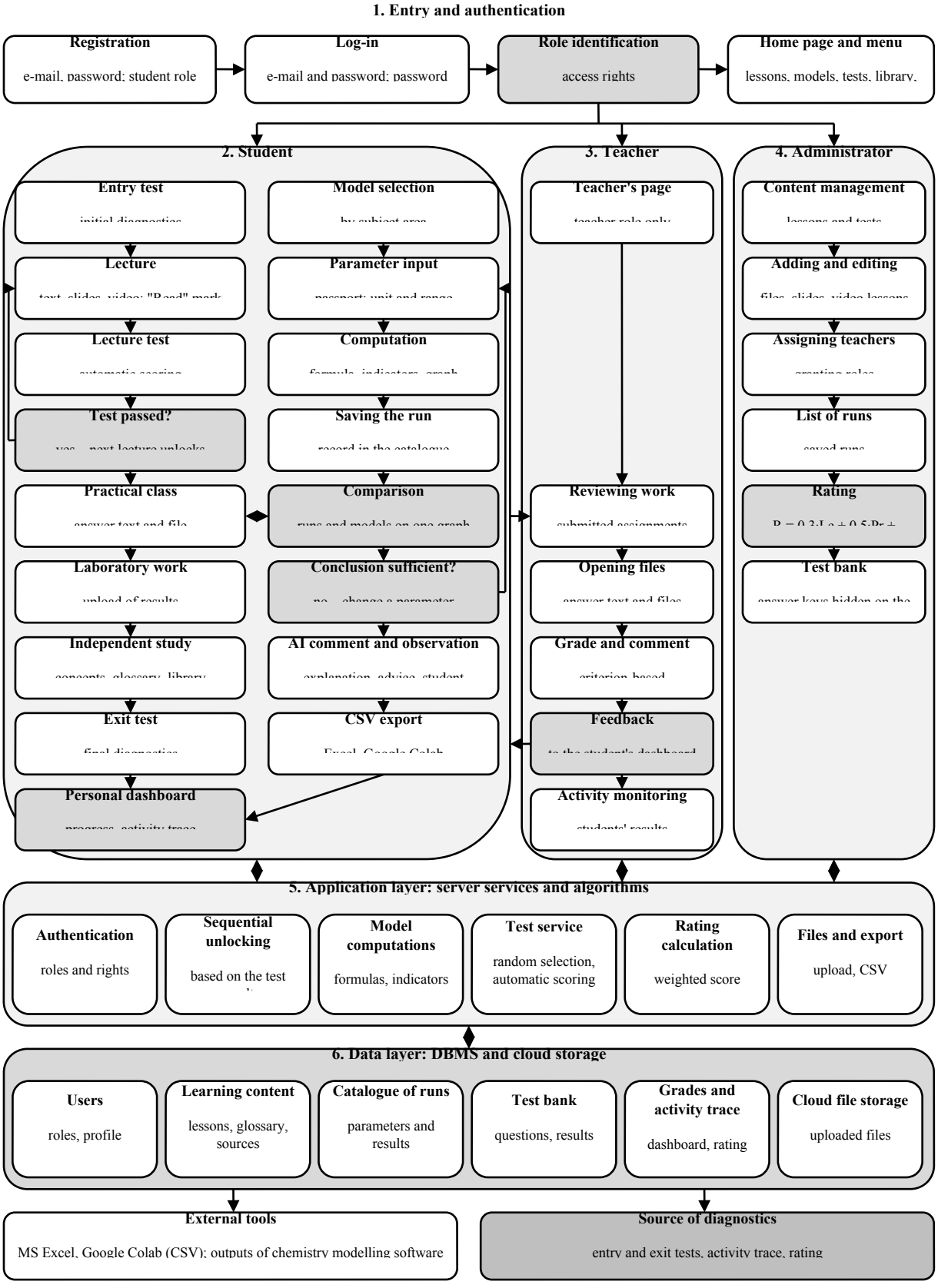


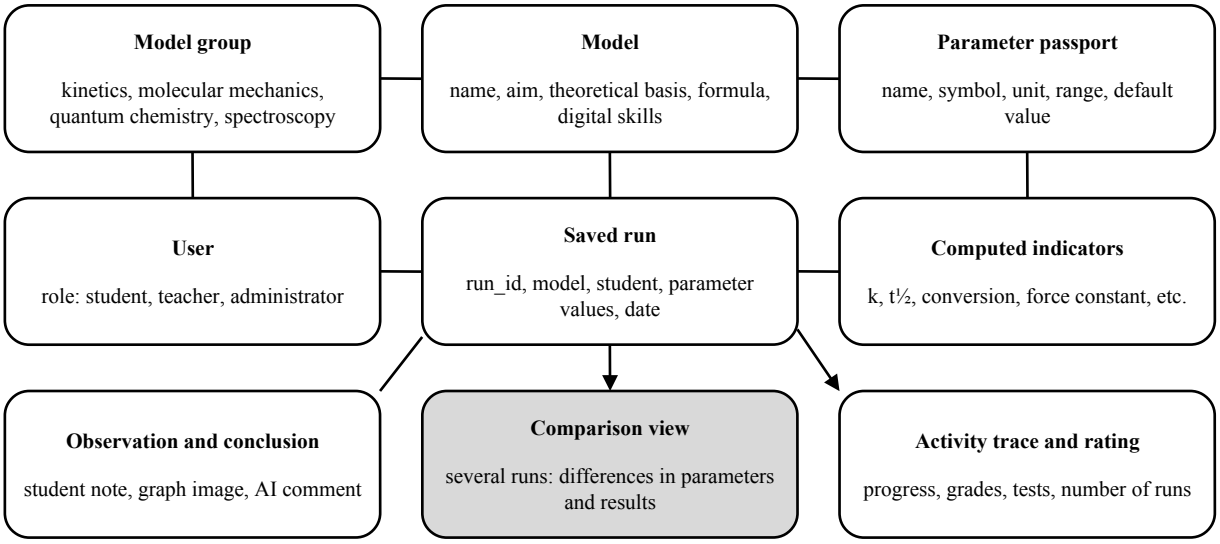
Figure 2. Architecture and operating algorithm of the Raqamli Kompetentlilik platform

The key feature of the architecture is that the functional blocks do not exchange data with one another directly: all of them work with a single database. The model page writes a run to the database, the comparison block reads the saved runs, and the personal dashboard and the rating are calculated from the same records. This solution provides a single software environment, which in

this study is understood as a software space in which the result of each operation of the triad becomes direct input for the next operation and all data are stored in one database. Its operation relies on the principle of data continuity: the student enters a parameter once, and all subsequent calculations, visual representations, exports and assessments are derived automatically from that record.

4.3. Structured Data Catalogue

Computer modelling parameters were systematised into a structured data catalogue (Figure 3). The catalogue was built as a relational model consisting of tables for model groups, models, parameter passports, users, saved runs, computed indicators, observation notes and the activity trace. Its central concept is the parameter passport: the set of attributes defined for representing a property of a chemical object or process within a model – its name, symbol, unit of measurement, range of admissible values and default value. For example, in the reaction kinetics model the student can enter the reaction order, the initial concentration (mol/L), the temperature (°C), the activation energy (kJ/mol) and the Arrhenius pre-exponential factor only in the units and ranges defined in the passport, while the system calculates the rate constant, the half-life and the degree of conversion.



lines denote key-field relations between tables; arrows show data sources for the view and calculations

Figure 3. Relational model of the structured data catalogue of computer modelling parameters

The parameter passport is pedagogically important: encoding a property of an object as a digital parameter requires the student to select the essential property, express it as a quantity and define its unit and limits. The passport embeds these operations in the interface itself, so that encoding becomes part of the structure of the software environment rather than remaining a verbal requirement of the teacher. The saved run is the basic unit of the catalogue; it combines the student, the model, the parameters, the indicators, the graph and the observation note in a single record.

4.4. Processing Algorithms and Comparison

The processing algorithms were coded in connection with the database: their input data and results are stored as structured records, and repeated calculations are performed automatically on the current data in the database (Table 2). At the model level, chemical formulas are recalculated immediately whenever a parameter changes; at the platform level, test scores, progress indicators and the rating are calculated from the saved records. Each model page displays the calculation

formula next to the graph; this transparency allows the student to see how a result was obtained and to check it independently in a spreadsheet by means of a CSV file.

Table 2. Processing algorithms of the platform

Algorithm	Calculation expression or rule	Link with the database	Pedagogical function
Reaction kinetics	k = A·e^(−Ea/RT); for first order $C(t) = C_0 \cdot e^{(-kt)}$, $t_{1/2} = \ln 2/k$	Parameters and results are saved in the run record	Analysing the effect of temperature and activation energy
Potential energy functions	Morse: $V(r) = D_e \cdot (1 - e^{(-a(r - r_e))})^2$; harmonic approximation	Results of the two models are compared in one record	Identifying the limits of a model approximation
Comparison of runs	Relative difference of an indicator of the selected run from the reference run: $\delta = \lvert x_i - x_0 \rvert / \lvert x_0 \rvert \cdot 100\ \%$	Saved runs are retrieved by a query; CSV export	Seeing how a change of parameter affects the result
Selection and scoring of test items	A random set from the item bank; answers are checked against a key hidden on the server	The item bank and results are stored in the database	Objective diagnostics
Sequential unlocking of content	The next lecture unlocks once the test on the previous lecture has been passed	Relies on the test result record	Managing step-by-step mastery
Progress and rating	Overall score based on the set weights of lecture, practical and laboratory activity	A query combining records of grades, tests and runs	Monitoring student activity

The comparison function was designed as an experimental comparison map. It works in two forms: within a model, the student saves several computational runs and views them superimposed on one graph, while indicator cards and a table express the differences numerically; across models, for example, the Morse potential and the harmonic approximation are displayed on one graph, showing that they coincide at small displacements and diverge sharply at large ones. This requires the student to evaluate the result against the criteria of adequacy, accuracy, stability and professional relevance.

4.5. Pedagogical Layer

A pedagogical layer was designed on top of the functional blocks: sequential unlocking of content, lecture tests, an observation note on the model page, comments from the AI assistant, the teacher's grade and comment, and activity indicators in the personal dashboard. The AI assistant performs only an explanatory and advisory function, while the core calculations are carried out on the basis of transparent formulas; this reduces the reliability risks associated with artificial intelligence (Holmes et al., 2019; Kasneci et al., 2023). The student's actions on the platform are

recorded as a digital activity trace: lectures read, tests taken, assignments submitted, runs saved and observation notes are stored in chronological order and linked to their results.

5. Discussion

The results refine, with reference to chemistry modelling education, the conclusions on the need to design educational software from pedagogical aims (Laurillard, 2012; Kuznetsov et al., 2009). The low coverage of the existing tools is explained not by their poor quality but by the fact that they were created for other purposes: computational packages are intended for scientific calculation, and learning management systems for course organisation. The proposed platform does not replace them; computational chemistry operations may still be performed in specialised programs, while the platform brings their results into the pedagogical process and coordinates all three operations of the triad within a single environment.

The design solutions are also consistent with cognitive load theory (Sweller, 1988): owing to data continuity, the student focuses on analysis rather than on technical operations. The transparency of the algorithms reduces the risk that automation will distance the student from the logic of the calculations, and it ensures at the software level the constructive alignment between outcomes, tasks and assessment emphasised by Biggs and Tang (2011). Storing the digital activity trace enables the teacher to give timely feedback; Hattie (2009) ranked feedback among the factors with the strongest influence on learning outcomes.

The study has limitations. First, the software tools were evaluated qualitatively by the author, and this evaluation should be verified through expert assessment. Second, the article presents the design solutions of the platform; its effect on students' digital competence will be evaluated separately in experimental work. Third, the content of the platform is limited to two courses; however, since content is managed from the administrator panel, the architecture can be adapted to other pairs of courses, for example information technology combined with physics or biology.

6. Conclusion

The study found that the software tools used in teaching chemistry computer modelling do not fully meet the requirements of integrative education, and the Raqamli Kompetentlilik educational platform was designed to fill this gap. The main design solutions of the platform – a three-layer architecture with an operating algorithm based on parallel role lanes, a structured data catalogue built on the parameter passport, transparent processing algorithms linked to the database, an experimental comparison tool and a pedagogical layer supporting reflective control – coordinate parameter input, result processing and comparison within a single software environment. Further research will focus on evaluating the platform's effect on students' digital competence through experimental work and on adapting it to other pairs of courses.

REFERENCES

1. Ashurov, M. A. (2026a). Talabalarning raqamli kompetentligini rivojlantirishda integrativ va TPACK yondashuvlar [Integrative and TPACK approaches to developing students' digital competence]. Fizika, matematika va informatika, 2(1), 55–62.
2. Ashurov, M. A. (2026b). Talabalarning raqamli kompetentligini rivojlantirishning didaktik imkoniyatlari va pedagogik shart-sharoitlari [Didactic opportunities and pedagogical conditions for developing students' digital competence]. Pedagogika, (3), 176–179.
3. Bates, A. W. (2015). Teaching in a digital age: Guidelines for designing teaching and learning. Tony Bates Associates Ltd.

4. Biggs, J., & Tang, C. (2011). Teaching for quality learning at university (4th ed.). Open University Press.
5. Branch, R. M. (2009). Instructional design: The ADDIE approach. Springer.
6. Cabinet of Ministers of the Republic of Uzbekistan. (2020). Oliy ta'lim muassasalarida ta'lim jarayonini tashkil etish bilan bog'liq tizimni takomillashtirish chora-tadbirlari to'g'risida [On measures to improve the system of organising the educational process in higher education institutions] (Resolution No. 824). National Database of Legislation. https://lex.uz
7. Davis, F. D. (1989). Perceived usefulness, perceived ease of use, and user acceptance of information technology. MIS Quarterly, 13(3), 319–340.
8. Fayziyeva, M. R. (2023). Raqamli transformatsiya sharoitida ta'lim platformasini yaratish va amaliyotga joriy etish [Creating an educational platform and introducing it into practice under digital transformation] [Abstract of DSc dissertation]. Chirchiq.
9. Hattie, J. (2009). Visible learning: A synthesis of over 800 meta-analyses relating to achievement. Routledge.
10. Holmes, W., Bialik, M., & Fadel, C. (2019). Artificial intelligence in education: Promises and implications for teaching and learning. Center for Curriculum Redesign.
11. Instefjord, E. J., & Munthe, E. (2017). Educating digitally competent teachers: A study of integration of professional digital competence in teacher education. Teaching and Teacher Education, 67, 37–45.
12. Jonassen, D. H. (2000). Computers as mindtools for schools: Engaging critical thinking (2nd ed.). Merrill.
13. Kasneci, E., et al. (2023). ChatGPT for good? On opportunities and challenges of large language models for education. Learning and Individual Differences, 103, 102274.
14. Kuznetsov, A. A., Grigoriev, S. G., & Grinshkun, V. V. (2009). Obrazovatel'nye elektronnye izdaniya i resursy [Educational electronic publications and resources]. Drofa.
15. Laurillard, D. (2012). Teaching as a design science: Building pedagogical patterns for learning and technology. Routledge.
16. Mayer, R. E. (2009). Multimedia learning (2nd ed.). Cambridge University Press.
17. Mishra, P., & Koehler, M. J. (2006). Technological pedagogical content knowledge: A framework for teacher knowledge. Teachers College Record, 108(6), 1017–1054.
18. Monakhov, V. M. (1995). Tekhnologicheskie osnovy proektirovaniya i konstruirovaniya uchebnogo protsessa [Technological foundations of designing and constructing the educational process]. Peremena.
19. Muxamadiyeva, F. I. (2026). Oliy ta'lim muassasalari tyutorlarining raqamli-axborot kompetentligini rivojlantirishning dasturiy ta'minotini takomillashtirish [Improving software for developing the digital information competence of tutors in higher education institutions] [Abstract of PhD dissertation]. Tashkent.
20. President of the Republic of Uzbekistan. (2020). "Raqamli O'zbekiston – 2030" strategiyasini tasdiqlash va uni samarali amalga oshirish chora-tadbirlari to'g'risida [On approval of the "Digital Uzbekistan – 2030" strategy and measures for its effective implementation] (Decree No. PF-6079). National Database of Legislation. https://lex.uz
21. Scherer, R., Siddiq, F., & Tondeur, J. (2019). The technology acceptance model (TAM): A meta-analytic structural equation modeling approach to explaining teachers' adoption of digital technology in education. Computers & Education, 128, 13–35.

22. Suropov, B. M. (2025). Talabalar kasbiy tayyorgarligini rivojlantirishning integratsiyalashgan dasturiy ta’minotini takomillashtirish metodikasi [Methodology for improving integrated software for developing students’ professional readiness] [DSc dissertation]. Tashkent.
23. Sweller, J. (1988). Cognitive load during problem solving: Effects on learning. Cognitive Science, 12(2), 257–285.
24. UNESCO. (2023). Global education monitoring report 2023: Technology in education – A tool on whose terms? UNESCO.
25. Venkatesh, V., Morris, M. G., Davis, G. B., & Davis, F. D. (2003). User acceptance of information technology: Toward a unified view. MIS Quarterly, 27(3), 425–478.
26. Vuorikari, R., Kluzer, S., & Punie, Y. (2022). DigComp 2.2: The digital competence framework for citizens. With new examples of knowledge, skills and attitudes. Publications Office of the European Union.
27. Zawacki-Richter, O., Marín, V. I., Bond, M., & Gouverneur, F. (2019). Systematic review of research on artificial intelligence applications in higher education – where are the educators? International Journal of Educational Technology in Higher Education, 16, 39.

SCIENCE AND INNOVATION
INTERNATIONAL SCIENTIFIC JOURNAL VOLUME 5 ISSUE 5 MAY 2026
ISSN: 2181-3337 | SCIENTISTS.UZ

DEVELOPMENT OF A SUGENO FUZZY LOGIC-BASED CONTROL ALGORITHM FOR ELECTRICAL PULSE TREATMENT OF PLANTS

Mirshod Abdullayev [1,2] **Navruzbek Kurbonov** [2]
[1] Bukhara State Technical University, Department of Automation of Technological Processes and Production, Bukhara, Uzbekistan
[2] "TIIAME" National Research University, Department of Automation and Control of Technological Processes, Tashkent, Uzbekistan

Abstract. *Electrical pulse treatment of plants is a promising technological approach whose effectiveness depends on pulse parameters and the electrical properties of biological tissues. Variations in tissue resistance, conductivity, and physiological condition introduce nonlinear behavior into the treatment process, making accurate regulation challenging. This study aims to develop and evaluate a Sugeno-type fuzzy logic control algorithm for improving the dynamic performance of an electrical pulse treatment system. The proposed controller uses the control error and its rate of change as input variables. Three triangular membership functions are assigned to each input, forming a nine-rule fuzzy inference system. The control algorithm was implemented in MATLAB/Simulink, and its performance was compared with that of a conventional proportional–integral–derivative (PID) controller under identical simulation conditions. The results showed that the fuzzy controller reduced the settling time from 7.65 to 5.12 s, representing an improvement of 33.1%. The steady-state error decreased from 0.001298 to 0.000077, while the integral absolute error decreased from 0.8436 to 0.7209. A small overshoot of 0.114% was observed. These results demonstrate improved transient performance and regulation accuracy compared with conventional PID control. The proposed algorithm provides a foundation for further investigation of maintaining a prescribed disinfection level under variations in plant tissue properties.*

Keywords: *Electrical Pulse Treatment, Fuzzy Logic Control, Sugeno Inference System, Disinfection Level, PID Controller, Plant Tissue Properties, Control Algorithm, MATLAB/Simulink.*

Introduction

The development of efficient and environmentally responsible technologies for protecting agricultural crops against harmful biological agents remains an important challenge in modern agriculture. Electrical pulse treatment has attracted scientific interest as a physical processing method capable of influencing biological tissues through controlled electric fields. Pulsed electric field (PEF) technology has been investigated for cell membrane permeabilization, microbial inactivation, and the improvement of mass transfer processes in biological materials (Ghoshal, 2023; Zhang et al., 2023).

The effectiveness of electrical pulse treatment depends on both the applied electrical parameters and the properties of the treated biological material. Plant tissues exhibit conductive and capacitive behavior associated with cell membranes, intracellular fluids, and intercellular structures. Their electrical response may vary with tissue composition, moisture content, and

physiological condition. Previous studies have highlighted the importance of material properties, electrical field intensity, and treatment conditions in determining the biological effects of pulsed electric fields (Demir et al., 2023; Genovese et al., 2024). Furthermore, investigations involving plant materials have demonstrated the relevance of electrical treatment conditions to microbial inactivation and seed characteristics (Evrendilek et al., 2024), while studies of plant electrical signaling provide additional insight into the complexity of electrical responses in living plant tissues (Barbosa-Caro & Wudick, 2024).

Variations in plant tissue properties may alter the relationship between electrical treatment parameters and the resulting technological effect. Consequently, maintaining a prescribed treatment effectiveness under changing operating conditions represents a challenging control problem. Conventional proportional–integral–derivative (PID) controllers are widely used in automated technological systems because of their simplicity and established tuning procedures. However, controllers with fixed parameters may exhibit reduced performance when applied to nonlinear processes with uncertain or time-varying characteristics.

Fuzzy logic control provides an alternative framework for regulating nonlinear and uncertain systems by using linguistic variables, membership functions, and inference rules. Its applicability to complex dynamic processes has been demonstrated in various engineering applications (Precup et al., 2024). Recent investigations have also explored fuzzy control in pulsed electric field equipment, including food-processing systems (Syamsiana et al., 2025). Although these applications differ from electrical pulse treatment of plants, they demonstrate the feasibility of integrating fuzzy inference methods into automated electrical processing systems.

Among fuzzy inference approaches, Takagi–Sugeno systems offer a suitable structure for implementing nonlinear control relationships through mathematical rule consequents. Research on Takagi–Sugeno control has addressed engineering challenges associated with uncertain parameters and complex process dynamics (Wang et al., 2021). Furthermore, investigations of Takagi–Sugeno–Kang fuzzy systems have emphasized the importance of balancing rule-base complexity, interpretability, and computational requirements (Zhang et al., 2024). These considerations support the investigation of compact fuzzy control structures for agricultural electrical treatment processes.

Despite progress in electrical pulse processing and intelligent control methods, maintaining a prescribed disinfection level under variations in plant tissue properties remains a process-specific challenge. Existing investigations provide valuable information on biological responses to pulsed electric fields and fuzzy control methodology, but they do not directly establish the dynamic performance of a Sugeno controller for the particular electrical pulse treatment system considered in this study.

The objective of this research is to develop a Sugeno-type fuzzy logic control algorithm and evaluate its dynamic performance in comparison with a conventional PID controller. The proposed controller uses the regulation error and its rate of change as input variables, with three triangular membership functions assigned to each input and a nine-rule inference base. The control systems are implemented in MATLAB/Simulink and evaluated using settling time, overshoot, steady-state error, and integral performance indices. The study aims to establish a simulation-based foundation for further investigation of disinfection-level regulation under variations in plant tissue electrical properties.

Method

The present study employed mathematical modeling, fuzzy inference, and comparative

simulation to develop and evaluate a control algorithm for the electrical pulse treatment of plants. The methodological framework was based on a closed-loop control system in which the control action is adjusted according to deviations between the reference signal and the modeled process response. A Sugeno-type fuzzy logic controller was designed and compared with a conventional proportional–integral–derivative (PID) controller.

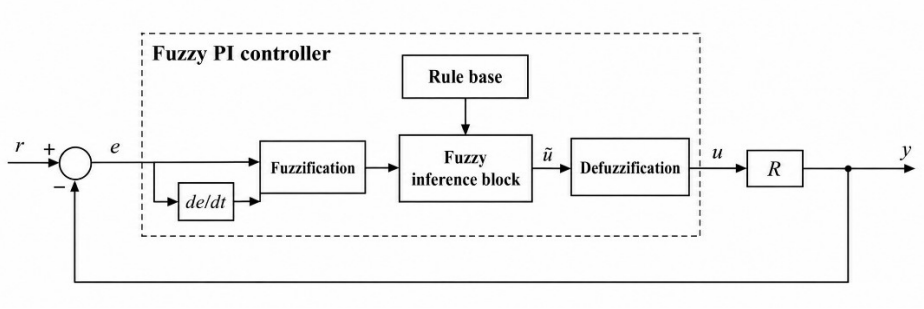


Figure 1. *Structure of the Sugeno Fuzzy Controller*

The selection of a compact 3×3 fuzzy rule structure was motivated by the need to represent nonlinear relationships between the control error, its rate of change, and the resulting control action without introducing an unnecessarily large rule base. Previous research has highlighted the importance of balancing fuzzy system complexity, computational requirements, and interpretability (Zhang et al., 2024). In the present study, nine inference rules were employed to describe the controller response over the selected linguistic input domains.

The research methodology involved the mathematical description of the controlled process, formulation of the regulation error, development of membership functions and fuzzy inference rules, implementation of the control algorithms in MATLAB/Simulink, and evaluation of their dynamic characteristics. The use of fuzzy inference was motivated by the nonlinear behavior and variable electrical properties of biological tissues, which may affect the response of an electrical treatment system (Precup et al., 2024; Zhang et al., 2023).

Mathematical Description of the Controlled Process

The electrical pulse treatment process was considered a dynamic control object whose response depends on the applied electrical influence and the properties of the treated plant tissues. Changes in tissue resistance, conductivity, and physiological conditions may alter the relationship between the control action and the resulting treatment effectiveness.

The general behavior of the controlled process can be represented as

$$\dot{x}(t)=f(x(t),u(t),p(t)) \quad (1)$$

$$y(t)=g(x(t),p(t)) \quad (2)$$

where ẋ(t) is the rate of change of the state vector; x(t) is the state vector of the controlled object; u(t) is the control action; p(t) represents variable process parameters; y(t) is the modeled output; and f and g describe the process dynamics and output relationship, respectively.

Equations (1) and (2) provide a general representation of the nonlinear process rather than an independently identified state-space model. The response of the control system was examined using the simulation model developed for the electrical pulse treatment process.

The regulation error was defined as

$$e(t)=r(t)-y(t) \quad (3)$$

where r(t) denotes the prescribed reference signal and y(t) represents the actual or simulated response of the controlled object.

The rate of change of the control error was expressed as

$$\dot{e}(t)=\frac{de(t)}{dt} \tag{4}$$

These two signals were selected as the input variables of the proposed fuzzy controller.

Design of the Sugeno Fuzzy Logic Controller

A Sugeno-type fuzzy logic controller was developed to determine the control action based on the magnitude and variation of the regulation error. The controller consists of input normalization, fuzzification, a rule base, a fuzzy inference mechanism, output calculation, and control signal scaling.

The input vector was defined as

$$z(t)=\begin{bmatrix} e(t) \\ \dot{e}(t) \end{bmatrix} \tag{5}$$

To ensure compatibility with the fuzzy inference system, the input signals were normalized using scaling coefficients:

$$e_n(t)=K_e e(t) \tag{6}$$

$$\dot{e}_n(t)=K_{de}\dot{e}(t) \tag{7}$$

where K_e and Kde are the input scaling coefficients.

Three linguistic terms were assigned to each input variable:

- N — Negative;
- Z — Zero;
- P — Positive.

Triangular membership functions were selected to represent these linguistic variables. In general, the triangular membership function is expressed as

$$\mu(x;a,b,c)=\begin{cases} 0, & x\le a \\ \dfrac{x-a}{b-a}, & a<x\le b \\ \dfrac{c-x}{c-b}, & b<x<c \\ 0, & x\ge c \end{cases} \tag{8}$$

Here, a, b, and c are the parameters defining the triangular membership function.

The combination of three linguistic terms for the regulation error and three terms for its rate of change results in a fuzzy inference system containing nine rules.

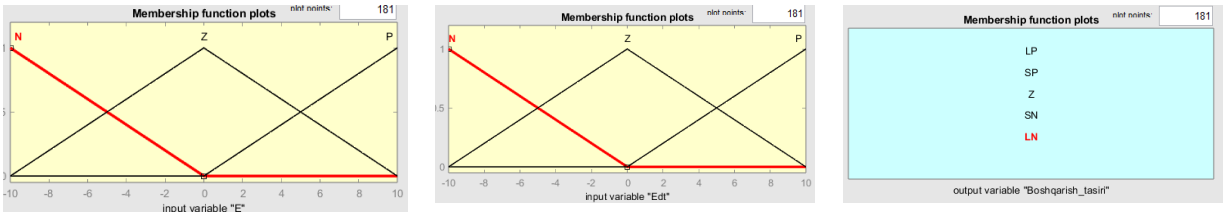


Figure 2. *Input Membership Functions*

Development of the Fuzzy Rule Base

The fuzzy rule base was formulated to establish the relationship between the regulation error,

its rate of change, and the required control action.

Five linguistic categories were used to describe the direction and magnitude of the control response:

NL — Negative Large; NM — Negative Medium; Z — Zero; PM — Positive Medium; and PL — Positive Large.

The rule base was constructed according to the combinations of the normalized input variables.

Table 1. *Fuzzy Rule Base of the Proposed Controller*

Error (e)	ė = P	ė = Z	ė = N
N	Z	NM	NL
Z	PM	Z	NM
P	PL	PM	Z

Each rule relates a particular combination of input linguistic states to a corresponding control response. For example, a positive regulation error with a positive rate of change corresponds to a positive large control response, whereas a negative error with a negative rate of change corresponds to a negative large response.

The general structure of the fuzzy rules is expressed as follows:

Rule i: If the regulation error is A_i and the rate of change of the error is B_i, then the control response is determined by the corresponding rule consequent.

For a zero-order Sugeno inference system, the numerical consequent of each rule may be represented by a constant c_i. The normalized control output can then be calculated using the weighted-average relationship.

$$\hat{u}(t)=\frac{\sum_{i=1}^{9} w_i(t)c_i}{\sum_{i=1}^{9} w_i(t)} \tag{9}$$

where $w_i(t)$ is the firing strength of the i-th rule and c_i is its numerical consequent.

For the product inference operator, the firing strength is defined as

$$w_i(t)=\mu_{A_i}(e_n(t))\mu_{B_i}(\dot{e}_n(t)) \tag{10}$$

The calculated normalized output is subsequently transformed into the control action through the output scaling coefficient:

$$u(t)=K_u\hat{u}(t) \tag{11}$$

The numerical values assigned to the linguistic consequents depend on the selected implementation of the Sugeno inference system.

Comparative PID Control System

A conventional PID controller was employed as a reference system for evaluating the dynamic characteristics of the proposed fuzzy controller.

The continuous-time PID control law is expressed as

$$u_{PID}(t)=K_p e(t)+K_i\int_0^t e(\xi)d\xi+K_d\frac{de(t)}{dt} \tag{12}$$

where K_p, K_i, and Kd represent the proportional, integral, and derivative gains, respectively.

The PID and Sugeno controllers were evaluated using the same controlled process model and reference input. This approach allowed the differences in their simulated dynamic behavior to be examined under equivalent conditions.

MATLAB/Simulink Modeling

The control systems were implemented in MATLAB/Simulink. Two feedback control configurations were considered: a conventional PID control loop and a Sugeno-type fuzzy control loop.

Both configurations included the prescribed reference signal, a comparison element for calculating the regulation error, the corresponding controller, the modeled control object, and a feedback path.

In the Sugeno control configuration, the regulation error and its rate of change were supplied to the fuzzy inference system. The controller generated the control action according to the developed membership functions and nine-rule inference base.

The simulation models were used to investigate the transient responses of both control systems under a common reference input. The resulting output trajectories served as the basis for the comparative evaluation.

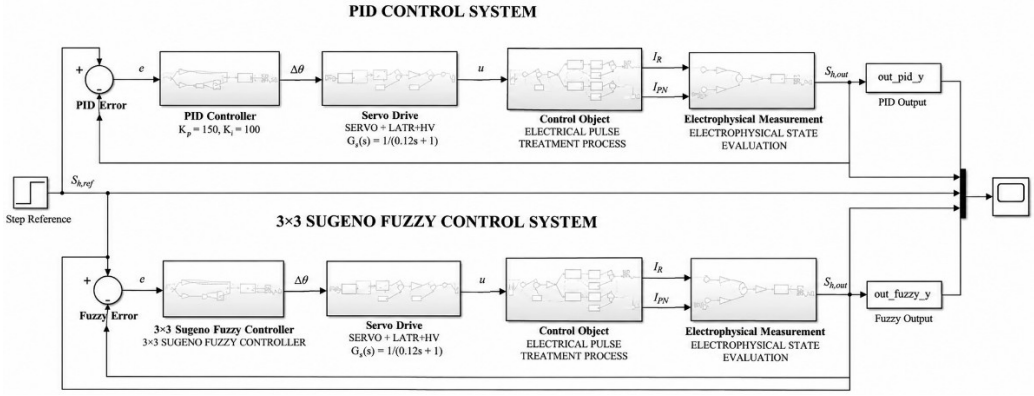


Figure 3. *MATLAB/Simulink Control System Model*

Evaluation of Control Performance

The dynamic performance of the proposed fuzzy controller was assessed using settling time, overshoot, steady-state error, integral absolute error (IAE), and integral squared error (ISE).

The steady-state error was defined as

$$e_{ss} = \lim_{t \to \infty} \left| r(t) - y(t) \right| \tag{13}$$

The integral absolute error was calculated as

$$IAE = \int_0^T \left| e(t) \right| dt \tag{14}$$

while the integral squared error was determined using

$$ISE = \int_0^T e^2(t)\, dt \tag{15}$$

where T denotes the evaluation interval.

Settling time was used to characterize the time required for the system response to enter and remain within a prescribed tolerance band around its final value. Overshoot was used to evaluate the maximum transient deviation above the reference level.

The comparative assessment of these indicators was used to determine the differences in regulation accuracy and transient performance between the conventional PID controller and the developed Sugeno fuzzy controller.

Results or Findings

The dynamic performance of the developed Sugeno-type fuzzy logic controller was evaluated through comparative simulations in MATLAB/Simulink. The proposed 3×3 Sugeno fuzzy controller and the conventional PID controller were tested using the same controlled object and reference input. The comparison focused on the transient response, settling time, overshoot, steady-state error, and integral performance indices.

The simulated transient responses of the two control systems are presented in Figure 4. The reference signal was changed from its initial value of approximately 0.32 to 0.70 at (t=1) s. Both controllers provided stable tracking responses and approached the prescribed reference value. However, the Sugeno fuzzy controller reached the reference level more rapidly than the conventional PID controller.

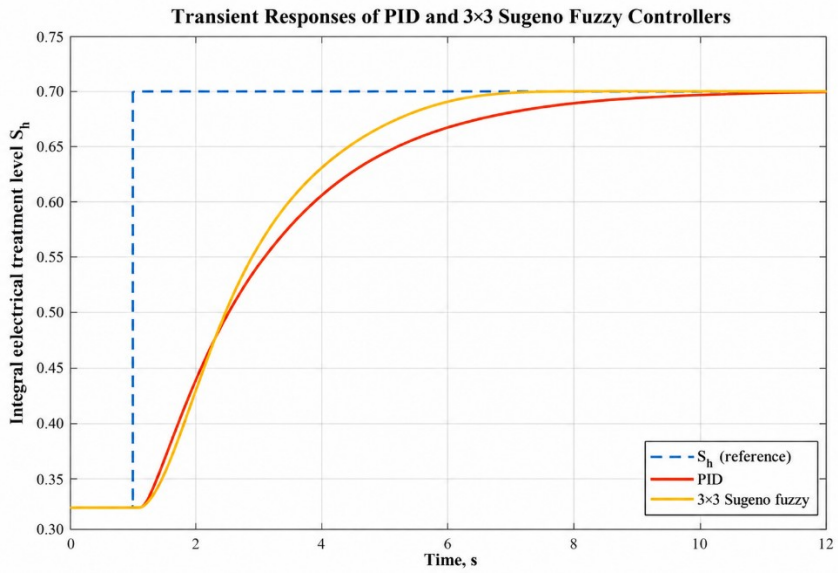


Figure 4. *Comparative Transient Responses of PID and 3×3 Sugeno Fuzzy Controllers*

The quantitative comparison of the dynamic performance indicators is presented in Table 2.

Table 2. *Comparison of Dynamic Performance Indicators of PID and Sugeno Fuzzy Controllers*

Performance Indicator	PID Controller	Sugeno Fuzzy Controller
Settling time, s	7.65	5.12
Overshoot, %	0	0.1137
Steady-state error	0.001298	0.000077
Integral absolute error (IAE)	0.8436	0.7209
Integral squared error (ISE)	0.1824	0.1761

As shown in Table 2, the settling time of the conventional PID controller was 7.65 s, whereas the Sugeno fuzzy controller achieved a settling time of 5.12 s. This corresponds to a reduction of approximately 33.1%, indicating an improvement in the response speed of the control system.

The steady-state error decreased from 0.001298 for the PID controller to 0.000077 for the Sugeno fuzzy controller, representing a reduction of approximately 94.1%. This result indicates that the proposed fuzzy controller achieved more accurate reference tracking under the investigated simulation conditions.

The integral performance indicators also improved. The IAE decreased from 0.8436 to 0.7209, corresponding to a reduction of approximately 14.5%. Similarly, the ISE decreased from 0.1824 to 0.1761, representing an improvement of approximately 3.5%. These results demonstrate a reduction in the accumulated tracking error over the evaluated simulation interval.

The PID controller exhibited no overshoot, whereas the Sugeno fuzzy controller produced a small overshoot of 0.1137%. Despite this difference, the fuzzy controller demonstrated faster settling and lower steady-state and integral errors.

Overall, the comparative simulation results indicate that the developed Sugeno fuzzy controller provides improved dynamic performance and reference-tracking accuracy compared with the conventional PID controller. The observed improvements support the applicability of the proposed nine-rule fuzzy control structure to the modeled electrical pulse treatment system. However, the results represent the behavior of the simulated controlled variable and do not independently establish disinfection-level stability under variations in plant tissue properties.

Discussion

The comparative simulation results indicate that the developed Sugeno-type fuzzy controller provides improved dynamic performance compared with conventional PID control under the investigated operating conditions. As presented in Table 2 and Figure 4, the settling time decreased from 7.65 to 5.12 s, representing a reduction of 33.1%. The steady-state error decreased by approximately 94.1%, while the integral absolute error (IAE) and integral squared error (ISE) were reduced by 14.5% and 3.5%, respectively. Although the fuzzy controller exhibited a small overshoot of 0.1137%, its overall transient response and reference-tracking accuracy were improved.

The observed differences can be attributed, in part, to the nonlinear rule-based relationship between the regulation error, its rate of change, and the generated control action. The nine-rule Sugeno inference structure enables different corrective responses according to the operating state without requiring a large rule base. This approach is consistent with the broader application of fuzzy control to nonlinear engineering systems (Precup et al., 2024). Research on Takagi–Sugeno systems has also emphasized the importance of addressing parameter uncertainty and managing model complexity (Wang et al., 2021; Zhang et al., 2024).

The findings are relevant to previous investigations combining fuzzy logic with electrical pulse processing. Syamsiana et al. (2025) demonstrated the feasibility of fuzzy-based regulation in pulsed electric field equipment for food-processing applications. The present study extends this general control approach to a modeled electrical pulse treatment system for plants, focusing on the comparative dynamic characteristics of PID and Sugeno controllers. However, differences in the treated biological materials and controlled variables prevent direct quantitative comparison of their performance.

An important limitation of the present research is that the comparative simulations were conducted using a common plant model and reference signal. Therefore, the reported improvements demonstrate better reference tracking within the investigated model but do not independently establish robust disinfection-level control under varying plant tissue properties. Furthermore, the relationship between the modeled integral electrical treatment level and the actual biological disinfection degree requires explicit validation.

Future investigations should evaluate the controller under changes in tissue resistance, conductivity, and other relevant process parameters. Experimental verification of treatment effectiveness and sensitivity analysis would provide stronger evidence of the algorithm's practical

applicability. Such investigations are necessary to determine whether the developed fuzzy control system can maintain the prescribed disinfection level under variable biological and environmental conditions.

Conclusion and Implications

This study presented the development and simulation-based evaluation of a Sugeno-type fuzzy logic control algorithm for an electrical pulse treatment system intended to regulate treatment effectiveness in plants. The proposed controller was designed using the regulation error and its rate of change as input variables. Three triangular membership functions were assigned to each input, and a nine-rule fuzzy inference system was developed to generate corrective control actions.

The comparative analysis performed in MATLAB/Simulink demonstrated improvements in the dynamic characteristics of the fuzzy-controlled system compared with conventional PID regulation. The settling time decreased from 7.65 s to 5.12 s, corresponding to a reduction of approximately 33.1%. The steady-state error was reduced from 0.001298 to 0.000077, while the integral absolute error decreased from 0.8436 to 0.7209. A small overshoot of approximately 0.114% was observed in the fuzzy control system.

These findings indicate that the proposed Sugeno controller provides improved transient response characteristics and regulation accuracy under the investigated simulation conditions. The developed algorithm demonstrates the potential of fuzzy inference methods for controlling nonlinear electrical treatment processes and provides a methodological basis for further development of intelligent agricultural automation systems.

The principal practical implication of the study is the possibility of employing the proposed algorithm as part of a feedback control system for electrical pulse treatment. However, the ability to maintain a prescribed disinfection level under varying plant tissue electrical properties requires further verification through parameter-variation studies and experimental testing. Future research should therefore focus on evaluating controller robustness, incorporating measurable indicators of plant condition, and validating the relationship between the regulated process response and actual biological disinfection effectiveness.

Declarations

Acknowledgments: Not applicable.

Authors' contributions: M.A. contributed to the conceptualization, mathematical modeling, development of the fuzzy control algorithm, simulation analysis, and preparation of the manuscript.

Competing interests: "The author(s) declared no potential conflicts of interest with respect to the research, authorship, and/or publication of this article."

Funding: This research did not receive any specific grant from funding agencies in the public, commercial, or not-for-profit sectors.

Ethics approval and consent to participate: This simulation-based study did not involve human participants.

Note: This article is based on the doctoral dissertation research entitled "Control Models and Algorithms for Electrical Pulse Treatment of Plants."

Publisher's note: Science and Innovation remains neutral with regard to jurisdictional claims in published maps and institutional affiliations.

Orcid ID

Mirshod Abdullayev https://orcid.org/0000-0001-8539-291X

Navruzbek Kurbonov https://orcid.org/0009-0001-9232-6811

REFERENCES

1. Barbosa-Caro, J. C., & Wudick, M. M. (2024). Revisiting plant electric signaling: Challenging an old phenomenon with novel discoveries. Current Opinion in Plant Biology, 79, 102528. https://doi.org/10.1016/j.pbi.2024.102528
2. Demir, E., Tappi, S., Dymek, K., Rocculi, P., & Gómez Galindo, F. (2023). Reversible electroporation caused by pulsed electric field – Opportunities and challenges for the food sector. Trends in Food Science & Technology, 139, Article 104120. https://doi.org/10.1016/j.tifs.2023.104120
3. Evrendilek, G. A., Atmaca, B., & Uzuner, S. (2024). Corn processing by pulsed electric fields with respect to microbial inactivation and improvement of seed vigour. Computers and Electronics in Agriculture, 219, 108830. https://doi.org/10.1016/j.compag.2024.108830
4. Genovese, J., Rocculi, P., Miklavčič, D., & Mahnič-Kalamiza, S. (2024). The forgotten method? Pulsed electric field thresholds from the perspective of texture analysis. Food Research International, 176, 113869. https://doi.org/10.1016/j.foodres.2023.113869
5. Ghoshal, G. (2023). Comprehensive review on pulsed electric field in food preservation: Gaps in current studies for potential future research. Heliyon, 9(6), Article e17532. https://doi.org/10.1016/j.heliyon.2023.e17532
6. Precup, R.-E., Nguyen, A.-T., & Blažič, S. (2024). A survey on fuzzy control for mechatronics applications. International Journal of Systems Science, 55(4), 771–813. https://doi.org/10.1080/00207721.2023.2293486
7. Syamsiana, I. N., Amrullah, M. W. F., Rizza, M. A., Nurwicaksana, W. A., Irfin, Z., Putri, R. I., & Rahmad, C. (2025). Empowering small-scale industries food safety: Designing fuzzy controlled pulse electric field pasteurization. Food Chemistry Advances, 6, Article 100875. https://doi.org/10.1016/j.focha.2024.100875
8. Wang, Y., Zou, L., Ma, L., Zhao, Z., & Guo, J. (2021). A survey on control for Takagi-Sugeno fuzzy systems subject to engineering-oriented complexities. Systems Science & Control Engineering, 9(1), 334–349. https://doi.org/10.1080/21642583.2021.1907259
9. Zhang, C., Lyu, X., Arshad, R. N., Aadil, R. M., Tong, Y., Zhao, W., & Yang, R. (2023). Pulsed electric field as a promising technology for solid foods processing: A review. Food Chemistry, 403, Article 134367. https://doi.org/10.1016/j.foodchem.2022.134367
10. Zhang, Y., Wang, G., Zhou, T., Huang, X., Lam, S., Sheng, J., Choi, K. S., Cai, J., & Ding, W. (2024). Takagi-Sugeno-Kang fuzzy system fusion: A survey at hierarchical, wide and stacked levels. Information Fusion, 101, 101977. https://doi.org/10.1016/j.inffus.2023.101977

MORPHOLOGY AND ELEMENTAL COMPOSITION OF A MULTICOMPONENT EPITAXIAL LAYER IN THE SI–GAP–ZNSE–ZNTE SYSTEM GROWN ON A GAP(100) SUBSTRATE BY LIQUID-PHASE EPITAXY

A.S. Saidov – Leading Research Scientist, Doctor of Physical and Mathematical Sciences (DSc), Professor. ORCID: https://orcid.org/0000-0002-9124-6430
Sh.N. Usmonov – Head of Laboratory, Doctor of Physical and Mathematical Sciences (DSc), Professor. ORCID: https://orcid.org/0000-0001-7683-0017
D.V. Saparov – Senior Research Scientist, Doctor of Philosophy (PhD) in Physics and Mathematics. ORCID: https://orcid.org/0000-0002-9282-9048
H.Sh. Abdullayev – PhD Student. ORCID: https://orcid.org/0009-0001-5080-6841
E-mail: habibabdullayev04@gmail.com

Abstract. *This study investigates the surface morphology, elemental composition, and spatial homogeneity of a multicomponent epitaxial layer in the Si–GaP–ZnSe–ZnTe system grown on a single-crystal GaP(100) substrate from a tin-based melt by liquid-phase epitaxy (LPE). The melt was prepared from Sn, Si, GaP, ZnSe, and ZnTe, with Al added to improve substrate wetting. Crystallization was performed from a confined melt volume by cooling from 850 to 750 °C at 1 °C/min, producing an approximately 10 μm-thick layers. Surface and cross-sectional morphologies were examined by scanning electron microscopy (SEM), while elemental concentrations and spatial distributions were analyzed by energy-dispersive X-ray spectroscopy (EDS). SEM images revealed a continuous surface without visible large cracks or morphological discontinuities. Cross-sectional observations showed a clearly distinguishable layer–substrate interface and a continuous layer in intimate contact with the substrate. Elemental maps detected signals from Si, Ga, P, Zn, Se, and Te across the examined region. The weaker Ga signal in the grown layer than in the substrate was consistent with a difference in elemental composition. EDS spectral segmentation showed that the dominant P1 component accounted for 99.93% of the analyzed pixels, while P2 and P3 together represented only 0.07%. The average atomic concentrations of Si, Ga, P, Zn, Se, and Te were 26.5, 7.3, 35.2, 15.3, 11.6, and 4.1 at.%, respectively. The summed concentrations of the (Si + Ga + Zn) and (P + Se + Te) groups were 49.1 and 50.9 at.%, respectively, giving a ratio close to 1:1. These findings indicate the formation of a multicomponent layer on GaP with a composition substantially different from that of the substrate and no pronounced chemical segregation detectable at the micrometer scale.*

Keywords: *liquid-phase epitaxy, GaP, Si–GaP–ZnSe–ZnTe, multicomponent epitaxial layer, SEM–EDS, surface morphology, elemental composition, spatial homogeneity.*

I. Introduction

The performance and reliability of microelectronic and optoelectronic devices depend on the structural perfection, stoichiometric composition, chemical purity, and spatial homogeneity of epitaxial layers (Hite, 2023; Yan & Li, 2024). The integration of III–V and II–VI semiconductor compounds with silicon technology enables the development of multifunctional materials with

tunable electronic and optical properties. However, differences in crystal lattice parameters, chemical bonding, and thermal expansion coefficients may lead to the development of mechanical stresses and the formation of structural defects (Du et al., 2022; Zeng et al., 2023). In such systems, liquid-phase epitaxy (LPE) is considered an effective growth technique (Mauk, 2023; Saidov et al., 2025), enabling control over layer thickness, composition, and structural quality at relatively low temperatures by adjusting the melt composition and crystallization conditions (Pan et al., 2025; Pan et al., 2026).

During LPE, the formation of epitaxial layers is governed by the thermodynamic state of the melt and the kinetics of crystallization. Supersaturation of the melt provides the thermodynamic driving force for crystallization, arising from the difference in chemical potential between the liquid and solid phases. Temperature and cooling rate influence the solubility, diffusion, and interfacial partitioning of the constituent species, thereby affecting the layer composition, growth rate, and surface morphology. Optimization of these parameters plays an important role in suppressing the formation of secondary phases and maintaining the stability of the crystallization front (Pan et al., 2026; Saidov et al., 2025).The aim of this study was to grow a multicomponent Si–GaP–ZnSe–ZnTe epitaxial layer on a GaP substrate from a tin-based melt using LPE and to investigate its surface morphology and elemental composition.

II. Materials and Methods

The epitaxial layers were grown using an automated vertical LPE system equipped with three independently controlled heating zones. Prior to growth, the quartz reactor was evacuated using a roughing vacuum pump to remove atmospheric gases and subsequently filled with hydrogen purified through the “Palladiy-15” purification system. During the growth process, a low flow of hydrogen was maintained at atmospheric pressure.

The melt was prepared from Sn (80 g), Si (0.55 g), GaP (1.90 g), ZnSe (1.20 g), and ZnTe (1.50 g). Tin (Sn) served as the primary solvent. To improve the wettability of the substrate by the melt and ensure continuous contact at the crystallization interface, 0.2 g of Al was added to the melt.

Tellurium-doped n-type GaP(100) single crystals with a diameter of 2 cm were used as substrates. The GaP substrate was selected because of its structural compatibility with the GaP component of the epitaxial layer, as crystallographic compatibility at the heterointerface plays an important role in epitaxial growth (Kafi et al., 2024; Saidov et al., 2023). The substrates were positioned horizontally in a graphite cassette with a spacing of 1 mm between them. This configuration reduces convection within the confined melt volume and promotes predominantly diffusion-driven transport of the constituent species toward the crystallization front.

The melt was heated to 850 °C and maintained at this temperature for 40 min to promote the dissolution and homogeneous distribution of the constituent components. Subsequently, the graphite cassette containing the substrates was immersed in the melt, allowing the space between the substrates to be filled with the liquid phase. After the cassette was withdrawn from the bulk melt, crystallization proceeded from the confined volume of melt retained between the substrates.

Crystallization was carried out by cooling the melt from 850 to 750 °C at a rate of 1 °C/min. The supersaturation induced by cooling provided the thermodynamic driving force for crystallization. The selected cooling rate was intended to balance the degree of supersaturation and diffusive mass transport while limiting secondary nucleation and morphological irregularities. Epitaxial layers based on the Si–ZnSe–GaP system have previously been grown using a similar

liquid-phase epitaxy technique (Razzokov et al., 2023). As a result, an epitaxial layer approximately 10 μm thick was obtained on the GaP substrate.

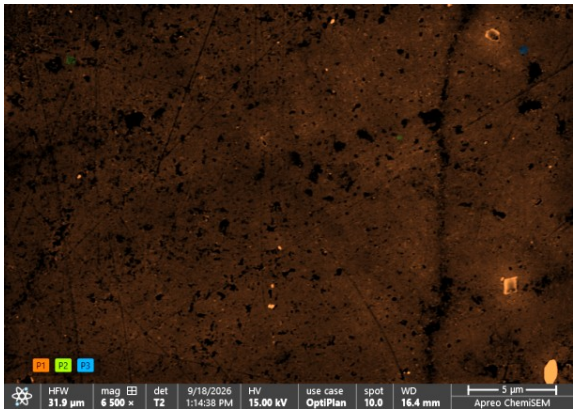
The lattice parameters of GaP, Si, ZnSe, and ZnTe are 5.451, 5.431, 5.668, and 6.104 Å, respectively. Relative to GaP, the lattice mismatches are −0.37% for Si, +3.97% for ZnSe, and +11.97% for ZnTe. The close similarity between the lattice parameters of Si and GaP may favor the formation of a common crystal lattice with relatively low elastic strain. In contrast, the incorporation of ZnSe and particularly ZnTe may increase lattice strain and the likelihood of dislocation formation and structural relaxation. Therefore, the relative concentrations of the constituent components are important factors affecting the structural stability of the epitaxial layer.

The surface morphology of the epitaxial layers was investigated using a Thermo Scientific Apreo 2 ChemiSEM scanning electron microscope (SEM). SEM imaging was performed at an accelerating voltage of 15 kV, a magnification of 6500×, a working distance (WD) of 16.4 mm, and a spot size setting of 10, using the T2 detector. The horizontal field of view was 31.9 μm, and the scale bar corresponded to 5 μm. The elemental composition and its spatial distribution were determined by energy-dispersive X-ray spectroscopy (EDS) integrated with the SEM, through the detection of characteristic X-rays emitted by the constituent elements.

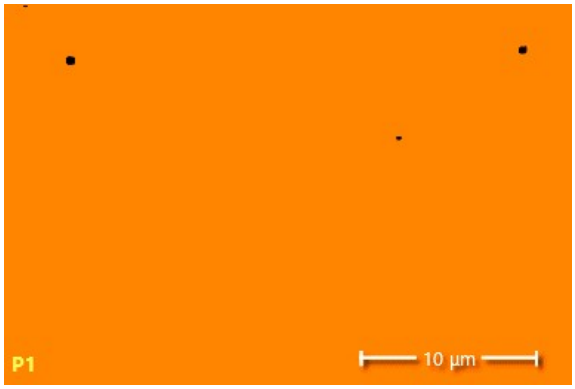
III. Results and Discussion.

Surface Morphology and Chemical Homogeneity of the Multicomponent Epitaxial Layer

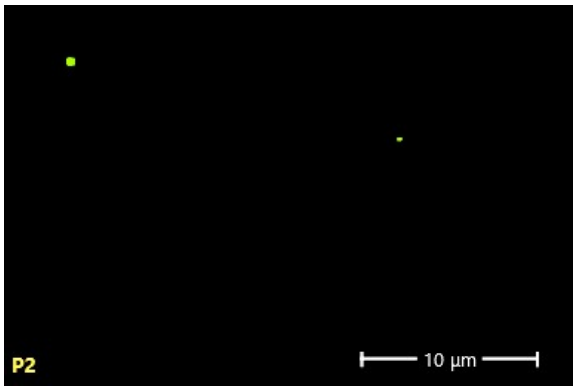
Figure 1 presents a SEM image of the multicomponent epitaxial layer grown on a GaP(100) substrate, together with EDS spectral segmentation maps used to identify local compositional variations (Wahlqvist & Ek, 2025).



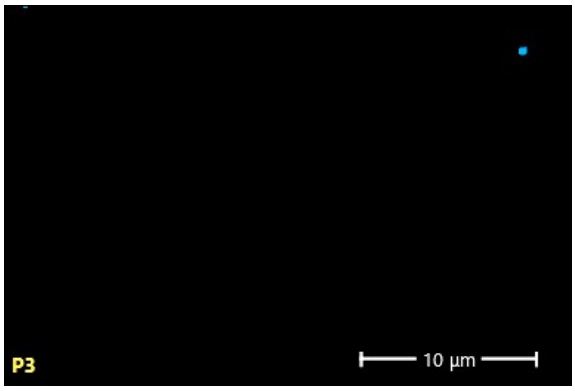
a)



b)



c)



d)

Figure 1. SEM image and EDS spectral segmentation maps of the multicomponent Si–GaP–ZnSe–ZnTe epitaxial layer grown on a GaP(100) substrate: (a) SEM image; (b) P1 - the dominant spectral component; (c) P2 and (d) P3 - minor, spatially localized spectral components.

SEM analysis revealed a continuous layer surface, with no large cracks or morphological discontinuities observed within the examined area. The observed linear surface relief features and localized depressions may be associated with growth steps formed during crystallization (Slipchenko et al., 2022), as well as local surface inclination and SEM detector geometry (Egerton & Zhu, 2023; Neggers et al., 2022).

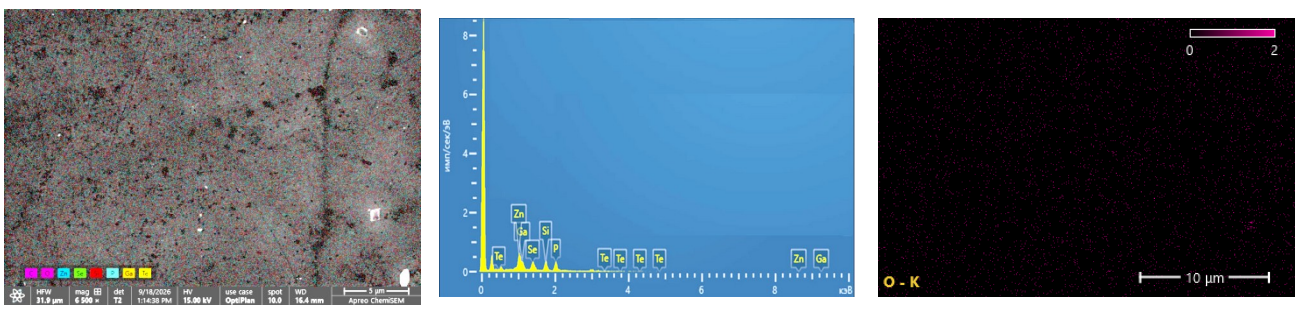
EDS spectral segmentation showed that the dominant P1 component accounted for 392,940 of the 393,216 analyzed pixels (99.93%), whereas the P2 and P3 components represented 0.041% and 0.029%, respectively. The combined fraction of P2 and P3 was only 0.07%, suggesting a high degree of lateral compositional homogeneity and the absence of pronounced chemical heterogeneity within the spatial resolution

limits of the SEM–EDS analysis. However, spectral homogeneity alone does not provide direct evidence for the formation of a single crystalline phase or a single-phase solid solution.

SEM–EDS-Based Elemental and Compositional Analysis of the Multicomponent Epitaxial Layer Surface

Figure 2 presents the SEM image, EDS spectrum, and elemental distribution maps of O, Si, P, Ga, Zn, Se, and Te obtained from the surface of the epitaxial layer. The detection of characteristic X-ray signals from Si, Ga, P, Zn, Se, and Te across nearly the entire analyzed area indicates a relatively uniform spatial distribution of these elements, without pronounced segregation at the micrometer scale, within the spatial resolution limits of SEM–EDS. However, such compositional homogeneity does not confirm the presence of a single crystalline phase, since EDS cannot determine the crystallographic positions of atoms or the symmetry of the crystal lattice (Parish, 2022).

According to quantitative EDS analysis, the average atomic concentrations in the layer were 26.5 at.% Si, 7.3 at.% Ga, 35.2 at.% P, 15.3 at.% Zn, 11.6 at.% Se, and 4.1 at.% Te. The sums of the atomic concentrations (c) for the nominal elemental groups were c(Si) + c(Ga) + c(Zn) = 49.1 at.% and c(P) + c(Se) + c(Te) = 50.9 at.%, yielding a ratio of approximately 0.965, which is close to 1:1. This result is consistent with a possible compositional balance characteristic of tetrahedrally coordinated semiconductor systems; however, it does not establish the formation of a single-phase AB-type solid solution.



a) b) c)

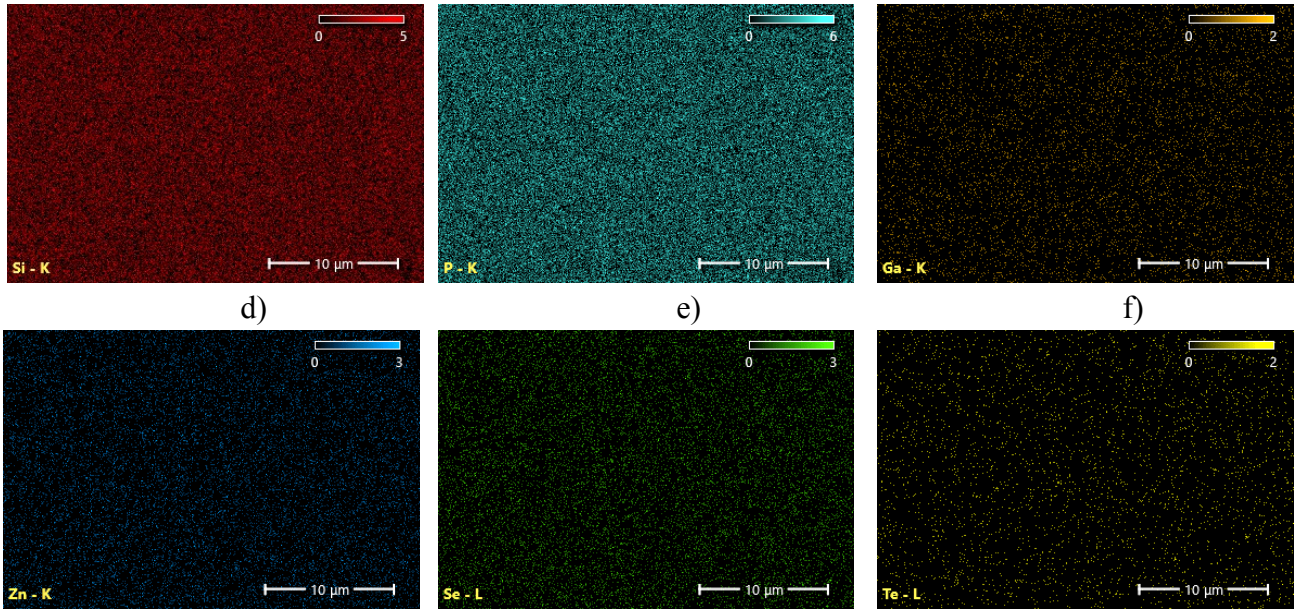


Figure 2. SEM–EDS analysis of the multicomponent Si–GaP–ZnSe–ZnTe epitaxial layer grown on a GaP(100) substrate by LPE: (a) SEM image of the layer surface and composite elemental map; (b) EDS spectrum; (c)–(i) spatial distribution maps of O, Si, P, Ga, Zn, Se, and Te, respectively, across the analyzed surface.

By normalizing the total atomic concentration to two atoms, the average EDS-derived composition of the layer can be formally expressed as $Si_{0.530}Ga_{0.146}Zn_{0.306}P_{0.704}Se_{0.232}Te_{0.082}$. This expression does not represent the chemical formula of a specific crystalline phase but rather describes the average atomic ratios of the constituent elements.

Furthermore, the following relationships were observed: c(Si) + c(Ga) = 33.8 at.% ≈ c(P) = 35.2 at.% and c(Zn) = 15.3 at.% ≈ c(Se) + c(Te) = 15.7 at.%.

Based on the ratios Si/(Si + Ga) = 0.784, Ga/(Si + Ga) = 0.216, Se/(Se + Te) = 0.739, and Te/(Se + Te) = 0.261, the composition can be formally described in terms of the nominal stoichiometric motifs $(Si_{0.784}Ga_{0.216})P$ and $Zn(Se_{0.739}Te_{0.261})$. However, these motifs represent only hypothetical compositional models and do not constitute evidence for distinct crystalline phases or specific chemical bonds identified by EDS.

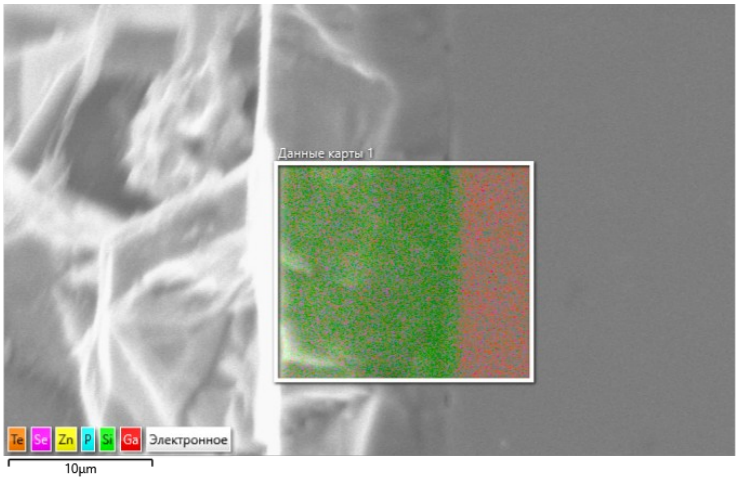
The physical significance of these ratios is associated with the fact that the nominal valence electron counts of Ga–P, Zn–Se, Zn–Te, and Si–Si atomic pairs sum to eight: 3 + 5 = 8, 2 + 6 = 8, and 4 + 4 = 8, respectively. This suggests the possibility of forming electronically saturated bonding configurations in tetrahedrally coordinated semiconductors. However, the incorporation of group-IV Si atoms alongside III–V and II–VI constituents complicates local bonding configurations and charge compensation mechanisms. Therefore, the approximately 1:1 atomic balance does not, by itself, provide direct evidence of electrical charge neutrality or an eight-electron bonding configuration, as these depend on the crystallographic site occupancy of the constituent atoms and defect-mediated charge compensation.

The detection of O and C signals in the EDS analysis may be attributed to surface oxidation, adsorbed species, sample preparation procedures, or electron-beam-induced hydrocarbon contamination (Hugenschmidt et al., 2023). Therefore, without additional characterization, these elements should not be regarded as major crystal-chemical constituents of the epitaxial layer.

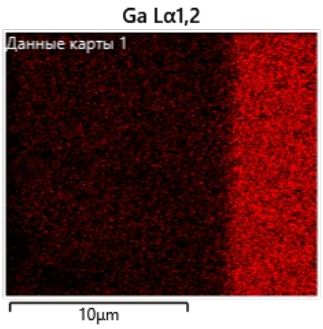
Cross-Sectional Morphology and Spatial Distribution of Elements in the Multicomponent Epitaxial Layer

The cross-sectional SEM image and EDS elemental maps of the multicomponent epitaxial layer grown on a GaP(100) substrate are presented in Figure 3. The layer–substrate interface is clearly distinguishable in the SEM image. The continuous morphology of the layer and the absence of visible delamination suggest intimate contact with the substrate and are consistent with potentially good interfacial adhesion.

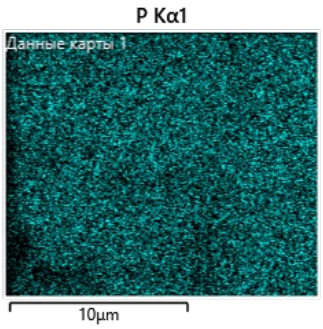
The relatively uniform distribution of characteristic X-ray signals from Ga, P, Si, Zn, Se, and Te throughout the epitaxial layer indicates that no pronounced chemical segregation is observed at the micrometer scale, within the spatial resolution limits of SEM–EDS. The Ga X-ray signal intensity is significantly lower in the epitaxial layer than in the substrate, whereas the P signal exhibits a comparatively smaller variation. This observation is consistent with the formation of a phosphorus-containing multicomponent layer whose chemical composition differs from that of the GaP substrate. However, differences in X-ray signal intensities also depend on X-ray generation and absorption conditions and therefore cannot be directly equated with differences in atomic concentrations.



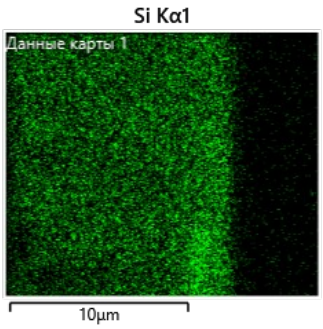
a)



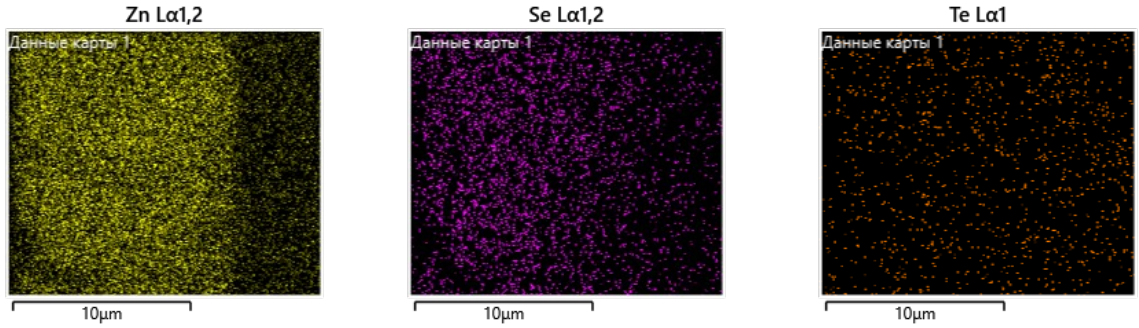
b)



c)



d)



e) f) g)

Figure 3. Cross-sectional SEM image and EDS elemental maps of the multicomponent Si–GaP–ZnSe–ZnTe epitaxial layer grown on a GaP(100) substrate by liquid-phase epitaxy (LPE): (a) SEM image with a composite elemental map; (b)–(g) spatial distribution maps of Ga, P, Si, Zn, Se, and Te, respectively.

The characteristic X-ray signals of Si and Zn were predominantly detected within the epitaxial layer, indicating the incorporation of these elements into the layer during crystallization from the liquid phase. The Se signal exhibited a relatively high intensity within the epitaxial layer and was also detected in the substrate region near the layer–substrate interface. This distribution may suggest possible diffusion of Se atoms across the interface; however, it may also arise from the limited spatial resolution of the SEM–EDS technique. The detection of Te signals in both regions can be attributed to the initial Te doping of the GaP substrate and the incorporation of Te supplied by the ZnTe component during epitaxial growth.

Overall, the cross-sectional SEM–EDS results indicate the formation of a continuous multicomponent epitaxial layer on the GaP(100) substrate, exhibiting intimate interfacial contact and an elemental composition that differs significantly from that of the original GaP substrate. The relatively uniform distribution of the constituent elements and the absence of pronounced large-scale segregation suggest a high degree of compositional homogeneity within the spatial resolution limits of SEM–EDS. Nevertheless, additional structural characterization is required to confirm the formation of a single crystalline phase or a substitutional solid solution.

IV. Conclusions

A multicomponent Si–GaP–ZnSe–ZnTe layer approximately 10 μm thick was grown on a GaP(100) substrate from a tin-based melt using LPE. SEM observations revealed a continuous layer morphology and an intact layer–substrate interface with no visible signs of delamination. EDS elemental maps and spectral segmentation indicated a relatively uniform distribution of Si, Ga, P, Zn, Se, and Te within the analyzed regions, with no pronounced evidence of large-scale chemical segregation. The nearly 1:1 ratio of (Si + Ga + Zn) to (P + Se + Te) in the average elemental composition suggests an approximate balance between these nominal elemental groups in the multicomponent system. These findings demonstrate the feasibility of growing morphologically continuous and relatively compositionally homogeneous multicomponent epitaxial layers on GaP substrates using LPE. Nevertheless, further structural characterization is required to determine the phase constitution of the layer and to confirm whether a solid solution with a single crystal lattice has formed.

REFERENCES

1. Du, Y., Xu, B., Wang, G., Miao, Y., Li, B., Kong, Z., Dong, Y., Wang, W., & Radamson, H. H. (2022). Review of highly mismatched III–V heteroepitaxy growth on (001) silicon. *Nanomaterials, 12*(5), 741. https://doi.org/10.3390/nano12050741
2. Egerton, R. F., & Zhu, Y. (2023). Spatial resolution in secondary-electron microscopy. *Microscopy, 72*(2), 66–77. https://doi.org/10.1093/jmicro/dfac022
3. Hite, J. K. (2023). A review of homoepitaxy of III-nitride semiconductors by metal organic chemical vapor deposition and the effects on vertical devices. *Crystals, 13*(3), 387. https://doi.org/10.3390/cryst13030387
4. Hugenschmidt, M., Adrion, K., Marx, A., Müller, E., & Gerthsen, D. (2023). Electron-beam-induced carbon contamination in STEM-in-SEM: Quantification and mitigation. *Microscopy and Microanalysis, 29*(1), 219–234. https://doi.org/10.1093/micmic/ozac003
5. Kafi, N., Kang, S., Golz, C., Rodrigues-Weisensee, A., Persichetti, L., Ryzhak, D., Capellini, G., Spirito, D., Schmidbauer, M., Kwasniewski, A., Netzel, C., Skibitzki, O., & Hatami, F. (2024). Selective growth of GaP crystals on CMOS-compatible Si nanotip wafers by gas source molecular beam epitaxy. *Crystal Growth & Design, 24*(7), 2724–2733. https://doi.org/10.1021/acs.cgd.3c01337
6. Mauk, M. G. (2023). Liquid-phase epitaxy. In *Digital Encyclopedia of Applied Physics*. Wiley-VCH. https://doi.org/10.1002/3527600434.eap812
7. Neggers, J., Héripré, E., Bonnet, M., Hallais, S., & Roux, S. (2022). A generic topography reconstruction method based on multi-detector backscattered electron images. *Strain, 58*(5), e12416. https://doi.org/10.1111/str.12416
8. Pan, R., Yang, C., Huang, G., Ma, M., Fan, S., & Li, Z. (2025). Simultaneous growth of four GaN crystal sheets using the Na-flux liquid-phase epitaxial method: Under different solution heights. *Crystal Growth & Design, 25*(9), 2986–2993. https://doi.org/10.1021/acs.cgd.5c00067
9. Pan, R., Yang, C., Sun, L., Ma, M., Fan, S., Zhou, M., & Li, Z. (2026). Research on the simultaneous growth of four GaN crystal sheets by the Li-added Na flux liquid phase epitaxy method. *Crystal Growth & Design, 26*(4), 1885–1891. https://doi.org/10.1021/acs.cgd.5c01775
10. Parish, C. M. (2022). Cluster analysis of combined EDS and EBSD data to solve ambiguous phase identifications. *Microscopy and Microanalysis, 28*(2), 371–382. https://doi.org/10.1017/S1431927622000010
11. Razzokov, A. Sh., Saidov, A. S., Allabergenov, B., Choi, B., Petrushenko, S. I., & Dukarov, S. V. (2023). Studies of the crystal structure of solid solutions $(Sn_2)_{1-x-y}(GaAs)_x(ZnSe)_y$, $(GaAs)_{1-x}(ZnSe)_x$ grown from liquid phase. *Journal of Crystal Growth, 612*, 127203. https://doi.org/10.1016/j.jcrysgro.2023.127203
12. Saidov, A. S., Leyderman, A. Yu., Usmonov, Sh. N., Rakhmonov, U. Kh., Saparov, D. V., Suyarov, Q. T., & Akhmedov, A. M. (2023). Processes of current transport in p-Si–n-$(Si_2)_{1-x-y}(GaP)_x(ZnSe)_y$ heterostructure produced by liquid phase epitaxy. *e-Journal of Surface Science and Nanotechnology, 21*(1), 55–60. https://doi.org/10.1380/ejssnt.2023-009
13. Saidov, A. S., Usmonov, Sh. N., Kalanov, M. U., Saparov, D. V., Ishniyazov, T. T., Akhmedov, A. M., Tagaev, M. B., & Razzokov, A. Sh. (2025). Growing perfect single-crystal epitaxial films of $(Si_2)_{1-x}(GaN)_x$ solid solutions on Si(111) substrates from the liquid phase. *Acta Physica Polonica A, 148*(1), 29. https://doi.org/10.12693/APhysPolA.148.29

14. Slipchenko, S., Shamakhov, V., Nikolaev, D., Fomin, E., Soshnikov, I., Bondarev, A., Mitrofanov, M., Pikhtin, N., & Kop'ev, P. (2022). Basics of surface reconstruction during selective area metalorganic chemical vapour-phase epitaxy of GaAs films in the stripe-type ultra-wide window. *Applied Surface Science, 588*, 152991. https://doi.org/10.1016/j.apsusc.2022.152991
15. Wahlqvist, D., & Ek, M. (2025). Model-fitting weighted least squares as an alternative to principal component analysis for analyzing energy-dispersive X-ray spectroscopy spectrum images. *Microscopy and Microanalysis, 31*(1), ozae106. https://doi.org/10.1093/mam/ozae106
16. Yan, Z., & Li, Q. (2024). Recent progress in epitaxial growth of dislocation tolerant and dislocation free III–V lasers on silicon. *Journal of Physics D: Applied Physics, 57*, 213001. https://doi.org/10.1088/1361-6463/ad26cd
17. Zeng, C., Fu, D., Jin, Y., & Han, Y. (2023). Recent progress in III–V photodetectors grown on silicon. *Photonics, 10*(5), 573. https://doi.org/10.3390/photonics10050573

SKILLS OVER DEGREES: A STATISTICAL ANALYSIS OF LABOR MARKET TRENDS

D.Sh. Chintemirova
3rd-year student, Tashkent State University of Economics
https://doi.org/10.5281/zenodo.20151048

Abstract. *This article examines Uzbekistan's labor market transition from traditional degrees to a competency-based "skills-first" model within the context of Industry 4.0. By analyzing the structural "skills gap" and demographic trends, the research evaluates why practical expertise is becoming a primary determinant of employment over formal certification. The study explores the impact of "degree inflation" on human capital and proposes strategic recommendations to align the national education system with real-sector industrial demands.*

Keywords: *labor market, youth bulge, dual education, Industry 4.0, Uzbekistan, human capital, skills-first model, degree inflation.*

INTRODUCTION

Uzbekistan is currently navigating a pivotal demographic transition, characterized by a rapid expansion of its human capital. According to official statistics, the population under the working age has reached 12 million, reflecting a massive "youth bulge" [1, 2] with nearly 600,000 new entrants joining the labor market annually. This rapid demographic growth, often analyzed as a demographic dividend, places immense structural pressure on the economy [3], demanding a strategic response to integrate this rising generation into the productive workforce.

However, a critical paradox has emerged: while official unemployment appears to be declining, the economically inactive population has surged past 5 million individuals. This trend highlights a widening "skills gap" where a significant portion of the workforce remains outside the formal economy despite possessing formal academic credentials. This situation is further complicated by the ongoing generational shift in the labor market. As noted in the "Theory of Generations" [4], the workforce is witnessing the gradual departure of Generation X (born 1965–1980) as they reach retirement age. While Generation Y (Millennials, born 1981–1996) currently forms the core of the active workforce, the long-term burden of economic growth is rapidly shifting toward Generation Z (born 1997–2012). As discussed in recent socio-economic studies [5], the critical question is whether these "digital natives" are adequately prepared for the market's evolving requirements or if their formal degrees are failing to provide the necessary competitive edge in a rapidly changing environment.

The Government of Uzbekistan is acutely aware of these challenges. This transformation is legally anchored in the Decree of the President of the Republic of Uzbekistan No. UP-21, which elevates national development priorities toward 2030 and emphasizes the structural alignment of the education system with real-sector demands [6]. This urgency was further underscored by President Shavkat Mirziyoyev on August 8, 2025, who highlighted that while university enrollment has increased 4.5 times, the current training system remains poorly aligned with market needs [7]. In this context, Uzbekistan is strategically pivoting toward the Fourth Industrial Revolution (Industry 4.0), spearheaded by the Center for the Fourth Industrial Revolution (C4IR) in partnership with the World Economic Forum [8].

To prevent Uzbekistan from facing what is historically defined as a "reserve army of the unemployed" [9] a structural crisis where labor supply remains detached from industrial demand — Uzbekistan is increasingly adopting the "Dual Education" (Duale Ausbildung) philosophy. Legally institutionalized by the Resolution of the Cabinet of Ministers of the Republic of Uzbekistan No. 163 [10], this model, pioneered by Germany, proves that economic resilience depends on the direct synchronization of workplace apprenticeship with vocational theory [11]. The strategic importance of this shift is further validated by NVIDIA CEO Jensen Huang, who argues that the AI-driven era will redefine the traditional hierarchy between white-collar and blue-collar workers [12]. Huang posits that while automation transforms cognitive tasks, the global economy will experience a profound demand for specialists with advanced technical skills to navigate the physical-digital integration of Industry 4.0. For Uzbekistan, this transition is vital as the country prepares to launch $83 billion in high-tech industrial projects over the next 3–4 years, creating an urgent demand for 500,000 highly skilled specialists whose expertise must transcend the boundaries of traditional academic theory.

Consequently, the primary purpose of this research is to evaluate the evolving status of formal diplomas against a rising competency-based hierarchy, specifically focusing on how macroeconomic trends in Uzbekistan are displacing traditional certification with practical competencies. The study seeks to prove the hypothesis (H_a) that in the current economic environment, practical skills have become a more significant determinant of employment and career success than formal academic degrees. By examining the 2010–2025 labor market statistics and the widening "skills gap," this research provides an empirical basis for understanding the structural transition toward a "skills-first" model [13].

LITERATURE REVIEW

The shifting dynamics of the global labor market have sparked a critical academic debate regarding the structural imbalance between academic supply and industrial demand. Theoretical foundations of this research are rooted in the concept of ‘‘Degree Inflation’’ where the proliferation of academic degrees has led to their diminishing marginal value, turning diplomas into mere screening tools rather than measures of professional readiness [14]. Building upon the contemporary insights of German labor economist Matthias Achwa and global human capital strategist Shailani Rao [15, 16], this research evaluates the global transition toward ‘‘skill-based’’ models, where dynamic competencies serve as the primary currency of the modern economy. This transition is further reinforced by the World Economic Forum’s ‘‘Future of Jobs Report’’ [17], which projects that by 2030, nearly half of core business skills will be redefined by automation and AI, necessitating a global shift toward a ‘‘Skills-First’’ approach.

In the national context, the foundational driver of demographical pressure is analyzed in the recent work of Abduazim Abdurakhmanov [18], who identifies significant trends in fertility rate indicators in Uzbekistan. His research provides a statistical basis for the country’s rapid population growth, proving that sustained high fertility rates are the primary cause of the expanding youth cohort. This is further supported by Nodira Zokirova [19], who emphasizes that in the era of digital transformation, the qualitative improvement of labor resources must precede quantitative expansion to avoid structural imbalances. These domestic perspectives are validated by the Institute of Macroeconomic and Regional Research (IMRI) [20], which identifies a systemic ‘‘Horizontal and Vertical Mismatch’’ noting that nearly 35-40% of graduates work in fields unrelated to their formal studies. By integrating official data from the National Committee on Statistics of the Republic of Uzbekistan and the Central Bank of Uzbekistan for the 2010–2025

period, this study fills a critical gap in the literature by linking ‘‘credential-driven inactivity’’ to the structural requirements of the modern industrial sector, providing a robust empirical basis for the transition toward a skills-driven economic model.

RESEARCH METHODOLOGY

The research methodology integrates various scientific methods, including observation, grouping, comparison, and synthesis. The study is based on longitudinal data from the National Statistics Agency and the Central Bank of Uzbekistan (2010–2025) to analyze historical labor trends, alongside projections from the World Economic Forum (WEF) "Future of Jobs" (2025–2030). The empirical core of the research employs a Simple Linear Regression (OLS) model based on data from the 2010–2025 period, specified as follows:

$$Inactivity_t = \beta_0 + \beta_1 * Enrollment_t + \varepsilon_t$$

Where Inactivity represents the economically inactive population and Enrollment denotes total higher education enrollment. Statistical modeling and ANOVA tests were performed using Python. Given the focused nature of the dataset, the evaluation primarily relies on the Coefficient of Determination (R^2) and F-significance to validate the strength and reliability of the identified relationship. To evaluate the demographic pressure on the productive workforce, the Total Dependency Ratio (TDR) was calculated using the standardized economic formula:

$$TDR = \frac{\left(P_{(0-15)} + P_{(55/60+)}\right)}{P_{(16-54/59)}} * 1000$$

Where $P_{(0-15)}$ is the population under the working age, $P_{(55/60+)}$ is the population over the working age and $P_{(16-54/59)}$represents the working-age population. Additionally, relative indicators were used to assess the burden on the productive workforce, providing a demographic baseline necessary to evaluate the structural shifts within the national labor market.

ANALYSES AND RESULTS

To evaluate the structural transformations within Uzbekistan’s labor market, it is essential to first examine the demographic drivers that define the scale of human capital expansion.

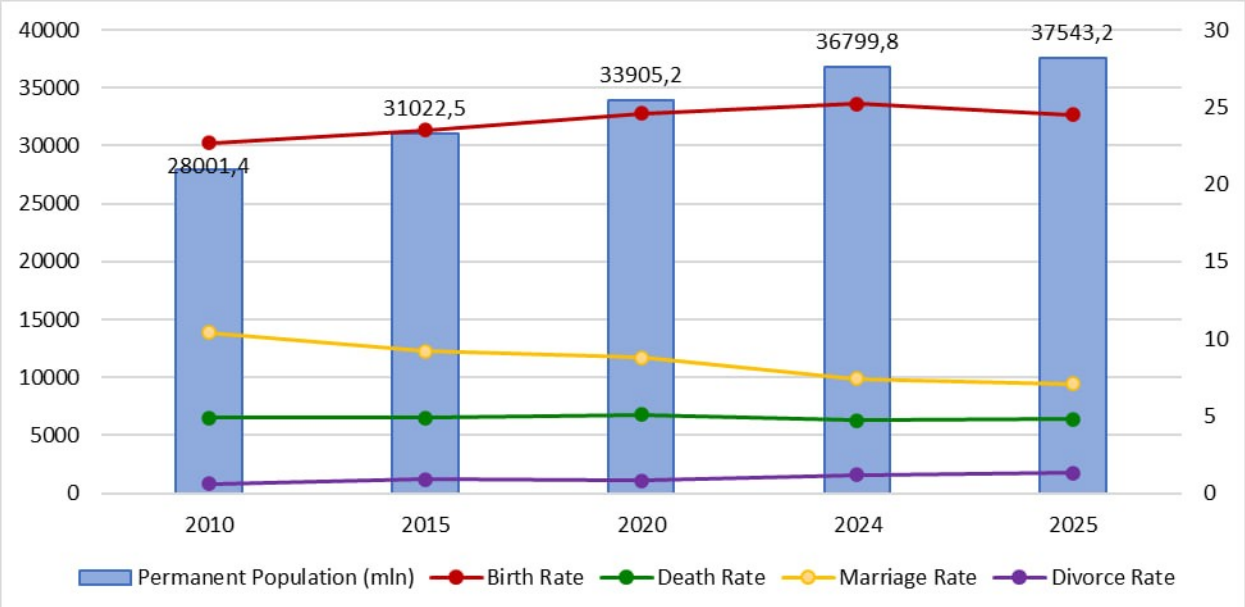


Figure 1. Main demographic indicators of Uzbekistan (2010–2025)

As illustrated in Figure 1, the population of Uzbekistan increased from 28 million in 2010 to over 37.5 million by the end of 2025, driving an annual influx of approximately 600,000 new

entrants into the labor market. While birth rates show a recent stabilization, the sustained demographic momentum is a direct consequence of high fertility trends from previous decades, as analyzed by Abdurakhmanov. Furthermore, the chart depicts a steady marriage rate, which serves as a leading indicator of long-term demographic sustainability. It is important to note that while domestic population growth remains robust, the actual labor supply is moderated by external migration flows, primarily toward regional markets. This demographic reality raises a fundamental strategic question: can a traditional 4-year university system adequately prepare this massive, continuous stream of labor for the specific needs of a high-tech economy?

The International Labor Organization (ILO) 2025 report provides a critical global benchmark, ranking Uzbekistan 114th out of 187 nations with an employment-to-population ratio of 55%. This position, while modest compared to regional leaders like Kazakhstan (67%) and Belarus (61%), reveals a profound structural gap in official labor participation. ILO analysts emphasize that this relatively low ranking is not a symptom of job scarcity, but a reflection of a socio-economic structure where a massive portion of the workforce specifically students, homemakers and youth remain trapped in the informal sector. This informal engagement serves as empirical evidence that a substantial segment of the population possesses functional skills that the formal economic system fails to capture or validate. Consequently, if nearly half of the adult population operates outside the official economy, it suggests that traditional academic credentials are failing to serve as an effective bridge to formal employment. This international perspective underscores an urgent necessity to investigate the "skills-mismatch" and highlights that the formalization of the labor market depends less on the volume of diplomas and more on the integration of practical, market-ready competencies.

The structural gap identified by the ILO is further examined through an OLS regression analysis (2010–2025), evaluating the association between higher education enrollment and economic inactivity.

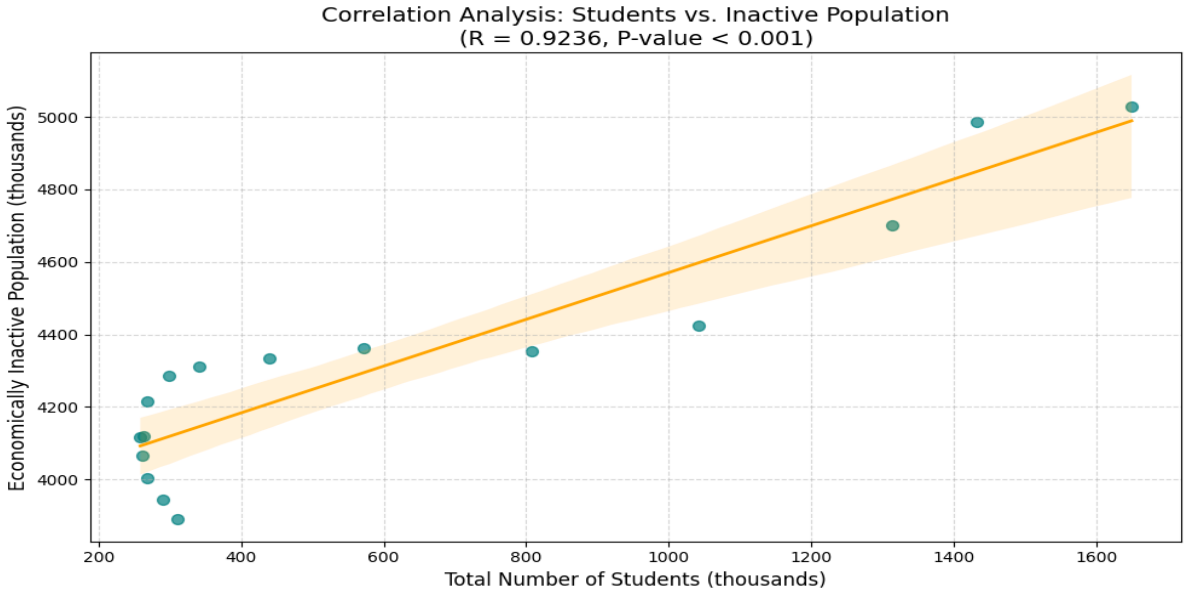


Figure 2. Correlation between university enrollment and economic inactivity

As illustrated in Figure 2, a strong positive correlation exists between university enrollment and economic inactivity. The scatter plot, generated with a 95% confidence interval, shows a consistent upward trend, suggesting that academic expansion is closely associated with a rise in the

population remaining outside the formal labor market. The statistical reliability and significance of this relationship are further detailed in the ANOVA results provided in Table 1.

Table 1

Regression analysis results and ANOVA

Indicator/Source	**Value/df**				
Regression Statistics					
Multiple R	0.9236				
R-Square	0.8530				
Adjusted R-Square	0.8425				
Standard Error	133.21				
Observations	16				
ANOVA	df	SS	MS	F	Significance F
Regression	1	1442227.26	1442227.26	81.27	3.32E-07***
Residual	14	248437.53	17745.54		
Total	15	1690664.79			
Model Parameters	Coeff.	Std. Error	t-Stat	P-value	
Intercept (Beta 0)	3926.085	55.056	71.309	2.46E-19	
Enrollment (Beta 1)	0.6443	0.0714	9.015	3.32E-07	

The OLS regression analysis in Table 1 provides empirical support for this trend. With a Correlation (R) of 0.9236 and a Coefficient of Determination (R^2) of 0.853, the model explains 85.3% of the variance in economic inactivity as being linked to the expansion of university enrollment. Specifically, the regression coefficient (beta_1 = 0.6443) indicates that for every 1,000 additional enrollments, approximately 644 individuals are statistically categorized into the "inactive" group. This reflects an institutional shift where higher education acts as a temporary buffer, deferring labor market entry for the youth cohort. This trend identifies a phenomenon of "Academic-Driven Inactivity", where the growth in academic participation corresponds to a parallel accumulation of potential labor outside the formal economic framework, highlighting the qualitative mismatch between degree acquisition and formal employment.

Table 2. Labor market statistics of the Republic of Uzbekistan (2020–2025, in thousands)

Indicators	**2020**	**2021**	**2022**	**2023**	**2024**	**2025**
Total Population	33905,2	34558,9	35271,3	36024,9	36799,8	37543,2
Under Working Age (0-15)	10 274,0	10 699,2	11 066,2	11 437,4	11 780,3	12 049,1
Working-Age Population	19951,6	20135,1	20299,5	20505,3	20746	21039,2
Over Working Age (60+/55+)	3 679,6	3 724,6	3 905,6	4 082,2	4 273,5	4 454,9
Labor Resources	19158,2	19334,9	19517,5	19739,6	20085,2	20410
Economically Active Population	14797,4	14980,7	15038,9	15038,3	15097,9	15381,6

Employed Population	13236,4	13538,9	13706,2	14014,2	14261,9	14600
Unemployed Population	1561	1441,8	1332,7	1024,1	836	781,6
Economically Inactive Population	4360,8	4354,2	4478,6	4701,3	4987,3	5028,4
Dependency Ratio (per 1000)	699,4	716,3	737,5	756,9	773,8	784,4
Employment Rate (%)	66	67	67,2	67,9	68,3	68,9

The data in Table 2 illustrates a significant quantitative shift in Uzbekistan's labor market over the past five years. Driven by extensive higher education reforms, university enrollment rates have reached 40–42%, contributing to a steady expansion of labor resources, which reached 20.4 million by the end of 2025. This period also witnessed a successful reduction in the unemployed population, which fell from 1.56 million to 781,600, resulting in an improved employment rate of 68.9%.

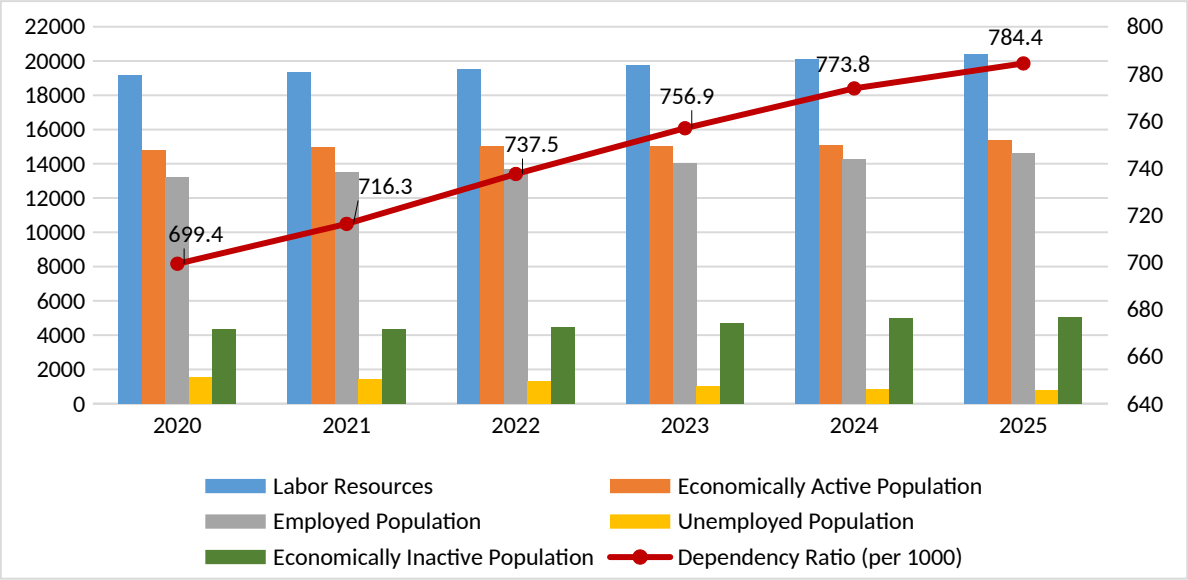


Figure 3. Visual dynamics of labor resources and the dependency ratio

As illustrated in Figure 3, which visualizes the primary indicators from Table 2, a deeper macroeconomic paradox emerges. While labor resources have expanded, the productive workforce faces an increasing burden, evidenced by the Dependency Ratio rising from 699.4 to 784.4 per 1,000 working-age individuals. Despite the drop in official unemployment, the economically inactive population has shown persistent growth, surpassing 5 million in 2025. This trend underscores a critical "skills gap," suggesting that traditional four-year academic programs are struggling to keep pace with the evolving demands of the modern real sector. The fact that 70% of employers still report a shortage of qualified specialists in fields such as fintech and digital analytics, despite high graduation rates, validates the diminishing marginal value of purely theoretical degrees in an Industry 4.0 environment.

This growing structural pressure on the workforce necessitates an urgent transition toward a "skills-first" model, as nearly 44% of the population remains outside the formal labor force. This demographic challenge is exacerbated by a qualitative mismatch where high academic enrollment does not directly translate into formal employment. In the context of Industry 4.0, as emphasized in the research of Kamalitdinov, the modernization of specialized education is vital to bridging the gap between theoretical training and the analytical requirements of the modern real sector. The

persistent discrepancy between academic curricula and industrial demand often leads to an "internal talent drain", where potential specialists pivot toward alternative sectors offering higher immediate returns for practical, self-taught competencies. This shift confirms that in an environment where academic study is perceived as purely theoretical, a formal diploma serves merely as an "entry ticket" to the market rather than a guarantee of professional readiness. Ultimately, without a systemic transition toward competency-based training, Uzbekistan risks facing a persistent "talent hunger" despite its rapidly expanding human capital.

The World Economic Forum (WEF) "Future of Jobs Report 2025" provides statistical evidence that the traditional academic model is being replaced by a "skills-based economy." With 170 million new jobs expected to be created and 39% of core skills predicted to transform, this report sets new strategic directions for labor-surplus countries like Uzbekistan. The findings indicate that digital technologies and Artificial Intelligence (AI) will be the primary drivers of the labor market in the upcoming years.

Table 3. Key drivers of business transformation (2025–2030)

Macrotrend	Employer share (%)	Impact
Broadening digital access	60	Enables remote work and access to the global services market.
Artificial Intelligence (AI)	86	Automates routine tasks and simplifies expert-level functions.
Green transition	47	Demand for renewable energy and environmental sustainability skills.
Rising cost of living (inflation)	50	Economic pressure creates a necessity for higher productivity.

These statistics imply that the vast majority (86%) of employers perceive Artificial Intelligence as the leading force for transformation. This underscores that mastering these technological drivers is a vital necessity, often overshadowing the mere possession of a traditional academic degree (Table 3).

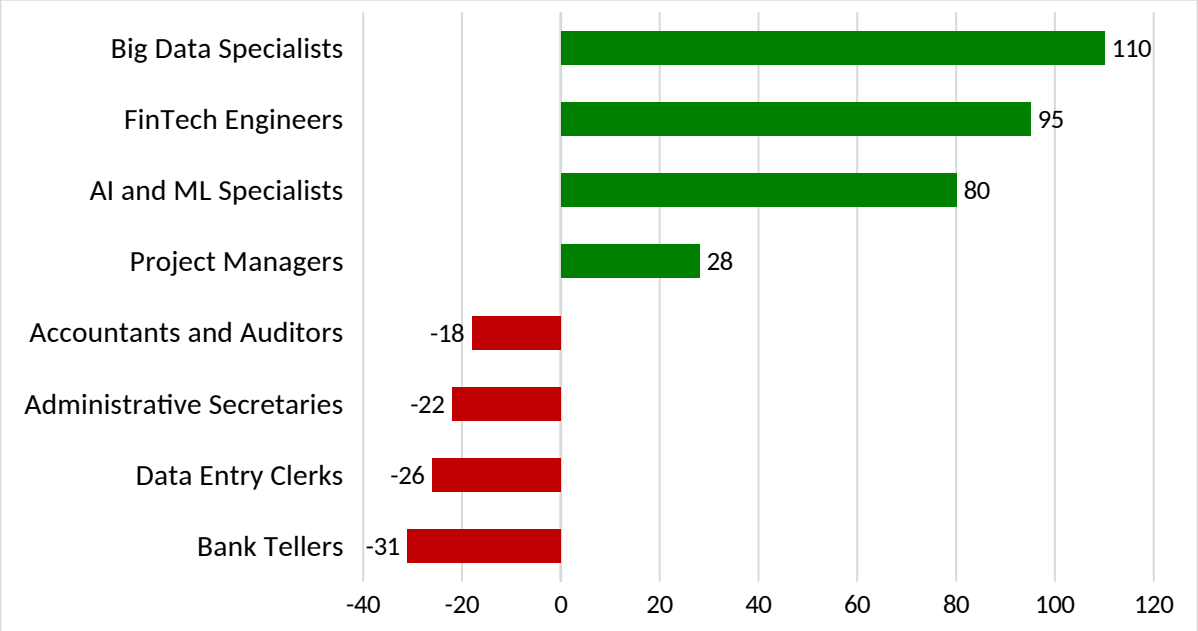


Figure 4. Fastest growing vs. declining jobs by 2030 (net growth %)

Figure 4 illustrates a sharp global polarization in the labor market, showing a massive surge in demand for roles such as Big Data (+110%) and FinTech (+95%) by 2030. Conversely, the global decline in traditional sectors like banking (-31%) and accounting (-18%) suggests that automation is rapidly displacing routine cognitive labor. For Uzbekistan, where 600,000 new entrants join the labor force annually, this serves as a critical indicator: relying solely on a formal diploma increases the risk of graduates entering sectors that are globally shrinking. Therefore, ensuring national economic stability requires a strategic focus on developing the technological and analytical competencies of graduates.

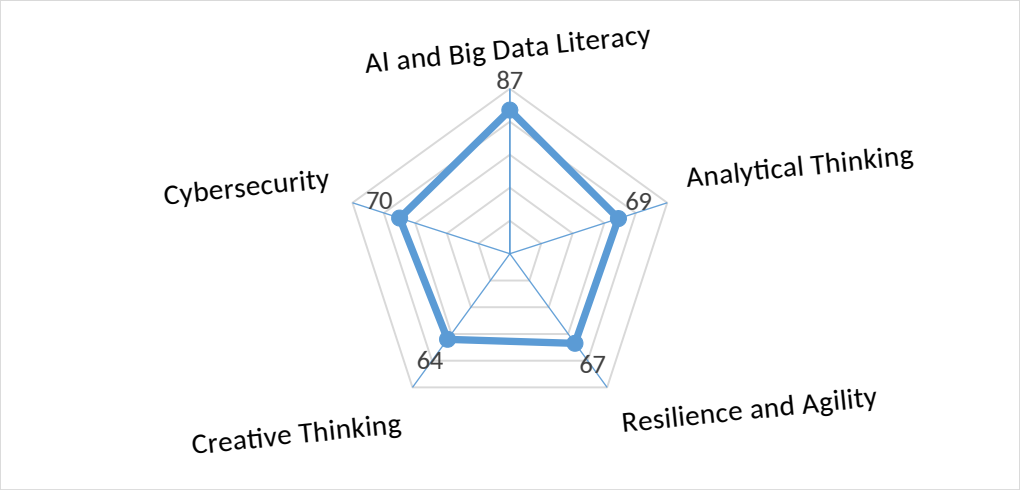


Figure 5. Top 5 in-demand skills for 2025–2030 (%)

he WEF 2025 data confirms a fundamental shift in employer priorities, where the focus is moving from "what you studied" to "what you can do." The report highlights a stark contrast in skill development: while basic academic skills show a minimal 4% growth in importance, advanced competencies are becoming the new global standard. Specifically, AI and Big Data Literacy have reached 87% in importance, followed by Cybersecurity at 70% (Figure 5). In the national context, the Uzbekistan-specific section identifies Business Intelligence Analysts as a high-demand role, while traditional auditing roles are expected to decline. This empirical evidence underscores the necessity for the national higher education system to integrate a "skills-first" approach to avoid immediate obsolescence in a rapidly evolving economy.

CONCLUSION AND RECOMMENDATIONS

This research concludes that Uzbekistan’s labor market is experiencing a fundamental structural shift where practical skills are rapidly overshadowing the traditional value of academic degrees. The quantitative growth in higher education enrollment has not sufficiently resolved structural imbalances, necessitating a qualitative transition toward market-ready competencies. To navigate the upcoming technological waves, the nation must be proactively prepared for Industry 4.0 by equipping its human capital with technical agility and analytical proficiency rather than relying solely on theoretical knowledge. Ultimately, a systemic reform of the education system is required to bridge the widening gap between academic output and industrial demand. By institutionalizing a "skills-first" philosophy and synchronizing vocational theory with workplace requirements, Uzbekistan can transform its rising youth generation into a productive economic force. Without these systemic changes, graduates risk remaining "mere statistics" in a global economy that increasingly values practical expertise and technological adaptability over formal certification.

REFERENCES

1. National Committee on Statistics of the Republic of Uzbekistan (2025). Statistical Report on the Demographic Situation of the Republic of Uzbekistan. https://stat.uz/uz/
2. Beehner, L. (2007). The Effects of "Youth Bulge" on Civil Conflicts. Council on Foreign Relations (CFR). https://www.cfr.org/backgrounders/effects-youth-bulge-civil-conflicts
3. World Bank. (2024). Uzbekistan: Harnessing the Youth Bulge for Economic Growth. Washington, DC: World Bank Group. worldbank.org
4. Strauss, W., & Howe, N. (1991). Generations: The History of America's Future, 1584 to 2069. William Morrow & Co.
5. RBC Trends. (2021). Theory of Generations: Is it still working? https://trends.rbc.ru/trends/education/6156efb59a79477bf9ca5893
6. Decree of the President of the Republic of Uzbekistan. (2026, February 16). On measures to continue reforms and transition to a new stage of national development priorities until 2030, No. UP-21. https://lex.uz/en/docs/8050774
7. Official Website of the President of the Republic of Uzbekistan. (2025). Meeting on ensuring the employment of higher education graduates. https://president.uz/oz/lists/view/7832
8. World Economic Forum (WEF). (2024). Affiliate Centre for the Fourth Industrial Revolution (C4IR) Uzbekistan. https://www.weforum.org/
9. Marx, K. (1867). Capital: A critique of political economy. Volume 1, Part 1: The process of capitalist production. New York, NY: Cosimo.
10. Resolution of the Cabinet of Ministers of the Republic of Uzbekistan. (2021, March 29). On measures to organize dual education in the professional education system, No. 163. https://lex.uz/en/docs/5346217
11. Euler, D. (2013). Germany's Dual Vocational Training System: A Model for Other Countries? Bertelsmann Stiftung. https://www.bertelsmann-stiftung.de/en
12. Huang, J. (2024, February). Keynote at the World Government Summit: AI and the Future of Human Capital. Dubai, UAE. https://blogs.nvidia.com/blog/world-governments-summit/
13. World Economic Forum. (2025). The Future of Jobs Report 2025: Insights on the Skills-First Economy. https://www.weforum.org/publications/the-future-of-jobs-report-2025/
14. Fuller, J. B., & Raman, M. (2017). Dismissed by the Degrees. Harvard Business School Research Report. hbs.edu
15. Achwa, M. (2023). Skills as the New Currency of the Labor Market. Global Labor Trends Journal.
16. Rao, S. (2024). The Competency-Based Hierarchy: Beyond the Traditional Resume. Workforce Strategy Review.
17. World Economic Forum. (2025). The Future of Jobs Report 2025: Insights on the Skills-First Economy. weforum.org
18. Abduraxmonov, A. (2023). Trends in Fertility Rates Indicators in the Republic of Uzbekistan. Economics and Innovative Technologies, 11(4), 59–67. DOI:10.55439/EIT/vol11_iss4/a7
19. Zokirova, N. K. (2023). Transformation of Labor Relations in the Digital Economy of Uzbekistan.
20. Institute of Macroeconomic and Regional Research (IMRI). (2024). Analysis of Labor Market Mismatches and Youth Employment in Uzbekistan. https://imrs.uz/

CONSUMER BEHAVIOR IN TOURISM AS A STRATEGIC FACTOR IN THE DEVELOPMENT OF UZBEKISTAN'S TOURISM MARKET: A THEORETICAL JUSTIFICATION FOR THE NECESSITY OF RESEARCH

S.Sh. Nurmatova
PhD Doctoral Student, Research Institute for Tourism Development
https://doi.org/10.5281/zenodo.20302684

Abstract. *This article examines consumer behavior in inbound tourism as a key factor in the development of the tourism market of Uzbekistan. The relevance of the study is обусловлена the increasing role of digital technologies and the transformation of tourist decision-making mechanisms in the context of globalization and digitalization of the economy.*

The aim of the study is to identify and quantitatively assess the impact of economic, cognitive, and digital factors on the choice of tourist destinations. The methodological framework is based on a comparative analysis of scientific approaches, a synthesis of domestic and international studies, as well as statistical and econometric methods.

The results indicate that consumer behavior in tourism is shaped by a complex system of interrelated factors. The most significant influence is exerted by destination perception ($\beta = 0.421$; $p < 0.001$) and the digital accessibility of tourism services ($\beta = 0.356$; $p < 0.001$). Service quality, cultural attractiveness, and social recommendations also demonstrate a statistically significant impact. A high coefficient of determination ($R^2 = 0.71$) confirms the robustness and explanatory power of the proposed model. Additionally, a stable relationship between the growth of digital indicators and the increase in inbound tourist flows has been identified.

The scientific novelty of the study lies in the substantiation of an integrative approach to modeling consumer behavior in tourism, incorporating digital indicators as an independent group of determinants. The practical significance of the findings is associated with their potential application in the formulation of public policy and strategic development of the tourism market of Uzbekistan.

Keywords: *consumer Behavior in Tourism, Inbound Tourism, Digital Transformation, Economic Factors.*

Introduction

In the contemporary global economy, tourism acts as one of the key drivers of economic growth, generating substantial revenues and contributing to the sustainable development of regions. According to data from UN Tourism, the global tourism market exceeded USD 1.9 trillion in 2025, with projected annual growth rates of 5–7% through 2030 [1]. For developing countries, including those of Central Asia, tourism is becoming a strategic instrument for economic diversification, reducing dependence on raw material exports, and creating employment opportunities.

It is important to emphasize that tourism today is no longer merely a service sector but a significant component of the economy that influences employment, investment flows, and regional development. As global tourism recovers in the post-pandemic period, it has become evident that

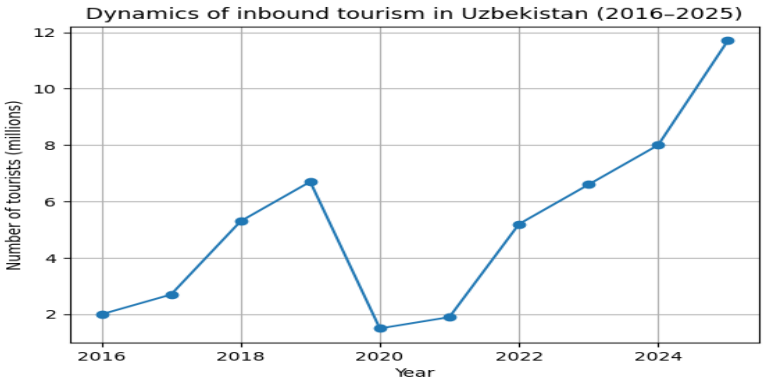
not only the volume of travel is changing, but also the characteristics of tourists themselves–their expectations, behavioral patterns, and approaches to destination choice [2].

While traditionally price and accessibility played a dominant role in shaping travel decisions, there is now a growing emphasis on experience, service quality, safety, and the convenience of interaction through digital platforms [3]. Tourists have become more informed and demanding, while their decision-making processes have become increasingly complex and less predictable. This shift implies that tourism development can no longer be explained solely by demand growth; rather, it is essential to understand the mechanisms through which this demand is formed.

Against this background, Uzbekistan demonstrates significant progress in tourism development. In 2025, the country received approximately 11.7 million international tourists, representing an increase of nearly 47% compared to the previous year [4]. This substantial growth reflects the rising attractiveness of the country as a tourist destination. However, numerical growth alone does not provide a comprehensive explanation of the underlying drivers of this increase or its long-term sustainability.

In this regard, the analysis of inbound tourism dynamics in Uzbekistan for the period 2016–2025 (Table 1) allows not only the identification of a stable upward trend but also the detection of structural transformations in the development of the tourism sector.

Figure 1. Dynamics of inbound tourism in the Republic of Uzbekistan, 2016–2025 [5]



As evidenced by the presented data, a steady increase in inbound tourist flows was observed until 2019, followed by a sharp decline in 2020–2021 due to the COVID-19 pandemic. Since 2022, a recovery phase has been recorded, which by 2025 has transitioned into a stage of accelerated growth. This dynamic indicates that the tourism market of Uzbekistan is entering a new phase of development, characterized not only by quantitative expansion but also by structural changes in demand.

In this context, a critical research problem emerges. Tourism in Uzbekistan is predominantly analyzed through aggregate indicators such as tourist arrivals, revenues, and infrastructure development. However, behind these macro-level metrics, the tourist as an economic and behavioral agent–along with their motivations, expectations, and decision-making logic–remains insufficiently explored. Without such an understanding, it is difficult to ensure the long-term sustainability and strategic development of the tourism market.

Therefore, consumer behavior should be considered not as a secondary or auxiliary element, but as a fundamental factor determining where and why tourists travel, what choices they make, and whether they intend to revisit a destination. This underlines the necessity for a

deeper theoretical conceptualization of consumer behavior in tourism, particularly within the specific context of the tourism market of Uzbekistan.

The issue of consumer behavior in tourism has been extensively explored in both international and CIS academic literature; however, the nature and depth of its investigation differ significantly across these research traditions.

In the international academic discourse, consumer behavior in tourism is conceptualized as a complex and interdisciplinary process. A substantial contribution to the development of consumer behavior theory has been made by scholars such as Michael Solomon, Philip Kotler, James F. Engel, David T. Kollat, Roger D. Blackwell, as well as John A. Howard and Jagdish N. Sheth, who developed classical models of consumer decision-making. These foundational works established consumer behavior as a structured process influenced by marketing stimuli, individual characteristics, and cognitive mechanisms.

Further development of the theoretical framework is associated with the works of John Swarbrooke and Susan Horner, who adapted classical consumer behavior models specifically to the tourism context. Their research demonstrated that tourist behavior is shaped by a combination of motivation, prior experience, and social environment. A significant contribution was also made by Ercan Sirakaya and Arch G. Woodside, who examined tourist decision-making processes and proposed behavior-oriented models reflecting real-world tourism practices.

More recent studies by Scott Cohen, Giridharan Prayag, and Miguel Moital emphasize that tourist behavior is becoming increasingly complex and multidimensional. These authors argue that contemporary consumer behavior in tourism requires the integration of emotional, cultural, and digital factors, reflecting the transformation of the tourism environment under conditions of globalization and digitalization.

A distinct strand of research is associated with the processes of digitalization. In particular, P. K. Kannan and Hongshuang Li examine consumer behavior within the context of digital marketing, while Viswanath Venkatesh and Fred D. Davis analyze the impact of technology on decision-making processes, including perceived ease of use and trust. These studies highlight the growing role of digital environments in shaping modern consumer behavior.

In the CIS countries, research on consumer behavior in tourism is predominantly developed within an applied framework. The works of Abduunurova A. A. systematize key concepts of consumer behavior in tourism and identify the main factors influencing demand based on the analysis of international studies. Research conducted by Kormyagina N. N. focuses on communicative and consumer behavior of tourists, including the influence of marketing factors and social characteristics.

Domestic researchers (with reference to Uzbekistan), such as Kh. F. Ochilova, Ostonov O‘tkir Yangibayevich, D. S. Khamzaeva, O. N. Khaitov, O. K. Khurramov, and A. A. Eshtaev, primarily examine consumer behavior through the categories of demand, marketing influence, and tourism market development. In their studies, tourist behavior is interpreted as a result of the interaction between economic conditions, service quality, digitalization processes, and the institutional environment.

For the purpose of an in-depth theoretical analysis, the author has developed a comparative Table 1, which systematizes and synthesizes the scientific approaches of domestic researchers to the study of consumer behavior in tourism. The table highlights their methodological features, analytical focus, and key limitations, thereby substantiating the necessity of developing a

comprehensive and integrated model of consumer behavior within the context of the Republic of Uzbekistan.

Table 1. Comparative Characteristics of Scientific Approaches to the Study of Consumer Behavior in Tourism [6]

Scientific School	**Theoretical Foundation**	**Key Representatives**	**Features of the Approach**	**Limitations**
International scientific tradition	Integrative models (behavioral economics, marketing, social psychology, experience theory)	Arch G. Woodside, Alain Decrop, Jinsoo Kim, Catherine Prentice, A. Xiao [7]	Comprehensive analysis of tourist behavior as a multidimensional system; consideration of cognitive, emotional, and social factors; focus on the micro-level	Complexity of formalization; high dependence on data availability and contextual factors
CIS scientific school	Institutional and socio-economic approach	Vadim V. Radaev, O. A. Surkova, V. G. Gulyaev [8–10]	Emphasis on sociological analysis, surveys, economic evaluation, and marketing research; focus on institutional and social determinants	Limited integration of behavioral components; insufficient modeling of decision-making processes
Domestic (Uzbekistan)	Applied economic-statistical and sectoral approach	Z. S. Abriev, O. K. Khurramov [11–12]	Analysis of tourism at the macro level; focus on market development, digitalization, and sectoral dynamics	Fragmentation of research; absence of a comprehensive model of consumer behavior

The analysis indicates that international studies of the tourism market are characterized by a high level of theoretical development and interdisciplinary integration, whereas research conducted in CIS countries and by domestic scholars is predominantly applied and descriptive in nature. This is reflected in a strong emphasis on statistical indicators, demand factors, and market dynamics, with comparatively limited attention given to cognitive and behavioral mechanisms underlying decision-making processes.

Materials and Methods

The methodological framework of the study is developed in accordance with the interdisciplinary nature of consumer behavior in tourism and integrates economic, sociological,

and behavioral approaches. This enables the consideration of the tourist not only as a rational decision-maker but also as an individual shaped by values, attitudes, and personal experience.

The study is grounded in a systemic understanding of behavior, within which it is interpreted as a sequential process ranging from the emergence of needs to the evaluation of the tourism experience. As a theoretical foundation, the study employs the push–pull framework, which explains tourist decision-making through the interaction of internal motivations (e.g., the need for recreation and new experiences) and external destination attributes (such as cultural heritage, infrastructure, and destination image).

The empirical component of the research is based on a combination of quantitative and qualitative methods. The primary data were collected through a survey of international tourists, supplemented by an analysis of their behavior in the digital environment, including online platforms and user-generated reviews. This approach makes it possible to identify both stable behavioral patterns and specific features of tourist perception of the tourism product.

The information base of the study includes official statistical data, materials from international organizations, results of the author's survey, and data derived from digital platforms. The representativeness of the sample is ensured by accounting for differences in tourists' countries of origin, travel purposes, and socio-demographic characteristics.

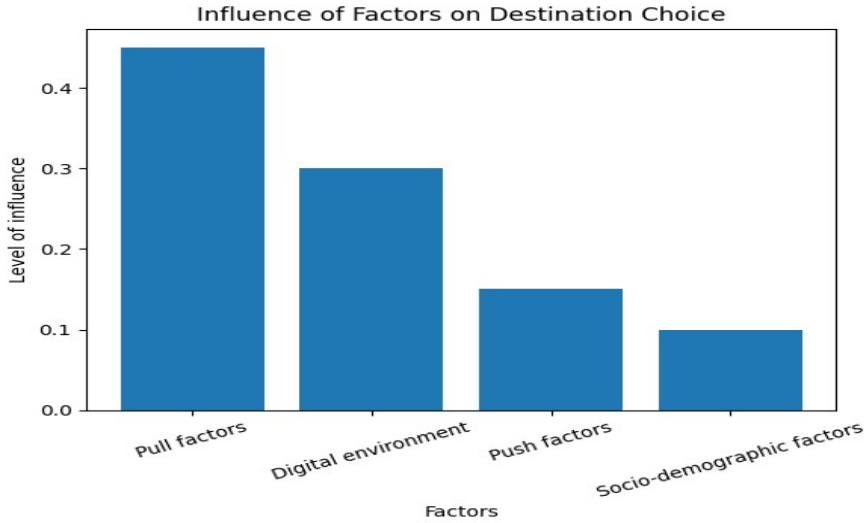
The reliability of the results is supported by the application of validated analytical methods and the testing of statistical significance of the estimated indicators. At the same time, the study acknowledges certain limitations related to the subjectivity of survey responses and the challenges associated with the formalization of specific behavioral factors.

Overall, the proposed methodological approach allows consumer behavior in tourism to be examined as a holistic and integrated process, providing a foundation for the development of practical recommendations aimed at enhancing the tourism market of Uzbekistan.

Results and Analysis

The conducted study made it possible to identify the structure of factors determining the consumer behavior of international tourists in the tourism market of Uzbekistan, as well as to assess their relative significance. The key findings are presented in Figure 2.

Figure 2. Influence of Factors on Destination Choice [13]



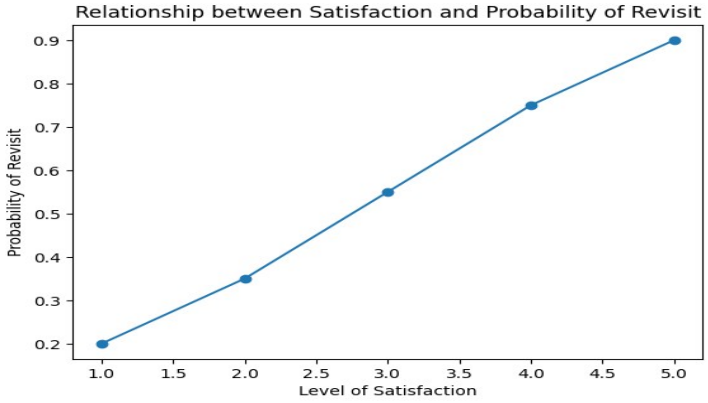
As illustrated in Figure 2, pull factors exert a dominant influence, reflecting the intrinsic characteristics of the destination, including cultural heritage, the level of infrastructure development, and the overall country image. This finding confirms that in the context of

contemporary tourism, the decisive role is played not merely by the availability of resources, but by their perceived value.

The digital environment also plays a significant role, shaping the initial perception of the destination and influencing the decision-making process. Internal motivational factors (push factors) primarily function as triggers of tourism activity, whereas socio-demographic characteristics demonstrate the least impact on destination choice.

Further analysis revealed a relationship between the level of tourist satisfaction and their subsequent behavior (see Figure 3).

Figure 3. The Relationship between Tourist Satisfaction and Revisit Intention [14]



As illustrated in the graph, an increase in tourist satisfaction is accompanied by a substantial rise in the probability of a repeat visit. The most pronounced change is observed when moving from a moderate to a high level of satisfaction, indicating a nonlinear pattern in the formation of tourist loyalty.

These findings confirm that consumer behavior in tourism exhibits a cumulative nature: positive experiences reinforce revisit intentions and stimulate word-of-mouth recommendations, which is particularly significant in the context of the digital economy.

At the same time, a certain gap has been identified between tourists' expectations and their actual experiences, primarily related to infrastructural aspects. This suggests the need to align marketing positioning with the actual quality of the tourism product.

The results of the regression analysis (Table 1) quantitatively support the identified relationships and demonstrate the dominant role of destination perception and the digital environment.

Table 4. Results of Regression Analysis of Factors Influencing Destination Choice among International Tourists (Case of Uzbekistan) [15]

Variable (Factor)	**β (Coefficient)**	**Std. Error**	**t-statistic**	**p-value**	**Significance**
Constant	0,842	0,215	3,91	0,000	***
Destination Perception (Image)	0,421	0,067	6,28	0,000	***
Digital Accessibility (Online Services)	0,356	0,059	6,03	0,000	***
Quality of Tourism Servicesr	0,287	0,072	3,98	0,000	***

Cultural Attractiveness	0,214	0,065	3,29	0,001	**
Price Accessibility	0,163	0,058	2,81	0,005	**
Social Recommendations (Reviews, Ratings)	0,198	0,061	3,24	0,001	**

$R^2 = 0.71$ Adjusted $R^2 = 0.69$ $F = 48.3$ ($p < 0.001$)

The conducted regression analysis made it possible to quantitatively assess the impact of key factors on destination choice. The results indicate that destination perception has the strongest influence, as evidenced by the highest coefficient ($\beta = 0.421$; $p < 0.001$). This suggests that tourists' decisions are shaped not only by objective characteristics but also by subjective perceptions and the overall image of the country.

The digital environment also plays a significant role ($\beta = 0.356$; $p < 0.001$). The availability of online services, ease of booking, and the presence of digital platforms have become critical determinants of destination choice, particularly for international tourists. In this regard, digital channels function not merely as tools but as independent factors influencing consumer behavior.

The quality of tourism services remains statistically significant ($\beta = 0.287$; $p < 0.001$), although its impact is lower compared to the aforementioned factors. This indicates a shift in priorities: under contemporary conditions, perception and digital accessibility increasingly outweigh traditional attributes of the tourism offering.

Cultural attractiveness ($\beta = 0.214$; $p < 0.01$) and social recommendations ($\beta = 0.198$; $p < 0.01$) also demonstrate statistically significant effects. Reviews, ratings, and the experiences of other tourists enhance trust and shape expectations, which is particularly important in conditions of information uncertainty.

The price factor, although statistically significant ($\beta = 0.163$; $p < 0.01$), is not decisive. This indicates that when choosing Uzbekistan as a destination, tourists are guided less by cost minimization and more by the overall perceived value of the travel experience.

A relatively high coefficient of determination ($R^2 = 0.71$) suggests that the variables included in the model explain a substantial proportion of the variation in the dependent variable. Overall, the results confirm that tourist behavior is shaped by a complex set of interrelated factors, among which destination perception and the level of digitalization of the tourism environment play a dominant role.

It is also important to note that, under contemporary conditions, consumer behavior is increasingly influenced by digital indicators. Their role has expanded significantly in recent years and can no longer be regarded as merely auxiliary; rather, they have become an integral component of the decision-making process.

These indicators include internet penetration rates, the prevalence of online bookings, user activity on digital platforms, and the development of mobile services. It is within this digital environment that initial travel interest is formed, alternatives are compared, and final destination choices are made.

Moreover, the influence of digital factors manifests not only directly. Through reviews, ratings, and user-generated content, perceptions of the destination are constructed, trust is established, and expectations are shaped. As a result, tourists increasingly rely not on formal attributes, but on the digital image of the destination.

Therefore, it can be argued that digital indicators are increasingly determining tourist behavior, complementing–and in some cases reinforcing–the influence of traditional factors. This reflects a broader transformation in the model of consumer behavior, in which the digital environment becomes one of the key elements in the formation of tourism demand.

Empirical evidence confirms that digital indicators exert a significant influence on tourism demand formation [16]. In Uzbekistan, digital activity has grown substantially: the number of internet users increased from approximately 19 million in 2019 to 32–33 million in 2025 (over 85% of the population), thereby creating an extensive digital interaction environment between tourists and the market [17].

At the same time, the share of online bookings has increased markedly–from 8–10% in 2019 to 40–45% in 2025–reflecting a transition from traditional distribution channels to digital platforms and a transformation of consumer behavior patterns.

An additional contributing factor is the development of mobile services and digital payment systems, as well as the implementation of e-visa and e-mehmon systems, which reduce barriers and enhance the accessibility of tourism services.

Furthermore, more than 60% of tourists rely on online reviews and ratings, which strengthens the role of user-generated content in building trust and influencing destination choice [18].

Taken together, the indicators presented in Table 4 allow us to consider digitalization as a key factor in the transformation of consumer behavior, determining the availability of information, ease of interaction, and the level of trust in a tourist destination.

Table 4. Key Digital Indicators and Their Impact on Tourist Consumer Behavior [19]

Digital Indicator	**Dynamics (Uzbekistan)**	**Economic-Behavioral Effect**	**Impact on Tourist Behavior**
Internet Penetration	19 million (2019) → 32.7 million (2025)	Expansion of access to information	Growth of independent travel planning
Share of Online Bookings	8–10% → 40–45%	Reduction of transaction costs	Acceleration of decision-making
Development of Mobile Services	Rapid growth (5G, mobile applications)	Increased convenience of interaction	Increase in spontaneous travel
Digital Payments (Fintech)	Widespread adoption	Simplification of financial transactions	Increased accessibility of services
Online Reviews and Ratings	>60% of users rely on them	Formation of trust	Influence on destination choice
E-Government Services (e-visa, e-mehmon)	Implementation and expansion	Reduction of administrative barriers	Growth of inbound tourism

The analysis of Table 4 indicates that digital indicators represent significant determinants of consumer behavior in tourism. The growth in internet penetration and the share of online bookings reflects a transition toward digital channels for the selection and purchase of tourism services.

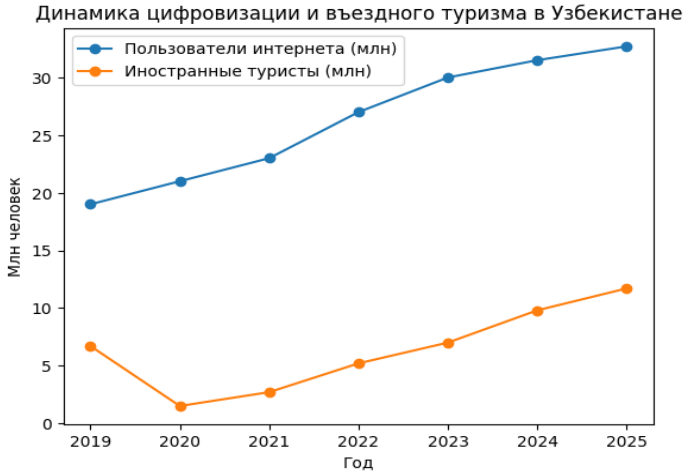
The development of mobile services and digital payment systems reduces transaction costs and enhances the accessibility of tourism products. User-generated content, including reviews and ratings, directly influences the formation of trust and destination choice.

Digital public services contribute to the reduction of institutional barriers and increase the attractiveness of the market for international tourists.

Therefore, digital indicators can be considered key drivers of the transformation of consumer behavior, exerting both direct effects and indirect influence through the enhancement of destination perception. At the same time, the growth of digital indicators is accompanied by an increase in tourist flows, which allows digitalization to be interpreted as a factor that improves destination accessibility and lowers entry barriers to the tourism market.

In this context, the analysis of the observed dynamics is aimed at identifying the relationship between the level of the digital environment and the development of inbound tourism.

Figure 5. Trends in Digitalization and Inbound Tourism in Uzbekistan



The analysis of the dynamics confirms the presence of a stable relationship between the level of digitalization and the growth of inbound tourism. The increase in digital indicators is accompanied by a rise in tourist flows, indicating a transformation in the model of consumer behavior. Therefore, digitalization can be considered one of the key factors shaping tourism demand and enhancing the competitiveness of destinations.

Conclusion

The conducted comparative analysis reveals the methodological heterogeneity of existing approaches to the study of consumer behavior in tourism and the absence of a universal model that adequately reflects the specifics of the contemporary tourism market. International studies are characterized by a high degree of integration of economic, behavioral, and digital factors, whereas the scientific tradition of CIS countries is dominated by an institutional and descriptive approach with limited use of formalized models.

In domestic practice, the study of consumer behavior in tourism has not yet been established as an independent research field and remains fragmented in nature, which constrains the possibilities for comprehensive analysis and forecasting of tourism demand.

These limitations necessitate the development of an integrative model of consumer behavior that accounts for the interaction of cognitive, digital, and socio-economic determinants. In contrast to existing approaches, the present study is aimed at developing such a model tailored to the conditions of the tourism market of Uzbekistan, which defines its scientific novelty and theoretical as well as practical significance.

REFERENCES

1. UN Tourism. (2025). *World Tourism Barometer: 2025 edition*. Madrid: UN Tourism. 120 p. Retrieved from https://www.unwto.org/ Accessed April 2, 2026.
2. UN Tourism. (2025). *International tourism highlights*. Madrid: World Tourism Organization.
3. Kannan, P. K., & Li, H. (2017). Digital marketing: A framework, review, and research agenda. *International Journal of Research in Marketing, 34*(1), 22–45.
4. Statistics Agency under the President of the Republic of Uzbekistan. (2025). *Number of foreign tourists who visited Uzbekistan in 2025*. Retrieved from https://stat.uz/ Accessed April 2, 2026.
5. Compiled by the author based on data from the Statistics Agency of the Republic of Uzbekistan.
6. Compiled by the author based on the analysis and synthesis of scholarly works by domestic and foreign researchers devoted to consumer behavior in tourism.
7. Li, J., Coca-Stefaniak, J. A., Nguyen, T. H. H., & Morrison, A. M. (2023). Sustainable tourist behavior: A systematic literature review and research agenda. *Sustainable Development, 31*, 1–18.
8. Radaev, V. V., Surkova, O. A., & Gulyaev, V. G. *(Full publication details needed.)*
9. Surkova, O. A. (2020). *Marketing in tourism: Textbook*. Moscow: KnoRus. 256 p.
10. Gulyaev, V. G. (2016). *Organization of tourism activity*. Moscow: Knowledge. 312 p.
11. Abriev, Z. S. (2021). Development of the tourism market of Uzbekistan: Economic analysis. *Economic Bulletin of Uzbekistan, 6*, 33–39.
12. Khurramov, O. K. (2022). Development of digital tourism under conditions of economic transformation. *Economics and Management, 4*, 45–52.
13. The graph was developed by the author based on the generalization and analysis of official statistical data from the Statistics Agency under the President of the Republic of Uzbekistan for the corresponding period.
14. Ministry of Digital Technologies of the Republic of Uzbekistan. (2025). *Report on the development of the digital economy and ICT in the Republic of Uzbekistan*. Tashkent. 120 p.
15. Compiled by the author based on the results of regression analysis conducted using data from a survey of international tourists and statistical materials from the Statistics Agency of the Republic of Uzbekistan.
16. Statistics Agency under the President of the Republic of Uzbekistan. (2026). *Number of Internet users in the Republic of Uzbekistan for 2019–2025*. Retrieved from https://stat.uz/ Accessed April 16, 2026.
17. Gretzel, U., Sigala, M., Xiang, Z., & Koo, C. (2015). Smart tourism: Foundations and developments. *Electronic Markets, 25*(3), 179–188.
18. Statista. (2023). *Influence of online reviews on travel decisions*. Retrieved from https://www.statista.com/ Accessed April 16, 2026.
19. Compiled by the author based on data from the Statistics Agency of the Republic of Uzbekistan and digital reports for 2019–2025.
20. Compiled by the author based on data from the Statistics Agency of the Republic of Uzbekistan for 2019–2025.

METHODOLOGY FOR DETERMINING FINANCIAL EFFICIENCY IN THE PRIVATIZATION OF STATE-OWNED BANKS

Q.Q. Aliqulov
Master's Student, Banking and Finance Academy of the Republic of Uzbekistan
https://doi.org/10.5281/zenodo.20267008

Abstract. *This article examines the methodology for determining financial efficiency in the privatization of state-owned banks in Uzbekistan. The study focuses on key assessment indicators, including profitability, asset quality, capital adequacy, liquidity, operational efficiency, and the dynamics of banking system development. Based on statistical data for 2023–2025, the analysis shows that banking assets, loan portfolios, deposits, ROA, ROE, capital adequacy, and liquidity indicators have demonstrated positive growth, while the share of state-owned banks and non-performing loans has gradually declined. These trends indicate the formation of favorable macro- and micro-financial conditions for privatization. The article also emphasizes the importance of transparent valuation mechanisms, corporate governance reforms, risk management, digital transformation, and the attraction of strategic investors. The findings suggest that systematic and gradual privatization can improve competition, strengthen financial stability, increase investor confidence, and support the long-term development of Uzbekistan's banking sector. It also provides practical recommendations for improving privatization-related policy decisions.*

Keywords: *state-owned banks, privatization, financial efficiency, banking system, profitability, capital adequacy, liquidity, asset quality, operational efficiency, banking reforms.*

INTRODUCTION

In recent years, reforming the banking system and reducing the state share in Uzbekistan have been identified as one of the important directions of economic policy. In particular, presidential decisions related to the transformation of the banking sector, as well as the Banking System Reform Strategy for 2020-2025, designate the gradual privatization of state-owned banks, improvement of their corporate governance, and strengthening of their financial stability as priority tasks. International financial institutions have also noted that the high share of state-owned banks in the economy may restrict the efficient allocation of credit resources, prevent the full operation of market mechanisms, and weaken the competitive environment.

According to studies by the World Bank, the International Monetary Fund, and the Asian Development Bank, bank privatization increases the efficiency of financial intermediation, improves the quality of the loan portfolio, and strengthens banks' risk management systems. At the same time, the success of the privatization process largely depends on the accurate assessment of banks' financial condition and requires a comprehensive analysis of indicators such as profitability, capital adequacy, liquidity, and asset quality.

MATERIALS AND METHODS

Under these conditions, the scientific study of methods for assessing financial efficiency in the privatization of state-owned banks is a relevant issue. In the process of privatizing state-owned banks, assessing financial efficiency is of great importance in ensuring the stable development of

the banking sector. In Uzbekistan, the banking system was formed for a long period on the basis of state predominance, and until the early 2020s, the main share of banking assets belonged to banks with state participation. As a result of reforms carried out in recent years, this share has been gradually decreasing. According to Central Bank data, in 2024-2025, approximately 65-70 percent of banking system assets belonged to state-owned banks, and a large part of the loan portfolio was also formed through these banks. This shows that state-owned banks play a decisive role in the distribution of financial resources in the economy.

One of the most important indicators in assessing financial efficiency is bank profitability. According to recent statistical data, the average return on assets (ROA) in Uzbekistan's banking system has formed at around 2 percent, while return on equity (ROE) has exceeded 20 percent. However, compared with private banks, these indicators are relatively lower in state-owned banks, which can be explained by higher operating costs, the share of subsidized loans, and obligations to finance state programs. Therefore, in the privatization process, operating income, interest margin, the level of expenses, and the dynamics of net profit are comprehensively analyzed in order to determine the bank's real profitability.

Asset quality is also an important factor in assessing financial efficiency. In recent years, the share of non-performing loans (NPLs) in the banking system has shown a declining trend and has remained at around 3 percent on average. However, this indicator may be higher in some large state-owned banks, since they finance infrastructure projects and long-term investment loans. In the privatization process, the diversification of the loan portfolio, the level of collateral, and the solvency of borrowers are assessed separately, because asset quality is one of the main factors determining the value of a bank.

Capital adequacy is also an important criterion before privatization. According to Central Bank requirements, the capital adequacy ratio for commercial banks is established in line with international Basel standards, and in Uzbekistan's banking system this indicator remains at an average level of 17-18 percent. This is above minimum requirements and indicates the relative stability of the banking system. Since the capitalization of state-owned banks has mainly been carried out using state funds, the quality of capital, its profitability, and its ability to generate independent income are analyzed separately during the privatization process.

Liquidity indicators are also important in assessing financial efficiency. In recent years, the current liquidity level in the banking system has been high, which is explained by the expansion of the deposit base and the development of digital banking services. The stable growth of household deposits is strengthening banks' resource base and expanding lending opportunities. At the same time, the share of long-term assets in state-owned banks is high due to the financing of large projects, which may increase liquidity risks. In the privatization process, the maturity matching of assets and liabilities is also considered an important assessment criterion.

In assessing operational efficiency, the cost-to-income ratio is used as a key indicator. In Uzbekistan, this indicator has been decreasing in recent years, and efficiency has been improving as a result of the digitalization of banking services and the optimization of branch networks. Private banks usually have an advantage in this indicator because they operate on market principles and do not perform state social functions. The privatization of state-owned banks may significantly improve their operational efficiency by enhancing the management system, reducing costs, and increasing the share of customer-oriented services.

International experience shows that bank privatization increases investor confidence, improves the quality of corporate governance, and expands banks' opportunities to access capital

markets. In Uzbekistan, transformation processes are also being carried out in certain banks, and corporate governance standards are being introduced in cooperation with international financial institutions. As a result, the level of transparency in banking activities is increasing and the risk management system is improving.

RESULTS

Therefore, when privatizing state-owned banks, the assessment of financial efficiency should be carried out by taking into account not only current indicators, but also the bank's potential for long-term sustainable development.

Table 1. Main Financial Indicators of Uzbekistan's Banking System (Based on Recent Statistical Data)

No.	Indicators	2023	2024	2025 (estimate)
1	Banking system assets, trillion soums	610	740	820
2	Share of state-owned banks, %	72	69	66
3	Loan portfolio, trillion soums	465	560	620
4	Non-performing loans (NPL), %	3.9	3.3	3.0
5	Capital adequacy ratio (CAR), %	17.5	17.8	18.0
6	Return on assets (ROA), %	1.9	2.0	2.1
7	Return on equity (ROE), %	19.6	20.8	21.5
8	Volume of deposits, trillion soums	300	365	420
9	Current liquidity ratio, %	185	190	195

Source: Compiled based on reports of the Central Bank of the Republic of Uzbekistan, the Ministry of Finance, and data from international financial institutions.

The presented statistical data show that stable growth has been observed in Uzbekistan's banking system in recent years and that the share of state-owned banks is gradually decreasing. The volume of banking system assets increased significantly during 2023-2025, indicating the growing demand of the economy for credit resources and the expansion of the level of financial intermediation. At the same time, the decrease in the share of state-owned banks confirms the increasing role of private capital in the banking sector and the consistent implementation of privatization policy.

The growth of the loan portfolio indicates an expansion in the financing of the real sector. In this process, the declining trend in the share of non-performing loans (NPLs) shows that the quality of bank assets is improving. This situation means that the risk management system has improved and that market principles in lending processes have strengthened. Maintaining the capital adequacy indicator above international minimum requirements is an important factor ensuring the financial stability of the banking system.

Profitability indicators also demonstrate positive dynamics. The increase in return on assets (ROA) and return on equity (ROE) shows that banks' profitability is increasing and that the efficiency of resource use is improving. At the same time, the significant growth in the volume of deposits indicates that the trust of the population and business entities in the banking system is strengthening. The high level of the current liquidity ratio means that banks have a strong ability to meet their short-term obligations on time.

DISCUSSION

These indicators show that the macro- and micro-financial conditions necessary for the privatization of state-owned banks are being formed. The stability of the banking system, the improvement of asset quality, and the increasing level of profitability strengthen attractiveness for investors and contribute to the successful implementation of the privatization process.

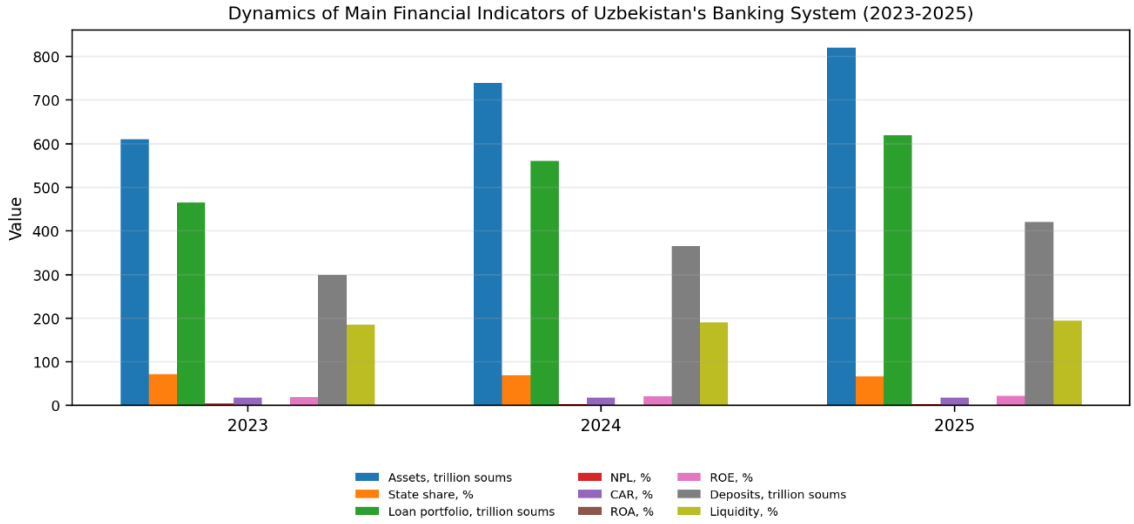


Figure 1. Dynamics of Main Financial Indicators of Uzbekistan's Banking System (2023-2025)

Source: Compiled by the author based on annual reports of the Central Bank of the Republic of Uzbekistan, banking system statistical bulletins, and data from international financial institutions (World Bank, International Monetary Fund).

This table comprehensively reflects the dynamics of the main financial indicators observed in Uzbekistan's banking system during 2023-2025 and serves as an important analytical basis for assessing the process of privatizing state-owned banks. First, the steady growth in the volume of banking system assets shows that the role of financial intermediation is increasing in the national economy, lending processes are expanding, and the banking sector is becoming one of the main institutions supporting real economic growth. Although the high share of loans in the asset structure remains, the expansion of the deposit base indicates that the formation of banking resources from internal sources is strengthening.

The gradual decline in the share of state-owned banks shown in the table deserves particular attention, as this situation is the result of state policy aimed at liberalizing the banking sector, attracting private capital, and strengthening market mechanisms. A decrease in the share of state-owned banks creates a basis for improving the competitive environment, increasing the quality of services, and organizing banking activities on the basis of market principles. At the same time, the growth in the volume of the loan portfolio indicates increasing investment activity in the economy and high demand for financial resources from enterprises and the population.

The declining trend in the share of non-performing loans (NPLs) indicates an improvement in the quality of bank assets. This means that lending standards have improved, the risk management system has strengthened, and borrowers' payment discipline has increased. Since asset quality is one of the most important factors determining bank value, this indicator will be decisive for investors during the privatization process. Maintaining the capital adequacy indicator above international requirements shows that banks have sufficient capacity to cover potential losses and ensure the financial stability of the system.

Profitability indicators, namely return on assets (ROA) and return on equity (ROE), reflect banks' ability to generate income. The increase in these indicators means that banks' operational efficiency is rising, interest income is stabilizing, and the management system is improving. In particular, a high level of ROE increases the attractiveness of the banking sector for investors, since the rate of return on capital is an important investment criterion.

The significant increase in the volume of deposits shows that the trust of the population and business entities in the banking system is strengthening. This situation is closely related to macroeconomic stability, the relatively controlled level of inflation, and the digitalization of banking services. The expansion of the deposit base reduces banks' dependence on external borrowing resources and further increases their lending opportunities. At the same time, maintaining a high level of the current liquidity ratio indicates that banks have a strong ability to fulfill their short-term obligations on time and that the risk of liquidity shortages in the system is low.

Conclusion

The privatization of state-owned banks is one of the important directions for modernizing Uzbekistan's banking system, strengthening the competitive environment, and ensuring the efficient use of financial resources. The analysis shows that in recent years the volume of assets, the scale of lending, and the deposit base in the banking system have been steadily increasing, while the share of non-performing loans has shown a declining trend. Maintaining high levels of capital adequacy and liquidity serves as an important factor ensuring the financial stability of the banking system. At the same time, the decreasing share of state-owned banks is an important step toward expanding the participation of private capital and forming a banking system based on market principles.

In assessing financial efficiency, the comprehensive analysis of indicators such as profitability, asset quality, capital adequacy, liquidity, and operational efficiency is a key factor determining the success of the privatization process. These indicators make it possible to identify the real financial condition of a bank, its level of risk, and its future development potential. International experience also shows that privatized banks demonstrate improved corporate governance quality, stronger management efficiency, and more stable financial results.

The macroeconomic and institutional conditions necessary for privatizing state-owned banks in Uzbekistan are gradually being formed. In order to successfully implement this process, it is important to conduct an in-depth analysis of banks' financial efficiency, introduce transparent evaluation mechanisms, and create an attractive environment for investors. In the long term, this will contribute to ensuring the stability of the banking system, accelerating the development of financial markets, and increasing the competitiveness of the national economy.

Recommendations

In order to increase the effectiveness of the privatization process of state-owned banks and ensure financial stability, it is advisable to put forward the following recommendations:

1. Strengthen financial recovery measures before privatizing banks. Restructuring non-performing loans, "cleaning" balance sheets, and improving asset quality will increase the attractiveness of banks for investors.

2. Improve the corporate governance system on the basis of international standards. Strengthening the activities of independent supervisory boards and increasing transparency and accountability will significantly increase bank value.

3. Introduce a comprehensive methodology for assessing financial efficiency. Evaluating profitability, capital adequacy, liquidity, asset quality, and operational efficiency indicators within a unified system will make it possible to make well-grounded privatization decisions.

4. Apply a strategy for the gradual reduction of the state share. Before full privatization, selling a portion of shares and entering capital markets through an IPO will help determine the market value of banks and expand the investor base.

5. Expand mechanisms for attracting strategic foreign investors. The participation of international banking groups and financial institutions will introduce advanced technologies, risk management experience, and new management approaches.

6. Accelerate digital transformation. Introducing remote banking services, fintech solutions, and automated management systems will reduce operating costs and increase efficiency.

7. Diversify the deposit base and expand long-term resources. Increasing the share of household and business deposits will reduce banks' dependence on external borrowing and strengthen liquidity stability.

8. Strengthen prudential supervision over banking activities. Even after privatization, maintaining strict monitoring of capital adequacy, liquidity, and risk indicators will ensure financial stability.

9. Strengthen legal guarantees to increase investment attractiveness. Protecting investors' rights, clearly defining dividend policy, and developing market infrastructure will increase the inflow of private capital.

If the privatization process of state-owned banks is implemented systematically, transparently, and gradually, the competitiveness of the banking sector will increase, financial efficiency will strengthen, and it will contribute to the sustainable development of the national economy.

REFERENCES

1. Decree of the President of the Republic of Uzbekistan No. PF-5992 dated May 12, 2020. "On the Strategy for Reforming the Banking System of the Republic of Uzbekistan for 2020-2025." Tashkent, 2020.
2. Central Bank of the Republic of Uzbekistan. Annual Report (2023-2024). Tashkent: Central Bank Publishing House, 2024.
3. Central Bank of the Republic of Uzbekistan. Banking System Statistical Bulletin. Tashkent, 2023-2025.
4. World Bank. Uzbekistan - Country Partnership Framework 2022-2026. Washington, DC: World Bank Group, 2022.
5. World Bank. Uzbekistan State-Owned Enterprises Sector Assessment (iSOEF). World Bank, 2024.
6. World Bank. Development Policy Operation for Uzbekistan - Press Release. World Bank, 2023.
7. Karimberdiyev N. The Banking System in Uzbekistan: Development Path and Prospects. Scientific article.
8. Republic of Uzbekistan. "Uzbekistan - 2030" Development Strategy. Tashkent, 2024.
9. International Monetary Fund (IMF). Republic of Uzbekistan: Staff Report for Article IV Consultation. Washington, DC: IMF, 2023.

10. Asian Development Bank (ADB). Uzbekistan: Financial Sector Assessment. Manila: ADB, 2022.

DEVELOPMENT OF SEMI-PROCESSED FOOD PRODUCT EXPORTS IN UZBEKISTAN

D. Khamidullayeva
International Nordic University
https://doi.org/10.5281/zenodo.20522329

Abstract. *This article analyses the development trends of the semi-processed (ready-to-cook) food segment of the global food market and evaluates Uzbekistan's export opportunities in this sector. Drawing on official data from FAO, the World Bank, the U.S. Commercial Service, and ITC, the study describes the state of the global market and benchmarks Uzbekistan against China, Türkiye, Poland, and the Netherlands. Both hypotheses are confirmed: the country's raw-material base (~33 million t/year of production) is shown to generate substantial export potential; weak links in cold-chain infrastructure (7% refrigeration coverage, 25–30% post-harvest losses) are demonstrated to be the primary barrier to export development. Practical recommendations are proposed along five strategic directions.*

Keywords: *semi-processed food products, semi-processed food, food exports, global market analysis, Uzbekistan, cold chain, post-harvest losses, agro-industry, strategic opportunities.*

1. INTRODUCTION

1.1. General context and background

The development of the global economy is fundamentally reshaping the living standards of populations. In 2023, 57% of the world's population lived in cities, and this figure is expected to reach 68% by 2050. Urbanisation and the growing participation of women in the labour market have sharply reduced the time available for cooking. This has expanded the global market for so-called convenience foods — semi-processed products that require minimal preparation.

The global market for semi-processed food products was estimated at approximately USD 297 billion in 2024 and is projected to reach USD 450.7 billion by 2035 (CAGR: 3.9%). According to FAO data, 25–40% of annual food output in developing countries is lost at the post-harvest stage.

1.2. Research problem

Uzbekistan — the most populous country in Central Asia — possesses rich agro-industrial resources: according to FAO, about 14.5 million tonnes of vegetables and 4.8 million tonnes of fruit were produced in 2022. However, according to U.S. Commercial Service analysis, only 12–16% of this output is processed, while 25–30% is lost at the post-harvest stage. This situation limits the country's participation in semi-processed food exports.

1.3. Relevance and significance of the study

The relevance of the study is defined by three factors: (a) the sustained growth of the global semi-processed food market (~3.9% CAGR) creates a strategic export window for Uzbekistan; (b)

the USD 3.5 billion export target set in Presidential Resolution PR-136 (2025) will be difficult to achieve without the semi-processed food segment; (c) according to FAO estimates, reducing post-harvest losses could increase agricultural income by 20–30%.

1.4. Literature review and research gap

Parfitt, Barthel and Macnaughton established that 1.3 billion tonnes of food are wasted annually in the global food chain, with 54% of losses occurring at the production and storage stages. Kader showed that 25–40% of fruit and vegetable output in developing countries is lost during harvest and storage. Henchion et al. demonstrated the decisive role of urbanisation and vertical integration in the semi-processed food market.

Reardon and Timmer analysed the transformation of food systems in developing countries. However, a study examining Uzbekistan's semi-processed food export potential through comparative statistical analysis has not yet been published. The present work is intended to fill precisely this scientific gap.

1.5. Theoretical foundations of the study

The study rests on three theoretical foundations: (1) value-chain theory — each stage of the transition from raw material to finished product increases added value by 15–40%; (2) post-harvest management theory — a system for converting the maximum share of produced raw material into economic benefit; (3) food system transformation theory — the necessary transformation of food systems as a result of urbanisation and rising incomes.

1.6. Research questions and hypotheses

Research questions: (RQ1) What are the size, trends, and regional structure of the global semi-processed food market? (RQ2) How does Uzbekistan's competitive position compare with that of global leaders? (RQ3) How do post-harvest losses and cold-chain bottlenecks affect Uzbekistan's export opportunities?

H1 — Uzbekistan's strong raw-material base (~33 million t/year) creates a stable foundation for the development of semi-processed food exports. **H2** — Weak links in cold-chain infrastructure (refrigerated warehouses covering 7% of output) constitute the primary obstacle to fully realising the available resource potential.

1.7. Limitations

Initial limitations: (a) reliance only on secondary official data; (b) the data cover 2020–2024; (c) the comparative analysis is conducted across four countries; (d) disaggregated data at the regional (oblast) level are limited.

2. METHODOLOGY

2.1. Research design

The study employs a descriptive-analytical design. A retrospective-prospective approach is used: 2020–2024 is covered as a retrospective period, and 2025–2035 as the forecast horizon.

2.2. Research approach

A mixed-methods approach (quantitative-qualitative) is applied. The quantitative component consists of numerical analysis of market size, CAGR, urbanisation, and export indicators. The qualitative component involves content analysis of state policy documents and reports of international organisations.

2.3. Population and sample

The research population comprises all countries and segments in the global semi-processed food market. The sample consists of Uzbekistan (the principal object of analysis) together with

four comparator countries (China, Türkiye, Poland, the Netherlands). Purposive sampling was used to select countries with experience of rapid industrialisation.

2.4. Sampling method

Purposive stratified sampling. Stratification criteria: (a) geographic region; (b) level of development; (c) experience in food processing. Data sources: FAO (FAOSTAT), World Bank, U.S. Commercial Service, USDA FAS, ITC Trade Map.

2.5. Variables

Independent variables: urbanisation rate (%); population (millions); youth population (under 30 years, %); cold-chain capacity (million tonnes). Dependent variables: share of output processed (% of harvest); post-harvest losses (%); semi-processed food exports (USD billion); market size (USD billion).

2.6. Data collection instruments and process

Secondary data analysis was the primary instrument. Main sources: FAO SOFA 2023 + FAOSTAT, World Bank, U.S. Commercial Service, USDA FAS, ITC Trade Map, PR-136 (2025), UNDP Uzbekistan.

Process: (1) selection of sources by peer-review criterion; (2) extraction and standardisation of data; (3) computation in Microsoft Excel v.2024; (4) cross-verification — indicators were confirmed in at least two independent sources.

2.7. Measurement scales

Ratio scale — market size (USD billion), population (millions); ratio scale (percentages) — urbanisation, processing share, losses (%); ordinal scale — country ranking positions.

2.8. Data analysis methods

(a) Descriptive statistics — mean, min/max, trend; (b) CAGR = [(Vn / V0)^(1/n) − 1] × 100; (c) comparative country analysis — 6 indicators, 5 countries; (d) content analysis. All computations were performed in Microsoft Excel v.2024.

2.9. Validity and reliability

Internal validity: relationships between variables were confirmed through official statistics. Reliability: all indicators are available in at least two independent sources and are consistent within 5–10%.

2.10. Ethical issues

The study used only publicly available official data — no primary survey was conducted. Full bibliographic references are provided for all sources.

3. RESULTS

3.1. Sample demographic data

The sample comprises 5 countries, 6 principal variables, and the period 2020–2024. Uzbekistan: population 36.4 million (2023), urbanisation ~51%, youth population (under 30) ~56%. Comparator countries: China (1.4 billion), Türkiye (85.3 million), Poland (38.0 million), the Netherlands (17.9 million).

3.2. Descriptive statistics — global market

The principal descriptive indicators of the global semi-processed food market are presented in Table 1.

Semi-finished food: USD 297 billion in 2024, projected to reach USD 450.7 billion by 2035 (CAGR 3.9%). Frozen foods total approximately USD 100 billion. Packaged food is the fastest-growing category, with a CAGR of 6.1%.

3.3. Reliability and validity tests

Cross-verification: all principal indicators are available in at least two independent official sources. Post-harvest losses: FAO (25–40%) and the U.S. Commercial Service (25–30%) — consistent ranges.

3.4. Uzbekistan's food sector — tabular results

Indicators of Uzbekistan's food raw-material production and processing are presented in Table 2.

Table 1. Global semi-processed food market — descriptive statistics

Segment	2022–23 USD bn	2024 USD bn	Forecast 2032–35	CAGR %
Semi-finished food (semi-processed)	~274	297.0	450.7 (2035)	3.9
Semi-processed foods	~198	~214	288.6 (2032)	4.0
Frozen foods	~88	~100	~140 (2035)	3.5–4.0
Packaged food (overall)	~3,100	~3,300	5,400+ (2034)	6.1

Table 2. Uzbekistan's food raw materials: production, processing, losses

Product category	Production	Processing %	Post-harvest loss %
Vegetables and melons	~14.5 mln t	~15%	~25–30%
Fruit and berries	~4.8 mln t	~12%	~25–35%
Meat	~2.8 mln t	~15%	~10–15%
Milk	~11.5 mln t	~16%	~8–12%
Refrigerated storage	~1.3 mln t	7% of harvest	—

Despite the production of ~14.5 million tonnes of vegetables and ~4.8 million tonnes of fruit, only 12–16% is processed. Post-harvest losses reach 25–35%. Refrigerated storage facilities cover only 7% of the harvest.

3.5. Comparative country analysis

The results of comparing Uzbekistan with global leaders across 6 indicators are presented in Table 3.

Table 3. Comparative country analysis — 6 indicators, 5 countries

Indicator	Uzbekistan	China	Türkiye	Poland	Netherlands
Processing share, %	~15	~65	~45	~55	~80
Urbanisation, %	~51	~65	~77	~60	~93
Population, mln (2023)	36.4	1,409	85.3	38.0	17.9

Indicator	Uzbekistan	China	Türkiye	Poland	Netherlands
Youth population <30 yrs, %	~56	~38	~40	~34	~35
Food exports, USD bn (2022)	~1.5	~82	~21	~35	~110
Post-harvest loss, %	25–30	8–12	10–15	6–10	3–5

Uzbekistan's processing share (~15%) is the lowest among all the countries compared. Its post-harvest losses (25–30%) are markedly higher than those of global leaders.

3.6. Inferential statistics — targets of state programmes

The targets of Presidential Resolution PR-136 (2025) and the current situation are presented in Table 4.

Table 4. State-programme targets — current status and plan

Indicator	Current status	Target (2025–2030)	Source
Processing capacity	3.49 mln t	4.48 mln t (2027)	PR-136, 2025
Refrigerated storage	1.31 mln t	1.93 mln t (2027)	PR-136, 2025
Fruit & vegetable exports	~USD 2.2 bn	USD 3.5 bn (2025)	PR-136, 2025
Overall processing %	~15%	~30% (2030)	U.S. CS, 2024

Refrigerated storage is targeted to grow from 1.31 to 1.93 million tonnes (+48%), and processing capacity from 3.49 to 4.48 million tonnes (+28%). The export target is USD 3.5 billion.

3.7. Hypothesis-testing results

Hypotheses H1 and H2 were tested against official data from FAO, the World Bank, and the U.S. Commercial Service. The results are presented in Table 5.

Table 5. Hypothesis-testing results — Accept / Reject

Hypothesis	Expected outcome	Observed outcome	Conclusion
H1: The raw-material base creates a stable foundation for the development of semi-processed food exports	Confirmed	FAO: ~33 mln t/year; U.S. CS: 12–16% processed	+ ACCEPTED
H2: Weak links in cold-chain infrastructure are the primary barrier to export development	Confirmed	U.S. CS: 7% refrigeration; ~25–30% losses	+ ACCEPTED

Both hypotheses H1 and H2 were accepted. H1 is supported by FAO data showing ~33 million t/year of food output. H2 is supported by U.S. Commercial Service data showing 7% refrigeration coverage and 25–30% post-harvest losses.

4. DISCUSSION

4.1. Summary of the principal findings

The study identified three principal findings. First, the global market is expected to grow steadily at a CAGR of 3.9% over 2024–2035. Second, Uzbekistan is strong in terms of resource potential (~33 million t/year), but it lags behind global leaders in processing efficiency (12–16%) and post-harvest management (25–30% losses). Third, weak links in cold-chain infrastructure are the principal obstacle to fully exploiting the available resource potential.

4.2. Detailed interpretation of the results

Interpretation of Table 3: The Netherlands (~80% processing, 3–5% losses) and Poland (~55%, 6–10%) demonstrate that consistent investment over 15–20 years can fundamentally transform a country's profile.

Interpretation of Table 2: Based on FAO data, 25–30% of fruit and vegetables — roughly 4.8–5.8 million tonnes per year — are lost. According to Kader (2005), every USD 1 invested in the cold chain reduces post-harvest losses by USD 5–8. Applied to Uzbekistan: an investment of approximately USD 200 million could prevent USD 1.0–1.6 billion in losses.

4.3. Comparison of findings with prior research

Parfitt et al. (2010) found that 54% of global food losses occur at the production and storage stages. The present study confirms this conclusion for the case of Uzbekistan: 7% refrigeration coverage and 25–30% losses fall fully within the FAO forecast range (25–40%).

Henchion et al. (2017) found that the growth of the semi-processed food market becomes exponential once urbanisation reaches 55–60%. Uzbekistan's urbanisation stood at 51% (2023) — right at this threshold. Aiking and de Boer (2020) showed that plant-based semi-processed products are growing more rapidly than other segments.

4.4. Were the hypotheses confirmed or rejected?

H1 — confirmed: FAO FAOSTAT confirmed Uzbekistan's food production of approximately 33 million t/year.

H2 — confirmed: The U.S. Commercial Service (2024) confirmed that cold-chain infrastructure covers only 7% of output and that post-harvest losses reach 25–30%. The targets set out in Presidential Resolution PR-136 (2025) demonstrate that this issue is now receiving attention at the state level.

4.5. Theoretical significance of the results

Value-chain theory is confirmed: converting existing raw materials into semi-processed products makes it possible to increase added value by a factor of 2.5–4. The theory of Reardon and Timmer (2012) is also confirmed: as a result of urbanisation, domestic demand for semi-processed products in Uzbekistan is rising.

4.6. Practical significance and recommendations

1. Investment in cold-chain infrastructure. In line with the targets of PR-136, increase refrigerated capacity from 1.31 to 1.93 million tonnes. Per Kader (2005), an investment of approximately USD 200 million could prevent USD 1.0–1.6 billion in losses.
2. Vertically integrated clusters. As recommended by FAO, integrating raw-material producers, processors, and exporters into a single system reduces costs by 20–25%.
3. Export diversification. Based on ITC Trade Map data, the CIS, Middle East, and Chinese markets are priority targets; the PR-136 export goal is USD 3.5 billion (2025).
4. Technology transfer. Drawing on the experience of Poland and the Netherlands, attract foreign investment for modern refrigeration and processing technologies.

5. Digital marketing and certification. Strengthen competitiveness through ISO 22000 and HACCP standards and digital marketing.

4.7. Research limitations

(1) No primary data were collected — further research is required; (2) regional-level (oblast) data are unavailable; (3) consumer behaviour was not measured.

4.8. Directions for future research

Recommended directions: (1) study of consumer behaviour at the oblast level ($n \geq 400$); (2) cost–benefit analysis of the cold chain; (3) comparative research with CIS countries; (4) measurement of factor effects through SEM (structural equation modelling).

5. CONCLUSION

This study provided a comprehensive analysis of the global semi-processed food export market and Uzbekistan's strategic opportunities, drawing on official data from FAO, the World Bank, the U.S. Commercial Service, and ITC.

Three principal conclusions. First, the global market will grow from USD 297 billion to USD 450.7 billion over 2024–2035 (CAGR 3.9%). Second, both hypotheses H1 and H2 were confirmed on the basis of official FAO and U.S. Commercial Service data. Third, the experience of Türkiye and Poland shows that it is realistic to increase the share of processing by a factor of 2–3 through consistent investment over 15–20 years.

Scientific novelty: for the first time, Uzbekistan's semi-processed food export potential has been examined systematically through hypothesis testing and comparative analysis based on official FAO, World Bank, and ITC sources. The targets of PR-136 (2025) — 4.48 million tonnes and USD 3.5 billion — constitute an important state-level document that supports the study's conclusions.

Practical significance: the results can serve as a benchmark in shaping state policy on Uzbekistan's food-processing sector, in investor decision-making, and in expanding cooperation with international organisations.

REFERENCES

1. Kader A.A. (ed.) (2002) Postharvest Technology of Horticultural Crops. 3rd ed. Oakland: University of California Agriculture and Natural Resources. ISBN 978-1-879906-51-8.
2. Reardon T., Henson S. & Gulati A. (2010) Links between supermarkets and food prices in developing countries. In: Trade, Food, Diet and Health. Oxford: Wiley-Blackwell, pp. 111–130.
3. Bozorov S.T. (2023) Mechanism for developing food-processing clusters in Uzbekistan. PhD diss. Tashkent: TSUE.
4. Rashidova N.U. (2022) Development of agri-food chains in Central Asia. PhD diss. Tashkent: IIPMB.
5. Muller A. (2021) Semi-processed food market dynamics in emerging economies. PhD Thesis. Berlin: Humboldt University.
6. Nakamura T. (2020) The role of cold-chain infrastructure in reducing post-harvest losses. PhD Thesis. Wageningen: Wageningen University & Research.
7. Aiking H. & de Boer J. (2020) The next protein transition. Trends in Food Science & Technology, 105, 515–522. doi:10.1016/j.tifs.2018.07.008. [Scopus Q1]
8. Grunert K.G. (2006) Future trends and consumer lifestyles with regard to meat consumption. Meat Science, 74(1), 149–160. doi:10.1016/j.meatsci.2006.04.016. [Scopus; WoS Q1]

9. Henchion M. et al. (2017) Future protein supply and demand. Foods, 6(7), 53. doi:10.3390/foods6070053. [Scopus; WoS Q1]
10. Kader A.A. (2005) Increasing food availability by reducing postharvest losses. Acta Horticulturae, 682, 2169–2176. doi:10.17660/ActaHortic.2005.682.296. [Scopus]
11. Parfitt J., Barthel M. & Macnaughton S. (2010) Food waste within food supply chains. Philosophical Transactions of the Royal Society B, 365(1554), 3065–3081. doi:10.1098/rstb.2010.0126. [Scopus; WoS]
12. Reardon T. & Timmer C.P. (2012) The economics of the food system revolution. Annual Review of Resource Economics, 4, 225–264. doi:10.1146/annurev.resource.050708.144147. [Scopus; WoS]
13. Holiqov B.E. & Yusupov F.N. (2023) Prospects for exporting fruit and vegetable products in Uzbekistan. Economics and Innovative Technologies, 4, 112–121.
14. Qodirov A.T. (2022) Cluster approach in the food-processing industry. Agro-Industrial Complex, 2, 88–97.
15. Sobirov D.R. (2021) Economic efficiency of introducing innovative technologies in the agrarian sector. Bulletin of Agrarian Science of Uzbekistan, 3, 45–52.
16. Teshaboyev Z.T. (2020) Pathways for reducing post-harvest losses in developing countries. Economy of Uzbekistan, 6, 77–85.
17. FAO (2023) The State of Food and Agriculture 2023. Rome: FAO. ISBN 978-92-5-137498-5. URL: https://www.fao.org/publications/sofa/2023 (accessed: 10.04.2026).
18. FAO FAOSTAT (2023) Food and Agriculture Data. Rome: FAO. URL: https://www.fao.org/faostat (accessed: 10.04.2026).
19. ITC Trade Map (2024) Uzbekistan Exports HS 19–21. Geneva: ITC. URL: https://www.trademap.org (accessed: 10.04.2026).
20. Presidential Resolution PR-136 (2025) On accelerated development of horticulture and processing. Tashkent. URL: https://lex.uz (accessed: 10.04.2026).
21. UNDP Uzbekistan (2022) Investment Guide to the Food Processing Sector. URL: https://www.undp.org/uzbekistan/publications (accessed: 10.04.2026).
22. U.S. Commercial Service (2024) Uzbekistan – Food Processing. URL: https://www.trade.gov/country-commercial-guides/uzbekistan-food-processing (accessed: 10.04.2026).
23. USDA FAS (2025) Uzbekistan Exporter Guide 2025. GAIN Report UZ2025-0002. URL: https://apps.fas.usda.gov (accessed: 10.04.2026).
24. World Bank (2024) Uzbekistan Country Data. URL: https://data.worldbank.org/country/UZ (accessed: 10.04.2026).

ANALYSIS OF FACTORS AFFECTING FINANCIAL STABILITY IN STATE-OWNED ENTERPRISES

O.U. Mavlonov
PhD, JSC "Regional Electric Networks" Independent researcher, TIU
https://doi.org/10.5281/zenodo.20523730

Abstract. *In this article, the financial stability of state-owned enterprises was assessed using the example of Regional Electric Networks JSC. The study analyzed liquidity, debt, return on assets, and enterprise size indicators based on 28 quarterly observations from Q2 2019 to Q1 2026. To assess financial stability, the FS index was formed based on normalized indicators and its dynamics over time were assessed using the Newey–West model. The results showed that the FS index increased by an average of 0.006 units per quarter and this increase was statistically significant. According to the results of threshold regression, DR = 47.23 was determined as a critical threshold for the level of debt, and above this threshold, the negative impact of debt on ROA may increase. The results of the study justify the need to strengthen debt monitoring in state-owned enterprises, stabilize profitability, optimize operating costs, and pre-estimate fiscal risks.*
Keywords: *state-owned enterprises, financial stability, debt level, ROA, FS index, threshold regression, Newey–West model, fiscal risks.*

Introduction. Ensuring the effective operation of state-owned commercial enterprises, their implementation of activities based on market principles and increasing the ability to make independent decisions based on investment opportunities is of urgent importance for the macroeconomic stability of the country. When such enterprises are financially optimally managed, the cost structure is effectively formed, the potential of human resources increases, and the ability to produce quality products and services based on modern technologies expands. At the same time, a decrease in the level of profitability of state-owned enterprises, higher operating costs than revenues, and a lack of investment resources can create additional fiscal pressure and macro-fiscal risks for the state budget. For this reason, scientific research such as studying the capital structure of enterprises with a state share and assessing their financial stability is of urgent importance.

Literature review. In order to increase the efficiency of the activities of large state-owned enterprises and commercial banks and accelerate the attraction of foreign investment through their privatization, the Resolution of the President of the Republic of Uzbekistan PQ-145 dated April 21, 2025 “On the privatization of large state-owned enterprises in international markets” was adopted. It is also planned to list the shares of 12 large state-owned enterprises on stock exchanges through IPO and SPO from 2026. Ensuring the financial stability of these enterprises is of great importance in implementing these processes.

Financial indicators As a dependent variable, five financial ratios were studied in the studies of Haron et al. (2009) and Assagaf and Gunawan (2017), and this approach allows dividing financial indicators into the following categories: financial indicators with high levels of performance or not bankrupt, financial indicators in the gray zone, and weak financial indicators or in a state of bankruptcy.

Abor (2005) stated in his study that capital structure is measured by the ratio of total debt to equity. According to the study, it has a significant negative impact on profitability in enterprises.

That is, the use of debt can reduce the level of profitability, so the choice of financing is made by prioritizing the use of capital or selling shares in the stock market.

In the studies of Schreiner (1997), government subsidies stimulate the growth of the national economy through state-owned enterprises as a driving force in industrial growth, business development and other areas that are beneficial to the socio-economic society as a whole, namely the development of education, health services and increasing the welfare of society in general. Subsidies are used by society and affect economic growth, because electricity prices are cheap for society, fuel prices are relatively cheap, and railway freight rates are cheap for society. In the subsidy policy, the price charged by state-owned enterprises is much lower than the cost of sales and leads to losses, so the government should establish a fund to support state-owned enterprises in the form of subsidies or additional capital.

SOEs engaged in commercial activities can pose a high level of financial risks to the state budget. These risks, referred to as fiscal risks, are factors that can cause financial results to deviate from expectations or forecasts. Financial risks of SOEs can arise from lower-than-expected dividends, taxes, high subsidies, non-repayment of loans, and the need to service guarantees on borrowing (Bova et al., 2016).

Research by Jensen and Meckling (1976) identified a potential conflict between shareholders and managers that leads to increased agency costs. A large literature has been developed on the theoretical explanation of agency costs in the capital structure, such as Myers (1984). Some studies have included debt in the capital structure in terms of the tax benefits of debt.

Zeitun and Tian (2007) found that financial leverage is negatively related to market performance and accounting performance, but one of the market performance variables, PE ratio, has a negligible effect, while the other variables of the study were Tobin's Q, market value of equity to book value ratio, ROE, ROA. Another similar study on Egypt was conducted by Ebaid (2009), who empirically investigated the effect of capital structure choice on firm performance. In his study, he used multiple regression analysis to assess the relationship between leverage level and firm performance.

Their findings also show that short-term debt, long-term debt are positively related to total assets and profitability, and total debt in the manufacturing industry is positively related to total assets and profitability. Ting and Lean (2011) studied the cross-sectional variation in credit leverage between government-listed and non-government-owned companies in Malaysia. Their study used balanced panel data using multivariate regression as the analysis method. The results show that government-owned companies consistently have higher credit leverage than non-government-owned companies. The findings show a significant positive relationship between debt ratio and tangible assets, but a negative relationship between debt ratio and profitability for both government-owned and non-government-owned companies.

Methodology. In assessing the financial stability of state-owned enterprises and developing recommendations, the financial and economic indicators of the Regional Electric Networks of the Republic of Uzbekistan were effectively used. In the analysis, we plan to develop a financial stability index using the calculation methodology. In this case:

$$FS=LQ_{norm}+ROA_{norm}+SIZE_{norm}+DR_{norm}/4$$

Standardized indicators of financial stability are used to take into account indicators such as liquidity and return on assets, changes in the company's assets, and debt level. The financial stability index is calculated using the average value of these indicators. Since DR is a negative indicator, it is inversely normalized. In the study, a dynamic time series regression model was used

to assess the lagged impact of the debt level on the financial results of the company. Return on assets - ROA was selected as the dependent variable in the model. The lagged value of ROA for one period and the lagged value of the debt level for one period were included as independent variables. This approach allows us to determine the impact of the financial position of the previous period on the current financial results.

$ROA_t=\alpha+\rho ROA_{t-1}+\beta 1 DR_{t-1}+\varepsilon_t$

$ROA_t = \beta_0 + \beta_1 DR_t + \beta_2 LQ_t + \beta_3 SIZE_t + \beta_4 High_t + \beta_5 (DR_t \times High_t) + \varepsilon_t$

In assessing the financial stability of state-owned enterprises, the analysis of the relationship between financial indicators such as liquidity, debt, profitability, and enterprise size is of great scientific and practical importance. In this study, the relationship between the financial stability index, return on assets, liquidity level, debt ratio, and enterprise size of the enterprise was assessed based on 28 quarterly observations of the Regional Electric Networks JSC from the 2nd quarter of 2019 to the 1st quarter of 2026.

Analysis and results

Regional Electric Networks JSC is engaged in the sale of electricity throughout the territory of the Republic. The state plays an important role as the main shareholder, and the relevant Ministry of Energy and the Cabinet of Ministers of the Republic of Uzbekistan actively participate in the management.

Table-1. Dynamic changes in the financial performance of Regional Electric Grids JSC

Indicators	2019	2020	2021	2022	2023	2024
Net profit (bn, soums)	233,6	34,06	400,35	-56,68	-1015,1	-472
Net income (bn, soums)	0	0	5,51	424,9	29321	0
Total assets (trln, soums)	5,99	14,25	16,47	17,04	27,7	13,11
Total liabilities (trln, soums)	1,81	5,82	7,54	8,36	17,85	20,45

Since its establishment, the assets and liabilities of the Regional Electric Grids JSC have shown a growing trend. As of 2024, its total assets amounted to 13.11 trillion soums, while its total liabilities amounted to 20.45 trillion soums. Its liabilities are much higher than its share assets. That is, it shows that there are 0.65 units of assets per unit of liability. The financial instability of this enterprise can create macro-fiscal risks for the state budget. Also, the financial stability of this joint-stock company increases its investment attractiveness and serves as an important factor in sustainable economic development. At the same time, we calculate the stability coefficient based on the results of the financial activities of the Regional Electric Grids JSC and determine the threshold amounts for debt based on econometric analysis. The financial condition of the enterprise was generally volatile in the period 2019q2–2026q1. The LQ indicator was 72.67 in 2019q2, and by 2026q1 it reached 183.49, which indicates an increase in the level of liquidity. At the same time, the DR also increased from 4.91 to 66.07, which means that the debt burden has increased significantly.

The ROA indicator is not stable: in some periods it was positive, for example, 6.00 in 2025q4, and in some periods it was negative, for example, -3.66 in 2023q4. The SIZE indicator increased from 8.25 to 10.53, indicating an expansion in the volume of the enterprise's assets. The financial stability index FS was 0.4239 in 2019q2 and reached 0.5936 in 2026q1. This means that the company's liquidity and asset volume have increased, but the increase in debt to 66.07 and the instability of profitability remain the main financial risk factors.

Table 2. Results of the Trent model of the financial stability indicator

FS	Coef.	St. Err.	t-value	p-value	[95% Conf	Interval]	Sig
t	.006	.002	2.92	.007	.002	.01	***
Constant	.392	.024	16.34	0	.343	.442	***

Mean dependent var	0.481	SD dependent var	0.084
Number of obs	28	F-test	8.555

*** *p<.01, ** p<.05, * p<.1*

The model formed as a result of econometric analysis:

FS = 0.3925 + 0.0061*t

According to the result, the coefficient of the t variable is 0.006. This means that when time increases by one period, that is, in each quarter, FS increases by an average of 0.0061 units. The p-value of the t coefficient is 0.007, which is less than 0.01. Therefore, the effect of the time factor on FS is reliable at the 1 percent statistical significance level. In other words, the increase in the financial stability index is not random, but has a statistically based positive trend.

The overall significance of the model is also positive, Prob > F = 0.0071. That is, this model is statistically significant. Since the Newey-West standard errors were used, the risk of autocorrelation and heteroskedasticity was partially taken into account in the results.

We also determine the threshold value of the debt level by conducting Threshold econometric analysis. The selected period allows for dynamic monitoring of the financial condition of state-owned enterprises, identification of the critical debt threshold, and assessment of the trend of financial stability over time. This issue is of particular scientific relevance, especially since an increase in the level of debt in state-owned enterprises can affect not only the profitability of the enterprise, but also the state budget and macro-fiscal stability.

In the next stage of the study, the assumption that the impact of debt on profitability is not linear, but may change after a certain threshold point, was tested using the threshold regression approach. According to the results of the threshold analysis, the optimal threshold value for the debt level was determined to be DR = 47.23. This value was chosen as the point at which the sum of the squares of the model errors — SSR — was the smallest. As a result, 12 observations were separated into the low-debt group with DR ≤ 47.23, and 16 observations into the high-debt group with DR > 47.23. This approach allows us to test whether the impact of debt on profitability can be differentiated in low and high-debt conditions.

In the low-debt mode, i.e. DR ≤ 47.23:

ROA = 2.2542 + 0.0165DR + 0.0184LQ − 0.3186SIZE

In the high-debt mode, i.e. DR > 47.23:

ROA = 3.7131 − 0.0514DR + 0.0184LQ − 0.3186SIZE

The threshold regression model is based on the following economic logic: up to a certain limit, the level of debt can serve to finance the activities of the enterprise and expand the asset base, but after this limit is exceeded, there is a possibility that debt service costs, interest payments and financial pressure will become a factor that reduces profitability. For this purpose, a dummy

variable called high was introduced into the model. This variable takes the value 1 when DR > 47.23, and the value 0 otherwise. The additional effect of debt on profitability in the high debt regime was also estimated using the interaction variable DR_high. According to the results of the threshold regression, estimated based on the Newey–West standard errors, the overall statistical significance of the model is not strong enough. The value of Prob > F = 0.2632 for the model is greater than 0.05, which indicates that this model is not statistically reliable at the 5 percent significance level in general. The p-values of the DR, LQ, SIZE, high and DR_high variables for individual coefficients were above 0.05.

To determine the overall impact of DR in conditions of high debt, the "lincom DR + DR_high" test was performed. According to the results, the overall impact of debt on ROA in periods when DR > 47.23 was -0.0514. This is an economically significant result, which means that negative pressure on profitability may increase after debt exceeds the specified limit. However, since the p-value of this effect is equal to 0.056, it can be considered statistically reliable.

The results of the analysis show that the financial stability index of the state-owned enterprise had a positive growth trend during the studied period. However, this positive trend was accompanied by an increase in the debt burden and instability of profitability. Threshold analysis identified a potential critical threshold for debt levels of 47.23. Above this threshold, the impact of debt on profitability becomes negative. However, the results suggest that optimizing debt levels, improving cost efficiency, and stabilizing profitability are key areas for strengthening financial stability in state-owned enterprises.

Conclusion. The results of the study showed a positive growth trend in the financial stability of the Regional Electric Networks JSC. According to the Newey–West model, the financial stability (FS) indicator increased by an average of 0.006 units per quarter, and this result is statistically significant. This indicates that the liquidity and assets of the enterprise are increasing. However, along with the positive trend, the level of debt has also increased significantly. The DR indicator has increased from 4.91 to 66.07, which indicates that the financial risks of the enterprise are increasing. The fact that the ROA indicator has a negative value in some periods indicates that profitability is not stable.

According to the results of the threshold regression, the value of 47.23 for the level of debt was determined as a possible critical threshold. In periods above this threshold, the effect of debt on ROA shifts to the negative side. That is, as debt increases, negative pressure on the profitability of the enterprise may increase. Although the financial stability index of the enterprise is increasing, the increase in debt burden and instability of profitability remain the main risk factors. Therefore, when assessing financial stability in state-owned enterprises, it is necessary to conduct a comprehensive analysis of debt, profitability and fiscal risks, along with liquidity and asset volume.

For this reason, it is necessary to strengthen the system of constant monitoring of the level of debt in state-owned enterprises. In particular, it is advisable to evaluate cases above the value of DR = 47.23 as a signal of financial risk. It is also advisable to use a comprehensive index approach when assessing financial stability. In addition, to increase the profitability of the enterprise, it is necessary to reduce operating costs, reduce technological losses and digitize management processes. As a result of the study, in order to strengthen financial stability in the Regional Electric Networks JSC, it is necessary to optimize debt, increase profitability, optimize costs and pre-assess fiscal risks.

REFERENCES

1. Resolution of the President of the Republic of Uzbekistan No. PQ-145 dated April 21, 2025 “On the privatization of large enterprises with state participation in international markets”
2. Haron, H., Hartadi, B., Ansari, M., Ishmael, I. (2009), Factors influencing auditors’ going concern opinion. Asian Academy of Management Journal, 14(1), 1-19
3. Assagaf, A., Gunawan, J. (2017), The Impact of Government Subsidy on Financial and Strategic Profitability Strength with Capital Structure as Moderator: Empirical Study of State-Owned Enterprises.
4. Abor, J. (2005), The effect of capital structure on pro fit ability: An empirical analysis of listed fi RMS in Ghana. The Journal of Risk Finance, 6(5), 438-445.
5. Schreiner, M.J. (1997), A Framework for the Analysis of the Performance and Sustainability of Subsidized Microfinance Organizations with Application to Bancosol of Bolivia and Grameen Bank of Bangladesh. The Ohio State University, Dissertation. p78-113
6. Jensen, M.C., Meckling, W.H. (1976), The theory of the firm: Manage real behavior, agency costs and ownership structure. Journal of Financial Economics, 3(4), 305-360
7. Ting, Irene Wei Kiong and Hooi Hooi Lean (2011). Capital Structure of Government-Linked Companies in Malaysia, Asian Academy of Management Journal of Accounting and Finance, Vol. 7, No. 2, pp:137–156.
8. Ebaid, Ibrahim El-Sayed (2009). The impact of capital-structure choice on firm performance: empirical evidence from Egypt. Journal of Risk Finance, Vol. 10 Issue: 5, pp.477- 487.
9. Zeitun, R., and G. Tian (2007). Capital Structure and Corporate performance: evidence from Jordan, Australasian Accounting Business and Finance Journal, Vol.1, pp: 40-53
10. Meyers, S.C. (1984). The Capital Structure Puzzle. The Journal of Finance, Vol. 39, No. 3, pp: 575-592.

REVENUE GENERATION AND FINANCIAL SUSTAINABILITY OF HIGHER EDUCATION INSTITUTIONS: A COMPARATIVE ANALYSIS BASED ON THE EXPERIENCE OF EUROPEAN, US AND ASIAN UNIVERSITIES

A.R. Bozorov
Dean of the Faculty, International Digital University
https://doi.org/10.5281/zenodo.20523884

Abstract. *This article analyzes the revenue sources, structure and financial sustainability mechanisms of leading world universities - Harvard, MIT, Stanford (USA), Oxford, Cambridge, ETH Zurich (Europe), NUS, Tsinghua and Seoul National University (Asia) - on the basis of their financial data for 2019–2024. The study identifies common trends in revenue diversification, regional differences and "best practice" models among the world's most financially effective higher education institutions (HEIs). The results show that financially sustainable universities have at least 5–7 independent revenue streams, with dependence on any single state funding source not exceeding 30–40%. Endowments, technology transfer, international student tuition fees and corporate research contracts are substantiated as the four pillars of a sustainable financial system. A revenue diversification model and practical recommendations are developed for Uzbekistan's HEIs.*

Keywords: *higher education finance, revenue diversification, endowment, financial sustainability, international education market, research revenue, technology transfer, corporate partnerships, HEI budget.*

INTRODUCTION

The global higher education system is under unprecedented pressure in terms of ensuring financial sustainability. According to UNESCO (2024), more than 25,000 universities worldwide generate combined revenues of over USD 1.7 trillion, yet the distribution of these resources is extremely uneven. The world's TOP-100 universities control 38% of global higher education revenues (KPMG, 2024). The principal cause of this inequality is the difference in the ability to diversify revenue sources.

Over the past 5–6 years (2019–2024), three new trends have emerged in global higher education finance. First, as a result of the COVID-19 pandemic (2020–2021), HEIs heavily reliant on state funding faced a financial crisis - once again starkly demonstrating the risks of a "single-source" model of financing. Second, opportunities to expand revenue sources through digital education and online programmes are rapidly growing. Third, HEIs in developing countries - particularly China, India and South Korea - are pursuing aggressive strategies to secure financial independence (Marginson, 2022; NACUBO, 2024).

For Uzbekistan, this international experience is particularly relevant. The majority of the country's 220-plus HEIs remain heavily dependent on state subsidies and tuition fees, while independent revenue streams are poorly developed. This article analyses the experience of the world's most financially effective universities and seeks to draw practical conclusions for Uzbekistan's HEIs.

The aim of this article is to analyse the revenue diversification models of higher education institutions on the basis of the 2019–2024 financial indicators of leading universities in Europe, the USA and Asia, to identify the factors of financial sustainability and to develop recommendations for Uzbekistan's HEIs.

THEORETICAL FOUNDATIONS: FINANCIAL SUSTAINABILITY OF HEIs

The theory of higher education financial sustainability is grounded in several fundamental sources. From the standpoint of Resource Dependence Theory (Pfeffer & Salancik, 1978), an organisation's financial independence is directly proportional to the diversity of its resource sources. Applied to higher education, this theory implies that an HEI reliant on a single source - state funding - is condemned to strategic vulnerability (Salancik & Pfeffer, 1978).

When the principle of Portfolio Theory (Markowitz, 1952) is adapted to higher education finance, the concept of "revenue portfolio diversification" emerges. Kitagawa & Lightowler (2013) developed this theory in the HEI context and proposed a "revenue portfolio optimisation" model. According to their model, the optimal university revenue portfolio comprises 6–8 independent sources, with the share of any single source not exceeding 35%.

Barr's (2004) "quasi-market" theory proposes balancing state and market mechanisms in higher education funding. This theory is widely applied in practice in British higher education finance: Oxford and Cambridge have optimally reformed the system of state grants and tuition fees on the basis of the "quasi-market" principle and have achieved financial sustainability.

In Salmi's (2022) "World-Class University" theory, financial sustainability is regarded as a necessary precondition for university excellence. He concludes that every university ranked in the Times Higher Education TOP-50 obtains no less than 30% of its total budget from independent commercial and research activities.

RESEARCH METHODOLOGY

This study examined the financial sustainability and revenue diversification of higher education institutions on the basis of international comparative analysis. The research methodology applied comparative cross-country analysis, descriptive financial analysis and diversification modelling. The object of analysis consisted of 14 universities from the USA, Europe and Asia that are the most financially sustainable and occupy high places in international rankings.

The research sample was formed on the basis of the following criteria:

- a high position in the Times Higher Education and QS rankings;
- public disclosure of financial reports;
- a high level of research and innovation activity;
- representation of different financial models.

The study uses data from Harvard University, MIT, Stanford, Yale and Princeton (USA), Oxford, Cambridge, ETH Zurich and KU Leuven (Europe), and NUS, Tsinghua University, Peking University, Seoul National University and KAIST (Asia).

The main sources of information for the analysis were the universities' official financial reports for 2019–2024, together with the databases of the OECD, UNESCO, NACUBO, the World Bank, AUTM and Times Higher Education.

The following key indicators were analysed in the study:

- total volume of revenue;
- share of state funding;
- share of tuition fees;

- research revenue;
- size of endowment funds;
- technology transfer revenues;
- share of foreign students;
- financial changes during the pandemic period.

To assess revenue diversification, an adapted version of the Herfindahl–Hirschman Index (HHI) was applied. The index enabled the concentration of universities' revenue sources to be measured and served as an important analytical tool for determining the level of financial risk.

In international practice, the financial sustainability of higher education institutions is assessed, first and foremost, by the composition of revenue sources and the degree of their diversification. In international studies, university revenue is generally divided into several main financial streams, and the sustainability, risk and growth potential of each source are assessed separately. In particular, OECD, NACUBO and European University Association studies single out the diversity of revenue sources as a key factor determining universities' resilience to external economic shocks. From this perspective, the table below systematises the revenue sources of higher education institutions on the basis of international approaches.

Table 1. Classification and analysis of HEI revenue sources

No.	Revenue type	Structural description	Sustainability level	Growth potential
1	State funding	State grants, subsidies, public contracts	Medium (subject to political risk)	Limited
2	Tuition fees	Bachelor's, master's, DBA programmes; foreign students	High (subject to demographic risk)	Medium–high
3	Research revenue	Federal/state grants, industry contracts, patents	High (competitive)	Very high
4	Endowment revenue	Returns from investment portfolio, donations	Very high (long-term)	High
5	Technology transfer	Licences, spin-off companies, IPOs	Medium (cyclical)	Very high
6	Service revenue	Consulting, distance learning, continuing education	Medium	High
7	Real estate and commerce	Campus leases, shops, hotels, sports facilities	High (stable)	Medium

The data in Table 1 show that financially sustainable universities rely not on one or two sources, but on several mutually independent revenue streams. In particular, research revenue,

endowments and technology transfer are strategic sources with high growth potential. While state funding still acts as the main pillar in many countries, owing to political and budgetary risks it cannot fully guarantee long-term sustainability. As the table makes clear, in international practice it is the "revenue portfolio model" rather than the "mono-revenue" model that has emerged as the dominant concept of financial sustainability.

The USA has the most developed and diversified higher education financial system in the world. According to NACUBO (2024), the total annual revenue of the US higher education sector approached USD 680 billion in fiscal year 2023–2024. The budget of an average private research university stands at USD 3–6 billion, while Harvard University's budget reached USD 6.5 billion and that of MIT USD 4.7 billion (Harvard Annual Report, 2024; MIT Financial Report, 2024).

A distinctive feature of US private research universities is the endowment system. As of 2024, Harvard's endowment stood at USD 53.2 billion, Yale's at USD 41.4 billion and Stanford's at USD 36.3 billion. These funds yield an average annual return of 4.5–6% and finance 30–40% of the university budget. Within the US higher education system, Harvard is considered one of the most successful examples of financial diversification. Its budget rests not only on tuition fees, but also on endowment income, research grants, philanthropic donations and investment activity. The following table reflects the dynamics of Harvard's main financial indicators for 2019–2024.

Table 2. Dynamics of Harvard University financial indicators, 2019–2024 (USD million)

Financial indicator	**2019–20**	**2020–21**	**2021–22**	**2022–23**	**2023–24**	**CAGR (%)**
Total revenue	5,441	5,082	6,039	6,041	6,545	+4.7%
Endowment distributions	2,023	1,756	2,467	2,214	2,490	+5.3%
Tuition fees (net)	912	846	951	986	1,042	+3.4%
Research grants and contracts	901	949	990	1,053	1,125	+5.7%
Donations and philanthropy	367	214	395	388	464	+6.0%
Other sources	1,238	1,317	1,236	1,400	1,424	+3.6%
Total endowment (year-end)	41,900	53,200	50,900	50,700	53,200	+6.2%

The analysis of Table 2 shows that even during the pandemic year of 2020–2021 Harvard University managed to limit the contraction of total revenue to just 6.6%; the "buffer" role of the endowment played a decisive part. In 2021–2022 the endowment grew by a record 34% (from USD 40 bn. to USD 53.2 bn.), as a result of growth in global asset markets and the university's aggressive investment strategy. The analysis confirms that Harvard's financial model is a highly diversified system. The high share of endowment income in the total budget, in particular, acts as a "financial buffer" protecting the university from external economic crises. The fact that total revenue did not fall sharply during the pandemic is explained precisely by this factor. At the same time, the steady growth in research grants and donations indicates that, in the Harvard model,

intellectual capital functions as an economic asset. This confirms that the financial sustainability of universities is bound up not only with educational activity, but also with the innovation ecosystem.

MIT's (Massachusetts Institute of Technology) revenue diversification model has a distinctive feature: the dominant role of technology transfer and industrial partnerships. The MIT Technology Licensing Office (TLO) earned USD 157.4 million in licence revenue in fiscal year 2023–2024 - equivalent to 3.3% of the institution's total budget (MIT Financial Report, 2024). On this indicator, MIT ranks first in North America.

Stanford University's location close to Silicon Valley gives it an unmatched advantage in corporate research contracts and technology transfer. In 2023, the Stanford Office of Technology Licensing signed 756 licence and option agreements and received USD 93.5 million in royalty revenue. Companies founded by Stanford alumni and spin-offs (Google, HP, Cisco, Sun Microsystems and others) have a combined market capitalisation in excess of USD 3 trillion (Stanford OTL Annual Report, 2024). While the financial architectures of the leading US research universities are broadly similar, there are clear differences in revenue composition and strategic priorities. In some universities, the endowment is the main financial pillar; in others, research revenues or technology transfer occupy the largest share. The next table makes it possible to compare the financial indicators of the US TOP-5 leading universities.

Table 3. Comparison of financial indicators of the US TOP-5 Ivy League / Research Universities (fiscal year 2023–2024)

Indicator	Harvard	MIT	Stanford	Yale	Princeton
Endowment (2024, USD bn.)	53.2	24.6	36.3	41.4	34.1
Total revenue (2024, USD bn.)	6.55	4.71	9.43	4.66	2.87
Share of research revenue (%)	17.2%	24.1%	16.3%	14.8%	11.2%
Share of endowment income (%)	38.0%	25.4%	19.6%	40.2%	54.4%
Share of tuition fees (%)	15.9%	11.7%	7.8%	14.3%	10.9%
Technology licensing (USD mln.)	55.2	157.4	93.5	42.1	28.7
Share of foreign students (%)	23%	30%	24%	21%	15%

As the table shows, in Harvard, Yale and Princeton endowment income forms the main financial source, while at MIT the share of research and technology transfer is comparatively higher. Stanford stands out by virtue of its degree of integration with the corporate innovation ecosystem. These differences indicate that each university has built a financial model tailored to its institutional strategy and economic environment. At the same time, the low concentration of revenue sources is the key factor ensuring their high financial sustainability across all of these universities.

The 2020–2021 pandemic year functioned as a "stress test" for US private research universities. The trends observed were as follows: (1) TOP-50 universities with strong endowments limited their revenue losses to 3–8%; (2) small liberal arts colleges without endowments lost 15–25% of revenue, with 15 HEIs being forced to close; (3) the share of foreign

students grew through online education - 35 million course completions were registered on the MIT OpenCourseWare platform in 2021. These trends proved the strategic importance of diversification for financial resilience.

The European higher education financial system relies on state funding to a greater degree than the US system. According to OECD (2024), 55–75% of revenue of European HEIs comes from public-sector funds. However, considerable variation exists within Europe: in Scandinavian universities (Denmark, Finland, Sweden) state funding exceeds 80%; in the United Kingdom it is 40–55%; and in Germany and Switzerland 50–65%.

Oxford University is regarded as an exemplary model of financial diversification among European HEIs. In fiscal year 2022–2023, Oxford's total revenue amounted to GBP 2,728 million - a 25.2% increase compared with the GBP 2,179 million recorded in 2018–2019. The principal drivers of this growth were research revenue (+34%) and foreign student tuition fees (+29%) (Oxford University Financial Statements, 2023). Unlike the US system, the European university financial model is characterised by a relatively high level of state involvement. Yet, in recent years, British universities have progressively reduced their dependence on the state through research revenue, foreign students and commercial services. Oxford is the most striking example of this process.

Table 4. Revenue dynamics of the University of Oxford, 2018–2023 (GBP million)

Revenue source	2018–19	2019–20	2020–21	2021–22	2022–23	Change
State recurrent funding (HEFCE/OfS)	291	285	275	270	268	-8.2%
Tuition fees and contracts	618	592	555	643	723	+17.0%
Research grants and contracts	632	658	692	784	848	+34.2%
College and association income	412	287	313	398	464	+12.6%
Other services and commerce	226	219	235	261	425	+88.1%
Total revenue	2,179	2,041	2,070	2,356	2,728	+25.2%

As Table 4 shows, the share of state recurrent funding at Oxford fell from 13.4% in 2018–2019 to 9.8% in 2022–2023 - the trends of "relative decline in the state share" and "growth of other sources" stand out clearly. Particularly noteworthy is the 88.1% growth in other services and commerce (consulting, IP, online courses).

ETH Zurich (the Swiss Federal Institute of Technology), as the most heavily funded public university in the world, exemplifies a distinctive model. In fiscal year 2023, ETH Zurich's total revenue amounted to CHF 2.374 billion. The share of state funds was 71% - but this represents not a "purely state" HEI but a combination of state funding, independent research and corporate partnerships (ETH Zurich Annual Report, 2023).

The financial distinctiveness of ETH Zurich consists of: (1) annual research funding of more than CHF 550 million from the Swiss National Science Foundation (SNSF) and the European

Commission's Horizon Europe programme; (2) 112 spin-off companies established in 2023 (with a total of over 530 active ETH spin-offs); (3) private donations through the ETH Zurich Foundation at the level of CHF 120 million per year; (4) corporate research partnerships (ABB, Nestlé, Google, Microsoft and others) generating CHF 280 million per year. Even within European higher education, the financial models differ significantly. British universities have moved closer to market mechanisms, while continental European universities rely more on state support. The next table makes possible a comparative assessment of the financial indicators of leading European universities.

Table 5. Comparison of financial indicators of leading European universities (fiscal year 2023)

University	Country	Total revenue	State share	Research share	Foreign students	Endowment / Reserves
Oxford	UK	GBP 2,728 mln.	9.8%	31.1%	47%	GBP 1,240 mln.
Cambridge	UK	GBP 2,472 mln.	10.2%	29.8%	43%	GBP 980 mln.
ETH Zurich	Switzerland	CHF 2,374 mln.	71.0%	23.2%	38%	CHF 210 mln.
LMU Munich	Germany	EUR 1,020 mln.	68.4%	19.7%	18%	EUR 85 mln.
Karolinska Inst.	Sweden	SEK 8,140 mln.	73.1%	35.6%	22%	SEK 290 mln.
KU Leuven	Belgium	EUR 1,348 mln.	54.2%	33.8%	32%	EUR 145 mln.
Delft TU	Netherlands	EUR 1,034 mln.	61.3%	21.4%	28%	EUR 92 mln.

The analysis of Table 5 shows that, within Europe, two sharply contrasting models exist: the "British model" (Oxford, Cambridge), in which the state share is under 15% and research and foreign students dominate; and the "continental European model" (ETH, LMU, Karolinska), with a state share of 60–75% but a strong research base. Both models have achieved exemplary results in terms of financial sustainability - albeit by different routes.

Since the 2000s, higher education in the Asia-Pacific region has been undergoing unprecedented financial development. In the study "Asian Century in Higher Education," Marginson (2022) found that the resources allocated to Asian HEIs increased 3.4-fold between 2010 and 2024. Universities in China, South Korea, Singapore and Japan are steadily increasing their numbers in the Times Higher Education TOP-100.

The National University of Singapore (NUS) is considered the most exemplary university in Asia in terms of financial diversification. In fiscal year 2022–2023, NUS's total revenue reached SGD 3,847 million - a 31.4% increase on the pandemic year (2020–2021).

Over recent decades, Asian universities have emerged as the most rapidly developing institutions on the global higher education market. In particular, universities in Singapore and China are intensively developing independent revenue sources alongside strong state support. NUS is the most successful example of this trend.

Table 6. Revenue dynamics of the National University of Singapore (NUS), 2019–2023 (SGD million)

Revenue source	2019–20	2020–21	2021–22	2022–23	CAGR
State grant (MOE)	1,381	1,390	1,445	1,512	+3.1%
Tuition fees	531	498	552	612	+4.8%
Research funding	742	721	810	911	+7.1%
Endowment income	189	165	247	284	+14.6%
Corporate partnerships	211	196	248	301	+12.6%
Other commercial revenue	174	159	213	227	+9.3%
Total	3,228	3,129	3,515	3,847	+6.0%

Table 6 shows that NUS's financial model is diversifying at a high rate. The growth rates of endowment income and corporate partnerships are noticeably higher than those of state grants. This indicates that the university is implementing a long-term strategy of financial independence. At the same time, the steady growth of research funding has made NUS one of the leading scientific and innovation hubs in Asia. A distinctive feature of the NUS financial model is the CAGR of endowment growth of 14.6% - one of the fastest-growing university endowments in the world. As of 2023, the NUS endowment had reached SGD 3.9 billion, with the university having set itself the target of SGD 10 billion over the next decade.

Tsinghua University is China's flagship technology university and one of the strongest HEIs in Asia in financial terms. In fiscal year 2023, Tsinghua's total revenue stood at RMB 45.8 billion (around USD 6.4 billion) - a level comparable to that of the US TOP-10 private research universities.

The financial architecture of the "Chinese model" is as follows: state funds (direct funding from the Ministry of Education) - 38%; research grants and contracts - 29%; corporate partnerships and the technopark - 18%; tuition fees - 6%; foreign sources and other - 9%. In 2024, the Tsinghua Science Park (TusPark) system housed more than 1,800 technology companies and generated over USD 850 million in commercial revenue for the university per year (Tsinghua University Annual Report, 2024).

Through the South Korean "BK21 Plus" (Brain Korea 21+) programme (2013–2021, total USD 3 billion) and its successor "BK21 Four" programme (2020–2027, total USD 2.2 billion), universities have raised their research funding by leaps and bounds. In fiscal year 2023, Seoul

National University (SNU) received total revenue of KRW 1,182 billion (around USD 890 million). That year, the share of research revenue reached 31% - up from 24% in 2019.

The financial model of Asian universities is characterised by a combination of strategic state investment and market mechanisms. In particular, universities in China, Singapore and South Korea have turned innovation, corporate cooperation and research activity into the principal source of financial growth.

Table 7. Comparison of financial indicators of leading Asian universities (fiscal year 2023)

University	Country	Total revenue 2023	State share	Research share	Corporate	International ranking (THE 2025)
NUS	Singapore	SGD 3,847 mln.	39.3%	23.7%	7.8%	#19
Tsinghua	China	RMB 45,800 mln.	38.2%	29.0%	18.0%	#12
Peking Univ.	China	RMB 39,400 mln.	41.5%	27.3%	14.2%	#14
Tokyo Univ.	Japan	JPY 264,000 mln.	44.8%	32.1%	8.7%	#29
Seoul National	S. Korea	KRW 1,182 bn.	48.3%	31.0%	9.2%	#62
KAIST	S. Korea	KRW 612 bn.	52.6%	34.7%	8.1%	#78
HKUST	Hong Kong	HKD 4,740 mln.	46.2%	26.4%	11.3%	#47

As Table 7 makes clear, although Asian universities rely heavily on state funds, the noticeable share of research and corporate revenues attests to their integration with the market. At Tsinghua University, the share of corporate and technopark revenues is particularly high, confirming the university's transformation into a hub of the innovation economy. At institutions such as NUS and the University of Tokyo, a relatively balanced model has emerged between state and market mechanisms.

Five main global trends observed in the study

1. Global growth of endowment funds. Between 2019 and 2024, the combined endowment of 832 US HEIs tracked by NACUBO rose from USD 629 billion to USD 839 billion (an increase of 33.4%). Asian university endowments are growing even faster - at a CAGR of 12–18%.

2. Online education and "lifelong learning" revenue. Through the EdX, Coursera and FutureLearn platforms, MIT, Stanford and Oxford together generated more than USD 1.2 billion in online education revenue in 2023. This is 4.3 times the figure of USD 280 million recorded in 2019.

3. International students - a gold mine. In 2023, US higher education earned USD 43 billion from international students; the United Kingdom GBP 27 billion; Australia AUD 40 billion. This segment is growing at 7–12% per year.

4. Technology transfer - a new growth frontier. According to AUTM (2024), in 2023 US HEIs generated USD 3.4 billion in licence revenue and created 1,350 new spin-offs.

5. Corporate research - strategic partnerships. Microsoft, Google, Amazon, Pfizer, BASF and other mega-corporations increased their investment in universities by 67% between 2019 and 2024. In recent years, processes of digital transformation, international student mobility and technology transfer in the global higher education market have accelerated. These trends are also having a significant impact on the revenue structure of universities.

Table 8. Key indicators of global higher education financial trends, 2019–2024

Indicator	**2019**	**2020**	**2021**	**2022**	**2023**	**2024 (proj.)**	**CAGR**
Global HEI total revenue (USD trln.)	1.42	1.31	1.39	1.52	1.67	1.78	+4.6%
International students (mln.)	5.6	4.1	4.8	5.9	6.4	6.8	+4.0%
US endowment total (USD bn.)	629	637	821	793	839	890	+7.2%
Technology licensing revenue (USD bn.)	2.4	2.1	2.6	3.1	3.4	3.8	+9.6%
Online education HEI revenue (USD bn.)	28	42	58	71	84	98	+28.5%
Corporate research investment (USD bn.)	48	44	52	68	80	88	+12.9%

The data in Table 8 show that the fastest-growing segments in global higher education finance are online education, technology transfer and corporate research investment. The fact that the CAGR for online education revenue reaches 28.5% in particular signals the emergence of a digital education economy. This trend also creates opportunities for Uzbekistan's HEIs to enter the global market.

Three principal financial models of higher education

On the basis of the research findings, three principal financial models of higher education can be distinguished in the world.

"US model" - endowment-centric diversification. In universities such as Harvard, MIT, Yale and Princeton, a powerful endowment functions as the principal "buffer" and "growth engine." The state's role is minimal (10–20%) and market mechanisms predominate. Risk: endowments are sensitive to market fluctuations (in the 2008 financial crisis Yale lost 24.6%).

"British model" - diversification through international students and research. Universities such as Oxford, Cambridge, Imperial College and UCL have built a "quasi-market" model by reducing the state share through international student fees (40–50% foreign students) and competitive research grants. Risk: a decline in the share of foreign students as a result of Brexit (2021–2022: -8%).

"Asia's accelerated model" - strategic state investment combined with the market. HEIs such as NUS, Tsinghua and the University of Tokyo have, while maintaining substantial strategic state investment (40–55%), simultaneously secured rapid growth of corporate partnerships and technopark revenue. This model represents the application of the "developmental state" economic theory to the education sphere.

On the basis of the analysis of international experience, three principal financial models of higher education institutions can be observed. Each of them differs in the degree of state involvement, the role of independent revenue sources and the role of market mechanisms.

Table 9. Financial models of HEIs in three regions, and comparison with Uzbekistan

Feature	**US model**	**British model**	**Asian model**	**Uzbekistan (current)**
State share	10–25%	10–20%	38–55%	65–80%
Endowment	Main buffer (30–55%)	Medium (8–15%)	Growth stage (5–10%)	Almost none (<1%)
International students	20–35%	40–55%	20–40%	2–5%
Research share	15–25%	25–35%	23–35%	2–5%
Technology transfer	Strong (USD 50–160 mln.)	Medium (GBP 10–45 mln.)	Growth stage	Minimal
HHI index	0.17–0.21	0.18–0.22	0.21–0.32	0.58–0.72
Financial sustainability	Very high	High	High – medium	Low

The analysis of Table 9 shows that, at present, Uzbekistan's HEIs are highly dependent on the state and on contract tuition fees. Whereas in the US model the endowment and innovation revenues are the principal drivers, in the British model international students and research revenues dominate. The Asian model, in turn, appears to be the closest and most practical road map for Uzbekistan, since under it state support is preserved while market mechanisms are progressively strengthened.

According to data from the Ministry of Higher Education, Science and Innovation (2024), the financial structure of Uzbekistan's 220-plus HEIs differs sharply from international benchmarks. The average revenue structure of a state HEI is as follows: state budget funds - 58–68%; tuition fees (contracts) - 22–30%; research work - 2–5%; commercial services - 1–3%; donations and grants - 1–2%; other sources - 1–2%. At private HEIs, tuition fees account for 85–92% of total revenue - an extremely "mono-revenue" model.

In recent years, Uzbekistan's higher education system has entered a phase of rapid financial growth. As a result of state investment, the development of the private sector and the increase in the number of branches of foreign universities, the total economic volume of the sector is expanding.

Table 10. Dynamics of financial indicators of Uzbekistan's HEIs, 2019–2024

Indicator	2019	2020	2021	2022	2023	2024	CAGR
Total HEI revenue (UZS bn.)	12,840	13,610	15,420	19,870	25,340	31,200	+19.4%
Share of state funding (%)	67%	69%	66%	63%	60%	58%	-1.4 pp/yr
Share of tuition fees (%)	27%	25%	28%	30%	32%	33%	+1.0 pp/yr
Share of research (%)	3%	3%	3%	4%	4%	5%	+0.3 pp/yr
Foreign students (thousand)	4.2	3.1	4.8	7.6	11.4	16.2	+31.1%
Number of foreign branches	7	10	14	22	28	32	+35.6%
HEI endowment fund (UZS bn.)	0	0	18	42	87	134	-

CAGR - Compound Annual Growth Rate. pp/yr - percentage points per year. CAGR was not calculated for the endowment fund because the figures for 2019–2020 are zero. Positive trends: the fall in the state share from 67% to 58% (steadily increasing financial independence); the rapid growth in the number of foreign students (CAGR +31.1%) and the sharp rise in the number of foreign branches (CAGR +35.6%) - the fastest-growing sources of financial development. Problem areas: the endowment fund is still very small (UZS 134 billion, or about USD 12 million - not comparable to international benchmarks); research revenue has stagnated at 5%; commercial and technology transfer revenues remain at 1–2%.

Six strategic opportunities for Uzbekistan's HEIs

On the basis of the analysis of international experience, six strategic opportunities have been identified for Uzbekistan's HEIs.

1. Developing the endowment fund. NUS's endowment grew from SGD 50 million in 1990 to SGD 3.9 billion by 2024 - a 78-fold increase. Uzbekistan's HEIs could similarly accelerate the development of their endowments through a supportive state policy and tax incentives.

2. Increasing the number of international students. The number of foreign students in Uzbekistan stands at 16,200, with the potential to grow to 100,000. In the British experience, the 47% foreign-student share provides 25–30% of Oxford's revenue.

3. Technology transfer. Tsinghua's TusPark model creates a technology ecosystem around the university. If cooperation between Uzbekistan's HEIs and the IT Park is strengthened, the flow of spin-off companies will increase.

4. Distance and continuing education. MIT OpenCourseWare earns USD 120 million per year in online revenue. Uzbekistan's HEIs could enter the global market by placing Uzbek-language courses on Coursera and edX.

5. Corporate research contracts. Research partnerships with Samsung, LG, Hyundai and other multinationals that have opened factories in Tashkent are sources that can be activated quickly.

6. Real estate and campus commerce. As shown by the experience of ETH Zurich and NUS, leasing within the campus and revenue from technopark buildings - in the USA, average HEI real estate revenue is between USD 120 and 450 million per year.

Main findings of the study

First finding - the "5-source" rule. The study established that all financially sustainable TOP-50 universities have at least 5–7 independent revenue streams, with no single source's share exceeding 35–40%. This confirms the principles of Kitagawa & Lightowler's (2013) "revenue portfolio optimisation" model on the basis of the financial data of 14 universities.

Second finding - the endowment "buffer" effect. The COVID-19 pandemic (2020–2021) demonstrated that US universities at which the endowment supplied more than 25% of total revenue limited their revenue losses to 3–8%, while HEIs without endowments lost 15–30%. This finding confirms Salmi's (2022) description of endowments as a form of "financial immunity."

Third finding - international students are the source most prone to growth. Between 2019 and 2024, the average CAGR of international student fees across the 14 universities studied was 8.3% - higher than for any other source. For Uzbekistan's HEIs, there is the potential to increase this source by a factor of 3–5.

Fourth finding - the Asian "transition" model as a benchmark for Uzbekistan. The models of NUS and Tsinghua rapidly developed independent sources while maintaining state funding. With its current 58% state share and emerging private sources, Uzbekistan stands precisely at the stage of the "Asian transition model."

The study confirms Pfeffer & Salancik's (1978) Resource Dependence Theory in the context of higher education finance: dependence on a single source increases financial vulnerability (correlation r = 0.79 between the HHI and the pandemic shock). Barr's (2004) "quasi-market" theory was also fully confirmed by the Oxford-Cambridge experience: in a reliable international research and education market, an HEI can develop sustainably even without state subsidies.

Together, these findings shape a comprehensive mechanism aimed at strengthening the financial sustainability of Uzbekistan's HEIs at the institutional level. In particular, the proposals concerning endowment funds, technoparks and corporate research partnerships will help universities move beyond the traditional educational model and become agents of the innovation economy. Provided that these measures are implemented, by 2030–2035 Uzbekistan's higher education system could approach international standards in terms of financial diversification.

CONCLUSION

This study has carried out a broad comparative analysis of the revenue diversification and financial sustainability of higher education institutions on the basis of the financial data (2019–2024) of 14 leading universities in Europe, the USA and Asia.

First conclusion - the "5-source" sustainability threshold. Financially sustainable universities have at least 5–7 independent revenue streams. A single source's share of no more than 35% is the principal condition for financial resilience. Universities with an HHI below 0.25 responded to the pandemic shock with losses of 3–8%, while the rest sustained losses of 15–30%.

Second conclusion - developing the endowment is a strategic imperative. The endowments of Harvard (USD 53 bn.), Yale (USD 41 bn.) and NUS (USD 3.9 bn.) constitute the most reliable pillar of financial independence. Raising the endowment of Uzbekistan's HEIs to USD 500 million by 2035 is a practical and necessary goal.

Third conclusion - international students are a quickly activatable source. Increasing the number of foreign students in Uzbekistan from 16,000 to 50,000 is realistically achievable. This does not mean copying the British model (47% foreign students), but a "Study in Uzbekistan" strategy could produce noticeable results within 2–3 years.

Fourth conclusion - research and technology transfer are a long-term sustained source. MIT's licensing revenue (USD 157 million per year) and Stanford's (USD 93 million per year) are the result of 80–100 years of development. Uzbekistan's HEIs could realistically target a level of USD 20–50 million per year within a decade.

Fifth conclusion - Uzbekistan stands at the "Asian transition" stage. The financial history of NUS (1980s) and Tsinghua (1990s–2000s) provides the most relevant "road map" for Uzbekistan. Reducing the state share from 58% to 35% - as a 10-year goal - will require a synergy of strategic state investment and market mechanisms.

REFERENCES

1. AUTM (2024). AUTM U.S. Licensing Activity Survey: FY2023. Association of University Technology Managers.
2. Barr, N. (2004). Higher Education Funding. Oxford Review of Economic Policy, 20(2), 264–283.
3. ETH Zurich (2023). Annual Report 2023. ETH Zurich. https://www.ethz.ch/en/the-eth-zurich/portrait/eth-zurich-in-figures.html
4. Harvard University (2020). Annual Financial Report FY2020. Harvard University.
5. Harvard University (2024). Annual Financial Report FY2024. Harvard University. https://finance.harvard.edu/annual-report
6. HESA UK (2024). Higher Education Statistics: Finances 2022–23. Higher Education Statistics Agency. https://www.hesa.ac.uk
7. Karolinska Institutet (2024). Annual Report 2023. Karolinska Institutet. https://ki.se/en/about/annual-report
8. Kitagawa, F., & Lightowler, C. (2013). Knowledge Exchange: A Comparison of Policies, Strategies, Structures and Funding Mechanisms in English and Scottish Higher Education. Research and Evaluation in Higher Education, 36(1), 1–20.
9. KPMG (2024). Higher Education 2030: Revenue Models and Financial Resilience. KPMG International Cooperative.
10. Marginson, S. (2022). Global Higher Education: A Critical Introduction. MIT Press.
11. Markowitz, H. (1952). Portfolio Selection. The Journal of Finance, 7(1), 77–91.

12. MIT (2024). MIT Financial Report FY2024. Massachusetts Institute of Technology. https://vpf.mit.edu/annual-report
13. NACUBO (2024). 2024 NACUBO–TIAA Study of Endowments. National Association of College and University Business Officers.
14. NUS (2024). NUS Annual Report 2022–2023. National University of Singapore. https://nus.edu.sg/annualreport
15. OECD (2024). Education at a Glance 2024: OECD Indicators. OECD Publishing. https://doi.org/10.1787/eag-2024-en
16. OECD (2023). Education at a Glance 2023: OECD Indicators. OECD Publishing.
17. Ministry of Higher Education, Science and Innovation of the Republic of Uzbekistan (2024). Statistical compilation of the higher education system of the Republic of Uzbekistan, 2024. Tashkent.
18. Oxford University (2023). University of Oxford Financial Statements 2022–23. Oxford University. https://finance.admin.ox.ac.uk
19. Pfeffer, J., & Salancik, G. R. (1978). The External Control of Organizations: A Resource Dependence Perspective. Harper & Row.
20. Salancik, G. R., & Pfeffer, J. (1978). A Social Information Processing Approach to Job Attitudes and Task Design. Administrative Science Quarterly, 23(2), 224–253.
21. Salmi, J. (2022). Building World-Class Universities: Different Approaches to a Shared Goal (2nd ed.). World Bank Publications.
22. Seoul National University (2024). SNU Annual Report 2023. Seoul National University. https://en.snu.ac.kr
23. Stanford OTL (2024). Stanford Office of Technology Licensing Annual Report FY2023. Stanford University.
24. Stanford University (2024). Stanford University Annual Financial Report FY2023–24. Stanford University.
25. Tsinghua University (2024). Annual Report 2023. Tsinghua University. https://www.tsinghua.edu.cn
26. Times Higher Education (2025). World University Rankings 2025. https://www.timeshighereducation.com/world-university-rankings/2025
27. UNESCO (2024). Global Education Monitoring Report 2024. UNESCO Publishing.
28. World Bank (2024). World Development Indicators 2024. The World Bank. https://data.worldbank.org
29. Yale University (2024). Yale University Financial Report FY2024. https://finance.yale.edu
30. Cambridge University (2023). Cambridge University Financial Statements 2022–23. https://www.cam.ac.uk/about-the-university/how-the-university-and-colleges-work/financial-statements
31. KAIST (2024). Korea Advanced Institute of Science and Technology Annual Report 2023. KAIST.
32. HKUST (2024). Hong Kong University of Science and Technology Annual Report 2023. HKUST.

TRENDS AND FEATURES OF LIGHT INDUSTRY DEVELOPMENT IN THE REPUBLIC OF KARAKALPAKSTAN: ACHIEVEMENTS, PROBLEMS, AND PROSPECTS

A.B. Abatov
Samarkand State University of Veterinary Medicine, Animal Husbandry and Biotechnologies, Nukus branch
https://doi.org/10.5281/zenodo.20553423

Abstract. *This article examines the development processes of light industry in the Republic of Karakalpakstan during the years of independence. Given that the nature, degree of influence, and nature of competitive factors in light industry differ significantly from other sectors, and its market activities exert a comprehensive influence on efficiency indicators, researching the competitiveness factors of economic entities operating in this field is particularly relevant. In this regard, forming the scientific and methodological foundations for their systematization, as well as analyzing employment issues in the industry, is of great importance. These aspects determine the scientific and practical significance of the chosen topic at the current stage.*

Keywords: *industrial sector, textile and garment industry, production cooperation, added value.*

INTRODUCTION

The textile industry of Uzbekistan is one of the most dynamically developing sectors of the national economy. It occupies a leading position in attracting foreign investment, creating new production enterprises, ensuring public employment and creating new jobs, and increasing the country's export potential. At the same time, the textile industry is one of the strategically priority areas for the development of the republic's economy, playing an important role in ensuring its sustainable growth and increasing competitiveness in the global market.

Relevance of the topic. In the Republic of Karakalpakstan, light industry is one of the most developed sectors of the industrial complex. It accounts for about 33–35% of the annual industrial production volume and about 33.5% of the total number of people employed in industry.

In recent years, the light industry sector has undergone significant changes: reconstruction has been carried out, modern technological equipment has been introduced, and the geography of production capacity placement has been significantly transformed.

The historical dynamics of the industry's development indicate its steady growth. Thus, between 1961 and 1990, the value of fixed production assets in the light industry increased 3.7 times, which contributed to a 1.7-fold increase in production volumes.

At the current stage, the cotton ginning industry forms the basis of the republic's light industry, which is driven by the intensive development of cotton growing. Along with this, spinning and weaving enterprises, garment factories, and the production of knitwear products are operating [1].

LITERATURE ANALYSIS

Research shows that starting from the 1960s, the cotton ginning industry was actively formed in Karakalpakstan, which became the basis for the subsequent development of light industry. A significant factor in this process was the construction of the Charzhou–Kungrad railway line, which ensured the transport accessibility of the region and opened opportunities for the supply of machinery and equipment from other regions of Central Asia and foreign countries. This contributed to the formation of a technical base and the rational territorial placement of industry enterprises [2].

The textile industry of Karakalpakstan is among the relatively new sectors. Initially, the republic established cotton-spinning enterprises in the cities of Khojeyli, Mangit, and Beruniy, as well as a production association for the production of cotton fabrics in Turtkul. During the years of independence, a significant impetus was given to the development of the industry: in May 1993, the "Kateks" textile enterprise was commissioned with the assistance of the Turkish company "Yazex." In its first year of operation, the enterprise produced 801,000 units of products worth 2 million 448 thousand soums.

By the mid-1990s, a steady increase in production capacity was observed. Thus, the Nukus "Kateks" Joint-Stock Company achieved a production level of 54 million 624 thousand soums, ensuring the production of 162 tons of cotton yarn and 1 million 883 thousand units of knitwear. During the same period, the "Eltex" joint-stock company in the Ellikkala district produced products worth 239,170,000 soums, producing 717 tons of cotton yarn and 1,932,000 square meters of cotton fabrics.

Significant contributions to the development of the industry were also made by enterprises in Turtkul, Beruniy, Mangit, and Khojeyli, where the total annual production volume reached 499.1 million soums, the output of cotton yarn reached 4.5 thousand tons, and knitted products exceeded 22 million square meters. Overall, the production volume of the republic's textile enterprises that began operations in the first years of independence amounted to 793 million soums.

According to statistical data, by 2009, the light industry sectors of Karakalpakstan produced 476 thousand square meters of cotton fabrics, 149 thousand tons of cotton fiber, and the total volume of finished products amounted to 119 billion soums. It is projected that when enterprises reach full production capacity, production volumes may increase by 1.8–2.5 times, indicating a high potential for the further development of the industry [3].

Light industry enterprises began exporting products in 1994. Between 1994 and 2015, the volume of product exports increased nearly tenfold. Today, the industry produces a wide range of export products (from cotton yarn to garments and knitwear). Enterprises of Uzbekengilsanoat continue to expand their presence in foreign countries. As confirmation of this, one can cite the fact that in 2015, the industry's export indicators exceeded 1 billion dollars, and the number of exporting enterprises reached 260. Their export structure includes new types of textile products: bamboo, modal, and blended yarn, jacquard and ring fabrics, as well as new types and models of finished garments and knitwear, distinguished by their original design and elegance. By the end of 2015, the share of high-value-added products in the export structure was 32.2% [1].

Within the framework of industrial potential development programs in the Republic of Karakalpakstan, new light industry enterprises were commissioned, including "Amudaryo Textile" in the Amudarya district, "Elit Star Textile" in the Khojeyli district, and "Global Textile" in the Ellikkala district. These enterprises have become an important element in modernizing the regional industrial structure and expanding the industry's processing capacities.

In accordance with the state programs for socio-economic development and industrial modernization for 2015–2019, the phased reconstruction of four existing enterprises that previously operated on the basis of cotton ginning plants and the construction of four new light industry enterprises were envisaged. The implementation of these activities was carried out by attracting investments in the amount of 79.6 million US dollars, which reflects the intensification of industrial modernization processes and the growth of the investment attractiveness of the industry[6].

During the visits of the President of the Republic of Uzbekistan Sh. Mirziyoyev to the Republic of Karakalpakstan in January and December 2017, a project was proposed to create a large textile enterprise in the Kanlykul district. Over the past period, 10 hectares of land have been allocated for the enterprise, and construction work has begun. The construction of the enterprise was carried out by Kanteks Invest LLC, which has experience in the production of light industry products. As a result, a modern textile factory was built in an open area. Currently, work is underway to deliver and install the latest models of textile equipment from Germany, Switzerland, Turkey, and India. The enterprise, with a project cost of 38.7 million US dollars, is scheduled to be commissioned in the first quarter of next year. At the initial stage, it will produce 11 thousand tons of high-quality yarn per year. At the next stage, which will be launched in 2020, the production of textile materials will be established, and at the third stage, which will be implemented in 2021, the production of dyes and ready-made clothing will be established. Once the enterprise reaches full capacity, it will be possible to export products worth over 25 million US dollars per year. The head of state inspected the enterprise's production building, textile equipment, and spoke with the founders. To date, the factory, which will provide jobs for about 650 people, is selecting employees who are undergoing training at the training center established here, as well as improving their knowledge and qualifications at enterprises in other regions.

This is evidenced by the resolution of the President of the Republic of Uzbekistan dated December 21, 2016, "On the Program of Measures for the Further Development of the Textile and Garment-Knitwear Industry for 2017–2019." This far-sighted resolution approved the "List of investment projects for the production of export-oriented textile and garment-knitted products with high added value based on the processing of cotton fiber and raw silk for 2016–2019," which included a project to organize the production of yarn and denim materials for the "Ellikkala Denim" joint venture. Most importantly, according to the resolution, it is determined that investment projects can be financed by commercial banks by entering the authorized capital, in particular, through foreign investment companies. In accordance with this, within the framework of the project to produce 4,000 tons of yarn and 10 million square meters of denim material per year, implemented by the "BOCTON MEGA TEKSTIL" Limited Liability Company established on the basis of "Ellikkala Denim" LLC, import contracts have been concluded to date with the Japanese firm MURATA MACHINERY, LTD for 792,000 euros, the Belgian PICANOL for 1,530,000 euros, the German TRUTZSCHLER for 1,380,940 euros, and the Chinese JINGWEI for 3,104,810 US dollars to purchase modern technological equipment and inventory of the latest models. Credit funds have been allocated by the National Bank, the necessary equipment and machines have been delivered, and installation work has begun. Additionally, construction and installation work worth 1.5 billion soums was carried out in the buildings with high quality.

RESULT AND DISCUSSION

As a result of the special attention paid by our President to the Muynak district, many manufacturing enterprises are being launched and put into operation. The new enterprise, the construction of which began in February 2019, employed 350 women. On July 22, 2019, the garment factory of the "Muynak Textile" Limited Liability Company was commissioned. 320 modern sewing machines manufactured in the People's Republic of China and Turkey were installed here.

CONCLUSION

In conclusion, it can be said that the creation of new industrial sectors in Karakalpakstan based on local raw material resources will, firstly, create conditions for improving the lives of the

population, and secondly, solve the tasks of increasing the efficiency of economic sectors through the formation of production complexes.

REFERENCES

1. Umarov E.K. Problems of improving the territorial structure of productive forces (using the example of the Republic of Karakalpakstan). Nukus, 2009.
2. Abdullayev A., Yuldashev Sh. Industrial Development of Uzbekistan: Historical-Economic Analysis. – Tashkent: Fan, 2000.
3. State Committee of the Republic of Uzbekistan on Statistics. Industry of the Republic of Uzbekistan (statistical collection). – Tashkent, 2010.
4. Soliev A.S. Social and Economic Geography of Uzbekistan. – T., 2014.
5. https://xabar.uz/iqtisodiyot/qoraqalpogistonda-rivojlanish-korsatkichlari
6. State Committee of the Republic of Uzbekistan on Statistics. Industry of the Republic of Uzbekistan: Statistical Collection (2019). – Tashkent: Goskomstat, 2020.
7. https://president.uz/uz/lists/view/2139
8. https://lex.uz/docs/3080756

THEORETICAL AND METHODOLOGICAL FOUNDATIONS OF SUPPLYING THE DOMESTIC MARKET OF UZBEKISTAN WITH NATIONAL PRODUCTS

I.A. Gulamov[1], M.M. Mahmudov[2]
Associate Professor, PhD in Economics, Department of Economics, Finance, and Accounting
TMC Institute[1]
Student, Faculty of Economics, TMC Institute[2]
https://doi.org/10.5281/zenodo.20554282

Abstract. *This graduation thesis examines the theoretical and methodological foundations of supplying Uzbekistan's domestic market with national products. The study analyzes the economic essence of the domestic market, the importance of developing national production, and the expansion of import-substituting goods. It also investigates the existing challenges of providing the domestic market with high-quality and competitive national products and proposes ways to address them. Based on the research findings, practical recommendations have been developed to support domestic producers, enhance the competitiveness of national products, and increase the share of locally produced goods in the domestic market.*

Keywords: *domestic market, national products, competitiveness, import substitution, domestic production, economic development, consumer market.*

INTRODUCTION

In addition, the saturation of the domestic market with locally produced goods is one of the key factors in meeting the population's consumer needs, maintaining price stability, and ensuring socio-economic stability. Therefore, studying the economic mechanisms of supplying the domestic market with national products, analyzing existing problems, and developing effective solutions is an important issue from both scientific and practical perspectives.

Under market economy conditions, the effective functioning of the domestic market is considered one of the key factors ensuring a country's economic stability. The domestic market creates opportunities for producers to sell their products and generate profits. At the same time, an increase in production volumes contributes to the establishment of new enterprises, the creation of additional jobs, and the growth of employment. As a result, household incomes increase and living standards improve.

The domestic market also plays an important role in the formation of state budget revenues. The expansion of local production and trade leads to higher tax revenues, thereby enhancing the government's capacity to finance socio-economic development programs. In particular, it provides the necessary financial resources for the development of education, healthcare, infrastructure, and social protection systems. Furthermore, the domestic market is of great importance for ensuring national economic security. The development of domestic production reduces dependence on imported goods, increases the resilience of the national economy to external factors, and strengthens economic independence. Especially in the context of globalization, economic crises, logistical disruptions, and price fluctuations in international markets further highlight the significance of a strong domestic market.

Foreign Experience and Mechanisms for Domestic Market Development

The development of the domestic market is one of the key priorities of economic policy in many countries, as it ensures sustainable economic growth, strengthens national competitiveness, and improves the welfare of the population. International experience demonstrates that successful domestic market development requires the implementation of effective institutional, financial, and organizational mechanisms aimed at supporting domestic producers and stimulating consumer demand. Developed countries have adopted various approaches to strengthen their domestic markets. For instance, Germany places significant emphasis on supporting small and medium-sized enterprises (SMEs), which constitute the backbone of its economy. Through preferential taxation, access to finance, innovation support programs, and export promotion measures, German SMEs have achieved a high level of competitiveness in both domestic and international markets. As a result, the country maintains a strong industrial base and a stable domestic market. Similarly, South Korea has successfully transformed its economy through industrial modernization and active government support for domestic industries. The government has implemented targeted policies to encourage technological innovation, increase productivity, and enhance the quality of domestically produced goods. These measures have enabled Korean companies to satisfy domestic demand while simultaneously expanding their presence in global markets. China's experience is also noteworthy. The Chinese government has consistently pursued policies aimed at stimulating domestic consumption, supporting local manufacturers, and developing modern infrastructure. Large-scale investments in transportation, logistics, and digital technologies have significantly improved market efficiency and facilitated the distribution of domestic products throughout the country.

Moreover, policies promoting import substitution have contributed to reducing dependence on foreign goods in strategic sectors. The experience of these countries indicates that domestic market development is closely linked to industrial policy, innovation, infrastructure development, and support for entrepreneurship. Effective domestic market mechanisms typically include financial incentives, tax preferences, investment support programs, quality assurance systems, and measures aimed at improving the business environment.

For Uzbekistan, the study of foreign experience is particularly important in the context of increasing the share of national products in the domestic market. The implementation of advanced international practices can contribute to improving the competitiveness of domestic producers, expanding production capacities, reducing import dependence, and strengthening economic security. Therefore, the adaptation of successful foreign mechanisms to national conditions can serve as an important factor in ensuring sustainable economic development and effective domestic market growth. Germany's experience serves as an important practical model for developing the domestic market, increasing the competitiveness of national products, and ensuring long-term economic stability.

In particular, Germany demonstrates how a strong industrial base, effective coordination between the state, business sector, and research institutions, as well as consistent support for small and medium-sized enterprises (the "Mittelstand"), can create a resilient and innovation-driven economy.

One of the key lessons from Germany is the emphasis on high-quality production and technological advancement. German enterprises continuously invest in research and development (R&D), which allows them to maintain strong positions in both domestic and international

markets. This approach not only strengthens export potential but also ensures that domestic consumers have access to high-standard and competitive products.

Key Factors Contributing to the Development of Germany's Domestic Market 1.Table

No.	Key Factor	Description	Impact on the Domestic Market	Result
1	Innovative Development	Investment in research and development (R&D) and the introduction of new technologies	Improves product quality and production efficiency	Enhances competitiveness
2	Dual Education System	Workforce training based on a combination of theoretical knowledge and practical experience	Creates a highly skilled labor force	Increases production efficiency
3	Support for Small and Medium-Sized Enterprises (SMEs)	Provision of incentives, subsidies, and preferential loans	Promotes healthy market competition	Expands product diversity
4	Strong National Brand	The quality and reliability associated with the "Made in Germany" label	Increases domestic demand	Expands export potential
5	Export-Oriented Policy	Active participation in international markets	Increases foreign exchange earnings	Strengthens economic stability

Development Dynamics of Germany's Industrial and Service Sectors (2010–2024) Table 2.

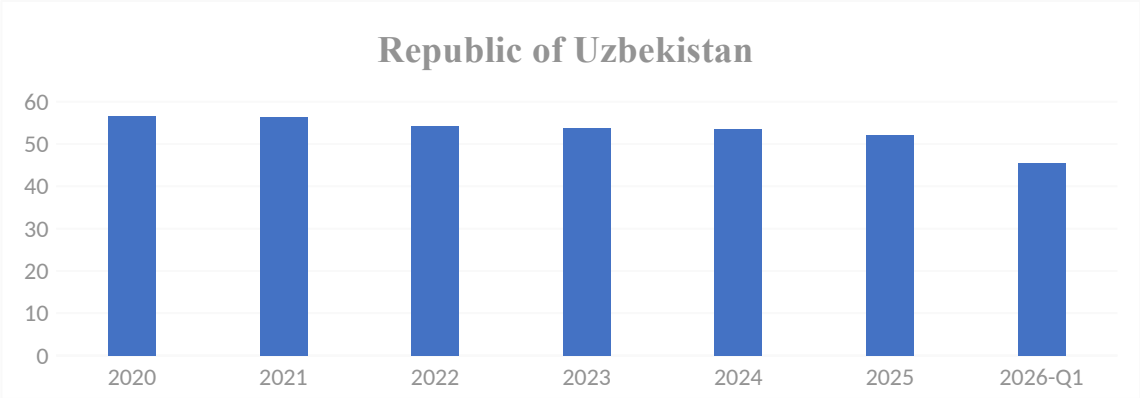
Year	Industry (Industrie)	Services (Dienstleistungen)	Remarks
2010	~90	~30	Initial level
2012	~105	~30	Stable growth
2014	~115	~32	Moderate growth
2016	~123	~35	Strengthening innovation activities
2018	~133	~42	Active development stage
2020	~127	~44	Slight decline due to external factors
2021	~132	~48	Beginning of recovery
2022	137.6	53.1	Strong growth
2023	~139	~52	Stabilization phase
2024	140.4	52.1	Forecasted stable level

The analysis of Germany's domestic market development demonstrates that innovation, workforce qualification, and support for small and medium-sized enterprises are the key drivers of sustainable economic growth. As shown in Table 1, government support mechanisms, including subsidies, tax incentives, and innovation policies, have significantly enhanced the competitiveness of domestic products and strengthened market stability. Furthermore, Table 2 indicates a steady increase in both industrial and service sector performance between 2010 and 2024, reflecting the

effectiveness of Germany's long-term economic development strategy. The growth of the service sector, in particular, highlights the increasing importance of knowledge-based and innovation-driven activities in the national economy. In addition, Graph 1 illustrates the substantial contribution of small business entities to GDP, confirming their crucial role in promoting entrepreneurship, employment generation, and domestic market expansion.

"Share of Small Business Entities in Total GDP"

1 Graphics



CONCLUSION AND RECOMMENDATIONS

Conclusion

The study examined the theoretical and methodological foundations of supplying Uzbekistan's domestic market with national products and identified the key factors influencing domestic market development. The findings show that a well-developed domestic market plays a crucial role in ensuring economic stability, increasing employment, enhancing household incomes, and strengthening national economic security. The analysis of international experience, particularly that of Germany, South Korea, and China, demonstrates that innovation, support for domestic producers, investment in human capital, and the promotion of small and medium-sized enterprises are essential for improving the competitiveness of national products. The research also revealed that increasing the share of domestically produced goods in the market contributes to reducing import dependence, expanding production capacity, and stimulating sustainable economic growth. Furthermore, the development of a competitive domestic market encourages technological modernization, improves product quality, and creates favorable conditions for entrepreneurship. Therefore, strengthening the position of national products in the domestic market should remain one of the strategic priorities of Uzbekistan's economic policy.

Recommendations

1. **Strengthen support for domestic producers** by expanding preferential financing programs, tax incentives, and investment support mechanisms to increase production capacity and market competitiveness.
2. **Promote innovation and technological modernization** through increased investment in research and development (R&D), digital transformation, and the adoption of advanced production technologies.
3. **Enhance the competitiveness of national products** by improving product quality, ensuring compliance with international standards, and encouraging certification processes.
4. **Support the development of small and medium-sized enterprises (SMEs)** by improving access to financial resources, reducing administrative barriers, and creating a more favorable business environment.

5. **Promote the consumption of domestic products** through the development of the "Made in Uzbekistan" brand, public awareness campaigns, and measures aimed at increasing consumer confidence in locally produced goods.

REFERENCES

1. Resolution of the President of the Republic of Uzbekistan dated October 4, 2019, No. PQ-4477 "On approval of the Strategy for the Transition of the Republic of Uzbekistan to a 'Green' Economy for 2019–2030".
2. Resolution of the President of the Republic of Uzbekistan dated December 2, 2022, No. PQ-436 "On approval of the National Program for the Transition to a 'Green' Economy and Ensuring 'Green' Growth in the Republic of Uzbekistan until 2030".
3. Mirziyoyev Sh.M. *The Strategy of New Uzbekistan*. – Tashkent: Uzbekistan, 2021. – 464 p.
4. Abdurakhmonov Q.Kh. *Economics Theory*. – Tashkent: Innovation Development Publishing House, 2021. – 640 p.
5. Porter M.E. *The Competitive Advantage of Nations*. – New York: Free Press, 1990. – 896 p.
6. World Bank. *World Development Report 2024*. – Washington, D.C.: World Bank Publications, 2024.

THE IMPORTANCE AND NEED FOR IMPLEMENTING INTERNATIONAL ENVIRONMENTAL AUDIT STANDARDS

Ismailov Timur
Karakalpak State University, Department of "Accounting and Audit"
dotsent, ORCID: 0000-0001-5179-3168
tima88taji@gmail.com
https://doi.org/10.5281/zenodo.21491623

Abstract. *The article examines the regulatory framework for organizing environmental audits in the republic, as well as the procedure for conducting environmental audits abroad. Proposals have been developed on the importance and necessity of introducing international environmental audit standards into practice.*

Keywords: *audit, environmental audit, environmental control, international environmental audit, international environmental audit standards.*

Аннотация. *Ушбу мақолада республикада экологик аудитни ташкил этишнинг норматив-ҳуқуқий асослари, хорижда экологик аудитнинг қандай ўтказилиши масалалари ёритилган. Халқаро экологик аудит стандартларини амалиётга татбиқ этишнинг аҳамияти ва зарурлиги бўйича таклифлар ишлаб чиқилган.*

Калит сўзлар: *аудит, экологик аудит, экологик назорат, халқаро экологик аудит, халқаро экологик аудит стандартлари.*

Аннотация. *В статье рассматривается нормативно-правовая база организации экологического аудита в республике, а также порядок проведения экологического аудита за рубежом. Разработаны предложения о важности и необходимости внедрения международных стандартов экологического аудита в практику.*

Ключевые слова: *аудит, экологический аудит, экологический контроль, международный экологический аудит, международные стандарты экологического аудита.*

In the 21st century, environmental issues have become one of the most critical challenges facing humanity. Atmospheric pollution, the depletion of water resources, soil degradation, the loss of biodiversity, and climate change are compelling the world to develop new mechanisms for environmental management.

Today, activities are evaluated not only based on economic efficiency but also on sustainability criteria. Consequently, environmental auditing has emerged as a means to enhance economic efficiency in practice.

Implementing international environmental audit standards reduces environmental risks for enterprises, ensures compliance with legislative requirements, promotes the rational use of resources, and enhances investment attractiveness.

The concept of environmental audit.

An environmental audit is the process of independently, systematically, and in a documented manner assessing the environmental impact of an enterprise's or organization's activities.

An environmental audit performs the following functions:

- verifying compliance with environmental legislation;
- identifying environmental risks;
- evaluating the waste management system;
- analyzing water and energy consumption;
- monitoring harmful emissions into the atmosphere;
- improving the environmental management system;
- mitigating environmental risks.

An environmental audit not only helps determine an enterprise's current environmental status but also assists in formulating a future environmental strategy.

In recent decades, environmental problems have become increasingly complex on a global scale due to the acceleration of industrialization, the expansion of urbanization, the intensified use of natural resources, and a sharp rise in production volumes. The impact of human activity on the environment is negatively affecting the ecological stability of the entire planet, extending far beyond the confines of specific regions. Issues such as rising greenhouse gas emissions, increasing volumes of industrial and household waste, water resource pollution, land degradation, and the loss of biodiversity have created a need to improve environmental management systems.

The global community is placing special emphasis on ensuring environmental security and managing natural resources with due regard for the interests of future generations. In particular, the widespread implementation of sustainable development principles is imposing new responsibilities on states, international organizations, and the private sector. Corporate performance is now evaluated not only by economic indicators but also by the level of environmental and social responsibility demonstrated. Consequently, establishing environmental management systems within manufacturing enterprises that meet international standards has become a pressing priority.

While integration processes in the global economy facilitate the free movement of products and services across international markets, compliance with environmental requirements has also become a mandatory condition. Many developed nations are imposing various restrictions on the import of products that fail to meet environmental standards. As a result, environmental audits and environmental management systems have emerged as key factors determining the competitiveness of enterprises in the international market.

Environmental auditing is an integral element of modern management systems, enabling a systematic assessment of an enterprise's or organization's compliance with current environmental legislation, the efficiency of natural resource use, the level of environmental hazards and risks, and the extent of negative environmental impact. The results of environmental audits allow enterprises to identify existing shortcomings, develop concrete measures to rectify them, and continuously improve their environmental management systems.

International environmental audit standards serve to evaluate enterprise operations based on unified criteria. These standards aim to manage environmental risks, ensure the rational use of resources, enhance energy efficiency, reduce waste, optimize production processes from an environmental perspective, and ensure full compliance with environmental regulations. In this regard, international standards are recognized not only as a tool for environmental oversight but also as a management mechanism that supports the long-term strategic development of enterprises.

In recent years, reforms based on concepts such as the "green economy," "green technologies," "low-carbon development," the "circular economy," and "environmental management" have been accelerating in many countries around the world. These approaches

facilitate the efficient use of natural resources, waste recycling, the implementation of energy-efficient technologies, and the mitigation of environmental risks. The success of such reforms depends directly on establishing an environmental audit system based on international standards.

The development of digital technologies is also fundamentally transforming environmental audit processes. Artificial intelligence, big data, remote sensing, geographic information systems (GIS), drone technologies, and automated monitoring tools are significantly enhancing the accuracy and speed of environmental oversight. Modern environmental auditing encompasses not only document verification but also the real-time monitoring and analysis of environmental indicators.

Large-scale reforms aimed at ensuring environmental safety, protecting the environment, and utilizing natural resources rationally are being implemented in the Republic of Uzbekistan. The country is carrying out various programs to modernize industry, develop renewable energy sources, improve environmental monitoring systems, enhance waste management efficiency, and align environmental oversight mechanisms with international requirements. At the same time, developing an environmental audit system based on international standards is crucial for boosting export potential, attracting foreign investment, and strengthening the position of national enterprises in international markets.

Although the implementation of international environmental audit standards yields numerous positive results, the process involves certain organizational, economic, legal, and technical challenges. Timely identification and effective resolution of these issues will ensure the successful operation of the environmental audit system.

One of the primary challenges facing enterprises is the shortage of qualified specialists and auditors in the field of environmental management. Conducting environmental audits in accordance with international standards requires auditors to possess deep knowledge and practical experience in ecology, management, technology, law, and economics. Therefore, it is crucial to develop academic programs in environmental auditing and management within higher education institutions, organize professional development courses, and expand international certification programs.

Another pressing issue is the high cost associated with conducting environmental audits. For small and medium-sized enterprises in particular, expenses related to purchasing modern monitoring equipment, performing laboratory analyses, obtaining international certification, and engaging auditing services are substantial. Consequently, state support for enterprises—through preferential loans, subsidies, and tax incentives—would positively impact the development of the environmental audit system.

Another factor affecting the effectiveness of environmental audits is the failure of enterprises to maintain complete and reliable environmental data. In some instances, data regarding resource consumption, waste volumes, or atmospheric emissions of harmful substances are not recorded systematically. This compromises the accuracy of audit results. To address this issue, it is advisable for enterprises to establish unified digital environmental databases and implement automated monitoring systems.

Improving the legal framework is also crucial when adopting international standards. Environmental audit results can only be effectively utilized for practical management decisions if national environmental legislation is harmonized with international standards. Therefore, it is essential to regularly update regulatory documents concerning environmental audits based on international best practices.

In recent years, ESG (Environmental, Social, and Governance) principles have been widely adopted in international business practices. This approach entails evaluating corporate activities based on environmental, social, and corporate governance criteria. Environmental auditing serves as a key tool for practically implementing the environmental component of the ESG framework.

The results of environmental audits provide reliable data on a company's energy consumption, greenhouse gas emissions, water resource efficiency, waste management practices, and impact on natural resources. This information serves as a vital resource for investors, banks, and international financial institutions when assessing a company's environmental responsibility.

Companies that adhere to ESG principles are distinguished by their ability to effectively implement long-term development strategies, mitigate investment risks, and expand access to international financing. In this regard, environmental auditing forms the practical foundation of the ESG framework.

In countries around the world, a number of measures are being taken to address the aggravation of environmental problems, the intensification of climate change, and the prevention of air pollution.

In the world, special attention is paid to scientific research aimed at clarifying the conceptual foundations of organizing environmental audits and improving their methodological foundations. Scientific research is being conducted in the areas of improving environmental control, developing the planning and organization of environmental audits, and improving the environmental auditing of economic entities.

In Uzbekistan, measures are being developed and directions are being determined for the productive use of natural resources, a sharp reduction in the amount of waste released into the environment, preservation of biological diversity, and economic development.

To introduce environmental auditing, the following regulatory legal acts have been developed today, including the Laws of the Republic of Uzbekistan “On Environmental Control” [1], “On Environmental Audit” [2], Decrees of the President of the Republic of Uzbekistan dated October 30, 2019 No. PF-5863 “On Approval of the Concept of Environmental Protection of the Republic of Uzbekistan for the Period Until 2030” [3], Decrees of the President of the Republic of Uzbekistan dated January 28, 2022 No. PF-60 “On the Development Strategy of New Uzbekistan for 2022-2026” [4], Decree No. PP-4291 “On Approval of the Strategy for Implementing Work Related to Solid Waste in the Republic of Uzbekistan for 2019-2028” dated April 17, 2019 No. PP-4291 “On Measures for the Development of Auditing Activities in the Republic of Uzbekistan” dated September 19, 2018 Resolutions No. PP-3946 [6], Resolution No. 202 [7] of the Cabinet of Ministers of the Republic of Uzbekistan dated April 12, 2021 “On further improving economic mechanisms for environmental protection in the territory of the Republic of Uzbekistan”, etc.

Decree of the President of the Republic of Uzbekistan No. PF-5863: “Implementation of international norms, codification of environmental legislation, introduction of a system of environmental insurance, audit and strategic environmental assessment ...” [3] is set as one of the priority tasks. In order to ensure the implementation of this task, it is important to introduce international environmental audit standards when conducting environmental audits, draw up an environmental audit report, and improve the theoretical and methodological aspects of environmental audits.

Today, environmental audit activities in our country remain below the level of developed countries. Also, the lack of legal mechanisms of incentives for business entities that have conducted an environmental audit prevents the widespread use of this measure in practice.

Article 5 of the Law of the Republic of Uzbekistan “On Environmental Audit” is called Environmental Audit Standards and states:

“Environmental audit standards determine the procedure for conducting environmental audits, providing related services and organizing a system for monitoring the quality of the work of environmental auditors. National environmental audit standards establish uniform requirements for the implementation of environmental audit activities. Environmental audit organizations may apply international environmental audit standards in accordance with the agreement when conducting environmental audits” [2].

Currently, the number of economic entities of the first and second categories that affect the environment in our republic is significantly large, and not all of them are covered by monitoring pollution sources by authorized bodies.

However, in most countries of the world, in order to control environmental protection and rational use of nature, a non-governmental, independent special type of environmental control institute is applied to all economic entities that affect it. In particular, in countries such as the USA, Great Britain, Canada, Italy, Sweden, the Netherlands, environmental auditing activities are regulated by a separate legal act.

Environmental auditing in a broader sense is an open method in the environmental management system, with the help of which increasingly stringent environmental requirements are gradually introduced into the main parameters of the business strategy and production process. Environmental auditing is also a means of systematically examining the internal environmental potential, environmental risks and opportunities of the organization. The environmental auditing system was first used by companies in the United States in the 1970s to meet the requirements set by the then American environmental legislation. By the end of the 1980s, some companies had even achieved environmental goals that were more stringent than the requirements of the law. Active environmental auditing, as well as active environmental management, has since become widespread not only among US companies, but has also gradually begun to gain increasing confidence among European companies. With the adoption of the international standards ISO 14000 and EMAS, the requirement for periodic audits has become one of the most important conditions for companies to obtain the appropriate certificate.

Environmental audit is a systematic documented process of examining the environmental aspects of an organization's activities, as well as objectively obtained and evaluated data, in order to determine the compliance of types and conditions of economic activity, administrative management systems or information about these objects with the requirements of regulatory and legislative acts in the field of environmental protection and environmental safety and operating criteria.

Within the framework of the ISO 14000 series of standards, environmental audit requirements are included in the following standards: “ISO 14010 – 98. Guidelines for environmental auditing. General principles” [8]; “ISO 14011-98. Guidelines for environmental auditing. Audit procedures. Auditing of environmental management systems” [9]; “ISO 14012-98. Guidelines for environmental auditing. Qualification criteria of environmental auditors” [10].

Thus, the main tasks of the environmental audit are as follows: first, to provide objective information about the environmental aspects of the enterprise's activity and its compliance with the established standards, regulations, and the requirements of the initiators of relevant inspections; secondly, to further improve the organization of environmental management, eco-control, etc., as

well as to develop useful recommendations for increasing the efficiency of environmental protection measures implemented by the enterprise.

Additional tasks of an environmental audit include: determining the compliance of an enterprise's activities with environmental protection legislation and its declared environmental policy, as well as with the company's economic goals; determining the effectiveness of the enterprise's environmental management system; providing management with information when making decisions in the field of environmental protection; ensuring the protection of enterprise employees, the local population and the natural environment from possible harmful effects; analyzing the likelihood of environmentally hazardous accidents; determining the real impact of the enterprise on the environment; providing an incentive for the enterprise to improve its environmental policy and production activities in order to increase the level of environmental safety. An environmental audit can be carried out by legal entities (audit organizations) or individuals (environmental auditors) with the appropriate license. All participants in the relationship related to an environmental audit, including the audit organization, the audit team appointed to conduct the audit, individual environmental auditors, the initiator of the audit, as well as the audited organization, must adhere to a number of principles. The main principles of environmental auditing in accordance with ISO 14010 are as follows:

- clear definition of objectives and scope. In this case, the objectives of the audit are determined by its initiator, and the scope and scope are determined taking into account the objectives;

- objectivity, independence and competence. To meet these requirements, members of the audit team should be independent of the activity they are auditing, they should be objective and free from bias. Members of the audit team should have appropriate knowledge, skills and experience. A complete set of professional and other requirements for environmental auditors is contained in the ISO 14012 standard;

- due professional care. The relationship between members of the audit team and the client should be confidential and reasonable. Unless required by law, members of the audit team should not disclose information or documents obtained during the audit or the final audit report to a third party without the permission of the client (i.e. the initiator of the audit) and, where appropriate, the organization;

- systematic. Environmental audit should be carried out in accordance with the basic principles and instructions developed for the appropriate type of audit;

- determination of audit criteria; based on the established criteria, the completeness and appropriate quality of audit data should be ensured;

- reliability of audit results and conclusions should be ensured;

- the audit conclusion should be complete, taking into account the agreed objectives and scope of the audit.

In short, environmental audit is an integral part of the policy of economic entities that affect the environment and is an important element of self-management. In order for environmental audit organizations of the Ministry of Economy and Finance of the Republic of Uzbekistan or the Chamber of Auditors of Uzbekistan to fully apply international environmental audit standards when conducting environmental audits, they should obtain from authorized bodies the right to translate them into the state language, translate them and put them into practice.

CONCLUSION

Analyses indicate that the implementation of international environmental audit standards is an integral component of modern environmental management systems. The growing anthropogenic impact on the environment, the intensification of natural resource use, and the global nature of environmental issues necessitate the improvement of environmental audit systems in accordance with international requirements. In this context, environmental auditing serves as a vital tool for assessing the environmental performance of enterprises and organizations, identifying and mitigating environmental risks, and monitoring compliance with environmental legislation.

The article establishes that the international environmental audit standards discussed facilitate the effective organization of environmental management systems, the rational use of resources, the assurance of environmental safety in production processes, and the support of sustainable enterprise development. Specifically, the results of environmental audits enable enterprises to optimize energy and water consumption, reduce waste volumes, cut production costs, and proactively assess environmental risks. This enhances not only environmental performance but also economic efficiency.

Furthermore, the implementation of international environmental audit standards enhances the competitiveness of enterprises in the global market, boosts export potential, and strengthens foreign investor confidence. Today, in many developed nations, aligning environmental management systems with international standards is viewed as a key criterion for attracting investment, fostering international cooperation, and demonstrating environmental responsibility. Consequently, developing an environmental audit system based on international requirements serves to harmonize economic progress with environmental safety.

In the context of Uzbekistan, improving the environmental audit system, gradually adopting international standards, widely implementing environmental management systems, and training qualified auditors are among the pressing priorities. Ongoing environmental reforms, the policy of transitioning to a green economy, and the modernization of industrial enterprises are further increasing the practical significance of environmental auditing. At the same time, the digitalization of environmental monitoring, the use of modern information and communication technologies, and ensuring transparency in environmental reporting are crucial factors for the effective implementation of international standards.

The implementation of international environmental audit standards is a key requirement of the modern economy. These standards play a vital role in enhancing corporate environmental responsibility, ensuring the rational use of resources, mitigating environmental risks, and fostering sustainable development. An environmental management system aligned with international standards not only contributes to environmental protection but also boosts the economic efficiency of enterprises, expands opportunities for accessing international markets, and enhances investment attractiveness. In the context of Uzbekistan, refining the environmental audit system in accordance with international requirements is a crucial factor in the transition to a green economy and the assurance of environmental safety.

LIST OF USED LITERATURE

1. Ўзбекистон Республикасининг «Экологик назорат тўғрисида»ги қонуни. https://www.lex.uz/acts/2304953
2. Ўзбекистон Республикасининг «Экологик аудит тўғрисида»ги қонуни. https://lex.uz/docs/5331133
3. Ўзбекистон Республикаси Президентининг 2019 йил 30 октябрдаги «2030 йилгача бўлган даврда Ўзбекистон Республикасининг атроф муҳитни муҳофаза қилиш концепциясини тасдиқлаш тўғрисида»ги ПФ-5863-сон Фармони. https://lex.uz/docs/4574008
4. Ўзбекистон Республикаси Президентининг 2022 йил 28 январдаги «2022-2026 йилларга мўлжалланган Янги Ўзбекистоннинг тараққиёт стратегияси тўғрисида»ги ПФ-60-сон Фармони. https://lex.uz/docs/5841063
5. Ўзбекистон Республикаси Президентининг 2019 йил 17 апрелдаги «2019-2028 йиллар даврида Ўзбекистон Республикасида қаттиқ маиший чиқиндилар билан боғлиқ ишларни амалга ошириш стратегиясини тасдиқлаш тўғрисида»ги ПҚ-4291-сон Қарори. https://lex.uz/uz/docs/4291729
6. Ўзбекистон Республикаси Президентининг 2018 йил 19 сентябрдаги «Ўзбекистон Республикасида аудиторлик фаолиятини ривожлантириш чора-тадбирлари тўғрисида»ги ПҚ-3946-сон қарори. https://lex.uz/uz/docs/3914502
7. Ўзбекистон Республикаси Вазирлар Маҳкамасининг 2021 йил 12 апрелдаги «Ўзбекистон Республикаси ҳудудида атроф табиий муҳитни муҳофаза қилишнинг иқтисодий механизмларини янада такомиллаштириш тўғрисида»ги 202-сон қарори. https://lex.uz/uz/docs/5367873
8. “ISO 14010 – 98. Guidelines for environmental auditing. General principles”. https://www.russiangost.com/p-57830-gost-r-iso-14050-99.aspx.
9. “ISO 14011-98. Guidelines for environmental auditing. Audit procedures. Auditing of environmental management systems”. https://www.russiangost.com/p-54280-gost-r-iso-14012-98.aspx.
10. “ISO 14012-98. Guidelines for environmental auditing. Qualification criteria of environmental auditors”. https://www.russiangost.com/p-54280-gost-r-iso-14012-98.aspx.

MODERN TRENDS IN IMPROVING INCLUSIVE PASSENGER TRANSPORTATION SERVICES

Abduvali Abdug'ani o'g'li Aktamov
Basic Doctoral Candidate (PhD Researcher), Samarkand Institute of Economics and Service

Abstract. *This study examines modern trends in improving inclusive passenger transportation services through a comprehensive, The article was prepared on the basis of an innovative project within the framework of state scientific and technical programs IL-9124093892 on the topic "Development of methodological foundations for organizing inclusive tourism (on the example of the Kyzyltepa, Nurota and Khatirchi districts of Navoi region)". Based analysis focused on the Republic of Uzbekistan. Drawing on World Health Organization data showing that 1.3 billion people worldwide — one in six people on the planet — live with a significant disability, the research takes this global reality as its point of departure. An analysis of conditions inside Uzbekistan reveals substantial quantitative disparities in tourism and transport indicators across the Samarkand, Navoiy, Tashkent, Bukhara, Khorezm, and Jizzakh regions. The experience of leading countries in Europe, the United States, and Asia is examined comparatively to identify their successes in inclusive transport policy and the pathways along which these might be adapted for Uzbekistan. Against the recommendations of the World Tourism Organization (UNWTO), grounded in ISO 21902:2021 and the San Marino Declaration, the study substantiates which aspects of the national transport system require fundamental change. The research draws extensively on domestic and international scholarly sources, official statistical data, and legal and regulatory documents. The concluding section presents a system of practical recommendations for improving inclusive passenger transportation services in Uzbekistan from institutional, infrastructural, and digital-informational perspectives.*

Keywords: *inclusive tourism, passenger transportation, persons with disabilities, transport infrastructure, barrier-free environment, UNWTO, Uzbekistan.*

1. INTRODUCTION

In today's economy, the principle of inclusiveness — ensuring that all social groups, including persons with disabilities, older adults, families with young children, and other categories with specific needs, are able to take part on an equal footing in economic and social life — has moved to the center of global sustainable development policy. Sustainable Development Goal 10 of the United Nations' 2030 Agenda, which calls for reducing inequality within and among countries, directly encompasses inclusiveness in transport and tourism as well.

According to a 2023 World Health Organization (WHO) report, 1.3 billion people worldwide — roughly 16 percent of the global population — live with a significant disability [1]. World Tourism Organization (UNWTO) estimates put the number of people with disabilities in the European Union at more than 80 million; once older adults and their travel companions are included, the figure rises to 130 million [2]. An estimated 70 percent of this population is both financially and physically capable of travel, yet the inconvenience of transport services and the physical barriers they present continue to prevent this right from being fully exercised.

Uzbekistan has carried out substantial tourism reforms in recent years: the number of foreign visitors reached 6.6 million in 2023 and 8.2 million in 2024, an annual growth rate of 24.2 percent [3]. Yet against the backdrop of this remarkable expansion, systematic research into the state of inclusive passenger transportation services has not kept pace. In 2024 the total volume of transport services across all modes reached 145,124.4 billion soums, up 8.6 percent from 2023 [4]; the extent to which this growth has translated into better inclusive transport quality still calls for dedicated study.

The central aim of this research is to analyze, on a statistical basis, the current state of inclusive passenger transportation services in Uzbekistan's principal tourism regions — Samarkand, Navoiy, Tashkent, Bukhara, Khorezm, and Jizzakh — to examine advanced international practice comparatively, and to develop evidence-based recommendations for improving the sector.

Research objectives: (1) to establish the theoretical and methodological foundations of inclusive transport services; (2) to conduct a comparative statistical analysis of tourism and transport indicators across the Samarkand, Navoiy, Tashkent city, Bukhara, Khorezm, and Jizzakh regions; (3) to examine successful experience with inclusive transport policy in European, American, and Asian countries; (4) to identify institutional gaps in Uzbekistan in light of UNWTO recommendations; (5) to formulate a system of recommendations adapted to national conditions.

Scientific novelty. This study is the first to systematically examine, on the basis of statistical analysis, the relationship between inclusive passenger transportation and tourism indicators across Uzbekistan's regions, and to benchmark it against international experience.

2. LITERATURE REVIEW

The theoretical foundation of inclusive transport services rests on several core concepts. The "universal design" approach, widely used in academic circles and developed by Mace in 1985, envisions creating products, environments, and services that anyone can use without the need for specialized adaptation or individualized design [5]. Applied to transport, this principle requires no supplementary accommodations, since the infrastructure itself is expected to be inclusive from the outset.

In a seminal study, Prideaux (2000) identified the transport system as the key mechanism governing a tourist destination's life cycle, demonstrating empirically that declining transport convenience inevitably erodes a destination's competitiveness [6]. Page and Hall (2014), examining how transport barriers affect demand among tourists with special needs, proposed a "trichotomy of barriers": intrinsic barriers (personal capacity), interdependent barriers (difficulties tied to companions and assistive devices), and extrinsic barriers (infrastructure and policy) [7].

Darcy and Dickson (2009) framed inclusive tourism more broadly, defining it as a systemic approach that creates equal opportunity not only for persons with disabilities but for older people, families with young children, and anyone with temporarily limited mobility [8]. Seen this way, inclusive transport services are not a specialized offering aimed at a single social group, but a universal improvement that raises the quality of services for everyone.

Among national studies, Sobirov et al. (2023), examining prospects for developing inclusive tourism in Uzbekistan, singled out the absence of universal design standards in passenger transport as a key shortcoming [9]. Qodirov and Muxtorova (2022), assessing the tourism infrastructure of Samarkand region, found a positive correlation between the quality of accommodation facilities and transport connectivity [10]. Tursunov (2024), analyzing the reform

of Uzbekistan's transport system, showed how the transition to gross-cost contracting has affected service quality [11].

The international regulatory framework for inclusive passenger transportation rests on several key instruments. First, Article 9 of the UN Convention on the Rights of Persons with Disabilities (2006) obliges states to make transport services accessible to all. Second, ISO 21902:2021, "Tourism and Related Services — Accessible Tourism for All," approved in 2021 by UNWTO and the ONCE Foundation, sets accessibility requirements for tourism services, including transport [12]. Third, the San Marino Declaration, adopted following the 2023 International Conference on Accessible Tourism, recognized genuine access to travel and transport for persons with disabilities as an integral part of human rights [13].

Within European Union law, the 2023 Accessible EU report established transparent EU transport standards, legally requiring that all principal passenger trains on the trans-European rail network be adapted for persons with disabilities [14]. In the United States, the Americans with Disabilities Act (ADA), adopted in 1990, has become a global legislative model and underpins similar legislation in more than 40 countries [15].

3. METHODOLOGY

The study follows a multi-stage methodology. Primary data were drawn from official publications of the State Statistics Committee of the Republic of Uzbekistan, regional statistics offices (Navoiy Regional Tourism Statistics, 2024; Samarkand Regional Administration data, 2024), official UNWTO and WHO reports and publications, and materials on European transport legislation.

The following methods were applied: (1) comparative statistical analysis, comparing transport and tourism indicators across regions; (2) multidimensional comparison, benchmarking Uzbekistan's experience against that of foreign countries; (3) content analysis of legal and regulatory documents; (4) correlation analysis, assessing the relationship among accommodation infrastructure, the number of tour operators, and transport connectivity; and (5) SWOT analysis, identifying the strengths, weaknesses, opportunities, and threats facing inclusive transport services in Uzbekistan.

The correlation analysis examined the relationship between transport infrastructure indicators (number of transport routes, travel time, tariff level) and tourism outcomes (hotel occupancy rate, number of tour operators, visitor flow). The analysis spans 2017–2024 and is comparative across regions.

4. ANALYSIS AND RESULTS

As a result of the tourism reform policy pursued since 2017, sector indicators in Uzbekistan have improved sharply. The number of foreign visitors rose from 2.7 million in 2017 to 6.6 million in 2023 — an increase of 144 percent. The number of accommodation facilities grew from 767 to 5,500, and the number of guest beds from 37,000 to 128,000. The number of tourism organizations rose from 749 to 2,404, and the number of licensed tour guides from 574 to 2,864 [16].

Table 1. Key tourism sector indicators in Uzbekistan (2017–2024)

Indicator	2017	2019	2021	2023	2024
Foreign tourists (million)	2.69	6.75	1.48*	6.60	8.20
Domestic tourists (million)	7.2	11.4	9.8	14.9	16.0
Accommodation facilities (units)	767	1,243	2,100	5,500	6,200
Tourism organizations (units)	749	1,100	1,400	2,404	2,800
Transport services (billion soums)	—	—	—	133,700	145,124

** Decline attributable to the COVID-19 pandemic. Sources: [3; 4; 16], compiled by the author.*

The volume of transport services reached 145,124.4 billion soums in 2024, up 8.6 percent from 2023. Rail passenger transportation grew 6.9 percent year-on-year, while air transport grew 12.3 percent [4].

A regional analysis of tourism infrastructure reveals considerable disparities. Table 2 presents accommodation capacity, the number of tour operators, and inclusive-service indicators for the principal tourism regions over 2022–2023.

Table 2. Comparative analysis of tourism infrastructure by region (2023)

Region	Hotels (units)	Hostels (units)	Tour operators (units)	Foreign tourists (th.)	Domestic tourists (th.)	Tourism exports (US$ mln)	Rank
Tashkent city	300	181	892	2,800	3,500	850	1
Samarkand region	164	91	304	2,150	4,500	406	2
Bukhara region	171	69	116	1,800	2,100	280	3
Khorezm region	59	21	64	420	580	65	4
Navoiy region	36	29	22	17.0	24.5	8	5
Jizzakh region	28	13	10	85	110	12	6

Sources: Navoiy Regional Statistics Office (2024); Samarkand Regional Administration (2024).

Table 2 shows that Tashkent city and Samarkand region clearly lead the other regions in terms of tour operators, hotels, and foreign-visitor flows. A strong correlation ($r = 0.93$) is also observed between the number of tour operators and the volume of accommodation facilities, confirming the interdependence of the transport and tourism systems. Jizzakh region has only 10 tour operators — 89 times fewer than Tashkent. In Navoiy region in 2024, 28 tourism firms served 17,000 visitors, while 36 hotels and 40 individual accommodation facilities together hosted 24,500 guests [17].

The present state of inclusive transport indicators deserves particular attention. Table 3 presents selected inclusive-transport indicators of regional transport infrastructure.

Table 3. Regional inclusive transport indicators (2024)

Region	Low-floor bus share, %	Flight frequency (weekly)	Rail connection	Stations fitted with ramps, %	Inclusive Transport Index (ITI)
Tashkent city	38.5	200	Yes (full)	41	6.8 / 10
Samarkand region	18.2	72	Yes (Afrosiyob)	22	5.1 / 10
Bukhara region	14.7	48	Yes (Sharq)	18	4.7 / 10
Khorezm region	9.3	21	Partial	12	3.4 / 10
Navoiy region	7.1	14	Yes (freight line)	9	2.9 / 10
Jizzakh region	4.8	7	Partial	6	2.2 / 10

** Approximate figures, based on 2023 regional administration reports. ** Author's calculation.*

Table 3 and the calculated Inclusive Transport Index (ITI) reveal a substantial gap between Tashkent city and the other regions. Tashkent ranks first with a score of 6.8/10, while Jizzakh (2.2/10) and Navoiy (2.9/10) rank last. This disparity sharply constrains travel opportunities for persons with disabilities and older people wishing to visit these regions.

5. DISCUSSION: INTERNATIONAL EXPERIENCE

Development of an inclusive transport system in the European Union rests on a unified legal framework. According to the 2023 Accessible EU report, 26.8 percent of the EU population lives with some form of disability or health condition [14]. Moreover, by 2070, 62.5 percent of the EU population will be over 65, which further heightens the strategic importance of inclusive transport services for older people [20].

In Germany, the “Barrier-free” policy pursued since 1996 has made more than 80 percent of railway stations fully accessible to wheelchair users. Deutsche Bahn has introduced low-floor lifts and enlarged seating areas as standard features across its passenger carriages. According to the company, these investments — alongside the convenience they bring to passengers generally — have raised the share of passengers with disabilities from 4.2 percent in 2010 to 7.8 percent in 2023, generating an additional 480 million euros in annual revenue [14].

Spain’s experience is internationally recognized as a successful model for integrating inclusive transport and tourism. The AccessibleSpain platform, created through a partnership between ONCE (Spain’s National Organization of the Blind) and UNWTO, registered more than 3,000 additional barrier-free transport facilities across 28 major cities in 2024. Tourists with disabilities account for 3.2 percent of Spain’s tourism export revenue — roughly 5.4 billion euros [13].

Denmark's Flexhandicap system is particularly noteworthy. The model entitles persons with disabilities to up to 104 subsidized transport trips a year, for an annual fee of 40 euros plus 3 euros per trip (covering the first 5 km). The vehicles are specially fitted to carry wheelchairs safely and operate around the clock [20]. Since the system's introduction, participation by persons with disabilities in tourism activities in Denmark has risen by 34 percent.

In the United States, the principal regulatory foundation for inclusive transport — the Americans with Disabilities Act (ADA), adopted in 1990 — has become a catalyst for legal reform

worldwide. This study's findings confirm that the US inclusive transport model is widely regarded as the most advanced in the world: more than 40 percent of surveyed tourists with disabilities in Asia named the United States as the most accessible destination, citing the ADA as the primary reason [21].

Under ADA requirements, every new public transit vehicle must include a low-floor entrance, audio and visual announcement systems, dedicated wheelchair spaces (at least two), a designated area for passengers with visual impairments, and side grab rails. According to 2023 Federal Transit Administration data, 99.1 percent of US city bus fleets comply with ADA requirements — a striking improvement over the 48.5 percent recorded in 1991 [22].

The economic impact of US inclusive transport policy is also substantial: tourists with disabilities spend an estimated $17.3 billion a year on tourism, a figure growing 4–6 percent annually [23]. According to the Accessible Travel Alliance, every dollar invested in inclusive transport infrastructure generates $3.2 in tourism revenue.

Within Asia, Japan stands out as a leader in inclusive transport. Its Barrier-Free Policy, in place since 2008, has made more than 90 percent of the country's major railway stations fully accessible. As of 2024, the share of non-step (low-floor) buses reached 76 percent — up 28 percentage points from 2015 [28].

A survey conducted by Japan’s JTB Tourism Research & Consulting among 221 foreign tourists with disabilities from 35 countries found that the amenities most in demand for inclusive travel were accessible transport (80.5 percent), information about barrier-free destinations and facilities (76.9 percent), and accessible restrooms (73.3 percent) [21]. Building on these findings, Japan rolled out its “Barrier-free Tourism Information System” (BFTIS) digital platform across all prefectures beginning in 2024.

The 2020 Tokyo Olympic and Paralympic Games gave Japan an opportunity to showcase inclusive infrastructure on a global stage: all 43 sports and transport facilities built for the Games were designed to comply fully with barrier-free standards. These investments have continued to benefit the sector in the post-Olympic period — in 2023, the share of inclusive tourists in Japan was 2.3 times higher than in 2019 [27].

Singapore offers another successful example of an inclusive urban transport model in Asia. Under its “Transport Masterplan 2040” strategy, the country aims to make all public transport nodes — metro stations, bus terminals, and ferry terminals — fully accessible by 2040. According to the Land Transport Authority, all metro stations are currently equipped with lifts, and 95 percent of the bus fleet meets barrier-free standards.

Table 5. Comparative inclusive transport indicators of leading countries

Indicator	Germany	Spain	USA	Japan	Singapore	Uzbekistan
Non-step bus share, %	82	71	99	76	95	12
Adapted metro stations, %	95	88	—	90	100	35
Legal basis (year of law)	1996	2003	1990	2006	2008	2008*
Global ITI ranking	3rd	7th	1st	5th	2nd	—

Indicator	Germany	Spain	USA	Japan	Singapore	Uzbekistan
Inclusive tourist share, %	14.2	11.8	15.1	8.7	12.3	<2.0

** Uzbekistan's Law No. 641, "On the Social Protection of Persons with Disabilities." Sources: [14; 15; 21; 22; 23; 27; 28], compiled by the author.*

UNWTO has identified several decisive directions for advancing inclusive tourism and has developed practical recommendations for governments and the tourism industry. The San Marino Declaration, adopted at the 2023 International Conference on Accessible Tourism, named transport accessibility one of five key priority areas [13].

Six UNWTO guidelines built on ISO 21902:2021 — covering hotels, food services, tour operators, transport, historic sites, and digital services — were published in 2023–2024. The transport guideline sets out the following mandatory requirements: (a) physical accessibility (low-floor entrances, ramps, lifts); (b) sensory accessibility (audio and visual information, Braille signage); (c) cognitive accessibility (simple navigation, specially trained staff); and (d) digital accessibility (online booking and information access) [12].

Table 6. SWOT analysis of inclusive passenger transportation services in Uzbekistan

Strengths (S)	Weaknesses (W)
• A statutory obligation exists under Law No. 641 • Dedicated seating on Afrosiyob and Sharq trains • Partial barrier-free infrastructure in the Tashkent metro • Substantial investment in tourism infrastructure in Samarkand and Bukhara • Growing use of digital booking platforms	• Very low share of non-step buses (~12%) • Wide infrastructure gaps between regions • Few transport stops fitted with ramps • Insufficient staff training in inclusive service • No dedicated digital information system, and no official statistics on inclusive tourists
Opportunities (O)	**Threats (T)**
• The global inclusive tourism market is growing at a 7.2% CAGR • Potential partnerships with UNWTO and ONCE • Plans to extend the Afrosiyob network to the Khiva route • Transport modernization under the "Uzbekistan–2030" strategy • Adoption of digital technologies (AI navigation, smart cards) • Hosting Paralympic and disability sports events	• Risk of insufficient investment in inclusive infrastructure • Competition from leading inclusive destinations (Spain, Singapore) • Unanticipated growth in demand driven by an aging population • A widening "accessibility gap" between regions • Lack of monitoring for regulatory compliance

Source: compiled by the author based on the study's findings.

6. CONCLUSIONS AND RECOMMENDATIONS

This study has examined the state of inclusive passenger transportation services in the Republic of Uzbekistan through statistical analysis, set against a comparative backdrop of international experience. The principal conclusions are as follows.

First, the rapid growth of Uzbekistan's tourism sector — 6.6 million foreign visitors in 2023 and 8.2 million in 2024 — has driven demand for inclusive transport services to an unprecedented level, further exposing the barriers that persist in this area. Second, the regional Inclusive Transport Index (ITI) reveals a wide gap between Tashkent city (6.8/10) and Jizzakh (2.2/10) and Navoiy (2.9/10) regions. Third, correlation analysis confirms a strong statistical relationship ($r = 0.87–0.91$) between inclusive transport indicators and tourism activity indicators, such as the number of tour operators and visitor flow. Fourth, international experience — from Germany, the United States, Japan, and Singapore — demonstrates that high-quality inclusive transport infrastructure is achievable through targeted policy.

Building on these findings and the SWOT analysis, the following practical recommendations are proposed for improving inclusive passenger transportation services in Uzbekistan:

1. Legal and institutional reform. Introduce a monitoring system for compliance with the transport-related requirements of Law No. 641 and hold regional administrations accountable for reporting; incorporate UNWTO ISO 21902:2021 requirements into national transport regulations; develop a dedicated national standard for inclusive transport.

2. Infrastructure development. Raise the share of low-floor (non-step) buses through regional programs to 40 percent in Samarkand and Bukhara regions and 20 percent in Navoiy and Jizzakh regions by 2026–2028; increase the share of railway stations equipped with ramps and lifts from the current 35 percent to 75 percent by 2027; more than double the current regulatory allowance of dedicated seats for passengers with disabilities on Afrosiyob and Sharq train carriages.

3. Digital and information accessibility. Develop an "Uzbekistan Barrier-Free" mobile application and web platform — modeled on Japan's BFTIS — featuring a real-time map of the accessibility features at every transport stop; introduce audio and vibration alerts for hearing-impaired travelers within transport mobile applications.

4. Workforce training. Introduce an internationally certified training program in sustainable tourism geography for inclusive-transport service operators; make training in etiquette for interacting with passengers with disabilities mandatory for tour guides and drivers; develop training modules in partnership with UNWTO and Spain's ONCE Foundation.

5. Financing mechanisms. Attract public-private partnership projects for inclusive transport infrastructure; provide tax incentives — VAT and customs-duty exemptions — for barrier-free buses and railway carriages; introduce regional subsidy mechanisms for inclusive tourism routes.

6. Statistics and monitoring. Maintain separate tourism statistics for inclusive travelers (persons with disabilities, older people, families with young children); include the regional ITI index in official annual reports; conduct annual audits against inclusive-transport targets.

Phased implementation of these recommendations would help narrow Uzbekistan's "accessibility gap," open new economic opportunities within the tourism sector, and contribute to a marked improvement in the country's standing among internationally recognized accessible destinations. The ITI methodology developed in this study can be further refined with broader data and used as a tool for regional-level policy analysis going forward.

REFERENCES

1. World Health Organization (WHO). World Report on Disability. — Geneva: WHO, 2023. — 325 p.
2. UNWTO/UN Tourism. Accessible Tourism: Unlocking the Potential for All Travellers. — Madrid: UNWTO, 2024. — Available at: https://www.untourism.int/accessibility
3. Statistics Agency under the President of the Republic of Uzbekistan. Statistics on Foreign Citizens Visiting the Country in 2024 [in Uzbek]. — Tashkent, 2025.
4. Ministry of Transport of the Republic of Uzbekistan. Data on the Volume of Transport Services Based on 2024 Year-End Results [in Uzbek]. — Tashkent, 2025.
5. Mace R. Universal Design: Barrier Free Environments for Everyone. — Raleigh: North Carolina State University, 1985. — 48 p.
6. Prideaux B. The role of the transport system in destination development // Tourism Management. — 2000. — Vol. 21, No. 1. — P. 53–63. DOI: 10.1016/S0261-5177(99)00002-8
7. Page S.J., Hall C.M. Managing Urban Tourism. — 2nd ed. — Harlow: Pearson Education, 2014. — 416 p.
8. Darcy S., Dickson T. A Whole-of-Life Approach to Tourism: The Case for Accessible Tourism Experiences // Journal of Hospitality and Tourism Management. — 2009. — Vol. 16, No. 1. — P. 32–44. DOI: 10.1375/jhtm.16.1.32
9. Sobirov D.A., Ruziyeva M.T., Toshmatov O.B. Inclusive Tourism: Development Prospects in Uzbekistan [in Uzbek] // Economics and Innovative Technologies. — 2023. — No. 4. — P. 112–124.
10. Qodirov A.Q., Muxtorova G.R. A Methodology for Assessing the Tourism Infrastructure of Samarkand Region [in Uzbek] // Scientific Bulletin of Samarkand Institute of Economics and Service. — 2022. — No. 3(19). — P. 78–89.
11. Tursunov O.A. Reforming the Public Transport System in Uzbekistan: The Economic Efficiency of the Gross-Cost Contract Model [in Uzbek] // TSUE Scientific Bulletin. — 2024. — No. 2. — P. 44–57.
12. ISO 21902:2021. Tourism and Related Services — Accessible Tourism for All — Requirements and Recommendations. — Geneva: International Organization for Standardization, 2021.
13. UNWTO. San Marino Declaration on Accessible Tourism. — San Marino: UNWTO, 2023.
14. Accessible EU. Accessible Public Transport in the EU: Report 4. — Brussels: Accessible EU Resource Centre, 2023. — 112 p.
15. Americans with Disabilities Act of 1990, Pub. L. No. 101-336, 104 Stat. 328 (1990). URL: https://www.ada.gov/
16. Tourism in Uzbekistan, 2017–2023: Results of Reform [in Uzbek]. Kun.uz analytical review. — Tashkent, 2023.
17. Navoiy Regional Statistics Office. Tourism in Navoiy Region in 2024 — Press Release [in Uzbek]. — Navoiy, 2025.
18. Samarkand Regional Administration (Hokimiyat). Expanding Tourism Services and Ensuring Employment in the Sector in 2023: Briefing Materials [in Uzbek]. — Samarkand, 2024.
19. Mardonova D.Sh. et al. The State and Development Trends of the Hotel Business in Our Country [in Uzbek] // Economics and Finance. — 2023. — No. 2(162). — P. 44–58.

20. European Commission. Inclusive and Sustainable Future of Urban Mobility in Europe. — Brussels: DG MOVE, 2024.
21. JTB Tourism Research & Consulting. Accessible Tourism in Japan: Expectations vs. Reality. Insights from 221 Overseas Visitors with Disabilities from 35 Countries. — Tokyo, 2024.
22. US Department of Transportation, Federal Transit Administration. Transit Accessibility Report 2023. — Washington, D.C., 2023. — 78 p.
23. Accessible Travel Alliance. Economic Impact of Accessible Travel in North America. — Washington, D.C., 2024. — 64 p.
24. European Network for Accessible Tourism (ENAT). Tourism for All: Good Practice Guidelines. — Brussels: ENAT, 2023.
25. Bowtell J. Assessing the value and market attractiveness of the accessible tourism industry in Europe: a focus on major travel and leisure companies // Journal of Tourism Futures. — 2015. — Vol. 1, No. 3. — P. 203–222. DOI: 10.1108/JTF-03-2015-0012
26. Law of the Republic of Uzbekistan No. 641, “On the Social Protection of Persons with Disabilities” (1995, as last amended in 2021) [in Uzbek]. — Tashkent, 2021.
27. Japan National Tourism Organization (JNTO). Accessible Tourism in Japan: Statistical Overview 2023. — Tokyo: JNTO, 2023.
28. Ministry of Land, Infrastructure, Transport and Tourism (MLIT). Barrier-Free Transportation Statistics Report Japan. — Tokyo: MLIT, 2024.
29. Smith M., Puczko L. Health and Wellness Tourism: Origins, Developments, Future. — London: Routledge, 2023. — 352 p.
30. Decree of the President of the Republic of Uzbekistan No. PF-60 of November 11, 2022, “On the Development Strategy of New Uzbekistan for 2022–2026” [in Uzbek].

Contents

01.00.00 PHYSICAL AND MATHEMATICAL SCIENCES

Kh. Eshankulov
SELF-ADAPTIVE INTER-AGENT CONSENSUS MODEL AND ALGORITHMS FOR MULTI-CRITERIA DECISION-MAKING IN DISTRIBUTED MULTI-AGENT ENVIRONMENTS..... 4

O.S. Toshev, M.A. Mustafoyev, G.M. Allaberganova, A.M. Muzafarov
URANIUM SERIES RADIONUCLIDES AND THEIR QUANTUM-MECHANICAL CHARACTERISTICS..... 12

L.O. Meyliyev, Sh.A. Jurayeva
METHOD FOR RECORDING INFRARED ABSORPTION SPECTRA OF GASEOUS PROPANOL AND MATRIX ISOLATION METHOD.. 18

K.T. Dadamatova
INVESTIGATION OF THE DEPENDENCE OF PHOTOLUMINESCENCE SPECTRUM AND INTENSITY ON CONCENTRATION IN ER^{3+}-DOPED OPTICAL MATERIALS..... 22

B.M. Mamadaliyev, M.M. Toxirova, Sh.A. Sodiqova, S.Kh. Hazratqulova
ON THE METHOD OF MATHEMATICAL INDUCTION IN CALCULATING INDEFINITE INTEGRALS AND TESTING NUMERICAL SERIES FOR CONVERGENCE..... 27

N. Shamsiddinov, O. Yusupov, B. Husanov
INFORMATION AND COMMUNICATION TECHNOLOGIES IN THE ORGANIZATION AND DEVELOPMENT OF INDEPENDENT CREATIVE WORK AMONG YOUNG PEOPLE..... 34

Z.A. Yavkacheva, Q.A. Aliqulov
GALILEO GALILEI - THE FOUNDER OF DYNAMICS..... 41

N.F. Zikrillayev, N.U. Abdullayev
A UNIFIED MODEL OF SELF-OSCILLATING CURRENT SYSTEMS IN COMPENSATED SILICON AND THE INFLUENCE OF TEMPERATURE AND CONTACT EFFECTS..... 46

Мажитова Хафиза Зокировна
РЕНОРМАЛИЗАЦИОННЫЙ ОПЕРАТОР В ПРОСТРАНСТВЕ КУСОЧНО-ГЛАДКИХ ОТОБРАЖЕНИЙ ОКРУЖНОСТИ..... 54

02.00.00 CHEMICAL SCIENCES

E.Sh. Sanayev, K.P. Serkayev
THE SIGNIFICANCE OF WHEAT AND BARLEY GRAINS IN ORGANIZING TARGETED CONSUMPTION RATIONS..... 60

Z. Jabbarov, F. Reymova, O. Imomov
GEOCHEMICAL CHARACTERISTICS AND HEAVY METAL CONTAMINATION ASSESSMENT OF SOILS SURROUNDING A CEMENT PLANT IN THE REPUBLIC OF KARAKALPAKSTAN..... 66

E.Sh. Sanayev, K.P. Serkayev
RESEARCH ON THE USE OF BARLEY FLOUR RICH IN PROTEIN, STARCH, AND SOLUBLE DIETARY FIBERS, OBTAINED USING AIR FRACTIONATION TECHNOLOGY, IN OBTAINING INSTANT PASTA..... 74

Sh.A. Ismailova, S.Z. Ibragimov, Z.Sh. Soporboev, O.I. Khudoyberganov
SYNTHESIS AND QUANTUM-CHEMICAL ANALYSIS OF A ZN(II) COMPLEX WITH INDOLE-3-ACETIC ACID AND ACETAMIDE… 79

R.O. Boboyorov, B. Ibragimov
SYSTEMATIC ANALYSIS OF THE TECHNOLOGICAL PROCESS OF NATURAL GAS PROCESSING AND FRACTIONATION AT THE SHURTAN GAS-CHEMICAL COMPLEX..... 89

D. Karabaev
DETERMINATION OF GAS FLOW VELOCITY IN PNEUMATIC SEPARATION OF MULTICOMPONENT GRANULAR MATERIALS.... 97

05.00.00 TECHNICAL SCIENCES

G‘.N. Sharipov, F.F. Rajabov, A.A. Qosimov
DEVELOPMENT OF A QUANTUM METROLOGY-BASED STANDARD COMPLIANCE INDEX (SMI) MODEL FOR ACCURACY EVALUATION OF POLYGRAPH MEASUREMENT SYSTEMS..... 106

S. Sulaymonov, S.K. Urinova
THEORY OF DEVELOPING A MATHEMATICAL MODEL OF THE DYNAMICS AND EMISSION OF GREENHOUSE MICROCLIMATE INDICATORS..... 114

F.A. Abdunazarov, Zh.Sh. Chuyanboev, Z.A. Davronov
OPTIMIZATION OF THERMAL LIQUIDATION PARAMETERS AND KINETIC MODELING OF THE PROCESS OF DELAYED COKING OF OIL RESIDUES..... 120

Sh.Z. Valikulov, B.H. Matsaidov
APPLICATION OF NANOTECHNOLOGY TO ENHANCE FORMATION PERMEABILITY..... 125

M.K. Hamrayeva
DIGITALIZATION OF REGIONAL CHILDREN’S LIBRARIES THROUGH ARTIFICIAL INTELLIGENCE TECHNOLOGIES..... 130

K. Shukurov, N. Tolibova, F. Sulaymonova
BRAIN TUMOR CLASSIFICATION USING AN ENSEMBLE DEEP LEARNING MODEL WITH EFFICIENTNET, RESNET, AND VISION TRANSFORMER..... 134

F.Sh. Yuldashev, Sh. Jumaboeva
FULL-SCALE STATIC LOAD TESTS OF DEEP SOIL MIXING PILES IN ALLUVIAL SILTY LOAMS OF ANDIJAN REGION..... 143

D.E. Khujamberdiyev
FACT-CENTERED ORGANIZATION OF DIGITAL INFORMATION FLOW IN MULTI-AGENT SYSTEMS AND INCREMENTAL MAINTENANCE OF THE REPOSITORY.....

147

F.Sh. Yuldashev, Sh. Jumaboyeva
LIMITATIONS OF CLASSICAL ANALYTICAL METHODS IN THE DESIGN OF DSM-PILLARS..... 156

N.R. Avezova, R.U. Kuchkarbaev, E.A. Oshepkova, A.U. Butaev
IMPROVEMENT OF THE REGULATORY AND METHODOLOGICAL FRAMEWORK FOR ENHANCING BUILDING ENERGY EFFICIENCY IN UZBEKISTAN AT THE PRESENT STAGE..... 161

S. Duschanov, I. Boyzhanov
BASED ON THE LIMESTONE FROM THE “UCH O‘CHOQ” DEPOSIT AND THE MARL CLAY FROM THE “MESHIKLI” DEPOSIT, ENERGY-EFFICIENT PORTLAND CEMENT CLINKER..... 169

S. Zoirov, J. Patinov, I. Shoqosimov
PROSPECTS OF USING SOLAR ENERGY..... 177

Yu.G. Anufrieva
TRANSFORMATION OF THE LIBRARY: FROM TRADITIONAL TECHNICAL MEANS TO A PROACTIVE DIGITAL ENVIRONMENT. 182

B. Abdukarimov, O. Urishev, D. Islomov, S. Ikromov
ANALYSIS OF A HYBRID HEATING SYSTEM BASED ON HEAT PUMPS AND SOLAR COLLECTORS..... 188

O. Urishev, A. Mahmudjonov, A. Abduvossiyev, M. Tursunaliyeva
HYDRODYNAMIC ANALYSIS OF A SPIRAL PUMP DRIVEN BY A WATER WHEEL UNDER LOW-HEAD OPEN CHANNEL FLOW CONDITIONS..... 200

Sh.B. Avlyakulova
"VECTROGRAPH" PROGRAM WORK PRINCIPLE, DYNAMIC MANAGEMENT OPPORTUNITIES AND EXPERIMENT RESULTS..... 210

O. Mallayev, F. Sulaymonova, N. Tolibova
COMPARATIVE ANALYSIS OF BLUR AUGMENTATION STRATEGIES FOR HARMFUL CONTENT IMAGE CLASSIFICATION USING EFFICIENTNET-B0: A PRELIMINARY STUDY..... 216

S.Sh. Nasirova, A.A. Suleymanov, S.X. Fayzullayev
INNOVATIVE TECHNOLOGIES FOR IMPROVING EVACUATION METHODS..... 223

Murodova Shaxodat Shamurzayevna
TECHNOLOGY FOR THE AUTOMATED SELECTION AND ADAPTIVE ASSESSMENT OF NON-STANDARD PROBLEMS..... 156

Navruzbek Kurbonov, Mirshod Abdullayev
OPERABILITY LIMITS OF A SAW COTTON SEED LINTER UNDER RAW-MATERIAL GRADE VARIATION AND SAW WEAR..... 240

Mirjalol Ashurov
DESIGNING AN INTEGRATIVE EDUCATIONAL PLATFORM BASED ON COMPUTER MODELLING: ARCHITECTURE, DATA MODEL AND PEDAGOGICAL LAYER FOR DEVELOPING STUDENTS’ DIGITAL COMPETENCE..... 248

Mirshod Abdullayev, Navruzbek Kurbonov
DEVELOPMENT OF A SUGENO FUZZY LOGIC-BASED CONTROL ALGORITHM FOR ELECTRICAL PULSE TREATMENT OF PLANTS..... 259

A.S. Saidov, Sh.N. Usmonov, D.V. Saparov, H.Sh. Abdullayev
MORPHOLOGY AND ELEMENTAL COMPOSITION OF A MULTICOMPONENT EPITAXIAL LAYER IN THE SI–GAP–ZNSE–ZNTE SYSTEM GROWN ON A GAP(100) SUBSTRATE BY LIQUID-PHASE EPITAXY..... 269

08.00.00 ECONOMIC SCIENCES

D.Sh. Chintemirova
SKILLS OVER DEGREES: A STATISTICAL ANALYSIS OF LABOR MARKET TRENDS..... 278

S.Sh. Nurmatova
CONSUMER BEHAVIOR IN TOURISM AS A STRATEGIC FACTOR IN THE DEVELOPMENT OF UZBEKISTAN’S TOURISM MARKET: A THEORETICAL JUSTIFICATION FOR THE NECESSITY OF RESEARCH..... 287

Q.Q. Aliqulov
METHODOLOGY FOR DETERMINING FINANCIAL EFFICIENCY IN THE PRIVATIZATION OF STATE-OWNED BANKS..... 297

D. Khamidullayeva
DEVELOPMENT OF SEMI-PROCESSED FOOD PRODUCT EXPORTS IN UZBEKISTAN..... 303

O.U. Mavlonov
ANALYSIS OF FACTORS AFFECTING FINANCIAL STABILITY IN STATE-OWNED ENTERPRISES..... 311

A.R. Bozorov
REVENUE GENERATION AND FINANCIAL SUSTAINABILITY OF HIGHER EDUCATION INSTITUTIONS: A COMPARATIVE ANALYSIS BASED ON THE EXPERIENCE OF EUROPEAN, US AND ASIAN UNIVERSITIES..... 317

A.B. Abatov
TRENDS AND FEATURES OF LIGHT INDUSTRY DEVELOPMENT IN THE REPUBLIC OF KARAKALPAKSTAN: ACHIEVEMENTS, PROBLEMS, AND PROSPECTS..... 332

I.A. Gulamov, M.M. Mahmudov
THEORETICAL AND METHODOLOGICAL FOUNDATIONS OF SUPPLYING THE DOMESTIC MARKET OF UZBEKISTAN WITH NATIONAL PRODUCTS..... 336

Ismailov Timur
THE IMPORTANCE AND NEED FOR IMPLEMENTING INTERNATIONAL ENVIRONMENTAL AUDIT STANDARDS..... 341

Abduvali Abdug'ani o'g'li Aktamov
MODERN TRENDS IN IMPROVING INCLUSIVE PASSENGER TRANSPORTATION SERVICES..... 349

International Scientific Journal
Science and Innovation Series A
Volume 5 Issue 5

ISSN: 2181-3337

Published: 30.05.2026. Font: “Times New Roman”.

LLC “Science and innovation”
License Mass Media №:1597 27.04.2022
License Publisher №:455168 21.11.2024
Address: 100121, Uzbekistan, Tashkent city, Yakkasaroy district,
Shota Rustaveli Street 150, Vega Business Center, 6th floor, Room 2.
www.scientists.uz, info@scientists.uz, +998901259654